National Research Council Canada
Conseil national de recherches Canada

NRC·CNRC

Canadian Journal of Fisheries and Aquatic Sciences

Journal canadien des sciences halieutiques et aquatiques

http://www.nrc.ca/cisti/journals

ISSN 0706-652X / CJFSDX 56(Suppl. 1) 1–198 (1999)

The *Canadian Journal of Fisheries and Aquatic Sciences*, previously published as *Contributions to Canadian Biology* 1901–1925, *Contributions to Canadian Biology and Fisheries* 1926–1934, *Journal of the Biological Board of Canada* 1934–1937, and *Journal of the Fisheries Research Board of Canada* 1938–1979, is issued monthly to form annual volumes of 12 numbers plus supplements.

Editorial policy: The Journal publishes original research articles, perspectives (syntheses, critiques, re-evaluations), discussions (comment and reply), and rapid communications. Manuscripts may concern cells, organisms, populations, communities, ecosystems, or processes that affect aquatic systems. They may cover a range of disciplines including biology and ecology of marine and freshwater organisms, limnology, oceanography, physiology, toxicology, genetics, economics, disease, and management. Preference will be given to manuscripts that emphasize understanding of observed phenomena and interpretation of experimental results. The Journal encourages papers that lead from clearly stated purpose or rationale and from testable hypotheses, concepts, or questions to identifiable conclusions or syntheses. Such papers may amplify, modify, question, or redirect accumulated knowledge embodied in contemporary perceptions of a particular state of aquatic sciences. The Journal discourages papers that are essentially descriptive, except in emerging disciplines; have only site-specific or local applications (a certain year, place, taxon, chemical compound, etc.); only confirm previously established principles; or apply standard techniques without breaking new methodological ground.

Manuscripts for publication should be submitted to the Editors, Canadian Journal of Fisheries and Aquatic Sciences, Department of Zoology, University of Guelph, Guelph, ON N1G 2W1, Canada (519-824-4120 ext. 2646; fax: 519-767-9798; e-mail: cjfas@uoguelph.ca).

Submissions in either English or French are acceptable. The information must be original, that is, not copyrighted, published, or submitted elsewhere except in abstract form or unless by written consent of the Editor. NRC accepts no responsibility for statements or opinions expressed by a contributor. Acceptance of an advertisement, announcement, or other material does not imply endorsement by either the *Journal*'s Editors or NRC. The use of proprietary names does not imply endorsement of the product or company.

Correspondence concerning accepted manuscripts and corrected proofs should be sent to NRC Research Press, National Research Council of Canada, Ottawa, ON K1A 0R6, Canada.

Instructions to Authors are published once a year in the first issue of each volume. Copies are available from NRC Research Press or from our Web site. The **Publication Policy** of NRC Research Press is also available at our Web site:
http://www.nrc.ca/cisti/journals/rj.html

Microfilm: Issues from 1934 through the current volume can be purchased on 16- or 35-mm microfilm. Photocopies of individual articles or issues can be purchased from University Microfilms International, 330 North Zeeb Road, Ann Arbor, MI 48106, U.S.A.

U.S. periodical postage paid at Champlain, N.Y., and at additional mailing offices. Attention U.S. POSTMASTER: Send address changes to **Canadian Journal of Fisheries and Aquatic Sciences**, c/o USACAN Media Distribution Center, P.O. Box 2888, Plattsburg, NY 12901, U.S.A.

Publié sans interruption depuis 1901, le *Journal canadien des sciences halieutiques et aquatiques* a paru sous plusieurs titres : *Contributions to Canadian Biology* 1901–1925, *Contributions to Canadian Biology and Fisheries* 1926–1934, *Journal of the Biological Board of Canada* 1934–1937, et *Journal of the Fisheries Research Board of Canada* 1938–1979. Le *Journal* paraît tous les mois, formant ainsi un volume de 12 numéros, et offre en plus jusqu'à deux suppléments par année.

Politique éditoriale : On publie, dans le Journal, des articles rendant compte de recherche originale, des perspectives (synthèses, critiques et réévaluations), des discussions (commentaires et réponses) et des communications rapides. Les documents peuvent porter sur les cellules, organismes, populations, communautés, écosystèmes ou processus qui affectent les systèmes aquatiques. Ils peuvent relever de divers domaines y compris la biologie et l'écologie des organismes marins et d'eau douce, la limnologie, l'océanographie, la physiologie, la toxicologie, la génétique, l'économie, la pathologie et la gestion. On accorde la préséance aux articles qui contribuent à la compréhension de phénomènes observés et à l'interprétation de résultats expérimentaux. On invite les auteurs à soumettre des articles ayant des objectifs précis ou relevant d'hypothèses, de concepts ou de questions vérifiables et se terminant par de solides conclusions ou d'utiles synthèses. Ces articles enrichissent, changent, mettent en question ou réorientent les connaissances acquises sur divers aspects des sciences aquatiques. On décourage toutefois la soumission d'articles simplement descriptifs (à moins qu'il ne s'agisse de nouvelles disciplines), d'application très limitée (applicables à une seule année, une seule région ou un seul taxon, portant sur un unique composé chimique, etc.); d'articles qui ne font que reprendre les principes énoncés dans des articles précédents; et d'articles rendant compte de l'application de normes sans gain de méthodologie.

Les auteurs voudront adresser leurs **manuscrits** aux directeurs scientifiques, Journal canadien des sciences halieutiques et aquatiques, Département de Zoologie, University of Guelph, Guelph, ON N1G 2W1, Canada (519-824-4120 poste. 2646; télécopieur : 519-767-9798; adresse électronique : cjfas@uoguelph.ca).

Les contributions peuvent être en anglais ou en français. Elles doivent être originales, c.-à.-d. qu'elles ne doivent pas avoir fait l'objet d'un copyright, avoir été publiées ou soumises ailleurs, sauf sous forme abrégée ou avec le consentement du rédacteur. Le CNRC ne se tient en aucune façon responsable des opinions exprimées par un collaborateur ou des déclarations qui pourrait faire ce dernier. La publication d'annonces publicitaires, d'avis et autres n'implique pas l'endossement de leur contenu par les directeurs du *Journal* ou du CNRC. L'utilisation des noms de marques de commerce ne signifie aucunement une sanction du produit en question ou de la compagnie qui le fabrique.

La correspondance ayant trait aux manuscrits acceptés et les **épreuves corrigés** doivent être envoyées aux Presses scientifiques du CNRC, Conseil national de recherches du Canada, Ottawa, ON K1A 0R6, Canada.

Recommandations aux auteurs sont publiés une fois par année dans le premier numéro de chaque volume. Des copies, ainsi que la **Politique de publication**, sont disponibles auprès des Presses scientifiques du CNRC ou au site Web :
http://www.nrc.ca/cisti/journals/rj.html

Microfilms : On peut acheter sur microfilms de 16 ou 35 mm tous les numéros depuis 1934. Des photocopies d'articles ou de numéros individuels sont aussi en vente auprès de University Microfilms International, 330 North Zeeb Road, Ann Arbor, MI 48106, É.-U.

This journal is indexed or abstracted in / Ce journal est signalé ou résumé dans
Aquatic Sciences and Fisheries Abstracts, Biological & Agricultural Index, CAB Abstracts (Centre for Agriculture and Biosciences), Chemical Abstracts, Current Awareness in Biological Sciences, Current Contents, FAO Freshwater and Aquaculture Contents Tables, FAO Marine Science Contents Tables, GEOBASE – Geo Abstracts, Meteorological and Geoastrophysical Abstracts, Oceanic Abstracts, Science Citation Index, Biological Abstracts, Environment Abstracts, Environmental Periodicals Bibliography, GEOREF, Life Sciences Collection, ABSEARCH, and PASCAL Database

Volume 56, Supplement 1, 1999

Canadian Journal of Fisheries and Aquatic Sciences

Published by the National Research Council of Canada

Volume 56, supplément 1, 1999

Journal canadien des sciences halieutiques et aquatiques

Publié par le Conseil national de recherches du Canada

Editors / directeurs scientifiques John C. Roff and Moira M. Ferguson

Assistant to the Editors / adjointe aux directeurs scientifiques **Holly Foster**

Associate Editors / directeurs scientifique associés

D. Boisclair, *Université de Montréal*
U. Borgmann, *Environment Canada, Burlington*
S.E. Campana, *DFO/MPO, Dartmouth*
D.G. Dixon, *University of Waterloo*
A.E. Dizon, *National Marine Fisheries Service, La Jolla, Calif.*
J.J. Dodson, *Université Laval*
J.A. Downing, *Iowa State University*
K.T. Frank, *DFO/MPO, Dartmouth*
D.F. Houlihan, *University of Aberdeen, Aberdeen, Scotland*
F.A. Huntingford, *University of Glasgow*
J.A. Hutchings, *Dalhousie University*
G.S. Jamieson, *DFO/MPO, Nanaimo*
B. Jonsson, *Norwegian Institute for Nature Research, Oslo, Norway*
L. Legendre, *Université Laval*
D.M. Mason, *Purdue University, West Lafayette, Ind.*
A. Mazumder, *University of Victoria*
D.L. Parrish, *Vermont Cooperative Fish and Wildlife Research Unit (USGS/BRD), University of Vermont*
P. Pepin, *DFO/MPO, St. John's*
R.M. Peterman, *Simon Fraser University*
E.E. Prepas, *University of Alberta*
T.M. Powell, *University of California, Berkeley, Calif.*
T.J. Quinn II, *University of Alaska–Fairbanks, Juneau, Alaska*
T.P. Quinn, *University of Washington*
R.D. Robarts, *Environment Canada, Saskatoon*
B. Sainte-Marie, *DFO/MPO, Mont-Joli*
P.F. Sale, *University of Windsor*
D.W. Schindler, *University of Alberta*
S.J. Smith, *DFO/MPO, Dartmouth*
W.G. Sprules, *University of Toronto*
R.J. Thompson, *Memorial University of Newfoundland*
C.J. Walters, *University of British Columbia*
R.D. Ward, *CSIRO Division of Fisheries, Australia*
C.M. Wood, *McMaster University*
B. de Young, *Memorial University of Newfoundland*

NRC Research Press / Presses scientifiques du CNRC

Editor-in-chief / directeur général **Bruce P. Dancik**

Assistant Editor-in-chief / directeur général adjoint **Iain E.P. Taylor**

Journals Program / Programme des revues

(Fax / télécopieur : 613-952-7656; e-mail / adresse électronique : research.journals@nrc.ca;
URL: http://www.nrc.ca/cisti/journals/)

Director / directrice **Aldyth Holmes**

Business Manager / gestionnaire des affaires **Paul McClymont**

Managing Editor / rédactrice administrative **Cecily M. Pearson (613-993-9099)**

Publication Officer / agente de publication **Jennifer McColl**

Advertising / annonces publicitaires **Judy Heyman (613-993-0151)**

Reprints / tirés à part **Roxanne Landriault (613-990-2254)**

Subscriptions / abonnements **Helen Goulet (613-993-9084)**

© National Research Council of Canada 1999. World rights reserved.
No part of this publication may be reproduced, stored, or transmitted in any form or by any means, without the written permission of the publisher, except as stated below.

The National Research Council of Canada grants **permission*** to individuals to make single copies of articles for personal use. Any person may reproduce short excerpts from articles in the journal for any purpose that respects the moral rights of authors, provided that the source is fully acknowledged. As a courtesy, the consent of authors of such material should be obtained directly from the author.

Authorization to reproduce items for other than personal use, as stated above, is granted by the National Research Council of Canada provided that the copyright fee of $7.00 per copy is paid directly to CANCOPY, One Yonge Street, Suite 1900, Toronto, ON M5E 1E5, Canada.

*The above permission does not extend to other kinds of copying, such as copying for general distribution, for advertising, or promotional purposes, for creating new collective works, or for resale. For such copying, arrangements must be made with the publisher, National Research Council of Canada, Ottawa, ON K1A 0R6, Canada.

© Conseil national de recherches du Canada 1999. Tous droits réservés.
Il est interdit de reproduire, de sauvegarder ou de transmettre quelque partie de la présente publication dans quelque format ou de quelque façon sans le consentement écrit de l'éditeur, à l'exception des conditions suivantes.

Le Conseil national de recherches du Canada accorde aux particuliers le droit de faire des copies individuelles pour leur usage personnel. Toute personne peut reproduire de courts extraits des articles de la Revue pour autant que les droits moraux de l'auteur soient respectés et que la mention de provenance soit clairement indiquée. Il est de convenance de demander le consentement de l'auteur avant de faire mention de son travail.

On obtiendra l'autorisation de reproduire des articles à d'autres fins que l'usage personnel (tel qu'on l'a décrit ci-dessus) auprès du Conseil national de recherches du Canada pour autant que des redevances de droits d'auteurs de 7,00 $/copie soient versées au CANCOPY, 1, rue Yonge, bureau 1900, Toronto, ON M5E 1E5, Canada.

*La permission ci-dessus ne s'applique pas à la reproduction à grande échelle, telle que la reproduction aux fins de distribution générale, publicitaire ou promotionnelle, de compilation de nouveaux ouvrages collectifs ou de revente. Dans de tels cas, il faudra ratifier une entente particulière avec l'éditeur, le Conseil national de recherches du Canada, Ottawa, ON K1A 0R6, Canada.

Subscription information

The *Canadian Journal of Fisheries and Aquatic Sciences* (ISSN 0706-652X) is published monthly by the National Research Council of Canada. 1999 annual subscription rates (second class postage) for Canada are $578CAN institutional and $182CAN personal, for US & foreign $578US institutional and $192US personal. For air mail add $150US to foreign rate. Canadian customers please include 7% GST (business no. 12149 1807 RT 0275). Subscriptions are entered for the calendar year. Remittances should be made payable to the Receiver General for Canada credit NRC. Price for regular single issues: institutional, $75.00; personal, $25.00. Supplements will be priced separately. Special rates apply to members of Canadian scientific and engineering societies if they subscribe through their respective societies.

There are no refunds on cancelled subscriptions once delivery has begun. Claims for missing issues should be made within four months (N. America) or six months (outside N. America) following the date of publication. The publisher expects to supply missing issues only when losses have occurred in transit and when the reserve stock will permit. For change of address and subscription enquiries: Subscription Office, NRC Research Press, National Research Council of Canada, Ottawa, ON K1A 0R6, Canada; tel: 613-993-9084; fax: 613-952-7656; e-mail: research.journals@nrc.ca.

Microform backfiles are available from UMI, P.O. Box 1346, Ann Arbor, MI 48106-1346, U.S.A., and Micromedia Ltd., 20 Victoria St., Toronto, ON M5C 2N8, Canada.

The 1998 issues of the *Canadian Journal of Fisheries and Aquatic Sciences* are available on the Web. Pricing information can be found at

http://www.nrc.ca/cisti/journals/

Renseignements sur l'abonnement

Journal canadien des sciences halieutiques et aquatiques (ISSN 0706-652X) est une publication mensuelle du Conseil national de recherches du Canada. Le prix de l'abonnement annuel au Canada (courrier de deuxième classe) est de 578 $CAN pour les organismes et de 182 $CAN pour les particuliers. À l'étranger (y compris les É.-U.), le prix de l'abonnement est de 578 $US pour les organismes et de 192 $US pour les particuliers. L'expédition par avion exige des frais de 150 $US en sus du prix d'abonnement à l'étranger. Les clients du Canada doivent ajouter la TPS de 7% (numéro d'entreprise 12149 1807 RT 0275). Les abonnements sont pour l'année civile. Tout paiement doit être adressé au Receveur général du Canada, crédit du CNRC. Le prix par numéro est de 75 $ pour les organismes et de 25 $ pour les particuliers. Le prix des hors-série varie. Les membres des sociétés canadiennes de sciences et de génie bénéficient de taux préférentiels en s'abonnant via leurs sociétés respectives.

Aucun remboursement ne sera accordé ni aucune annulation acceptée une fois que les livraisons auront commencé. Les réclamations de numéros manquants devront être soumises dans les quatre mois (Amérique du Nord) ou dans les six mois (à l'extérieur de l'Amérique du Nord) suivant la date de publication. L'éditeur ne fournira de numéros manquants que si le document a été perdu pendant l'expédition et que si le stock le permet. Adressez tout changement d'adresse ou toute question quant à l'abonnement au : Bureau des abonnements, Presses scientifiques du CNRC, Conseil national de recherches Canada, Ottawa, ON K1A 0R6, Canada; téléphone : 613-993-9084; télécopieur : 613-952-7656; adresse électronique : research.journals@nrc.ca.

On peut obtenir les fichiers rétrospectifs sur **microforme** auprès de UMI, P.O. Box 1346, Ann Arbor, MI 48106-1346, É.-U., et auprès de Micromedia Ltée, 20 rue Victoria, Toronto, ON M5C 2N8, Canada.

Les numéros de 1998 de *Journal canadien des sciences halieutiques et aquatiques* sont accessibles sur le Web. On trouvera des renseignements sur les tarifs à

http://www.nrc.ca/cisti/journals/rjfr.html

Supplement Price
Canada: $49.95CAN
Other countries: $49.95US
NRC No. 42740

Prix du supplément
Au Canada : 49,95 $CAN
À l'étranger : 49,95 $US
N° de CNRC 42740

Selected proceedings of the symposium entitled "Space, time, and scale: new perspectives in fish ecology and management"

Sélection de comptes rendus du symposium intitulé «Espace, temps échelle : nouvelles perspectives pour l'écologie et la gestion des pêches»

Special Editors/Directeurs scientifiques spéciaux

Doran M. Mason
Purdue University, West Lafayette, Ind.

and

Stephen B. Brandt
NOAA – Great Lakes Environmental Research Laboratory, Ann Arbor, Mich.

Space, time, and scale: new perspectives in fish ecology and management

Doran M. Mason and Stephen B. Brandt

Abstract: This supplement is the product of a special symposium organized on "Space, time, and scale: new perspectives in fish ecology and management" held during the 127th annual meeting of the American Fisheries Society in Monterey, California, August 1997. The purpose of this supplement is to illustrate the breadth and diversity of ideas and applications being explored for integrating space, time, and scaling issues and to highlight future directions. Topics cover a variety of studies, techniques, and applications from salt water to freshwater, from lotic to lentic habitats, and across various scales that can be used as background for integrating space, time, and scale in ongoing and future fish research and management.

Résumé : Le présent supplément est le fruit du symposium spécial <<Espace, temps, échelle : nouvelles perspectives pour l'écologie et la gestion des pêches>>, qui s'est déroulé durant la 127e réunion annuelle de l'American Fisheries Society à Monterey, en Californie, en août 1997. Ce supplément veut refléter l'étendue et la diversité des nouvelles idées et applications en matière d'intégration des questions d'espace, de temps et d'échelle, et indiquer les orientations futures en cette matière. Les thèmes abordés couvrent diverses études, techniques et applications relatives au milieu marin et aux eaux douces, aux habitats lotiques et lénitiques sur des échelles diverses qui peuvent servir de base pour l'intégration de l'espace, du temps et de l'échelle dans les activités présentes et futures de recherche et de gestion concernant le poisson.

[Traduit par la Rédaction]

Fish ecologists and managers realize that all ecological systems exhibit heterogeneity and patchiness on a broad range of spatial and temporal scales (Haury et al. 1978). We all recognize that these patterns have fundamental effects on biological processes (Brandt et al. 1992; Mason and Brandt 1996), dynamics of populations and ecosystems (Walters and Juanes 1993), our perception of the environment (Levin 1992), and, ultimately, how we sample and manage natural resources (Steele 1978; Loehle 1991). Incorporation of space, time, and scale (and their interactions) in theories, modeling, and sampling has improved our understanding of how population dynamics and species interactions respond to the physical (e.g., temperature) and biological (e.g., prey density) spatial structure in the environment. Multiscale analysis has shown the existence of scale-dependent patterns (Weins 1989; Rastetter et al. 1992) that can be of biological or physical origin and that can have significant effects on biological processes (Turner and Gardner 1991). Recent advances in hardware and software technologies and analytical techniques have contributed to our abilities to acquire and analyze complex spatial data sets, and to model ecological processes, over a wide range of spatial and temporal scales. Despite these advances and our growing appreciation for the importance of space, time, and scale, it is still often ignored in field sampling and modeling programs that attempt to evaluate predator–prey interactions, fish growth and production, and sustainability of a fishery. The purpose of this supplement is to highlight how explicit considerations of space, time, and scale and use of various analysis tools can improve our understanding of species interactions and linkages between biological and physical processes, as well as provide critical data and information for the management of fisheries resources in complex ecosystems.

This supplement is a product of a special symposium organized on "Space, time, and scale: new perspectives in fish ecology and management" held during the 127th annual meeting of the American Fisheries Society in Monterey, California, during 24–28 August 1997. Many of the invited papers presented in the symposium, now peer-reviewed, are published in this supplement of the *Canadian Journal of Fisheries and Aquatic Sciences*. Contributions to the symposium were by invitation. We were particularly looking for a diverse array of research and approaches that represent a gradient from measures to quantify pattern and scale to models that explore the consequences of pattern. We did not intend for the symposium to cover all aspects of space and scaling issues or to be a comprehensive summary of the state of the art. Other reviews on space, time, and scaling issues in ecology and resource management can be found in Wiens (1989), Levin (1992), Kolasa and Pickett (1991), Levin et al. (1993), Schneider (1994), Hanski and Gilpin (1997), and Tilman and Kareiva (1997). Moreover, the symposium does not include all of the innovative technologies being used in aquatic ecosystems (e.g., LIDAR). Rather, our purpose was

Received August 31, 1999. Accepted September 1, 1999.
J15333

D.M. Mason.[1] Department of Forestry and Natural Resources, Purdue University, 1159 Forestry Building, West Lafayette, IN 47907-1159, U.S.A. e-mail: doran@fnr.purdue.edu
S.B. Brandt. National Oceanic and Atmospheric Administration, Great Lakes Environmental Research Laboratory, 2205 Commonwealth Blvd., Ann Arbor, MI 48105, U.S.A. e-mail: brandt@glerl.noaa.gov

[1]Author to whom all correspondence should be addressed.

© 1999 NRC Canada

Table 1. Papers in the symposium "Space, time, and scale: new perspectives in fish ecology and management."

	System			Scale		Analysis		
Authors of papers	River	Lake	Ocean*	Spatial	Temporal	Models	Data	General topic
Ault et al.			✓	10–100 m	Days–months	✓		Predator–prey/spatial distribution/recruitment
Beauchamp et al.		✓		1–100 m	Hours	✓		Foraging
Essington and Kitchell		✓		10–100 m	Hours–months	✓	✓	Spatial distribution/horizontal migration
Horne et al.			✓	10^{-4}–10^{11} m^2	Milliseconds–centuries		✓	Critical scales
Hrabik and Magnuson		✓		1–1000 m	Years–decades	✓		Species dispersal/invasion
Kline			✓	100 km	Months–years		✓	Food web/stable isotopes
Lamon and Stow		✓		1–100 m	Years	✓	✓	Contaminants/trend detection
Luecke et al.		✓		1–100 m	Days–years	✓		Foraging/bioenergetics/growth
Nøttestad et al.			✓	1–1000 km	Days–months	✓		Spatial distribution/horizontal migration
Rahel and Nibbelink	✓			1 km	Years		✓	Habitat gradients/species occurrence
Rose and Kulka			✓	1–1000 km	Years		✓	Commercial fisheries
Schindler		✓		1 m	Hours–months	✓		Habitat selection/overwinter mortality
Schneider et al.			✓	1 m – 100 km	Hours–years		✓	Critical scales
Steinhart and Wurtsbaugh		✓		1 m	Hours		✓	Vertical migration
Stockwell and Johnson		✓		1–10 m	Hours–months	✓		Foraging/bioenergetics/growth
Swartzman et al.			✓	1–1000 m	Days		✓	Predator–prey/spatial distribution/tools
Zlokovitz and Secor	✓		✓	10 km	Years		✓	Contaminants/otolith analysis

*Includes estuaries.

to illustrate the breadth and diversity of ideas and applications being explored and to highlight future directions.

The papers presented in this volume cover a variety of studies, techniques, and applications from salt water to freshwater, from lotic to lentic habitats, and across various scales ranging from milliseconds to centuries and millimetres to thousands of kilometres (Table 1). Topics covered in this supplement include the following.

(1) Schindler, Essington and Kitchell, Ault et al., Nøttestad et al., and Hrabik and Mangnuson use contrasting modeling techniques to explore the potential mechanisms for small- and large-scale horizontal migration/dispersal patterns and the corresponding patterns in spatial distribution at scales ranging from metres to thousands of kilometers and from hours to decades. The consequences of these migrations are evaluated in the context of foraging, predator–prey interactions, survival, recruitment, and exotic species invasions. In contrast, Rahel and Nibbelink use Geographic Information System (GIS) technology to predict the landscape-level spatial distribution of brown trout (*Salmo trutta*) and explore the role of smaller-scale regional processes when predictions fail.

(2) Lamon and Stow, and a paper by Zlokovitz and Secor, highlight the advantages of reducing variance in estimates of contaminant concentrations in fish tissue by considering spatial location of samples and identify distinct "hot spots" that may be responsible for contributing to high contaminant levels. In addition, both papers highlight two very different, yet innovative approaches (classification and regression trees and electron microanalysis of otolith strontium) for understanding spatial complexity in contaminant body burden. Both papers emphasize the need to understand better the life stage dependent migratory behavior of fishes in space and time to predict changes in polychlorinated biphenyl levels.

(3) Kline uses stable-isotope ratios of carbon and nitrogen from zooplankton and fish samples to identify seasonal and spatial trends in the source of energy (Prince William Sound versus the Gulf of Alaska) for juvenile Pacific herring (*Clupea pallasi*) and juvenile walleye pollock (*Theragra chalcogramma*) in Prince William Sound, Alaska. Based on his results, he conjectures that recruitment and nutritional processes in fishes residing in Prince William Sound are closely linked to cross-shelf transport of zooplankton, from Gulf of Alaska to Prince William Sound.

(4) Rose and Kulka explore the role of spatial processes in fisheries-dependent data on our ability to interpret overexploitation in a fishery. They provide an important lesson on how ignoring spatial issues in a fishery may have devastating consequences to fish populations.

(5) Beauchamp et al., Luecke et al., Steinhart and Wurtsbaugh, and Stockwell and Johnson explore how fine-scale processes affect the vertical spatial distribution of fishes and highlight the implications for foraging and growth. These contributions demonstrate the behavioral plasticity of fishes to changes in their local environment over diel and seasonal time steps, demonstrate the interactive effect of prey abundance and environmental conditions in mediating predator–prey interactions, provide

© 1999 NRC Canada

insight into the spatial scale at which visual predators experience patchiness of prey, and provide relevance for the use of spatially explicit models of growth rate potential (Brandt et al. 1992) for quantifying pelagic habitat and changes in quantity and quality of habitat.

(6) Horne et al. and Schneider et al. provide insight into the identification of key processes controlling populations over various spatial and temporal scales. Horne et al. use dimensionless ratios of rates to determine the relative importance of biological and physical processes across scales and demonstrate that dominant processes differ across various scales, life history stages, and species. Schneider et al. use a recently developed graphical technique to quantify how critical scales change with fish ontogeny. The two papers combine to demonstrate that critical time and space scales are linked and cannot be taken as constants.

(7) Swartzman et al. develop computer-based tools for the analysis and exploratory comparisons of spatial data sets, patch identification, and quantifying spatial and scale-dependent proximity between predators and prey. These tools may be used for scale-robust hypothesis formulation and testing of spatial patterns of predators and prey.

We hope that the papers in this supplement of the *Canadian Journal of Fisheries and Aquatic Sciences* will provide the motivation to incorporate space, time, and scaling issues in research and management. We expect that our understanding and appreciation of spatial and temporal processes occurring at various scales (dictated by relevant fluid and ecological dynamics) in aquatic ecosystems will dramatically improve in concert with continued development of three-dimensional spatial and temporal modeling and expanded coupling of physical and biological processes.

Acknowledgments

We thank John B. Dunning, Jr. for comments on a previous version of this paper. This research was funded by the University of Wisconsin Sea Grant Institute under grants from the National Sea Grant College Program, National Oceanic and Atmospheric Administration, U.S. Department of Commerce, and from the State of Wisconsin, federal grant No. NA46RG0481, project No. R/LR-72, to D.M.M. and by NSF grant No. OCE9417540 to S.B.B. This is publication No. 1146 of the National Oceanic and Atmospheric Administration Great Lakes Environmental Research Laboratory.

References

Brandt, S.B., Mason, D.M., and Patrick, E.V. 1992. Spatially-explicit models of fish growth rate. Fisheries (Bethesda), **17**: 23–35.

Hanski, I.A., and Gilpin, M.E (*Editors*). 1997. Metapopulation biology: ecology, genetics, and evolution. Academic Press, San Diego, Calif.

Haury, L.R., McGowan, J.A., and Wiebe, P.H. 1978. Patterns and processes in the time–space scales of plankton distributions. *In* Spatial pattern in plankton communities. *Edited by* J.H. Steele. Plenum Press, New York. pp. 277–327.

Kolasa, J., and Pickett, S.T.A (*Editors*). 1991. Ecological heterogeneity. Spring-Verlag, New York.

Levin, S.A. 1992. The problem of pattern and scale in ecology. Ecology, **73**: 1943–1967.

Levin, S.A., Powell, T.M., and Steele, J.W. (*Editors*). 1993. Patch dynamics. Springer-Verlag, New York.

Loehle, C. 1991. Managing and monitoring ecosystems in the face of heterogeneity. *In* Ecological heterogeneity. *Edited by* J. Kolasa and S.T.A Pickett. Springer-Verlag, New York. pp. 144–159.

Mason, D.M., and Brandt, S.B. 1996. Effects of spatial scale, capture efficiency, and the spatial distribution of predators on the predictions made by spatially-explicit models of fish growth rate. Environ. Biol. Fishes, **45**: 283–298.

Rastetter, E.B., King, A.W., Cosby, B.J., Hornberger, G.M., O'Neill, R.V., and Hobbie, J.E. 1992. Aggregating fine-scale ecological knowledge to model coarser-scale attributes of ecosystems. Ecol. Appl. **2**: 55–70.

Schneider, D.C. 1994. Quantitative ecology: spatial and temporal scaling. Academic Press, San Diego, Calif.

Steele, J.H. 1978. Some comments on plankton patches. *In* Spatial pattern in plankton communities. *Edited by* J.H. Steele. Plenum Press, New York. pp. 1–20.

Tilman, D., and Kareiva, P. (*Editors*). 1997. Spatial ecology: the role of space in population dynamics and interspecific interactions. Princeton University Press, Princeton, N.J.

Turner, M.G., and Gardner, R.H. 1991. Quantitative methods in landscape ecology: the analysis and interpretation of landscape heterogeneity. Ecological studies. Vol. 82. Springer-Verlag, New York.

Walters, C.J., and Juanes, F. 1993. Recruitment limitations as a consequence of natural selection for use of restricted feeding habitats and predation risk taking by juvenile fishes. Can. J. Fish. Aquat. Sci. **50**: 2050–2070.

Wiens, J.A. 1989. Spatial scaling in ecology. Funct. Ecol. **3**: 385–397.

© 1999 NRC Canada

A spatial dynamic multistock production model[1]

Jerald S. Ault, Jiangang Luo, Steven G. Smith, Joseph E. Serafy, John D. Wang, Robert Humston, and Guillermo A. Diaz

Abstract: We developed a generalized spatial dynamic age-structured multistock production model by linking bioenergetic principles of physiology, population ecology, and community trophodynamics to a two-dimensional finite-element hydrodynamic circulation model. Animal movement is based on a search of an environmental–habitat feature vector that maximizes cohort production dynamics. We implemented a numerical version of the model and used scientific data visualization to display real-time results. As a proxy for larger regional-scale dynamics, we applied the model to study the space–time behavior of recruitment and predator–prey production dynamics for cohorts of spotted seatrout (*Cynoscion nebulosus*) and pink shrimp (*Penaeus duorarum*) in the tropical waters of Biscayne Bay, Florida.

Résumé : Nous avons élaboré un modèle de production spatial et dynamique généralisé pour stock mixte, structuré selon l'âge, en liant des principes bioénergétiques de physiologie, l'écologie des populations et la trophodynamique des communautés à un modèle de circulation hydrodynamique d'éléments finis à deux dimensions. Les déplacements des animaux sont fondés sur la recherche d'un vecteur de caractéristiques lié à l'environnement et à l'habitat qui maximise la dynamique de production des cohortes. Nous avons appliqué une version numérique du modèle et utilisé la visualisation de données scientifiques pour afficher les résultats en temps réel. Comme approximation de la dynamique plus vaste à l'échelle régionale, nous avons appliqué le modèle pour étudier le comportement spatio-temporel de la dynamique de production en rapport avec le recrutement et les relations prédateurs–proies chez des cohortes d'acoupa pintade (*Cynoscion nebulosus*) et de crevette rose du Nord (*Penaeus duorarum*) dans les eaux tropicales de la baie Biscayne, en Floride.

[Traduit par la Rédaction]

Introduction

Traditionally, water quality, critical habitats, and fish stocks have each been treated as separate management issues. However, pervasive declines in fishery production and widespread habitat degradation have emphasized the importance of taking a more holistic view. The new paradigm focuses assessment and modeling efforts on linking the production dynamics of fish populations, fishing, the biological community, the physical environment, and essential habitat (Department of Commerce 1997).

Such an approach is clearly needed in South Florida's coastal ocean ecosystem, which supports a wide diversity of tropical marine organisms, productive multispecies fisheries, and a multibillion dollar tourist economy. The ecosystem and its economically valuable fisheries are currently under siege from intense human development and increasing usage. Regional fishing effort has increased in proportion to staggering human population growth, which has had significant fisheries impacts. For example, Ault et al. (1998) found that 13 of 16 species of grouper and seven of 13 snapper species in the Florida Keys were overfished according to federal guidelines. The Florida Keys have been given the dubious distinction of being an "ecosystem-at-risk," ranking it as one of the nation's most significant yet most stressed marine resources under NOAA and National Park Service management (NOAA 1995). An additional concern is the restoration of the Florida Everglades (Harwell et al. 1997). Hydrologic projects of historic proportions are expected to substantially change the volume and timing of freshwater outflows into the coastal bays, thereby affecting many important inshore and reef fish populations directly and indirectly through environmental changes and food web interactions.

To address these issues, in this paper, we develop a model that extends traditional fish population dynamics theory using fundamental principles of bioenergetics, population ecology, and community trophodynamics. The numerical model strikes a balance between the highly articulated individual-based models (e.g., DeAngelis and Gross 1992) and contemporaneous applied population and community models (e.g., Gutierrez 1996). Our model divides each of n population cohorts into a number of patches and follows each of these patches over both space and time with fewer tactical assumptions about animal behavior than individual-based models. We link the environment and prey dynamics to fish (predator) production through a spatial distribution of growth rate potential (Brandt et al. 1992) to explore the extent to which physics and biology couple to determine spatial and temporal effects on the growth and survival of each patch. In addition, by summing individual patches over space, we can obtain information on the survivorship and

Received January 6, 1998. Accepted September 8, 1998. J14362

J.S. Ault,[2] J. Luo, S.G. Smith, J.E. Serafy, J.D. Wang, R. Humston, and G.A. Diaz. University of Miami, Rosenstiel School of Marine and Atmospheric Science, 4600 Rickenbacker Causeway, Miami, FL 33149, U.S.A.

[1]Invited Paper: 127th Annual American Fisheries Society, Monterey, Calif., Symposium: Space, Time and Scale: New Perspectives in Fish Ecology and Management (D.M. Mason and S.B. Brandt, Organizers).

[2]Author to whom all correspondence should be addressed. e-mail: ault@shark.rsmas.miami.edu

© 1999 NRC Canada

variability of cohort growth and recruitment. Summing the cohorts considers the population, while comparison of prey and predator reflects community dynamics. We use the model to understand how physics and biology contribute to growth, mortality, and development of a year-class by focusing our analysis on a key trophodynamic linkage between an important predator (spotted seatrout, *Cynoscion nebulosus*) and prey (pink shrimp, *Penaeus duorarum*) in the tropical waters of Biscayne Bay, Florida.

Methods

Physical setting

Biscayne Bay is a relatively shallow (<5 m) 750-km^2 subtropical lagoon adjacent to Miami on the southeastern coast of Florida, U.S.A. (Fig. 1). A wide variety of substrates (e.g., rocky outcrops, sand, silt–clay) and associated floral and faunal assemblages (e.g., seagrasses, sponges, soft corals, mangroves) provide a mosaic of habitats for over 150 species of fishes and macroinvertebrates (J.S. Ault et al., unpublished data). Average water temperatures range from 21°C in winter to 30°C in summer. Currents are driven by winds and semidiurnal tides (Fig. 2). Water exchange with the ocean is by way of numerous passes between the eastern barrier islands or Keys, and mean flushing time is about 2–3 months (Lee and Rooth 1976). A few kilometres to the east of Biscayne Bay is the northern boundary of the Florida Keys coral reef tract. Along the Bay's western shore is an extensive network of water management canals that regulate freshwater discharges into the Bay (Fig. 1). These canals facilitate agriculture and provide flood control. Episodic canal freshwater releases contribute to the development of ephemeral salinity gradients that range from freshwater on the Bay's western side to undiluted salt water to the east. Salinity patterns fluctuate seasonally between wet (June–November) and dry (December–May) seasons (Chin-Fatt 1986). We simulated water currents and salinities with a two-dimensional finite-element model of Biscayne Bay (Wang et al. 1988). The model space domain consisted of 6364 triangular elements and 3407 nodes, with grid spacings between nodes on the order of 500 m. The hydrodynamics model was parameterized for calendar year 1995 using tides predicted from harmonic constants, wind observations from the Rosenstiel School of Marine and Atmospheric Science dock on Virginia Key, and canal freshwater discharge data from the South Florida Water Management District. The hydrodynamics simulation model was run on 1-min time steps with currents and salinities output at 10-min intervals.

Biological setting

Pink shrimp (prey) and spotted seatrout (predator) both utilize similar nearshore bay environments as nursery areas. Adult pink shrimp spawn offshore (Munro et al. 1968; Kennedy and Barber 1981), and fertilized ova hatch and progress through a series of planktonic larval stages while being transported towards the coast by prevailing ocean currents (Jones et al. 1970). Postlarvae settle onto relatively shallow (<1 m) seagrass beds in coastal bays (Costello et al. 1986). Juvenile pink shrimp occupy this habitat until the onset of sexual maturity, which occurs at about 6 months of age and 85 mm total length (TL) (Eldred et al. 1961). Individuals then move to offshore grounds where they remain through adulthood (maximum age about 3 years) and are intensively fished (Iversen and Idyll 1960; Tabb et al. 1962*b*; Beardsley 1970). Spotted seatrout spend their entire life within coastal bays, and adults spawn in seaward entrance channels (Saucier and Baltz 1993). Fertilized ova hatch and within 2 weeks progress through planktonic larval stages as they are advectively transported shoreward by currents (Peebles and Tolley 1988). Larvae settle onto nearshore seagrass beds and unvegetated silt–clay substrates (McMichael and Peters 1989; Rutherford et al. 1989). Juveniles remain in these nearshore habitats for several months (Rutherford et al. 1989) and then gradually move to vegetated bottoms throughout the Bay as they grow older and larger (McMichael and Peters 1989). Seatrout reach sexual maturity at about 2.5 years, recruit to the fishery at 380 mm TL (about 3.5 years), and live to a maximum age of 9 years (Johnson and Seaman 1986; Maceina et al. 1987; Murphy and Taylor 1994).

Pink shrimp are omnivores, feeding mainly on detritus, algae, small benthic worms, molluscs, and crustaceans (Eldred et al. 1961). Pink shrimp are the principal food of juvenile spotted seatrout (Pearson 1929; Tabb 1961; Hettler 1989) and many other fishes harvested in the bays and coral reefs (Costello and Allen 1970; Bielsa et al. 1983).

Model overview

We develop a spatial dynamic multistock production model that includes demographic attributes of growth, survivorship, recruitment, and spatial movements, which are explicitly linked to "habitat features" of the physical and biological environment. The numerical version of the spatial dynamic model tracks cohorts of pink shrimp (prey, $N(a,t)$) and spotted seatrout (predator, $P(a,t)$) at age a and time t in space from spawning, through settlement and recruitment, and as they grow. To simplify the presentation, we begin with development of the multistock predator–prey model in dimensions of age and time, but independent of space. Subsequently, in describing larval transport and recruitment, all aspects of the coupled biophysical model are referenced in age, time, and space.

Predator–prey dynamics

We model predator growth using a bioenergetic framework to facilitate explicit coupling with the prey and the physical and biological environment. Traditional models describe the growth of fish with respect to time as the difference between rates of tissue synthesis (anabolism) and degeneration (catabolism) (von Bertalanffy 1949). Both anabolic and catabolic rates are considered to be allometric functions of individual weight (Jobling 1994). This allows age-structured growth to be written as a general conservation equation following Ault and Olson (1996):

$$(1)\qquad \mathrm{d}W(a,t) = \text{anabolism} - \text{catabolism}$$
$$= \lambda W(a,t)^m - \eta W(a,t)^n$$

where $W(a,t)$ is weight at age a and time t and λ and η are scalar coefficients. The anabolism power coefficient m relates to the proportionality between gut surface area of digestion and body volume, whereas catabolism is assumed to be proportional to body volume (e.g., the von Bertalanffy model assumes that $m = 2/3$ and $n = 1$). Equation 1 is in the form of the Chapman–Richards generalized growth equation (Gulland 1983) fundamental to many traditional fishery stock production models (Schaefer 1954; Pella and Tomlinson 1969; Fox 1970, 1975; Ault and Olson 1996). Dividing eq. 1 by $W(a,t)$ produces the weight-specific growth rate:

$$(2)\qquad \frac{1}{W(a,t)}\frac{\mathrm{d}W(a,t)}{\mathrm{d}t} = \lambda W(a,t)^{m-1} - \eta W(a,t)^{n-1}.$$

Equation 2 provides equivalency between the Chapman–Richards equation and the bioenergetic modeling framework (e.g., Kitchell et al. 1977; Bartell et al. 1986; Adams and Breck 1990; Hewett and Johnson 1992; Houde 1996):

$$(3)\qquad \frac{\mathrm{d}W(a,t)}{W(a,t)\mathrm{d}t} = (C - E - U) - R$$

where C is consumption, E is egestion, U is excretion, and R is respiration or total metabolic costs. Rate functions E and U are usually modeled as relative proportions of C (following Hewett and

© 1999 NRC Canada

Fig. 1. Map of the South Florida region with inset showing the Biscayne Bay study area. Coral reef, seagrass, hardbottom, and barebottom habitat types are indicated. Seagrass habitat is characterized by sandy or silt–clay sediments vegetated by three main varieties of seagrasses (i.e., *Thalassia*, *Halodule*, *Syringodium*). Hardbottom consists of a foundation of oolitic limestone covered by a thin sediment layer populated with sponges and soft corals. Barebottom is substrate generally devoid of large benthic organisms. Bay depth contours are shown. The water management overland canal network is indicated by dashed lines.

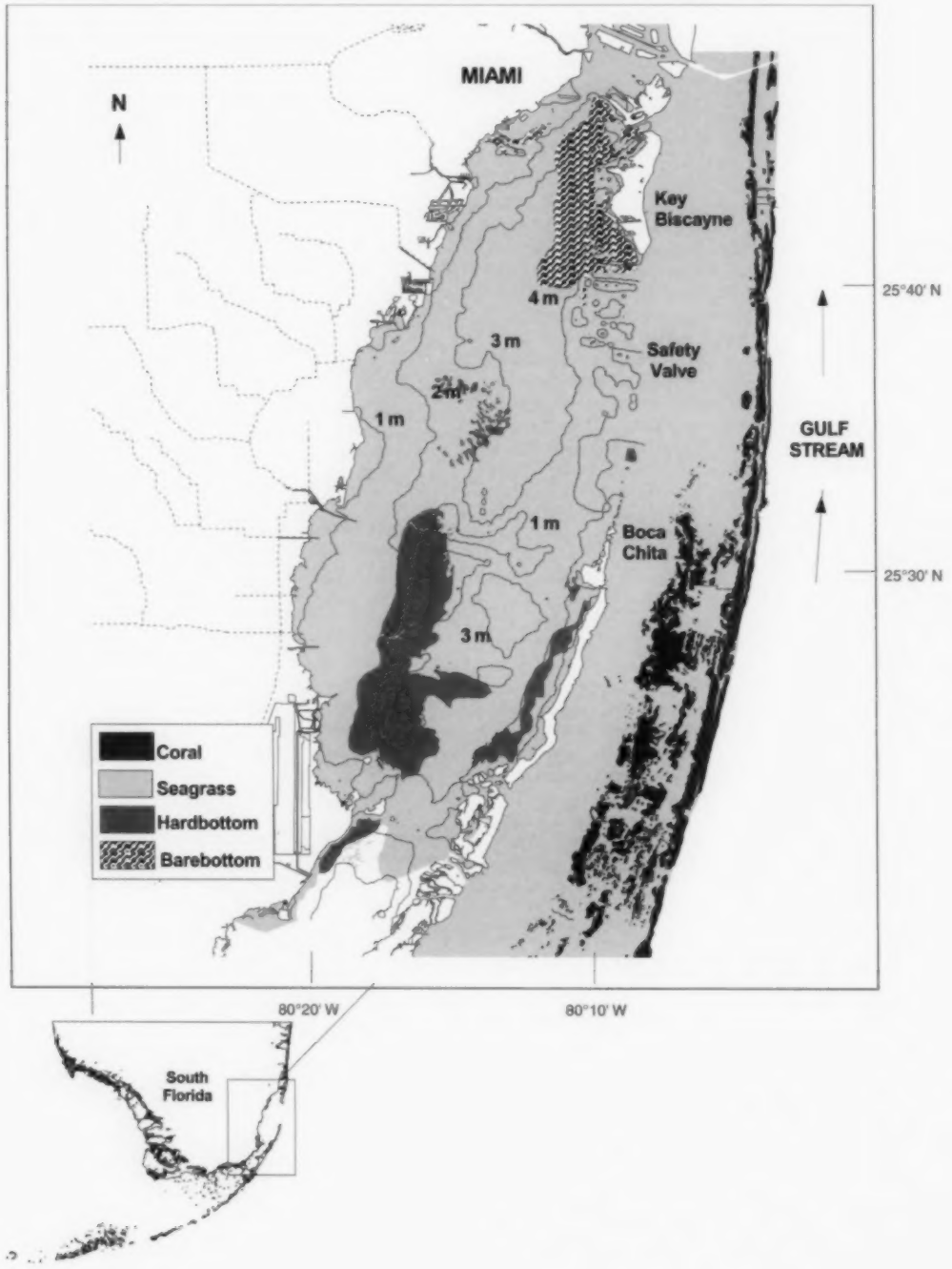

© 1999 NRC Canada

Fig. 2. Biscayne Bay hydrodynamic model outputs showing typical daily current patterns of (A) flood tide and (B) ebb tide and seasonal salinity patterns ranging between 0 and 36‰ for the (C) dry season (December–May) and (D) wet season (June–November). The vector arrows in Figs. 2A and 2B show the direction and magnitude of currents at particular locations; large arrows indicate a scale of 1 $m \cdot s^{-1}$.

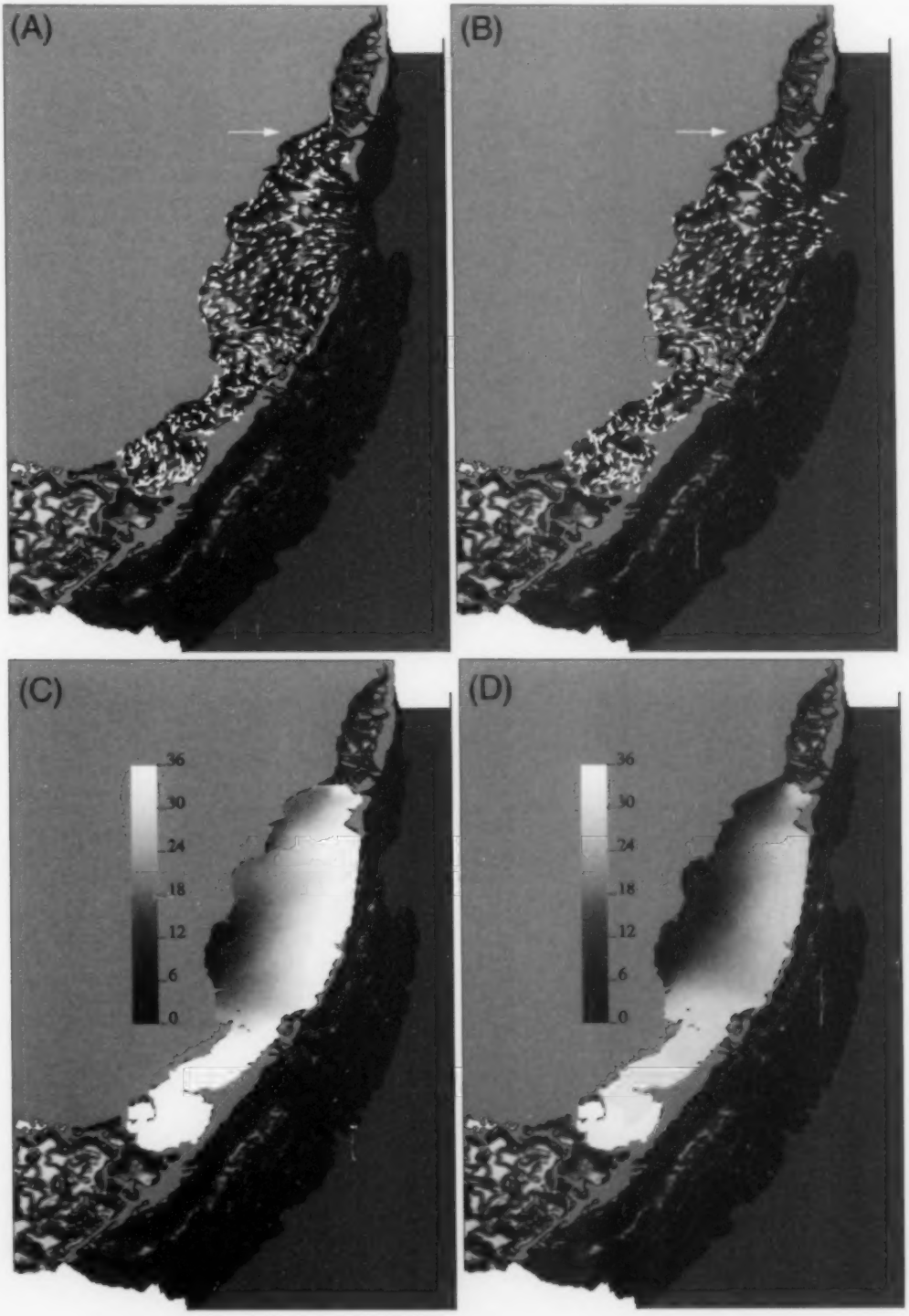

© 1999 NRC Canada

Johnson 1992), i.e., $E = Cp_E$ and $U = Cp_U$, each function ranging between 0 and 1. This allows eq. 3 to be rewritten as

$$(4)\quad \frac{dW(a,t)}{W(a,t)dt} = (C - Cp_E - Cp_U) - R$$
$$= C(1 - p_E - p_U) - R$$
$$= CA - R$$

where $A = (1 - p_E - p_U)$ is food assimilation efficiency, a quantity that reflects what is consumed minus what the body cannot process or does not use.

Predator consumption rate C was modeled as a function of fish size in weight $W(a,t)$, water temperature $T(t)$, salinity $S(t)$, and prey abundance $N(a,t)$. The maximum consumption rate C_{max} was considered to be an allometric function of weight, written

$$(5)\quad C = ([C_{max} f_C(N)][f_C(T) f_C(S)]) = \alpha_C[f_C(T) f_C(S) f_C(N)]W(a,t)^{\beta_C}$$

where α_C is the maximum consumption rate of a 1-g fish at the optimal temperature and salinity and β_C is the exponent for the size (i.e., weight) dependence of consumption. The water temperature dependence function $f_C(T)$ was defined by the Thornton and Lessem (1978) algorithm, a function describing the ascending and descending portions of a parabolic curve. The term $f_C(S)$ is a salinity-dependent consumption function derived from field and laboratory experiments. The predator "functional response" $f_C(N)$ relates the average spatial arrangement of predator to prey (Cosner et al. 1999). We made the simplest assumption that both predator $P(a,t)$ and prey $N(a,t)$ were distributed homogeneously in a unit area described by a type II functional response:

$$(6)\quad f_C[N(a,t)] = \left[\frac{N(a,t)}{N(a,t) + \rho}\right]$$

where ρ is the half-saturation constant. In this context, eq. 6 is the numerical response of the predator to prey density (Gutierrez 1996).

Respiration rate R was modeled as an allometric function of body weight, water temperature $T(t)$, salinity $S(t)$, and average swimming speed $V_P(a)$:

$$(7)\quad R = \alpha_R[f_R(T) f_R(S) f_R(V_P)]W(a,t)^{\beta_R}$$

where α_R is the standard respiration rate of a 1-g fish at the optimal temperature and salinity, β_R is the exponent for the weight dependence of respiration, $f_R(T)$ and $f_R(S)$ are temperature- and salinity-dependent proportional adjustment factors of the respiratory rate, and $f_R(V)$ is an activity-dependent proportional adjustment to specify respiration rate above the standard reference level. Combining eqs. 5, 6, and 7 into eq. 4, we obtain

$$(8)\quad \frac{dW(a,t)}{W(a,t)dt} = CA - R$$
$$= [\alpha_C[f_C(T) f_C(S) f_C(N)]W(a,t)^{\beta_C}]A - \alpha_R[f_R(T) f_R(S) f_R(V_P)]W(a,t)^{\beta_R}.$$

Thus, eq. 8 is in the general form of eq. 2 and captures fundamental bioenergetic growth principles into the ensemble weight equation.

While it would be desirable to model shrimp growth as a bioenergetic function of salinity, temperature, and food quality, these data are not currently available. Therefore, we modeled pink shrimp growth with a temperature-dependent length $L(a,t)$ on age a function following Smith (1997) using a piecewise linear relationship:

$$(9)\quad L(a_{dd}(a,t)) = \begin{cases} b_{01} + b_{11} a_{dd}(a,t) \text{ if } L(a,t) < 45 \text{ mm} \\ b_{02} + b_{12} a_{dd}(a,t) \text{ if } L(a,t) \geq 45 \text{ mm}. \end{cases}$$

This is accomplished by recasting chronological age as the cumulative sum of daily temperatures:

$$(10)\quad a_{dd}(a,t) = \int_{t=a_1}^{t=a} (T(t) - T_{min})dt$$

following Curry and Feldman (1987), where a_1 is age at immigration, a is postimmigration age in chronological units, t is Julian day, $a_{dd}(a,t)$ is age in degree-days (dd), $T(t)$ is temperature, and T_{min} is the minimum temperature at which physiological growth occurs. Model parameters were developed from laboratory data of Teinsongrusmee (1965) and field-based growth projections of Eldred et al. (1961). Animal weight dependence on length follows an allometric relationship.

Cohort abundance at age over time for both predator and prey was represented by the McKendrick – von Forester (Murray 1989; Ault and Olson 1996) population conservation equation:

$$(11)\quad dP(a,t) = -Z(a,t)P(a,t)dt = -[M(a,t) + F(a,t)]P(a,t)dt$$

where the total mortality rate $Z(a,t)$ is the sum of natural $M(a,t)$ and fishing $F(a,t)$ mortalities. The base natural mortality rate M (i.e., the rate for average environmental conditions) for both species was estimated using maximum average life span methods (Alagaraja 1984; Vetter 1988). The realized natural mortality rate was determined as the base rate modulated as a function of the physical (e.g., "habitat quality") and biological (predator and prey densities) features of the environment. In our model, we linked predator $P(a,t)$ natural mortality to growth by making the magnitude of realized M proportional to optimum size of a fish at age $W(a,t)$ relative to a current size:

$$(12)\quad \frac{dP(a,t)}{dt} = -M\left[1 - \gamma\left(\frac{W(a,t) - W_{opt}(a)}{W_{opt}(a)}\right)\right]P(a,t)$$

where $W_{opt}(a)$ is the optimum weight at age of a fish growing in an environment with no competitive effects (i.e., unlimited food resources) and γ is a mortality scale factor to weight the factor response. Predator stock biomass at age is the product of numbers at age times weight at age. Since weight at age is an "environment-dependent" function, this arrangement explicitly makes predator stock biomass a function of predator density, prey density, age, time, location, bottom type, salinity, temperature, and swimming velocity.

Prey natural mortality rate M was separated into two components: environmental M_H and predation M_P mortalities. Neither dynamic models nor appropriate data are available to make primary production and benthic detritus functions of current transport and salinity regimes. Thus, we computed environmental mortality of prey as

$$(13)\quad M_H = Mf(D, S, B)$$

where $f(D,S,B)$ relates mortality rates to features of the environment: depth $D(x,y,t)$, salinity $S(x,y,t)$, and bottom substrate $B(x,y,t)$ at location (x,y) at time t, where x and y are coordinates on a two-dimensional grid (Figs. 1 and 2). Bottom substrate is taken from the static habitat map. Using a conservation principle, predation mortality M_P was computed as

$$(14)\quad M_P = M\Psi f_C(N)$$

© 1999 NRC Canada

where this mortality is proportional to the consumption rate calculated in the predator energetic submodel (eq. 8), $f_C(N)$ is the functional response of predator P to prey density N, and Ψ is a mortality effect weighting factor. This arrangement makes prey mortality a function of the redistribution of predators due to changing environmental fields. In essence, the mortality rates of predator and prey are higher while searching to reflect the basic foraging–movement risk notion that most juvenile mortality is likely to occur while feeding or dispersing. This creates an explicit link between feeding and mortality rate. Total mortality Z was computed from catch curve analysis of abundance estimates from our fishery-independent trawl surveys conducted in Biscayne Bay during November 1996 and March 1997 (Ault et al. 1999). Fishing mortality F was obtained by difference, i.e., $F = Z - M$, and adjusted for gear size selectivity.

Larval transport and recruitment

We define "larval immigration" as the arrival of fertilized eggs (seatrout) or postlarvae (shrimp) into Biscayne Bay. The timing and magnitude of seatrout immigration were principal factors in the simulation experiments described below. One cohort of postlarval shrimp was assumed to arrive each month. Numbers of immigrating shrimp postlarvae were obtained from back-projections of trawl survey abundance data (Ault et al. 1999) combined with seasonal immigration pattern data from Allen et al. (1980). For both seatrout and shrimp populations, total immigrants in a cohort were divided into 1000 patches of equal density and then distributed in a rectangle 100 patches long by 10 patches wide covering the entire Safety Valve entrance channel on the Bay's eastern edge (Fig. 1). The initial east–west and north–south interpatch distance was 125 m. The spatial movement of each patch was then tracked during the pelagic larval transport period, which began with the event of immigration and concluded with the event of demersal settlement. Horizontal patch movements in continuous two-dimensional space were modeled as the distance change (∂x and ∂y) along the x and y coordinate axes during a 10-min time interval (dt):

$$(15)\quad \frac{\partial x}{\partial t} = X = X_c + (X_b + X_r)$$

$$\frac{\partial y}{\partial t} = Y = Y_c + (Y_b + Y_r)$$

where X and Y are the x and y coordinate velocities for a patch, respectively. Subscripts "c," "b," and "r" respectively denote velocity components due to water currents X_c (i.e., passive movements), behavioral taxis X_b (i.e., directed movements towards optimal conditions by active swimming), and diffusion X_r (i.e., purely random movements). Water current velocity components were obtained from the Biscayne Bay hydrodynamic model (Wang et al. 1988). The terms X_r and Y_r are velocity components of density diffusion of the whole patch that were simulated as a two-dimensional random walk (Berg 1993):

$$(16)\quad X_r = \Lambda_r \cos(\xi)$$

$$Y_r = \Lambda_r \sin(\xi)$$

where $\Lambda_r = \sqrt{2\delta\tau}$ is the linear distance moved per time interval, δ is the relative diffusion coefficient, τ is equal to dt, and ξ is a uniform random variable ranging between 0 and 2π.

We modeled a seatrout spawning event (i.e., egg immigration) to occur at night on the incoming tide. Seatrout patch movements were tracked over a continuous spatial domain at 10-min time intervals until all individuals either settled on the bottom or died. For seatrout eggs and yolk-sac larvae, we assumed that horizontal movements were advective (i.e., due to currents and diffusion) and not behavioral (i.e., $X_b = Y_b = 0$) and that no vertical movements occurred during the seatrout pelagic life stage. At 5–8 days of age, seatrout larvae will actively settle onto seagrass in depths less than 2 m (Peebles and Tolley 1988). At 9 days postspawn, we modeled seatrout larvae to settle regardless of substrate and depth.

Postlarval shrimp transport was modeled by incorporating behaviorally mediated movements. The behavioral taxis component comprised two parts: swimming velocity and a net resultant angular direction of movement (i.e., the angle of motion). This idea can be written in polar coordinate form as

$$(17)\quad X_b = \Lambda_b \cos(\theta)$$

$$Y_b = \Lambda_b \sin(\theta)$$

$$\Lambda_b = V_N \left[\frac{S_{opt} - S(x,y,t)}{\mathrm{Max}[S(x,y,t)] - S_{opt}} \right]$$

$$\theta = \sin^{-1}\left(\frac{\phi_y}{\sqrt{\phi_x^2 - \phi_y^2}} \right) + \epsilon\pi$$

where, Λ_b is a function that modulates the maximum average swimming speed V_N, $S(x,y,t)$ is salinity at location (x,y) at time t, S_{opt} is the optimal salinity for growth, $\mathrm{Max}[S(x,y,t)]$ is the maximum salinity for the entire grid, and ϕ_x and ϕ_y are salinity gradients along x and y coordinate axes where $\phi_x = \dfrac{\partial S(x,y,t)}{\partial x}$. The parameter ϵ is a normally distributed random deviate that allows for behavioral error in directional movement. Pink shrimp postlarvae regulate their horizontal position with precisely timed vertical movements. Postlarvae remain on the bottom during the day and vertically migrate and enter the water column at night (Tabb et al. 1962*b*; Hughes 1968). We assumed that some amount of random horizontal movement (X_r,Y_r) is always in effect. Water current (X_c,Y_c) and behavioral (X_b,Y_b) velocities were only invoked at night when shrimp were in the water column. Water current velocities usually dominate X and Y component velocities. Laboratory studies by Hughes (1969) suggested that nocturnal vertical movements by pink shrimp postlarvae are modulated by the prevailing tidal cycle in several ways: (*i*) postlarvae can detect relatively small salinity changes (i.e., ≤1‰), (*ii*) during flood tides, they vertically migrate in response to increasing salinity, and (*iii*) during ebb tides, they remain on the bottom in response to decreasing salinities. In the model, vertical migration was assumed to begin after dusk coinciding with the onset of flood tides. We assumed that once suspended in the water column, postlarvae cannot detect subsequent tidal cycle shifts that may occur during the rest of the night. Horizontal movement occurs until dawn when postlarvae migrate to the sea floor. After each nocturnal transport period, a proportion of postlarvae p[settle] within a given patch settle out to the benthic environment. Settling probability was described by three component functions based on bottom substrate type B, depth D, and postlarvae total length L:

$$(18)\quad p[\mathrm{settle}] = \omega = \begin{cases} \omega[B]\omega[D]\omega[L] & \text{if } L_1 \le L \le L_\omega \\ 1.0 & \text{if } L > L_\omega \end{cases}$$

in accordance with field and laboratory observations (Hughes 1969; Allen et al. 1980; Costello et al. 1986). Since settlement occurs over a limited range of postlarval lengths, functions for substrate and depth were modeled with size-dependent probabilities that increased proportional to reported preferences. At 11 mm TL, all postlarval shrimp settled regardless of substrate and depth.

© 1999 NRC Canada

Postsettlement movements

The fish movement model describes the ability of seatrout to detect gradients of habitat quality that provide stimuli for the fish to move. We considered the factors that affect fish growth rate dW/dt to be essential fish habitat variables (i.e., salinity, substrate, temperature, prey density, etc.). To determine the compound effect of these habitat variables, we used a modification of a spatially explicit model (Brandt et al. 1992) to integrate our physiologically based models of predator growth with the spatial distribution of prey and the physical information into a single variable for each location in space termed "growth rate potential" (Ω). These computations produce a spatial map of growth rate potential that provides a quantitative index of habitat quality (Berryman and Brown 1981; Brandt et al. 1992; Brandt and Kirsch 1993). Fish movement was based on an optimization search by the animal at its present location relative to the growth rate potential of alternative locations in the surrounding environment. We modeled each patch of fish of a cohort as an object on continuous two-dimensional coordinate space with behavioral movement described mathematically by

$$(19)\quad X_b(f[\Omega]) = \left(\tilde{V}(a,t)\left[1 - e^{\Phi\left(\frac{\Omega(t)-\Omega_{max}}{\Omega_{max}}\right)}\right]\right)(\cos[\theta_{max} + \epsilon\pi])$$

$$Y_b(f[\Omega]) = \left(\tilde{V}(a,t)\left[1 - e^{\Phi\left(\frac{\Omega(t)-\Omega_{max}}{\Omega_{max}}\right)}\right]\right)(\sin[\theta_{max} + \epsilon\pi])$$

where X_b is the x coordinate velocity component due to behavior, Y_b is the y coordinate velocity component, ϵ is a random normal variate, Ω_{max} is the maximum growth rate potential within the detection range of the fish, $\tilde{V}(a,t)$ is the net displacement velocity of the fish at age a, Φ is a scalar multiplier, and θ_{max} is the heading to the location of maximum growth rate potential within the detection range of the fish. The first term on the right-hand side of eq. 19 is the velocity of fish as a function of growth rate potential $\Omega(t)$, while the second is the directional heading of fish as a function of habitat quality. We assumed that animals evaluated their "environment" daily to determine movements and that juvenile and adult fish movements were not affected by hydrodynamic currents. The net displacement velocity is the actual distance moved between two points from the start and end of one time interval, recognizing that substantial searching may occur during this time.

Shrimp postsettlement movements were modeled following Ruxton (1996) by a discrete transform two-dimensional cellular automaton method that divides the spatial domain into j grid cells each with dimensions 0.0025° latitude × 0.0025° longitude (i.e., about 278 × 250 m). At each 1-day time step, a proportion of animals move to and from neighboring grid cells. The probability of an individual of length L staying in cell j at time t is defined as

$$(20)\quad p[\text{stay}] = \psi = \psi[\mathbf{H}(j,t)]\psi[L(a,t)]\psi[\epsilon]$$

where $\psi[\mathbf{H}(j,t)]$, $\psi[L(a,t)]$, and $\psi[\epsilon]$ are the respective habitat-dependent, size-dependent, and random stay probabilities. Probability $\psi[\mathbf{H}(j,t)]$ is a function of environmental variables (e.g., depth, substrate, salinity) that define habitat quality measured by observed animal density distributions. To reflect the increasing movement capabilities of pink shrimp as they grow (Eldred et al. 1961; Costello et al. 1986), $\psi[L(a,t)]$ decreases with increasing length L. The number of animals of size L departing cell j at time t is

$$(21)\quad N_d(L,j,t) = N(L,j,t)(1 - p[\text{stay}])$$

where $N(L,j,t)$ is the number of animals of size L in cell j at time t. For juvenile size-classes ($L \leq 85$ mm), $N_d(L,j,t)$ are distributed among neighboring cells k according to stay probabilities given the triplet (L,k,t). For emigrating subadult shrimp greater than 85 mm, animals departing cell j move to a single neighboring cell k determined by a transport factor $\zeta(k,t)$, here defined as a function of salinity and currents in accordance with the transport studies of Hughes (1969) and Beardsley (1970).

Habitat and fishery-independent databases

We acquired a comprehensive habitat and fishery-independent survey database to assess shrimp and fish abundance and habitat preferences. Essential fish "habitat" was described as a feature vector comprising six principal variables: bathymetry, substrate type, water temperature, water currents, salinity, and prey or predator density. Gridded bathymetry data for Biscayne Bay were obtained from the National Ocean Service hydrographic database (NOAA National Geographic Data Center, Boulder, Co.) and the Office of Naval Research. Areal benthic habitat coverages for Biscayne Bay were provided by Dade County and the Florida Marine Research Institute. Daily temperature was modeled by a periodic function fit to observations for 1990–1994. Water current velocity and salinity distributions were modeled at 10-min intervals for the simulated year 1995 with the Biscayne Bay numerical hydrodynamic model (Wang et al. 1988).

Since April 1996, we have conducted quarterly baywide fishery-independent trawl surveys of fish and macroinvertebrate populations in Biscayne Bay (for details, see Ault et al. 1999). This was the primary biological data source for animal densities by habitat type and season used in the model development and parameterization. March 1997 survey data were used to initialize pink shrimp spatial densities for model simulations. We also used the fishery-independent database to empirically validate model simulation results. Model parameters, functional forms, and initial conditions were developed from a number of published field and laboratory sources to represent the population dynamics and spatial movement behaviors for spotted seatrout and pink shrimp (Tables 1 and 2). The scientific data visualization package IDL (Interactive Data Language, Research Systems Inc., Boulder, Co.) was used on a Digital Equipment Corporation alpha workstation (model 3000/400) to view the data and animate the coupled biophysical simulation model.

Experimental design

Simulation experiments varying two factors were conducted to explore the model's dynamic behavior: (*i*) timing of spawning of a seatrout cohort and (*ii*) the relative magnitude of that seatrout cohort. Pink shrimp were recruited into the bay during every month of the year in numbers proportional to the distribution shown in Fig. 4, while seatrout were spawned on the new moon in either June or August. We set fish predation mortality (i.e., shrimp natural mortality) to be 10 times greater for the high versus low mortality factor runs. In each run the nominal natural mortality rate was set to $0.5M$ and predation mortality then varied from 0 to $0.5M$. Four types of model runs were conducted: (*i*) June seatrout recruitment with low predation mortality, (*ii*) June seatrout recruitment with high predation mortality, (*iii*) August seatrout recruitment with low predation mortality, and (*iv*) August seatrout recruitment with high predation mortality. Simulations were run for a 1-year time period.

Results

Model performance

A spatially independent simulation of the bioenergetic growth model for spotted seatrout using annual average en-

© 1999 NRC Canada

Table 1. Glossary of model variables.

Variable	Description	Units
t	Time	Julian day
(x,y)	Spatial position coordinates	Longitude, latitude
$j(x,y)$	Spatial grid cell	Dimensionless
$k(x,y)$	Neighboring grid cell	Dimensionless
$B(x,y)$	Substrate	Dimensionless
$D(x,y)$	Depth	m
$S(t,x,y)$	Salinity	‰
$T(t)$	Water temperature	°C
$P(a,t,x,y)$	Predator abundance	Numbers of fish
$N(a,t,x,y)$	Prey abundance	Numbers of shrimp
$L(a,t,x,y)$	Animal total length	mm
$W(a,t,x,y)$	Animal weight	g
$C(a,t,x,y)$	Consumption rate	$g \cdot g^{-1} \cdot day^{-1}$
E	Egestion rate	$g \cdot g^{-1} \cdot day^{-1}$
U	Excretion rate	$g \cdot g^{-1} \cdot day^{-1}$
$R(a,t,x,y)$	Respiration rate	$g\ O_2 \cdot g^{-1} \cdot day^{-1}$
A	Assimilation efficiency	Dimensionless
V_P	Predator average swimming speed	Body lengths$\cdot s^{-1}$
$f_C(T)$	Temperature-dependent function for consumption	Dimensionless
$f_C(N)$	Prey-dependent functional response for consumption	Dimensionless
$f_R(T)$	Temperature-dependent function for respiration	Dimensionless
$f_R(S)$	Salinity-dependent function for respiration	Dimensionless
$f_R(V_P)$	Activity-dependent function for respiration	Dimensionless
$Z(a,t,x,y)$	Total instantaneous mortality rate	$Year^{-1}$
$M(a,t,x,y)$	Natural mortality rate	$Year^{-1}$
$f(P)$	Predation mortality functional response	Dimensionless
$F(a,t)$	Fishing mortality rate	$Year^{-1}$
$s(a,t)$	Size selectivity of fishing gear	Dimensionless
$X(t,x,y)$	Velocity along the X-axis (longitude)	$cm \cdot s^{-1}$
$Y(t,x,y)$	Velocity along the Y-axis (latitude)	$cm \cdot s^{-1}$
$X_c(t,x,y)$	Velocity component due to water currents	$cm \cdot s^{-1}$
$X_b(a,t,x,y)$	Velocity component due to animal behavior	$cm \cdot s^{-1}$
X_r	Velocity component due to random dispersion	$cm \cdot s^{-1}$
V_N	Prey maximum average swimming speed	$cm \cdot s^{-1}$
$\omega(a,t,x,y)$	Settlement probability	Dimensionless
$\Omega(a,t,x,y)$	Growth rate potential	Dimensionless
$\bar{V}_{max}(a,t)$	Maximum net displacement velocity	$mm \cdot day^{-1}$
$\psi(a,t,j)$	Stay probability	Dimensionless
$\zeta(t,k)$	Transport factor	Dimensionless

vironmental conditions was consistent with empirical growth data and demonstrated the seasonal dynamics of seatrout growth (Fig. 3). In general, seatrout in Biscayne Bay grew fast in spring and fall when water temperatures ranged from 24 to 29°C. Growth slowed in summer when the water temperature was over 29°C, and there was little or no growth in winter when the water temperature dropped below 23°C.

The transport of postlarval shrimp showed strong seasonal and semilunar periodicities (Fig. 4). The seasonal periodicity indicates that the magnitude of advective transport was at a general maximum from early May to late July. The semilunar periodicity indicated that shrimp recruitment, which is facilitated by shoreward transport, occurs optimally during two short time windows each month. The dashed line in Fig. 4 indicates the relative monthly recruitment estimated from postlarval shrimp abundance sampled at the Long Key channel (Allen et al. 1980). Shrimp recruitment peaks during the period of maximum net shoreward transport. This period also corresponds closely to the period of maximum seatrout spawning. The transport distance was simulated with behavioral response of postlarval shrimp to tidal currents and diel light cycles at the main entrance of Biscayne Bay (Safety Valve). In general, it takes about 3 days for a postlarval shrimp with behavior to reach suitable settling habitat, whereas it takes more than 7 days for a passively drifting particle to reach similar areas.

A generalized picture of pink shrimp cohort dynamics is represented by a 1-year simulation of a June cohort (Fig. 5). Pink shrimp in Biscayne Bay possess the temporal and spatial dynamics of a typical species that uses the estuarine nursery grounds. At recruitment, postlarvae settle in concentrated bands on seagrass beds along the western side of Biscayne Bay (Fig. 5A). At 150 days postsettlement, pink shrimp are about 85 mm TL and are still concentrated in

© 1999 NRC Canada

Table 2. Parameters of the spatial multistock production model for predator and prey.

Symbol	Description	Function/value	Units	Reference
Predator (spotted seatrout, *Cynoscion nebulosus*)				
Cohort dynamics				
a_f	Age at fertilization	0	Days	
a_λ	Maximum age	9	Years	Murphy and Taylor 1994
$T(t)$	Water temperature	$T(t) = 4.2707 \sin\left[\left(\frac{2\pi t}{365}\right) - 2.5075\right] + 25.9876$	°C	
α_C	Intercept for maximum consumption	0.492	$g \cdot g^{-1} \cdot day^{-1}$	Hartman 1993
β_C	Weight exponent for maximum consumption	–0.268		Hartman 1993
$f_C(T)$	Function for consumption temperature dependence	$f_C(T) = f(O_{C1},O_{C2},O_{C3},O_{C4},K_{C1},K_{C2},K_{C3},K_{C4})$		Thornton and Lessem 1978
O_{C1}	Temperature for K_{C1} in $f_C(T)$	18.87*	°C	Hartman 1993
O_{C2}, O_{C3}	Temperature for K_{C2} and K_{C3} in $f_C(T)$	28.3*	°C	Hartman 1993
O_{C4}	Temperature for K_{C4} in $f_C(T)$	31.7*	°C	Hartman 1993
K_{C1}	Proportion of C_{max} at O_{C1}	0.0334		Hartman 1993
K_{C2}, K_{C3}	Proportion of C_{max} at O_{C2} and O_{C3}	0.98		Hartman 1993
K_{C4}	Proportion of C_{max} at O_{C4}	0.561		Hartman 1993
$f_C(S)$	Function for consumption salinity dependence	$f_C(S) = (1.22 - 0.2004S + 0.0004575S^2)^{-1}$	g	Lankford and Targett 1994
ρ	Half-saturation constant	0.5		
A	Assimilation efficiency	0.7		Hewett and Johnson 1992
α_R	Intercept for maximum standard respiration	0.0107	$g\ O_2 \cdot g^{-1} \cdot day^{-1}$	Wohlschlag and Wakeman 1978
β_R	Weight exponent for maximum standard respiration	–0.151		Wohlschlag and Wakeman 1978
$f_R(T)$	Function for respiration temperature dependence	$f_R(T) = f(O_{R1},O_{R2},O_{R3},O_{R4},K_{R1},K_{R2},K_{R3},K_{R4})$		Thornton and Lessem 1978
O_{R1}	Temperature for K_{R1} in $f_R(T)$	18.1*	°C	Hartman 1993
O_{R2}	Temperature for K_{R2} in $f_R(T)$	29.0*	°C	Hartman 1993
O_{R3}	Temperature for K_{R3} in $f_R(T)$	29.1*	°C	Hartman 1993
O_{R4}	Temperature for K_{R4} in $f_R(T)$	34.0*	°C	Hartman 1993
K_{R1}	Proportion of R at O_{R1}	0.0334		Hartman 1993
K_{R2}, K_{R3}	Proportion of R at O_{R2} and O_{R3}	0.98		Hartman 1993
K_{R4}	Proportion of R at O_{R4}	0.561		Hartman 1993
$f_R(S)$	Function for respiration salinity dependence	$f_R(S) = 1.679 - 0.01468S - 0.003158S^2 + 0.0001504S^3 - 0.0000174S^4$		Wohlschlag and Wakeman 1978
$f_R(V_P)$	Function for respiration activity dependence	$f_R(V_P) = e^{0.8329V_P^{0.3918}}$	Dimensonless	Wohlschlag and Wakeman 1978
V_P	Average swimming speed	1.0	Body lengths·s^{-1}	Wohlschlag and Wakeman 1978
$W(L)$	Weight–length relationship	$W(a,t) = 0.00000439L(a,t)^{3.1169}$	g	Data source: Murphy and Taylor 1994
M	Base natural mortality rate	0.33	$Year^{-1}$	Method: Alagaraja 1984; Vetter 1988
γ	Natural mortality weighting factor	1.0		
Postlarval transport and settlement				
δ	Relative diffusion coefficient	8.33×10^{-4}	$cm^2 \cdot s^{-1}$	Berg 1993
Postsettlement movement				
$\vec{V}_{max}(a,t)$	Net displacement velocity	$\vec{V}_{max}(a,t) = 2000L(a,t)$	mm·day^{-1}	
Φ	Behavioral movement weighting factor	5.0		

© 1999 NRC Canada

Table 2 (*continued*).

Symbol	Description	Function/value	Units	Reference
Prey (pink shrimp, *Peneaus duorarum*)				
Cohort dynamics				
a_1	Age at immigration	0	Days	Model starting value
a_λ	Maximum age	2.75	Years	Bielsa et al. 1983
T_{min}	Physiological minimum temperature	17.2	°C	Method: Curry and Feldman 1987; data source: Teinsongrusmee 1965
b	Growth model coefficients	$b_{01} = 8.1$ $b_{11} = 0.05$ $b_{02} = 19.2$ $b_{12} = 0.035$	mm	Data sources: Eldred et al. 1961; Teinsongrusmee 1965
$W(a,t)$	Animal weight	$W(a,t) = 0.00000535L(a,t)^{3.05}$	g	J.S. Ault, unpublished data
M	Base natural mortality rate	1.09	Year^{-1}	Method: Alagaraja 1984; Vetter 1988
$f(D,S,B)$	Natural mortality environmental function	$f(D,S,B) = \begin{cases} 0.5 \text{ if } D < 1 \text{ m}, B = \text{seagrass}, S < 34‰ \\ 1.0 \text{ if } 1 \le D \le 2 \text{ m}, B = \text{seagrass}, S < 34‰ \\ 1.5 \text{ if } D > 2 \text{ m}, B = \text{seagrass}, S < 34‰ \\ 2.0 \text{ if } B = \text{hardbottom}, S < 34‰ \\ 2.5 \text{ if } S \ge 34‰ \\ 3.0 \text{ if } B = \text{barebottom} \end{cases}$		Data source: Ault et al. 1999
$f(P)$	Predation mortality functional response	$f(P) = 1 - e^{-4.0\left(\frac{P(t,x,y)}{P_{max}(t)}\right)^{1.5}}$		
Z	Base total mortality rate	1.27	Year^{-1}	Data source: J.S. Ault et al., unpublished
F	Base fishing mortality rate	0.18	Year^{-1}	
$s(a,t)$	Size selectivity of fishing gear	$s(a,t)\frac{1}{1+e^{-(-7.96+0.169L(a,t))}}$		J.S. Ault, unpublished data
$F(a,t)$	Age-specific fishing mortality	$F(a,t) = Fs(a,t)$	Year^{-1}	
Postlarval transport and settlement				
L_1	Mean length at immigration	8	mm	Allen et al. 1980
L_∞	Maximum length at settlement	11	mm	Hughes 1969; Costello et al. 1986
S_{opt}	Optimum salinity	20.0	‰	Tabb et al. 1962*a*; Gunter et al. 1964
V_N	Swimming speed	1.0	cm·s^{-1}	Hughes 1969
δ	Relative diffusion coefficient	8.33×10^{-4}	cm^2·s^{-1}	Berg 1993
$\omega[B(x,y)]$	Substrate-dependent settlement probability	$\omega[B(x,y)] = \begin{cases} 1.0 \text{ if } B = \text{seagrass} \\ 0.5 \text{ if } B = \text{hardbottom} \\ 0.0 \text{ if } B = \text{barebottom} \end{cases}$		Data source: Costello et al. 1986

© 1999 NRC Canada

Table 2 (*concluded*).

Symbol	Description	Function/value	Units	Reference
$\omega[D(x,y)]$	Depth-dependent settlement probability	$\omega[D(x,y)] = \begin{cases} 1.0 & \text{if } D \le 2\text{ m} \\ e^{-3.0(D(x,y)-2.0)} & \text{if } D > 2\text{ m} \end{cases}$		Data source: Costello et al. 1986
$\omega[L(a,t)]$	Length-dependent settlement probability	$\omega[L(a,t)] = 10^{-22}\ e^{4.61L(a,t)}$		Data sources: Hughes 1969; Costello et al. 1986
Postsettlement movement				
$\psi[B(j)]$	Substrate-dependent stay probability	$\Psi[B(j)] = \begin{cases} 1.0 \text{ if } B = \text{seagrass} \\ 0.5 \text{ if } B = \text{hardbottom} \\ 0.1 \text{ if } B = \text{barebottom} \end{cases}$		Data source: Ault et al. 1999
$\psi[S(t,j)]$	Salinity-dependent stay probability	$\psi[S(t,j)] = \begin{cases} 1.0 & \text{if } S > 7‰ \\ \dfrac{1}{e^{(7-S(t,j))}} & \text{if } S \le 7‰ \end{cases}$		Data sources: Tabb et al. 1962*a*; Gunter et al. 1964
$\psi[\mathbf{H}(t,j)]$	Habitat-dependent stay probability	$\psi[\mathbf{H}(t,j)] = \psi[B(j)]\psi[S(t,j)]$		
$\psi[L(a,t)]$	Size-dependent stay probability	$\psi[L(a,t)] = \begin{cases} 1.0 \text{ if } L \le 45\text{ mm} \\ 0.5 \text{ if } 45 < L \le 85\text{ mm} \\ 0.2 \text{ if } L > 85\text{ mm} \end{cases}$		Data sources: Eldred et al. 1961; Joyce 1965; Costello et al. 1986
$\overline{V}_c(k)$	Annual average current speed		$cm \cdot s^{-1}$	Hydrodynamics model
$\zeta(t,k)$	Emigration transport factor	$\zeta(t,k) = \left(\dfrac{S(t,k)}{\text{Max}(S(t))}\right)\left(\dfrac{\overline{V}_c(k)}{\text{Max}(\overline{V}_c)}\right)$		Data sources: Hughes 1969; Beardsley 1970

Note: Asterisks denote temperature values that were adjusted for the warmer tropical waters of Biscayne Bay, Florida.

© 1999 NRC Canada

Fig. 3. Simulated growth for spotted seatrout from birth to 3 years of age (solid line) compared with empirical size estimates at age (triangles) for Everglades fish as reported by Stewart (1961), Rutherford (1982), and Johnson and Seaman (1986). The dashed line shows ambient water temperature. Start date is 1 June, salinity is 25‰, and prey density is constant.

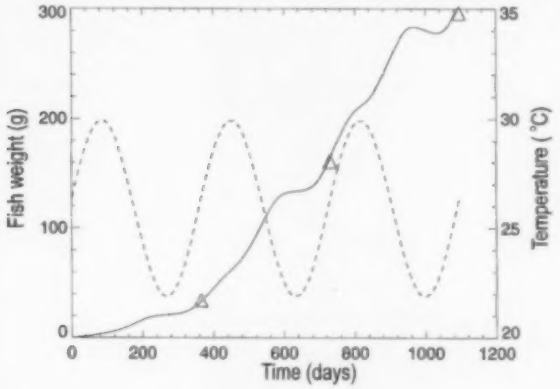

seagrass beds, but the total spatial abundance distribution has expanded and diffused outward into deeper waters (Fig. 5B). At about 180 days or 6 months postsettlement, shrimp have begun an easterly ontogenetic migration where animals begin inhabiting deeper channelized areas with high salinity and strong currents (Fig. 5C). By age 270 days the majority of a pink shrimp cohort has left the Bay for oceanic habitats for adult feeding and spawning grounds.

The empirical shrimp spatial density (number of shrimp per 600 m^2) distribution, sample locations, and the distribution of average size at those sampling locations estimated from stratified sampling surveys for August and November 1996 are shown in Fig. 6. Highest shrimp densities were found in relatively shallow seagrass beds located on the western side of the Bay in areas of moderate salinity regimes (10–20‰) (Figs. 6A and 6C), although the center of abundance moves somewhat between August and November, presumably influenced strongly by varying salinity regimes. Figures 6B and 6D suggest that shrimp move eastward towards more oceanic habitats as they grow.

Simulation experiments

Simulated average size of fish in patches and spatial patterns of seatrout recruits are different for cohorts spawned during June (Figs. 7A and 7B) and August (Figs. 7C and 7D). For the June cohort, 817 out of 1000 patches were transported into Biscayne Bay and settled in suitable habitat 9 days after spawning. For the August seatrout cohort, 642 out of 1000 patches were transported into the Bay and settled 9 days after spawning. Differences in spawning time also resulted in differences in the spatial distributions of fish. Seatrout cohorts spawned in June settled over a wider range of Bay habitats than those spawned in August (cf., Fig. 7), principally due to the differences in water circulation patterns. These differences at settlement combined with their subsequent exposure to different environmental conditions postsettlement produced different spatial patterns of recruitment and size range of fish in a cohort at 365 days between

Fig. 4. Hydrodynamic model simulated net transport of particles at the main oceanic connection (Safety Valve) to Biscayne Bay. Positive values indicate westward transport into the Bay. The solid line represents the nighttime transport pattern of particles with vertical movement behavior of pink shrimp postlarvae, the dashed line shows the relative monthly pink shrimp postlarvae recruitment estimated from channel net samples collected at the Long Key channel of Florida Bay (Allen et al. 1980), and the dotted line represents the advective transport pattern of pure passive particles (e.g., spotted seatrout eggs); circles indicate the time of the new moon in 1995, and the two vertical arrows indicate the timing (June 27 and August 25) of spotted seatrout spawning in biological model simulations.

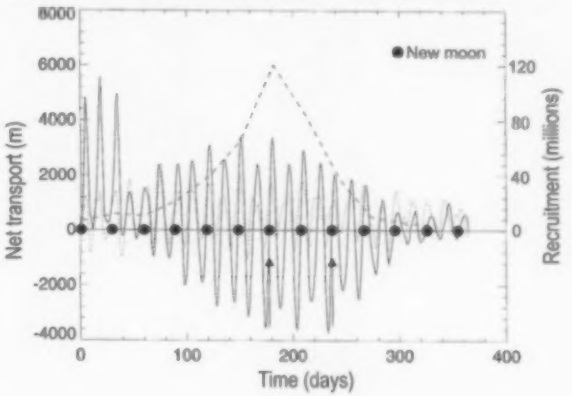

the June and August spawnings. Furthermore, the 2-month difference in spawning time affected seatrout growth. More seatrout grew to a larger size by age 365 days for the June cohort (Figs. 7A and 7B) than for the August cohort (Figs. 7C and 7D), since the former were exposed to better water temperatures and prey abundances. The temporal pattern of habitat quality and seatrout abundance for a June cohort is shown in Fig. 8. Fish near high habitat quality environments in general had highest growth and survivorship.

Seatrout larval densities affected the growth of juvenile seatrout (Figs. 7 and 9). Higher larval densities led to fewer large fish regardless of spawn time (Figs. 9B and 9D). Although seatrout within a given cohort started out at exactly the same size in the simulations, the growth history of any individual patch is an integration of all different conditions (both biological and physical) that were encountered after settlement in the Bay. The "observed" differences in growth among patches from a cohort increased as the patches of fish aged (Fig. 9). At 365 days of age, the size range was from 100 to 250 mm TL for the June cohort with low larval density (Fig. 9A), from 100 to 220 mm TL for a June cohort with high larval density (Fig. 9B), from 90 to 200 mm TL for an August cohort with low larval density (Fig. 9C), and from 90 to 180 mm TL for an August cohort with high larval density (Fig. 9D). Also, larger fish were mostly associated with seagrass habitats on the western side of the Bay (Fig. 8) where shrimp are abundant (Fig. 6). Seatrout larval density also affected pink shrimp population dynamics (Fig. 10). Higher seatrout larval densities induced higher mortalities on pink shrimp, as indicated by the steeper slopes of the abundance surface plots, and reduced shrimp survival by the end of simulations (Figs. 10B and 10D).

© 1999 NRC Canada

Fig. 5. Simulated pink shrimp population spatial abundance distributions over time for a June immigrating cohort: (A) day 0 (birth); (B) day 150; (C) day 180; (D) day 250. Note that all animals from a given cohort are assumed to have left the Bay by 270 days after birth. Color scale indicates densities from 0 to 1.0 shrimp·m^{-2}.

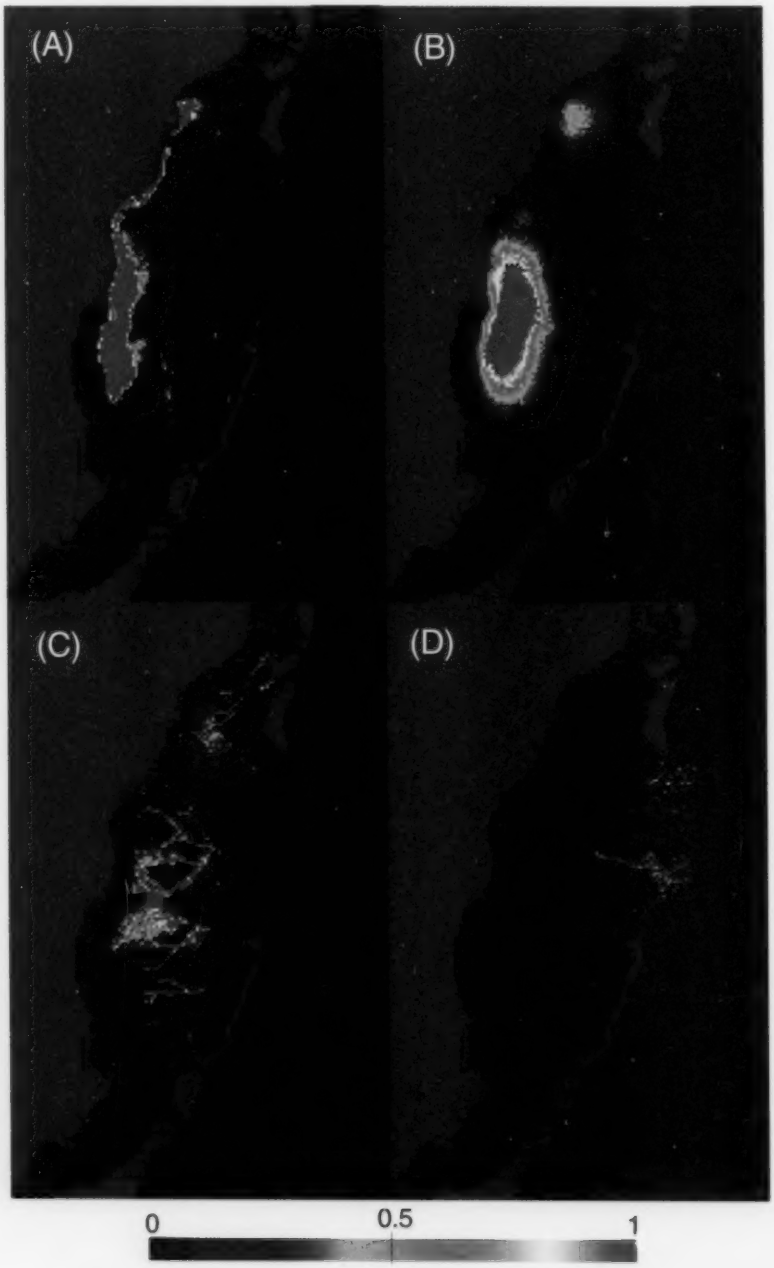

Discussion

Model dynamics

The model presented in this study is still in the early stages of development. This type of dynamic spatial model requires a large number of known parameters derived from empirical studies, makes important assumptions as to which attributes of the ecosystem should be modeled, and demands computer intensive programming. At several junctures, we made many simplifications to avoid an unmanageable number of state variables. Our results indicate that, despite these simplifications, the model provides a quantitative framework for assessing predator–prey population responses to dynamic physical and biological environments. The model provided

© 1999 NRC Canada

insight into two key population-dynamic phenomena: spawning time effects on larval transport and settlement and the influence of time–space history of habitat quality on animal growth and survivorship.

Spawning date determines the transport rate of larvae from the spawning grounds to the nursery grounds. In our system, advected particles moved shoreward at a far slower rate than particles with vertical movement behaviors of postlarval pink shrimp. For biological particles with behavior, spawning date has a strong effect on net movement rates, and these rates appear to be correlated with moon phase and time of year. The net effect is that different spawning dates can result in different spatial distributions of larvae and juveniles. Many economically and ecologically important tropical marine fishes and macroinvertebrates recruit over protracted periods of the year (e.g., Ault and Fox 1990; Sparre and Venema 1992). Johannes (1978) stated that many tropical species spawn at times and locations that favor the advective transport of their pelagic eggs and larvae to offshore environments where predation is reduced. By contrast, we note that many economically important South Florida fishes and invertebrates (e.g., groupers, snappers, grunts, bonefish, lobsters, and shrimp) spawn offshore at the shelf edge, but their developing larvae are then advected inshore into nearshore and coastal bay nursery areas (e.g., Lee et al. 1992). In our model, cohorts spawned at different times differentially spread out in space over the range of the prey resource. Such a reproductive strategy may serve to reduce intraspecific competition within the seatrout population by providing higher energetic input to the average larvae than if they all were to settle out at the same location. Not surprisingly, we found that the annual cycles of net advective hydrodynamic nighttime transport and the observed spawning habits of both shrimp and seatrout are highly correlated.

Our spatially independent runs of the seatrout bioenergetic growth model produced results consistent with empirical data of average growth at age determined from "annual rings" on otoliths (Tabb 1966). Variations of growth derived from annual ring methods are usually neglected in practice because it is believed that those variations result from differences in spawning dates (i.e., protracted spawning seasons) and inaccuracies of the methodologies. However, our spatial model runs suggest that relatively small variations in the physical and biological environment can result in large variations in the growth of fish from the same spawning date. In model runs, we initially set all patches comprising a cohort to be equal in numbers of animals and their biological nature; thus, any differences in abundance or growth between patches observed in later life stages were due strictly to the environment. The distribution of effects and responses in growth and mortality by individuals comprising a given cohort was regulated by the explicit coupling of the biophysical environment, and these linkages resulted in seasonal variations in stock biomass. This suggests that the distribution of sizes at given ages in a population may be a genotypical or phenotypical expression of animal size as modulated by environmental variability in space and time. In spatial model runs, we showed that fish spawned in August grew slower than June-spawned cohorts due primarily to different water temperature histories during their first year of life. The mean and variance of size were positively corre-

Fig. 6. Empirical pink shrimp population spatial density and size distributions estimated from survey sampling conducted during (A and B) August and (C and D) November 1996; (A and C) contoured shrimp density (numbers per 600 m^2); (B and D) spatial distribution of average size (mm). For August, the color scale reports densities ranging from 1 to 162 shrimp and sizes ranging from 9 to 17 mm carapace length (CL). For November, the color scale reports densities ranging from 2 to 390 shrimp and average sizes ranging from 12 to 21 mm CL. $TL = 1.616 + 4.503CL$ for $C \leq 17$ mm; $TL = 11.636 + 3.985CL$ for $CL > 17$ mm.

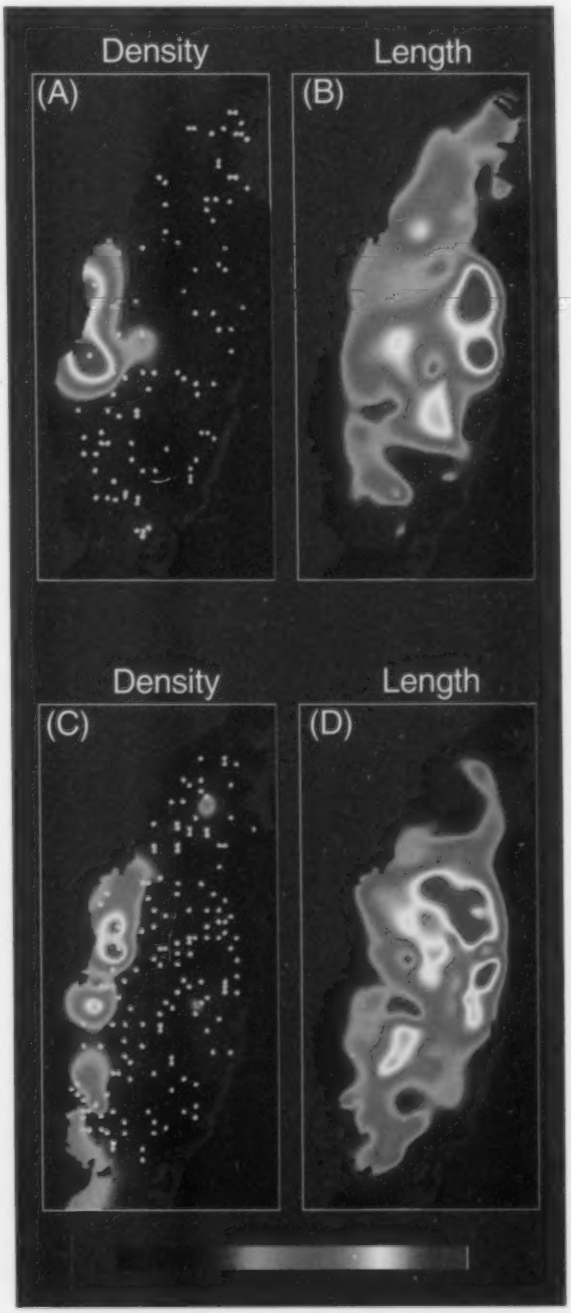

© 1999 NRC Canada

Fig. 7. Simulated spatial distribution of spotted seatrout sizes in weight for June- and August-spawned cohorts at low and high recruitment densities: (A) June low density, (B) June high density, (C) August low density, and (D) August high density. The color scale represents fish weights ranging from 10 to 40 g.

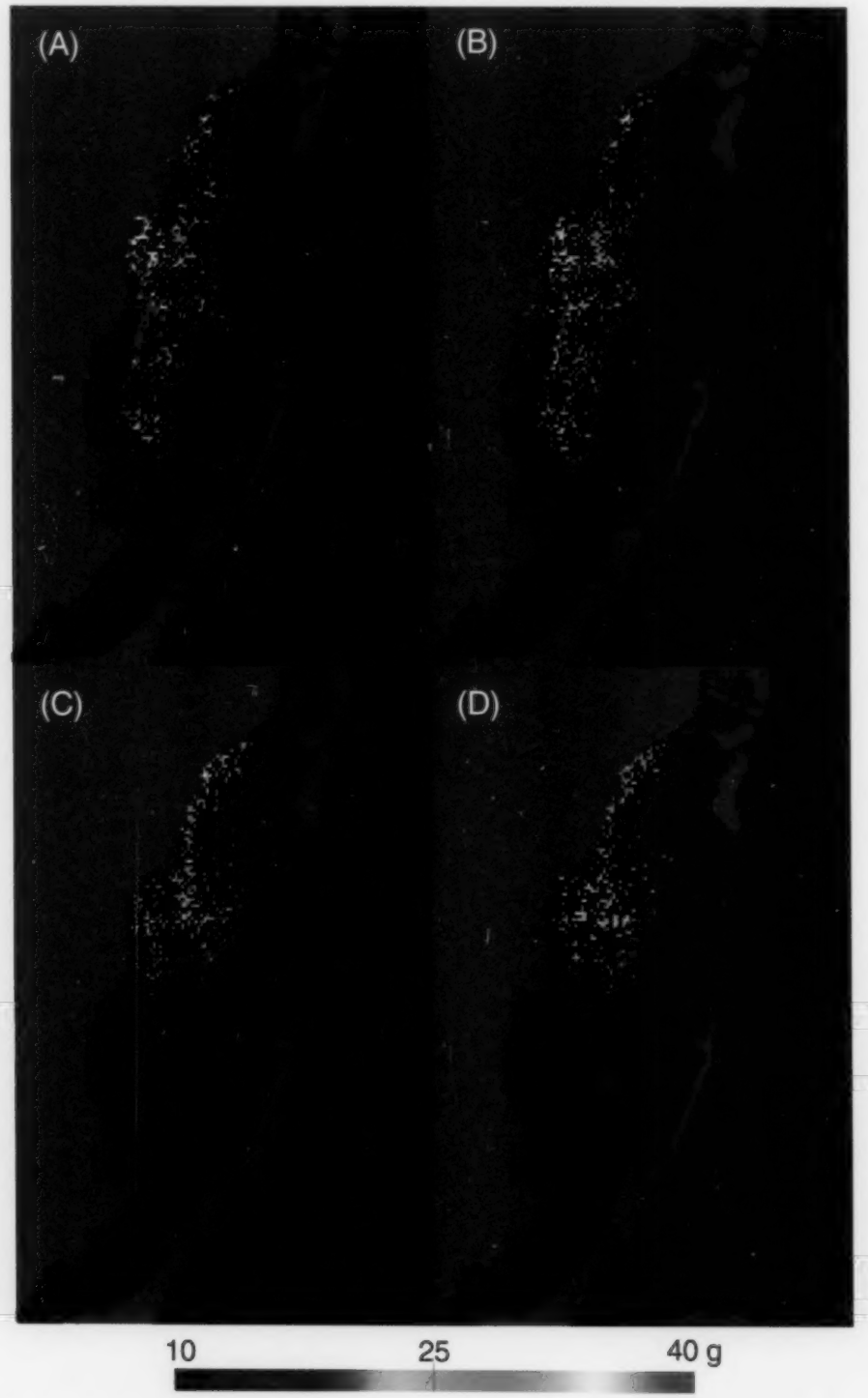

© 1999 NRC Canada

Fig. 8. Simulated spatial distributions of spotted seatrout "habitat quality" (i.e., spatial growth rate potential) and density and for (A) 1 day, (B) 150 days, (C) 300 days, and (D) 360 days. The color scale shows habitat quality ranging from 0 (low) to 1 (high) and densities ranging from 0 to 100 fish·km^{-2}.

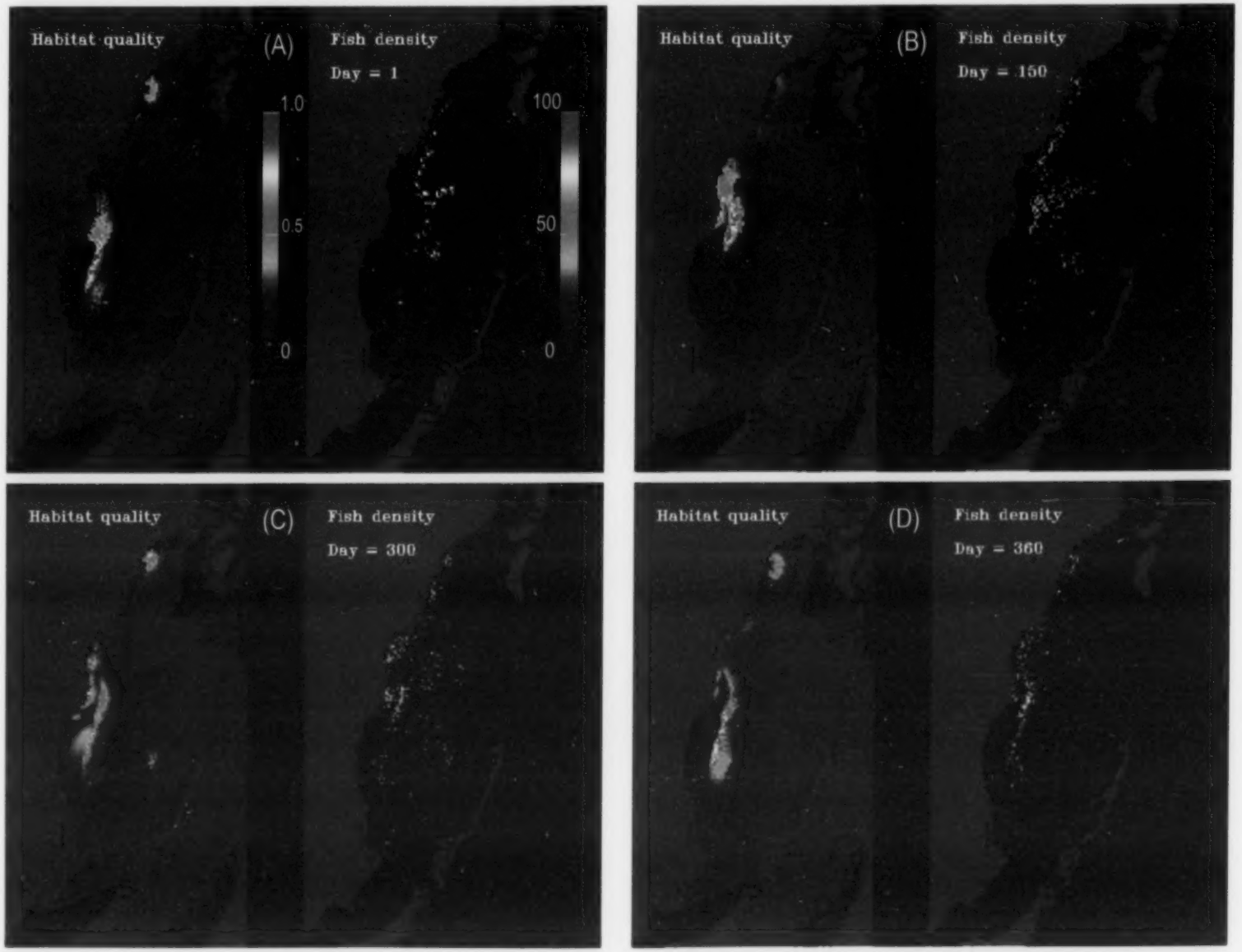

© 1999 NRC Canada

Fig. 9. Simulated spotted seatrout abundance as a function of time and total length for spatial simulations following recruited cohorts: (A) June low density, (B) June high density, (C) August low density, and (D) August high density.

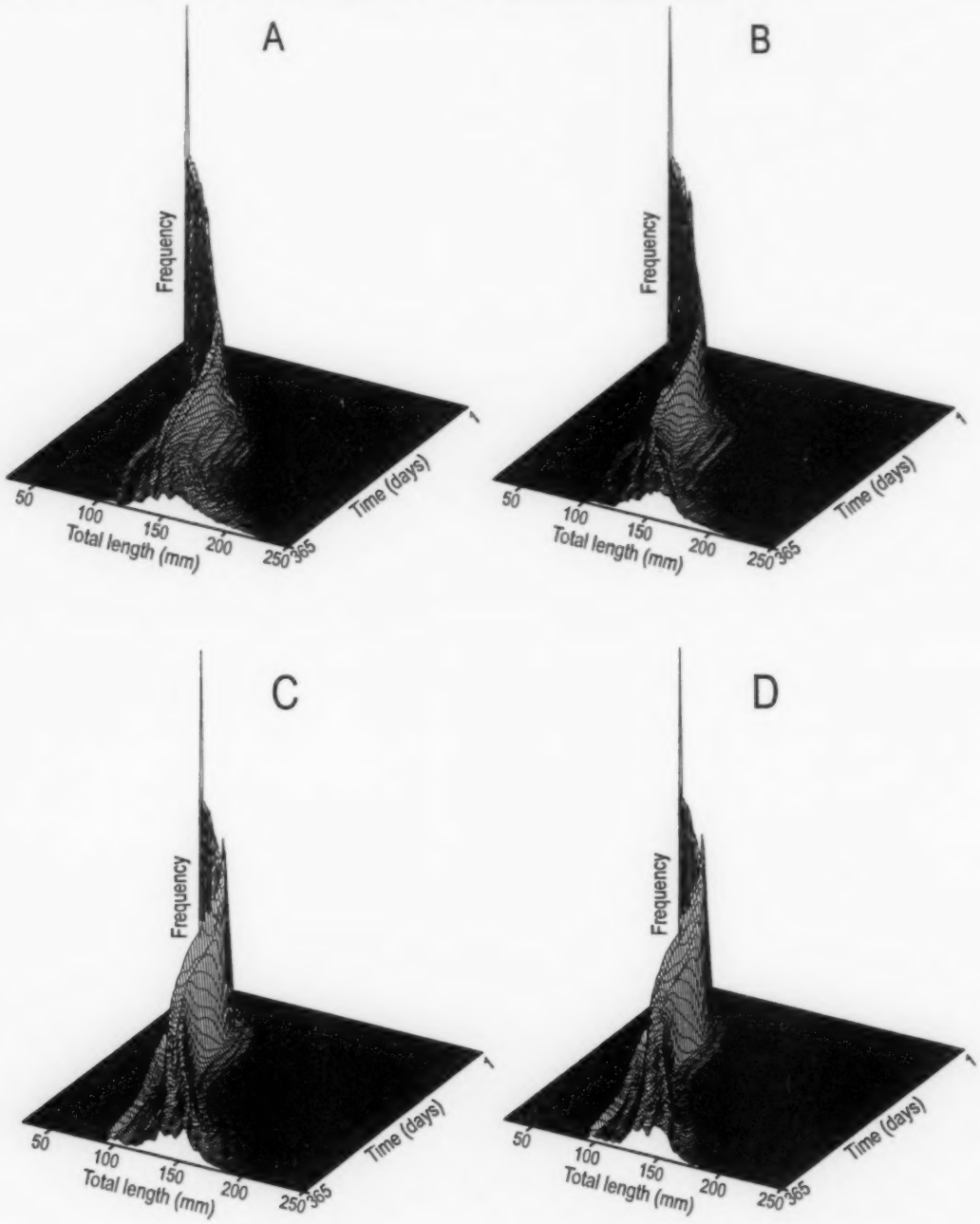

lated. Reductions in growth resulted from both physical environmental variability and spatial mismatches of settling predators with prey density distributions. These reductions led to decreased survivorship that directly modulated the spread of size at age distributions. The upper end of the distribution is dominated by individuals who have found favorable environmental conditions for growth and survivorship over their lifetime.

Data and model needs

A basic need of models as sophisticated as those presented here is population dynamics and bioenergetics param-

© 1999 NRC Canada

Fig. 10. Simulated pink shrimp abundance as a function of time and total length for spatial simulations following the total population comprising 12 cohorts of shrimp. Fish are recruited (A) June low density, (B) June high density, (C) August low density, and (D) August high density. The peaks and valleys are functions of seasonal magnitudes of cohort recruitment.

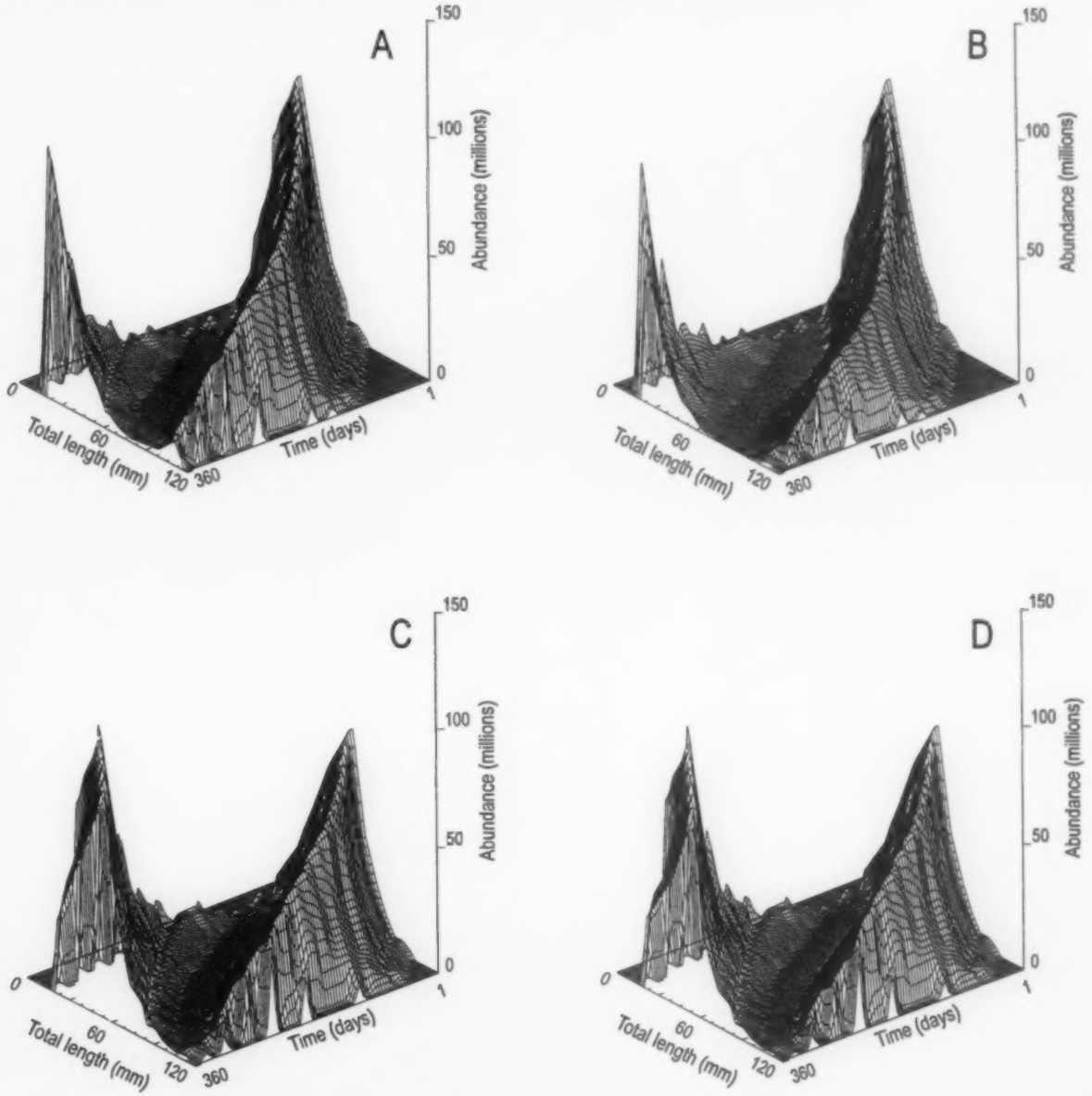

eters that cover the breadth of the trophic network representative of the ecosystem components of interest. To estimate model parameters in this study, we used relatively precise data from our fishery-independent field surveys (Ault et al. 1999) and information from published literature on both pink shrimp and spotted seatrout or related species (such as weakfish, *Cynoscion regalis*) when data for the target species were not available. As a result, the predicted outputs presented here are not intended to necessarily represent realistic spotted seatrout – pink shrimp community dynamics per se, but are representative of the kinds of dynamics that a predator–prey community with these demographic and behavioral characteristics would be expected to display in a coupled physical and biological environment. Better predictions of both predator and prey spatial and temporal dynamics will require more precise demographic, bioenergetic, and movement data that facilitate a deeper understanding of inter- and intra-specific relationships. A central area of research will be on taxa-specific bioenergetic rates of consumption, respiration, and osmoregulation and their variabil-

© 1999 NRC Canada

ity, since these processes ultimately drive somatic and gonadal growth. In addition, more concise definitions of what constitutes "essential habitat" on appropriate space scales are also required. This is because determination of the covariance structure between animals and their environment is a critical first principle for design of efficient sampling surveys, and as such, these data can provide more accurate and precise initial conditions and parameter estimates for model runs.

Two aspects of spatial fishery models are underdeveloped: the mechanisms underlying animal movements and predator–prey trophodynamics. Improved knowledge is required of animal swimming speeds and behaviors related to a suite of environmental stimuli and how these factor arrangements influence or change movement or migration patterns (Videler 1993). Significant opportunities for model exploration remain and involve analytical treatments of the sensitivity of spatial and model dynamics to parameter ranges, time steps, initial conditions, and boundary conditions (Bartell et al. 1986; Rothschild and Ault 1992, 1996). Our numerical model's structure is also amenable to analyses of emergent spatial pattern behaviors because the timing mechanisms for events at different sites within the model are believed to have substantial impacts on large-scale model predictions (e.g., Brown and Rothery 1993; Ruxton 1996). Prey encounters and spatial growth rate potentials are of critical importance to the survivorship and growth of juvenile predators. The difficulty in modeling these processes is tied to knowledge of the spatial arrangement of prey and predator to facilitate choice of the predator functional response (Cosner et al. 1999). More rigorous analyses will likely involve incorporation of three-dimensional encounter probability theory into bioenergetic consumption rate dynamics of predators (Gerritsen and Strickler 1977; Luo et al. 1996). Such population dynamic behaviors are fundamental determinants of spatial distribution (Rothschild and Ault 1996).

The model's utility will be enhanced by adopting a systems approach that coordinates field, laboratory, and modeling efforts in a rigorous quantitative framework. This approach will result in more precise and accurate databases and models that represent the structure, function, and dynamics of the fishery ecosystem. "New" data will require that spatially articulated biological sampling be conducted at the same times and locations as oceanographic and meteorological sampling to couple physical and biological response functions. To ensure that forecasts are reliable, numerical model results must be validated with empirical information in both space and time (e.g., Figs. 5 and 6).

Future applications

Our model was developed to explore the space–time behavior of recruitment and predator–prey production dynamics. But the model has a number of other potential applications in terms of assessing water quality and fishing. A restudy is underway to determine the effects of modifications to the Central and Southern Florida project, which includes physical alterations to the drainage, flood control, and water supply system of southeast Florida. The restudy examines a present-day base case (i.e., no modifications to the system, but with 2050 projected development) and several alternatives that will change the quantity and timing of freshwater flowing to the South Florida coastal estuaries, in particular Biscayne Bay and Florida Bay. Salinity is an important environmental parameter affecting the health of the coastal marine ecosystem and its fishery resources (Montague and Ley 1993; Livingston 1997; Livingston et al. 1997; Serafy et al. 1997; Young et al. 1997). Our coupled biophysical model of Biscayne Bay will facilitate evaluation of expected impacts of various proposed water management alternatives on biological resource sustainability. In addition, the environmental impact of expanding an airport near Homestead, Fla., on Biscayne Bay fisheries may also be explored using the model in its current formulation.

Another concern is widespread serial overfishing of coral reef fishes in the Florida Keys (Ault et al. 1998). Our age-structured predator–prey model enables fishery management decision makers to assess quantitative multistock indicator statistics such as spatial yield-per-recruit and spawning potential ratios. Regional-scale hydrodynamic models are being developed to describe circulation patterns in the Intra-American Seas (Mooers and Maul 1998) and the coral reef tract adjacent to the Straits of Florida (Mooers and Ko 1994). These could be coupled to our existing biophysical model domain to incorporate the biological interconnectedness of coastal bays with the Florida Keys coral reef tract and the pelagic realm. For example, this model could be configured to understand the dynamic linakges between the coastal bay bait shrimp fishery and impacts on the habitat, reef fish community dynamics and production, and commercial food shrimp fishery.

Our model can also address additional management concerns regarding space, including definition of essential fish habitat, design of marine protected areas, and assessment of ecological risks. Spatial growth rate potential provides a clear quantitative understanding of habitat quality over space. This could be viewed as a formal definition of essential fish habitat. Using the concept of spatial growth rate potential as a guide, the model could also be useful for designing the location and size of marine protected areas (Bohnsack and Ault 1996; Ballantine 1997). Such a suitably structured model could also be used in ecological risk assessments to conduct natural resource damage resulting from the fate and transport of oil and other pollutants.

However, to accomplish these goals requires a systems approach to resource assessment using an adaptive management procedure that emphasizes strategy over tactics (Ault 1996; Bohnsack and Ault 1996; Rothschild et al. 1996). This approach will ensure that key hypotheses are clearly articulated and supported by efficient sampling designs in support of model building that will enable fishery management to provide more realistic assessments of the entire fish community in dynamically coupled biophysical environments. Adherence to this view is a critical step towards building sustainable fisheries.

Acknowledgments

We thank Donald B. Olson and Chris Cosner for their sage advice on the coupling of physics and biology and Carl J. Walters and an anonymous referee for their critical review of the manuscript. This work was sponsored by the NOAA Coastal Ocean Program (grant No. NA37RJO2000), the U.S.

© 1999 NRC Canada

Army Corps of Engineers (grant No. DACW 39-94-K0032), and the NOAA South Florida Ecosystem Restoration Prediction Modeling (grant No. NA67RJ0149).

References

Adams, S.M., and Breck, J.E. 1990. Bioenergetics. *In* Methods for fish biology. *Edited by* C.B. Schreck and P.B. Moyle. American Fisheries Society, Bethesda, Md. pp. 389–415.

Alagaraja, K. 1984. Simple methods for estimation of parameters for assessing exploited fish stocks. Indian J. Fish. **31**: 177–208.

Allen, D.M., Hudson, J.H., and Costello, T.J. 1980. Postlarval shrimp (*Penaeus*) in the Florida Keys: species, size, and seasonal abundance. Bull. Mar. Sci. **30**: 21–33.

Ault, J.S. 1996. A fishery management system approach for Gulf of Mexico living resources. *In* GIS applications for fisheries and coastal resources management. *Edited by* P.J. Rubec and J. O'Hop. Gulf States Mar. Fish. Comm. **43**: 106–111.

Ault, J.S., and Fox, W.W., Jr. 1990. Simulation of the effects of spawning and recruitment patterns in tropical and subtropical fish stocks on traditional management assessments. Gulf Carib. Fish. Inst. **39**: 361–388.

Ault, J.S., and Olson, D.B. 1996. A multicohort stock production model. Trans. Am. Fish. Soc. **125**: 343–363.

Ault, J.S., Bohnsack, J.A., and Meester, G.A. 1998. A retrospective (1979–1996) multispecies assessment of coral reef fish stocks in the Florida Keys. Fish. Bull. U.S. **96**: 395–414.

Ault, J.S., Diaz, G.A., Smith, S.G., Luo, J., and Serafy, J.E. 1999. An efficient sampling design for estimating pink shrimp abundance in Biscayne Bay, Florida. N. Am. J. Fish. Manage. **19**: 696–712.

Ballantine, W.J. 1997. "No take" marine reserve networks support fisheries. *In* Developing and sustaining world fisheries resources: the state of science and management. *Edited by* D.A. Hancock, D.C. Smith, A. Grant, and J.P. Beumer. 2nd World Fisheries Congress, Brisbane, Australia. pp. 702–706.

Bartell, S.M., Breck, J.E., Gardner, R.H., and Brenkert, A.L. 1986. Individual parameter perturbation and error analysis of fish bioenergetics models. Can. J. Fish. Aquat. Sci. **43**: 160–168.

Beardsley, G.L., Jr. 1970. Distribution of migrating juvenile pink shrimp, *Penaeus duorarum duorarum* Burkenroad, in Buttonwood Canal, Everglades National Park, Florida. Trans. Am. Fish. Soc. **99**: 401–408.

Berg, H.C. 1993. Random walks in biology. Princeton University Press, Princeton, N.J.

Berryman, A.A., and Brown, G.C. 1981. The habitat equation: a useful concept in population modeling. *In* Quantitative population dynamics. *Edited by* D.G. Chapman and V.F. Gallucci. International Co-operative Publishing House, Fairland, Md. pp. 11–24.

Bielsa, L.M., Murdich, W.H., and Labisky, R.F. 1983. Species profiles: life histories and environmental requirements of coastal fishes and invertebrates (south Florida) — pink shrimp. U.S. Fish Wildl. Serv. FWS/OBS-82/11, U.S. Army Corps Eng. TR EL-82-4.

Bohnsack, J.A., and Ault, J.S. 1996. Management strategies to conserve marine biodiversity. Oceanography, **9**: 73–82.

Brandt, S.B., and Kirsch, J. 1993. Spatially explicit models of striped bass growth potential in Chesapeake Bay. Trans. Am. Fish. Soc. **122**: 845–869.

Brandt, S.B., Mason, D.M., and Patrick, E.V. 1992. Spatially-explicit models of fish growth rate. Fisheries (Bethesda), **17**: 23–33.

Brown, D., and Rothery, P. 1993. Models in biology: mathematics, statistics and computing. John Wiley & Sons, New York.

Chin-Fatt, J. 1986. Canal impact on Biscayne Bay salinities. M.Sc. thesis, University of Miami, Coral Gables, Fla.

Cosner, C., DeAngelis, D.L., Ault, J.S., and Olson, D.B. 1999. Effects of spatial grouping on the functional response of predators. Theor. Popul. Biol. **56**: 65–75.

Costello, T.J., and Allen, D.M. 1970. Synopsis of biological data on the pink shrimp *Penaeus duorarum duorarum* Burkenroad, 1939. FAO Fish. Rep. **57**(4): 1499–1537.

Costello, T.J., Allen, D.M., and Hudson, J.H. 1986. Distribution, seasonal abundance, and ecology of juvenile northern pink shrimp, *Peneaus duorarum*, in the Florida Bay area. NOAA Tech. Memo. NMFS-SEFC-161.

Curry, G.L., and Feldman, R.M. 1987. Mathematical foundations of population dynamics. Texas A&M University Press, College Station, Tex.

DeAngelis, D.L., and Gross, L.J. 1992. Individual-based models and approaches in ecology. Chapman and Hall, New York.

Department of Commerce. 1997. NOAA fisheries strategic plan. National Oceanic and Atmopsheric Administration, Washington, D.C.

Eldred, B., Ingle, R.M., Woodburn, K.W., Hutton, R.F., and Jones, H. 1961. Biological observations on the commercial shrimp, *Penaeus duorarum* Burkenroad, in Florida waters. Mar. Lab. Fla. Prof. Pap. Ser. 3.

Fox, W.W., Jr. 1970. An exponential surplus yield model for optimizing exploited fish populations. Trans. Am. Fish. Soc. **90**: 80–88.

Fox, W.W., Jr. 1975. Fitting the generalized stock production model by least-squares and equilibrium approximation. U.S. Natl. Mar. Fish. Serv. Fish. Bull. U.S. **73**: 23–37.

Gerritsen, J., and Strickler, J.R. 1977. Encounter probabilites and community structure in zooplankton: a mathematical model. J. Fish. Res. Board Can. **34**: 73–82.

Gulland, J.A. 1983. Fish stock assessment: a manual of basic methods. John Wiley & Sons, New York.

Gunter, G., Christmas, J.R., and Killebrew, R. 1964. Some relations of salinity to population distributions of motile estuarine organisms, with special reference to penaeid shrimp. Ecology, **45**: 181–185.

Gutierrez, A.P. 1996. Applied population ecology: a supply-demand approach. John Wiley & Sons, New York.

Hartman, K. 1993. Striped bass, bluefish, and weakfish in the Chesapeake Bay: energetics, trophic linkages, and bioenergetic model applications. Ph.D. dissertation, University of Maryland, College Park, Md.

Harwell, M.A., Long, J.F., Bartuska, A.M., Gentile, J.H., Harwell, C.C., Myers, V., and Ogden, J.C. 1997. Ecosystem management to achieve ecological sustainability: the case of South Florida. Environ. Manage. **20**: 497–521.

Hettler, W.F., Jr. 1989. Food habits of juvenile spotted seatrout and gray snapper in western Florida Bay. Bull. Mar. Sci. **44**: 155–162.

Hewett, S.W., and Johnson, B.L. 1992. Fish bioenergetics model 2: a generalized bioenergetics model of fish growth for microcomputers. Univ. Wis. Sea Grant Inst. WIS-SG-92-250.

Houde, E.D. 1996. Evaluating stage-specific survival during the early life of fish. *In* Survival strategies in early life stages of marine resources. *Edited by* Y. Watanabe, Y. Yamashita, and Y. Oozek. A.A. Balkema, Rotterdam, The Netherlands. pp. 51–66.

Hughes, D.A. 1968. Factors controlling emergence of pink shrimp (*Penaeus duorarum*) from the substrate. Biol. Bull. **134**: 48–59.

Hughes, D.A. 1969. Responses to salinity change as a tidal transport mechanism of pink shrimp, *Penaeus duorarum*. Biol. Bull. **136**: 43–53.

Iversen, E.S., and Idyll, C.P. 1960. Aspects of the biology of the Tortugas pink shrimp, *Penaeus duorarum*. Trans. Am. Fish. Soc. **89**: 1–8.

© 1999 NRC Canada

Jobling, M. 1994. Fish bioenergetics. Fish Fish. Ser. 13. Chapman and Hall, New York.

Johannes, R.E. 1978. Reproductive strategies of coastal marine fishes in the tropics. Environ. Biol. Fishes, **3**: 65–84.

Johnson, D.R., and Seaman, W., Jr. 1986. Species profiles: life histories and environmental requirements of coastal fishes and invertebrates (south Florida) — spotted seatrout. U.S. Fish. Wildl. Serv. Biol. Rep. 82(11.43), U.S. Army Corps Eng. TR EL-82-4.

Jones, A.C., Dimitriou, D.E., Ewald, J.J., and Tweedy, J.H. 1970. Distribution of early developmental stages of pink shrimp, *Penaeus duorarum*, in Florida waters. Bull. Mar. Sci. **20**: 634–661.

Joyce, E.A., Jr. 1965. The commercial shrimps of the northeast coast of Florida. Mar. Lab. Fla. Prof. Pap. Ser. 6.

Kennedy, F.S., Jr., and Barber, D.G. 1981. Spawning and recruitment of pink shrimp, *Peneaus duorarum*, off eastern Florida. J. Crustacean Biol. **1**: 474–485.

Kitchell, J.F., Stewart, D.J., and Weininger, D. 1977. Applications of a bioenergetics model to yellow perch (*Perca flavescens*) and walleye (*Stizostedion vitreum vitreum*). J. Fish. Res. Board Can. **34**: 1922–1935.

Lankford, T.E., Jr., and Targett, T.E. 1994. Suitability of estuarine nursery zones for juvenile weakfish (*Cynoscion regalis*): effects of temperature and salinity on feeding, growth and survival. Mar. Biol. **119**: 611–620.

Lee, T.M., and Rooth, C.G. 1976. Circulation and exchange processes in southeast Florida's coastal lagoons. Biscayne Bay Symposium. Univ. Miami Sea Grant Spec. Rep. 5.

Lee, T.M., Rooth, C.G., Williams, E., McGowan, M., Szmant, A., and Clarke, M.E. 1992. Influence of Florida current, gyres and wind-driven circulation on transport of larvae and recruitment in the Florida Keys coral reefs. Continental Shelf Res. **12**: 971–1002.

Livingston, R.J. 1997. Trophic response of estuarine fishes to long-term changes in river runoff. Bull. Mar. Sci. **60**: 984–1004.

Livingston, R.J., Niu, X., Lewis, F.G., III, and Woodsum, G.C. 1997. Freshwater input to a gulf estuary: long-term control of trophic organization. Ecol. Appl. **7**: 277–299.

Luo, J., Brandt, S.B., and Klebasko, M.J. 1996. Virtual reality of planktivores: a fish's perspective of prey selection. Mar. Ecol. Prog. Ser. **140**: 271–283.

Maceina, M.J., Hata, D.N., Linton, T.L., and Landry, A.M., Jr. 1987. Age and growth analysis of spotted seatrout from Galveston Bay, Texas. Trans. Am. Fish. Soc. **116**: 54–59.

McMichael, R.H., Jr., and Peters, K.M. 1989. Early life history of spotted seatrout, *Cynoscion nebulosus* (Pisces: Sciaenidae), in Tampa Bay, Florida. Estuaries, **12**: 98–110.

Montague, C.L., and Ley, J.A. 1993. A possible effect of salinity fluctuation on abundance of benthic vegetation and associated fauna in northeastern Florida Bay. Estuaries, **16**: 703–717.

Mooers, C.N.K., and Ko, D.S. 1994. Nowcast system development for the Straits of Florida. *In* Estuarine and coastal modeling III. *Edited by* M.L. Spaulding, K. Bedford, A. Blumberg, R. Cheng, and S. Swanson. American Society of Civil Engineers, New York. pp. 158–171.

Mooers, C.N.K., and Maul, G.A. 1998. Intra-Americas sea circulation. Chap. 7. *In* The sea. Vol. 11. *Edited by* A.R. Robinson and K.H. Brink. John Wiley & Sons, New York. pp. 183–208.

Munro, J.L., Jones, A.C., and Dimitriou, D. 1968. Abundance and distribution of the larvae of the pink shrimp (*Penaeus duorarum*) on the Tortugas Shelf of Florida, August 1962 – October 1964. Fish. Bull. U.S. **67**: 165–181.

Murphy, M.D., and Taylor, R.G. 1994. Age, growth, and mortality of spotted seatrout in Florida waters. Trans. Am. Fish. Soc. **123**: 482–497.

Murray, J.D. 1989. Mathematical biology. Springer-Verlag, New York.

NOAA. 1995. Our living oceans. NOAA/NMFS, Department of Commerce, Washington, D.C.

Pearson, J.C. 1929. Natural history and conservation of the redfish and other commercial sciaenids on the Texas coast. Bull. U.S. Bureau Fish. **4**: 129–214.

Peebles, E.B., and Tolley, S.G. 1988. Distribution, growth, and mortality of larval spotted seatrout, *Cynoscion nebulosus*: a comparison between two adjacent estuarine areas of southwest Florida. Bull. Mar. Sci. **42**: 397–410.

Pella, J.J., and Tomlinson, P.K. 1969. A generalized stock production model. Inter-Am. Trop. Tuna Comm. Bull. **13**: 419–496.

Rothschild, B.J., and Ault, J.S. 1992. Linkages in ecosystem models. S. Afr. J. Mar. Sci. **12**: 1101–1108.

Rothschild, B.J., and Ault, J.S. 1996. Population-dynamic instability as a cause of patch structure. Ecol. Model. **93**(1–3): 237–249.

Rothschild, B.J., Ault, J.S., and Smith, S.G. 1996. A systems science approach to fisheries stock assessment and management. *In* Stock assessment: quantitative methods and applications for small scale fisheries. *Edited by* V.F. Gallucci, S. Saila, D. Gustafson, and B.J. Rothschild. Lewis Publishers (Division of CRC Press), Chelsea, Mich. pp. 473–492.

Rutherford, E.S. 1982. Age, growth, and mortality of spotted seatrout, *Cynoscion nebulosus*, in Everglades National Park, Florida. Masters thesis, University of Miami, Coral Gables, Fla.

Rutherford, E.S, Schmidt, T.W., and Tilmant, J.T. 1989. Early life history of spotted seatrout (*Cynoscion nebulosus*) and gray snapper (*Lutjanus griseus*) in Florida Bay, Everglades National Park, Florida. Bull. Mar. Sci. **44**: 49–64.

Ruxton, G.D. 1996. Effects of the spatial and temporal ordering of events on the behaviour of a simple cellular automaton. Ecol. Model. **84**: 311–314.

Saucier, M.H., and Baltz, D.M. 1993. Spawning site selection by spotted seatrout, *Cynoscion nebulosus*, and black drum, *Pogonias cromis*, in Louisiana. Environ. Biol. Fishes, **36**: 257–272.

Schaefer, M.B. 1954. Some aspects of the dynamics of populations important to the management of the commercial marine fisheries. Inter-Am. Trop. Tuna Comm. Bull. **1**: 27–56.

Serafy, J.E., Lindeman, K.C., Hopkins, T.E., and Ault, J.S. 1997. Effects of freshwater canal discharge on fish assemblages in a subtropical bay: field and laboratory observations. Mar. Ecol. Prog. Ser. **160**: 161–172.

Smith, S.G. 1997. Models of crustacean growth dynamics. Ph.D. dissertation, University of Maryland at College Park, College Park, Md.

Sparre, P., and Venema, S.C. 1992. Introduction to tropical fish stock assessment. Part I — manual. FAO Fish. Tech. Pap. No. 306.1, rev. 1. FAO, Rome.

Stewart, K.W. 1961. Contributions to the biology of the spotted seatrout (*Cynoscion nebulosus*) in the Everglades National Park, Florida. Masters thesis. University of Miami, Coral Gables, Fla.

Tabb, D.C. 1961. A contribution to the biology of the spotted seatrout, *Cynoscion nebulosus* (Cuvier), of east-central Florida. Fla. Board Conserv. Mar. Res. Lab. Tech. Ser. 35.

Tabb, D.C. 1966. The estuary as a habitat for spotted seatrout (*Cynoscion nebulosus*). Am. Fish. Soc. Spec. Publ. **3**: 59–67.

Tabb, D.C., Dubrow, D.L., and Manning, R.B. 1962*a*. The ecology of northern Florida Bay and adjacent estuaries. Fla. State Board Conserv. Tech. Ser. 39.

Tabb, D.C., Dubrow, D.L., and Jones, A.E. 1962*b*. Studies on the biology of the pink shrimp, *Penaeus duorarum* Burkenroad, in Everglades National Park, Florida. Fla. State Board Conserv. Tech. Ser. 37.

Teinsongrusmee, B. 1965. The effect of temperature on growth of

© 1999 NRC Canada

post-larval pink shrimp, *Penaeus duorarum* Burkenroad. M.S. thesis, Univesity of Miami, Coral Gables, Fla.

Thornton, W., and Lessem, A.S. 1978. A temperature algorithm for modifying biological rates. Trans. Am. Fish. Soc. **107**: 284–287.

Vetter, E.F. 1988. Estimation of natural mortality in fish stocks: a review. Fish. Bull. U.S. **86**: 25–83.

Videler, J.J. 1993. Fish swimming. Fish Fish. Ser. 10. Chapman and Hall, New York.

von Bertalanffy, L. 1949. Problems of organic growth. Nature (Lond.), **163**: 156–158.

Wang, J.D., Cofer-Shabica, S.V., and Chin-Fatt, J. 1988. Finite element characteristic advection model. J. Hydraul. Eng. **114**: 1098–1114.

Wohlschlag, D.E., and Wakeman, J.M. 1978. Salinity stress, metabolic responses and distribution of the coastal spotted seatrout, *Cynoscion nebulosus*. Contrib. Mar. Sci. **21**: 171–185.

Young, G.C., Potter, I.C., Hyndes, G.A., and de Lestang, S. 1997. The ichthyofauna of an intermittently open estuary: implications of bar breaching and low salinities on faunal composition. Estuarine Coastal Shelf Sci. **45**: 53–68.

© 1999 NRC Canada

A length-based hypothesis for feeding migrations in pelagic fish

Leif Nøttestad, Jarl Giske, Jens Chr. Holst, and Geir Huse

Abstract: We evaluated the costs and benefits of long-distance horizontal migration by pelagic planktivores, Atlantic herring (*Clupea harengus*), blue whiting (*Micromesistius poutassou*), mackerel (*Scomber scombrus*), and capelin (*Mallotus villosus*) in the Norwegian and Barents seas using a numerical model and tested model predictions against field observations. Specifically, we considered (*i*) energetic costs as a function of body size, water currents, swimming speed, and distance, (*ii*) time costs as a function of speed and distance, and (*iii*) energetic gain in terms of differences in food intake between areas. The model demonstrates how body size restricts large-scale horizontal migration patterns. Model and field results suggest that the extent of migration will increase with increasing body length. The model predicts that long-distance migration costs may exceed energy intake for fish <20 cm, due to increased hydrodynamical drag with decreasing fish size. Field results suggest that migration distance is a function of length, weight, and age. Food abundance and distribution, current speed and direction, and differences in day length at boreal latitudes are believed to be the major driving forces influencing large-scale migration distance, direction, and timing in pelagic planktivores. Northwards latitudinal rather than longitudinal feeding migrations are explained by the improved feeding opportunities with increased day lengths.

Résumé : Nous avons évalué les coûts et les avantages de la migration horizontale à longue distance de poissons pélagiques planctivores, à savoir le hareng (*Clupea harengus*), le merlan bleu (*Micromesistius poutassou*), le maquereau (*Scomber scombrus*) et le capelan (*Mallotus villosus*), dans la mer de Norvège et la mer de Barents. Nous avons comparé les prévisions obtenues d'un modèle numérique et d'un modèle fondé sur les observations aux valeurs observées sur le terrain. Plus précisément, nous avons examiné (*i*) les dépenses énergétiques en fonction de la taille, du courant, de la vitesse de nage et de la distance, (*ii*) les dépenses de temps en fonction de la vitesse et de la distance et (*iii*) le gain énergétique en fonction des écarts de la consommation alimentaire entre les zones. Le modèle montre comment la taille limite la migration horizontale à grande échelle. Le modèle et les résultats obtenus sur le terrain portent à croire que l'importance de la migration s'accroît avec la longueur du poisson. Selon le modèle, les coûts d'une migration sur une longue distance peuvent être supérieurs à l'énergie absorbée chez les poissons de moins de 20 cm de longueur, étant donné que la traînée hydrodynamique s'accroît à mesure que la taille du poisson décroît. Les résultats obtenus sur le terrain indiquent que la distance de migration est fonction de la longueur, du poids et de l'âge. L'abondance et la répartition de la nourriture, la vitesse et la direction du courant de même que la durée du jour, différente sous les latitudes boréales, semblent constituer les principales forces qui influent sur la distance, la direction et le moment des migrations à grande échelle chez les planctivores pélagiques. Les migrations d'alimentation en direction des latitudes nordiques plutôt qu'en longitude sont expliquées par les meilleures possibilités d'alimentation découlant de jours plus longs.

[Traduit par la Rédaction]

Introduction

Large-scale horizontal migrations (>1000 km occurring over several months) have evolved in response to predictable oceanic features such as frontal areas where food is expected to be abundant, overwintering areas where conditions are favourable for energy saving and survival, and spawning areas where partners are expected to be found and conditions for spawning as well as larval drift routes are benign (Harden Jones 1968; Fernö et al. 1998). But migrations are energetically demanding (Weihs 1987; Jobling 1994), with smaller fish incurring greater swimming costs than larger fish (Videler 1993). High energetic costs may be offset by swimming in the same direction as the transporting tide (Weihs 1978; Metcalfe et al. 1990; Castonguay and Gilbert 1995) or by taking advantage of favourable coastal (Nøttestad et al. 1996) and oceanic (Thomson et al. 1995; Walter et al. 1997) currents. This energy saving could confer a selective advantage by increased allocation to growth and reproduction and by reducing starvation risk (Harden Jones 1984).

For long-distance migrators with distinct spawning and feeding seasons, time use may be as equally important as energy use in an environment with short feeding durations. During the summer, day length increases the further north the fish travel, thus potentially increasing the feeding duration for pelagic visual predators. In situations with similar

Received October 3, 1997. Accepted July 15, 1999.
J14231

L. Nøttestad[1] **and J.Chr. Holst.** Institute of Marine Research, P.O. Box 1870 Nordnes, N-5817 Bergen, Norway. **J. Giske and G. Huse**. Department of Fisheries and Marine Biology, University of Bergen, P.O. Box 7800, N-5020 Bergen, Norway.

[1]Author to whom all correspondence should be addressed.
e-mail: leif.nottestad@imr.no

© 1999 NRC Canada

concentrations of food everywhere, the visual predator would benefit energetically from staying in areas where the day length is longest, unless the uniform concentration of prey is sufficiently high to maximize energy ingestion or growth even for shorter daylight periods.

All horizontally migrating planktivorous fish species in the Nordic Seas, Atlantic herring (*Clupea harengus*), blue whiting (*Micromesistius poutassou*), mackerel (*Scomber scombrus*), and capelin (*Mallotus villosus*), are larger than the nonmigratory planktivores, the northern lightfish *Benthosema glaciale*, and the lightfish *Maurolicus muelleri* (Skjoldal et al. 1993). We therefore hypothesize that fish length may be a vital parameter for long-distance horizontal migration for pelagic fish, as fish length strongly influences the costs of swimming.

This paper focuses on the energetic cost–benefit relationship in long-distance migration in pelagic fish. In particular, we focus on time, size, and current constraints. Migration is hence analysed for its value in growth enhancement, which is likely to be an important motivation for migration in the Northeast Atlantic, since the productive time span for food of planktivorous fishes is very short (Skjoldal et al. 1993; Fernö et al. 1998). A numerical model was developed that analyses time and energy costs and benefits of migration for different sized fish, and this model was applied to invoke predictions about migration direction, routes, and physical and hydrodynamical constraints. Field data collected from Atlantic herring, blue whiting, mackerel, and capelin were then used to test the model predictions.

Material and methods

Model of migration

Energy minimization

The energetic costs of horizontal migration is a function of distance traveled (D), swimming speed (U), and energetic costs of swimming at speed U. Cost of locomotion (swimming) can be approximated by calculating the power (P) required to overcome drag. Power needed to overcome the drag of a moving object increases with the length of the object and with its swimming speed. For sockeye salmon (*Oncorhynchus nerka*) >10 cm, Ware (1978) used the empirical relationship

$$P = a_1 L^{\alpha} U^{\beta} \quad (1)$$

where a_1, α, and β are coefficients and L is fish length (all symbols used in all equations are explained in Table 1). Standard metabolism of a fish may be expressed from fish length (Brett 1964):

$$z = a_2 L^{\gamma}. \quad (2)$$

However, cost of migration must also consider water movements. If we denote the average directional speed of the current by u and the total travel speed by U_T, we have $U_T = U + u$ (current speed may be positive or negative, but to migrate in the right direction, $U + u > 0$). Following Ware (1978), we may express optimum cruising speed (U^*) as the speed where cost (sum of standard metabolic rate and power output) per distance travelled is minimum. By solving

$$\frac{d\left(\frac{U_T}{z+P}\right)}{dU_T} = 0 \quad (3)$$

we obtain an expression for the most cost-effective cruising speed depending on fish length and water current:

$$U^* = \left[\frac{a_1 L^{\alpha}\left(\beta + \frac{u}{U^*} - 1\right)}{z}\right]^{\frac{-1}{\beta}} \quad (4)$$

(an asterisk is used to indicate the optimum value of a parameter under energy minimization). We assume that fish may assess the current speed, but if fish are unable to do so, the estimated U^* (eq. 4) would tend to be underestimated, and consequently, the migration cost would be underestimated. For each fish species, a weight–length function $W = a_3 L^b$, where W is body wet weight, can be described. The energy cost per body mass during cruising at optimal speed in a current can be expressed as

$$\frac{C^*}{W} = \frac{P^* + z}{W} \quad (5)$$

where P^* is found from eq. 1 by use of U^* and where C^* ($= P^* + z$) is total energy costs at optimum speed. The cost per distance is C^*/U^*W, and the minimum total energy (E^*) use for migrating the distance D is

$$E^* = \frac{DC^*}{U^* + u}. \quad (6a)$$

The most cost-efficient time for this migration (T_m^*) is

$$T_m^* = \frac{D}{U^* + u} = \frac{E^*}{C^*}. \quad (6b)$$

U^* is optimal only in the sense of energy efficiency. For long-distance migrating fish in a highly seasonal environment, time use may be as equally important as energy use. This is not considered here but would tend to increase swimming speed.

Given that the main purpose of the migration away from the spawning area in spring and summer is increased feeding (Skjoldal et al. 1993; Fernö et al. 1998), the energetic cost must be offset by an energetic gain (ultimately to reduce time to maturation and increase survival and fecundity). We will analyse this decision under two different assumptions: (*i*) that fish at the spawning grounds decide to make a horizontal migration to a distant feeding area or (*ii*) that feeding fish on a daily basis decide whether to remain for another day or swim towards a less food deprived area.

Fish in the first scenario must also cover the cost of the return migration. Thus, swimming a distance D from an area with feeding rate F_1 and standard metabolic cost z_1 to feed in an area with feeding rate F_2 and standard metabolic cost z_2 and then back again during the time period T is energetically beneficial if

$$F_2 T_f - 2PT_m - z_2 T > F_1 T - z_1 T \quad (7a)$$

where T is total time and T_f is the time available for feeding ($T - 2T_m$). The feeding season in the Norwegian Sea is usually from April to August (Skjoldal et al. 1993; Fernö et al. 1998), about T = 5 months. Note that eq. 7*a* assumes no swimming cost (but still standard metabolic costs z) for fish that choose to remain on the spawning grounds during the feeding season. If we further assume equal standard metabolic costs for the two localities (i.e., no temperature effects, as in eq. 2), we have a metabolic benefit of migration to a distant feeding area when

$$F_2 > \frac{F_1 T(U^* + u) + 2DP}{T(U^* + u) - 2D}. \quad (7b)$$

© 1999 NRC Canada

Table 1. Symbols used in the equations in the text.

Symbol	Explanation	Value	Units
	Length – swimming cost allometry exponent	1.42[a]	
	Swimming speed – swimming cost allometry exponent	2.42[a]	
	Length–metabolism allometry exponent	2.47[b]	
a_1	Swimming cost allometry constant	5.18×10^{-3}[a]	
a_2	Length–metabolism allometry constant	1.47×10^{-5}[b]	
a_3	Length–weight allometry constant	Species specific	
b	Length–weight allometry exponent	Species specific	
C	Total energy cost		$J \cdot s^{-1}$
C/W	Energy cost per body weight		$J \cdot g^{-1} \cdot s^{-1}$
$C/(UW)$	Energy cost per distance		$J \cdot g^{-1} \cdot m^{-1}$
c	Conversion factor from energy contents to wet weight of prey	1800	J·g wet weight^{-1}
D	Horizontal migration distance		m
E	Energy use by migrating distance D		J
F_i	Feeding rates at site i		$J \cdot s^{-1}$
L	Fish body length		cm
N_i	Prey concentration at site i		Individuals$\cdot m^{-3}$
P	Power needed to overcome the drag of a moving object		$J \cdot s^{-1}$
R_i	Feeding rations at site i		g wet weight prey·g wet weight fish^{-1}·day^{-1}
r	Sensory range of fish		m
s_f	Part of the diel cycle that is allocated to feeding		s
T	Time available for migration and feeding = $T_f + T_m$		s
T_f	Time available for feeding		s
T_m	Migration time		s
U	Individual swimming speed		$m \cdot s^{-1}$
U_T	Total travel speed = $U + u$		$m \cdot s^{-1}$
u	Average directional speed of the current		$m \cdot s^{-1}$
W	Fish weight		g
W_{prey}	Prey weight		g
z, z_i	Standard metabolism of the fish (at site i)		$J \cdot s^{-1}$

Note: Symbols with an asterisk in equations refer to parameter values under optimal cruising speed U^*.
[a]Ware (1978).
[b]Brett (1964).

If the current speed and direction experienced by the fish are constant during migration (feeding and spawning migration), then we may exclude u from eq. 7*b*. On the other hand, if the fish may take advantage of horizontal or vertical variation in u, e.g. in a horizontal gyre or in a vertical countercurrent system (Harden Jones 1957, 1963, 1965, 1968; McCleave et al. 1984), this behaviour may be of great biological importance by saving travel time and travel costs and increasing feeding time.

The daily feeding ration R can be expressed from the instantaneous feeding rate F by

$$(8) \qquad R_i = \frac{F_i s_f}{Wc}$$

(i = 1 or 2 as in eqs. 7*a* and 7*b*) where feeding rate is scaled against the weight of the fish, the energy concentration of the prey (c), and the fraction of the day spent feeding (s_f). Minimum required daily increase in ration to offset the cost of migration can now be calculated from eq. 7*b*. If day length increases along the feeding migration route, then a smaller increase in F_2 is needed to obtain a sufficiently high R_2 to facilitate migration.

The second scenario describes the choice for an individual that shall decide whether to migrate a smaller distance D to feed there for today or remain where it is for at least one more day. Standard metabolic costs may be considered constant over this distance. If we further assume that migration time is at the expense of feeding time, we may express a different criterion for horizontal migration based on eq. 7*a*:

$$(7c) \qquad F_2 > \frac{F_1 T(U^* + u) + DP}{T(U^* + u) - D}$$

That is, migration will occur if feeding rate at area 2 can replace energy lost due to migration. Note that eq. 7*c* does not assume that the fish will have to reserve energy for the return migration. Neither is the cost of a countercurrent ($-u$, metres per second) in the homing migration included.

If feeding rate approaches stomach capacity, the feeding motivation for further migration will cease. Feeding rate will depend on a series of factors, including sensory range of the fish (r), food concentration (N), swimming speed of the predator (U), and prey size (W_{prey}) (Giske and Salvanes 1995; Aksnes and Utne 1997). To obtain an encounter-limited feeding at a rate of F (joules per second), a predator will need a concentration (individuals per cubic metre) of

$$(9) \qquad N_i = \frac{F_i}{\pi r^2 (U + u) c W_{prey}}.$$

Both U and to a smaller extent r are length dependent (sensory range will predominantly be depth dependent, Aksnes and Utne 1997). Although swimming speed under feeding (U) will differ

© 1999 NRC Canada

from optimum cruising speed U^*, size differences will probably remain. Optimum swimming speed is twice as high for a 50-cm fish as for a 10-cm fish and three times as high if $u = 0.5$ m·s^{-1}. Hence, a 10-cm fish will probably need more than twice the prey concentration to achieve the same feeding rate F as a 50-cm fish.

Current speed (u) in the Northeast Atlantic between 55°N and 80°N and from 5°W to 15°E including the main 20- to 50-km branch of the strong Atlantic current was calculated by taking average speed and direction for every 1°N from available field data (Poulain et al. 1996) and model simulations (E. Svendsen and M. Skogen, Institute of Marine Research, Bergen, Norway, personal communication). The average current speed in a northerly direction during the period from April to August from 1993 to 1996 was estimated by vector analysis. Arrays indicating current speed and direction were vectored into a north–south and east–west component. From this contribution the northern component was calculated.

Field sampling

Model predictions were tested using acoustic and trawl data for four Atlantic species (Atlantic herring, blue whiting, mackerel, and capelin) collected from scientific cruises on R/V *Johan Hjort* and R/V *G.O. Sars*. The goal of these surveys was to estimate the abundance of commercially important pelagic species over a broad geographical range (Anonymous 1996*a*, 1996*b*; Monstad et al. 1996; Fernö et al. 1998; Gjøsæter 1998). Thus, these data sets are ideal for testing our model predictions. For Norwegian spring-spawning Atlantic herring, data are from April–May (spring feeding) and July–August (late-summer feeding) 1993–1996 cruises. Data were used to calculate overall migration distances and to determine geographic patterns of length, weight, and age. Average lengths (±SE) for every 1.0°N from 62°N to 80°N and between 5°W and 15°E were calculated from subsamples (N = 100·trawl^{-1} in 146 trawl hauls). The distance that an individual shoal migrates was not available from the data set. Thus, we assumed that spawning is limited in space and time for each species; this has been shown to be a good approximation (Fernö et al. 1998). Atlantic herring (as well as blue whiting, mackerel, and capelin) have reasonably defined spawning sites (Fig. 1). Although variations in spawning locations do exist both within and between years (Dragesund et al. 1997; Gjøsæter 1998), the majority of spawning is concentrated within a small geographical location providing a core spawning site from which to estimate migration distance. Moreover, all species in this study have a pronounced south–north migration pattern. The end result is a data set from which we can estimate migration distance and the relationship between length and latitude.

A similar procedure was applied to blue whiting, mackerel, and capelin. Data from July–August 1993–1996 (late-summer feeding) were applied for blue whiting, while data from July–August 1991, 1993, 1995, and 1996 (late-summer feeding) and September–October 1990–1992 (most northern extent of the migration) were applied for mackerel and capelin, respectively. The time periods chosen for each species reflect maximum spatial coverage. Capelin in the Barents Sea ecosystem achieve the most northerly extent of their migration later than Atlantic herring, blue whiting, and mackerel studied in the Norwegian Sea. This information is used to include only those data from the feeding period where these species are distributed furthest to the north. The years used represent periods when population size was high and long-distance feeding migration was pronounced for each species applied in the analysis.

For Atlantic herring, we have also included a westerly migration during the feeding migration in addition to the pronounced northerly migration (Misund et al. 1997). Atlantic herring migrate to the polar front area in the western part of the Norwegian Sea (Fig. 1), where they feed during late spring and early summer. Later, they swim further north. This migration pattern is not as pronounced as for blue whiting and mackerel in the Norwegian Sea. Capelin prefer the productive areas connected to the Arctic ice edge during summer feeding, giving a more pronounced northward feeding migration. Thus, in blue whiting, mackerel, and capelin, we have only incorporated a northerly migration pattern from the spawning sites. Again, this is believed to represent conservative minimum values on migration distance for each length group and species. A simplistic northward migration route may nevertheless reveal important aspects of long-distance migration. Repeated surveys over subsequent years also indicate this to be appropriate (Anonymous 1996*a*).

Results

Model simulations

Assumption 1. Long-distance migration

The migration model predicts a decrease in swimming cost per body mass with increasing size of fish, so that the most optimal swimming speed is size dependent (cf. Ware 1978; Videler 1993). Effects of current speed override size effects at high currents in the swimming direction, while size differences are maximized for the expensive countercurrent swimming (Fig. 2). The time needed to swim D = 500 km will be length dependent in the absence of water currents, while strong currents in the swimming direction reduce differences in migration time between sizes (Fig. 3).

Minimum ration to offset a horizontal migration does not vary significantly among species. Figure 4 is based on length–weight relationships for Atlantic herring ($a_3 = 6.9 \times 10^{-3}$, $b = 3.04$) but on sockeye salmon data in eqs. 1 and 2. The parameters a_3 and b were also measured from the other three species, with only small differences found in swimming costs. The maximum difference between species in minimum ration to offset migration was found to be 6% between 10-cm capelin and mackerel at low R_1 and $u = 0$. The increase in minimum ration to initiate an energetically beneficial feeding migration of $2D$ = 1000 km is about 40–65%, without help from currents, for fish <20 cm (Fig. 4). However, if fish use prevailing currents ($u = 0.5$ m·s^{-1}), without the penalty of a countercurrent spawning migration, the minimum increase in ration to initiate a feeding migration is only 15% and essentially independent of fish size (Fig. 4).

Assumption 2. Short daily migrations

Daily decision to migrate will depend on body size, water currents, day length, and expected differences in feeding rates (Fig. 5). (The nonlinearities in Fig. 5 appear when F_1 is close to standard metabolic demands z. At such very low feeding rates, the small amount of energy required to transport the fish 1 km is big relative to the low F_1.) Food competition in a large resident population will drive F_1 to the left in Fig. 5, so that a smaller absolute difference between R_2 and R_1 will initiate a migration (eq. 7*a*). Although any food density N gives twice as high F_1 for a 50-cm than for a 10-cm fish (eq. 9), this advantage is counteracted by the far higher energy demands of the larger fish. Smaller individuals, with both smaller stomachs and lower swimming speed, will experience satiation at far lower feeding rates (measured as joules per second) than larger fish. As the initial food density in a virgin area decreases due to feeding, the larger fish will experience nonsatiating food concentration and thereby food competition first. Large individuals can therefore be expected to continue their swimming towards areas

© 1999 NRC Canada

Fig. 1. Migration patterns of pelagic fish in the Northeast Atlantic. Atlantic herring, blue whiting, and mackerel migrations are shown for the Norwegian Sea, while capelin migration is shown for both the Barents Sea and Icelandic stocks. Different shading and symbols used to indicate feeding migration, feeding area, spawning migration, and spawning area for each species. Spawning areas: SH, Atlantic herring; SBW, blue whiting; SM, mackerel; SC, capelin. Migration data collected from Gjøsæter (1980), Loeng (1981), FAO (1983), Ozhigin and Luka (1984), Monstad (1990), Holst and Iversen (1992), Røttingen (1992), Vilhjàlmsson (1994), Walsh et al. (1995), Anonymous (1996*a*, 1996*b*), and Monstad et al. (1996).

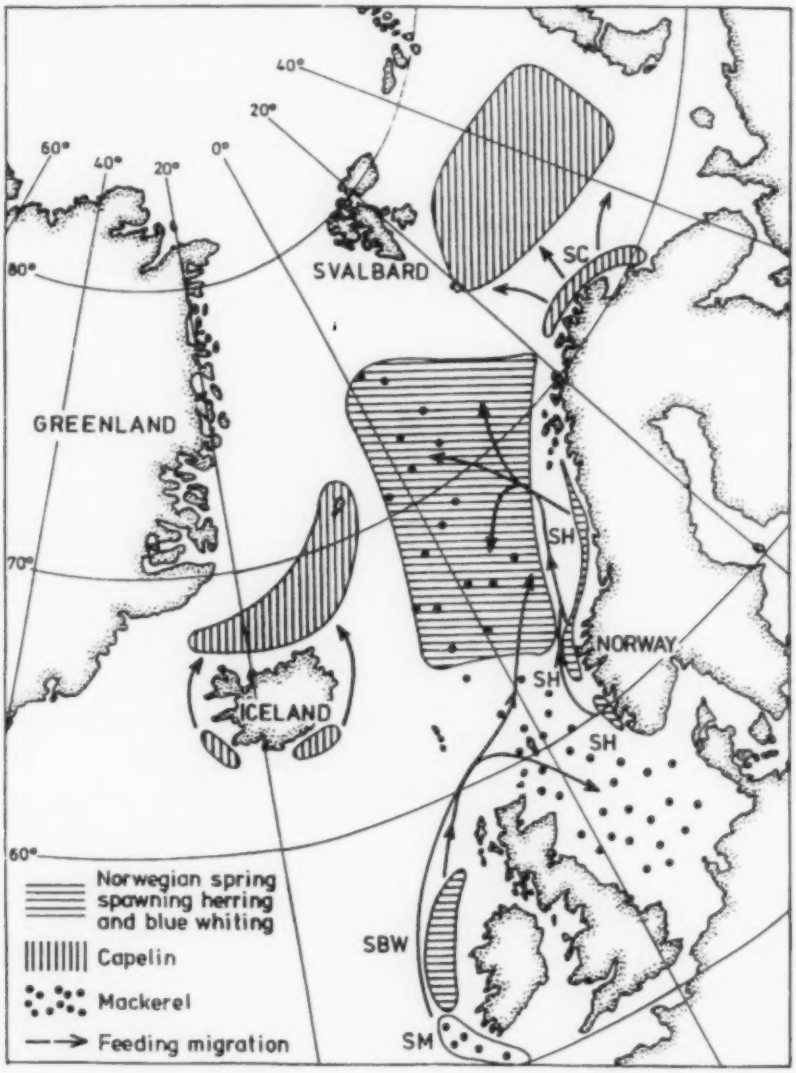

with more food and for longer days of feeding opportunity before the smaller fish experience any competition, creating a size-dependent horizontal migration. Following currents will reduce the size-dependent difference in feeding rates needed for migration.

Since longer days give visual predators more time to feed, migration will be directed northward if the food gradients change in the same manner in all directions away from the present feeding area (compare Figs. 5A and 5B with Figs. 5C and 5D). Expectations with increasing day length are far more reliable than expectations with feeding rates and currents. The predictable seasonal northward propagation of phytoplankton and zooplankton production present in the Northeast Atlantic during the feeding season may also influence the migration pattern of pelagic planktivores.

Model predictions

Based on the model results, three predictions emerge as follows.

(1) Due to time constraints, visual predators under equal feeding conditions (given that food concentration is sufficiently low to impact feeding rate) will migrate pole-

© 1999 NRC Canada

Fig. 2. Swimming speed for which energy cost per distance travelled is minimum for various sizes of fish as a function of current speed u.

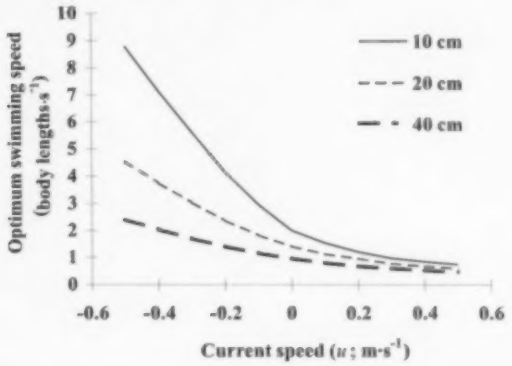

Fig. 3. Duration (T_m) to migrate 500 km, swimming at optimal migration speed U^*, as a function of fish length L and current velocity u. Current speed may override size effects on days used for a 500-km migration at the most energy-efficient swimming speed.

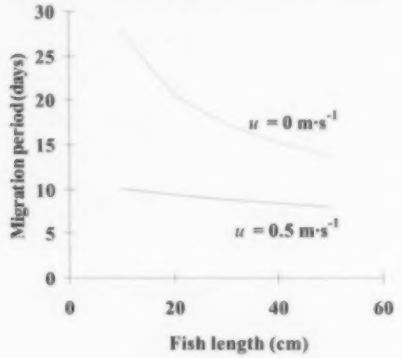

wards in the feeding season to obtain longer days and feeding periods. This will apply to areas with pronounced latitudinal variation in day length and in particular to 40–70°N or S.

(2) Larger individuals will experience food competition at higher food concentrations than smaller fish and will therefore benefit most from continual horizontal (northwards) feeding migration during summer. We therefore expect to find the average size of the individuals in a species to increase northwards.

(3) Consistent variation in current speed u in the vertical or transverse to the direction of migration may enable individuals to utilize different migratory routes in feeding migrations and in the spawning migrations. This will benefit smaller individuals more than larger ones and will counteract some of the strongest size selection in prediction 2.

Field data

Length-dependent migration

Average fish length increased significantly with latitude

Fig. 4. Minimum food ration R_2 at the destination to initiate a migration given food ration R_1 at the present location and average current speed u.

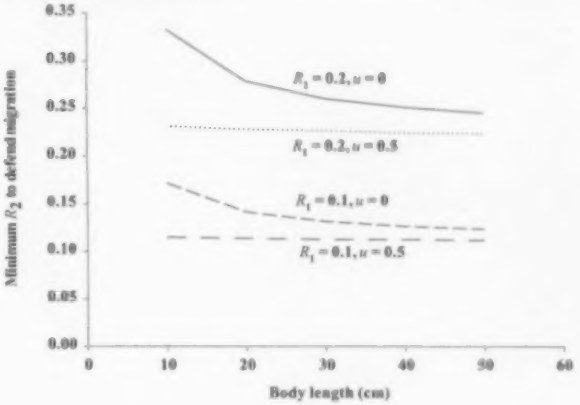

for Atlantic herring, blue whiting, mackerel, and capelin (Fig. 6). Fish length (±SE) increased 0.71 ± 0.28, 1.01 ± 0.08, 0.99 ± 0.10, and 0.50 ± 0.05 cm for each 1°N for Atlantic herring, blue whiting, mackerel, and capelin, respectively.

Currents

Current speed in April–July 1990–1993 at 1°N intervals from 55°N to 80°N and from 5°W to 15°E in the Northeast Atlantic is given in for depths of 20 and 250 m (Fig. 7). The chosen current depths are directly related to average migration depth for the selected species during the feeding period. We assume a migration depth for Atlantic herring, mackerel, and capelin to be around 20 m, while the migration depth for blue whiting is at about 250 m depth. Based on acoustic measurements, visual observations, and biological samples, there should be a good approximation between applied current depth and migration depth.

Discussion

Feeding migrations may be looked upon as opportunistic. The hunt for food drives pelagic fish in a northerly and northwesterly direction during spring and summer for several reasons: (*i*) inter- and intra-specific competition is forcing fish to move to new feeding areas (Wootton 1990), (*ii*) the zooplankton production cycle is initiated in the south and propagates northwards during spring and summer (Mann and Lazier 1991), thus forcing pelagic planktivorus fishes to follow the production of zooplankton, and (*iii*) prolonged day length increases the feeding period for visually feeding planktivorous fish, providing increased energy ingestion and energetic benefits (Suthers and Sundby 1996). Since day length increases significantly when heading north in boreal waters, fish may decide to swim towards north rather than west, even though the food concentration may be similar in other areas. However, Atlantic herring have a pronounced westerly migration pattern towards the polar front area during spring and early summer (Misund et al. 1997). This may be linked to higher phytoplankton and zooplankton produc-

© 1999 NRC Canada

Fig. 5. Energetic motivation to initiate small-scale migration to a new feeding area. The fish may at sunrise decide to stay where it is and feed all day (T = 12 or 18 h of daylight) or migrate at optimum speed to a new area D = 1 km away and feed there for the remaining hours of daylight ($T_f = T - T_m^*$). If the difference in feeding rates ($F_2 - F_1$) between these locations is above a threshold defined by the line for each fish size (eq. 7*c*), then horizontal migration is energetically profitable. The threshold for migration is lowest at long days and swimming with a current (Fig. 5D). Differences between size-classes are most pronounced in the absence of a following current (Figs. 5A and 5C).

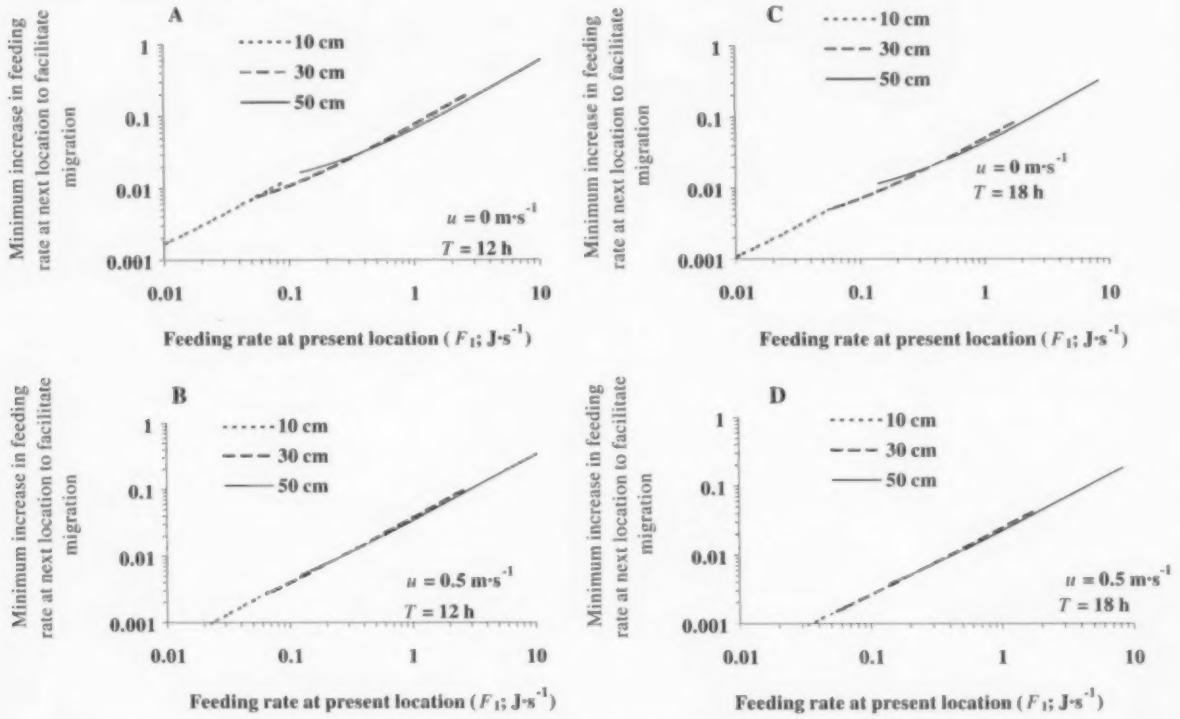

tion in the polar front areas in the western part of the Northeast Atlantic, where relatively warm Atlantic water mixes with colder Arctic water (Blindheim 1989; Fernö et al. 1998). There may be different plausible explanations for northward migrations in boreal waters during the summer feeding period. Random dispersal of fish within the Atlantic current system could be another explanation. Nevertheless, based on our field data on length-dependent migration pattern and model results, we strongly argue that food, together with favourable current and light conditions, predominantly influences the active migration pattern for pelagic fish.

Prediction 1

The field data for the Atlantic species support the first prediction that fish in general should swim northwards during summer to obtain longer days and thus more time to feed compared with areas further south. One should note that expectations with increasing day length are far more reliable than expectations with feeding rates and currents. A predictable seasonal northward propagation of phytoplankton and zooplankton production present in the Northeast Atlantic during the feeding season may also influence the migration pattern of pelagic planktivores. Highly productive polar front areas in the mixed region between Atlantic and Arctic water masses in the western part of the Norwegian Sea slightly modify this picture (see Fig. 1). Atlantic herring prefer to feed in polar front areas during part of the summer feeding as opposed to blue whiting and mackerel in the Norwegian Sea. This may result in a more western distribution of Atlantic herring, at least when food is abundant in the polar front area. Nevertheless, Atlantic herring have a pronounced northward migration pattern during the feeding season, without considering their extensive western migration route. In all species, our estimates of length-dependent migration are most probably significantly underestimated and conservative.

Prediction 2

The longest individuals of each species were consistently found furthest to the north. This supports the second prediction and relates to the greater swimming efficiency of longer fish as well as to the higher sensitivity to food concentrations. Pacific herring in British Columbia do not seem to migrate outside the continental shelf area (D. Hay, Department of Fisheries and Oceans, Victoria, B.C., personal communication), suggesting that they may be too small (<22 cm) to beneficially undergo such long-distance migrations. In addition to swimming more efficiently, large fish generally have greater fat reserves than small fish so that the capability for long-distance feeding migrations should increase with size (Videler 1993). It is possible that small fish cannot store or expend sufficient energy to travel long distances. Larger fish

© 1999 NRC Canada

Fig. 6. Latitudinal variation in average length of Atlantic herring, blue whiting, mackerel, and capelin. The linear equation $y = ax + b$ and values of the correlation coefficient R^2 for each species are as follows: Atlantic herring, $y = 0.73x - 18.17$ ($R^2 = 0.94$, $n = 4696$); blue whiting, $y = 1.01x - 41.56$ ($R^2 = 0.79$, $n = 5969$); mackerel, $y = 0.99x - 30.61$ ($R^2 = 0.92$, $n = 4002$); capelin, $y = 0.50x - 25.23$ ($R^2 = 0.90$, $n = 5905$). Data are from scientific cruises in 1990, 1992, 1993, 1994, and 1996 (Institute of Marine Research, Bergen, Norway).

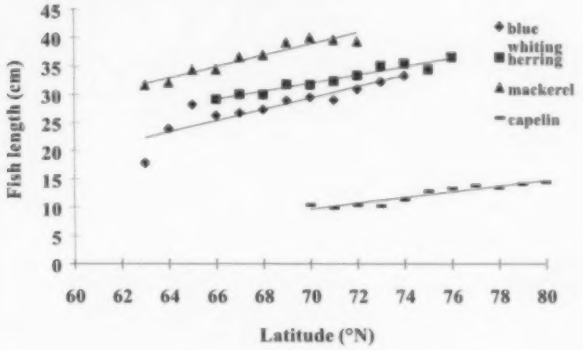

may swim longer distances at suboptimal swimming speeds without losing much energy, while smaller fish are much more sensitive to swimming speed energetics. Trump and Leggett (1980) predicted that with respect to distance, larger fish will have higher optimal swimming speeds and lower minimum specific energy expenditures and will experience smaller energetic penalties for swimming at speeds other than the optimal. Larger fish seem to benefit first by leaving an area with food competition (Fig. 5), so larger fish will then first occupy new and possibly highly productive feeding areas. Competition between species may also be important during the feeding season and influence migration patterns. In practice, Atlantic herring, blue whiting, and mackerel are competing for the same food resources (Fig. 1), thus creating an interspecific competition for zooplankton in the Norwegian Sea (Fernö et al. 1998).

Prediction 3

The general size-specific migration shown in this study may be closely connected to the prevailing current system of the Norwegian and Barents seas. Adult planktivores rarely swim against the prevailing currents (Harden Jones 1968). A recent report on near-surface circulation of the Nordic seas by Poulain et al. (1996) gives the highest resolution and most detailed description of circulation patterns including the Norwegian and Barents seas. From the Faeroe–Shetland channel, Atlantic water will spread towards the northeast. The current spreads outside Stad (62°N), and the easterly border of the current follows the continental edge north along the continental slope. After spawning, Atlantic herring, blue whiting, and mackerel seem to associate with strong currents (>40 cm·s^{-1}) up to 66–67°N, where the flow changes direction towards the west/northwest. Interestingly, after detailed tracking of Atlantic herring schools during the whole feeding period in 1995 and 1996, the Atlantic herring headed westward after reaching 66–66.30°N (Anonymous 1996*a*; Poulain et al. 1996). Not surprisingly, Atlantic herring and possibly blue whiting and mackerel take advantage of the strong current flowing north and then westward to the polar front areas. Passive advection requires current speeds in the range of 10–20 cm·s^{-1}, which is possible in the Continental Slope Current (Hansen and Jàkupsstovu 1991). Weihs (1978) demonstrated that substantial (40–90%) energy savings can be achieved by migrating fish that move at a constant velocity relative to the bottom where both fish and tide are moving in the same direction. Presently, there exists no evidence on how pelagic fish navigate in the ocean, apparently without any external reference points such as the bottom or the coastline (see Harden Jones 1968). One challenge for future science is whether or how pelagic fish assess the current speed ("ground speed" versus "through-the-water speed") and how these aspects may influence our understanding and quantification of fish migration. More synoptic field data on variation in the current system compared with the migration routes on proper spatiotemporal scales are required in order to establish how and to what extent fish may take advantage of the current system. However, field data from Poulain et al. (1996) and simulation models support the hypothesis that consistent variation in current speed may enable individuals to use different migratory routes in feeding migrations and in spawning migrations.

Fig. 7. Average current speed in the northern direction from April to July 1990–1993 at 20 and 250 m depth from 5°W to 15°E.

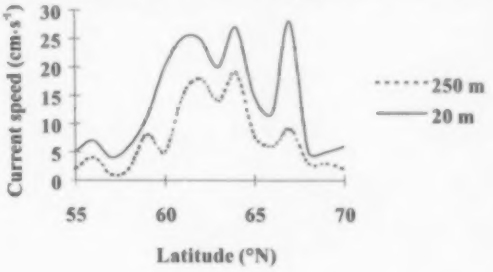

Acknowledgements

We would like to thank Anders Fernö, Steven Mackinson, Tony Pitcher, Doran Mason, and two anonymous referees for valuable comments and suggestions on the manuscript.

References

Aksnes, D.L., and Utne, A.C.W. 1997. A revised model of visual range in fish. Sarsia, **82**:137–147.

Anonymous. 1996*a*. Report of the Northern Pelagic and Blue Whiting Fisheries Working Group. ICES C.M. 1996/Assess: 14.

Anonymous. 1996*b*. Report of the Working Group on the Assessment of Mackerel, Horse Mackerel, Sardine and Anchovy. ICES C.M. 1996/Assess: 3.

Brett, J.R. 1964. The respiratory metabolism and swimming performance of young sockeye salmon. J. Fish. Res. Board Can. **21**: 1183–1226.

Dragesund, O., Johannessen, A., and Ulltang, Ø. 1997. Variation in migration and abundance of Norwegian spring spawning herring (*Clupea harengus* L.). Sarsia, **82**: 97–105.

FAO. 1983. FAO species catalogue: Scombrids of the world. Vol. 2. No. 125. FAO, Rome.

© 1999 NRC Canada

Fernö, A., Pitcher, T.J., Melle, W., Nøttestad, L., Mackinson, S., Hollingworth C., and Misund O.A. 1998. The challenge of the herring in the Norwegian Sea: making optimal collective spatial decisions. Sarsia, **83**: 149–167.

Giske, J., and Salvanes, A.G.V. 1995. Why pelagic planktivores should be unselelctive feeders. J. Theor. Biol. **173**: 41–50.

Gjøsæter, H. 1998. The population biology and exploitation of capelin (*Mallotus villosus*) in the Barents Sea. Sarsia, **83**: 453–496.

Hansen, B., and Jakupsstovu, S.H. 1991. Availability of blue whiting (*Micromestistius poutassou*) in Faroese waters in relation to hydrography. ICES 1991/Variability Symp. No. 28/Session 3.

Harden Jones, F.R. 1957. Movements of herring shoals in relation to tidal currents. J. Cons. Perm. Int. Explor. Mer, **22**: 322–328.

Harden Jones, F.R. 1963. The reaction of fish to moving backgrounds. J. Exp. Biol. **34**: 259–275.

Harden Jones, F.R. 1965. Fish migration and water currents. Spec. Publ. Int. Commun. NW Atl. Fish. **6**: 257–266.

Harden Jones, F.R. 1968. Fish migration. Edward Arnold (Publishers) Ltd., London, U.K.

Harden Jones, F.R. 1984. A view from the ocean. *In* Mechanisms of migration in fishes. *Edited by* J.D. McCleave, G.P. Arnold, J.J. Dodson, and W.H. Neill. Plenum Press, New York. pp. 1–26.

Holst, J.C., and Iversen, S. 1992. Distribution of Norwegian spring-spawning herring and mackerel in the Norwegian Sea in late summer, 1991. ICES C.M. 1992/H: 13. Pelagic Fish Committee.

Jobling, M. 1994. Fish bioenergetics. London. Chapman and Hall, London, U.K.

Loeng, H. 1981. Nordlig utbredelse av lodde og temperaturforholdene i Barentshavet om høsten. Fisken Havet, **1**: 1–10. (In Norwegian.)

Mann, K.N., and Lazier, J.R.N. 1991. Dynamics of marine ecosystems. Blackwell, London, U.K.

McCleave, J.D., Arnold, G.P., Dodson, J.J., and Neill, W.H. (*Editors*). 1984. Mechanisms of migration in fishes. Plenum Press, New York.

Metcalfe, J.D., Arnold, G.P., and Webb, P.W. 1990. The energetics of migration by selective tidal stream transport:an analysis for plaice tracked in the southern North Sea. J. Mar. Biol. Assoc. U.K. **70**: 149–162.

Misund, O.A., Melle, W., and Fernö, A. 1997. Migration behaviour of Norwegian spring spwning herring entering the cold front in the Norwegian Sea. Sarsia, **82**: 107–112.

Monstad, T. 1990. Distribution and growth of blue whiting in the northeast Atlantic in 1980–1988. *In* Biology and fisheries of the Norwegian spring spawning herring and blue whiting in the northeast Atlantic. Proceedings of the Fourth Soviet–Norwegian Symposium, Bergen, 12–16 June 1989. *Edited by* T. Monstad. Institute of Marine Research, Bergen, Norway. pp. 227–267.

Monstad, T., Belikov, S.V., and Shamrai, E.A. 1996. Report of the Norwegian–Russian acoustic survey on blue whiting during spring 1996. ICES C.M. 1996/H: 12.

Nøttestad, L., Aksland, M., Beltestad, A., Fernö, A., Johannessen, A., and Misund, O.A. 1996. Schooling dynamics of Norwegian spring spawning herring (*Clupea harengus* L.) in a coastal spawning area. Sarsia, **80**: 277–284.

Ozhigin, V.K., and Luka, G.I. 1984. Some pecularities of capelin migrations depending on thermal conditions in the Barents Sea. *In* The Proceedings of the Soviet–Norwegian Symposium on the Barents Sea Capelin. *Edited by* H. Gjøseter. Institute of Marine Research, Bergen, Norway. pp. 135–148.

Poulain, P.-M, Warn-Varnas, A., and Niiler, P.P. 1996. Near-surface circulation of the Nordic seas as measured by Lagrangian drifters. J. Geophys. Res. **101**(C8): 18 237 – 18 258.

Røttingen, I. 1992. Recent migration routes of Norwegian spring spawning herring. ICES C.M. 1992/H:18.

Skjoldal, H.R., Noji, T.T., Giske, J., Fosså, J.H., Blindheim, J., and Sundby, S. 1993. Mare Cognitum science plan for research on marine ecology of the Nordic seas (Greenland, Norwegian, Iceland seas). Institute of Marine Research, Bergen, Norway.

Suthers, I.M., and Sundby, S. 1996. Role of the midnight sun: comparative growth of pelagic juvenile cod (*Gadus morhua*) from the Arcto-Norwegian and a Nova Scotian stock. ICES J. Mar. Sci. **53**: 827–836.

Trump, C.L., and Leggett, W.C. 1980. Optimum swimming speeds in fish: the problem of currents. Can. J. Fish. Aquat. Sci. **37**: 1086–1092.

Videler, J.J. 1993. Fish swimming. Chapman and Hall, London, U.K.

Vilhjàlmsson, H. 1994. The Icelandic capelin stock. Rit Fiskideildar **13.**

Walsh, M., Reid, D.G., and Turrell, W.R. 1995. Understanding mackerel migration off Scotland: Tracking with echosounders and commercial data, and including environmental correlated and behaviour. ICES J. Mar. Sci. **52**: 925–940.

Walter, E.E., Scandol, J.P., and Healey, M.C. 1997. A reappraisal of the ocean migration patterns of Fraser River sockeye salmon (*Oncorynchus nerka*) by individual based modelling. Can. J. Fish. Aquat. Sci. **54**: 847–858.

Ware, D. M. 1978. Bioenergetics of pelagic fish: theoretical change in swimming speed and ration with body size. J. Fish. Res. Board Can. **35**: 220–228.

Weihs, D. 1978. Tidal stream transport as an efficient method of migration. J. Cons. Int. Explor. Mer, **38**: 92–99.

Weihs, D. 1987. Hydromechanics of fish migration in variable environments. Am. Fish. Soc. Symp. Ser. **1**: 254–261.

Wootton, R.J. 1990. Ecology of teleost fishes. Fish and Fisheries Series 1. Chapman and Hall, London, U.K.

© 1999 NRC Canada

Simulated dispersal of exotic rainbow smelt (*Osmerus mordax*) in a northern Wisconsin lake district and implications for management

Thomas R. Hrabik and John Magnuson

Abstract: We simulated geographic dispersal of exotic rainbow smelt (*Osmerus mordax*) as a function of present introduction rates, the probability of invasion through stream connections among lakes and watersheds, and survival based on physical and chemical factors of lakes within a northern Wisconsin watershed. One fourth of the habitable lakes contained rainbow smelt after 1000 years if dispersal was restricted to stream corridors. In contrast, with present rates of human transport, half contained rainbow smelt after 200 years, three quarters after 300 years, and all after 1000 years. Simulated human introductions increased the number of epicenters for spread and were the most influential parameter in the model. Stream connections between lakes increased the number of lakes colonized; decreases in migration ability led to fewer invaded lakes. Although extinction was operating, human introductions outweighed extinction and led to a saturation of rainbow smelt across all habitable lakes within the watershed within 1000 years. Our results highlight the importance of human vectors in driving exotic fish dispersal, suggest that isolated lakes are important refuges for species negatively affected by rainbow smelt, and show that agencies interested in controlling the spread of exotic fishes need to strongly consider the human vector of transport.

Résumé : Nous avons simulé la dispersion géographique d'une espèce d'éperlan arc-en-ciel (*Osmerus mordax*) exotique en fonction des taux d'introduction actuels, de la probabilité d'invasion par les voies de communication entre les lacs et les bassins hydrographiques et de la survie fondée sur les facteurs physiques et chimiques des lacs d'un bassin hydrographique situé dans le nord de l'État du Wisconsin. Dans ce bassin, seul le quart des lacs habitables contenaient des éperlans arc-en-ciel après 1000 ans si la dispersion était limitée aux corridors des cours d'eau. Par contraste, avec les taux actuels de déplacement des êtres humains, la moitié des cours d'eau contenaient des éperlans arc-en-ciel après 200 ans, les trois quarts après 300 ans et tous en contenaient après 1000 ans. La simulation d'introductions par les êtres humains a augmenté le nombre d'épicentres de distribution et constituait le paramètre du modèle ayant la plus grande influence. Les voies de communication interlacustres ont augmenté le nombre de lacs colonisés; la diminution de la capacité de migration a entraîné l'invasion d'un moins grand nombre de lacs. Même si le phénomène d'extinction était actif, les introductions par l'être humain ont été supérieures à l'extinction et ont entraîné une saturation en éperlan arc-en-ciel de tous les lacs habitables du bassin hydrographique en moins de 1000 ans. Les résultats obtenus soulignent l'importance de vecteurs humains commandant la dispersion de poissons exotiques, ce qui laisse supposer que les lacs isolés constituent des refuges importants pour les espèces qui sont affectées négativement par la présence de l'éperlan arc-en-ciel et montrent que les organisations intéressées à contrôler la dispersion des poissons exotiques doivent prendre en compte sans réserve le vecteur du transport humain.

[Traduit par la Rédaction]

Introduction

Introductions of exotic fishes are commonplace; exotics are spreading at a rapid rate worldwide (Moyle 1986; Lodge 1993*a*; Bruton 1995) and often cause negative impacts on native fauna and existing fisheries (Magnuson 1976; Moyle et al. 1986; Kaufman 1992; Lodge 1993*b*; Moyle and Moyle 1995). The addition of exotic species changes community composition and structure in many ecosystems as spread occurs across a landscape (Skellum 1951; Elton 1958; Mooney and Drake 1986).

The exotic rainbow smelt (*Osmerus mordax*) now exists in all of the Laurentian Great Lakes and is spreading secondarily to smaller, more isolated lakes within the Great Lakes region (Evans and Loftus 1987; Mayden et al. 1987; Franzin et al. 1994). Reproductive success of lake whitefish (*Coregonus clupeaformis*) and cisco (*Coregonus artedi*) has declined dramatically owing to predation by rainbow smelt on their larval stages (Loftus and Hulsman 1986; Hrabik et al. 1998). Predation by rainbow smelt has led to the rapid decline and probable extinction of cisco in Sparkling Lake, Wisconsin. The effects of competition by rainbow smelt on yellow perch (*Perca flavescens*) also have been observed in Crystal Lake, Wisconsin (Hrabik et al. 1998). Understanding processes governing the dispersal of rainbow smelt is of interest to fisheries managers, ecologists, and conservationists

Received October 8, 1997. Accepted June 10, 1999.
J14242

T.R. Hrabik[1] and J. Magnuson. Center for Limnology, 680 N. Park Street, Madison, WI 53706, U.S.A.

[1]Author to whom all correspondence should be addressed.
e-mail: habik@macc.wisc.edu

© 1999 NRC Canada

concerned with preserving the integrity of native fish communities.

Spatially explicit population models can provide insight into the effects of alterations in landscape characteristics on spatial distribution of species (Dunning et al. 1995). Such models can characterize patch use by organisms, which is important for visualizing the effects of management strategies and determining the most important factors shaping distribution patterns (Turner et al. 1995). Currently, few models are available to predict or visualize the spread of exotic fishes across lake districts. Dispersal across a heterogeneous lake district is a slow process; lakes often are isolated to varying degrees by streams and land barriers (Magnuson et al. 1998). Because rainbow smelt dispersal is occurring within the Bear River watershed in northern Wisconsin and because it is reasonably well documented, we constructed a spatially explicit simulation model of dispersal to assess possible future rainbow smelt distributions over periods of time longer than practical through empirical measurement. We also evaluate potential methods of controlling the rates of dispersal within and across watershed boundaries through systematic manipulation of the model parameters and the time course for the persistence of lakes not invaded by rainbow smelt. We present data from field collections and reports documenting the spread of rainbow smelt in three adjacent watersheds in Vilas County, Wisconsin, and discuss the application of spatially explicit population models for use in management strategies to control the spread of exotic fishes.

Methods

Study area

Field studies were conducted in the Bear River and Manitowish River watersheds in western Vilas County. This 1556-ha area contains 507 lakes larger than 0.75 ha and has a maximum difference in elevation among lakes of 52 m (North Temperate Lakes Long-Term Ecological Research project (NTL-LTER) database). Of these lakes, 29% have stream outlets and or inlets (NTL-LTER database). The area was deglaciated 10 000 – 12 000 years ago and is characterized by noncalcareous soils composed of postglacial till, moraine, and outwash material and irregular topographic relief (Bowen 1978; Attig 1985). We constructed a simulation model of rainbow smelt dispersal within the Bear River watershed (Fig. 1), the only watershed for which we had information on both physical and chemical properties and approximate dates of rainbow smelt invasion of each lake to date.

Field collections

We documented the dispersal and present distribution of rainbow smelt in lakes and streams through interviews and our own collections (Tables 1–3). We collected rainbow smelt during the spring spawning migrations in headwater streams and channels between lakes using a 12 × 1 m beach seine and long-handled dip nets. We collected rainbow smelt during the summer using five single-mesh, 4-m-wide vertical gill nets of 19-, 25-, 32-, 51-, and 64-mm stretch mesh that extended from the surface to the bottom (see Rudstam and Magnuson 1985). Personal communication with fisheries biologists from the Lac du Flambeau Natural Resource Department, the Wisconsin Department of Natural Resources, and local fishers who collected rainbow smelt during spring spawning migrations provided approximate dates of rainbow smelt invasions.

Model and assumptions

The model was constructed to represent rainbow smelt dispersal among lakes in a low-gradient glacial outwash area containing small, low-gradient streams, lakes connected via streams, and lakes without stream connections. Assumptions related to the habitat characteristics suitable for rainbow smelt, the ability of rainbow smelt to move through connecting streams, and the habitability of lakes for rainbow smelt were estimated from characteristics of the lakes and the surrounding landscape.

The suitability of lakes for rainbow smelt habitation was estimated from physical and chemical characteristics of the lakes. In a study of 187 Canadian lakes that contained rainbow smelt, Evans and Loftus (1987) presented minimum and maximum values for pH, minimum depth, and minimum lake area. We used these values to constrain acceptable lake habitats for rainbow smelt. In our model, each of the three parameters had to lie within the minimum and maximum values to be considered acceptable. Physical and chemical data for most of the lakes in the watershed were available from the eastern lakes survey (Linthurst et al. 1986). Of about 114 lakes larger than 0.75 ha within the Bear River watershed, 41 met all three suitability criteria and 23 had stream outlets or inlets.

Stream connections between lakes were separated into their upstream and downstream components. Upstream movement to another lake is possible for adult rainbow smelt that migrate upstream through tributary streams during spring spawning migrations (Becker 1983; Nellbring 1989). Newly hatched rainbow smelt larvae can be washed out of the outlet downstream for several kilometres into downstream lakes (Naesje et al. 1987).

Given these life history and dispersal characteristics, we developed equations to estimate the probability of rainbow smelt using each stream as a dispersal route. The stream connectivity parameters varied from 0 to 1 based on the equations

$$U_i = \left(\left(1 - \frac{\min(g_i, g_m)}{g_m} \right) \left(1 - \frac{\min(l_i, l_m)}{l_m} \right) \right)^{1/2}$$

$$D_i = \left(1 - \frac{\min(l_i, l_{md})}{l_{md}} \right)$$

where U_i is the probability of rainbow smelt migrating upstream through a stream connection, g_i is the gradient for each individual stream between two lakes estimated from topographic maps, g_m is the maximum gradient against which a rainbow smelt can migrate upstream, l_i is the length of each individual stream between two lakes estimated from topographic maps, l_{md} is the maximum distance that rainbow smelt will wash downstream in the Bear River watershed, l_m is the maximum distance that rainbow smelt will migrate upstream in the Bear River watershed, and D_i is the probability of rainbow smelt larvae being washed downstream to the next lake.

Streams in the Bear River watershed are small with discharges generally less than 75 m^3/s. Thus, we have not included a component that accounts for high-discharge events because the study area is characterized by stable and low flows. For application in large river systems, additional parameters accounting for increased downstream dispersal of larvae could be added by altering the downstream dispersal equation.

For baseline simulations, we used parameter values that were reasonable based on the known distribution of rainbow smelt and chronology of invasions in the Bear River watershed. Using this scenario, we were able to simulate an invasion into Fence Lake and the dispersal to connected lakes over 30 years (the duration since rainbow smelt were introduced into Fence Lake). The model consistently replicated what apparently happened naturally within the lakes connected to Fence Lake (Fig. 1). The rate of human intro-

© 1999 NRC Canada

Fig. 1. Map of the Bear River watershed in Vilas County, Wisconsin, showing (*a*) the present distribution of rainbow smelt in the watershed (lakes in black are those that contain rainbow smelt) and (*b* and *c*) the observed spread of rainbow smelt through connected lakes within the Fence Lake chain and the results of model simulations under baseline parameter settings where an introduction of rainbow smelt into Fence Lake and invasions of connected lakes are compared with what actually occurred.

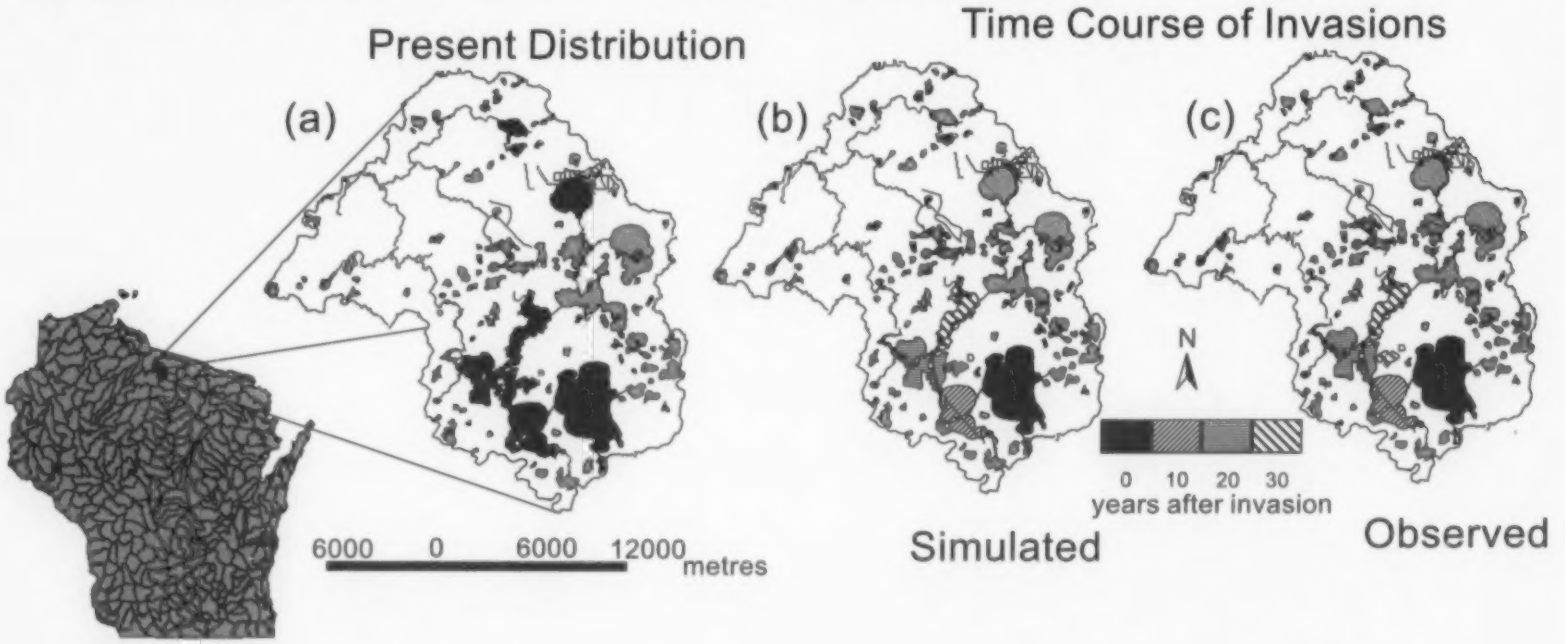

© 1999 NRC Canada

Table 1. Site, dates, and presence or absence of rainbow smelt at channel locations within the Bear River, Trout Lake, and Manitowish River watersheds sampled during field surveys.

Lake or stream	Date	Rainbow smelt	Sampling gear
Long Interlaken/Big Crawling Stone Lake channel	April 23, 1996	Yes	Beach seine
Flambeau/Pokegamma Lake channel	April 23, 1996	Yes	Beach seine
Moss/Long Interlaken Lake channel	April 21, 1995	Yes	Beach seine, dip net
Little Crawling Stone/Big Crawling Stone Lake channel	April 30, 1995	Yes	Dip net
Bolton/Fence Lake stream	April 30, 1995	Yes	Dip net
Bolton Creek (upstream from state highway 47)	April 30, 1995; April 23, 1996	No	Beach seine, dip net
Fence/North Twin Placid Lake channel	April 24, 1996	Yes	Dip net
Alder/Wild Rice Lake channel	April 24, 1996	No	Dip net
Manitowish/Spider Lake channel	April 25, 1996	No	Beach seine, dip net

Note: The timing of sampling with beach seines and dip nets coincided with spawning runs of rainbow smelt in nearby lakes.

Table 2. Sites, dates, and presence or absence of rainbow smelt at locations within the Bear River, Trout Lake, and Manitowish River watersheds in northern Wisconsin during field sampling surveys.

Lake	Date	Rainbow smelt	Sampling gear or data source
Fence Lake	July 21, 1993	Yes	Vertical gill nets
Crawling Stone Lake	August 28, 1993	Yes	Vertical gill nets
Manitowish Lake	June 24, 1996	No	Vertical gill nets
Little Star Lake	July 10, 1996	No	Vertical gill nets
Clear Lake	July 5, 1996; July 11, 1997	No	Vertical gill nets
Dead Pike Lake	July 15, 1996	Yes	Vertical gill nets
Big Lake	July 21, 1997	No	Vertical gill nets
Sparkling Lake	1982 to present	Yes	LTER database
Trout Lake	1981 to present	No	LTER database
Allequash Lake	1981 to present	No	LTER database
Big Muskellunge Lake	1981 to present	No	LTER database
Crystal Lake	1985 to present	Yes	LTER database
Papoose Lake	June 24, 1997	No	Vertical gill nets
Little Trout Lake	May 1990	Yes	L.Wawronowicz, personal communication

Note: The timing of sampling with beach seines and dip nets coincided with spawning runs of rainbow smelt in nearby lakes. Sampling with gill nets occurred during thermal stratification in each lake.

Table 3. Approximate year that rainbow smelt were first noted in lakes within the Bear River watershed.

Lake	Year	Source	Method of collection
Fence Lake	1968	Becker 1983	Unknown
Big Crawling Stone Lake	1975	W. Wolfe, personal communication	Beach seine
Little Crawling Stone Lake	1982	T.R. Hrabik, personal observation	Dip net
Long Interlaken Lake	1983	T.R. Hrabik, personal observation	Beach seine
Moss Lake	1989	T.R. Hrabik, personal observation	Dip net
To To Tom Lake	1990	G. Fidiment, personal communication	Hook and line
North Twin Placid Lake	1996	T.R. Hrabik, field collection	Dip net
Pokegamma Lake	1996	T.R. Hrabik, field collection	Beach seine

ductions within the watershed was estimated from the number of isolated lakes within the watershed containing rainbow smelt and was based on the following equation:

$$H = \frac{(L/L_t)}{T}$$

where H is the rate of human introductions, L is the number of lakes that were successfully invaded by rainbow smelt from human introductions, L_t is the total number of habitable lakes within the watershed, and T is number of years since the rainbow smelt were first introduced into the watershed.

The theory of island biogeography suggests that the extinction of a species is more likely on small islands than on large ones (MacArther 1972), and lakes can be considered as islands of water within the landscape (e.g., Magnuson 1976). We included an extinction function that fit this theory for the purpose of weighing its importance relative to other functions in the model. Based on this general contention, the probability of the extinction of rainbow smelt after an invasion had taken place in each lake was assumed to be inversely proportional to lake area and varied from 0 to 1 where extinction was equal to (lake area (ha))$^{-1.1}$.

Lakes that lacked stream connections to lakes containing rainbow smelt but still acquired rainbow smelt were assumed to have received introductions by humans. No observable lake characteristic seemed to make a lake more likely to receive rainbow smelt from human introductions, and no discernible pattern to these introductions was observed. Introductions might be expected to oc-

© 1999 NRC Canada

Fig. 2. Results of a sensitivity analysis from model simulations performed by changing each parameter by 20% while holding all others constant. Proportions shown are the mean number of lakes invaded from 100 simulations over 100 simulation years for each parameter setting divided by the mean number of lakes invaded under baseline parameter settings. Labels with upward pointing arrows represent scenarios with 20% increases in human introductions, rainbow smelt migration ability against gradient and length of streams, downstream dispersal ability, and increases in extinction rate. Labels with downward pointing arrows represent means from scenarios with a 20% decrease from each baseline setting.

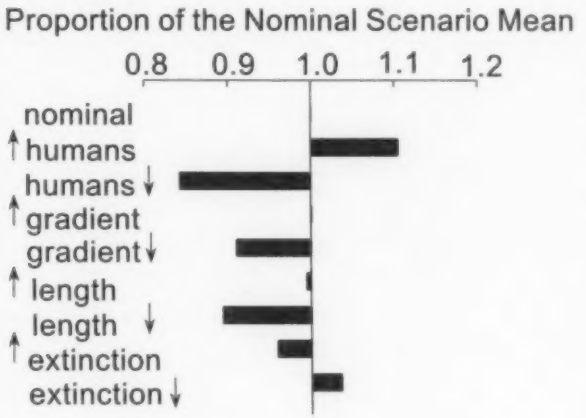

cur in connection with sport fishing; rainbow smelt have a reputation as good forage for predatory fish (e.g., Jones et al. 1994). However, of the lakes in our study area that have received rainbow smelt introductions, 60% have been smaller than 70 ha. Thus, our model assumed that human introductions occurred randomly with respect to the size of the lake and that each lake had an equal probability of being invaded through human introductions at each time step. The probability of each event in the model was determined by drawing a random probability between 0 and 1 from a uniform distribution; if the random probability was less than the probability of an individual process (e.g., U_i, D_i, H) determined by the output of each model function, the process occurred.

Once rainbow smelt invade a lake, further dispersal from the lake may "lag" or be limited for several years by low abundance and the absence of mature adults. We simulated the lag by allowing rainbow smelt to disperse from a newly invaded lake after having been established for 6 model years. This represented about two generations: one to reproduce and the other to represent a cohort of spreading adults.

A sensitivity analysis was performed by individually varying g_m, l_m, l_{md}, and H by ±20% from the nominal parameter values. The response variable used for the analysis was the mean number of lakes invaded based on 100 simulations run for 100 years. The upstream and downstream dispersal components through streams were combined into a total stream dispersal component to be compared with the human dispersal and the extinction components in a systematic way.

The trend of modeled invasions through time was well represented by an asymptotic function. The number of new lakes invaded by rainbow smelt was a function of time:

$$N_t = N_m\ (1 - e^{-a(T)})$$

where N_t is the number of lakes invaded at time t, N_m is asymptote parameter representing the maximum number of lakes to be invaded under current parameter settings, T is time (years), and a is a constant. The parameters in the model were estimated by fitting the function to the average number of lakes invaded at 50-year intervals for 100 simulations under the nominal parameter scenario. The fit resulted in an r^2 of 0.98 and parameter values of $N_m = 43.3$ and $a = 0.004$ (Nonlin-Systat v.7, SPSS Inc.). This model also was fit to data from 100 individual simulations under the nominal parameter settings to observe the distribution and variability of estimates of N_m (see Results).

Results

Observed rainbow smelt distributions

Rainbow smelt were present in 6 of 9 creeks and channels sampled between lakes (Table 1). Rainbow smelt were numerous in the channels between Fence Lake and Big Crawling Stone Lake and between Big Crawling Stone Lake and Long Interlaken Lake, where they were observed in spawning masses. Rainbow smelt were present in 6 of 14 lakes sampled (Table 2). The chronology of the rainbow smelt invasions in each lake was estimated from personal communications with Lac du Flambeau tribal fisheries biologists (L. Wawronowicz) and Wisconsin Department of Natural Resources fisheries biologists (H. Carlson) and through interviews with local fishers who had caught rainbow smelt (Table 3).

Simulated rainbow smelt invasions

The mean number of simulated invasions varied with changes in each model parameter. The largest variation in the number of invasions occurred due to changes in the human introduction rates (Fig. 2). Changes in the dispersal ability of rainbow smelt led to relatively smaller changes in the mean number of lakes invaded (Fig. 2). Changes in the extinction rate led to the smallest changes in the number of lakes invaded relative to either stream connections or human introductions (Fig. 2).

Model simulations in which human introductions and immigration parameters were changed concurrently led to the largest response in the number of lakes invaded (Fig. 3). The greatest number of lakes were invaded in simulations where human introduction rates and immigration parameters were increased, with the fewest invaded in simulations where human introduction rates and immigration parameters were concurrently decreased (Fig. 3). Changes in the human introduction rates affected the number of invaded lakes more dramatically than alterations of the connectivity parameters (Fig. 3). The importance of stream connections varied along the gradient of human introductions. At low levels of human introduction, stream invasions increased the number of lakes invaded. Increases in rainbow smelt migration ability at higher levels of human introduction rates had little additional effect (Fig. 3). Changing the level of human introductions was more important than changes in stream passability under several different levels of each parameter.

The rate of new invasions decreased over time, with the cumulative number of rainbow smelt lakes showing a curvilinear trend (Fig. 4). Under the nominal scenario, the model of invasions through time predicted that rainbow smelt would invade all of the habitable lakes after 1000 years

© 1999 NRC Canada

Fig. 3. Mean number of lakes invaded for 100 simulations over 100 years in response to (*a*) three levels of human introductions and (*b*) three levels of rainbow smelt migration ability showing the effect of concurrently varying each parameter. Hatched bars indicate results for a 20% reduction in human introduction rates and migration ability, solid bars indicate results for a nominal human introduction rate and migration ability, and open bars indicate results for a 20% increase in human introduction rates and migration ability.

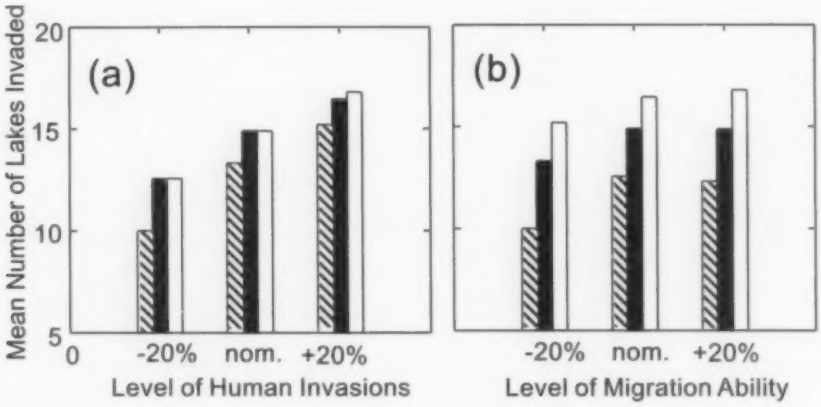

Fig. 4. Mean number of invasions for 100 simulations at 50-year intervals over 1100 years under the nominal parameter settings presented as a function of time. Error bars represent standard deviations of the mean. The curvilinear line represents a nonlinear model (see Methods) fit to output. The broken line indicates the number of habitable lakes within the watershed.

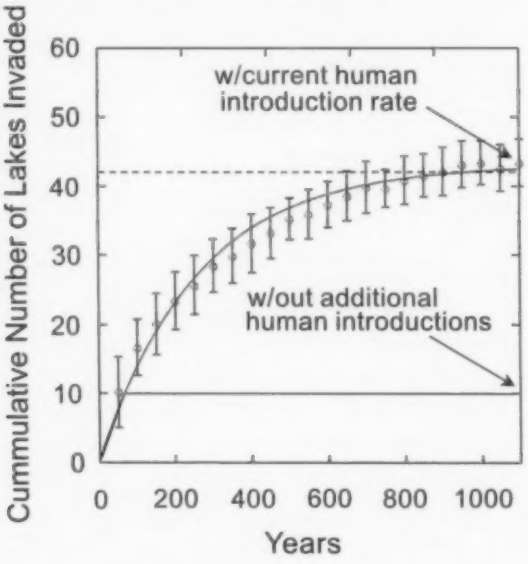

Fig. 5. Distribution of estimated asymptote values for 100 individual simulations run for 1100 years. The broken line indicates the total number of habitable lakes within the watershed.

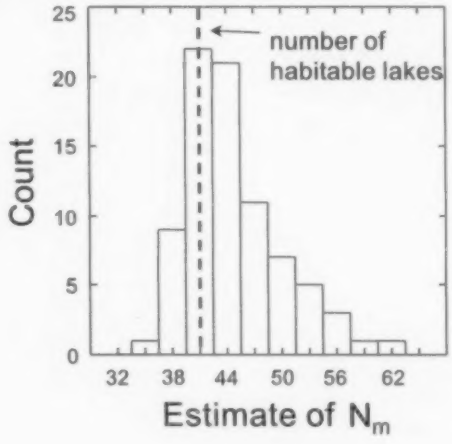

(Fig. 4). If no other human invasions had occurred within the model watershed after Fence Lake was invaded, less than 25% of the lakes would have been invaded by rainbow smelt over 1000 years (Fig. 4). The distribution of maximum number of lakes invaded (N_m) from 100 simulations under nominal parameter settings over 1100 years of invasion suggests that extinction may occur but that the lakes often are reinvaded via humans or streams after an extinction takes place (Fig. 5).

Discussion

Rainbow smelt dispersal across isolated lakes depends primarily on transport and introductions by humans. In the Bear River watershed, only one fourth of the habitable lakes contained rainbow smelt after 1000 years if dispersal was restricted to stream corridors. In contrast, with the present rates of human transport, half contained rainbow smelt after 200 years, three quarters after 300 years, and all after 1000 years. This suggests that lakes isolated from humans will be the only refuge for fishes negatively influenced by rainbow smelt and that they should be managed as such; little can be done once rainbow smelt are in a lake. Human transport creates new epicenters for rainbow smelt to reach new sets of lakes by stream corridors or further human transport and is the only way for rainbow smelt to be dispersed to

© 1999 NRC Canada

lakes without stream connections. Clearly, the first priority in the management of exotic rainbow smelt is to eliminate or reduce random dispersal by humans through education of humans about potential vectors.

Human behavior and rainbow smelt spawning habits may be the most important factors contributing to the regional spread of rainbow smelt. Rainbow smelt are caught recreationally each year in the tributaries of the Great Lakes (Becker 1983). They also are caught by the growing numbers of people fishing for them in streams and channels within the Bear River watershed and other watersheds (T.R. Hrabik, personal observation). Rainbow smelt caught during spawning runs are sexually mature adults that contain gametes that, when mixed, may lead to thousands of viable zygotes. After cleaning their catch, people often discard rainbow smelt viscera by tossing them into a nearby waterbody. Introductions from dumping, the use of ripe rainbow smelt as bait, intentional introductions, and accidental introductions all are enhanced by the gathering of the rainbow smelt in shallow tributaries and channels used as spawning habitat by adult rainbow smelt.

Increasing the maximum stream length and gradient through which rainbow smelt migrate during spawning runs did little to influence the simulated dispersal of rainbow smelt through the Bear River watershed, but decreasing each did reduce the average number of lakes invaded. Gradient and stream length may be important considerations in areas with higher topographic relief and longer streams between lakes. In our simulations, the change in number of lakes invaded caused by altering migratory ability was less than that caused by altering human introduction rates. This suggests that the dispersal of rainbow smelt through streams is highly efficient and happens quickly in lake districts where the gradient is slight and stream length between lakes is less than a few kilometres. In large river systems that experience much higher discharge and flooding, downstream dispersal may occur even more rapidly and efficiently over much greater distances (see Mayden et al. 1987; Franzin et al. 1994).

The lakes suitable for habitation by rainbow smelt may be invaded repeatedly over several hundred years through human introduction and from connected lakes. Increasing the rate of introductions by humans led to a proportionately smaller change in the number of new lakes invaded than a decrease in the rate, suggesting a saturation effect at high human introduction rates. Through time, the rate of invasions to new lakes or lakes that had experienced an extinction also decreased. However, based on model output, estimates of the total number of new lakes invaded often exceed the number of habitable lakes (Fig. 5), suggesting that the extinctions were occurring and that lakes were subsequently reinvaded. Given that little is known about the rate of extinctions in rainbow smelt populations, we used estimates that may have overestimated actual rates. Even so, the mode of the asymptote distribution (see Fig. 5) of the number of invaded lakes after 1000 years is roughly equal to the habitable lakes within the Bear River watershed. This suggests that at current rates of human introductions, lakes with suitable habitat that experience an extinction of rainbow smelt will likely be repeatedly reinvaded over longer time scales. In effect, even moderate rates of human introduction may lead to a relatively rapid "saturation" of watersheds. Saturation is likely to occur more quickly under a combination of high human introductions and efficient spread through stream connections and be maintained as long as human introduction rates continue unchecked.

In watersheds like the Bear River watershed, dispersal could be slowed if temporary physical barriers such as low head dams could be placed in areas likely to experience rainbow smelt swimming upstream during spring spawning migrations. At the risk of prohibiting migration of native species that spawn at the same time, these barriers could be maintained for the short duration of rainbow smelt spawning runs and subsequently removed, allowing subsequent runs of native fish to use the streams for spawning habitat. For example, a simple flume with a removable face capable of holding a head of water 3 ft high would likely stop the upstream movement of rainbow smelt in regions that do not experience floods. Downstream movement by larvae will be the most difficult aspect of rainbow smelt dispersal to control because larvae are small, eurythermal, and abundant. Downstream spread is likely responsible for the rapidity of rainbow smelt spread throughout the Missouri, Mississippi (Mayden et al. 1987), English (Campell et al. 1991; Franzin et al. 1994), and Nelson rivers (Remnant et al. 1997).

Assessment and prediction of the most important factors influencing the spread of exotic fishes will continue to be an important aspect of fisheries ecology and fisheries management. Most studies on exotic species focus on how the exotic influences the native biota or ecosystem dynamics. However, conservation and management strategies must focus on reducing the spread of harmful exotics. Observing how spatially explicit population models represent fish dispersal can be used as a method to systematically vary and weigh each parameter and examine the importance of potential factors governing the spread of an exotic species. This method is useful because equations and parameter settings can be altered to simulate dispersal of different species or the same species in very different types of lake districts, making the approach more generally applicable. This approach makes possible projections of potential distributions and the planning of management scenarios prior to likely invasions taking place. Knowing how dispersal of a harmful exotic is represented by a model may help set conservation priorities for vulnerable species in lakes less likely to be invaded and preserve species and populations that might otherwise be locally lost. Accurate prediction of likely invasions may allow unique populations to be conserved through management, a more productive activity than observing the negative effects of rainbow smelt on yet another lake.

References

Attig, J.W. 1985. Pleistocene geology of Vilas County, Wisconsin. Wis. Geol. Nat. Hist. Surv. Inf. Circ. 50.

Becker, G.C. 1983. Fishes of Wisconsin. University of Wisconsin Press, Madison, Wis.

Bowen, D.G. 1978. Quaternary geology — a stratigraphic framework for multidisciplinary work. Pergamon Press, New York.

Bruton, M.N. 1995. Have fishes had their chips? The dilemma of threatened fishes. Environ. Biol. Fishes, **43**: 1–27.

Campbell, K.B., Derkson, A.J., Remnant, R.A., and Stewart, K.W. 1991. First speciments of the rainbow smelt, *Osmerus mordax*

© 1999 NRC Canada

new record, from Lake Winnipeg, Manitoba. Can. Field Nat. **105**(4): 568–570.

Dunning, J.B., Jr., Stewart, D.J., Danielson, B.J., Noon, B.R., Root, R.L., Lamberson, R.H., and Stevens, E.E. 1995. Spatially explicit population models: current forms and uses. Ecol. Appl. **5**: 3–11.

Elton, C.S. 1958. The ecology of invasions by animals and plants. John Wiley & Sons, New York.

Evans, D.O., and Loftus, D.H. 1987. Colonization of inland lakes in the great lake region by rainbow smelt, *Osmerus mordax*: their freshwater niche and effects on indigenous fishes. Can. J. Fish. Aquat. Sci. **44**(Suppl. 2): 249–266.

Franzin, W.G., Barton, B.A., Remnant, R.A., Wain, D.B., and Pagel, S.J. 1994. Range extension, present and potential distribution, and possible effects of rainbow smelt in Hudson Bay drainage waters of Northwestern Ontario, Manitoba, and Minnesota. N. Am. J. Fish. Manage. **14**: 65–76.

Hrabik, T.R., Magnuson, J.J., and McLain, A.S. 1998. Predicting the effects of rainbow smelt on native fishes in small lakes: evidence from long-term research on two lakes. Can. J. Fish. Aquat. Sci. **55**: 1364–1371.

Jones, M.S., Goettl, J.P., and Flickinger, S.A. 1994. Changes in walleye food habits and growth following a rainbow smelt introduction. N. Am. J. Fish. Manage. **14**: 409–414.

Kaufman, L. 1992. Catastrophic change in species-rich freshwater ecosystems. BioScience, **42**: 846–858.

Linthurst, R.A., Landers, D.H., Eilers, J.M., Brakke, D.F., Overton, W.S., Meier, E.P., and Crowe, R.E. 1986. Characteristics of lakes in the eastern United States. Vol. 1. Population descriptions and physico-chemical relationships. U.S. Environ. Protect. Agency Publ. 600/4-86/007a.

Lodge, D.M. 1993*a*. Biological invasions: lessons for ecology. Trends Ecol. Evol. **8**: 133–136.

Lodge, D.M. 1993*b*. Species invasions and deletions: community effects and responses to climate and habitat change. *In* Biotic interactions and global change. *Edited by* P.M. Karieva, J.G. Kingslover, and R.B. Heuy. Sinauer Associates, Sunderland, Mass. pp. 376–387.

Loftus, D.H., and Hulsman, P.F. 1986. Predation on larval lake whitefish (*Coregonus clupeaformis*) and lake herring (*Coregonus artedii*) by adult rainbow smelt (*Osmerus mordax*). Can. J. Fish. Aquat. Sci. **43**: 812–818.

MacArther, R.H. 1972. Geographical ecology. Patterns in the distribution of species. Harper Row, New York.

Magnuson, J.J. 1976. Managing with exotics: a game of chance. Trans. Am. Fish. Soc. **105**: 1–9.

Magnuson, J.J., Tonn, W.M., Banerjee, A., Toivonen, J., Sanchez, O., and Rask, M. 1998. Isolation vs. extinction in the assembly of fishes in small northern lakes. Ecology, **79**: 2941–2956.

Mayden, R.L., Cross, F.B., and Gorman, O.T. 1987. Distributional history of the rainbow smelt, *Osmerus mordax* (Salmoniformes: Osmeridae), in the Mississippi River basin. Copeia, **1987**: 1051–1054.

Mooney, H.A., and Drake, J.A. (*Editors*). 1986. Ecology of biological invasions of North America and Hawaii. Springer-Verlag, New York.

Moyle, P.B. 1986. Fish introductions into North America: patterns and ecological impact. *In* Ecology of biological invasions of North America and Hawaii. *Edited by* H.A. Mooney and J.A. Drake. Springer-Verlag, New York.

Moyle, P.B., and Moyle, P.R. 1995. Endangered fishes and economics: intergenerational obligations. Environ. Biol. Fishes, **43**: 29–37.

Moyle, P.B., Li, H.W., and Barton, B.A. 1986. The Frankenstien effect: impact of introduced fishes on native fishes in North America. *In* Fish culture in fisheries management. American Fisheries Society, Bethesda, Md. pp. 415–426.

Naesje, T.F., Jonsson, F., Klyve, B.L., and Sandlund, O.T. 1987. Food and growth of age-0 smelts, *Osmerus eperlanus*, in a Norwegian fjord lake. J. Fish Biol. **30**: 119–126.

Nellbring, S. 1989. The ecology of smelts (genus *Osmerus*): a literature review. Nord. J. Freshwater Res. **65**: 116–145.

Remnant, R.A., Graveline, P.G., and Bretecher, R.L. 1997. Range extension of the rainbow smelt, *Osmerus mordax*, in the Hudson Bay drainage of Manitoba. Can. Field Nat. **111**(4): 660–662.

Rudstam, L.G., and Magnuson, J.J. 1985. Predicting the vertical distribution of fish populations: analysis of cisco, *Coregonus artedii*, and yellow perch, *Perca flavescens*. Can. J. Fish. Aquat. Sci. **42**: 1178–1198.

Skellum, J.G. 1951. Random dispersal in theoretical populations. Biometrika, **38**: 196–218.

Turner, M.G., Arthaud, G.H., Engstrom, R.T., Hejl, S.J., Liu, J., Loeb, S., and McKelvey, K. 1995. Usefulness of spatially explicit population models in land management. Ecol. Appl. **5**: 12–16.

© 1999 NRC Canada

Spatial patterns in relations among brown trout (*Salmo trutta*) distribution, summer air temperature, and stream size in Rocky Mountain streams

Frank J. Rahel and Nathan P. Nibbelink

Abstract: Stream size interacted with mean July air temperature to influence the distribution of brown trout (*Salmo trutta*) in southeastern Wyoming streams. The geographic range of brown trout was positively associated with mean July air temperatures of 19–22°C. Within this thermal zone, brown trout were more likely to occur in large streams (>4 m wetted width) than in small streams. We used a geographic information system to examine spatial patterns in the distribution of anomalous sites (i.e., sites predicted to have brown trout but which lacked this species). Sites that lacked brown trout but contained brook trout (*Salvelinus fontinalis*) tended to be on small streams at the cold margin of the 19–22°C thermal window. Sites lacking both brown trout and brook trout tended to be on small streams clustered in three of the six study drainages. The spatial aggregation of these sites suggests that additional regional factors influence the occurrence of brown trout in southeastern Wyoming. It is hypothesized that these factors could involve land-use practices interacting with basin geology and geomorphology. Classification models that incorporate a few general habitat factors are useful for identifying stream reaches with the potential to support brown trout and for directing management efforts to sites where this potential is not realized.

Résumé : La taille du cours d'eau a interagi avec la température moyenne de l'air en juillet pour influer sur la répartition de la truite brune (*Salmo trutta*) dans des cours d'eau du sud-est de l'État du Wyoming. L'aire de répartition géographique de cette espèce était corrélée positivement avec les températures moyennes de l'air en juillet, comprises entre 19 et 22°C. Dans cette zone thermique, la probabilité était plus grande de rencontrer cette espèce dans les grands cours d'eau (>4 m de largeur mouillée) que dans les petits cours d'eau. Nous avons utilisé un système d'information géographique pour examiner les profils spatiaux de la répartition de sites aberrants (c.à.d. des sites dans lesquels il devait y avoir de la truite brune mais qui n'en contenaient pas). Les sites sans truite brune mais qui renfermaient de l'omble de fontaine (*Salvelinus fontinalis*) tendaient à être de petits cours d'eau à la limite inférieure de la fenêtre thermique 19–22°C. Les sites sans truite brune ni omble de fontaine se trouvaient en général dans de petits cours d'eau regroupés dans trois des six bassins à l'étude. D'après l'agrégation spatiale de ces sites, d'autres facteurs régionaux influeraient sur la présence de la truite brune dans le sud-est du Wyoming. Ces facteurs pourraient être liés à des pratiques d'utilisation des sols qui agiraient sur les caractéristiques géologiques et géomorphologiques du bassin. Les modèles de classification qui intègrent quelques facteurs généraux concernant l'habitat sont utiles pour déterminer les tronçons de cours d'eau susceptibles d'héberger la truite brune et orienter les efforts de gestion sur les sites où ce potentiel n'est pas réalisé.

[Traduit par la Rédaction]

Introduction

Understanding fish–habitat relationships is a major focus of fishery management efforts in streams. Numerous models have been developed that relate fish abundance to reach-level habitat features such as the amount of woody debris, types of substrates present, and water velocity (Fausch et al. 1988; Hubert et al. 1996). With the development of landscape perspectives in stream fish ecology, there is renewed interest in how large-scale habitat features and land-use patterns influence the distribution and abundance of fish (Schlosser 1991; Rieman and McIntyre 1995; Maret et al. 1997). For example, Lanka et al. (1987) observed that geomorphic variables such as basin relief and drainage density were useful in predicting standing stock of trout at the reach level in Wyoming streams. The geomorphic variables appeared to determine local site characteristics such as stream width, gradient, and substrate composition that were important determinants of trout habitat.

One large-scale habitat feature long considered important in determining regional fish distribution patterns is temperature (Ferguson 1958; Huet 1959; MacCrimmon and Campbell 1969; Keleher and Rahel 1996). Because fish are ectothermic, temperature mediates all physiological processes and strongly influences the geographic range that a

Received January 7, 1998. Accepted March 17, 1999.
J14380

F.J. Rahel[1] and N.P. Nibbelink. Department of Zoology and Physiology, University of Wyoming, Laramie, WY 82071, U.S.A.

[1]Author to whom all correspondence should be addressed.
e-mail: frahel@uwyo.edu

© 1999 NRC Canada

Fig. 1. Map of the study region in southeastern Wyoming indicating the six study drainages that flow into the North Platte River. Study drainages were the North Laramie River, Laramie River, Sybille Creek, Chugwater Creek, Bear Creek, and Horse Creek.

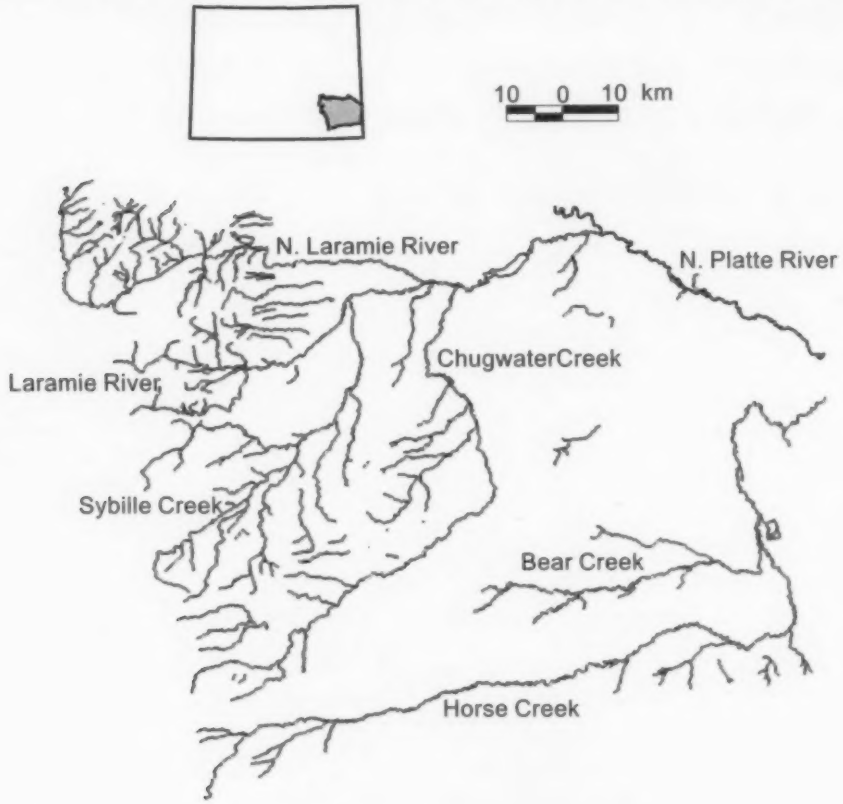

species can inhabit. The distributions of many warmwater fishes in North America appear to be determined by overwinter starvation of young fish. This is evidenced by the fact that species distributions tend to follow mean annual air temperature isotherms rather than landform or watershed boundaries (Shuter and Post 1990). The distribution of cold-water fishes often reflects their inability to survive high summer water temperatures (Meisner 1990; Eaton et al. 1995; Taniguchi et al. 1998). Again, regional distributions often are correlated with air temperature isotherms. For example, MacCrimmon and Campbell (1969) reported that the native range of brook trout (*Salvelinus fontinalis*) in North America is delimited to the south by a mean July air temperature of 21°C. Rieman and McIntyre (1995) observed that the lower elevation limit for bull trout (*Salvelinus confluentus*) in the Boise River basin in Idaho corresponded to a mean annual air temperature of 5°C.

Stream size also can be an important factor determining the distribution of stream fishes. Larger streams typically have more fish species than smaller streams, and this has been attributed to an increase in living space and habitat complexity as stream size increases (Schlosser 1987; Rahel and Hubert 1991). Also, larger streams are more likely to have deep pools that provide refuges during periods of thermal stress or dewatering in summer (Fausch and Bramblett 1991; Matthews et al. 1994) or freeze-up during winter (Cunjak 1996).

In this study, we examined the distribution of brown trout (*Salmo trutta*) in relation to mean July air temperature and stream size in a set of adjacent drainages in the Rocky Mountains of Wyoming. We focused on these factors because of the extensive literature indicating their importance to the distribution of cold-water fishes in the Rocky Mountain region (Vincent and Miller 1969; Lanka et al. 1987; Fausch 1989; Hubert and Kozel 1993). We also used a geographic information system (GIS) to explore spatial patterns in anomalies of brown trout distribution (i.e., the absence of brown trout in areas considered thermally suitable). Spatial distribution of these anomalies could give insights into the relative importance of local versus regional factors in determining fish presence–absence. For example, clustering of anomalous sites would suggest that one or more regional features overlooked in the initial analysis may be controlling fish distributions. By contrast, random distribution of anomalous sites throughout the drainage would suggest that localized, site-specific factors play a major role in determining fish distributions. Such factors could include land-use practices such as livestock grazing that strongly influence fish habitat quality at the local scale (Wesche et al. 1987; Platts 1991).

© 1999 NRC Canada

Fig. 2. Brown trout abundance in relation to predicted mean July air temperature at 182 sites within the study region.

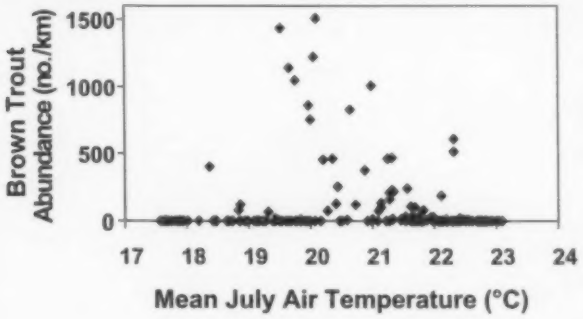

Methods

Study area and data sources

The study area consisted of six contiguous drainages that flow into the North Platte River in southeastern Wyoming (Fig. 1). Brown trout have established naturalized populations throughout the study area and are not stocked in the study streams. The other major trout species present consisted of naturalized populations of brook trout that were limited to headwater reaches in some of the study streams.

Information on fish populations, elevation, and stream width for 182 sites was obtained from a database maintained by the Wyoming Game and Fish Department. Fish populations had been sampled by electrofishing. Because many sites had been sampled using only one-pass electrofishing, we could not calculate population estimates for the stream reaches. Instead, we used the number of brown trout caught during the first pass with electrofishing gear as an index of abundance. Four sites on the Laramie River downstream of Grayrocks Reservoir had been stocked with adult brown trout (Patton 1991), and brown trout were eliminated from the fish survey data at those sites. In a few streams, stocked rainbow trout (*Oncorhynchus mykiss*) were present in low numbers, but we did not include this species in our analyses because it had not established naturalized populations in the study streams.

Brown trout occurrence in relation to air temperature, stream size, and brook trout presence

To examine the influence of thermal limits on brown trout distribution, we developed a regression equation relating mean July air temperature to elevation in southeastern Wyoming. Temperature data encompassed the period 1961–1990 and came from 27 weather stations ranging in elevation from 1186 to 2481 m above mean sea level. We calculated mean July air temperature at each of the 182 fish sampling sites using the regression equation and site elevation. We then plotted brown trout abundance in relation to mean July air temperature to identify the thermal window where brown trout were likely to occur in southeastern Wyoming.

The influence of stream size and brook trout presence on the distribution of brown trout was examined by noting the presence–absence of both species in a plot of stream size versus mean July air temperature for the 182 study sites. As a measure of stream size, we used wetted stream width measured at the time of fish population sampling. Because fish populations generally were sampled during July–October, wetted stream width was a measure of stream size during baseflow conditions. We also plotted brown trout abundance directly against brook trout abundance at the 182 study sites.

GIS analyses

We used a GIS running ARC/INFO and ARCVIEW software (Environmental Systems Research Institute, Inc. 1995) to examine brown trout presence–absence in relation to mean July air temperature across the study region. We created a coverage of mean July air temperature using a digital elevation map (DEM) available from the U.S. Geological Survey. Resolution of the DEM was 90 × 90 m. The DEM was converted to a grid in ARC/INFO where each grid cell has an elevation value corresponding to its location. The elevation grid was converted to a grid of mean July air temperature using the regression equation. This temperature grid was converted to a contour coverage in which contours represented isopleths of predicted mean July air temperature in the same manner that contours on a topographic map represent elevation.

The coverage of mean July air temperature was combined with a coverage of hydrologic features of the study drainages derived from 1 : 100 000 scale topographic maps of the U.S. Geological Survey. This resulted in a map showing the stream drainages in relation to thermal zones based on mean July air temperature. Plotting the 182 fish sampling sites on this map allowed us to look for spatial patterns in the presence versus absence of brown trout throughout the study region.

Spatial patterns in the distribution of anomalous sites

Anomalous sites were defined as sites that contained no brown trout even though they were located within the moderate thermal zone where mean July air temperatures were considered suitable for brown trout. We used a χ^2 statistic to test the hypothesis that anomalous sites were distributed randomly across the landscape with respect to the six drainage basins in the study area. A two-way contingency table was developed with one category being drainage basin and the other category being the presence or absence of brown trout. The expected number of anomalous sites within a drainage was computed by multiplying the total number of fish sampling sites in that drainage by the proportion of anomalous sites across all drainages.

Spatial patterns were examined for three groups of anomalous sites. The first group consisted of sites within the moderate thermal zone on large streams (width >4 m). The second group consisted of sites within the moderate thermal zone on small streams (width ≤4 m) that lacked brown trout but contained brook trout. The third group consisted of sites within the moderate thermal zone on small streams that lacked both brown trout and brook trout. We choose a width of 4 m to delineate small versus large streams because brook trout were absent in streams >4 m wide.

Results

Brown trout occurrence in relation to air temperature and stream size

Mean July air temperature in southeastern Wyoming was related to elevation as follows ($r^2 = 0.877$, $P < 0.001$):

$$\text{JulyC} = 29.343 - 0.00502(\text{elevation})$$

where JulyC is mean July air temperature (degrees Celsius) and elevation is given as metres above mean sea level. This regression equation was used to calculate mean July air temperature for 182 sites where fish populations had been sampled. The relationship between brown trout abundance and summer air temperature indicated upper and lower thermal limits associated with the distribution of brown trout in the six drainages (Fig. 2). Brown trout generally were not present where mean July air temperatures were predicted to be <19°C or >22°C. Within the range of 19–22°C, brown trout

© 1999 NRC Canada

Fig. 3. Map of the study area showing the location of the 182 sampling sites across the six drainage basins. Streamflow generally is from left to right. The shaded area indicates the moderate thermal zone where mean July air temperature is predicted to be 19–22°C. Solid circles indicate sites where brown trout were present. Open circles indicate sites where brown trout were absent.

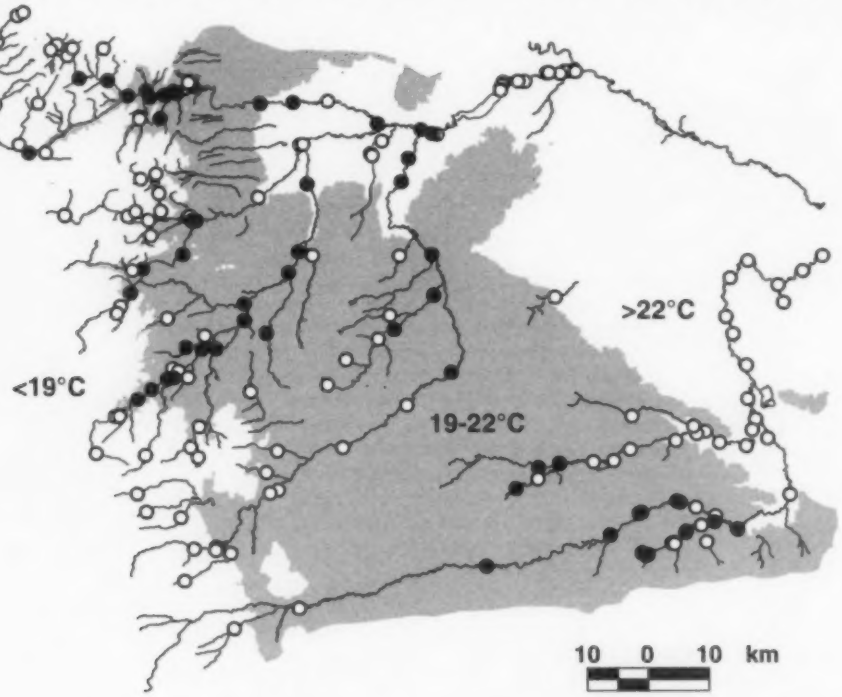

Fig. 4. Abundance of brown trout and brook trout at the 182 study sites.

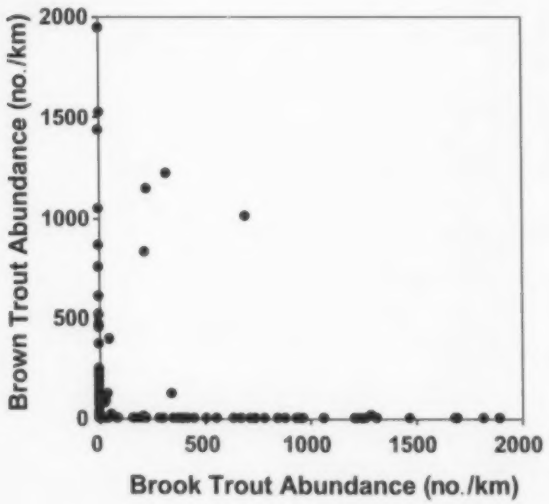

were present at 50 of 98 sites and sometimes achieved a high abundance.

We examined the distribution of brown trout in relation to three thermal zones based on mean July air temperature: a "cool thermal zone" with temperatures <19°C, a "moderate thermal zone" with temperatures between 19 and 22°C, and a "warm thermal zone" with temperatures >22°C. Within the cool thermal zone, brown trout were present at three of 36 sites (Fig. 3). All three sites were located in the North Laramie River drainage near the transition between the cool and moderate thermal zones. Within the moderate thermal zone, brown trout were present at 50 of 98 sites distributed throughout the study region. Within the warm thermal zone, brown trout were present at eight of 48 sites clustered in the northern portion of the region (Laramie River and its tributaries).

There was a strong, negative relationship between the abundance of brown trout and brook trout (Fig. 4). To explore how the distribution of these two species was related to stream size and thermal zone, we plotted the presence–absence of both species in relation to these two factors. Brook trout generally were restricted to small streams (≤4 m wide) at cool temperatures whereas brown trout were less likely to be present in small streams (Fig. 5). Based on the patterns in Figs. 2 and 5, we classified the 182 sampling sites into three thermal zones (cool, moderate, and warm) and two size categories (≤4 and >4 m). The probability of brown trout occurrence was high in large streams within the moderate thermal zone, intermediate in small streams within the moderate thermal zone or large streams in the warm thermal zone, and low in the other categories (Fig. 6).

Spatial patterns in the distribution of anomalous sites

To examine spatial patterns among the sites lacking brown trout, we used the GIS to divide the moderate thermal zone

© 1999 NRC Canada

Fig. 5. Occurrence of brown trout and brook trout in relation to stream width and mean July air temperature across the study area.

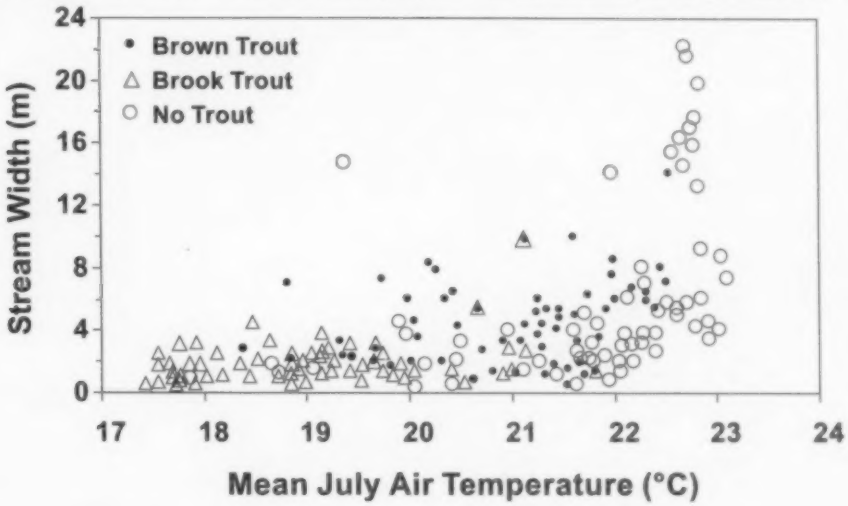

Fig. 6. Percent occurrence of brown trout and brook trout at sampling sites in relation to stream width and mean July air temperature. Thermal categories are cool (<19°C), moderate (19–22°C), and warm (>22°C). Stream width categories are large (>4 m wetted width) and small (≤ 4 m wetted width).

Stream Size \ Thermal Category	Cool	Moderate	Warm
Large	Insufficient Data n = 2	Brown = 74.1% Brook = 0% Both = 7.4% Neither = 18.5% n = 27	Brown = 23.5% Brook = 0% Both = 0% Neither = 76.5% n = 34
Small	Brown = 0% Brook = 85.3% Both = 5.9% Neither = 8.8% n = 34	Brown = 26.8% Brook = 28.2% Both = 12.7% Neither = 32.4 % n = 71	Brown = 0% Brook = 0% Both = 0% Neither = 100% n = 14

into 1°C intervals of predicted mean July air temperature. For large streams within the moderate thermal zone, there was no obvious pattern of spatial aggregation among the five sites that lacked brown trout (Fig. 7). For small streams within the moderate thermal zone, two patterns were observed. In the first pattern, the 20 sites that contained brook trout were clustered near the 19°C margin of the moderate thermal zone (Fig. 8). The distribution of these 20 sites across the drainages was nonrandom, mainly because there were no sites in the Bear Creek or Horse Creek drainages (Table 1). In the second pattern, 23 sites lacking both brown trout and brook trout were not randomly distributed across the study area but were clustered in the Chugwater Creek, Bear Creek, and Horse Creek drainages (Fig. 9; Table 1).

Discussion

Our results indicate that a few general habitat factors can provide significant insights into the regional distribution of brown trout. We focused on temperature and stream size as critical habitat factors because of the extensive literature indicating the importance of these factors in determining trout biomass in streams (Lanka et al. 1987; Fausch 1989; Kozel and Hubert 1989; Meisner 1990; Rahel et al. 1996). Other large-scale habitat factors also can play a critical role in determining fish distribution patterns. For example, biomass of brown trout in streams differed among land-type associations in the Black Hills National Forest of South Dakota and Wyoming (Modde et al. 1991). Differences in brown trout biomass primarily reflected differences in the proportion of pool habitat in streams from different land-type associations. Patch size influenced the probability of bull trout occurrence in watersheds of the Boise River basin in Idaho, with bull trout less likely to be present in small patches compared with large patches (Rieman and McIntyre 1995). The distribution of Yellowstone cutthroat trout (*Oncorhynchus clarki bouvieri*) was negatively related to stream gradient in the Greybull–Wood River drainage in Wyoming, and extremely high gradients functioned as migration barriers that prevented the occurrence of cutthroat trout in upstream reaches (Kruse et al. 1997).

In our study, the geographic distribution of brown trout was largely bounded by the 19 and 22°C isotherms of mean July air temperature (Fig. 3). The upper thermal limit probably reflects physiological limitations, as the upper critical temperature maximum for brown trout is near 26°C (Eaton et al. 1995). The upper thermal limit for the distribution of brown trout also may be affected by competition with warmwater fishes such as creek chub (*Semotilus atromaculatus*). In a laboratory stream tank, Taniguchi et al. (1998) noted that brown trout dominated creek chub through interference competition for foraging sites over the range of 3–22°C, but creek chub began to have competitive success over the range of 24–26°C. Thus, there may be a narrow thermal window just below lethal conditions where brown trout may be physiologically stressed and unable to compete with warmwater fishes.

Lower thermal limits to the distribution of brown trout in the study drainages probably reflect the combined effects of

© 1999 NRC Canada

Table 1. Analyses of spatial aggregation in the occurrence of anomalous sites involving the distribution of trout: (A) distribution of 20 anomalous stream sites that were within the moderate thermal zone (19–22°C) and ≤4 m wide and lacked brown trout but contained brook trout and (B) distribution of 23 anomalous sites that were within the moderate thermal zone (19–22°C) and <4 m wide and lacked both brown trout or brook trout.

	Distribution A		Distribution B	
Drainage	No. of sites	No. of anamolous sites	No. of sites	No. of anamolous sites
North Laramie River	5	2	5	0
Laramie River	8	5	8	0
Sybille Creek	21	8	21	4
Chugwater Creek	14	5	14	7
Bear Creek	8	0	8	6
Horse Creek	15	0	15	6
χ^2_3		15.44		16.95
P		<0.01		<0.01

Note: A χ^2 statistic was used to test the null hypothesis that anomalous sites were randomly distributed across drainages.

Fig. 7. Map of the study area showing the moderate thermal zone divided into three regions representing mean July air temperatures of 19–19.9, 20–20.9, and 21–21.9°C. Circles represent sampling locations where stream width was >4.0 m and neither brown trout nor brook trout were present (n = 5).

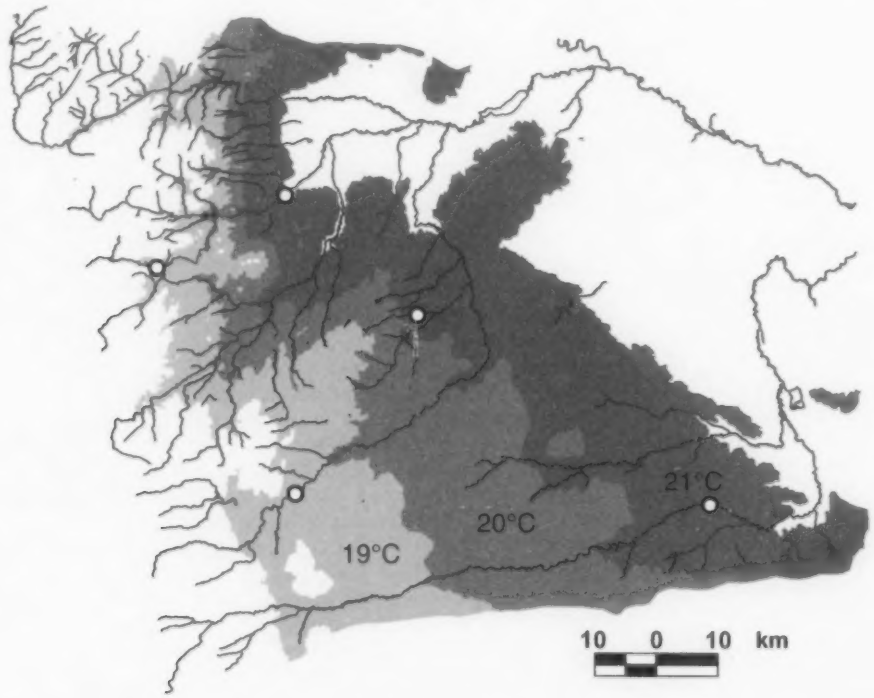

temperature, stream size, and competition with brook trout. Temperature alone is not likely to restrict brown trout to regions where mean July air temperature is ≥19°C as Fausch (1989) found little evidence of an upper elevational limit for brown trout in western North America. Also, in their native range in Europe, brown trout populations occur north of the Arctic Circle where mean July air temperatures are 10–15°C (MacCrimmon and Marshall 1968).

Our results point to an interaction between temperature and stream size in determining the upper elevational limit for brown trout, as they were more likely to be present in large streams than in small streams within the moderate thermal zone (Fig. 6). Small streams near the 19°C isotherm often were dominated by brook trout (Fig. 8). Brook trout often occur upstream of the upper elevational limit of brown trout in Rocky Mountain streams (Vincent and Miller 1969; Fausch 1989), but whether they play a role in excluding brown trout is unclear. At low elevations with moderate water temperatures, brown trout are behaviorally dominant over brook trout (Fausch and White 1981; Waters 1983). It

© 1999 NRC Canada

Fig. 8. Map of the study area showing the moderate thermal zone divided into three regions representing mean July air temperatures of 19–19.9, 20–20.9, and 21–21.9°C. Triangles represent sampling locations where stream width was ≤4 m and brown trout were absent but brook trout were present (n = 20).

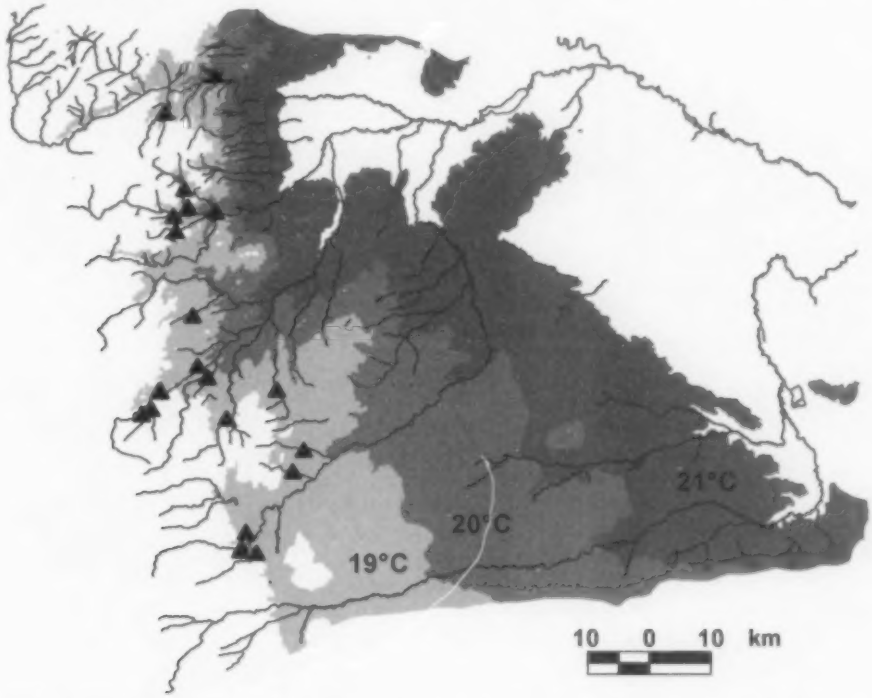

has been speculated that at high elevations with cold water temperatures, the competitive balance may shift in favor of brook trout (Fausch 1989). However, when this hypothesis was tested in a laboratory stream tank, brown trout did not become subordinate to brook trout at temperatures as cold as 3°C (Taniguchi et al. 1998). Cold temperatures may favor brook trout from a bioenergetics perspective, or small stream size may favor a species such as brook trout that matures at a small body size and thus can reproduce in shallow systems with limited spawning habitat. These hypotheses remain to be examined before we can understand how temperature, stream size, and brook trout interact in determining the geographic distribution of brown trout.

In our analysis, the highest probability of brown trout occurrence was at sites with mean July air temperature of 19–22°C and stream width >4 m. It is interesting to note, however, that five of the 27 stream reaches in this category lacked trout. This suggests that, although stream size and summer air temperature must be within a suitable range to support a brown trout population, these habitat conditions are not, by themselves, sufficient to guarantee a viable trout population. The absence or rarity of trout at sites where width and temperature appear suitable indicates that additional factors are influencing trout populations.

Examining spatial patterns in the distribution of anomalous sites provides insight into the role of local versus regional factors in determining why brown trout may be absent from a site. For example, we found no spatial aggregation among the five sites that lacked brown trout despite being in the moderate thermal zone and having a stream width >4 m (Fig. 7; Table 1). This suggests that local factors such as intensive livestock grazing or irrigation withdrawal are likely reasons for the absence of brown trout.

We hypothesize that degradation of streambanks due to livestock grazing may be a major reason why brown trout are absent from sites with suitable widths and thermal conditions. Undercut banks and overhanging vegetation are important components of habitat for brown trout in Rocky Mountain streams (Wesche et al. 1987; Hubert et al. 1996). Livestock grazing in the riparian zone eliminates these habitat features and thus reduces the abundance of trout (Platts 1991). In Arizona, Clarkson and Wilson (1995) reported that standing stocks of trout in streams with low gradients and suitable thermal conditions were more than twice as high in ungrazed reaches compared with grazed reaches.

Quantitative data on riparian condition were not collected during the fish surveys in the drainages that we examined. However, field notes by management agency personnel indicated that siltation and degraded streambanks often were associated with livestock grazing in the riparian zone (Snigg 1993; Meyer 1994). Because livestock grazing is a major land use in the study drainages, a quantitative examination of relationships among livestock grazing, riparian condition, and brown trout abundance would be a logical next step in determining why some stream reaches lacked brown trout despite favorable width and summer temperatures.

By contrast, two spatial patterns were evident among the sites that lacked brown trout despite being within the moder-

© 1999 NRC Canada

Table 1. Analyses of spatial aggregation in the occurrence of anomalous sites involving the distribution of trout: (A) distribution of 20 anomalous stream sites that were within the moderate thermal zone (19–22°C) and ≤4 m wide and lacked brown trout but contained brook trout and (B) distribution of 23 anomalous sites that were within the moderate thermal zone (19–22°C) and <4 m wide and lacked both brown trout or brook trout.

	Distribution A		Distribution B	
Drainage	No. of sites	No. of anamolous sites	No. of sites	No. of anamolous sites
North Laramie River	5	2	5	0
Laramie River	8	5	8	0
Sybille Creek	21	8	21	4
Chugwater Creek	14	5	14	7
Bear Creek	8	0	8	6
Horse Creek	15	0	15	6
χ^2_3		15.44		16.95
P		<0.01		<0.01

Note: A χ^2 statistic was used to test the null hypothesis that anomalous sites were randomly distributed across drainages.

Fig. 7. Map of the study area showing the moderate thermal zone divided into three regions representing mean July air temperatures of 19–19.9, 20–20.9, and 21–21.9°C. Circles represent sampling locations where stream width was >4.0 m and neither brown trout nor brook trout were present (n = 5).

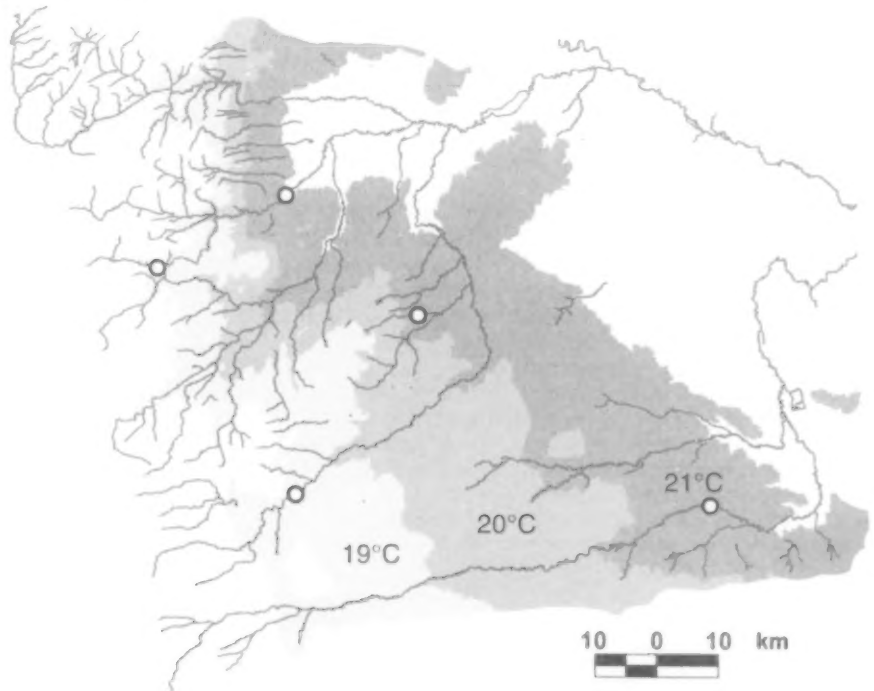

temperature, stream size, and competition with brook trout. Temperature alone is not likely to restrict brown trout to regions where mean July air temperature is ≥19°C as Fausch (1989) found little evidence of an upper elevational limit for brown trout in western North America. Also, in their native range in Europe, brown trout populations occur north of the Arctic Circle where mean July air temperatures are 10–15°C (MacCrimmon and Marshall 1968).

Our results point to an interaction between temperature and stream size in determining the upper elevational limit for brown trout, as they were more likely to be present in large streams than in small streams within the moderate thermal zone (Fig. 6). Small streams near the 19°C isotherm often were dominated by brook trout (Fig. 8). Brook trout often occur upstream of the upper elevational limit of brown trout in Rocky Mountain streams (Vincent and Miller 1969; Fausch 1989), but whether they play a role in excluding brown trout is unclear. At low elevations with moderate water temperatures, brown trout are behaviorally dominant over brook trout (Fausch and White 1981; Waters 1983). It

© 1999 NRC Canada

Fig. 8. Map of the study area showing the moderate thermal zone divided into three regions representing mean July air temperatures of 19–19.9, 20–20.9, and 21–21.9°C. Triangles represent sampling locations where stream width was ≤4 m and brown trout were absent but brook trout were present (n = 20).

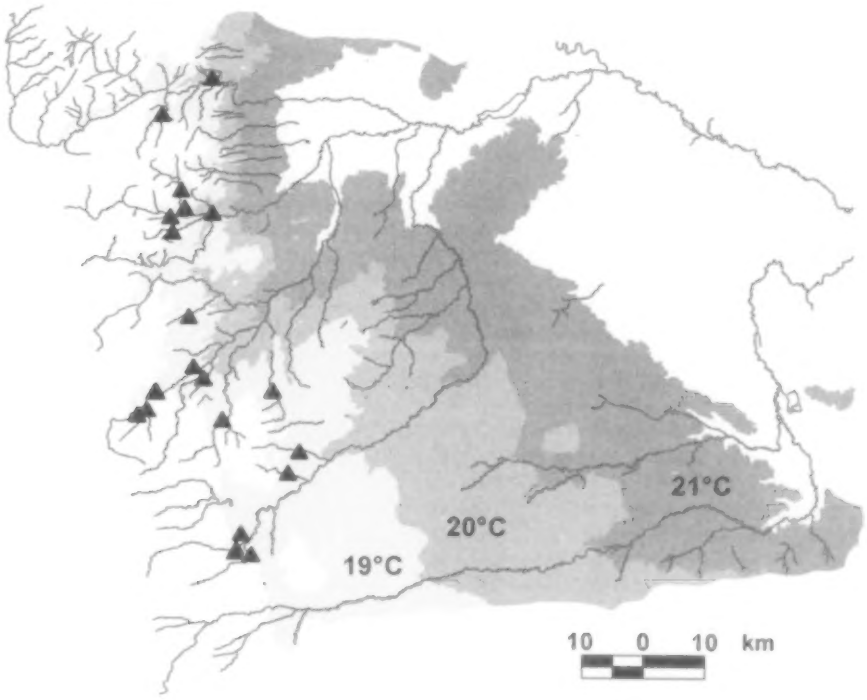

has been speculated that at high elevations with cold water temperatures, the competitive balance may shift in favor of brook trout (Fausch 1989). However, when this hypothesis was tested in a laboratory stream tank, brown trout did not become subordinate to brook trout at temperatures as cold as 3°C (Taniguchi et al. 1998). Cold temperatures may favor brook trout from a bioenergetics perspective, or small stream size may favor a species such as brook trout that matures at a small body size and thus can reproduce in shallow systems with limited spawning habitat. These hypotheses remain to be examined before we can understand how temperature, stream size, and brook trout interact in determining the geographic distribution of brown trout.

In our analysis, the highest probability of brown trout occurrence was at sites with mean July air temperature of 19–22°C and stream width >4 m. It is interesting to note, however, that five of the 27 stream reaches in this category lacked trout. This suggests that, although stream size and summer air temperature must be within a suitable range to support a brown trout population, these habitat conditions are not, by themselves, sufficient to guarantee a viable trout population. The absence or rarity of trout at sites where width and temperature appear suitable indicates that additional factors are influencing trout populations.

Examining spatial patterns in the distribution of anomalous sites provides insight into the role of local versus regional factors in determining why brown trout may be absent from a site. For example, we found no spatial aggregation among the five sites that lacked brown trout despite being in the moderate thermal zone and having a stream width >4 m (Fig. 7; Table 1). This suggests that local factors such as intensive livestock grazing or irrigation withdrawal are likely reasons for the absence of brown trout.

We hypothesize that degradation of streambanks due to livestock grazing may be a major reason why brown trout are absent from sites with suitable widths and thermal conditions. Undercut banks and overhanging vegetation are important components of habitat for brown trout in Rocky Mountain streams (Wesche et al. 1987; Hubert et al. 1996). Livestock grazing in the riparian zone eliminates these habitat features and thus reduces the abundance of trout (Platts 1991). In Arizona, Clarkson and Wilson (1995) reported that standing stocks of trout in streams with low gradients and suitable thermal conditions were more than twice as high in ungrazed reaches compared with grazed reaches.

Quantitative data on riparian condition were not collected during the fish surveys in the drainages that we examined. However, field notes by management agency personnel indicated that siltation and degraded streambanks often were associated with livestock grazing in the riparian zone (Snigg 1993; Meyer 1994). Because livestock grazing is a major land use in the study drainages, a quantitative examination of relationships among livestock grazing, riparian condition, and brown trout abundance would be a logical next step in determining why some stream reaches lacked brown trout despite favorable width and summer temperatures.

By contrast, two spatial patterns were evident among the sites that lacked brown trout despite being within the moder-

© 1999 NRC Canada

Fig. 9. Map of the study area showing the moderate thermal zone divided into three regions representing mean July air temperatures of 19–19.9, 20–20.9, and 21–21.9°C. Circles represent sampling locations where stream width was ≤4 m and neither brown trout nor brook trout were present (n = 23).

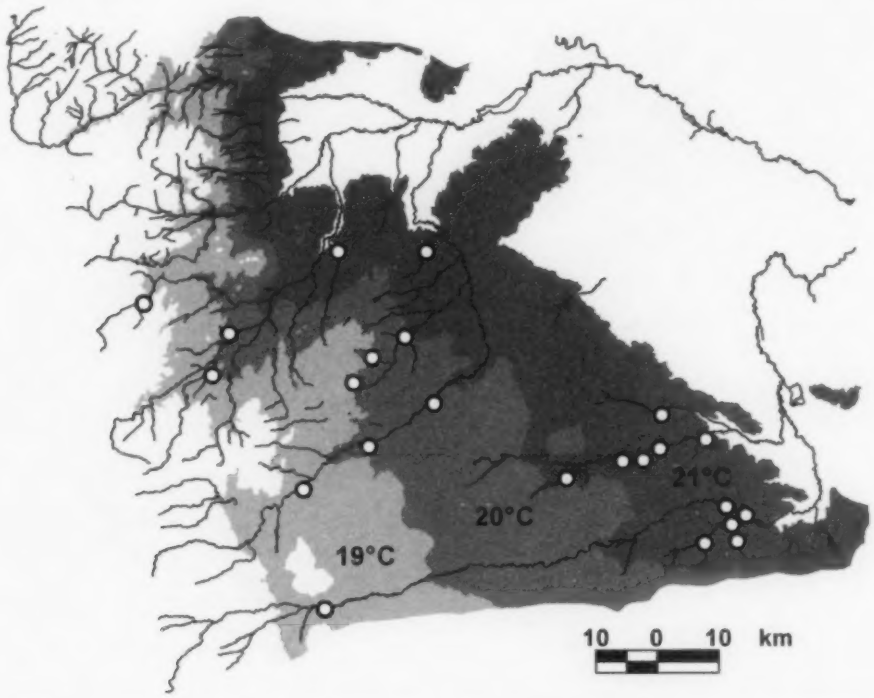

ate thermal zone and having a stream width ≤4m. First, the 20 sites that contained brook trout were on small streams near the 19°C isotherm (Fig. 8). As discussed above, this suggests some interaction among stream size, thermal conditions, and the presence of brook trout in determining the cold thermal limit to the distribution of brown trout. Second, streams lacking both brown trout and brook trout were not randomly distributed across the study area but were clustered in three drainages (Fig. 9). This pattern suggests some regional influences that are more important in these drainages compared with the other study drainages. We do not know what these regional influences are, but possibilities include widespread livestock grazing and irrigation withdrawal, perhaps interacting with drainage basin geomorphology. Nelson et al. (1992) found that interaction of land use with basin geology determined the distribution of trout in northeastern Nevada. In particular, cattle grazing appeared less detrimental to fish populations in a sedimentary district (where weathering produced riparian soils dominated by gravel) compared with a detrital district (where weathering produced riparian soils dominated by silts that eroded into the stream with cattle trampling). Examining the influence of land-use practices on fish habitat in relation to basin geomorphology and geology would be a useful area for future research efforts.

In summary, large-scale habitat features provide a useful means of identifying stream reaches likely to contain populations of brown trout in southeastern Wyoming and for directing management efforts to stream reaches far below their potential standing stock of trout. Such stream reaches offer the greatest opportunity for increasing trout abundance through reach-level habitat improvement (Hubert et al. 1996). Fish–habitat models can be enhanced by considering spatial patterns in the distribution of anomalous sites, i.e., sites that differ from model predictions of species occurrence. A GIS can provide a powerful method for displaying spatial patterns in the location of anomalous sites and exploring the extent to which anomalies are due to local versus regional factors.

Acknowledgements

Christopher Keleher and Jeffry Anderson helped create coverages used in the GIS analyses. Curt Meyer, Dirk Miller, and Ronald Remmick facilitated access to data of the Wyoming Game and Fish Department. Wayne Hubert, Douglas Novinger, and two anonymous reviewers provided helpful comments on the manuscript. Funding was provided by grants from the U.S. Department of Agriculture and the Wyoming Game and Fish Department to F.J. Rahel.

References

Clarkson, R.W., and Wilson, J.R. 1995. Trout biomass and stream habitat relationships in the White Mountains area, east-central Arizona. Trans. Am. Fish. Soc. **124**: 599–612.

Cunjak, R.A. 1996. Winter habitat of selected stream fishes and potential impacts from land-use activity. Can. J. Fish. Aquat. Sci. **53**(Suppl 1): 267–282.

Eaton, J.G., McCormick, J.H., Goodno, B.E., O'Brien, D.G., Stefany, H.G., Hondzo, M., and Scheller, R.M. 1995. A field information-

© 1999 NRC Canada

based system for estimating fish temperature tolerances. Fisheries (Bethesda), **20**(4): 10–18.

Environmental Systems Research Institute, Inc. 1995. Understanding GIS: the ARC/INFO method. Environmental Systems Research Institute, Inc., Redlands, Calif.

Fausch, K.D. 1989. Do gradient and temperature affect distributions of, and interactions between, brook charr (*Salvelinus fontinalis*) and other resident salmonids in streams? Physiol. Ecol. Jpn. **1**(Spec. Vol.): 303–322.

Fausch, K.D., and Bramblett, R.G. 1991. Disturbance and fish communities in intermittent tributaries of a western Great Plains river. Copeia, **1991**: 659–674.

Fausch, K.D., and White, R.J. 1981. Competition between brook trout (*Salvelinus fontinalis*) and brown trout (*Salmo trutta*) for positions in a Michigan stream. Can. J. Fish. Aquat. Sci. **38**: 1220–1227.

Fausch, K.D., Hawkes, C.L., and Parsons, M.G. 1988. Models that predict standing crop of stream fish from habitat variables: 1950–85. U.S. For. Serv. Gen. Tech. Rep. PNW-213.

Ferguson, R.G. 1958. The preferred temperature of fish and their midsummer distribution in temperate lakes and streams. J. Fish. Res. Board Can. **15**: 607–624.

Hubert, W.A., and Kozel, S.J. 1993. Quantitative relations of physical habitat features to channel slope and discharge in unaltered mountain streams. J. Freshwater Ecol. **8**: 177–184.

Hubert, W.A., Marwitz, T.D., Gerow, K.G., Binns, N.A., and Wiley, R.W. 1996. Estimation of potential maximum biomass of trout in Wyoming streams to assist management decisions. N. Am. J. Fish. Manage. **16**: 821–829.

Huet, M. 1959. Profiles and biology of Western European streams as related to fish management. Trans. Am. Fish. Soc. **88**: 155–163.

Keleher, C.J., and Rahel, F.J. 1996. Thermal limits to salmonid distributions in the Rocky Mountain region and potential habitat loss due to global warming: a geographic information system (GIS) approach. Trans. Am. Fish. Soc. **125**: 1–13.

Kozel, S.J., and Hubert, W.A. 1989. Factors influencing the abundance of brook trout (*Salvelinus fontinalis*) in forested mountain streams. J. Freshwater Ecol. **5**: 113–122.

Kruse, C.G., Hubert, W.A., and Rahel, F.J. 1997. Geomorphic influences on the distribution of Yellowstone cutthroat trout in the Absaroka Mountains, Wyoming. Trans. Am. Fish. Soc. **126**: 418–427.

Lanka, R.P., Hubert, W.A., and Wesche, T.A. 1987. Relations of geomorphology to stream habitat and trout standing stocks in small Rocky Mountain streams. Trans. Am. Fish. Soc. **116**: 21–28.

MacCrimmon, H.R., and Campbell, J.S. 1969. World distribution of brook trout, *Salvelinus fontinalis*. J. Fish. Res. Board Can. **26**: 1699–1725.

MacCrimmon, H.R., and Marshall, T.L. 1968. World distribution of brown trout, *Salmo trutta*. J. Fish. Res. Board Can. **25**: 2527–2548.

Maret, T.R., Robinson, C.T., and Minshall, G.W. 1997. Fish assemblages and environmental correlates in least-disturbed streams of the Upper Snake River basin. Trans. Am. Fish. Soc. **126**: 200–216.

Matthews, K.R., Berg, N.H., Azuma, D.L., and Lambert, T.R. 1994. Cool water formation and trout habitat use in a deep pool in the Sierra Nevada, California. Trans. Am. Fish. Soc. **123**: 549–564.

Meisner, J.D. 1990. Potential loss of thermal habitat for brook trout, due to climate warming, in two southern Ontario streams. Trans. Am. Fish. Soc. **119**: 282–291.

Meyer, C. 1994. A fisheries inventory of the Chugwater Creek drainage, Platte, Laramie, and Albany counties, Wyoming. Admin. Rep. 5094-01-9301, Fish Division, Wyoming Game and Fish Department, Cheyenne, Wyo.

Modde, T., Ford, R.C., and Parsons, M.G. 1991. Use of a habitat-based stream classification system for categorizing trout biomass. N. Am. J. Fish. Manage. **11**: 305–311.

Nelson, R.L., Platts, W.S., Larsen, D.P., and Jensen, S.E. 1992. Trout distribution and habitat in relation to geology and geomorphology in the North Fork Humbolt River drainage, northeastern Nevada. Trans. Am. Fish. Soc. **121**: 405–426.

Patton, T.M. 1991. Potential for sport fisheries in the Laramie River downstream from Grayrocks Reservoir. Thesis, University of Wyoming, Laramie, Wyo.

Platts, W.S. 1991. Livestock grazing. Am. Fish. Soc. Spec. Publ. **19**: 389–424.

Rahel, F.J., and Hubert, W.A. 1991. Fish assemblages and habitat gradients in a Rocky Mountain – Great Plains stream: biotic zonation and additive patterns of community change. Trans. Am. Fish. Soc. **120**: 319–332.

Rahel, F.J., Keleher, C.J., and Anderson, J.L. 1996. Potential habitat loss and population fragmentation for cold water fish in the North Platte River drainage of the Rocky Mountains: response to climate warming. Limnol. Oceanogr. **41**: 1116–1123.

Rieman, B.E., and McIntyre, J.D. 1995. Occurrence of bull trout in naturally fragmented habitat patches of varied size. Trans. Am. Fish. Soc. **124**: 285–297.

Schlosser, I.J. 1987. A conceptual framework for fish communities in small warmwater streams. *In* Community and evolutionary ecology of North American stream fishes. *Edited by* W.J. Matthews and D.C. Heins. University of Oklahoma Press, Norman, Okla. pp. 17–24.

Schlosser, I.J. 1991. Stream fish ecology: a landscape perspective. BioScience, **41**: 704–712.

Shuter, B.J., and Post, J.R. 1990. Climate, population viability, and the zoogeography of temperate fishes. Trans. Am. Fish. Soc. **119**: 314–336.

Snigg, M.A. 1993. A fisheries survey of the Sybille Creek drainage, Albany and Platte County, Wyoming. Admin. Rep. 5093-01-9101, Fish Division, Wyoming Game and Fish Department, Cheyenne, Wyo.

Taniguchi, Y., Rahel, F.J., Novinger, D.C., and Gerow, K.G. 1998. Temperature mediation of competitive interactions among three fish species that replace each other along longitudinal stream gradients. Can. J. Fish. Aquat. Sci. **55**: 1894–1901.

Vincent, R.E., and Miller, W.H. 1969. Altitudinal distribution of brown trout and other fishes in a headwater tributary of the South Platte River, Colorado. Ecology, **50**: 464–466.

Waters, T.F. 1983. Replacement of brook trout by brown trout over 15 years in a Minnesota stream: production and abundance. Trans. Am. Fish. Soc. **112**: 137–146.

Wesche, T.A., Goertler, C.M., and Frye, C.B. 1987. Contribution of riparian vegetation to trout cover in small streams. N. Am. J. Fish. Manage. **7**: 151–153.

© 1999 NRC Canada

New perspectives in the analysis of fish distributions: a case study on the spatial distribution of largemouth bass (*Micropterus salmoides*)

Timothy E. Essington and James F. Kitchell

Abstract: Analyses of fish distributions rarely account for spatial arrangement of habitat types, are typically conducted at a single scale, and use a null model of random distributions without considering other null models. This study demonstrates a procedure to circumvent these difficulties by analyzing telemetry data collected on largemouth bass (*Micropterus salmoides*) in Long Lake, Michigan. Bass were highly aggregated within the littoral region, showing peaks of aggregation at small (<60 m) and large (>160 m) spatial scales. A neutral movement model (no taxis or kinesis within habitat types) could explain some of the observed aggregation, yet substantial aggregation remains unexplained. Much of the large-scale aggregation could be generated by including a taxis towards the eastern half of the basin, but taxes towards shallower cells or cells containing woody emergent macrophytes were unable to generate the observed degree of small-scale aggregation. Our results highlight the utility of analyzing spatial distributions at multiple scales and the importance of the spatial arrangements of habitat types and suggest that nonrandom distributions at one scale may be due to processes occurring at different scales.

Résumé : Les analyses des distributions des poissons rendent rarement compte de l'organisation spatiale des types d'habitat, sont généralement effectuées à une seule échelle, et ont recours à une hypothèse nulle de distribution aléatoire sans considérer d'autres hypothèses nulles. Nous présentons ici une méthode permettant de contourner ces difficultés en analysant des données télémétriques recueillies sur l'achigan à grande bouche (*Micropterus salmoides*) du lac Long (Michigan). Les achigans étaient fortement regroupés dans la zone littorale, et montraient des pics de regroupement à des échelles spatiales petite (<60 m) et grande (>160 m). Un modèle de déplacement neutre (ni taxie ni cinèse au sein des types d'habitat) a pu expliquer une partie du regroupement observé, mais non l'importance de cette agrégation. Une bonne portion de ce phénomène pourrait être engendrée par une taxie orientée vers la moitié est du bassin, mais l'intégration de taxies orientées vers des cellules peu profondes ou des cellules contenant des macrophytes ligneux émergés n'a pas pu générer le degré observé d'agrégation à petite échelle. Nos résultats soulignent l'utilité d'une analyse des distributions spatiales à des échelles multiples et l'importance de la configuration spatiale des types d'habitats, et font ressortir que les distributions non aléatoires observées à une seule échelle peuvent être dues à des processus survenus à des échelles diverses.

[Traduit par la Rédaction]

Introduction

Despite the applied and ecological implications of the spatial distribution of organisms (Hassell and Pacala 1990; Ives 1992; Murdoch et al. 1992; McCauley et al. 1996), we have only modest understanding of the processes underlying causes of aggregation, avoidance, or preference for different habitats for many fish species. To some extent, this may be a consequence of methodological problems in the analysis of spatial distribution data; accounts of fish distribution and habitat tend to be descriptive, and habitat preferences are often ascertained from correlations between local abundance and physical or biological attributes of that locality. This approach does not account for the spatial arrangement of habitat types present and thereby ignores the spatial autocorrelation in the data. Moreover, nonrandom distributions of fishes are routinely attributed to habitat preferences, yet alternative hypotheses are rarely addressed. Finally, most habitat analyses are conducted at a single spatial scale, and these scales may not be the same between studies. Collectively, these shortcomings make descriptive accounts of fish distributions limited in their ability to provide general conclusions about where fish are likely to be located and the underlying processes responsible for observed distributions.

Excellent examples of these difficulties come from studies on the role of structural habitat complexity in the spatial distribution of largemouth bass (*Micropterus salmoides*). Conventional wisdom holds that bass most commonly associate with areas of structural complexity. Indeed, some telemetry studies have indicated that bass associate with areas containing macrophytes (Mesing and Wicker 1986), areas with

Received October 14, 1997. Accepted September 8, 1998. J14253

T.E. Essington[1] **and J.F. Kitchell.** University of Wisconsin-Madison, Center for Limnology, 680 N. Park St., Madison, WI 53706, U.S.A.

[1]Author to whom all correspondence should be addressed. e-mail: teessing@facstaff.wisc.edu

© 1999 NRC Canada

shoreline brush (Schlagenhaft and Murphy 1985), or artificial reef habitats (Prince and Maughan 1979). However, Bains and Boltz (1992) found no response of radiotagged bass to removal of macrophytes, suggesting that structural habitat may not always be important. Also, Fish and Savitz (1983) found that edges of habitat between open water and macrophyte beds were most important for bass, and Schlagenhaft and Murphy (1985) claimed that the importance of structural cover varies seasonally. Rather than providing strong support for the view that bass associate with structural attributes of the habitat, these descriptive studies have only indicated that habitat preferences may be highly variable both within and between lakes. Consequently, the literature provides little insight into the conditions and scales at which structural complexity is important.

An alternative approach that avoids these shortcomings comes from an extensive body of work on terrestrial insects, which considers how random and nonrandom movement of individuals within landscapes produces spatial patterns in insect abundance (Karieva and Shigesada 1983; Cain 1985; Karieva and Odell 1987; Turchin 1991). This approach uses a null model of neutral movement (no taxis towards or kinesis within habitat types) and then explores how movement biases, either towards or within certain habitat types, account for the observed distribution. The strengths of this approach are that it explicitly accounts for the spatial arrangement of habitat types and it more accurately represents how habitat preferences are manifest as patterns in animal abundance. Further, this approach uses the spatial distributions resulting from neutral movement as the null model, and this distribution may not be random (Gardner and O'Neill 1991). Because neutral movement is typically the hypothesis that researchers want to test, this approach provides a more appropriate null model than the random spatial distributions often used in correlative studies.

In this study, we illustrate the neutral movement approach by using data collected on the spatial distribution, movement, and habitat of largemouth bass in a small lake in northern Wisconsin. Further, we describe statistical tools for analyzing spatial distributions at multiple spatial scales. The concepts and procedures presented here are taken from the extensive literature on insect ecology, landscape ecology, and spatial statistics, but we are unaware of any instances in which these approaches have been used to assess fish distributions. Ultimately, our hope is that the ideas presented in this paper will stimulate new ideas and new ways of thinking about the processes governing the distribution of fish.

We first describe our study site and our data collection procedures, summarize the observed distribution of bass, and identify possible habitat preferences using a simple correlative approach. We then describe the neutral movement model and demonstrate how the neutral movement model generates nonrandom spatial distributions. Finally, we evaluate the ability of models containing nonneutral movement to generate spatial distributions that are similar to the observed distribution of Long Lake bass.

Study site

Long Lake is a 7.3-ha kettle lake located in Gogebic County, Michigan, at the University of Notre Dame Environmental Research Center (UNDERC). A neoprene curtain divides the lake into two basins, 5.8 ha (west basin) and 2.5 ha (east basin) for other experimental purposes (Carpenter et al. 1996). This study was conducted in the west basin, which has a mean depth of 3.14 m and a maximum depth of 17.7 m (Fig. 1). Secchi depth averaged 2.25 m, and thermocline depth averaged 2.2 m. Epilimnetic water temperature averaged 21°C and ranged from 19 to 24°C. The fish community consisted almost entirely of largemouth bass and brook stickleback (*Culaea inconstans*). All telemetry data were collected between June 20 and August 27, 1996.

Spatial distribution of Long Lake largemouth bass

Data collection and analysis

We implanted radio transmitters into eight largemouth bass, six of which were transplanted from a nearby lake because of low densities of large fish following a mild winterkill. The six transplanted fish ranged in size from 114 to 449 g and were surgically implanted with miniature (3 g) transmitters on June 13, 1996. Each transmitter had a unique frequency that allowed each fish to be individually identified. Fish were held for 2 days after surgery to allow recovery and were then released into Long Lake. On July 15, 1996, two additional 120-g bass were collected from Long Lake and implanted with transmitters. These two fish were members of a large 1995 year-class that were the numerically dominant piscivores in Long Lake in 1996. All fish were released at the same location, positioned on the north bank just east of the narrowing between the basins. Fish distributed throughout the lake within 1 day after release.

To locate radiotagged bass, we used a hand-held loop antenna and a Fieldmaster receiver (Advanced Telemetry Systems). We patrolled the lake in a john boat equipped with a small electric motor until we found a strong signal. We then carefully approached the fish, and when within about 20 m, triangulated to determine its precise position. This method was necessary because the low conductivity of Long Lake made the range of the radio signals too short to allow us to triangulate from distant, predetermined stations. Each located fish was assigned to a 10 × 10 m cell (Fig. 1). We marked the intersection between grid cells and the shoreline by surveying, and fish were assigned to cells using these markers and approximating the distance offshore. We were typically able to locate all bass within 25–30 min.

To describe the spatial distribution of bass and to identify any weekly or diel trends in fish distributions, we located fish at 4-h intervals from 08:00 to 16:00 three times weekly. On two dates (August 25 and 26, 1996) we located fish at 2-h intervals from 08:00 to 02:00 the following day to verify that locations determined during the aforementioned sampling period were representative of locations used during other periods of the day. The sampling protocol precluded analysis of movement and spatial distributions during dawn. The overall distribution pattern was determined by counting the number of times individuals were located in each cell.

One difficulty in determining whether a spatial distribution deviates from random is that the result of any such analysis is dependent on the scale at which it is conducted. A statistic that circumvents this difficulty is Ripley's K

© 1999 NRC Canada

Fig. 1. Map of Long Lake, Michigan, and the observed spatial distribution of largemouth bass in the lake, 1996. The eastern edge of the map represents where the west basin is separated from the east basin by a neoprene curtain. The intensity of the shading reflects the number of visits received by each cell.

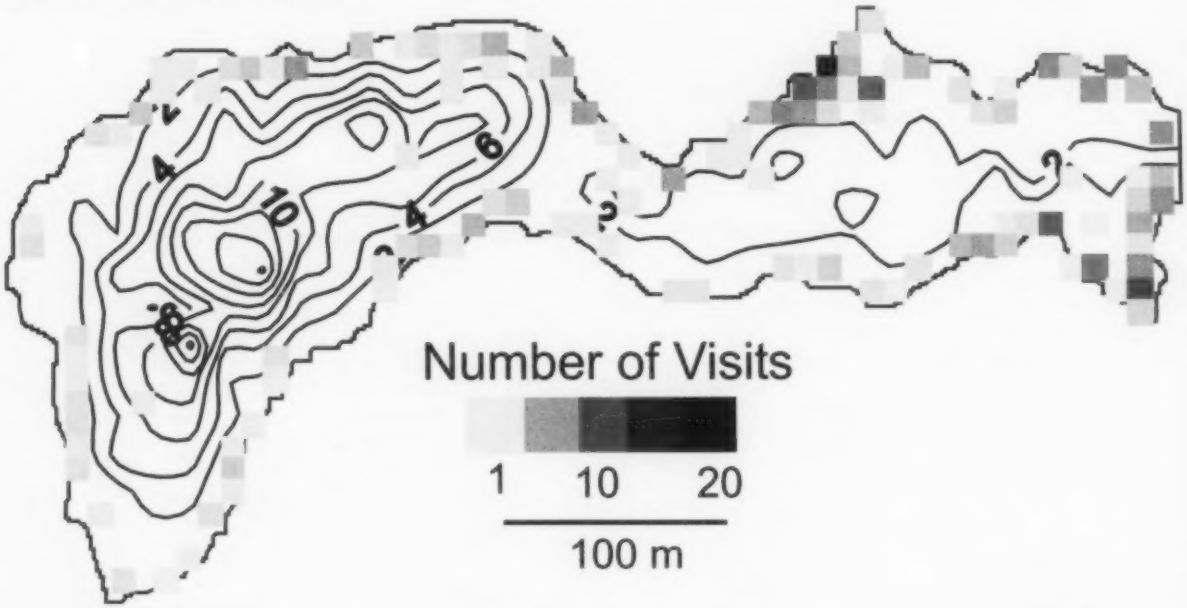

(Cressie 1993); $K(h)$ is a statistic that quantifies the degree of aggregation at a spatial resolution of h, such that the degree of aggregation can be measured at several scales simultaneously. The formal expression for $K(h)$ is

$$(1a) \quad K(h) = \lambda^{-1} \Sigma\Sigma w(s_i, s_j)^{-1} I(\|s_i - s_j\| \leq h)/N$$

$$(1b) \quad \lambda = N/A$$

where A is the area of a circle of radius h centered at cell s_i, N is the number of observations of bass in A, $\|s_i - s_j\|$ is the distance between cells i and j, $I(\|s_i - s_j\| \leq h)$ is the indicator function, which equals 1 if $\|s_i - s_j\| \leq h$ and 0 otherwise, and $w(s_i, s_j)$ is a weighting function, which is the proportion of the circumference of a circle centered at s_i that passes through s_j.

The $K(h)$ was calculated using the spatial statistics module in Splus© v. 3.3 (1995, MathSoft Inc.). Inferences are drawn by comparing $K(h)$ for the observed distribution to Monte Carlo simulations of random spatial distributions. For all of our analyses, these consisted of 500 random distributions of bass among all cells shallower than 2 m and were either in contact with the shoreline or adjacent to a cell that was (see Results of telemetry study). We then calculated a standardized aggregation parameter defined as follows:

$$(2) \quad K(h)'_{obs} = \frac{K(h)_{obs} - \overline{K(h)_{rand}}}{K(h)^{(0.975)}_{rand} - \overline{K(h)_{rand}}}$$

where $\overline{K(h)_{rand}}$ is the mean $K(h)$ of the null (random) distributions and $K(h)^{0.975}_{rand}$ is the 97.5th percentile of the null distribution. Thus, $K(h)'_{obs}$ is the standardized deviation from a random distribution. Values greater than 1 indicate significant aggregation at that scale.

We performed a simple correlative analysis to assess the preference for habitat attributes that we could readily measure: coarse woody debris, emergent woody macrophytes (leatherleaf (*Chamaedaphne calyculata*)), and depth. To describe the abundance of structural cover in each shoreline cell, we snorkeled the entire shoreline and counted the number of logs in each cell that were at least 5 m long and 15 cm in diameter. Leatherleaf was noted as present or absent. Other macrophytes were relatively scarce in Long Lake and were therefore not addressed in this study. We estimated mean cell depth by using topographic maps with 2-m depth contours and calculated the depth at the center of each cell. Depths were estimated by linearly interpolating between the shoreline and the 2-m isocline.

We used a general linear model to identify which habitat attributes were correlated with the number of times each cell was visited. Parameter estimates of the linear model were fit by the method of least squares. This procedure does not account for spatial autocorrelation and consequently underestimates the uncertainty in the parameter estimates (Thomson et al. 1996). Thus, this procedure gives "optimistic" p values, so significant p values need to be interpreted with caution. However, we used this method only as an exploratory tool to identify what habitat types might be associated with bass distributions.

Results of telemetry study

We collected 324 observations of bass locations. Individuals were found in cells widely dispersed throughout the lake such that the maximum distance between cells visited by individual fish ranged from 415 to 515 m. We assessed whether individuals exhibited any apparent home ranges within the lake by plotting the cumulative number of cells

© 1999 NRC Canada

Fig. 2. Aggregation of largemouth bass ($K(h)'$) at scales (h) ranging from 10 to 200 m. The standardized aggregation parameter $K(h)'$ is the standardized deviation from random distributions, such that values greater than 1 indicate statistically significant aggregation. Bass in Long Lake were significantly aggregated at all scales and showed peaks of aggregation at h = 0, 30, and 180 m.

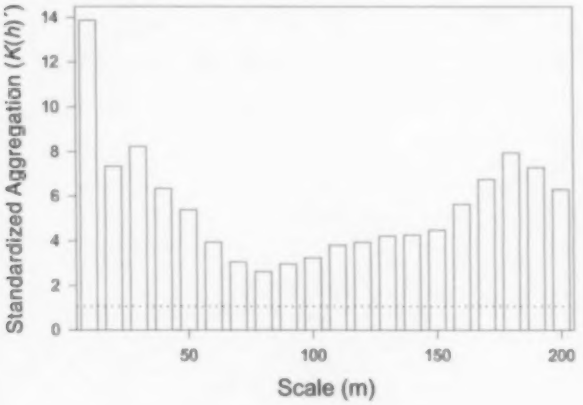

visited versus the number of observations of each fish. An asymptotic curve suggests that individuals were restricting their movements to a few cells (i.e., a home range; Winter 1977). For every fish in this study, this relationship was nearly linear, even after 60 observations for some fish (data not shown). This indicates that even if fish were using home ranges smaller than the entire lake, our data would be insufficient to identify them. Further, only one fish exhibited any strong site fidelity. This fish (mass = 137 g) was found in 11 cells located in the southeastern portion of the lake for 23 of the 29 times that that fish was located. However, this fish was also found in cells located 500 m away. Because there was little evidence that individuals were using home ranges smaller than the lake, we described the overall spatial distribution of bass by pooling all 4 h-interval telemetry data.

Fish exhibited a strong preference for the shoreline; 255 (79%) of the observations were located in shoreline cells (Fig. 1). Nearly all of the remaining observations were in cells located adjacent to shoreline cells, but within the 2-m isocline. Bass were located in cells deeper than 2 m on only nine occasions. Thus, 97% of the observations were located in cells shallower than 2 m and either directly in contact with the shoreline or adjacent to cells that were.

Visual assessment of the observed distribution suggested nonrandom distributions at two or three scales. At smaller scales, two bays in the eastern basin received 30% of all cell visits, and one of these cells was visited 19 times, representing 6% of all fish locations (Fig. 1). At a larger scale, we also noted that the western half of the lake was infrequently visited. Ripley's K confirmed that these patterns represent significant deviations from random distributions (Fig. 2). The observed spatial distribution was significantly aggregated at all scales, and there were three notable peaks in the degree of aggregation across scales that corresponded to the patterns observed from visual inspection of the bass distribution. The first (and largest) peak occurred at the smallest spatial scale, which corresponds to the scale of our 10 × 10 m grid. A second, slightly smaller peak centered at 30 m was also observed, likely representing the aggregation in the bays and aggregation among the cells within them. The third peak corresponded to a spatial scale of 170–190 m, representing the aggregation in the eastern basin.

Within the 203 cells described above, leatherleaf presence (T = 3.71, $p < 0.001$) and cell depth (T = 2.85, p = 0.005) were positively and negatively correlated with the number of cell visits, respectively. Cells with leatherleaf were visited an average of 4.35 (SD = 5.2) times whereas the remaining cells were visited on average 1.65 (SD = 2.08) times. Coarse woody debris was not correlated with the number of cell visits. The general linear model with a constant, leatherleaf, and cell depth as predictors explained only 13% of the variation in cell visits.

In summary, bass were found throughout Long Lake, and there was little evidence that fish were using home ranges smaller than the entire lake. Bass tended to be found in cells adjacent to the shoreline and were rarely found in cells deeper than 2 m. The observed spatial distribution was highly aggregated among shoreline cells and cells adjacent to shoreline cells within the 2-m isocline. Simple correlative analyses suggested that the presence of leatherleaf and cell depth might explain the variation in the number of cell visits at the spatial resolution of 10 × 10 m (i.e., the cell size).

Neutral movement model

Model description

We now demonstrate a procedure for generating spatial distributions resulting from neutral movement. We refer to this as a neutral movement model to reflect that movement is not affected by taxes or kinesis and is analogous to the terminology used in landscape ecology literature (Gardner and O'Neill 1991). The strategy in constructing this type of model is to identify habitable cells, empirically estimate the propensity of individuals to move among cells, and then simulate fish movement within these cells. Because bass were located in shoreline or shallow (<2 m) adjacent cells on 97% of the observations, these criteria were used to define habitable cells. We hereafter refer to cells that meet these criteria as "habitable."

The central concept underlying the model structure is that the probability of a individual moving into a cell is solely a function of the distance between that cell and the cell in which the individual resides. This necessitated that we estimate the probability function $p_i(d_i)$, which indicates the probability that cell i would be visited (p_i) by an individual residing in cell j, given that the distance between cells i and j is d_i. To obtain data needed to estimate this probability function, we collected additional telemetry data by locating individual fish at 30-min intervals for 2–4 h on eight dates (all data collected between 08:00 and 19:00). From these data, we determined the proportion of individuals that remained in the same cell for successive sampling intervals and, for those individuals that did move, how far they travelled. The observed frequency distribution of movement distances could not be satisfactorily fit to a single probability distribution (Fig. 3). Instead, we treated the frequency distribution as consisting of two components. The first component was the probability that an individual would remain in the same cell

© 1999 NRC Canada

Fig. 3. Movement patterns of Long Lake largemouth bass over 30-min sampling intervals. The line shows the best fit to the probability function $p_i(d_i)$, which denotes the probability of a cell being visited by an individual as a function of distance between that cell and the individual. See text for details.

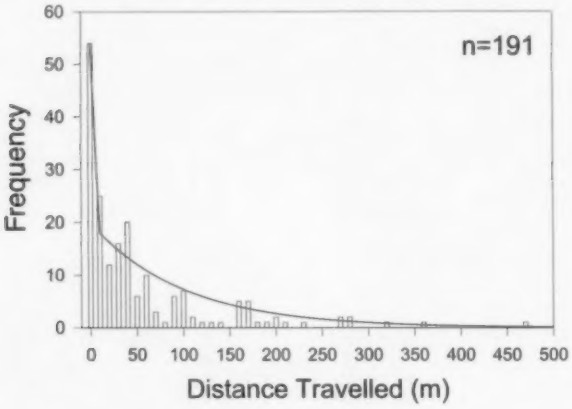

for consecutive sampling intervals, denoted p_0. The second component was the probability distribution of distances travelled for bass that moved into new cells. This was approximated as a gamma distribution. Thus, the overall probability function, $p_i(d_i)$, was

$$(3a) \quad p_i(d_i) = p_0 \qquad \text{for } d_i = 0$$

$$(3b) \quad p_i(d_i) = (1 - p_0)\frac{a^n}{\Gamma(n)}\exp(-ad_i)d_i^{n-1} \qquad \text{for } d_i > 0$$

where a and n are parameters describing the shape of the gamma distribution. These parameters were fit to the movement data by simulating the distance travelled by each fish for 50 combinations of a and n and then comparing the simulated distances with the observed distances using a Kolmogorov–Smirnov test. For each combination of a and n, this procedure was run 10 times, and the combination of parameters that resulted in the lowest test statistic (i.e., highest p value) was used. For our data, the best fit was obtained by setting $p_0 = 0.3$, $a = 0.01$, and $n = 1$ (Fig. 3).

Now that habitable cells have been identified, and the function $p_i(d_i)$ has been defined and parameterized, we can simulate movement of fish among habitable cells. We placed one fish in each habitable cell and simulated the movement of each individual for 200 iterations, where each iteration represented a 30-min time step. Movement of individual fish was simulated by calculating p_i for each cell based on the probability function $p_i(d_i)$ and then randomly selecting a cell from this probability distribution. We integrated over values of d_i at 10-m intervals to calculate p_i for each cell. The model counted the number of times that each cell was visited, and from this calculated the probability of finding a fish in each cell at any given time, $P_{t,i}$, as the proportion of the simulated visits in which individuals visited cell i. For each individual, we simulated 200 movements, and preliminary model runs indicated that 200 iterations was sufficient to reach equilibrium.

We generated 100 spatial distributions by randomly selecting 324 cells (to match our observed telemetry data) based on the $P_{t,i}$ and then calculated standardized aggregation, $K(h)'$, for each distribution. We considered the model to generate significantly greater aggregation than random when the mean $K(h)'$ of the 100 simulations exceeded 1 (i.e., the average $K(h)$ exceeded the 97.5th percentile of the random distributions).

Spatial distribution generated by the neutral movement model

At all scales, the mean aggregation generated by the neutral movement model was greater than the mean aggregation generated from random distributions, and at spatial resolutions greater than 160 m, the neutral model generated spatial distributions that were significantly more aggregated than random (Fig. 4A). The process by which this occurs is straightforward. When individuals are more likely to move into nearby cells than into distant cells, regions of lake in which there are large patches of habitable cells receive more visits than expected if individuals were randomly distributed among these cells. At small spatial resolutions, one can think of this phenomenon in terms of the number of cells that potentially act as "sources" of individuals to cells; those cells that have many cells in close proximity have several sources of individuals that may visit them. On a larger scale, these large patches of habitable cells can "trap" individuals within them. In other words, individuals are less likely to move to more distant cells if there are several cells nearby that each has a high probability of being visited.

If we had made the function $p_i(d_i)$ a uniform probability distribution, the neutral movement model would generate completely random distributions because each cell would be equally likely to be visited. Thus, the random spatial distribution is a special case of the neutral movement model wherein the probability of each cell being visited is independent of distance. Thus, the appropriateness of a random spatial distribution as a null model depends on whether a uniform probability distribution is a reasonable approximation for $p_i(d_i)$.

Evaluating the effect of nonneutral movement on the spatial distribution of largemouth bass

Incorporating taxes into the movement model

We evaluated the spatial distribution that resulted from incorporating three taxes into the neutral movement model: taxes towards the eastern half of the lake, shallower cells, and cells containing leatherleaf. The latter two preferences derived from our correlative analysis. The hypothesis that there may have been a preference for the eastern half was derived from our observation that this half of the lake received disproportionately greater visits than the western half. Taxes were incorporated into the model by adding an additional term, $I(c)$, to the probability function $p_i(d_i)$:

$$(4) \quad p_i(d_i)' = p_i(d_i)I(c)$$

where $I(c)$ is an indicator function that changes values depending on cell depth, position in the lake, and the presence

© 1999 NRC Canada

Fig. 4. Standardized aggregation of largemouth bass predicted by (A) the neutral movement model, (B) the model with taxis towards cells with leatherleaf, and (C) the model with taxis towards the eastern half of the basin. Each bar represents the mean of 100 simulations. Values above the broken line ($K(h)' > 1$) indicate significantly greater aggregation than random at that scale.

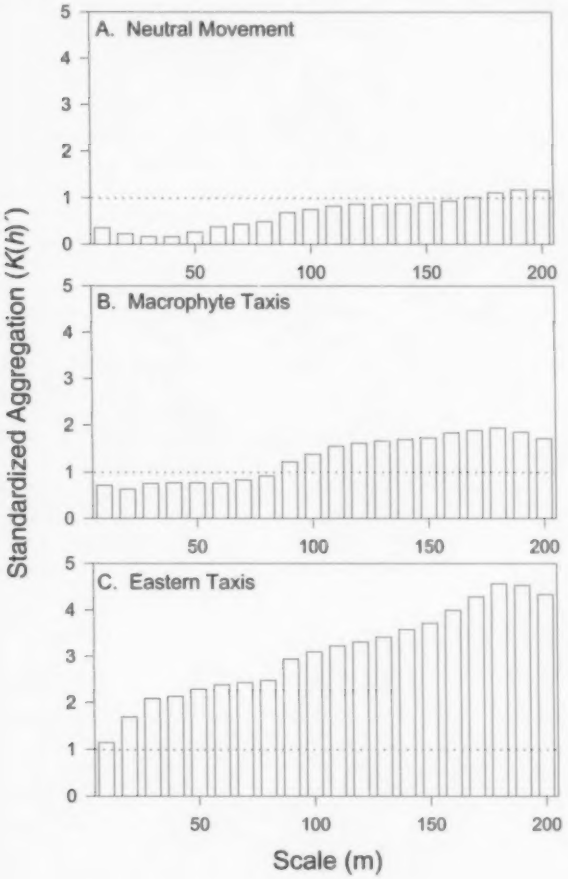

of leatherleaf. For the leatherleaf taxis, $I(c) = 2$ if the cell contained leatherleaf and $I(c) = 1$ otherwise. In other words, cells with leatherleaf were twice as likely to be visited than those that did not contain leatherleaf. Preliminary analysis indicated that this resulted in optimal model performance. For the depth preference scenario, $I(c) = 1.35$ if the mean cell depth was less than 1.0 m, $I(c) = 1$ if the mean cell depth was between 1.0 and 1.5 m, and $I(c) = 0.65$ if the mean cell depth exceeded 1.5 m. These numbers were derived by comparing the observed use of each depth category with the proportional availability of cells in each depth category. For the eastern taxis, we made $I(c)$ a function of the position in the lake:

$$(5a) \quad I(c) = 0.5 + 0.002 l_i \quad \text{if } l_i < 250\,\text{m}$$

$$(5b) \quad I(c) = 1 \quad \text{if } l_i > 250\,\text{m}$$

where l_i is the eastward component of the distance vector from cell i to the westernmost edge of the lake. Note from eq. 5*b* that within the eastern half of the lake, $p_i(d_i)$ was no different from that in the neutral movement model, i.e., bass moved neutrally within cells in the eastern half of the lake. For each model scenario, we generated 100 random distributions in the same manner described for the neutral movement model.

We first evaluated the pattern of aggregation produced by two of these taxes, the leatherleaf preference and the eastern preference. These two were selected because they provided a contrast between small-scale (leatherleaf) and large-scale (eastern preference) taxes and thus allowed us to evaluate how the effects of these taxes vary across all scales. We then evaluated the goodness-of-fit between the observed distribution and the distributions simulated from neutral movement and the three scenarios described above. For this, we used a modification of a procedure outlined by Turner et al. (1989). The test statistic F_w ranges from 0 (no fit) to 1 (perfect fit) and like $K(h)$ is calculated at several scales. This procedure aggregates the 10 × 10 m cells into successively larger cells (20 × 20 m, 30 × 30 m, etc.), and at each level of aggregation, the test statistic F_w is calculated. In other words, F_w denotes the similarity of two spatial distributions at a resolution (cell dimension) of $10w \times 10w$ m, where w indicates the size of the cells. The F_w is calculated as follows:

$$(6) \quad F_w = 1 - \frac{\sum \left| n_{i,1} - n_{i,2} \right|}{N}$$

where $n_{i,j}$ represents the number of observations of fish in cell i of spatial distribution j and N is the total number of fish in each of the spatial distributions being compared (for our analyses, N was the same for the simulated and observed distributions).

For illustrative purposes, we used random distributions as our null model. This allowed us to compare the improvement of fit provided by the neutral movement model and the taxes incorporated within it. We calculated F_w for 500 random distributions and the simulated distributions generated by the movement models. We define the standardized goodness-of-fit as follows:

$$(7) \quad F'_{w,\text{obs}} = \frac{F_{w,\text{obs}} - \overline{F_{w,\text{rand}}}}{F^{(0.975)}_{w,\text{rand}} - \overline{F_{w,\text{rand}}}}$$

where $\overline{F_{w,\text{rand}}}$ is the mean F_w of the random distributions and $F^{(0.975)}_{w,\text{rand}}$ is the 97.5th percentile of the random distributions. Thus, $F'_{w,\text{obs}}$ is the standardized deviation from a random distribution, and values greater than 1 indicate significant goodness-of-fit. We considered the goodness-of-fit to be significantly greater than random when the mean $F'_{w,\text{obs}}$ of the simulation exceeded 1.

Aggregation and goodness-of-fit of model scenarios

Not surprisingly, there was greater aggregation at small scales when we included a taxis towards cells containing leatherleaf (Fig. 4B) and at large scales when we included a taxis towards the eastern half of the basin (Fig. 4C) compared with the random or neutral movement model. However, both scenarios resulted in increased aggregation at

© 1999 NRC Canada

Fig. 5. Goodness-of-fit (F'_w) between the observed largemout bass distribution and the distributions simulated by the three model scenarios at different spatial resolutions. Paremeter w indicates the cell size ($10w \times 10w$) used in each comparision. Solid bars represent goodness-of-fit for neutral movement alone. Open bars represent goodness-of-fit for the model containing (A) taxis towards woody macrophytes, (B) taxis towards cells shallower than 1 m and avoidance of cells deeper than 1.5 m, and (C) taxis towards cells in the eastern half of Long Lake. Each bar represents the mean of 100 simulations. Values above the broken line ($F'_w > 1$) indicate significantly better fit than random distributions.

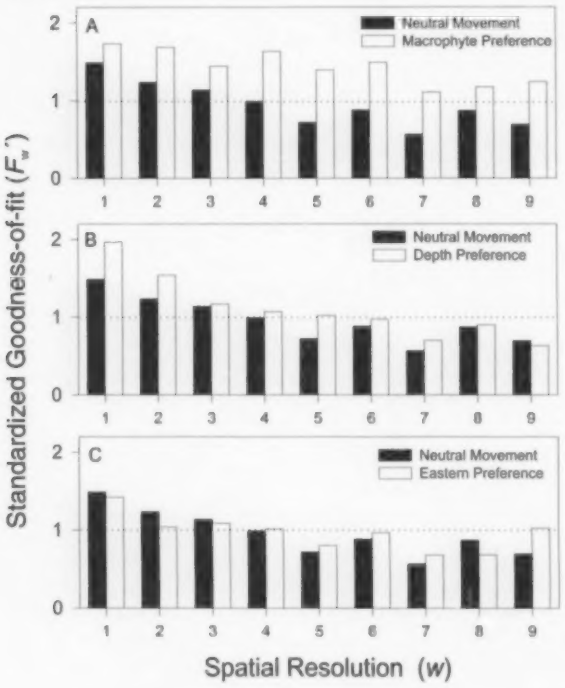

scales markedly different from the scale at which they operated. This was especially striking for the eastern taxis scenario, in which the aggregation was significant at all scales. Thus, the effect of a taxis was manifest at scales markedly different from the scale at which it was operating. These results occurred in our model because many of the large patches of habitable cells were located in the eastern half of the lake. We have already discussed how these large patches caused the neutral movement model to generate nonrandom distributions. The eastern taxis, by further "pushing" individuals into these patches, caused that process to be even more pronounced. Similarly, much of the leatherleaf was located within these patches of habitable cells. Thus, the juxtaposition of these large patches of habitable cells and preferred habitat played a large role in governing the simulated spatial distributions.

At all scales, the neutral movement model alone generated spatial distributions that were more similar to the observed distribution than were random distributions and provided a significantly better fit at small spatial resolutions (Fig. 5). The macrophyte taxis improved the model fit at all spatial scales and always fit the observed data better than random distributions (Fig. 5A). The depth taxis resulted in the largest observed F'_w at the smallest spatial resolution (Fig. 5B). However, the improvement over the neutral model was only modest at spatial resolutions greater than 30 × 30 m. The eastern taxis had little effect on the goodness-of-fit at any spatial resolution (Fig. 5C).

Discussion

Our results shed some light on why simple correlative analyses between local abundance and habitat attributes can provide misleading conclusions about the processes causing nonrandom fish distributions. One reason is that the null model typically used in correlative analyses is a random spatial distribution, yet our results show that this is only appropriate when the probability function $p_i(d_i)$ is a uniform probability distribution. Granted, there are some instances in which this is a reasonable approximation of fish behavior. For example, if home ranges are small relative to the individuals' movement rate, then the distribution of individuals within the home range can be approximated with a Poisson (random) distribution (de Roos and Sabelis 1995). However, the assumption of a uniform probability distribution is often an poor approximation of $p_i(d_i)$, as was the case for largemouth bass in Long Lake. Another problem with correlative analyses is they are typically conducted at a single spatial resolution, yet our results indicate that taxes operating at one scale can generate nonrandom distributions at very different scales. Thus, nonrandom attributes at small scales may be attributable to small-scale habitat variability, when a much larger scale taxis may be responsible for the observed distribution. Finally, simple correlative analyses do not account for the spatial arrangement of habitat types, although theoretical (Lavorel et al. 1994; this study) and experimental results (Fahrig and Paloheimo 1988; Lavorel et al. 1994) indicate that patchiness plays a key role in dictating the local abundance of individuals. The neutral movement approach, coupled with more sophisticated spatial statistics circumvents these difficulties by explicitly incorporating these processes to generate predictions about the distribution of fish.

It is important to note the limitations of the modelling approach employed in this study. The probability function $p_i(d_i)$ is a coarse approximation of individual movement and is best used to evaluate spatial distribution patterns integrated over long (seasonal) time periods. As such, this approach is not likely to be useful in evaluating short-term distributions and movement patterns (e.g., diel patterns), unless the approximation $p_i(d_i)$ is sufficiently supported by the data. Clearly, at very short temporal scales (seconds to minutes), $p_i(d_i)$ is inappropriate. Instead, a different model structure that evaluates movement vector distances, angles, and frequencies of turns should be used to predict animal abundances from these data (Karieva and Shigesada 1983; Cain 1985; Karieva and Odell 1987; Turchin 1991).

We gained several insights into the processes governing the spatial distribution of bass through this analysis. The most important insight was that bass distributions were the product of several processes operating at multiple spatial scales. The observed distribution showed peaks in aggrega-

© 1999 NRC Canada

tions centered at three spatial scales: 10, 30, and 180 m. Some of the small-scale aggregation may be attributable to a preference for areas containing leatherleaf, thereby supporting the contention that bass associate with areas of structural complexity. However, we found only a modest increase in small-scale aggregation when this taxis was incorporated into the model, suggesting that this preference accounts for only a small component of the observed aggregation. We have some evidence that small-scale kinesis may have played a role in these aggregations; 16 cells received 30% of fish visits, and our movement data indicated that fish in these cells were more than twice as likely to remain in the same cell for consecutive sampling intervals. These cells shared little similarities in terms of habitat attributes, suggesting that factors such as prey availability may have been responsible.

There also appeared to be a larger-scale preference for fish to be located in the eastern half of the lake, and this model scenario was the only one that generated aggregation close to the observed aggregation. This may reflect a thermal preference for warmer water, as the prevailing winds push warmer water into the eastern basin, and on moderately windy days (15–20 mi/h), we have noted a temperature gradient from 23 to 25°C from the westernmost to the easternmost edge during the midafternoon (T.E. Essington, unpublished data). Given that the bioenergetic optimal temperature for largemouth bass is about 27°C, it seems reasonable that bass may have responded to this gradient. Interestingly, our statistical procedure did not indicate an improvement in the model fit by including this taxis. This may be a shortcoming of the statistical procedure used to compare the two spatial distributions. Turner et al. (1989) suggested that cells not be aggregated into cells greater than one third the size of the shortest dimension of the landscape. For Long Lake, this meant that we could only aggregate cells to 90 × 90 m. Larger-scale aggregation may have yielded significant improvements in model fit.

Another important insight was that the simulated spatial distributions were very sensitive to the extent of individual movement (i.e., the shape of the $p_i(d_i)$), and placing relatively small biases resulted in very different spatial distributions than the neutral movement model. Thus, small changes in fish behavior may ultimately result in large, surprising changes in fish distributions. Behavior, in turn, can be influenced by food availability (Savitz et al. 1983) and limnological conditions (Rogers and Bergesen 1995). There is considerable evidence that bass movement is highly variable within and between lakes. In some lakes, largemouth bass have been shown to exhibit extensive movement (Diana et al. 1990; this study) whereas in other lakes, bass move very little, restricting movement to small home ranges (Warden and Lorio 1975; Fish and Savitz 1983; Mesing and Wicker 1986; Bain and Boltz 1992; Demers et al. 1996). Some of these differences could be due to differences in foraging strategy. Largemouth bass are known to exhibit either a sit-and-wait strategy or a cruising strategy (Savino and Stein 1982). Thus, the type of foraging strategy used may ultimately have considerable consequences on bass distributions.

Most importantly, our results suggest that the spatial pattern of habitat types likely plays a key role in determining the spatial distribution of bass. One hypothesis that derived from these analyses is that large patches of habitable cells that also contain some cells with preferred habitat attributes (i.e., leatherleaf) will contain very high fish densities. Thus, the effect of removing habitat on fish distributions may depend entirely on the location of that habitat within the lake landscape. This phenomenon has been widely recognized by landscape ecologists, but correlative studies of fish distributions rarely account for this phenomenon. Given this oversight, it is not surprising that the literature provides little consensus on the processes underlying the spatial distribution of fish. Greater appreciation of the importance of the lake landscape, as well as the other issues raised in this paper, should dramatically improve our understanding of the processes governing the distribution of fish.

Acknowledgements

We thank Ron Hellenthal and Jeff Runde for accommodating our field studies at the University of Notre Dame Environmental Research Center (UNDERC) and M. Peterson for assisting with the data collection. We thank Chris Harvey, Conrad Lamon, Tim Johnson, and two anonymous reviewers for providing helpful comments on the manuscript. This project was supported by an NSF Graduate Research Traineeship awarded to T.E.E.

References

Bain, M.R., and Boltz, S.E. 1992. Effect of aquatic plant control on the microdistribution and population characteristics of largemouth bass. Trans. Am. Fish. Soc. **121**: 94–103.

Cain, M.L. 1985. Random search by herbivorous insects: a simulation model. Ecology, **66**: 876–888.

Carpenter, S.R., Kitchell, J.F., Cottingham, K.L., Schindler, D.E., Christensen, D.L., Post, D.M., and Voichick, N. 1996. Chlorophyll variability, nutrient input, and grazing: evidence from whole-lake experiments. Ecology, **77**: 725–735.

Cressie, N.A. 1993. Statistics for spatial data. John Wiley & Sons, New York.

Demers, E., McKinley, R.S., Weatherley, A.H., and McQueen, D.J. 1996. Activity patterns of largemouth and smallmouth bass determined with electromyogram biotelemetry. Trans. Am. Fish. Soc. **125**: 434–439.

de Roos, A.M., and Sabelis, M.W. 1995. Why does space matter? In a spatial world it is hard to see the forest before the trees. Oikos, **74**: 347–348.

Diana, J.S., Clapp, D.F., Hay-Chmielewski, E.M., Schnicke, G., Siler, D., Ziegler, W., and Clark, R.D. 1990. Relative success of telemetry studies in Michigan. Am. Fish. Soc. Symp. **7**: 346–352.

Fahrig, L., and Paloheimo, J. 1988. Effect of spatial arrangement of habitat patches on local population size. Ecology, **69**: 468–475.

Fish, P.A., and Savitz, J. 1983. Variations in home ranges of largemouth bass, yellow perch, bluegills and pumpkinseeds in an Illinois lake. Trans. Am. Fish. Soc. **112**: 147–153.

Gardner, R.H., and O'Neill, R.V. 1991. Pattern, process, and predictability: the use of neutral models for landscape analysis. *In* Quantitative methods in landscape ecology. *Edited by* M.A. Turner and R.H. Gardner. Springer-Verlag, New York. pp. 289–307.

© 1999 NRC Canada

Hassell, M.P., and Pacala, S. 1990. Heterogeneity and the dynamics of host–parasitoid interactions. Philos. Trans. R. Soc. Lond. B, Biol. Sci. **330**: 203–220.

Ives, A.R. 1992. Density-dependent and density-independent parasitoid aggregation in model host–parasitoid systems. Am. Nat. **140**: 912–937.

Kareiva, P., and Odell, G. 1987. Swarms of predators exhibit "prey-taxis" if individual predators use area-restricted search. Am. Nat. **130**: 233–270.

Kareiva, P.M., and Shigesada, N. 1983. Analyzing insect movement as a correlated random walk. Oecologia, **56**: 234–238.

Lavorel, S., O'Neill, R.V., and Gardner, R.H. 1994. Spatio-temporal dispersal strategies and annual plant species coexistence in a structured landscape. Oikos, **71**: 75–88.

McCauley, E., Wilson, W.G., and de Roos, A.M. 1996. Dynamics of age-structured predator–prey populations in space: asymmetrical effects of mobility in juvenile and adult predators. Oikos, **76**: 485–497.

Mesing, C.L., and Wicker, A.M. 1986. Home range, spawning migrations, and homing of radio-tagged Florida largemouth bass in two central Florida lakes. Trans. Am. Fish. Soc. **115**: 286–295.

Murdoch, W.M., Briggs, C.J., Nisbet, R.M., Gurney, W.S.C., and Stewart-Oaten, A. 1992. Aggregation and stability in metapopulation models. Am. Nat. **149**: 41–58.

Prince, E.D., and Maughan, O.E. 1979. Telemetric observations of largemouth bass near underwater structures in Smith Mountain Lake, Virginia. *In* Response of fish to habitat structure in standing water. *Edited by* D.L. Johnson and R.A. Stein. N. Cent. Div. Am. Fish. Soc. Spec. Publ. **6**: 26–32.

Rogers, K.B., and Bergersen, E.P. 1995. Effects of a fall drawdown on movement of adult northern pike and largemouth bass. N. Am. J. Fish. Manage. **15**: 596–600.

Savino, J.F., and Stein, R.A. 1982. Predator–prey interaction between largemouth bass and bluegills as influenced by simulated, submersed vegetation. Trans. Am. Fish. Soc. **111**: 255–266.

Savitz, J., Fish, P.A., and Weszely, R. 1983. Effects of forage on home-range size of largemouth bass. Trans. Am. Fish. Soc. **112**: 772–776.

Schlagenhaft, T.W., and Murphy, B.R. 1985. Habitat use and overlap between adult largemouth bass and walleye in a West Texas reservoir. N. Am. J. Fish. Manage. **5**: 465–470.

Thomson, J.D., Weiblen, G., Thomson, B.A., Alfaro, S., and Legendre, P. 1996. Untangling multiple factors in spatial distributions: lilies, gophers, and rocks. Ecology, **77**: 1698–1715.

Turchin, P. 1991. Translating foraging movements in heterogeneous environments into the spatial distribution of foragers. Ecology, **72**: 1253–1266.

Turner, M.G., Costanza, R., and Sklar, F.H. 1989. Methods to evaluate the performance of spatial simulations models. Ecol. Model. **48**: 1–18.

Warden, R.L., and Lorio, W.J. 1975. Movements of largemouth bass (*Micropterus salmoides*) in impounded waters as determined by underwater telemetry. Trans. Am. Fish. Soc. **104**: 696–702.

Winter, J.D. 1977. Summer home range movements and habitat use by four largemouth bass in Mary Lake, Minnesota. Trans. Am. Fish. Soc. **106**: 323–330.

© 1999 NRC Canada

Migration strategies of young fishes under temporal constraints: the effect of size-dependent overwinter mortality

Daniel E. Schindler

Abstract: Habitat selection by fishes involves balancing the benefits of foraging opportunities and the risk of predation. Size-dependent overwinter mortality imposes a time constraint on behavioral programs of juvenile fishes: individuals must achieve a sufficient size by the end of the growing season to survive. I developed a dynamic optimization model to evaluate how severity of size-dependent overwinter mortality alters habitat use by minnows. The littoral zone was the safest habitat with respect to predation. In lakes where zooplankton exhibit diel vertical migration, fish migrate to the pelagic at night and return to the littoral during the day to maximize foraging rates. Model results demonstrated that size-dependent overwinter mortality should lead to development of more pronounced predation risk-taking by fishes in lakes with severe winters. Individuals are predicted to initiate diel littoral–pelagic migrations at smaller sizes as winter severity increases or as hatch date within a season increases. This analysis suggests that the time constraint imposed by size-selective overwinter mortality has important consequences for life history strategies of juvenile fishes. The effects of time constraints on behavior are expected to be especially important near the high latitudinal limits of a species' geographic distribution.

Résumé : La sélection de l'habitat par les poissons suppose un équilibre entre les avantages des possibilités de recherche de nourriture et le risque de prédation. Chez les poissons, le taux de mortalité hivernale liée à la taille impose une limite de temps aux régimes comportementaux des juvéniles : les individus doivent atteindre une taille suffisante avant la fin de la saison de croissance pour être capables de survivre. J'ai développé un modèle d'optimisation dynamique pour évaluer dans quelle mesure l'ampleur de la mortalité hivernale liée à la taille modifie l'utilisation de l'habitat par les ménés. La zone littorale représentait l'habitat le moins dangereux sur le plan de la prédation. Dans les lacs à migration verticale nycthémérale du zooplancton, les poissons migrent vers la zone pélagique pendant la nuit et reviennent dans la zone littorale pendant le jour pour maximiser le taux de quête de nourriture. Les résultats du modèle ont montré que, dans le cas de mortalité hivernale liée à la taille, les poissons vivant dans les lacs où les hivers sont rigoureux devraient développer des dispositions à prendre plus de risques face à la prédation. On prévoit que les individus entreprendront des migrations nycthémérales zone littorale – zone pélagique à une taille plus petite à mesure que les hivers seront plus rigoureux ou lorsque la date d'éclosion est plus tardive dans la saison. Selon la présente analyse, les limites de temps dues à la mortalité hivernale selon la taille auraient d'importantes conséquences sur les stratégies vitales des juvéniles. Les effets des limites de temps sur le comportement devraient être particulièrement importants à proximité des limites septentrionales de la distribution géographique d'une espèce.

[Traduit par la Rédaction]

Introduction

Fish population dynamics are often driven by early life history success (May 1974; Lasker 1981). Early life history success in turn is often strongly size dependent (Werner and Gilliam 1984; Miller et al. 1988) whereby small differences in growth and mortality processes can have important effects on annual recruitment (Shepherd and Cushing 1980; Houde 1987, 1989; Luecke et al. 1990). Vital rates of young fishes are highly correlated with body size such that larger fish have higher prey capture rates, lower probability of starvation, and decreased vulnerability to predators than smaller individuals (Miller et al. 1988).

In lakes, pelagic and littoral habitats offer different levels of prey availability and refuge from predators for juvenile fishes. Because many physiological and ecological features of juvenile fishes change substantially in their first year of life, the preferred habitats of juvenile fishes often change as they grow through early life stages (Werner and Gilliam 1984). Werner and Gilliam (1984) presented a model to predict ontogenetic habitat shifts in fishes whose body size changes several orders of magnitude over their lifetime. This simple model predicts that foragers should choose habitats that minimize the instantaneous ratio of mortality (μ) to growth rate (g) based on size-specific rules of foraging return and predation vulnerability to maximize their lifetime fitness. This model predicts that foragers will expose themselves to higher risks of predation if their own foraging returns are sufficiently high. Alternatively, "...animals could

Received October 8, 1997. Accepted June 10, 1999.
J14235

D.E. Schindler.[1] Center for Limnology, 680 N. Park Street, Madison, WI 53706, U.S.A.

[1]Present address: Department of Zoology, University of Washington, Box 351800, Seattle, WA 98195, U.S.A.
e-mail: deschind@u.washington.edu

© 1999 NRC Canada

Table 1. Description of parameters used in dynamic optimization model, with units and values used in the simulations presented in this paper.

Parameter	Description	Value	Units
a_m	Exponent of overwinter mortality function	–26.6	None
b_m	Inflection point of overwinter mortality function	Variable	mm
d	Average day length during growing season	15	h
n	Average night length during growing season	9	h
f_i	Intercept of function relating prey density to feeding rate	0.98	None
f_s	Exponent of function relating prey density to feeding rate	0.278	$mg \cdot L^{-1}$
s_s	Slope for size dependency of swimming speed	1.07	s^{-1}
s_i	Intercept for size dependency of swimming speed	1.11	$cm \cdot s^{-1}$
v_e	Exponent for size dependency of predation vulnerability	–2.28	None
v_s	Coefficient for size dependency of predation vulnerability	44.76	None
v_i	Intercept for size dependency of predation vulnerability	3.37	None
δ	Migration distance to switch habitats	50	m
o_l	Proportion of space overlap with predators in littoral habitat	0.19	None
o_p	Proportion of space overlap with predators in pelagic habitat	0.2	None
g_l	Littoral prey density	0.076	$mg \cdot L^{-1}$
g_{pn}	Pelagic prey density during night	0.115	$mg \cdot L^{-1}$
g_{pd}	Pelagic prey density during day	0.053	$mg \cdot L^{-1}$
z	Predator size	170	mm

avoid patches that risk exposure to a predator...[living] in energetically poor habitats...[where] they would grow slowly but live a long time" (Abrahams and Dill 1989). Because this "minimize μ/g" rule is intuitively simple and easily testable, it has been well supported with field and laboratory experiments (reviewed by Lima and Dill 1990). However, one limiting assumption made in the derivation of this model is that reproduction (fitness payoff) is continuous and extends over an infinite time horizon. This assumption ignores the fact that foraging decisions might be subject to time constraints, a phenomenon that is relatively common in many taxa at a variety of time scales (Ludwig and Rowe 1990).

Fish populations often suffer severe overwinter mortality for young-of-the-year stages in temperate and arctic systems. This overwinter mortality generally removes small individuals with low energy reserves (Lindroth 1965; Forney 1966; Chevalier 1973; Oliver et al. 1979; Toneys and Coble 1979; Shuter et al. 1980; Toneys and Coble 1980; Post and Prankevicius 1987; Henderson et al. 1988; Post and Evans 1989; Johnson and Evans 1990, 1991). To survive, young-of-the-year fishes must therefore achieve a threshold size by late fall of their first growing season. Such a time constraint makes a highly conservative strategy of avoiding predators by remaining in refuges with low food availability (Abrahams and Dill 1989) unlikely to be adaptive.

In this study, I use a dynamic optimization model to evaluate how the time constraint imposed by overwinter mortality affects ontogenetic habitat shifts by young-of-the-year minnows. A variety of minnow species are widely distributed throughout North America and represent an important component of many fish communities. Some minnow species (e.g., northern redbelly dace (*Phoxinus eos*) and golden shiner (*Notemigonus crysoleucas*)) exhibit pronounced ontogenetic niche shifts. Newly hatched individuals remain in littoral habitats (e.g., Hall et al. 1979; Hatch 1988) and within their first 2 years of growth usually begin to migrate to pelagic habitats at night to forage on zooplankton and then return to littoral habitats during the daylight (Hall et al. 1979; Naud and Magnan 1988). The model I develop evaluates the effects of predation risk and food availability in littoral and pelagic habitats on the timing of this behavioral shift. I use dynamic programming to impose the time constraint caused by size-dependent overwinter mortality on behavioral decisions by young minnows (Mangel and Clark 1988). My analysis of the effects of time constraints on behavioral programs is analogous to that of Ludwig and Rowe (1990). However, I have focussed the model on the effects of overwinter mortality on early life history characteristics of freshwater fishes, a subject that has not been previously investigated. Specifically, I evaluated how the severity of overwinter mortality affects the size at which juvenile minnows initiate diel littoral–pelagic migrations in lakes. Model results demonstrate that size-dependent overwinter mortality should cause minnows to adopt behavioral strategies that expose them to higher risk of predation by initiating diel migrations at smaller sizes than in the absence of this time constraint.

Model

Dynamic programming is a method of dynamic optimization that allows behavioral programs to be determined in a way that they are sensitive to (1) the fitness payoff that results from a series of short-term behavioral decisions, and (2) time constraints on achieving that fitness payoff (Mangel and Clark 1988; Mangel and Ludwig 1992). In this model-

© 1999 NRC Canada

Fig. 1. Scaling of size-dependent processes accounted for in the dynamic optimization model. All rates are shown relative to the rate at hatching. Consumption (C) and respiration (R) rates are mass specific ($g \cdot g^{-1} \cdot day^{-1}$) (Post 1990), swimming speed is in units of $cm \cdot s^{-1}$, and the size component of vulnerability to predation (PV) is calculated assuming a 170-mm-long predator (Miller et al. 1988).

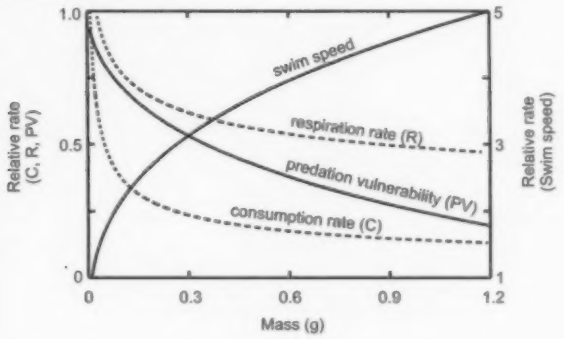

ing framework, short-term behavioral decisions are dependent on the current state (e.g., physiological condition) of the organism that is accounted for by a state variable $X(t)$ (Mangel and Clark 1988). Here, I use body mass as the state variable in the model. Body mass has important effects on the physiology and ecology of fishes, especially of juveniles, which change several orders of magnitude in size during their first year of life (Werner and Gilliam 1984; Miller et al. 1988).

I use the dynamic programming algorithm presented by Mangel and Clark (1988) to evaluate the ontogeny of littoral–pelagic migrations in juvenile minnows. Wherever possible, I have used the notation of Mangel and Clark (1988) in describing my model. A thorough description of the derivation and mechanics of dynamic programming is found in Mangel and Clark (1988).

The model I present accounts for the trade-offs between risk of predation, foraging success, and energetic costs associated with different behavioral strategies (i). The parameters used to describe the behavioral strategies are (1) α_i, the energetic cost per time period of choosing strategy i, (2) β_i, the probability of predation per time period if strategy i is chosen, (3) λ_i, the probability of feeding per time period if strategy i is chosen, and (4) Y_i, the increment in the state variable (mass) if strategy i is chosen and food is encountered. The dynamic programming algorithm uses a lifetime fitness function $F(x,t,T)$ to describe mathematically the "maximum value of the probability that the forager survives from period t to period T, given that at period t the forager is alive, and the value of the state variable $X(t)$ is x" (Mangel and Clark 1988).

The general form of the dynamic programming algorithm is written

$$(1) \quad F(x,t,T) = \max(1-\beta_i)[\lambda_i F(x_i', t+1, T) + 1 - \lambda_i) F(x_i'', t+1, T)]$$

where the state variable $X(t+1)$ takes one of two values determined by whether the forager finds food (with probability λ_i) or does not feed (with probability $1 - \lambda_i$) according to

$$(2) \quad x_i' = (x - \alpha_i + Y_i)$$

$$x_i'' = (x - \alpha_i)$$

Therefore, x_i' describes the value of the state variable if the forager finds food (i.e., current mass – energetic costs + increment in mass from feeding) and x_i'' describes the value of the state variable if the forager does not find food (i.e., current mass – energetic costs). Thus, the maximum probability of surviving from time t to the end (T) is the product of (1) the probability of surviving predation in time period t $(1 - \beta_i)$ and (2) the expected future value of the fitness function at time $t + 1$. This expected future value of the fitness function integrates across all events that affect the fitness function between $t + 1$ and T. As a result, the behavioral decision at time t is a function of both the temporal proximity to the time of fitness payoff (T) and the current state of the organism $X(t)$. Given a possible end state of the organism at time T, the optimal behavioral program is obtained by a straightforward iterative procedure that runs backward in time from $t = T$ to $t = 1$ (the day of hatch).

Characterization of behavioral strategies (i)

I assumed that young minnows perform one of four behavioral strategies (i) to distribute themselves between littoral and pelagic habitats during the daylight and night. In the first strategy, minnows remain in the littoral zone for the entire 24-h day. In the second strategy, minnows are dispersed throughout the pelagic habitat for the entire day. In the third strategy, minnows are located in the littoral zone during the daylight, migrate offshore to the pelagic habitat at night, and return to the littoral zone at dawn. The fourth strategy involves moving to the littoral zone at night and back to the pelagic habitat during the daylight. Each of these four strategies involves alternative costs and benefits. The benefits of choosing a given behavioral pattern are manifest in feeding rate, while the costs are associated with the risk of predation and the energetic costs of migrating between habitats. The rules that describe the characteristics of behavioral strategies change as a function of the size of the organism (Fig. 1).

Risk of predation of strategy i (β_i)

Total risk of predation in any one time period in strategy i (β_i) was calculated as

$$(3) \quad \beta_i = \text{overlap}_i \times \text{capture success} \times \text{pred}$$

where overlap_i accounts for the spatial and temporal overlap of juvenile minnows and their predators in strategy i, capture success is a function to describe the ability of predators to capture juvenile minnows once they have encountered each other, and pred is a parameter to vary the encounter rate between predators and juvenile minnows (Table 1). The parameter overlap_i was set such that littoral habitat represented a predation refuge compared with the pelagic habitat. Behavioral strategies that involved migration between these two habitats used a value of overlap_i that was weighted for the fraction of each day that the juvenile minnows spent in each of the habitats. Capture success was modeled according to Miller et al. (1988) as dependent on the ratio of predator length to prey length according to

$$(4) \quad \text{Capture success} = 100 - ((\text{ratio} + 3.37)/44.76)^{-2.28}$$

© 1999 NRC Canada

Table 2. Parameters used in the bioenergetics model of growth, respiration, and consumption by juvenile fishes (from Post 1990).

Parameter	Description	Value	Units
CA	Intercept of mass dependency of maximum consumption rate	0.51	$g^{-1} \cdot day^{-1}$
CB	Slope of mass dependency of maximum consumption rate	–0.42	None
CTO	Optimum temperature for consumption	29	°C
CTM	Maximum temperature for consumption	32	°C
CQ	Slope of temperature dependency of consumption	2.3	None
RA	Intercept for standard respiration	0.035	$g^{-1} \cdot day^{-1}$
RB	Slope for standard respiration	–0.20	None
RTO	Optimum temperature for standard respiration	32	°C
RTM	Maximum temperature for standard respiration	35	°C
RQ	Slope of temperature dependence of maximum respiration	2.1	None
ACT_1	Active respiration multiplier	4.4	None
ACT_2*	Enhanced respiration multiplier during migration	8	None
SDA	Cost of specific dynamic action	0.15	None
U	Cost of excretion	0.15	None
F	Cost of egestion	0.15	None

*Additional parameter added to the Post (1990) bioenergetics model for this study.

where ratio is the ratio of the average predator length over the minnow body length. For all simulations presented in this paper, I set the predator length to 170 mm. Therefore, as juvenile minnows get larger, they outgrow their vulnerability to predators (Fig. 1). I used the relationship wet mass = $4.475 \times 10^{-6} \times \text{length}^{3.147}$ (where length is in millimetres and mass is in grams, D.E. Schindler, unpublished data) to relate minnow mass to total length throughout the simulations.

Energetic cost of strategy *i* (α_i)

I divided the energetic costs for minnows choosing each of the behavioral strategies into two components. The first component described the energetic costs of routine metabolism. This metabolic cost is associated with respiration (which includes the costs of routine activity), energetic costs of digestion (which depend on the feeding rate), excretion, and fecal losses. Fecal losses, excretion losses, and cost of digestion were each calculated as 0.15 of consumed mass (Post 1990) (Table 2).

I modeled total respiration (grams per gram per day) as

$$\text{(5)} \quad \text{Respiration} = 0.035 \times \text{mass}^{-0.2} \times \text{activity}$$

where mass is in grams wet mass (Post 1990). I accounted for the costs of activity for a nonmigrating juvenile minnow by setting activity to 4.4 (Post 1990). The cost associated with migrating between habitats was added to the activity multiplier in eq. 5 in proportion to the time required for the minnow to switch habitats, which was inversely related to its swimming speed:

$$\text{(6)} \quad \log_{10}\text{speed} = 1.07 \log_{10}\text{length} - 1.11$$

where length is in millimetres and swim speed is in centimetres per second (Miller et al. 1988). Therefore, the activity multiplier in eq. 5 was incremented by the proportion of each 24-h period that the fish was involved in migration between habitats times a multiplier of basal respiration to describe the enhanced respiration rate due to migration activity. The proportion of each day spent migrating between habitats was calculated as the distance between habitats divided by the swimming speed and then multiplied by 2. Because respiration rates of young fishes increase sharply with increases in swimming speed (Dabrowski et al. 1988), I assumed that respiration of migrating minnows equaled eight times their basal respiration rate. Total respiration was rescaled to account for temperature dependence according to Kitchell et al. (1977). In all simulations presented here, I assumed that juvenile minnows experienced a constant 23°C environment and that temperature differences between littoral and pelagic habitats are negligible. Small temperature differences (i.e., 1–3°C) can develop between littoral and pelagic habitats during the day in some lakes (e.g., James and Barko 1991). Although these temperature gradients cause diurnal, convective circulation between littoral and pelagic habitats (MacIntyre and Melack 1995), I have not included any physical mixing processes in the model I describe here because I have assumed that young fishes can control their spatial positions within the weak currents that develop from this type of circulation. I have also assumed that the small temperature differences between littoral and pelagic habitats are not important to the behavior of juvenile minnows. Instead, I assumed that habitat choices are based entirely on differences in feeding potential and vulnerability to predators in different habitats.

Daily increment in state variable of strategy *i* (Y_i)

The state variable, body mass ($X(t)$), was incremented through prey consumption. I used the consumption model of Post (1990) to account for the allometric and temperature scaling of feeding rates by juvenile fish. Maximum possible consumption rate (grams prey per gram predator per day) was modeled as

$$\text{(7)} \quad \text{Maximum consumption} = 0.51 \times \text{mass}^{-0.42}$$

which was then adjusted to a 23°C environment according to the method of Kitchell et al. (1977). Post (1990) presented a saturating function to relate the realized consumption rate of juvenile fish to the density of their zooplankton prey. This function is expressed in units of the proportion of the maximum consumption rate (P). I adjusted the intercept of this

© 1999 NRC Canada

Fig. 2. Size-dependent overwinter mortality of juvenile golden shiner in Peter Lake, Michigan, over the 1991–1992 winter. Minnows were captured with trap nets on October 1, 1991, and on May 18, 1992. I measured 300 individuals on each sampling date. Growth was negligible during this time period due to low water temperatures. All length measurements were taken to the nearest millimetre of total length. Only young-of-year are shown. A sigmoid function (eq. 10) was fit by nonlinear least squares to describe this relationship (R^2 = 0.98). Parameter values for eq. 10 were a = 26.1 mm (SE = 6.2) and b = 47.8 mm (SE = 0.4).

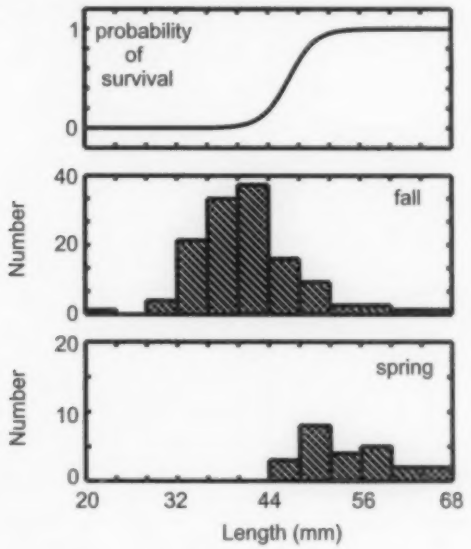

function to make the range of growth rates predicted by the model overlap with the range of growth rates of juvenile minnows observed in northern Wisconsin lakes (D.E. Schindler, unpublished data). The modified function was

$$(8) \qquad P = 0.98 \times \text{food}^{0.278}$$

where food is the density of prey (milligrams dry mass per litre) experienced by the predator.

Minnows migrate to pelagic habitats at night to capitalize on the upward migration of zooplankton into the surface water of lakes (Hall et al. 1979; Naud and Magnan 1988). Minnows have the ability to filter-feed (Ehlinger 1989), so I assumed that nocturnal feeding rates were not limited by nighttime light intensity. Habitats may differ greatly in their relative profitability (e.g., Werner et al. 1983), but these relative profitabilities are extremely difficult to assess due to the problems associated with determining prey availability to predators, especially in benthic habitats (Ware 1973). Therefore, I took a parsimonious approach and assumed that littoral and pelagic habitats had the same mean profitability but that the two habitats differed only in the temporal availability of prey. I assumed that littoral prey were equally available throughout all 24-h periods. I simulated diel vertical migration of zooplankton in the pelagic habitat by increasing prey availability at night and decreasing it during the day. Therefore, foraging rate of an individual in this model is maximized by feeding offshore at night when zooplankton are abundant and foraging inshore during the day. For all

Fig. 3. Possible variation in the size-dependent overwinter mortality functions to describe the terminal fitness function ($\phi(x)$) in the dynamic optimization model. The broken curve represents the function fitted to the overwinter mortality of golden shiner in Peter Lake, Michigan, shown in Fig. 2.

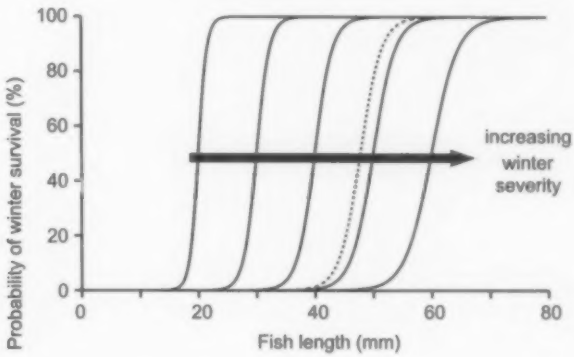

simulations in this paper, I used values of food representative of zooplankton concentrations in northern Wisconsin lakes (Carpenter and Kitchell 1993). I assumed food for the pelagic habitat had a value of 0.053 (milligrams dry mass per litre) at daytime and a value of 0.115 during the night. In the littoral habitat, food was assigned a value of 0.076 for the entire 24-h period. Although the model ignores many complexities associated with the value of different habitats to foraging fish, it gives a reasonable first approximation for describing different habitats.

I assumed that the probability of finding food in any of the strategies was proportional to the relative net energy gain that resulted from choosing that strategy. Therefore, λ_i from eq. 1 was calculated as

$$(9) \qquad \lambda_i = \frac{(Y_i - \alpha_i)}{(Y - \alpha)_{\max}}$$

where $(Y - \alpha)_{\max}$ is the maximum energetic increment possible among the four behavioral options at time period t. Thus, for the energetically most profitable habitat, λ_i = 1.

Terminal fitness function

This model simulates habitat use by minnows through their first growing season. I assume that these fish are not capable of reproducing in their first summer of life. I also assume that behavioral decisions in the first growing season are made with size-dependent, overwinter survival as the long-term fitness payoff (Figs. 2 and 3). Size-dependent overwinter mortality was modeled as a sigmoid relationship according to

$$(10) \qquad P(\text{mortality}) = (1 + e^{a})/(1 + e^{[a(1-\text{length}/b)]})$$

where parameter a was fit to the data from Peter Lake in northern Wisconsin (Carpenter and Kitchell 1993) (Fig. 2) and parameter b was treated as a variable that took on values between 20 and 60 mm (see Model results). Parameter b can be viewed as a size threshold below which the probability of overwinter mortality is very high. Therefore, large values of

© 1999 NRC Canada

Fig. 4. Data output from a typical model run. The mass and fitness increase to a maximum at time *T*. Juvenile minnows are predicted to remain in the littoral zone until they reach a mass of 275 mg on day 27, at which point they begin to perform diel onshore–offshore migrations. This behavioral switch is illustrated by the step in the solid line. For this example, mass at the end of the growing season was 1000 mg, predation intensity (pred) was 1, and the overwinter size threshold (*b*) was 40 mm.

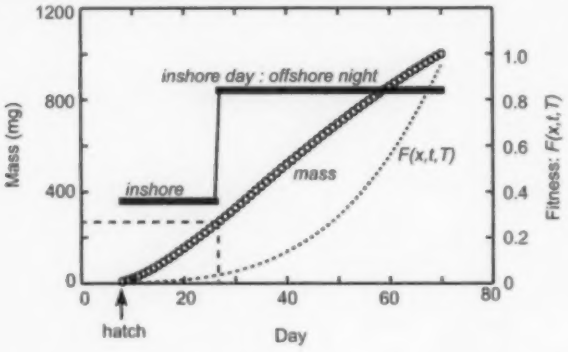

b reflect winters with high severity (e.g., long duration), and low values of *b* reflect mild or short-duration winters (Fig. 3). The terminal fitness function $\phi(x)$ was defined as 1 – *P*(mortality) and represents the payoff associated with making a defined series of behavioral decisions (i.e., a behavioral program). The terminal fitness function is employed in the dynamic programming algorithm by equating $F(x,t,T)$ to $\phi(x)$ in eq. 1 (Mangel and Clark 1988).

I ran model simulations to evaluate interactions between the intensity of predation, winter severity, and mass at the terminal time period (*T*) in determining the timing of the initiation of onshore–offshore migrations by juvenile minnows. Winter severity was varied by systematically changing parameter *b* (eq. 10) from 20 to 60 mm. The mass of minnows at the terminal time period (*T*) was systematically varied between values of 200 and 1400 mg. Fifty combinations of the mass at the terminal time period and winter severity were run at four levels of predation intensity, which was altered by setting values of pred (eq. 3) to 0.1, 1, 3, and 5. For all strategies, I assumed that the length of daylight is 15 h and the length of night is 9 h. For all results presented in this paper, I ran the model at a 1-day time step.

Model results

The dynamic optimization model predicted that only two of the four possible behavioral strategies were ever considered the best migration strategy. In all simulations, juvenile minnows were predicted to remain in the littoral zone for the entire 24-h day immediately after hatching. At an older stage, juvenile minnows began to migrate offshore at night and inshore during the day (Fig. 4). I will refer to the mass where minnows begin to perform diel littoral–pelagic migrations as the "mass-at-migration." The model predicted that juvenile minnows initiate littoral–pelagic migrations at masses between 180 and 350 mg.

Winter severity, hatch date, and predation intensity all had substantial effects on mass-at-migration (Fig. 5). Model results also demonstrated strong interactions between these three variables in altering mass-at-migration. Increased predation intensity increased mass-at-migration for all possible combinations of hatch date and winter severity. Mass-at-migration decreased with increasing winter severity, especially in low-predation environments. Thus, juvenile minnows are predicted to evolve behaviors that expose them to greater predation risks (i.e., move out of littoral zone refuges at smaller sizes) when the probability of overwinter mortality is high.

In low-predation environments, hatch date interacted strongly with winter severity to alter mass-at-migration. When winters were severe (i.e., the front edge of Figs. 5A and 5B), minnows initiated offshore migrations at smaller sizes as hatch date increased. However, when winters were mild (i.e., back edge of Figs. 5A and 5B), minnows initiated offshore migrations at larger sizes as hatch date increased. In contrast, the model predicted that under extremely high predation intensity, mass-at-migration is insensitive to winter severity and hatch date and that initiation of offshore migrations largely occurs when minnows have grown out of their vulnerable sizes. At predation intensities greater than that shown in Fig. 5, the model predicted that minnows would evolve behaviors whereby they remain in the littoral zone for their entire first year.

For all of the simulation results I have presented in this paper, I have assumed that the temperature experienced by young fishes is a constant 23°C. I ran an additional set of model simulations to evaluate the effects of a seasonal temperature regime on the model predictions of the mass-at-migration. Model simulations with a constant temperature were compared with those run with a seasonal temperature regime characteristic of the changes in epimnetic temperatures from northern Wisconsin lakes. For this comparison, mass-at-migration was calculated across a range of winter severity (i.e., by varying *b* from 20 to 60 mm), with pred = 1 and the mass at $t = T$ set to 1000 mg. The model results showed a weak but interesting interaction between the winter severity and thermal seasonality with the predicted mass-at-migration. For relatively severe winters ($b > 50$ mm), seasonality had less than a 5% effect on the mass-at-migration for young fishes: severe winters always caused fishes to initiate migrations at small sizes (e.g., Fig. 5). For relatively mild winters ($b < 50$ mm), mass-at-migration was reduced by 10% in a seasonal environment from that predicted from a constant thermal environment, but the effect on mass-at-migration was weaker than that of winter severity. This predicted decrease in the mass-at-migration for seasonal environments reflects the decreased growth capacity of fishes during autumn cooling. Taken together, these model results reinforce the prediction that increased winter severity should cause fishes to develop risk-prone behaviors and that fishes may become more risk sensitive in systems with decreased winter severity.

Discussion

Habitat selection by juvenile fishes is often dependent on the risk associated with predation and profitability for growth in alternative habitats. In many cases, habitat selection that minimizes the ratio of the instantaneous predation

© 1999 NRC Canada

Fig. 5. Effects of winter severity and hatch date on the mass (mg) when juvenile minnows initiate diel littoral–pelagic migrations. Panels A–D are ordered with increasing predation intensity (pred reflects the relative predation intensity experienced by minnows (eq. 3)). Winter severity corresponds to the value of b in eq. 10, which is the threshold below which juvenile minnows are too small to survive the winter. Large values of winter severity therefore represent winters with long duration, and small values represent short-duration winters. Hatch date refers to the number of days after June 1.

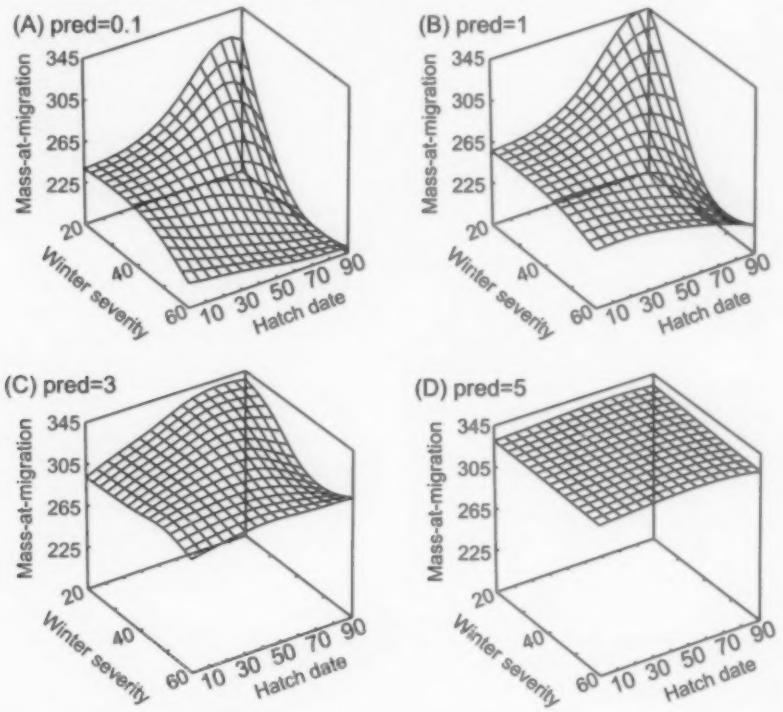

risk to foraging profitability appears to be an adaptive behavior in fishes (Werner and Gilliam 1984; Gilliam and Fraser 1987; Lima and Dill 1990). The results of the model presented in this paper demonstrate that time constraints imposed by size-dependent overwinter mortality alter the balance in trade-offs between avoiding predators and maximizing growth rate. Although I have not explicitly evaluated the ratio of μ/g (sensu Werner and Gilliam 1984), I have modeled behavioral decisions based on a trade-off between the expected net energetic return and the expected probability of predation in a common currency that links short-term behavioral decisions to long-term fitness (McNamara and Houston 1986). The important result that derives from dynamic programming is that predation risk-taking by juvenile fish should be sensitive to both the expected fitness payoff of a given behavioral program (i.e., probability of overwinter survival) and the temporal proximity to the payoff period (i.e., end of the growing season). It is important to note that this analysis does not require that individual fish have perfect knowledge of expected fitness payoffs, but rather that life history strategies will evolve in a manner adaptive to local conditions (Stearns 1993). For example, rapid evolution of reproductive effort and timing in response to altered predation regimes has been documented for guppies (Reznick et al. 1990). Also, Conover and colleagues (Conover 1992; Present and Conover 1992; Schultz and Conover 1997) have shown that growth potential and allocation of energy to somatic storage prior to winter increase with latitude for estuarine Atlantic silverside (*Menidia menidia*) along the east coast of North America. These genetic and physiological changes are apparently adaptive responses to changes in the time constraints imposed by the length of the growing season and the severity of size-dependent overwinter mortality along this latitudinal gradient (Conover 1992). Although I am unaware of any documented cases of the effects of time constraints on ontogenetic niche shifts or maturation in fishes, spadefoot toad larvae metamorphose at smaller sizes and younger ages in desert pools of short duration than in pools of long duration (reviewed by Stearns et al. 1991). Interestingly, *M. menidia* from a high-latitude population consumed substantially more food than individuals from southern populations, when reared in the same environment (Present and Conover 1992), suggesting that evolution of foraging behaviors may also respond to latitudinal variation in climate. Thus, life history strategies in fishes are probably responsive to a variety of changing environmental conditions. The time constraint imposed by size-selective overwinter mortality is one of these potentially important selection pressures that will vary among lakes depending on local climate conditions that change with latitude and elevation.

Two specific and testable hypotheses concerning timing of ontogenetic habitat selection by juvenile fishes derive from the model results. These hypotheses address the variation in

© 1999 NRC Canada

ontogenetic niche shifts as a function of winter severity among lakes and as a function of hatch date within lakes. First, in lakes where size-dependent overwinter mortality is an important mechanism that regulates survival of juvenile fishes, individuals that are hatched late in the growing season should take greater predation risks than those hatched early in the growing season (Fig. 5). Ontogenetic habitat switches should therefore occur at smaller sizes for fishes that are hatched late than for those that are hatched early. Thus, the magnitude of the difference in mass-at-migration due to hatching date will be inversely related to predation intensity.

The model predicted that individual behaviors become more sensitive to predation risks when size-dependent overwinter mortality is low. In fact, model simulations that incorporated low winter mortality predicted that early-hatched individuals took larger predation risks than those that were hatched late (i.e., early-hatched individuals "switched" at smaller sizes than late-hatched individuals). This result was produced because the dynamic programming algorithm imposes a risk of starvation in predation refuges that occurs with probability $1 - \lambda_i$ (eq. 1). Therefore, individuals that have high fitness close to the payoff time (T) are expected to develop safe behaviors (Ludwig and Rowe 1990). This result is due to the assumption that overwinter survival is the ultimate fitness payoff. A more realistic elaboration of my model would include an expected reproductive output in adult stages by sequentially coupling adult stages to the juvenile model that I have presented (Mangel and Clark 1988). By elaborating the model in this manner, the response surfaces in Fig. 5 would lose the peaks found at low values of winter severity and late hatching dates. However, for lakes with severe winters, the results would not change, as surviving the first winter is a major fitness bottleneck in the populations (Shuter et al. 1980; Henderson et al. 1988; Post and Evans 1989).

The second hypothesis derived from this model is that timing of ontogenetic habitat shifts in minnows should vary among systems depending on winter severity. Specifically, juvenile fishes should demonstrate behaviors that put them at higher risk to predation in lakes with severe winters than in those with mild winters. Winter severity is related to a variety of environmental parameters that are generally correlated with latitude (Shuter et al. 1980). Therefore, ontogenetic habitat shifts should occur at smaller sizes for individuals from populations at high latitudes (especially near the high-latitude edges of geographic ranges) if predation risk and relative habitat profitability are otherwise similar. These two hypotheses concerning the expected changes in foraging strategies with increases in latitude build on the important observation that growth rate potential increases with latitude in some fishes (Conover 1992). In this model analysis, I have evaluated the interaction between the risk of overwinter mortality and the risk of predation in shaping the life history strategies of young fishes. Given that predator-sensitive foraging is so common in fishes (e.g., Werner and Gilliam 1984; Lima and Dill 1990), future empirical research on the latitudinal changes of life history strategies in fishes should account for interactions between the constraints imposed on fishes by their predators and the time constraints imposed by overwinter starvation.

Model limitations

The model that I have presented greatly simplifies the interactions between predator avoidance, foraging, and habitat choice in juvenile minnows. For example, I assumed that there was no density dependence in foraging returns among juvenile fishes. This assumption may not be valid when juvenile fishes forage in very small habitat volumes where prey are easily depleted (Walters and Juanes 1993). The fact that the model never predicted the entirely pelagic behavioral strategy as the best decision may reflect the lack of density dependence in the littoral habitat. Fish species whose larvae spend their early life history in pelagic habitats (e.g., *Lepomis* and *Perca* species) may have evolved this strategy as a mechanism to avoid density dependence in restricted littoral refuges (Walters and Juanes 1993). Therefore, although littoral refuges may provide shelter from predators, growth potential may not be as great due to intense intracohort competition in refuges. Linking a population model that included feedbacks between predator consumption and prey availability to the model presented here might identify critical population phenomena that lead to the pelagic larval life history strategy.

In formulating this model, I only considered the fitness and behavioral decisions of the juvenile (prey) fish. An alternative approach would have been to use a frequency-dependent approach where predator behaviors are dependent on the behavior of their prey and vice versa (Hugie and Dill 1994). However, because predation risk detection by minnows is largely via chemical communication (Brown et al. 1995), predator avoidance behaviors by juvenile minnows may largely be threshold responses to the mere presence of predators (He and Kitchell 1990). Therefore, behavioral responses by minnow populations may be reasonably simulated without invoking frequency-dependent behavioral programs. The differences in responses of young fishes to various levels of predation depicted in Fig. 5 can, therefore, be thought of as the differences in response to the presence of predators that are a product of long-term selection pressures due to predation.

Implications of refuging behavior

Risk-sensitive behavior by juvenile minnows may have important effects on other components of lake food webs and ecosystem processes. For example, prey fish that respond to predators by remaining in littoral refuges may reduce predation pressure on open-water zooplankton communities (Turner and Mittelbach 1990). Changes in timing of when dominant cohorts of juvenile fishes change habitats or migration strategies may also have important implications for the seasonal timing of zooplankton dynamics in lakes. Therefore, timing of ontogenetic niche shifts by minnows has important implications for food web interactions in plankton communities. Refuging behavior by juvenile fishes may also make them more susceptible to parasite-induced mortality (Brabrand et al. 1994), thereby further reducing their potential to have long-term effects on pelagic communities.

Migrating fishes may also alter the spatial and temporal patterns of nutrient recycling in lakes (Schindler 1995; Vanni 1995). Therefore, ontogenetic niche shifts by minnows may cause changes in the patterns of nutrient recycling experi-

© 1999 NRC Canada

enced by pelagic phytoplankton. Because fishes that migrate between pelagic and littoral habitats represent an important component of littoral–pelagic coupling in lakes (Lodge et al. 1988), processes that alter these behaviors also potentially alter littoral–pelagic links in lakes. My analyses demonstrate that the time constraints imposed by size-dependent overwinter mortality on young fishes may reinforce the strength of littoral–pelagic links in temperate lake ecosystems by causing juvenile fishes to engage in strong littoral–pelagic migrations at early stages in their lives.

Given the genetic variability and phenotypic plasticity of life history characteristics of many fish species (Policansky 1983), we should expect that life history strategies within fish species or closely related groups of fishes will vary seasonally and with local environmental factors. I argue that minnows and other fishes in north-temperate ecosystems should evolve behaviors that are adaptive to the time constraints imposed by size-dependent overwinter mortality. As a result, we should expect some of the variation, with respect to geographic location, in life history characteristics of fishes to be due to the indirect effects that seasonally extreme environments have on organism behaviors.

Acknowledgments

I am thankful to S. Carpenter, J. Kitchell, C. Madenjian, L. Rudstam, and R. Wright for help in development of the model and to S. Arnott, S. Carpenter, T. Essington, J. Fischer, A. Ives, and J. Kitchell for helpful reviews of this manuscript. I am grateful to S. Brandt and D. Mason for the opportunity to participate in the special symposium focussed on spatial processes in fish ecology. Support for this work was provided by a Natural Sciences and Engineering Research Council of Canada graduate fellowship and grants from the NSF to J. Kitchell and S. Carpenter.

References

Abrahams, M.V., and Dill, L.M. 1989. A determination of the energetic equivalence of the risk of predation. Ecology, **70**: 999–1007.

Brabrand, Å, Bakke, T.A., and Faafeng, B.A. 1994. The ectoparasite *Ichthyophthirius multifiliis* and the abundance of roach (*Rutilis rutilis*): larval fish epidemics in relation to host behaviour. Fish. Res. **20**: 49–61.

Brown, G.E., Chivers, D.P., and Smith, R.J.F. 1995. Fathead minnows avoid conspecific and heterospecific alarm pheromones in the faeces of northern pike. J. Fish Biol. **47**: 387–393.

Carpenter, S.R., and Kitchell, J.F. (*Editors*). 1993. The trophic cascade in lakes. Cambridge University Press, Cambridge, U.K.

Chevalier, J.R. 1973. Cannibalism as a factor in first year survival of walleye in Oneida Lake. Trans. Am. Fish. Soc. **102**: 739–744.

Conover, D.O. 1992. Seasonality and the scheduling of life history at different latitudes. J. Fish Biol. **41**(Suppl. B): 161–178.

Dabrowski, K., Takashima, F., and Law, Y.K. 1988. Bioenergetic model of planktivorous fish feeding, growth and metabolism: theoretical optimum swimming speed of fish larvae. J. Fish Biol. **32**: 443–458.

Ehlinger, T.J. 1989. Foraging mode switches in the golden shiner (*Notemigonus crysoleucas*). Can. J. Fish. Aquat. Sci. **46**: 1250–1254.

Forney, J.L. 1966. Factors affecting first-year growth of walleyes in Oneida Lake, New York. N.Y. Fish Game J. **13**: 146–167.

Gilliam, J.F., and Fraser, D.F. 1987. Habitat selection under predation hazard: test of a model with foraging minnows. Ecology, **68**: 1856–1862.

Hall, D.J., Werner, E.E., Gilliam, J.F., Mittelbach, G.G., Howard, D., Doner, C.G., Dickerman, J.A., and Stewart, A.J. 1979. Diel foraging behavior and prey selection in the golden shiner (*Notemigonus crysoleucas*). J. Fish. Res. Board Can. **36**: 1029–1039.

Hatch, J.T. 1988. Ontogenetic shifts in feeding habits of mixed cohort schools of larval golden shiners. Ver. Theor. Angew. Limnol. Verh. **23**: 1704–1709.

He, X., and Kitchell, J.F. 1990. Direct and indirect effects of predation on a fish community: a whole lake experiment. Trans. Am. Fish. Soc. **119**: 825–835.

Henderson, P.A., Holmes, R.H.A., and Mamber, R.N. 1988. Size-related overwintering mortality in the sand smelt, *Atherina boyeri* Risso, and its role in population regulation. J. Fish Biol. **33**: 221–233.

Houde, E.D. 1987. Fish early life dynamics and recruitment variability. Am. Fish. Soc. Symp. **2**: 17–29.

Houde, E.D. 1989. Comparative growth, mortality, and energetics of marine fish larvae: temperature and implied latitudinal effects. Fish. Bull. U.S. **87**: 471–495.

Hugie, D.M., and Dill, L.M. 1994. Fish and game: a game theoretic approach to habitat selection by predators and prey. J. Fish Biol. **45**(Suppl. A): 151–169.

James, W.F., and Barko, J.W. 1991. Estimation of phosphorus exchange between littoral and pelagic zones during nighttime convective circulation. Limnol. Oceanogr. **36**: 179–187.

Johnson, T.B., and Evans, D.O. 1990. Size dependent winter mortality of young-of-the-year white perch: climate warming and invasion of the Laurentian Great Lakes. Trans. Am. Fish. Soc. **119**: 301–313.

Johnson, T.B., and Evans, D.O. 1991. Behaviour, energetics, and associated mortality of young-of-the-year white perch (*Morone americana*) and yellow perch (*Perca flavescens*) under simulated winter conditions. Can. J. Fish. Aquat. Sci. **48**: 672–680.

Kitchell, J.F., Stewart, D.J., and Weininger, D. 1977. Application of a bioenergetic model to yellow perch (*Perca flavescens*) and walleye (*Stizostedion vitreum vitreum*). J. Fish. Res. Board Can. **34**: 1922–1935.

Lasker, R. 1981. Marine fish larvae. University of Washington Press, Seattle, Wash.

Lima, S.L., and Dill, L.M. 1990. Behavioral decisions under the risk of predation: a review and prospectus. Can. J. Zool. **68**: 619–640.

Lindroth, A. 1965. First winter mortality of Atlantic salmon parr in the hatchery. Can. Fish Cult. **36**: 23–26.

Lodge, D.M., Barko, J.W., Strayer, D., Melack, J.M., Mittelbach, G.G., Howarth, R.W., Menge, B., and Titus, J.E. 1988. Spatial heterogeneity and habitat interactions in lake communities. *In* Complex interactions in lake communities. *Edited by* S.R. Carpenter. Springer-Verlag, New York. pp. 181–208.

Ludwig, D., and Rowe, L. 1990. Life-history strategies for energy gain and predator avoidance under time constraints. Am. Nat. **135**: 686–707.

Luecke, C., Rice, J.A., Crowder, L.B., Yeo, S.E., and Binkowski, F.P. 1990. Recruitment mechanisms of bloater in Lake Michigan: an analysis of the predatory gauntlet. Can. J. Fish. Aquat. Sci. **47**: 524–532.

MacIntyre, S., and Melack, J.M. 1995. Vertical and horizontal transport in lakes: linking littoral, benthic, and pelagic habitats. J. North Am. Benthol. Soc. **14**: 599–615.

© 1999 NRC Canada

Mangel, M., and Clark, C.W. 1988. Dynamic modeling in behavioral ecology. Princeton University Press, Princeton, N.J.

Mangel, M., and Ludwig, D. 1992. Definition and evaluation of the fitness of behavioral and development programs. Annu. Rev. Ecol. Syst. **23**: 507–536.

May, R.C. 1974. Larval mortality in marine fishes and the critical period concept. *In* The early life history of fish. *Edited by* J.H.S. Blaxter. Springer-Verlag, New York. pp. 3–19.

McNamara, J.M., and Houston, A.I. 1986. The common currency for behavioral decisions. Am. Nat. **127**: 358–378.

Miller, T.J., Crowder, L.B., Rice, J.A., and Marschall, E.A. 1988. Larval size and recruitment mechanisms in fishes: toward a conceptual framework. Can. J. Fish. Aquat. Sci. **45**: 1657–1670.

Naud, M., and Magnan, P. 1988. Diel onshore–offshore migrations in northern redbelly dace, *Phoxinus eos* (Cope), in relation to prey distribution in a small oligotrophic lake. Can. J. Zool. **66**: 1249–1253.

Oliver, J.D., Holeton, G.F., and Chua, K.E. 1979. Overwinter mortality of fingerling smallmouth bass in relation to size, relative energy stores, and environmental temperatures. Trans. Am. Fish. Soc. **108**: 130–136.

Policansky, D. 1983. Size, age and demography of metamorphosis and sexual maturation in fishes. Am. Zool. **23**: 57–63.

Post, J.R. 1990. Metabolic allometry of larval and juvenile yellow perch (*Perca flavescens*): in situ estimates and bioenergetic models. Can. J. Fish. Aquat. Sci. **47**: 554–560.

Post, J.R., and Evans, D.O. 1989. Size-dependent overwinter mortality of young-of-the-year yellow perch (*Perca flavescens*): laboratory, in situ enclosure, and field experiments. Can. J. Fish. Aquat. Sci. **46**: 1958–1968.

Post, J.R., and Prankevicius, A.B. 1987. Size-selective mortality in young-of-the-year yellow perch (*Perca flavescens*): evidence from otolith microstructure. Can. J. Fish. Aquat. Sci. **44**: 1840–1847.

Present, T.M.C., and Conover, D.O. 1992. Physiological basis of latitudinal growth differences in *Menidia menidia*: variation in consumption or efficiency? Funct. Ecol. **6**: 23–31.

Reznick, D.A., Bryga, H., and Endler, J.A. 1990. Experimentally induced life-history evolution in a natural population. Nature (Lond.), **346**: 357–359.

Schindler, D.E. 1995. The role of fishes in littoral–pelagic coupling in lakes. Dissertation, University of Wisconsin-Madison, Madison, Wis.

Schultz, E.T., and Conover, D.O. 1997. Latitudinal differences in somatic energy storage: adaptive responses to seasonality in an estuarine fish (Atherinidae: *Menidia menidia*). Oecologia, **109**: 516–529.

Shepherd, J.G., and Cushing, D.H. 1980. A mechanism for density-dependent survival of larval fish as the basis of a stock–recruitment relationship. J. Cons. Cons. Int. Explor. Mer, **39**: 160–167.

Shuter, B.J., MacLean, J.A., Fry, F.E.J., and Regier, H.A. 1980. Stochastic simulation of temperature effects on first-year survival of smallmouth bass. Trans. Am. Fish. Soc. **109**: 1–34.

Stearns, S.C. 1993. The evolution of life histories. Oxford University Press, Oxford, U.K.

Stearns, S.C., de Jong, G., and Newman, R. 1991. The effects of phenotypic plasticity on genetic correlates. Trends Ecol. Evol. **6**: 122–126.

Toneys, M.L., and Coble, D.W. 1979. Size-related first winter mortality of freshwater fishes. Trans. Am. Fish. Soc. **108**: 415–419.

Toneys, M.L., and Coble, D.W. 1980. Mortality, haematocrit, osmolality, electrolyte regulation, and fat depletion of young-of-the-year freshwater fishes under simulated winter conditions. Can. J. Fish. Aquat. Sci. **37**: 225–232.

Turner, A.M., and Mittelbach, G.G., 1990. Predator avoidance and community structure: interactions among piscivores, planktivores, and plankton. Ecology, **71**: 2241–2254.

Vanni, M.J. 1995. Nutrient transport and recycling by consumers in lake food webs: implications for algal communities. *In* Food webs: integration of pattern and process. *Edited by* G.A. Polis and K.O. Winemiller. Chapman and Hall, New York. pp. 81–95.

Walters, C.J., and Juanes, F. 1993. Recruitment limitation as a consequence of natural selection for use of restricted feeding habitats and predation risk taking by juvenile fishes. Can. J. Fish. Aquat. Sci. **50**: 2058–2070.

Ware, D.M. 1973. Risk of epibenthic prey to predation by rainbow trout (*Salmo gairdneri*). J. Fish. Res. Board Can. **30**: 787–797.

Werner, E.E., and Gilliam, J.F. 1984. The ontogenetic niche and species interactions in size-structured populations. Annu. Rev. Ecol. Syst. **15**: 393–425.

Werner, E.E., Mittelbach, G.G., Hall, D.J., and Gilliam, J.F. 1983. Experimental tests of optimal habitat use in fish: the role of relative habitat profitability. Ecology, **64**: 1525–1539.

© 1999 NRC Canada

Sources of variability in microcontaminant data for Lake Michigan salmonids: statistical models and implications for trend detection

E. Conrad Lamon III and C.A. Stow

Abstract: Variability in Lake Michigan salmonid microcontaminant data may arise from differences in contaminant concentrations in the water column, fat content, diet, age, location, and species-specific factors. Polychlorinated biphenyl (PCB) concentrations for salmonids in Lake Michigan have been determined for fish collected from a wide variety of locations and sizes for each of five species. Lake managers and policy makers wishing to evaluate trends in these concentration data must either remove this variability before trend assessment or leave it and settle for less statistical power for identifying the underlying time trend. Classification and regression trees (CART) have proven to be a useful tool for identifying nonlinear patterns of variability in these data and portraying them graphically. We used CART to study patterns of variability in PCB concentrations in five species of Lake Michigan salmonids, using data collected from 1972 to 1994 by both the Michigan and Wisconsin Departments of Natural Resources. For most of the species studied here, length was the major source of variability, followed by location.

Résumé : La variabilité des données sur les microcontaminants des salmonidés du lac Michigan peut être attribuable à des differences dans les concentrations des contaminants dans la colonne d'eau ou dans les teneurs en matières grasses des poissons, leur régime alimentaire, leur âge, le lieu ou des facteurs propres à l'espèce. Les concentrations de polychlorobiphényles (PBC) chez les salmonidés du lac Michigan ont été mesurées chez des poissons prélevés à divers endroits et de diverses tailles appartenant à chacune des cinqs espèces. Les gestionnaires de lacs et les décisionnaires qui veulent évaluer les tendances de ces concentrations doivent éliminer cette variabilité avant d'évaluer une tendance ou la laisser et accepter une puissance statistique moindre pour établir la tendance temporelole sous-jacente. Les arbres de classification et de régression (CART) se sont révélés un outil précieux pour établir les profils non linéaires de variabilité de ces données et les présenter sous forme de graphiques. Nous avons utilisé le système CART pour étudier les profils de variabilité des concentrations de PCB chez cinq espèces de salmonidés du lac Michigan, au moyen des données recueillies entre 1972 et 1994 par les ministères des Richesses naturelles des États du Michigan et du Wisconsin. Chez presque toutes les espèces étudiées, la longueur était la principale source de variabilité, suivie du lieu.

[Traduit par la Rédaction]

Introduction

Numerous factors have been hypothesized as determinants of fish tissue contaminant concentration. Fish tissue concentrations have been related to contaminant concentrations in the water column (Barber et al. 1991; LeBlanc 1995) and the diet (Madenjian et al. 1994), guild or trophic level of the fish (Rasmussen et al. 1990), age (Stow and Carpenter 1994; Stow et al. 1995), lipid content (Reinert 1969; Larsson et al. 1996), and reproductive status (Larsson et al. 1993). Many of the proposed determinants vary both spatially and temporally, complicating the identification of polychlorinated biphenyl (PCB) concentration patterns and trends. Fisheries managers wishing to assess patterns in microcontaminant concentrations often must use data collected from a variety of times, locations, age-classes, and fish conditions. The result can be a signal that is lost in "noise" due to the variability caused by the various ages, conditions, and locations at which the fish were obtained. Thus, removal of deterministic patterns of variability in a data set before trend assessment has been suggested (e.g., Hirsch et al. 1982; Reckhow and Stow 1990). Linear regression, which assumes that effects are additive and that the functional form of these effects is well represented by a straight line, has been a frequent method for modeling such deterministic patterns (e.g., Stow 1995; Stow et al. 1997). Our work relaxes these assumptions by studying factors related to fish tissue PCB concentration while assuming neither additivity nor linearity.

The objective of this study was to explore potential sources of variability in fish PCB concentration data for the purpose of removing explained variability to facilitate trend assessment. In the following sections, we present a brief background of classification and regression trees (CART) and describe the data used in this work. We then outline the procedure used to fit classification trees for prediction of fish tissue PCB concentration, present our results, and provide a discussion. A simplified example using spatial coordinates

Received October 15, 1997. Accepted August 4, 1998. J14258

E.C. Lamon III.[1] Center for Limnology, University of Wisconsin, 680 N Park St., Madison, WI 53706, U.S.A.
C.A. Stow. Nicholas School of the Environment, Duke University, Box 90328, Durham, NC 27708–0328, U.S.A.

[1]Author to whom all correspondence should be sent at the following address: Institute for Environmental Studies, Louisiana State University, 42 Atkinson Hall, Baton Rouge, LA 70803, U.S.A. e-mail: eclamon@lsu.edu

© 1999 NRC Canada

Fig. 1. Sampling locations for Lake Michigan salmonids collected by the Wisconsin and Michigan Departments of Natural Resources.

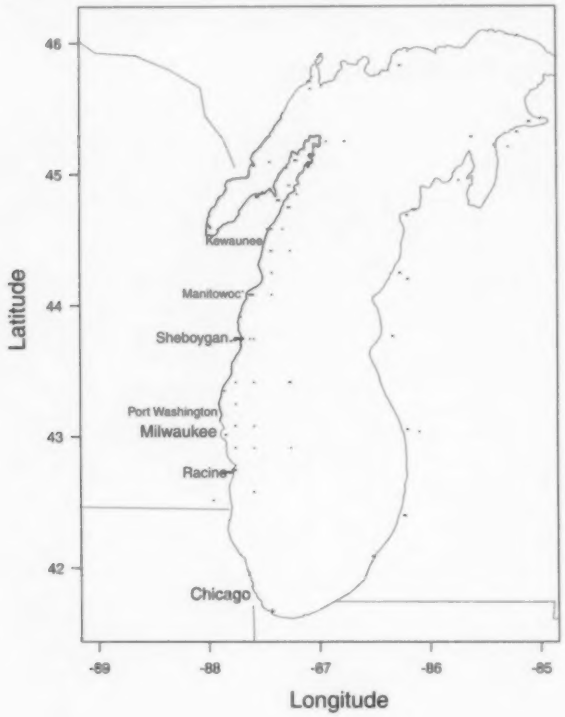

as predictors with a subset of these data is presented in the Appendix.

Materials and methods

CART: background

Tree-based models are useful for classification and regression problems in which the analyst cannot (or does not want to) specify a priori the form of important interactions between predictors (explanatory or independent variables). Tree models are easy to interpret, invariant to monotone transformations of the predictors, and able to capture nonadditive behavior (interaction effects among the predictors). Sonquist and Morgan (1964) first introduced tree-based models in statistics, with much of their recent development due to the work of Brieman et. al. (1984). A description of CART, along with examples, is provided in Clark and Pregibon (1992).

Tree-based methods use recursive algorithms to split the data along the axes of the predictor variables, **x**, into disjoint partitions within which the conditional distribution of response variable y given **x**, $f(y|\mathbf{x})$, does not depend on **x**. The recursive partitioning regression model takes the form

$$(1) \qquad \text{If } \mathbf{x} \in R_m, \text{ then } \hat{f}(\mathbf{x}) = f_m(\mathbf{x}|\{a_j\}_1^q)$$

where $\{R_m\}_1^M$ are M disjoint partitions of the data, j is a subscript describing that partition, a is an empirically derived coefficient, and q is the degree of the spline function. Tree models are the simplest case of recursive partitioning regression (with $q = 0$) in which the

$$(2) \qquad f_m(\mathbf{x}|a_m) = a_m$$

where a_m is a constant, the mean of y within the partition.

Fitting of a regression tree proceeds from the root or parent node, which contains all observations and associated variability, splitting the data set by binary recursive partitioning into increasingly homogeneous subsets until within-node variability is below some user-specified value. When a node cannot be split further according to the user-specified rules, it is called a terminal node, or leaf in keeping with the tree analogy. The model used for regression is based on the Gaussian (normal) distribution and consists of a stochastic component:

$$(3) \qquad y_i \sim N(\mu_i, \sigma^2),\ i = 1, \ldots, N$$

and a structural component:

$$(4) \qquad \mu_i = \tau(\mathbf{x}_i).$$

The stochastic component describes variability about the mean (μ). The structural component describes what data are being modeled, by which predictors (**x**), and in what form. The deviance function for an observation is

$$(5) \qquad D(\mu_i; y_i) = (y_i - \mu_i)^2.$$

The root node has an estimated mean value $\hat{\mu}$. The deviance of a node is the sum of the deviances for all observations in that node. The deviance of the data before partitioning (the root node deviance) is analogous to sample variance, but the analogy fails for subsequent nodes. The algorithm uses all unique values of each predictor variable as candidate values for splitting the data set. Splitting of a given node proceeds by evaluating the deviance of the two nodes resulting from each candidate split:

$$(6) \qquad D(\hat{\mu}_L, \hat{\mu}_R; Y) = \sum_L D(\hat{\mu}_L; y_i) + \sum_R D(\hat{\mu}_R; y_i)$$

where subscripts L and R refer to left- and right-hand nodes, respectively. The split is chosen that maximizes

$$(7) \qquad \Delta D = D(\hat{\mu}; y) - D(\hat{\mu}_L, \hat{\mu}_R; y)$$

such that ΔD is greater than some small fraction of the root deviance.

Some qualitative insight into the CART procedure may be gained by a comparison with ANOVA. ANOVA involves models of numeric variables by factors, which are variables that take on one of a specified set of levels. These data may be the result of an experiment, in which observations of one or more responses are made for changing values of several factors. The variation in the response is then studied in order to understand how it depends on the underlying phenomena that the levels of the factors represent (Chambers et al. 1990). For this analysis to proceed, the experimenter must specify the set of levels for each factor a priori, before the data are seen. Interactions between factors are restricted to be additive and linear. In contrast, the specific levels of a factor are selected by the CART procedure. Further, nonlinear interactions are allowed by CART. In other words, ANOVA attempts to answer the question "is the mean response different among the various levels of the chosen factors?" CART searches for the levels of the factors (defined by splits) that have different means.

Lake Michigan salmonid data

We used PCB concentration data from five salmonid species collected from Lake Michigan (Fig. 1) by the Wisconsin and Michigan Departments of Natural Resources: brown trout (*Salmo trutta*), lake trout (*Salvelinus namaycush*), rainbow trout (*Oncorhynchus mykiss*), chinook salmon (*Oncorhynchus tshawytscha*), and coho salmon (*Oncorhynchus kisutch*). Sample collection and analysis of the data through 1992 have been previously detailed (Stow et al. 1995). This data collection and analysis have been updated to include additional data collected by the Wisconsin Department of

© 1999 NRC Canada

Fig. 2. Boxplots of $\log_{10}$[PCB] for five species of Lake Michigan salmonids. Box width is proportional to the square root of n, the number of samples. A notch represents an approximate 95% confidence interval about the median. Upper and lower ends of the box represent the upper and lower quartiles. Horizontal lines at the ends of the broken vertical lines represent ±1.5 times the interquartile range from the median. Horizontal lines beyond the 1.5 interquartile range represent individual observations beyond that range.

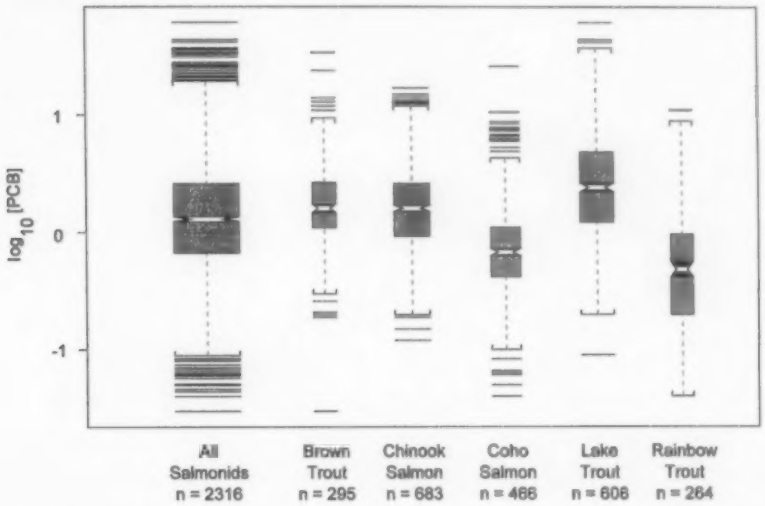

Fig. 3. Plot of deviance versus size for sequences of pruned trees evaluated using a 50-fold cross-validation for the all-salmonids data set. The plot suggests that deviance for trees with 10–15 terminal nodes is similar, as is deviance for trees of 20–35 terminal nodes.

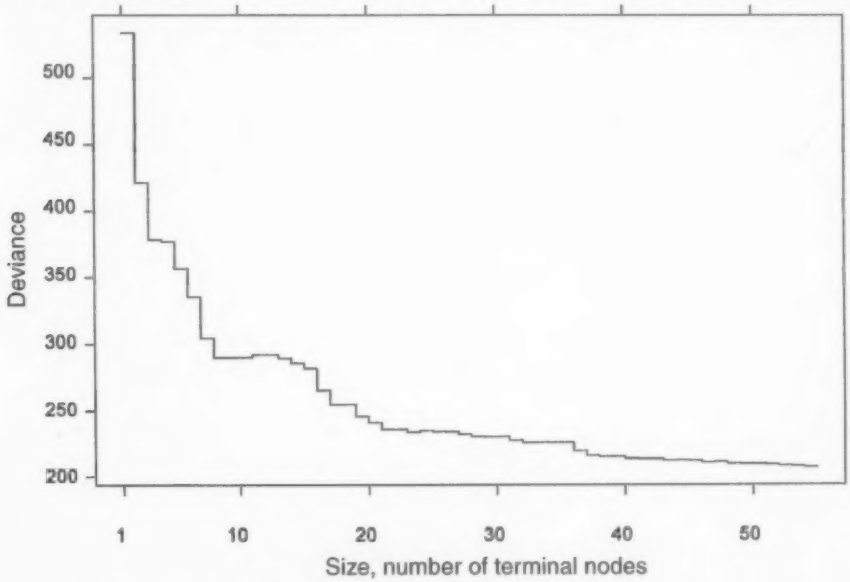

Natural Resources through 1994. The data are $\log_{10}$-transformed PCB concentrations (micrograms per gram) from skin-on filets for each fish species. As such, model predictions presented here will be for $\log_{10}$[PCB]. Due to transformation bias, $\log_{10}$[PCB] predictions will represent annual median concentrations when transformed back to the original metric (micrograms per gram). If annual mean PCB concentrations are needed, a correction factor can convert the medians to approximate means (Miller 1984). Figure 2 presents box-and-whisker plots summarizing the $\log_{10}$[PCB] data used in this study and illustrates the extreme variability in $\log_{10}$[PCB].

Procedure

We fit a regression tree to the $\log_{10}$[PCB] response for the combined data set consisting of all five fish species (Fig. 2) using both continuous predictors (latitude, longitude, length, and fat content as percent lipid) and categorical predictors (source agency and species). For each species, we also fit a regression tree to predict $\log_{10}$[PCB] for each of the five species using all of these predictors except species. The result in each of these six cases is a regression tree that can be represented as a dendrogram. For each tree, a cross-validation procedure was used to explore the relationship between model size (number of terminal nodes or leaves) and resid-

© 1999 NRC Canada

Fig. 4. Dendrogram of 11 terminal node regression tree fit to all-salmonid data showing splits at interior nodes (ovals) and mean $\log_{10}$[PCB] values at the terminal nodes, or leaves (rectangles). Species are represented by letters assigned in alphabetical order (BT, brown trout; CHIN, chinook salmon; COHO, coho salmon; LT, lake trout; RT, rainbow trout). The mean value is indicated in each node with the deviance below the node. The first split separates coho salmon and rainbow trout from the other three species and explains the most deviance of all splits.

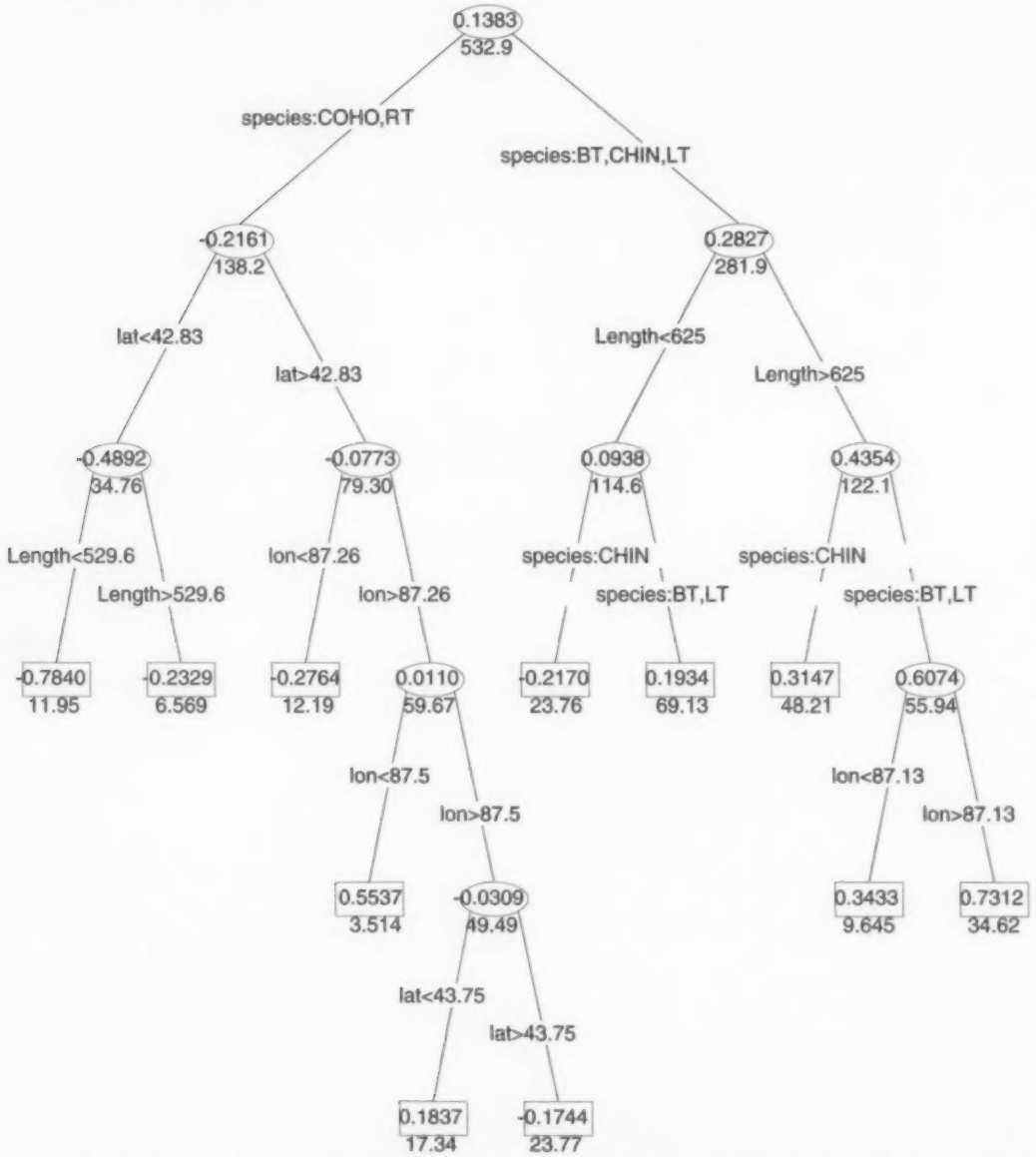

ual deviance. In this procedure the data were subsampled into 50 mutually exclusive sets containing equal numbers of observations. A tree was fit to each set and that tree was evaluated with the 49 unused subsets. This process was repeated for each of the 50 subsets. The result of this procedure is a plot of deviance versus tree size (number of terminal nodes), which we then used to determine a tree size that balanced low deviance and parsimony. With this information, regression trees fit to the entire data set and to each species separately were pruned to the indicated size. The plot of deviance versus size is presented for the tree fit to the entire data set to demonstrate this procedure but has been omitted for the individual species tree models.

Results

All salmonids

When all species were combined for analysis, the cross-validation procedure indicated that the trees with 10–15 terminal nodes (leaves) resulted in similar model residual devi-

© 1999 NRC Canada

Table 1. Summary of model residuals.

Model	Minimum	1st Quartile	Median	Mean	3rd Quartile	Maximum
All salmonids	−1.716	−0.2247	−0.0181	6.76×10^{-17}	0.2045	1.375
Brown trout	−1.5767	−0.1555	−0.0176	-7.447×10^{-1}	0.1634	0.8268
Chinook salmon	−0.876	−0.1765	−0.0057	6.859×10^{-17}	0.1622	1.187
Coho salmon	−1.244	−0.1641	0.0119	5.111×10^{-17}	0.1827	1.157
Lake trout	−1.0827	−0.1984	−0.012	-5.973×10^{-1}	0.1832	1.183
Rainbow trout	−1.2787	−0.1976	0.0015	-7.251×10^{-1}	0.1926	1.008

Fig. 5. Dendrograms for the tree models selected for (*a*) all salmonids, (*b*) brown trout, (*c*) chinook salmon, (*d*) coho salmon, (*e*) lake trout, and (*f*) rainbow trout. Length of vertical lines in these dendrograms is proportional to the amount of deviance explained by each split.

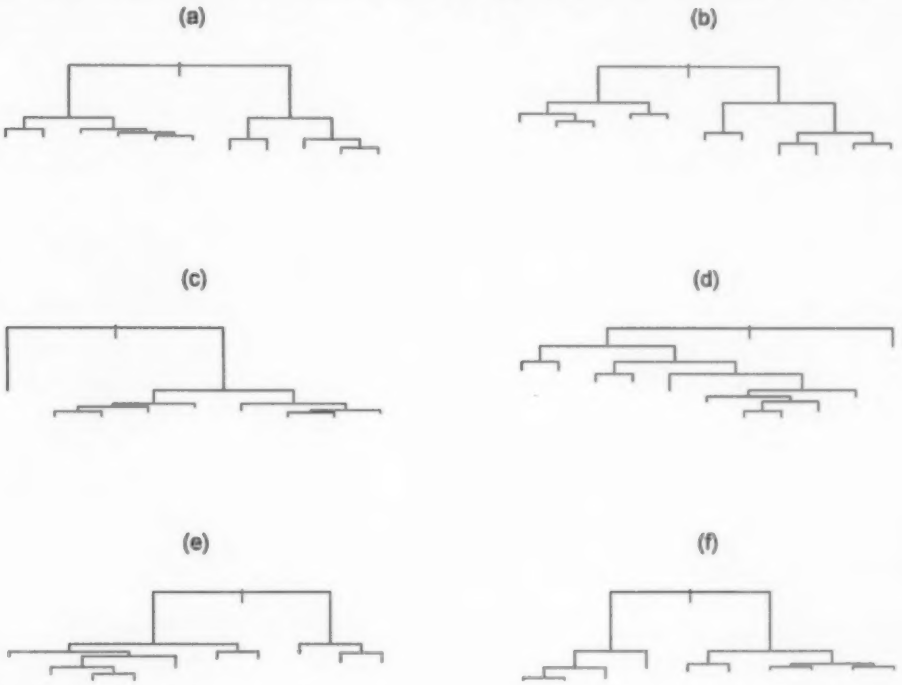

ance (Fig. 3). The number of terminal nodes in a tree is selected by balancing model fit and parsimony. The tree selected as a result of such a balance is the regression tree with 11 leaves and is presented as a dendrogram in Fig. 4. The first split in this tree is on the categorical variable species, with coho salmon and rainbow trout going to the left and brown trout, chinook salmon, and lake trout going to the right. This split explains more of the deviance than any other split in this regression tree. The split reflects the low median $\log_{10}$[PCB] for coho salmon and rainbow trout relative to the other three species (Fig. 2). The next split chosen for coho salmon and rainbow trout is on the variable latitude, while for brown trout, chinook salmon, and lake trout the next split is on the variable length. The length split explains nearly as much deviance as the next three splits of the node containing coho salmon and rainbow trout. This indicates a strong length versus $\log_{10}$[PCB] relationship and that $\log_{10}$[PCB] is more variable in these three species. It is interesting to note that the predictor variable fat (percent lipid) is not selected by the CART procedure for the all-salmonid regression tree (Fig. 4).

Individual species trees

A variety of different tree topologies are associated with the individual species trees, as indicated by the dendrograms plots of the regression trees (Fig. 5). For chinook salmon, coho salmon, and lake trout the models have initial splits on the variable length. Among this group, the coho salmon tree (Fig. 5*d*) does not fit well with the trees for chinook salmon (Fig. 5*c*) and lake trout (Fig. 5*e*), since the initial split in the coho salmon regression tree explains much less deviance than the initial splits for the other two. For coho salmon, subsequent splits on the length and geographic coordinates produced a model that fits the data better than the lake or rainbow trout models when model fit is measured by the interquartile range of the model residuals (Table 1). The coho salmon tree model does not fit as well as the brown trout or chinook salmon model.

© 1999 NRC Canada

Fig. 6. Best nine terminal node tree model for chinook salmon $\log_{10}$[PCB].

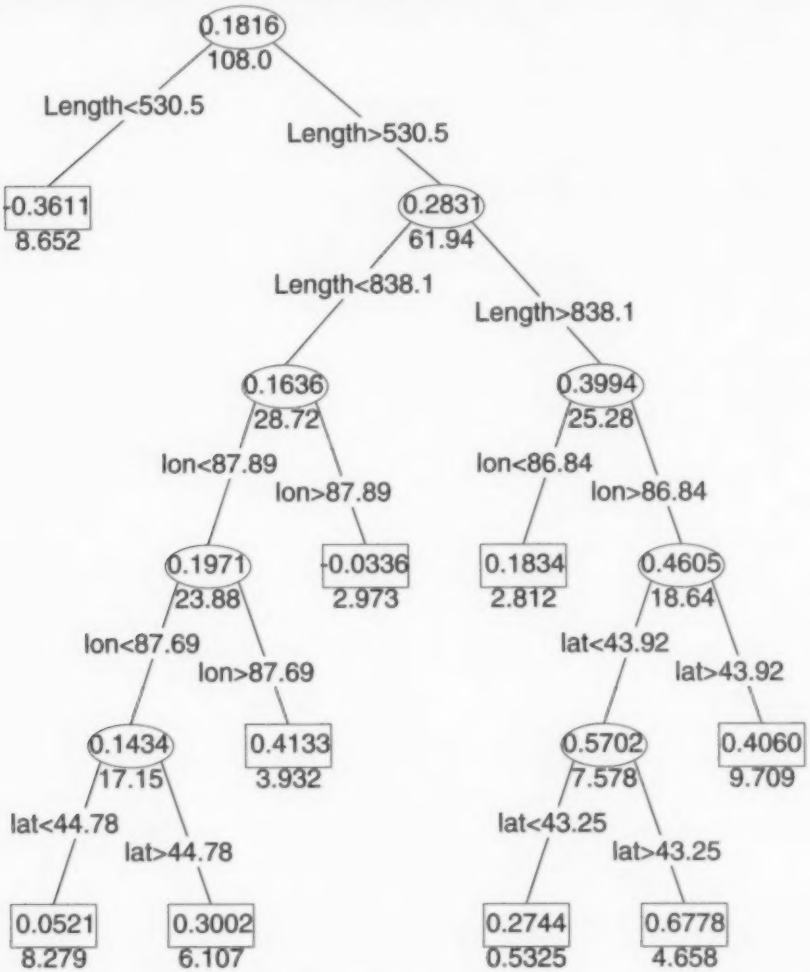

The first split in the tree model selected for chinook salmon (Figs. 5*c* and 6) explains much more deviance in $\log_{10}$[PCB] than that of the coho salmon tree model (Figs. 5*d* and 7). This model indicates that chinook salmon collected nearshore from north of Milwaukee to south of Manitowoc have a mean $\log_{10}$[PCB] of 0.68 (median of 4.76 ppm) for fish larger than about 838 mm in length.

Like chinook salmon, the model selected for lake trout (Figs. 5*e* and 8) contains an initial split on length that explains much more deviance in $\log_{10}$[PCB] than that for the coho salmon model (Figs. 5*d* and 7). An area of rather high concentrations in lake trout (Fig. 8) occurs nearshore from about Milwaukee (>42.97°N) to about Kewaunee (<44.5°N), with a mean $\log_{10}$[PCB] of 0.78 (median of 5.65 ppm) for fish *less than* about 627 mm in length. Longer fish (>673 mm) collected by the Wisconsin Department of Natural Resources (agency "wi" in Fig. 8) north of about 44.2°N have a mean $\log_{10}$[PCB] of 1.05 (median of 11.22 ppm).

In contrast with coho salmon, chinook salmon, and lake trout, initial splits for brown trout (Fig. 9) and rainbow trout (Fig. 10) are on geographical coordinates (longitude and latitude, respectively). For brown trout the initial split on longitude at 87.26° creates a node with a mean $\log_{10}$[PCB] of 0.35 (median of 2.24 ppm) to the west and 0.06 (median of 1.15 ppm) to the east. The western node is split on the variable latitude at 42.83°, with the northern node having a mean $\log_{10}$[PCB] of 0.425 (median of 2.66 ppm) and the southern node a mean $\log_{10}$[PCB] of –0.037 (median of 0.92 ppm). This north and west node is split again such that the brown trout collected west of longitude 87.26°, north of latitude 42.83°, and south of 43.75° have a mean $\log_{10}$[PCB] of 0.59 (median of 3.88 ppm). This node is split again on latitude such that fish collected from the nearshore area from just north of Port Washington to north of Sheboygan have a mean $\log_{10}$[PCB] of 0.76 (median of 5.81 ppm). The eastern node resulting from the initial split is split further on the variable length, as is the southern node split from the western node created by the initial split.

Rainbow trout are split initially on the variable latitude at 42.83° (Fig. 10), a split value also found in the individual

© 1999 NRC Canada

Fig. 7. Best 10 terminal node tree model for coho salmon $\log_{10}$[PCB].

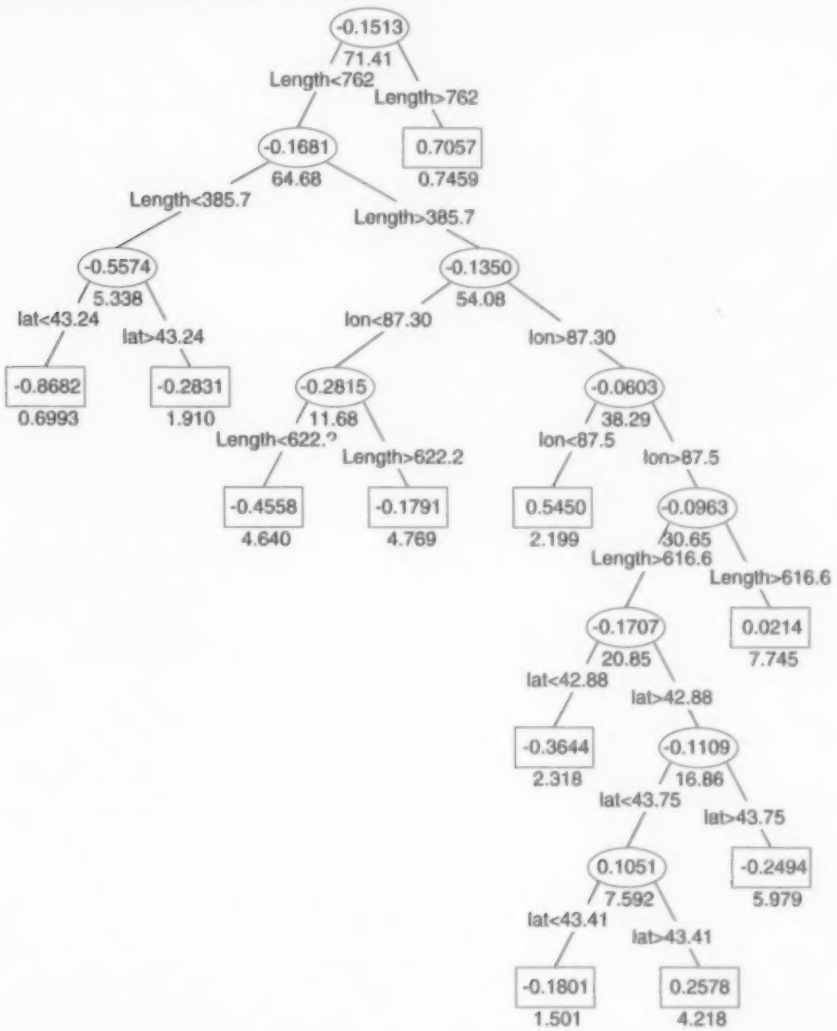

species tree fit to brown trout (Fig. 9). Subsequent splits in the rainbow trout tree model create a node that represents fish collected *offshore* (east of longitude 87.72°) between Racine and Sheboygan, with a mean $\log_{10}$[PCB] of 0.54 (median of 3.5 ppm). The split on the predictor fat (percent lipid), given that latitude is >43.75°, explains relatively little deviance and has a counterintuitive mean value for lipid >9.5%. For fat content <9.5% lipid, there is a split on the predictor fat at 3.9% lipid, where mean $\log_{10}$[PCB] is lower in the mode corresponding to lowest percent lipid and higher when percent lipid is higher.

Discussion

Spatial "hot spots", or areas of high fish tissue PCB concentration, are apparent from our analyses, and they are most pronounced for small lake trout, medium-sized coho salmon, large chinook salmon, and all sizes of rainbow and brown trout. The hot spots tend to be located on the western shore of the lake from Milwaukee to Manitowoc, in the vicinity of the Milwaukee Estuary and Sheboygan River areas of concern (AOCs). The remedial action plan (RAP) for the Milwaukee Estuary AOC (Wisconsin Department of Natural Resources 1994*a*) and the RAP public review draft for the Sheboygan River AOC (Wisconsin Department of Natural Resources 1994*b*) both identify PCB-contaminated sediments as pollutants of concern. The deviance explained by splits on spatial coordinates that define these hot spots is also greatest for the iteroparous species, rainbow, brown, and lake trout. These species would likely be exposed to higher water column and diet PCB concentrations relative to coho and chinook salmon. The location of these AOCs, along with the behavior of these three species, provides evidence of spatial variability in PCB concentrations in Lake Michigan fishes.

Temporal trends for PCB concentrations exist in these

© 1999 NRC Canada

Fig. 8. Best 10 terminal node tree model for lake trout $\log_{10}$[PCB].

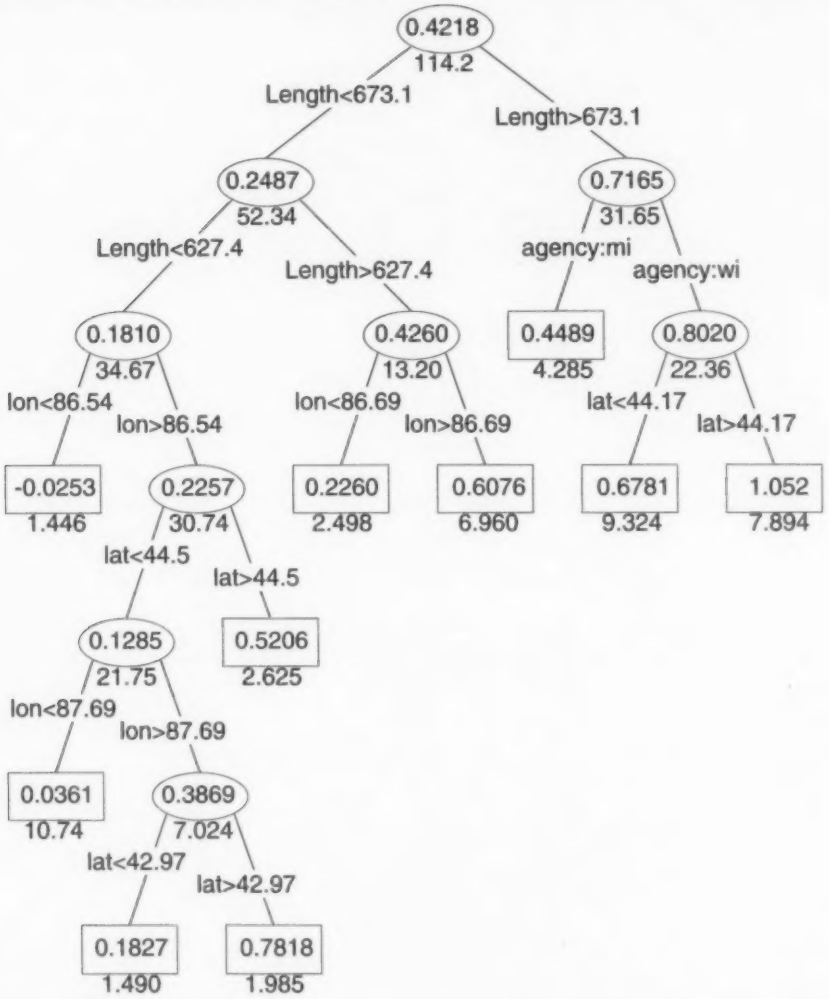

data (Stow et al. 1995; Lamon et al. 1998, 1999), but date of collection was intentionally omitted as a potential regressor when the tree models were fit. This was done for two reasons. First, retrospective assessment of $\log_{10}$[PCB] trends will be facilitated by reducing variability in the trend signal. Residuals from these tree models can be evaluated for a trend signal that is considerably less noisy than that before variance reduction. Second, by selecting size-classes and locations whose mean $\log_{10}$[PCB] closely approximates that of all fish of a species during the final year of collection (1994), considerable savings may be realized in future monitoring (Fig. 11). The splits used in these trees can serve as a guide in selecting size-classes and locations for future fish collection. This twofold approach will provide more precise prospective and retrospective estimates of trend, along with substantial savings in monitoring effort and laboratory analyses.

Brown and rainbow trout are the two species with the fewest observations and are the only species for which the initial splits were made on geographical coordinates in the individual species tree models. The near-linear and noisy relationship between length and $\log_{10}$[PCB], combined with relatively few observations and the difficulty in fitting linear relationships with a parsimonious tree model, could be responsible for the selection of geographic coordinates as initial splits in the tree models for these species.

Due to the presence of temporal trend, the apparent existence of spatial hot spots for $\log_{10}$[PCB] in several species could be the result of spatially or temporally biased sample collection. If many samples had been collected from one location early in the time series, when PCB concentrations were higher, with subsequent collections omitting these areas, the trend effect would have been confounded by the haphazard sampling in space and time. If this were the case, we suspect that the magnitude of the temporal trend in the tree model residuals would differ from that seen in the trend assessments done on the unadjusted data (Stow et al. 1995; Lamon et al. 1998, 1999). We constructed time series plots

© 1999 NRC Canada

Fig. 9. Best 11 terminal node tree model for brown trout $\log_{10}$[PCB].

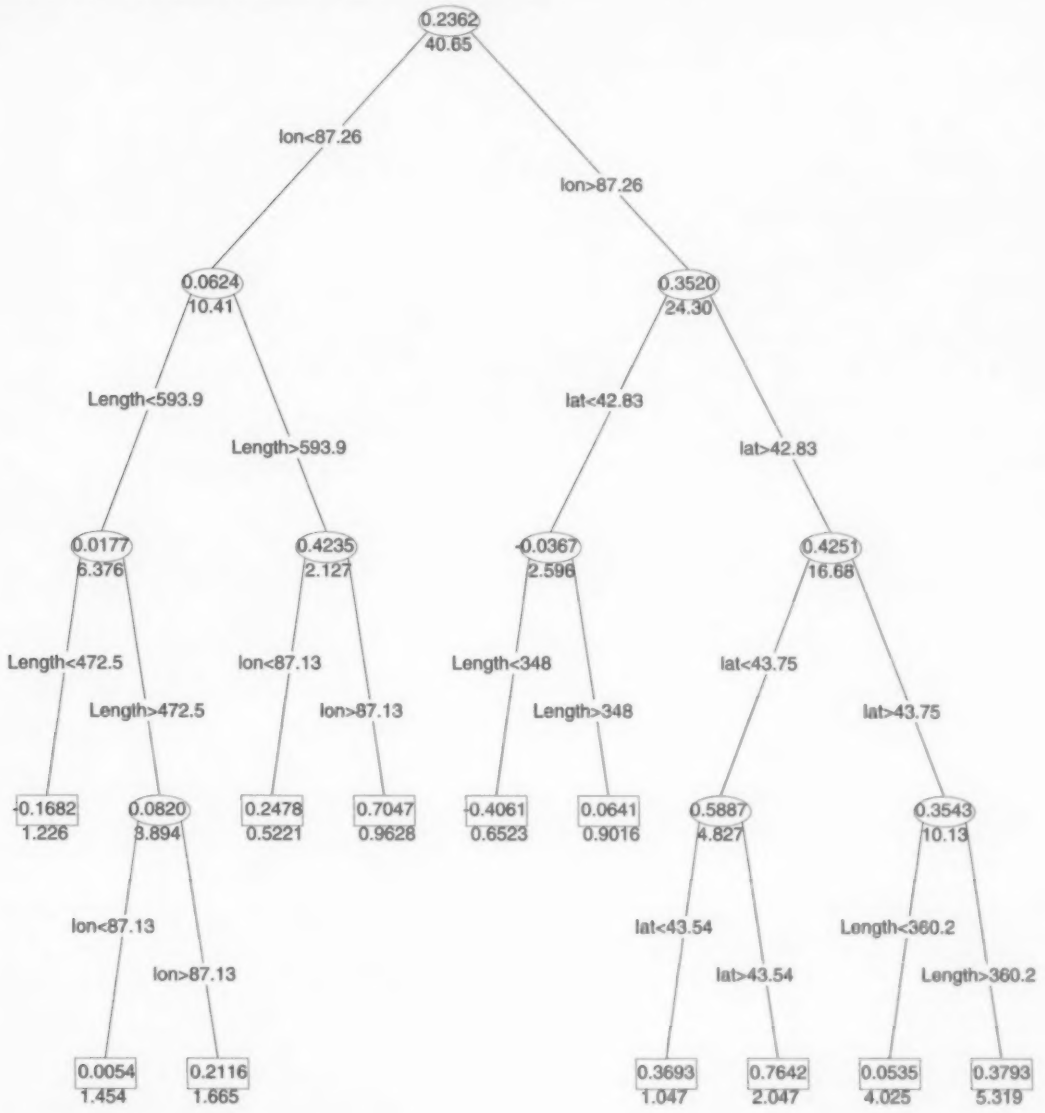

of annual average CART model residuals to investigate the possibility of confounding by haphazard sampling (Fig. 12). Full trend assessment of these residuals has been reserved for a later date, as it is beyond the stated goals of this effort. Visual inspection of these plots indicates that the time trends are preserved.

It is not entirely clear what the identified spatial patterns indicate. Location of capture may be considered a random event if salmonids in Lake Michigan migrate throughout the lake. Spatial patterns found for various size-classes in several species may indicate site fidelity *during specific life stages*. Such site fidelity is illustrated by lake trout <627 mm long, which seem to have an area of high PCB concentration off the western shore near Milwaukee (Fig. 13). Furthermore, the splits on geographic coordinates for the smaller lake trout explain more deviance than do those for the medium-sized or larger fish, suggesting a stronger spatial pattern for younger (i.e., smaller) lake trout. Evidence for site fidelity is strong for only smaller lake trout, which likely would have been missed or dismissed as insignificant if linear and additive assumptions had been made about this relationship. Miller et al. (1992) found significant differences between the PCB bioaccumulation rate of lake trout inhabiting shallow nearshore (Clay Banks Reef area) and deep offshore (Sheboygan Reef area) waters of Lake Michigan and attributed this difference to the effect of dissimilar diets on contaminant uptake. They also found higher PCB concentrations at age in the nearshore waters, which agrees with our result

© 1999 NRC Canada

Fig. 10. Best 10 terminal node tree model for rainbow trout $\log_{10}$[PCB].

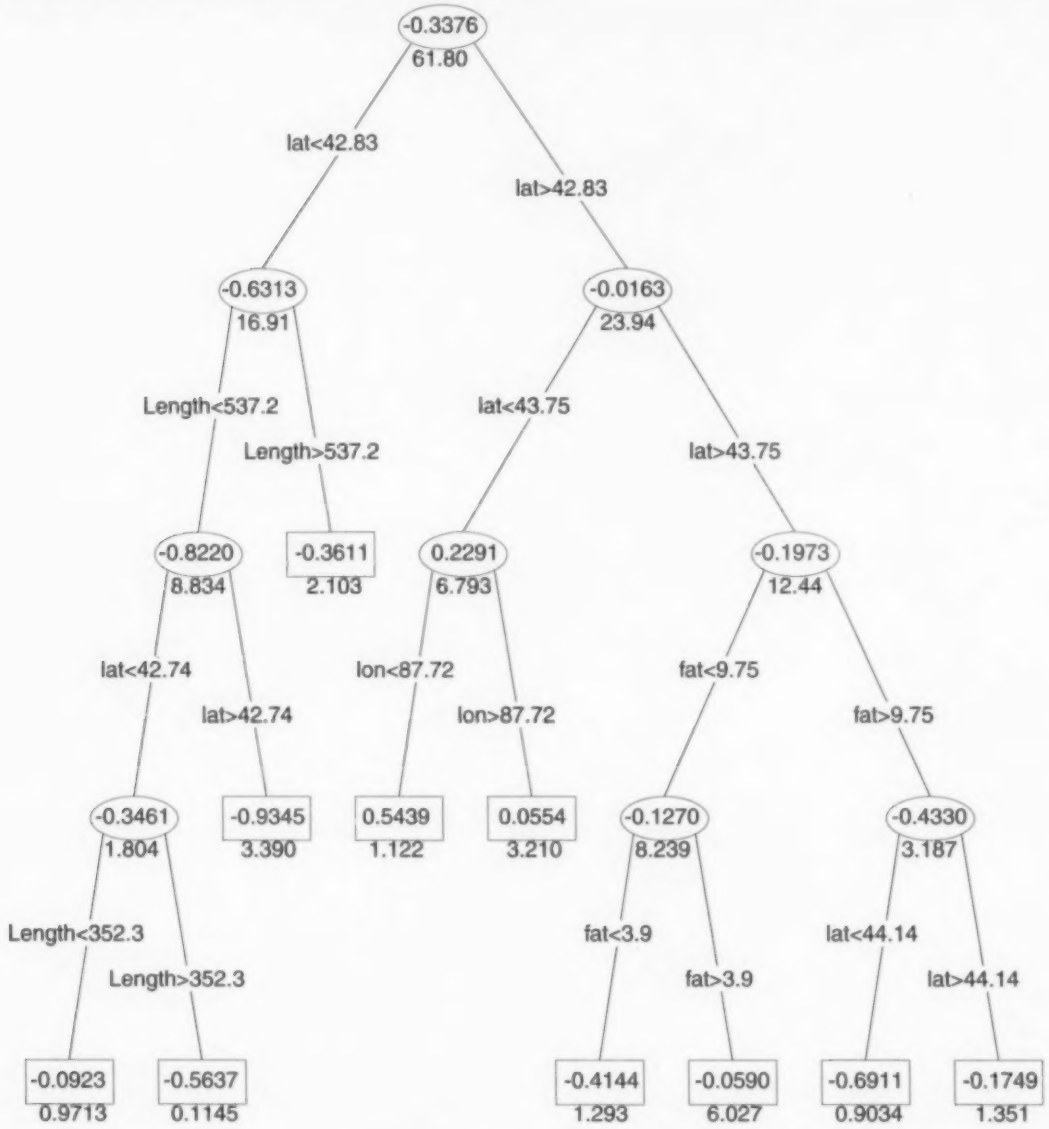

(Fig. 13) and provides a possible mechanism to explain the spatial differences in PCB concentrations.

It is interesting to note that for lake trout the CART procedure chose a split on length at 673.1 mm and at 627.4 mm (Figs. 8 and 13). The resulting interior nodes have a mean $\log_{10}$[PCB] of 0.181 (fish <627.4 mm), 0.426 (fish >627.4 and <673.1 mm), and 0.7165 (fish >673.1 mm). Madenjian et al. (1998*a*) found that the diet shifts from small to large alewife (*Alosa pseudoharengus*) when lake trout reach about 600 mm. Similar results have been found for coho salmon when they reach about 500 mm in length (Madenjian et al. 1998*b*). Alewife contaminant concentrations increase with increasing age, as with any individual fish, and large bloater (*Coregonus hoyi*) and large alewife exhibit higher PCB concentrations than any other prey species (Madenjian et al. 1998*a*, 1998*b*). The diet shift determinations of Madenjian et al. (1998*a*, 1998*b*, 1998*c*) were obvious and made without rigourous statistical procedures, size-classes were determined a priori based on diet protocol for Lake Michigan piscivorous fish (Elliot et al. 1996), and differences among the size-classes were then examined. The CART procedure identified size-classes that maximize the difference in PCB concentration between classes, and using the data of Madenjian et al. (1998*a*), it would be possible to let the CART procedure determine the size-classes at which diet shifts are most pronounced.

The absence of the predictor fat (percent lipid) in the all-salmonid regression tree is in general agreement with the

© 1999 NRC Canada

Fig. 11. Log_{10}[PCB] probability density estimates: (*a*) all samples of lake trout from 1994 (solid line: low, flat curve) and for lake trout 618.5–718.8 mm in length sampled in 1994 (broken line: more sharply peaked curve), (*b*) all samples of chinook salmon (solid line: low, flat curve) and for chinook salmon 622.2–762 mm in length sampled east of longitude 87.3° (broken line: more sharply peaked curve), and (*c*) all coho salmon samples (solid line: low, flat curve) and coho salmon 627.4–673 mm in length (broken line; more sharply peaked curve). By collecting fish selectively by size, variability is reduced.

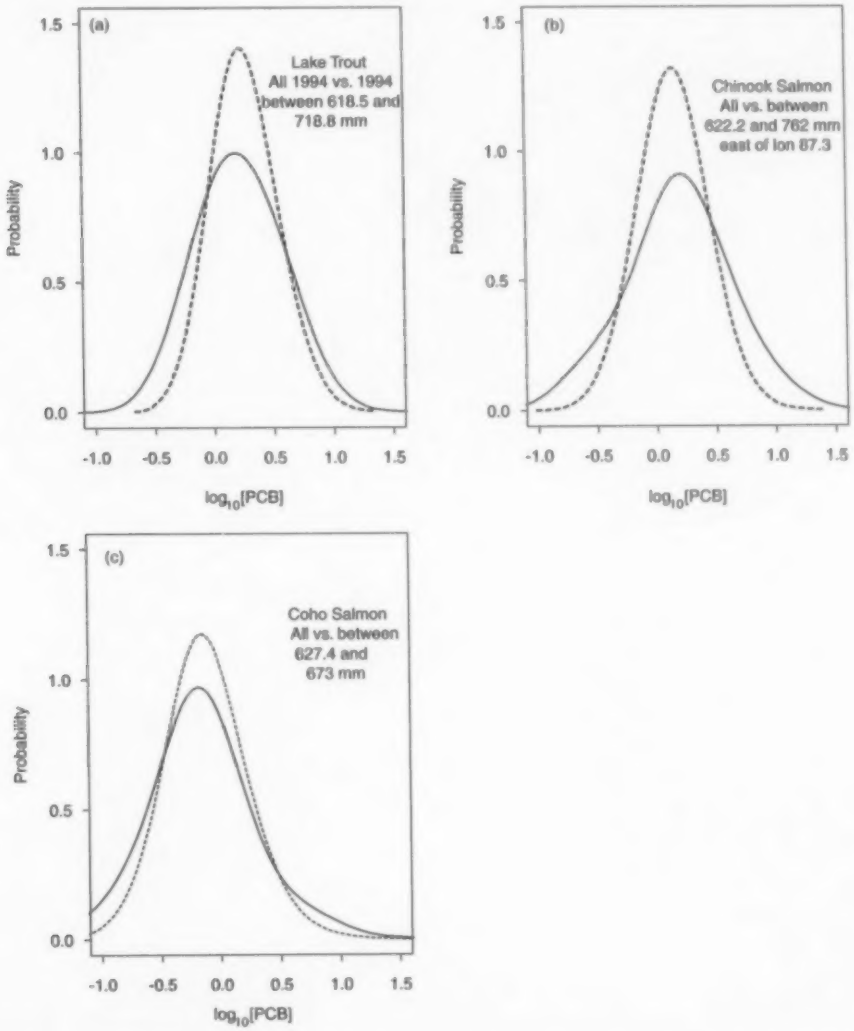

findings of Stow et al. (1997), who found no linear relationship between PCB concentration and lipid content within nonspawning individuals of these species. A strong linear correlation was found between mean species lipid and PCB values without accounting for other factors. Between-species differences in mean log_{10}[PCB] values can be found here (Fig. 2) that may be attributable to percent lipid, among many other factors, but between-species lipid effects on PCB concentrations are confounded by the categorical predictor variable species. In other words, if we know the species, knowing the percent lipid content of a fish will not tell us anything more regarding PCB concentration. Since species was chosen in the CART model and not percent lipid, this indicates that species is actually a better predictor of PCB concentration.

There are some attractive features of the recursive partitioning regression models presented here. Even though the functional relationship between predictors and response may depend on many variables throughout the domain of observed PCB concentrations, the dependence is strong only on, at most, a few variables locally. This leads to local variable subset selection, and therefore, global variable subset selection. Recursive partitioning regression models can also be represented on a binary tree, which allows easy interpre-

© 1999 NRC Canada

Fig. 12. Time series plots of CART model residuals for brown trout, chinook salmon, coho salmon, lake trout, and rainbow trout. Residuals were calculated as $Y_{pred} - Y_{obs}$ for each species' CART model. Points on these plots represent the average residual for each year.

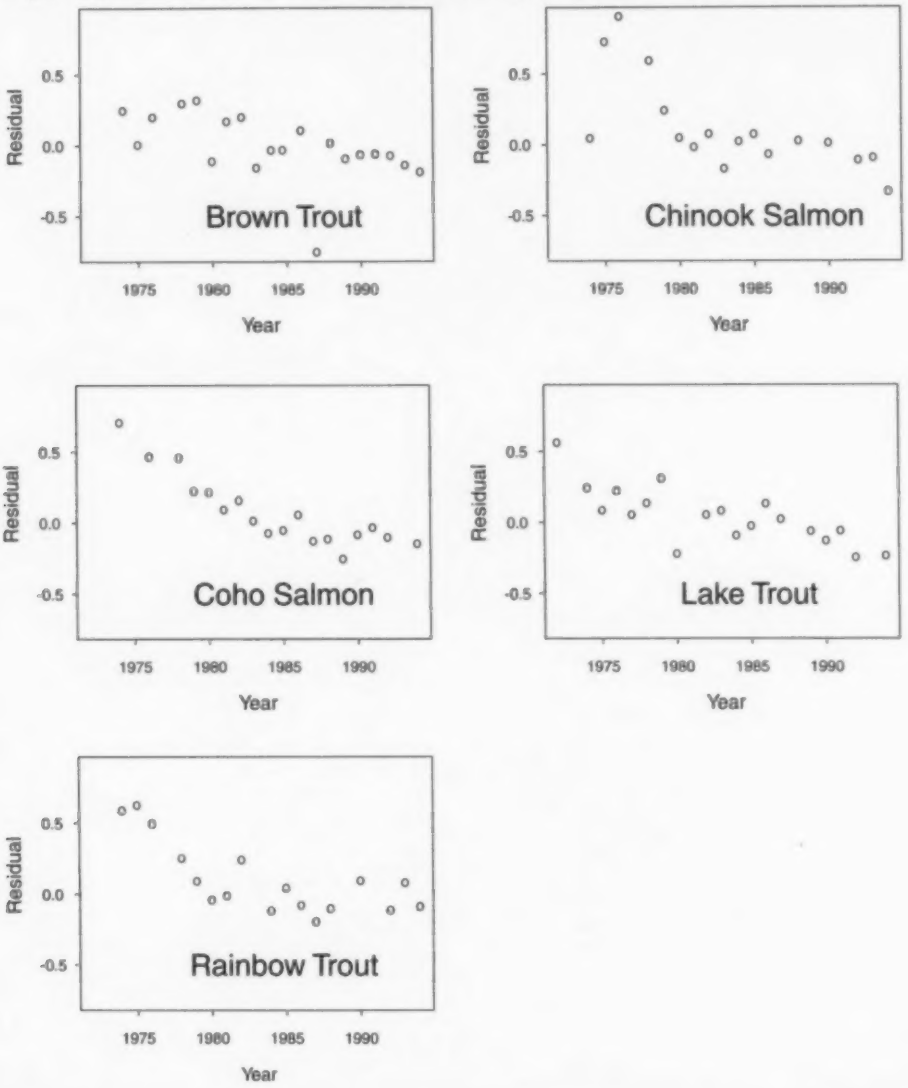

tation of the model. When there is just one predictor variable, tree models are step functions, and with two predictors the disjoint partitions of a tree model may be plotted on a bivariate plot of the two predictor variables.

Unfortunately, there are also some limitations including discontinuities at the subregion (partition) boundaries and the inability to provide good approximations to some classes of commonly occurring functions (as mentioned previously, linear and additive functions are among them). Uncertainty regarding selection of the predictor variable upon which to partition the data, as well as the value at which to make the split once the variable is chosen, is dealt with in CART models only one node at a time. This decision is based on maximizing ΔD in eq. 7. Since ΔD is calculated considering only the current node and the resulting daughter nodes, there may be a split of the current node that yields a less than maximum ΔD in the two daughter nodes but provides a much better (i.e., larger) ΔD in subsequent splits. Such uncertainties will be addressed with a Bayesian approach in a forthcoming version of the CART algorithm (Chipman et al. 1998). Unquantified uncertainties associated with the methods of data collection and analysis used here should be weighed against the possibility of site fidelity among salmonids and known areas of PCB contamination when fisheries managers design programs to assess PCB trends in the Lake Michigan food web.

Acknowledgments

Thanks are due to Steve Carpenter, Tim Essington, and

© 1999 NRC Canada

Fig. 13. Combination of dendrogram and map representation of the $\log_{10}$[PCB] regression tree for lake trout. For smaller fish (<627.4 mm), there is a "hot spot," or region of high PCB concentration, near the western shore north of Milwaukee.

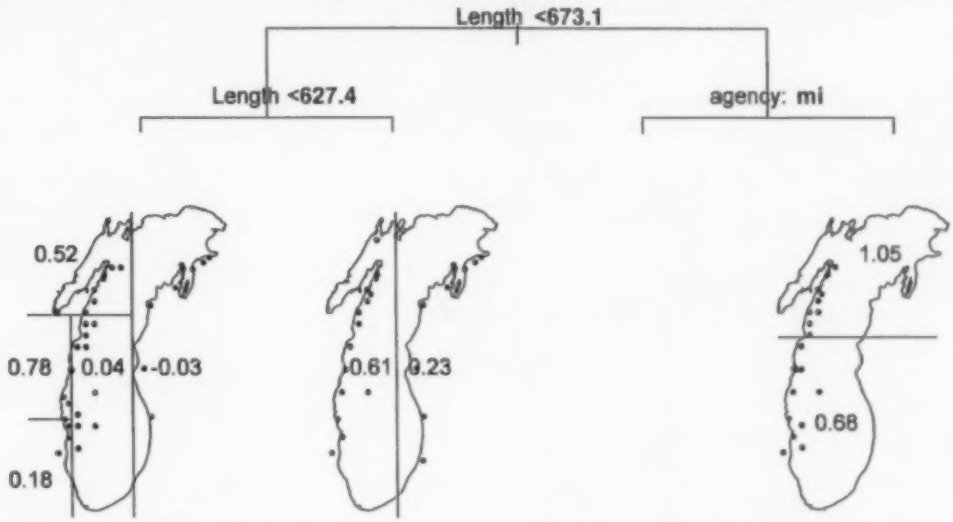

Tom Hrabik for helpful reviews of earlier versions of this manuscript. CART models were fit using Splus for Windows, version 3.2. This work was funded by the University of Wisconsin Sea Grant Institute, under grants from the National Sea Grant College Program, National Oceanic and Atmospheric Administration, U.S. Department of Commerce, and the State of Wisconsin. Federal grant No. NA46RG0481, project No. R/MW-59.

References

Barber, M.C., Suarez, L.A., and Lassiter, R.R. 1991. Modelling bioaccumulation of organic pollutants in fish with an application to PCBs in Lake Ontario salmonids. Can. J. Fish. Aquat. Sci. **48**: 318–337.

Brieman, L., Friedman, J.H., Olshen, R.A., and Stone, C.J. 1984. Classification and regression trees. Wadsworth International Group, Belmont, Calif.

Chambers, J.M., Freeny, A.E., and Heiberger, R.M. 1992. Analysis of variance: designed experiments. *In* Statistical models in S. *Edited by* J.M. Chambers and T.J. Hastie. Wadsworth and Brooks/Cole Advanced Books and Software, Pacific Grove, Calif.

Chipman, H., George, E.I., and McCulloch, R.E. 1998. Bayesian CART model search (with discussion). J. Am. Stat. Assoc. **93**: 935–956.

Clark, L.A., and Pregibon, D. 1992. Tree based models. *In* Statistical models in S. *Edited by* J.M. Chambers and T.J. Hastie. Wadsworth and Brooks/Cole Advanced Books and Software, Pacific Grove, Calif.

Elliot, R.F., Peeters, P.J., Ebener, M.P., Rybicki, R.W., Schneeberger, P.J., Hess, R.J., Francis, J.T., Eck, G.W., and Madenjian, C.P. 1996. Conducting diet studies of Lake Michigan piscivores — a protocol. Rep. 96-2, U.S. Fish and Wildlife Service, Green Bay, Wis.

Hirsch, R.M., Slack, J.R., and Smith, R.A. 1982. Techniques of trend analysis for monthly water-quality data. Water Resour. Res. **18**: 107–121.

Lamon, E.C., Carpenter, S.R., and Stow, C.A. 1998. Forecasting PCB concentrations in five species of Lake Michigan salmonids: a dynamic linear model approach. Ecol. Appl. **8**: 659–668.

Lamon, E.C., III, Carpenter, S.R., and Stow, C.A. 1999. Rates of decrease of polychlorinated biphenyl concentrations in five species of Lake Michigan salmonids. Can. J. Fish. Aquat. Sci. **56**: 53–59.

Larsson, P.L., Okla, L., and Colvin, L. 1993. Reproductive status and lipid content as factors in PCB, DDT and HCH contamination of a population of pike (*Esox lucius* L.). Environ. Sci. Technol. **12**: 855–861.

Larsson, P., Backe, C., Bremle, G., Eklov, A., and Okla, L. 1996. Persistent pollutants in a salmon population (*Salmo salar*) of the southern Baltic Sea. Can. J. Fish. Aquat. Sci. **53**: 62–69.

LeBlanc, G.A. 1995. Trophic-level differences in the bioconcentration of chemicals: implications in assessing biomagnification. Environ. Sci. Technol. **29**: 154–160.

Madenjian, C.P., Carpenter, S.R., and Rand, P.S. 1994. Why are the PCB concentrations of salmonine individuals from the same lake so highly variable? Can. J. Fish. Aquat. Sci. **51**: 800–807.

Madenjian, C.P., Hesselberg, R.J., DeSorcie, T.J., Schmidt, L.J., Stedman, R.M., Quintal, R.T., Begnoche, L.J., and Passino-Reader, D.R. 1998*a*. Estimate of net trophic transfer efficiency of PCBs to Lake Michigan lake trout from their prey. Environ. Sci. Technol. **32**: 886–891.

Madenjian, C.P., Elliot, R.F., Schmidt, L.J., DeSorcie, T.J., Hesselberg, R.J., Quintal, R.T., and Benoche, L.J. 1998*b*. Net trophic transfer efficiency of PCBs to Lake Michigan coho salmon from their prey. Environ. Sci. Technol. **32**: 3063–3067.

Madenjian, C.P., DeSorcie, T.J., and Stedman, R.M. 1998*c*. Ontogenic and spatial patterns in diet and growth of lake trout from Lake Michigan. Trans. Am. Fish. Soc. **127**: 236–252.

Miller, D.M. 1984. Reducing transformation bias in curve fitting. Am. Stat. **38**: 124–126.

Miller, M.A., Madenjian, C.P., and Masnado, R.G. 1992. Patterns of organochlorine contamination from Wisconsin waters of the Great Lakes. J. Gt. Lakes Res. **18**: 742–754.

Rasmussen, J.B., Rowan, D.J., Lean, D.R.S., and Carey, J.H. 1990. Food chain structure in Ontario lakes determines PCB levels in lake trout (*Salvelinus namaycush*) and other pelagic fish. Can. J. Fish. Aquat. Sci. **47**: 2030–2038.

Reckhow, K.H., and Stow, C.A. 1990. Monitoring design and data analysis for trend detection. Lake Reservoir Manage. **6**: 49–60.

© 1999 NRC Canada

Reinert, R.E. 1969. Insecticides and the Great Lakes. Limnos, **2**: 3–9.
Sonquist, J.N., and Morgan, J.N. 1964. The detection of interaction effects. Monogr. 35, Survey Research Center, Institute of Social Research, University of Michigan, Ann Arbor, Mich.
Stow, C.A. 1995. Factors associated with PCB concentrations in Lake Michigan salmonids. Environ. Sci. Technol. **29**: 522–527.
Stow, C.A., and Carpenter, S.R. 1994. PCB accumulation in Lake Michigan coho and chinook salmon: individual-based models using allometric relationships. Environ. Sci. Technol. **28**: 1543–1549.
Stow, C.A., Carpenter, S.R., Eby, L.A., Amrhein, J.F., and Hesselberg, R.J. 1995. Evidence that PCBs are approaching stable concentrations in Lake Michigan fishes. Ecol. Appl. **5**: 248–260.
Stow, C.A., Jackson, L.J., and Amrhein, J.F. 1997. An examination of the PCB:lipid relationship among individual fish. Can. J. Fish. Aquat. Sci. **54**: 1031–1038.
Wisconsin Department of Natural Resources. 1994*a*. Milwaukee Estuary remedial action plan. Wisconsin Department of Natural Resources, Madison, Wis.
Wisconsin Department of Natural Resources. 1994*b*. Sheboygan River remedial action plan. Wisconsin Department of Natural Resources Madison, Wis.

Appendix. Regression trees: a simplified spatial example

For the purpose of developing a simplified example regression tree model, a subset of the previously described data was chosen at random (Table A1), consisting of latitude and longitude as predictor variables and $\log_{10}$[PCB] as the response. A regression tree model was fit to this subset, progressively splitting the data into increasingly homogeneous subsets, but stopping for simplicity with a model consisting of only three terminal nodes (partitions). Two graphical representations of the resulting model are presented in Fig. A1. The left-hand side of Fig. A1 is the binary tree graphical depiction of regression trees responsible for their name. It is helpful to think of individual data points being dropped into the root node at the top of the tree and then shunted to the right or left at each interior node based on the decision rule (splits) determined by the recursive partitioning algorithm. This continues until the observation lands in a terminal node (leaf). The model prediction for that observation is the mean value of the leaf in which it lands. The right-hand side of Fig. A1 shows the resulting partitions on the predictor space (latitude and longitude) with the mean value of the $\log_{10}$[PCB] response centered in each partition. This sort of representation of a regression tree model may be made only with two predictor variables.

Basis functions are vector transformations of the original predictors (vectors) that span the original predictor space and are linearly independent. The basis functions associated with the three terminal node regression tree example are presented in Table A1. These consist of a product of one or more terms in which the predictor value (data) for an observation minus the split is evaluated by the $H(\eta)$ operator, which is an indicator function. If the sign of the result of this subtraction does not match the sign within the square brack-

Fig. A1. Two graphical representations of the example regression tree, $\log_{10}$[PCB] ~ lat + lon. The left-hand side is a dendrogram showing splits at the interior nodes (ovals) and mean $\log_{10}$[PCB] values at the terminal nodes, or leaves (rectangles). The mean value is indicated in each node with the deviance in parentheses. The right-hand side shows the partitions of the bivariate plot of the predictor space (latitude versus longitude). Mean $\log_{10}$[PCB] values are shown in each partition.

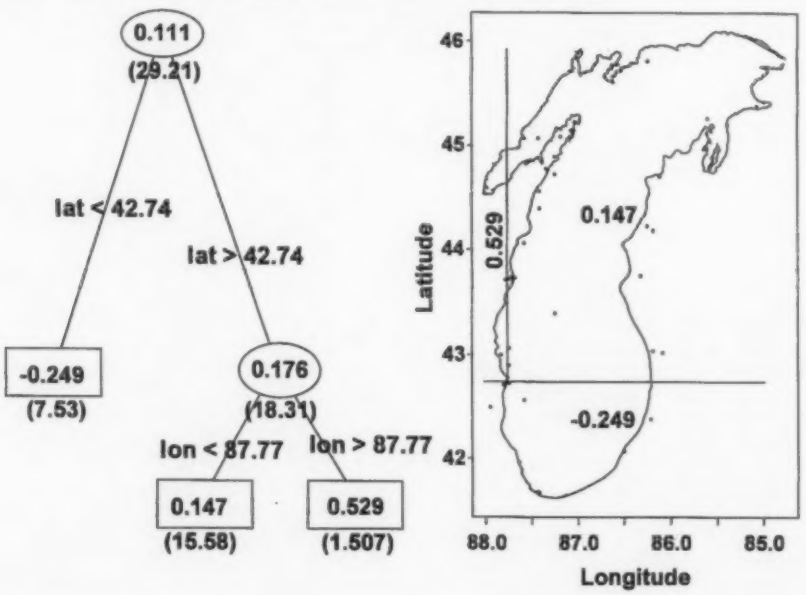

© 1999 NRC Canada

Table A1. Ten observations used to construct the example regression tree.

$\log_{10}$[PCB]	Latitude	Longitude
0.28330	44.2040	–86.18
0.11394	44.2490	–86.25
0.66276	43.7533	–87.72
–0.40894	43.7333	–87.78
0.04139	44.0833	–87.58
–0.23657	43.7407	–87.74
0.71600	43.7500	–87.68
0.20412	43.7333	–87.78
0.17609	44.0833	–87.58
0.98677	42.5167	–87.95

Table A2. Basis functions for regression tree model, $\log_{10}$[PCB] ~ lat + lon.

$B_1 = H[-(\text{lat} - 42.74)]$
$B_2 = H[+(\text{lat} - 42.74)]H[-(\text{lon} - (-87.77))]$
$B_3 = H[+(\text{lat} - 42.74)]H[+(\text{lon} - (-87.77))]$

Note: $H(\eta) = 1$ if the sign of η matches the sign within the square brackets and $H(\eta) = 0$ if the sign of η does not match the sign withinin the square brackets.

ets, the indicator function evaluates the term to 0, and the entire basis function is also 0 for that observation, since the basis function is a product of one or more of these terms. On the other hand, if the sign of result of the subtraction matches the sign within the square brackets, the term evaluates to 1, and if all other terms do likewise, the entire basis function evaluates to 1. For the first observation ($i = 1$) in the example data given in Table A1, the three basis functions of Table A2 are evaluated as follows:

$$B_1 = H[-(\text{lat} - 42.74)] = H[-(44.20 - 42.74)] = H[-(+1.46)] = 0$$

$$B_2 = H[+(\text{lat} - 42.74)]H[-(\text{lon} - 87.77)] = H[+(44.20 - 42.74)]H[-(-86.18 - (-87.77))] = H[+(+1.46)]H[-(+1.59)] = 1 \times 0 = 0$$

$$B_3 = H[+(\text{lat} - 42.74)]H[+(\text{lon} + 87.77)] = H[+(44.204 - 42.74)]H[+(-86.18 - (-87.77))] = H[+(+1.46)]H[+(+1.59)] = 1 \times 1 = 1.$$

It may be seen from the example regression tree design matrix of our example (Table A3) that only one basis function evaluates to a value of 1 per observation, with the rest being 0, which ensures linear independence of the columns of the design matrix. With all the observations classified into only one basis function, an ordinary least squares procedure can be used to estimate the mean value for each column of the design matrix (basis function). This results in a model that is not linear in the original predictors but is linear in the basis functions.

Table A3. First 10 rows of a design matrix for an example tree regression model, $\log_{10}$[PCB] ~ lat + lon.

B_1	B_2	B_3
0	0	$H[+(\text{lat} - 42.74)]H[+(\text{lon} - (-87.77))]$
0	0	$H[+(\text{lat} - 42.74)]H[+(\text{lon} - (-87.77))]$
0	0	$H[+(\text{lat} - 42.74)]H[+(\text{lon} - (-87.77))]$
0	$H[+(\text{lat} - 42.74)]H[-(\text{lon} - (-87.77))]$	0
0	0	$H[+(\text{lat} - 42.74)]H[+(\text{lon} - (-87.77))]$
0	0	$H[+(\text{lat} - 42.74)]H[+(\text{lon} - (-87.77))]$
0	0	$H[+(\text{lat} - 42.74)]H[+(\text{lon} - (-87.77))]$
0	0	$H[+(\text{lat} - 42.74)]H[+(\text{lon} - (-87.77))]$
0	0	$H[+(\text{lat} - 42.74)]H[+(\text{lon} - (-87.77))]$
$H[-(\text{lat} - 42.74)]$	0	0

$$\begin{matrix} B_1 & B_2 & B_3 \end{matrix}$$
$$\begin{bmatrix} 0 & 0 & 1 \\ 0 & 0 & 1 \\ 0 & 0 & 1 \\ 0 & 1 & 0 \\ 0 & 0 & 1 \\ 0 & 0 & 1 \\ 0 & 0 & 1 \\ 0 & 0 & 1 \\ 0 & 0 & 1 \\ 1 & 0 & 0 \end{bmatrix}$$

© 1999 NRC Canada

Effect of habitat use on PCB body burden in Hudson River striped bass (*Morone saxatilis*)

Erik R. Zlokovitz and David H. Secor

Abstract: The Hudson River commercial striped bass (*Morone saxatilis*) fishery has been closed since 1976 due to high polychlorinated biphenyl (PCB) contamination. Accurate forecasting of PCB levels in striped bass has been confounded by high variance in contamination among individuals. We investigated the relationship between habitat use and PCB contamination in Hudson River and Long Island Sound striped bass using electron microanalysis of otolith strontium to generate time series of individual salinity habitation. Males with highly contaminated levels (mean PCB = 8.3 ppm) showed freshwater resident behavior, rarely experiencing salinities >5 ppt. Several individuals showed large habitat shifts. Shifts from brackish or marine habitats to freshwater habitats were often associated with high PCB levels. A third pattern was apparent in large females, where polyhaline/euhaline salinity habitation was associated with lower PCB levels. Total PCB body burden was inversely correlated with mean salinity encountered during the most recent growth season prior to capture. Fish with recent exposure to polyhaline salinities showed high variability in PCB body burdens (0.4–9.0 ppm), suggesting a local source of PCB contamination in the New York Harbor region.

Résumé : La pêche commerciale du bar rayé (*Morone saxatilis*) dans l'Hudson est interdite depuis 1976 en raison d'une forte contamination par les polychlorobiphényles (PCB). La forte variance de la contamination entre individus a rendu difficile l'établissement de prévisions précises des niveaux de PCB chez les bars rayés. Nous avons étudié la relation entre l'utilisation de l'habitat et la contamination par les PCB chez les bars rayés de l'Hudson et de Long Island Sound au moyen de la microanalyse électronique du strontium des otolithes pour générer des séries temporelles de résidence des individus dans des milieux de salanités diverses. Les mâles fortement contaminés (concentration moyenne de PCB = 8.3 ppm) résidaient en eau douce et étaient rarement exposés à des salinités supérieures à 5 parties par millier. Plusieurs individus ont montré d'importants changements d'habitats. Les passages des habitats saumâtres ou marins aux habitats dulcicoles étaient souvent associés à des niveaux élevés de PCB. Une troisième situation a été observée dans le cas des grosses femelles, chez lesquelles le séjour dans les conditions polyhalines ou euhalines était associé avec des niveaux plus bas de PCB. La charge corporelle totale de PCB était corrélée négativement avec la salinité moyenne à laquelle les poissons étaient exposés durant la plus récente saison de croissance avant la capture. Les poissons récemment exposés à des conditions polyhalines ont montré une forte variabilité de leurs charges corporelles de PCB (0,4–9,0 ppm), ce qui laisse penser qu'il existe une source locale de contamination par les PCB dans la région du port de New York.

[Traduit par la Rédaction]

Introduction

The Hudson River commercial striped bass (*Morone saxatilis*) fishery has been closed since 1976 due to high levels of polychlorinated biphenyl (PCB) contamination (Brown et al. 1985; Limburg 1986). The mean PCB body burden in Hudson River striped bass continues to exceed the current U.S. Food and Drug Administration action limit of 2.0 ppm (Bush et al. 1989; Fabrizio et al. 1991). PCB contamination has resulted in an estimated annual loss of US$0.75–3.7 million to New York recreational and commercial striped bass fisheries (Kahn and Buerger 1994). In addition, recreational striped bass fishers have been issued annual fish consumption health advisories since 1976 (Sloan et al. 1986).

Received November 27, 1997. Accepted October 14, 1998. J14324

E.R. Zlokovitz and D.H. Secor.[1] University of Maryland Center for Environmental Science, Chesapeake Biological Laboratory, P.O. Box 38, Solomons, MD 20688-0038, U.S.A.

[1]Author to whom all correspondence should be addressed. e-mail: secor@cbl.umces.edu

A total of 2.7×10^5 kg of PCBs was discharged into the Hudson River estuary from about 1947 to 1987 (Thomann et al. 1991). The majority of PCB contamination to the Hudson River estuary resulted from a solvent washing process at the General Electric Corporation capacitor facility above the Troy Dam (river kilometre (Rkm) 246) (Bush et al. 1989). High levels of PCBs (mean 18.1 ppm total PCBs) were found in the edible flesh of the striped bass in 1978 (Horn and Sloan 1985; Bush et al. 1989). As a condition of the 1975 Settlement Agreement signed by General Electric Corporation and the New York State Department of Environmental Conservation, discharge of PCBs from the General Electric Corporation capacitor manufacturing plant was terminated in June 1977 (Hetling et al. 1978; Armstrong and Sloan 1988). PCB concentrations in striped bass initially declined with the significant reduction in upstream loadings. However, concentrations through the 1980s showed little decline and have persisted above levels considered unsafe for human consumption (Sloan et al. 1995).

High-discharge events and dredging projects in the upestuary region have exacerbated contamination throughout the Hudson River by reintroducing buried contaminants. This has resulted in a PCB gradient within the biota that is

© 1999 NRC Canada

positively related to river kilometre (Limburg 1986; Bush et al. 1989). For instance, in 1994, total PCB concentrations in striped bass were highest (mean = 6.4 ppm wet weight) in the Albany/Troy region (Rkm 246) and concentrations decreased with distance downstream to about 1.9 ppm in the Tappan Zee region (Rkm 40) (Sloan et al. 1995). In 1994, mean PCB levels in striped bass were <2.0 ppm in Long Island Sound and New York's marine district.

Levels of PCB contamination are expected to be affected by patterns of habitat use by striped bass, which often undertake coastal migrations away from the Hudson River system. The current model of the long-term behavior of PCBs in Hudson River striped bass assumes that striped bass >2 years old occur in coastal habitats during the summer months and use coastal habitats for the majority of the year by age 6 (Thomann et al. 1989). Using otolith microanalysis to investigate migrations, Secor and Piccoli (1996) observed a contingent of resident fish in the upper estuary near the Troy Dam (Rkm 246) that did not participate in coastal migrations. They hypothesized that these fish were most vulnerable to PCB contamination because they fed and grew in close proximity to the most highly contaminated sediments in the Hudson River estuary. Conversely, we expected that fish that participated in regular coastal migrations, or fish that established long-term residence in polyhaline/euhaline habitats, would have lower PCB body burdens due to growth dilution in relatively "clean" habitats.

The objective of this study was to use otolith microanalysis to (*i*) verify the proposed link between habitat use and PCB body burden in Hudson River striped bass (i.e., resident fish should have high PCB body burden) and (*ii*) examine the effects of season, sex, and place of collection on habitat use and PCB body burden.

Methods

The New York State Department of Environmental Conservation has routinely sampled striped bass in the Hudson River, south shore of Long Island, and Long Island Sound for PCB contamination since 1976. Most fish are collected by beach haul seine (150 m long × 3.7 m deep), although some coastal samples were provided by fishers. Fish selected for PCB analysis were filleted (skin not removed) and then frozen. Muscle tissue from fillets was shipped to Hazleton Laboratories America, Inc., Madison, Wis., for gas chromatography PCB analysis (Aroclor method). We used total PCB values, based on wet weight (measured in parts per million), which is a sum of major Aroclors.

We subsampled 1994 and 1995 samples to represent season, sex, collection site, and PCB level as homogeneously as possible (Table 1). Individuals with PCB burden ≥1.8 ppm were considered "hot" and those with <1.8 ppm were considered "cold." This criterion was close to the U.S. Food and Drug Administration's action limit and represented the 50th percentile in PCB levels in the striped bass analyzed for otolith Sr (Fig. 1). Adult females (n = 43) and males (n = 45) were sampled from the Troy Dam region (Rkm 246), Catskill (Rkm 179), Poughkeepsie (Rkm 122), Haverstraw Bay (Rkm 64), Tappan Zee bridge (Rkm 43), Manhattan (Rkm 19), New York City Harbor, eastern Long Island Sound, and Long Island's south shore (Fig. 2; Table 1). Females ranged in size from 463 to 1007 mm total length and in age from 3 to 15 years. Males ranged in size from 457 to 858 mm and in age from 3 to 16 years (Table 1).

Table 1. Sample of spring- and fall-collected Hudson River striped bass.

	Females				Males			
	"Hot" (≥1.8 ppm PCBs)		"Cold" (<1.8 ppm PCBs)		"Hot" (≥1.8 ppm PCBs)		"Cold" (<1.8 ppm PCBs)	
	≥Rkm 90	<Rkm 90	≥Rkm 90	<Rkm 90	≥Rkm 90	<Rkm 90	≥Rkm 90	<Rkm 90
Fall (August–December, n = 47)								
Total PCB (ppm)	7.6±0.68	3.54±0.59		0.49±0.08	8.34±1.10	4.64±0.80		0.51±0.04
n	3	9	0	13	8	8	0	6
Total length (cm)	872.67±53.48	711.89±42.78		641.08±47.27	588.25±22.25	700±35.27		561.67±41.23
Weight (g)	7476.67±969.64	4138.89±686.77		3080.77±725.92	2093.75±299.31	4031.25±726.82		2295±616.76
Age (years)	12.33±1.67	8.00±1.03		6.15±1.10	7.63±0.82	9.13±0.93		4.33±0.33
Lipid (%)	4.98±1.01	5.12±0.64		3.77±0.54	3.41±0.76	5.41±1.45		5.82±0.52
Spring (April–June, n = 41)								
Total PCB (ppm)	4.88±1.00		1.07±0.09	1.03±0.17	6.78±1.31	2.51±0.01	0.86±0.09	0.7312±0.03
n	3	0	10	5	10	2	6	5
Total length (cm)	664.33±58.67		787.8±26.12	682±75.37	617.7±17.54	583.0±62.0	639.17±35.0	610.0±21.48
Weight (g)	3206.67±719.48		5926.9±701.76	4262.8±1806.09	2740±219.63	2650.0±450.0	3000.0±480.64	2528.0±324.32
Age (years)	6.33±0.88		7.8±0.55	6.6±1.36	8.5±1.14	6.5±1.5	5.67±0.76	5.00±0.32
Lipid (%)	6.34±0.66		4.50±0.37	5.842±1.09	6.33±1.08	7.08±1.42	5.56±0.65	5.49±0.93

© 1999 NRC Canada

Fig. 1. Total wet PCBs in an examined sample of Hudson River striped bass. The modeled lognormal distribution is presented by the curve.

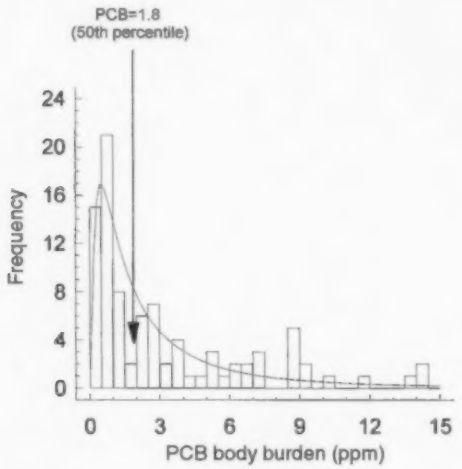

Sagittal otoliths were removed from striped bass carcasses that had been sampled previously for PCB analysis. Otoliths were cleaned with 10% bleach solution and embedded in Spurr low-viscosity resin. Otoliths were sectioned transversely (sections were about 1 mm thick) through the otolith cores using a low-speed diamond metallurgical wafering saw. Sections were mounted on glass slides, polished initially with wet 600-grit sandpaper to remove major marks and scratches, and then polished in a slurry of 0.3-μm alumina until their surfaces were free of pits and abrasions. This polishing method was used to minimize artifacts in microprobe analysis (Kalish 1990). Finally, sections were rinsed with deionized water and placed in an ultrasonic cleaner to remove any residue resulting from the polishing procedure.

Annuli in striped bass otoliths have been verified to form at an annual rate, and precision in age determination was estimated to exceed 95% (Secor et al. 1995*a*). Each annulus comprised a narrow opaque zone and a wide translucent zone when viewed under transmitted light microscopy. Annuli were counted once for each fish under light microscopy (magnification 60 or 150×) along the sulcal ridge in transverse sections by a single reader.

Electron probe otolith microanalysis of Sr and Ca was performed by X-ray wavelength dispersive spectrometry using a JEOL JXA-840A microprobe (Center for Microanalysis, University of Maryland, College Park, Md.). Measurement of atomic weights of Sr and Ca was standardized using strontianite ($SrCO_3$) and calcite ($CaCO_3$) standards (Secor 1992). We routinely used two transects per otolith, spacing each point of measurement 25 μm apart for the initial transect, which ran from the first to fifth annulus. The second transect traversed narrower annuli corresponding to older ages; spacing between points was set at 13 μm. Each point was about 5 μm in diameter. To reduce error between machine runs, Sr was expressed as a ratio, Sr:Ca. Backscatter electron micrographs for each analyzed otolith showed series of low relative atomic mass (dark) zones that corresponded to the optically opaque zones of annuli. Each 5-μm measured "point" was visible in electron micrographs. These points were related to the distance from succeeding opaque zones. Points directly within an opaque zone were considered to represent early spring, prior to spawning (Secor et al. 1995*a*), and were thus the last points associated with a given year of life. Points immediately succeeding the opaque zone were considered to form just after the spawning season and represent the first part of a given year of life (i.e., spring). Points between opaque zones were assumed to sample age in linear proportion. For example, if four points were measured from annulus 7 to 8, then points were assigned ages 7.0, 7.25, 7.50, and 7.75.

Time series data of Sr:Ca were compiled for each striped bass. Based on laboratory and field experiments, Secor et al. (1995*b*) developed a logistic relationship between salinity and otolith Sr:Ca:

$$\text{Salinity habitation (ppt)} = 40.302$$

$$(1 + 56.337\ e^{-1523.310(\text{Sr/Ca})})^{-1};\ r^2 = 0.94,\ n = 54.$$

This model was used to convert Sr:Ca values to salinity chronologies. Salinity habitation estimated the salinity inhabited for the period of time represented by each Sr:Ca datum. Residuals from the logistic model indicated that Sr:Ca typically predicted salinity habitation with a precision error of less than ±6 ppt.

Mean salinities of the most recent growth season, the last two growth seasons, and the last three growth seasons were used as measures of recent habitat use. These variables were regressed against PCB level and contrasted using sequential sums of squares. The most recent growth season's habitat history explained most variance in PCB level, and this response was used to test season, sex, and site effects. To conduct a nested analysis of variance (ANOVA), fish were sampled across seasons (fall–winter versus spring), sexes (males versus females), PCB levels (<1.8 versus ≥1.8 ppm), and zone (<Rkm 90 versus ≥ Rkm 90). Fish analyzed from New York City Harbor, Long Island Sound, and the south shore of Long Island were only collected in fall and thus were excluded from the nested ANOVA. This reduced sample size from 88 to 63. The nested design directed the ANOVA to occur in hierarchal order at four levels:

$$\gamma_{ijklm} = \mu + \gamma_i + \beta_{j(i)} + \gamma_{k(ij)} + O_{\lambda(ijk)} + \xi_{(ijk\lambda)m}$$

where γ_{ijklm} is the salinity experienced by an individual during its last growth season, μ is the overall mean, γ_i is the effect of the ith season, $\beta_{j(i)}$ is the effect of the jth sex, $\gamma_{k(ij)}$ is the effect of the kth zone, $O_{\lambda(ijk)}$ is the effect of the λth PCB level, and $\xi_{(ijk\lambda)m}$ is the random error component.

Statistical significance for factors was accepted at $\alpha = 0.05$ (type I sum of squares for type I error). Analysis of covariance was also performed to examine the effects of season, sex, and site on the relationship between total PCB body burden and recent salinity history. Site categories were Troy/Catskill/Poughkeepsie (≥ Rkm 90), Haverstraw/Tappanzee (≥ Rkm 20, <Rkm 90), Manhattan/NYC Harbor (<Rkm 20), and Long Island (coastal). The response variable was $\log_{10}$ transformed to normalize residuals.

Results

Salinity chronologies from individual striped bass showed three distinct migratory behaviors. All fish captured during fall and winter in the upper estuary in the vicinity of the Troy Dam had high PCB levels. Fish were predominately resident, inhabiting salinities of 5 ppt or less throughout most of their lives (Fig. 3). A single female (PCB = 7.3 ppm) sampled from this region during fall also exhibited resident behavior. Resident behaviors associated with high PCB contamination also occurred for spring-collected males and females but were less dependent on site of collection. In some individuals, salinity chronologies indicated a habitat shift from either low to high or high to low salinity (Fig. 4). One individual captured in the Troy region (Rkm 246) with a PCB level of 10.5 ppm used mesohaline habitats early in life and then suddenly shifted to freshwater/oligohaline habitats. Alternatively, an individual with low PCB body burden (0.4 ppm) inhabited freshwater for its first two growth sea-

© 1999 NRC Canada

Fig. 2. Collection sites (triangles) in the Hudson River estuary.

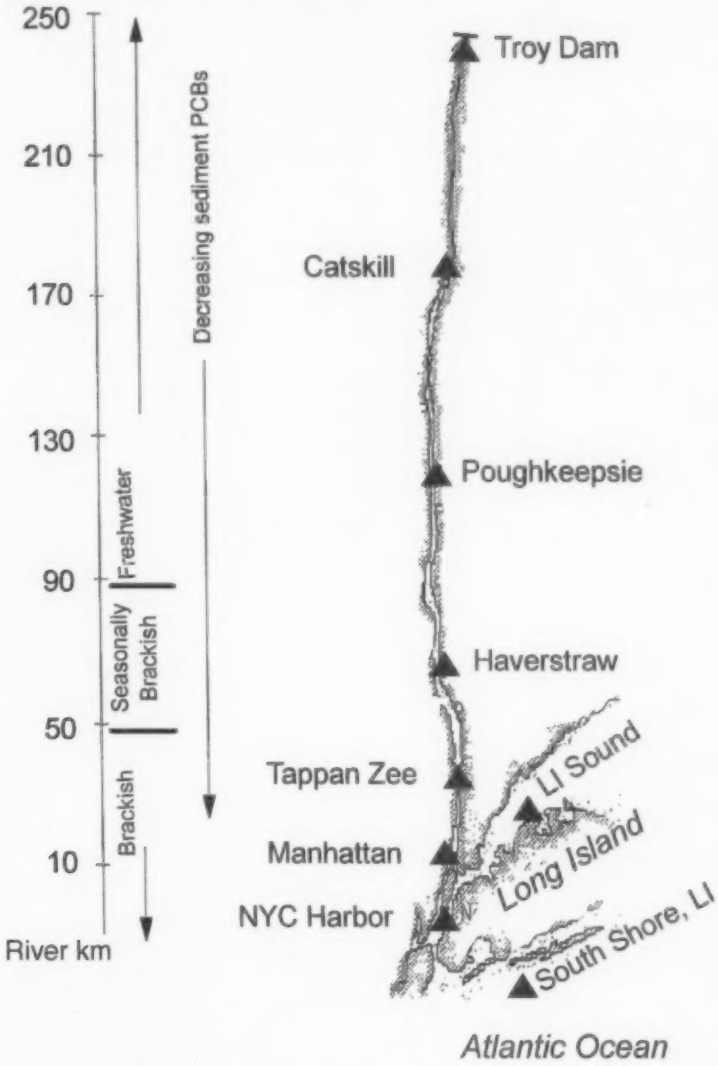

sons and then emigrated to marine or polyhaline habitats for the rest of its life. Shifts from low to high salinity were not always associated with low PCB body burdens. A Long Island captured fish with a relatively high PCB body burden (2.7 ppm) inhabited freshwater/oligohaline habitats early in life and then shifted to polyhaline/euhaline regions for most of the remainder of its lifetime (Fig. 4). A third pattern in migration was annual cycles from brackish to marine habitats, indicating possible spawning migrations (Secor and Piccoli 1996). Two such migrating females showed strong cyclic behavior (Fig. 5); the female with higher PCB body burden (7.2 ppm) inhabited lower salinity waters over its lifetime.

Salinity records for each individual were used to compute lifetime means, an overall index of an individual's past habitat use. Frequency distributions of lifetime salinities showed that fish classified as cold (<1.8 ppm) tended to grow in mesohaline/polyhaline environments (Fig. 6). Individuals classified as hot (≥1.8 ppm) and highly contaminated (≥4 ppm) tended to use predominately freshwater and oligohaline environments throughout their lives.

Salinity history over the most recent growth season explained slightly more variance in PCB level than other measures of recent habitat use and was used as an index of recent habitat history (Fig. 7). The PCB classification effect on recent habitat history was highly significant, explaining 22% of model variance. There was a significant, albeit highly variable, effect of total length ($p = 0.03$) on recent salinity history. Therefore, total length was included in the ANOVA as a covariate. ANOVA showed significant effects due to all factors except season (Table 2). Therefore, the nested analysis showed that PCB level was significantly influenced by recent habit history regardless of effects due to

© 1999 NRC Canada

Fig. 3. Representative time series of salinity habitation for resident striped bass. Salinity habitation was determined based on microanalysis of Sr:Ca. Total PCB body burdens (wet weight based) are indicated. Total PCB body burden was determined through the Aroclor method on a single fillet with skin on and scales removed (muscle tissue).

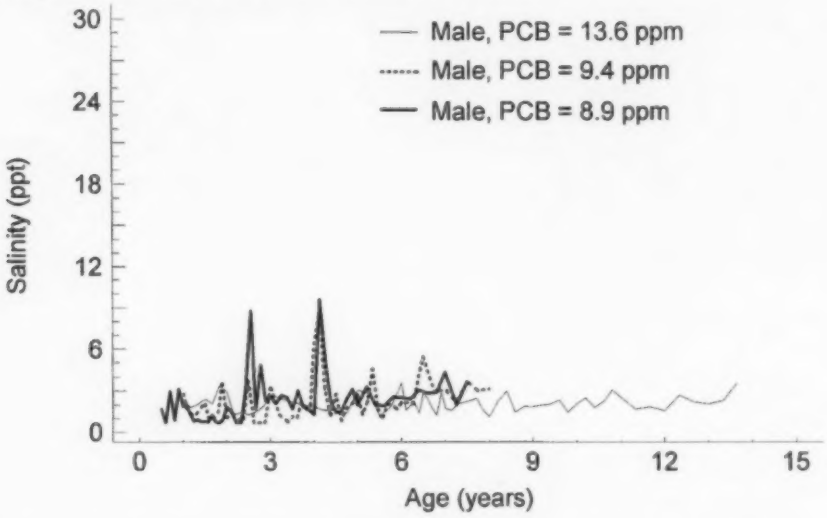

Fig. 4. Representative time series of salinity habitation of striped bass showing habitat shifts. Salinity habitation was determined based on microanalysis of Sr:Ca. Total PCB body burdens (wet weight based) are indicated.

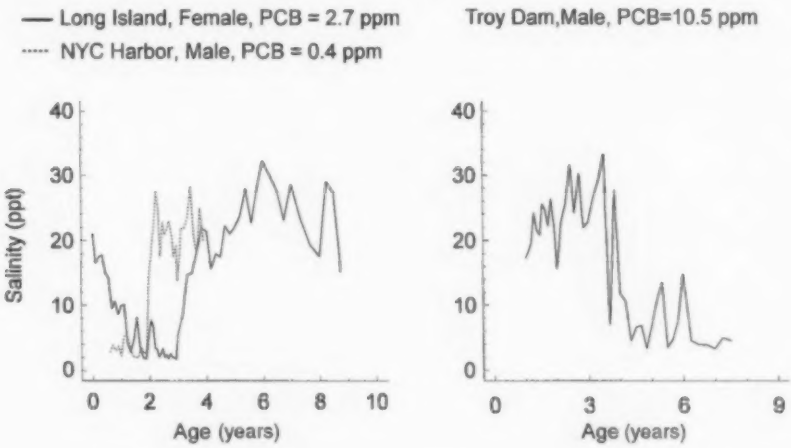

size, sex, or site of collection. Site of collection explained most variance (36%); where fish are collected was largely influenced by where they had recently occurred.

PCB body burden was strongly and inversely related to recent salinity history ($r = -0.71$, $p < 0.001$). There was no significant effect of season on the relationship between recent salinity history and total PCBs (Fig. 7). In an ANOVA using salinity history as a covariate, sex did not significantly affect total PCBs ($p < 0.42$). Similarly, no season effect was observed on the relationship between recent habitat history and total PCBs ($p > 0.32$) (Figs. 7 and 8). Site did significantly influence the relationship between total PCBs and recent habitat history ($p = 0.05$). The site effect was due to fish collected in the upper Hudson River estuary (≥Rkm 90), which showed resident behaviors and high PCB contamination (Fig. 8).

Discussion

A previous model of PCB contamination in Hudson River striped bass (Thomann et al. 1991) assumed that the entire population of striped bass began emigrating into coastal environments following sexual maturity. However, salinity chronologies determined for striped bass collected during 1994–1995 corroborate recent findings (Secor and Piccoli 1996), which indicated that Hudson River striped bass migratory behavior is highly variable. We observed a resident contingent of fish, predominately males, in the upper Hudson

© 1999 NRC Canada

Fig. 5. Representative time series of salinity habitation of female striped bass showing anadromous migratory behavior. Salinity habitation was determined based on microanalysis of Sr:Ca. Total PCB body burdens (wet weight based) are indicated.

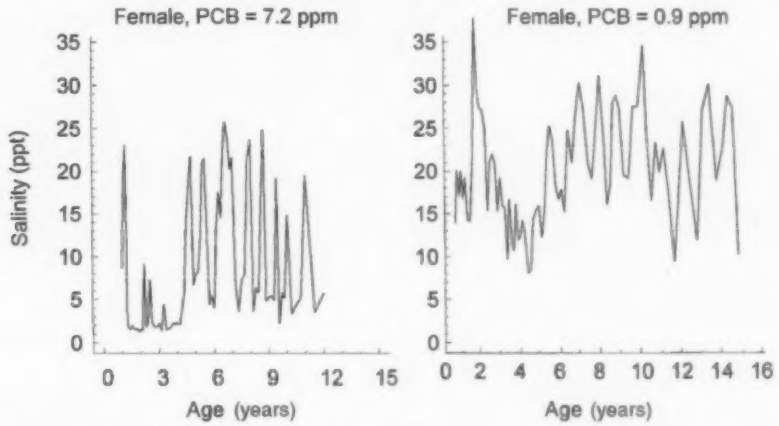

Fig. 6. Frequency histogram of lifetime salinity habitation for "cold" (<1.8 ppm PCBs), "hot" (≥1.8 ppm PCBs), and highly contaminated (≥4 ppm PCBs) Hudson River striped bass.

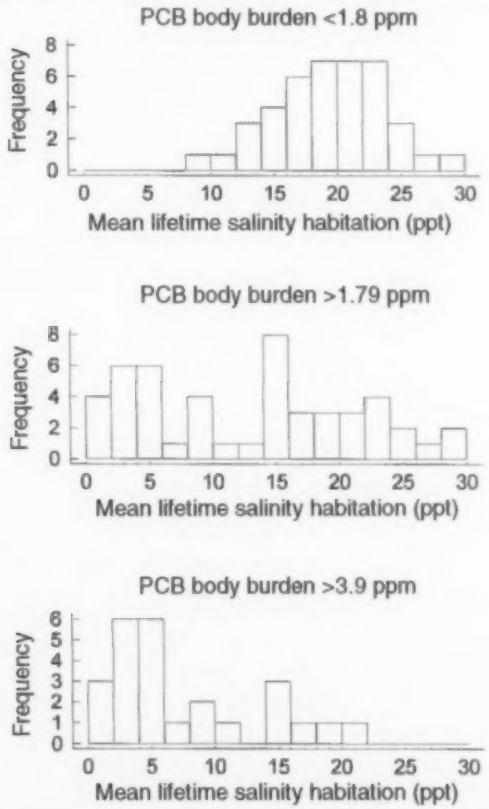

Fig. 7. Mean salinity history of the most recent growth season versus total PCB body burden in striped bass by season and sex. The coefficient of determination for a power function is indicated.

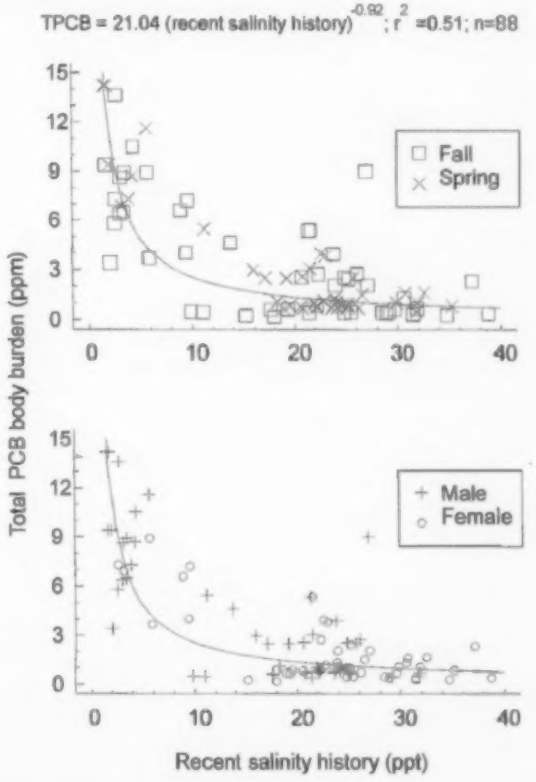

River estuary that were apparently susceptible to high PCB contamination. This trend is supported by the close proximity of this contingent to the most highly contaminated sediments in the Hudson River estuary. Important forage fish for striped bass, blueback herring (*Alosa aestivalis*) and alewife (*Alosa pseudoharengus*) congregate below Troy Dam and

© 1999 NRC Canada

Table 2. Nested ANOVA of season, sex, site of collection, and level of PCB contamination effects on recent salinity history (n = 63).

Variable	df	Sum of squares	Significance level (p)
Covariate			
Total length	1	336.1	0.002
Class variable			
Season	1	394.6	0.001
Sex (season)	2	155.9	0.11
Site (season–sex)	4	790.8	0.001
PCB (season–sex–site)	6	487.7	0.04

Note: Striped bass total length was used as a covariate in the analysis. Season levels were fall and spring, site levels were ≥Rkm 90 and <Rkm 90, and PCB levels were <1.8 and ≥1.8 ppm. Factors in parentheses indicate the nesting procedure. For example, PCB (season–sex–site) refers to variance explained by PCB level nested within combinations of season, sex, and site.

Fig. 8. Mean salinity history of the most recent growth season versus total PCB body burden in striped bass by collection site.

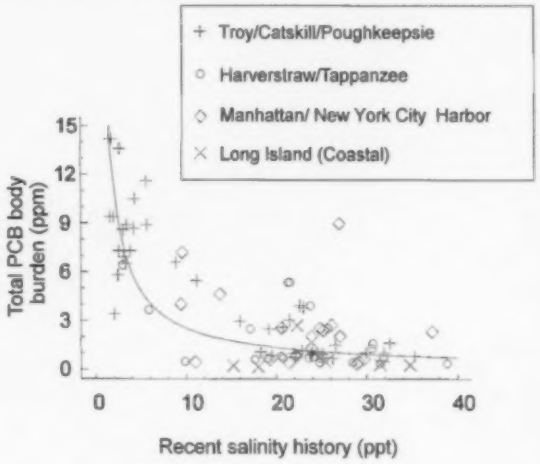

may play a role in the resident behavior of striped bass and their high contaminant levels (K. Hattala, New York State Department of Environmental Conservation, New Paltz, N.Y., personal communication). Sloan and Armstrong (1988) reported total PCB levels of 2–5 ppm for these species from 1980 collections.

In our application of otolith microanalysis, we assumed that Sr in striped bass otoliths was reflective of where the fish lives. This assumption is based on laboratory and field studies (Secor et al. 1995*b*) that showed a strong positive relationship between salinity and Sr:Ca in striped bass otoliths. We have also assumed that otolith microanalysis proportionately sampled all seasons. For instance, otolith growth probably slows or ceases during the midwinter months. Therefore, we are not sampling each season equally. Nevertheless, because PCB uptake is expected to occur primarily in growing fish, we believe that otolith microanalysis serves as a useful measure of habitat history in contaminant studies.

Recent habitat use was a strong determinant of PCB contamination. ANOVA and regression tests showed that recent salinities at which striped bass grew were strongly and negatively related to PCB levels independent of any effects due to season, sex, site of collection, or fish size. Results supported the expectation that fish inhabiting highly contaminated freshwater regions during the growth season before capture will not be able to significantly reduce body burden due to growth dilution. In some cases, otolith microanalysis revealed that fish that shifted from coastal or brackish habitats to up-estuary freshwater habitats were likely to show high PCB levels. However, the converse was not always true: fish that shifted from freshwater to brackish marine habitats did not always reduce their PCB levels, again indicating the possibility of a down-estuary source of PCBs. This result corresponds to recent observations of relatively high mean PCB levels in fish collected in the New York Harbor region (Skinner et al. 1996). For instance, in 1993, mean PCB level for this region was 3.4 ppm (Sloan et al. 1995), a level much higher than adjacent up-estuary regions. This level is in contrast with the overall pattern of down-estuary dilution of PCBs and indicates other sources of PCBs in the Hudson River estuary.

Unlike commercial fishing in the Hudson River, recreational angling for striped bass has become an increasingly important industry over the past decade. At present, the New York State Department of Environmental Conservation allows anglers possession of two fish of at least 71 cm total length. High fishing effort by charter, party, and private vessels as well as shore angling exists in the Hudson River estuary and along both coasts of Long Island (B. Young, New York State Department of Environmental Conservation, East Setauket, personal communication). Striped bass collected in the upper estuary (≥Rkm 90) during the fall are likely to be resident fish that are highly contaminated. Fishing in the upper estuary should continue to be restricted. In addition, health warnings could be revised to reflect the increased likelihood of contaminated striped bass collected in up-estuary regions during fall. Fishing effort in the lower estuary (Rkm 0–60) and Long Island Sound predominantly targets fish that are part of a more highly migratory contingent. Therefore, fish captured in these regions are less likely to be highly contaminated.

Previous models of the long-term behavior of PCBs in striped bass were biased towards coastal habitat use in adult striped bass and underrepresented PCB burdens in the overall Hudson River population. The fraction of the population that is resident (or spends parts of its life in the New York Harbor region) is unknown and would be expected to vary on an annual and generational time frame based on changes in recruitment and exploitation of the more migratory contingents of the population. The high degree of variability and unpredictability in the spatial dynamics of the Hudson River striped bass prescribes more intensive monitoring of migration patterns and individual-based modeling approaches (Van Winkle et al. 1993) to predict future rates of PCB loss.

Acknowledgments

Dr. Phil Piccoli provided expertise and training on X-ray wavelength dispersive spectrometric electron microanalysis. We are grateful to K. Hattala and R. Sloan of the New York Department of Environmental Conservation who provided

© 1999 NRC Canada

access to striped bass sampled for PCBs. This research was sponsored by the Hudson River Foundation and is contribution number 3237 of the University of Maryland Center for Environmnetal Science.

References

Armstrong, R.W., and Sloan, R.J. 1988. PCB patterns in Hudson River fish. *In* Fisheries Research in the Hudson River. *Edited by* C.L. Smith. State University of New York Press, Albany, N.Y.

Brown, M.P., Werner, M.B., Sloan, R.J., and Simpson, K.W. 1985. Polychlorinated biphenyls in the Hudson River. Environ. Sci. Technol. **19**: 656–661.

Bush, B., Streeter, R.W., and Sloan, R.J. 1989. Polychlorobiphenyl (PCB) congeners in striped bass (*Morone saxatilis*) from marine and estuarine waters of New York State determined by capillary gas chromatography. Arch. Environ. Contam. Toxicol. **19**: 49–61.

Fabrizio, M.C., Sloan, R.J., and O'Brien, J.F. 1991. Striped bass stocks and concentrations of polychlorinated biphenyls. Trans. Am. Fish. Soc. **120**: 541–551.

Hetling, L.J., Horn, E., and Tofflemire, T.J. 1978. Summary of Hudson River PCB study results. Tech. Pap. 52. New York State Department of Environmental Conservation, Albany, N.Y.

Horn, E.G., and Sloan, R.J. 1985. PCB in Hudson River striped bass — 1984. Division of Fish and Wildlife, New York State Department of Environmental Conservation. Albany, N.Y.

Kahn, J.R., and Buerger, R.B. 1994. Valuation and the consequences of multiple sources of environmental deterioration: the case of the New York striped bass fishery. J. Environ. Manage. **40**: 257–273.

Kalish, J.M. 1990. Use of otolith microchemistry to distinguish progeny of sympatric anadromous and non-anadromous salmonids. Fish. Bull. US. **88**: 657–666.

Limburg, K.E. 1986. PCBs in the Hudson River. *In* The Hudson River ecosystem. *Edited by* K.E. Limburg, M.A. Mosan, and W.H. McDowell. Springer-Verlag, New York. pp.83–130.

Secor, D.H. 1992. Application of otolith microchemistry analysis to investigate anadromy in Chesapeake Bay striped bass, *Morone saxatilis*. Fish. Bull. U.S. **90**: 798–806.

Secor, D.H., and Piccoli, P.M. 1996. Age and sex dependent migrations of striped bass in the Hudson River as determined by chemical microanalysis of otoliths. Estuaries, **19**: 778–793.

Secor, D.H., Trice, T.M., and Hornick, H.T. 1995*a*. Validation of otolith-based aging in Chesapeake Bay striped bass by mark–recapture with a comparison of otolith and scale-based aging. Fish. Bull. US. **93**: 186–190.

Secor, D.H., Henderson-Arzapalo, A., and Piccoli, P.M. 1995*b*. Can otolith microchemistry chart patterns of migration and habitat utilization in anadromous fishes? J. Exp. Mar. Biol. Ecol. **192**: 15–23

Skinner, L.C., Jackling, S.J., Kimber, G., Waldman, J., Shastay, J., Jr., and Newell, A.J. 1996. Chemical residues in fish, bivalves, crustaceans and a cephalopod from the New York – New Jersey Harbor Estuary: PCB, organochlorine pesticides, and mercury. New York State Department of Environmental Conservation, New York, N.Y.

Sloan, R.J., and Armstrong, R.W. 1988. PCB patterns in Hudson River fish: II. Migrant and marine species. *In*. Fisheries Research in the Hudson River. *Edited by* C.L. Smith. State University of New York Press, Albany, N.Y. pp. 325–350.

Sloan, R.J., Horn, E.G., Young, B., Zawacki, C., and Forti, A. 1986. PCB in striped bass from the marine district of New York – 1985, and contaminants in Hudson River striped bass: 1978–1985. Tech. Rep. 86-1(BEP). New York State Department of Environmental Conservation, Albany, N.Y.

Sloan, R., Young, B., and Hattala, K. 1995. PCB paradigms for striped bass in New York State. Tech. Rep. 95-1 (BEP). New York State Department of Environmental Conservation, Division of Fish and Wildlife, Division of Marine Resources, Albany, N.Y.

Thomann, R.V., Mueller, J.A., Winfield, R.P., and Huang, C. 1989. Mathematical model of the long-term behavior of PCBs in the Hudson River estuary. Hudson River Foundation Rep. Hudson River Foundation, New York.

Thomann, R.V., Mueller, J.A., Winfield, R.P., and Huang, C. 1991. Model of fate and accumulation of PCB homologues in the Hudson estuary. J. Environ. Eng. **117**: 161–178.

Van Winkle, W., Rose, K.A., and Chambers, R.C. 1993. Individual-based approaches to fish population dynamics. Trans. Am. Fish. Soc. **122**: 397–404.

© 1999 NRC Canada

Temporal and spatial variability of $^{13}C/^{12}C$ and $^{15}N/^{14}N$ in pelagic biota of Prince William Sound, Alaska

Thomas C. Kline, Jr.

Abstract: Stable isotope ratios of carbon and nitrogen were used to identify seasonal and spatial patterns in carbon and nitrogen and to determine source of energy (Prince William Sound (PWS) versus the Gulf of Alaska (GOA)) for juvenile fishes in PWS. PWS-wide samples of bulk net zooplankton (all noncalcareous zooplankton collected in 335-μm-mesh nets), individual late copepodid stage of the large herbivore *Neocalanus cristatus*, juvenile Pacific herring (*Clupea pallasi*), and juvenile walleye pollock (*Theragra chalcogramma*) were collected in spring, summer, and fall in 1994 and 1995. For bulk zooplankton and *N. cristatus*, there was a strong $^{13}C/^{12}C$ gradient but weak $^{15}N/^{14}N$ gradient within PWS and GOA. Zooplankton $^{15}N/^{14}N$ was positively correlated with $^{13}C/^{12}C$ during the phytoplankton bloom but was not correlated during the zooplankton bloom, suggesting a decoupling of nitrogen and carbon cycles. Plankton isotopic signatures suggested a diagnostic $^{13}C/^{12}C$ for GOA carbon. For juvenile fishes and diapausing copepods in PWS, $^{13}C/^{12}C$ varied between years, suggesting that the origin of carbon differed between years (GOA more so in 1995 than in 1994). Use of a natural stable isotope tracer provided evidence for biophysical coupling via inferred fluctuations in oceanographic processes.

Résumé : Des ratios d'isotopes stables du carbone et de l'azote ont été utilisés pour établir les profils saisonniers et spatiaux de ces deux éléments et déterminer la source d'énergie (baie Prince-William par rapport au golfe de l'Alaska) de poissons juvéniles de la baie Prince-William. Des échantillons de zooplancton en vrac (tous les organismes zooplanctoniques non calcaires recueillis dans des filets à mailles de 335 μm), des spécimens du dernier stade copépodite du gros herbivore *Neocalanus cristatus*, des harengs du Pacifique juvéniles (*Clupea pallasi*) et des goberges de l'Alaska juvéniles (*Theragra chalcogramma*) ont été recueillis au printemps, en été et à l'automne, en 1994 et 1995. Dans le cas du zooplancton en vrac et de *N. cristatus*, on a observé un fort gradient du ratio $^{13}C/^{12}C$ mais un gradient faible du ratio $^{15}N/^{14}N$ dans la baie Prince-William et le golfe de l'Alaska. Chez le zooplancton, le ratio $^{15}N/^{14}N$ était corrélé positivement avec le ratio $^{13}C/^{12}C$ pendant la prolifération phytoplanctonique; il ne l'était pas pendant la prolifération zooplanctonique, ce qui indiquerait un découplage des cycles de l'azote et du carbone. Les signatures isotopiques du plancton indiquent que le ratio $^{13}C/^{12}C$ donne des renseignements significatifs sur le carbone dans le golfe de l'Alaska. Chez les poissons juvéniles et les copépodes en diapause de la baie Prince-William, le ratio $^{13}C/^{12}C$ variait d'une année à l'autre; ainsi l'origine du carbone serait différente d'une année à l'autre (encore plus dans le golfe de l'Alaska en 1995 qu'en 1994). Cette utilisation d'un traceur isotopique stable naturel a révélé l'existence d'un couplage biophysique établie par inférence de fluctuations des processus océanographiques.

[Traduit par la Rédaction]

Introduction

Prince William Sound (PWS) is a complex and dynamic ecosystem that is influenced by oceanographic processes occurring in the Gulf of Alaska (GOA). Montague and Hinchinbrook islands form the southern boundary separating PWS from the GOA. The Alaska Coastal Current (ACC) transports oceanic waters into this fjordlike inland sea through the gap between the two islands known as Hinchinbrook Entrance (Niebauer et al. 1994). Variability in the effects of the ACC-driven circulation is being examined in an ecosystem-level study called Sound Ecosystem Assessment (SEA). SEA is examining trophic interactions to see if the flow of energy through the food web is impeding recovery of fish stocks in PWS. For example, Pacific herring (*Clupea pallasi*) populations have supported important commercial and subsistence fisheries. However, since 1993, Pacific herring have not been abundant enough to harvest. Furthermore, the failure of populations of many PWS vertebrate consumers of Pacific herring and other fishes to recover from moralities induced by the 1989 oil spill of the T/V *Exxon Valdez* may, in part, be due to physically forced ecosystem-level shifts occurring in the GOA (Brodeur and Ware 1992; Francis and Hare 1994; Ingraham et al. 1998).

The principal SEA hypothesis, known as the river–lake hypothesis, states that spatial and temporal variability in regional oceanographic conditions controls production in PWS. Conditions are postulated to vary from lentic (lake-

Received October 8, 1997. Accepted September 17, 1998.
J14234

T.C. Kline, Jr. Prince William Sound Science Center, P.O. Box 705, Cordova, AK 99574, U.S.A. e-mail: tkline@.pwssc.gen.ak.us

© 1999 NRC Canada

like, weak ACC) to lotic (riverlike, strong ACC) in relation to the strength and influence of the ACC on PWS. These processes are further hypothesized to affect both bottom-up and top-down biological processes that in turn affect recruitment of exploited fish stocks. The advective regime connecting the northern GOA with PWS is postulated to control recruitment and nutritional processes in fishes. Since interzonal copepods (Miller and Terazaki 1989) are the dominate larger copepods of the subarctic Pacific (Miller et al. 1984), their role in the zooplankton advected from the GOA (Cooney 1988) was of special interest.

The natural abundance of nitrogen and carbon stable isotope ratios measured in aquatic biota is useful for reconstructing the flow of organic material in food webs. There may be considerable carbon and nitrogen isotopic variability in the supply of organic material for marine pelagic food webs that is passed on to higher trophic levels with consistent enrichment of ^{13}C and ^{15}N effecting $\delta^{13}C$ and $\delta^{15}N$ (eq. 1) increases of about 1 and 3.4‰ per trophic level, respectively (DeNiro and Epstein 1978, 1981; McConnaughey and McRoy 1979; Rau et al. 1983; Minagawa and Wada 1984; Wada et al. 1991; Hobson and Welch 1992; Cabana and Rasmussen 1994). Determination of temporal and spatial patterns of carbon and nitrogen stable isotope variability at the food web base in an ecosystem study provides a context for tracing material flow to higher trophic levels (Fry 1988; Dunton et al. 1989). Isotopic signatures are generated by primary producers, which are then transferred to consumers such as microcrustacea (Fry and Sherr 1984; Fry 1988; Goering et al. 1990; Wu et al. 1997) that are an important forage base for fishes. Isotopic characterization of the food web base using herbivores provides a good ecosystem baseline (Vander Zanden et al. 1997). For example, analysis of herbivorous zooplankton eliminates the compositional uncertainty associated with particulate organic material samples typically used as a proxy for phytoplankton and its consequential confounding effects on data (Owens 1987). Furthermore, an isotopic context based on the temporal and spatial variability in zooplankton is appropriate for using isotope techniques to understand material flow in fish food webs that are dependent on a zooplankton forage base.

The overall objective of this study was to assess the temporal and spatial variability of carbon and nitrogen stable isotope abundance in the pelagic ecosystem. The spatial and temporal patterns in the variability of the isotopic composition of zooplankton were determined from bulk net zooplankton collections made on research cruises before, during, and after the spring zooplankton bloom (March–June) as well as during late summer (September). Individual zooplankters of various taxa were collected initially to assess effects of zooplankton species composition on isotopic signatures, and later only a large interzonal (Miller and Terazaki 1989) copepod of the genus *Neocalanus*, an important taxon that dominates the zooplankton of the epipelagic North Pacific (Miller et al. 1984). Zooplankton were then compared isotopically with juvenile Pacific herring and walleye pollock (*Theragra chalcogramma*) sampled within the same geographical area to assess their linkages with carbon sources represented by zooplankton. This provided a context for assessing carbon source dependencies by rapidly growing juvenile pelagic fishes, Pacific herring and walleye pollock, in PWS, since they were predicted by the river–lake hypothesis to change from year to year.

Materials and methods

Field sampling

Zooplankton

Zooplankton were collected during April, May, September, and November of 1994 at sampling stations in western PWS and in March, April, May, June, September, and October of 1995 at sampling stations in PWS and the adjacent GOA (Fig. 1; Appendix) from the F/V *Alaska Beauty* and R/V *Bering Explorer*. Sampling techniques varied according to month, year, and target taxa. A 0.5-m-diameter, 335-μm-mesh plankton net was towed from 50 m (determined by meter wheel and wire angle) to the surface and from about 20 m above the bottom to the surface at 1 $m \cdot s^{-1}$ to collect upper 50 m and water column bulk zooplankton samples, respectively. Bulk samples collected from March to June 1995 were immediately inspected for all late-stage (copepodite stages IV–VI) *Neocalanus cristatus* and other large (length greater than about 7 mm) zooplankters. Macrozooplankters were also removed (by forceps, but in the laboratory) from the bulk zooplankton collections made in 1994. Macrozooplankers were also collected using a beam trawl (5-mm mesh) towed from about 200 m depth at station SEA4 (Fig. 1) in April 1994 and Tucker trawls (1-mm mesh) towed to 400 m at stations SEA22 and SEA27 (Fig. 1) in November 1994. Diapausing *N. cristatus* were collected using a closing Puget Sound net (Miller et al. 1984) towed from about 20 m above the bottom to 200 m below the surface in September 1995.

Removal of nondietary carbon from bulk plankton samples was effected by removal of shelled pteropods. This approach was used instead of acid treatment in order to avoid potential artifacts (Goering et al. 1990; Bunn et al. 1995). Shelled pteropods were removed from bulk plankton samples by (*i*) forcepting, (*ii*) screening with a 2-mm-mesh sieve after selective removal of macrozooplanton, and (*iii*) decanting after allowing the sample to settle in a beaker.

Bulk zooplankton samples (after removal of macrozooplankters and pteropods) were placed in 125-mL polyethelene jars (VWR Trace-clean) and frozen in shipboard freezers (–20°C). *Neocalanus cristatus* and other macrozooplanter samples were placed in polyethylene Omni-vials (Wheaton) and frozen. In the laboratory, frozen bulk samples were thawed and rinsed in tap water to remove salts using a 223-μm-mesh Nitex sieve. Rinsed samples were returned to their jars, frozen, and then freeze-dried in a Labconco Shelf Drier – 6 Liter Freeze Drier unit. Bulk freeze-dried samples were ground to a fine powder using a dental amalgamator (Crescent Dental Wig-L-Bug) and returned to their jars. Omni-vial samples were uncapped and freeze-dried without rinsing. Freeze-dried samples were inventoried and all selected samples shipped to the University of Alaska Fairbanks Stable Isotope Facility for isotopic analysis.

Juvenile Pacific herring and walleye pollock

Juvenile Pacific herring (N = 360) and walleye pollock (N = 287) were collected throughout PWS opportunistically during 1994 and from a multivessel broadscale survey (Norcross et al. 1996) conducted from October to November 1995 (Fig. 1). During the broadscale survey, a lead acoustic vessel located concentrations of fishes, which were then sampled with a purse seine (50 m diameter by 4 m deep with 3-mm mesh (stretched)). On the trailing vessel, a random sample of 200 Pacific herring (range about 70–150 mm standard length (ages 0 and 1)) and 200 walleye pollock (range about 70–100 mm fork length (age 0)) were immediately frozen

© 1999 NRC Canada

Fig. 1. Sampling stations and potential copepod diapause habitat in PWS, Alaska. Zooplankton were sampled at designated oceanographic stations that had alphanumeric names (listed in the Appendix). Fishes were sampled near map symbols consisting of single letters (A–N). The names of these sites are given in Table 6. Potential diapause habitat is the area of PWS deeper than 400 m, as indicated by shading.

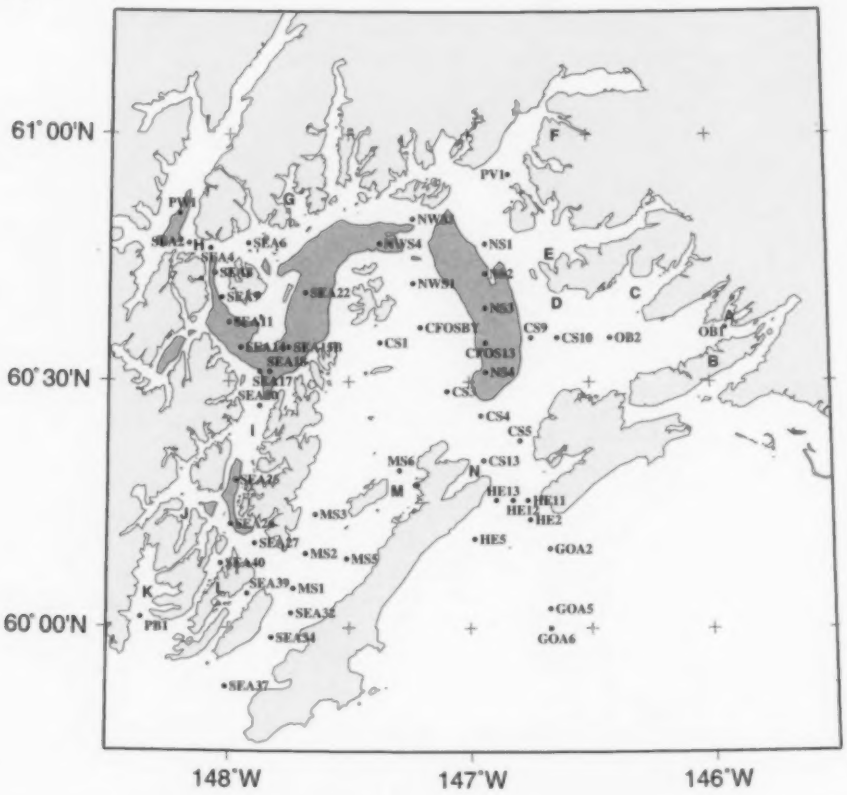

(–20°C) in seawater at each study site for paired energetic (Paul et al. 1998) and isotopic analysis (this study). Laboratory handling procedures were described by Paul et al. (1998). Following energetic analysis (Paul et al. 1998), dried fish samples were sent from Seward, Alaska, to Cordova, Alaska, for isotopic analysis preparation. For 1995 sampling, 25 Pacific herring and 25 walleye pollock were randomly selected from each sampling area, ground to a fine powder, sealed in polyethylene LSC (Wheaton) vials, and shipped to the University of Alaska Fairbanks Stable Isotope Facility for isotopic analysis. In 1994, fish samples were obtained using similar gear and analysis techniques.

Isotopic analysis and data modeling

Replicate subsamples of about 1.5 mg were taken from all samples except individual macrozooplankters, since the entire organism was required for a single analysis. Subsamples or whole zooplankters, as appropriate, were weighed to the nearest 1 μg and loaded into combustion boats for mass spectrometric analysis. Isotopic analyses were performed using a semiautomated stable isotope analyzer (Europa Scientific 20/20 equipped with a Roboprep sample combustion and purification unit). A single isotopic analysis generated the following data: $^{13}C/^{12}C$ and $^{15}N/^{14}N$ ratios expressed in standard delta units, $\delta^{13}C$ and $\delta^{15}N$, respectively, and %C and %N. The conventional delta notation used to express stable isotope ratios is reported relative to international standards (air for nitrogen and Vienna Peedee belemnite for carbon) and defined by the following expression:

$$(1) \qquad \delta^{15}N \text{ or } \delta^{13}C\ (‰) = \left(\frac{R_{sample}}{R_{standard}} - 1\right) \times 1000$$

where $R = {}^{15}N/{}^{14}N$ or $^{13}C/^{12}C$. By definition, the isotope standards have delta values of zero, i.e., $\delta^{15}N = 0$ for atmospheric N_2. Typically, instrument replication is <0.2‰. The %C and %N data were used to calculate C/N atomic ratios. The data presented consist of mean $\delta^{13}C$, $\delta^{15}N$, and C/N for all replicated samples.

Removal of lipid (DeNiro and Epstein 1977) and trophic level (see Introduction) effects from $\delta^{13}C$ values of fish made it possible to assess carbon source (Kline 1997). $^{13}C/^{12}C$ content of PWS nekton was correlated with C/N (a proxy for lipid content) and $^{15}N/^{14}N$ content (a proxy for trophic level), thus requiring lipid and trophic level normalization (Kline 1997). The method of McConnaughey and McRoy (1979) was used to calculate lipid-normalized $^{13}C/^{12}C$, while the method of Kline (1997) was used to normalize for trophic level. Lipid normalization was based on C/N using a C/N = 4 as the base level (McConnaughey and McRoy 1979). Normalization for trophic level effects used (*i*) the $\delta^{15}N$ value of the herbivore *N. cristatus* as the trophic level baseline (Vander Zanden et al. 1997) and (*ii*) an assumed constant nitrogen and carbon trophic fractionation factor ratio of 3.4:1. In general, normalization reduces sources of ^{13}C variability, enabling comparisons among species without the confounding effects of trophic level and lipid content (Kline 1997). Thus, normalized $^{13}C/^{12}C$ values of fishes

© 1999 NRC Canada

could be compared directly with those of *N. cristatus* at a consistent lipid storage level.

The expressions $\delta^{13}C$, $\delta^{13}C'$, $\delta^{13}C_{TL}$, and $\delta^{13}C'_{TL}$ denote $^{13}C/^{12}C$ abundance in relation to the international standard, normalized for lipid content, normalized for trophic level, and normalized for lipid content and trophic level, respectively. Whereas $\delta^{13}C'$, $\delta^{13}C_{TL}$, and $\delta^{13}C'_{TL}$ are used in accordance with a particular data analysis context, ^{13}C is used to reflect generic $^{13}C/^{12}C$ isotopic trends irrespective of normalization.

Data mapping

Areal distributions of isotopic data were mapped and contoured using the Generic Mapping Tools computer program (Smith and Wessel 1990; Wessel and Smith 1995).

Data analyses and modeling

Correlation analyses aided the data comparisons. Assessment of isotopic shifts occurring during the spring bloom followed the analysis technique of Goering et al. (1990) using $\delta^{13}C$ versus $\delta^{15}N$ regressions. Data were regressed collectively and by month. To eliminate confounding effects of higher trophic level taxa found in bulk net samples, isotopic analysis in 1995 focused on the large interzonal copepod *N. cristatus*. Correlation analysis was used to compare the isotopic values of *N. cristatus* with those of the bulk net samples from which they were collected.

An empirical model was developed to integrate spatial and temporal variability using statistics calculated from third-order polynomial regressions for $\delta^{13}C$, $\delta^{13}C'$, and $\delta^{15}N$ values of upper 50 m bulk zooplankton versus time (day of the year, Julian day) during the spring of 1995. The correlation coefficients (r^2) were incorporated as V_t in a simple variability model:

$$(2) \qquad V_s + V_t + V_o = V_b$$

where V_s was the spatial variability, V_t was the temporal variability, V_o was variability not otherwise accounted for (e.g., isotopic variability due to species composition), and V_b was the total bloom period (integrated) variability.

Results

Zooplankton species and within-station variability

The following sections deal with species composition as a significant source of within-station variability in bulk plankton samples. The trophic levels of species comprising the bulk samples were a source for increased $\delta^{15}N$ variability, while significant ^{13}C variability occurred within single-taxon samples.

Bulk plankton

The within-station variability of $\delta^{15}N$, $\delta^{13}C$, and $\delta^{13}C'$ measured in upper 50 m net zooplankton over the 1994–1995 period was suggested by the standard deviation (SD) value for each station to range up to 2‰, while annual mean isotopic value differences for each station ranged up to 3.4‰ (Table 1). Values and ranges of the isotopic composition of net zooplankton sampled over the water column were similar to those of upper 50 m samples (Table 1). However, water column net zooplankton $\delta^{15}N$ values were poorly correlated ($r^2 = 0.1$, $P < 0.05$) (Table 2) with those from 50-m tows from the same station and date. Correlations between $\delta^{13}C$ and $\delta^{13}C'$ were better ($r^2 = 0.3$ and 0.5, respectively, $P < 0.05$) (Table 2).

Macrozooplankton

Macrozooplankton consisted of various taxa extracted from plankton tows made in 1994 and individually isotopically analyzed (Table 3). These macrozooplankters consisted largely of diel migrators, as they were found in 50-m tows at night as well as in tows made over the water column. Macrozooplankters other than interzonal copepods had $\delta^{15}N$ values (Table 3) that were more positive than was typical of bulk net samples (Table 1). Interzonal copepods were consistently lower in $\delta^{15}N$ than other taxa, with a mean value of about +8‰. Euphausiids (*Euphausia pacifica* and *Thysanoessa* spp.) had mean $\delta^{15}N$ of about +10‰, whereas amphipods (principally *Cyphocaris challengeri*) and decapods were about +11‰. Carnivorous copepods (*Euchaeta elongata*) had the most positive macrozooplankter $\delta^{15}N$ value of about +12‰. The range in macrozooplankter $\delta^{15}N$ values is similar to that observed by Wu et al. (1997) and likewise was probably due to trophic level differences among the taxa. Macrozooplankter $\delta^{13}C$ and $\delta^{13}C'$ values were similar to those of bulk samples (Tables 1 and 2). Their $\delta^{13}C$ values ranged from about –19 to –23‰ but were reduced to –18 to –21‰ when normalized ($\delta^{13}C'$). The only macrozooplankters with mean $\delta^{13}C'$ values less than –20‰ were interzonal copepods.

Neocalanus cristatus

Neocalanus cristatus were found in both water column and 50 m net plankton tows (Tables 4 and 5). These data are presented separately because samples from the upper 50 m contained actively feeding individuals, whereas samples from the complete water column tow included copepods undergoing diapause at depth as well as those actively feeding near the surface (the latter principally in May; Table 4).

Counts of copepodite stage IV and V *N. cristatus* were highest in the PWS 50-m tows in May (Table 4). A total of 56 were found in fifteen 50-m tows in May compared with 8, 15, and 22 found in 16, 15, and fifteen 50-m tows made in March, April, and June, respectively (Table 4). Monthly mean $\delta^{13}C$ and $\delta^{13}C'$ values of bulk zooplankton and *N. cristatus* collected from March through June 1995 were correlated ($r^2 = 0.4$ and 0.5, respectively), while $\delta^{15}N$ values were not ($r^2 << 0.1$) (Table 2). Varying trophic level composition of bulk samples probably contributed to the reduced $\delta^{15}N$ correlations. Four 50-m tows produced large samples of *N. cristatus* ($N \geq 12$) (Table 4). The SDs of these samples were small: 0.5–0.7 for $\delta^{15}N$, 0.3–1.4 for $\delta^{13}C$, and 0.4–1.3 for $\delta^{13}C'$ (see comparison with water column *N. cristatus* below).

Unlike the 50-m samples, regressing the mean $\delta^{15}N$, $\delta^{13}C$, and $\delta^{13}C'$ values of *N. cristatus* and net plankton samples collected at each station suggested that *N. cristatus* from the water column were unlike the bulk net samples from which they were collected (Table 2). Furthermore, unlike upper 50 m samples, the $\delta^{15}N$ and $\delta^{13}C$ values of *N. cristatus* from the water column were not correlated (Table 2). A number of the deep *N. cristatus* tows produced large samples (Table 5). The SDs of these samples were greater than those of the 50-m samples with $N \geq 12$, ranging up to 4.3 (Table 5).

Zooplankton temporal variability

The following sections deal with temporal variability, reflecting changes in the seasonal production cycle, depending on sample type.

© 1999 NRC Canada

Table 1. Overall interannual differences in isotopic composition (mean and SD, ‰) in PWS, Alaska, at oceanographic stations with $N > 1$ (1994–1995) (Fig. 1).

Station	1994 N^a	1995 N^a	All observations						Difference in annual means (1994–1995)[b]		
			$\delta^{15}N$	SD	$\delta^{13}C$	SD	$\delta^{13}C'_{TL}$	SD	$\delta^{15}N$	$\delta^{13}C$	$\delta^{13}C'_{TL}$
Upper 50 m											
CFOS13	3	4	7.9	1.1	−21.7	1.0	−19.6	1.3	0.5	0.9	−0.1
CFOSBY		4	8.4	0.6	−21.2	1.7	−18.6	1.7			
CS3	1	3	8.6	0.8	−21.6	1.0	−18.6	1.6	1.0	0.6	1.8
CS9		4	7.9	1.0	−21.6	1.1	−19.4	1.5			
GOA6		3	6.7	0.9	−24.3	1.2	−21.9	1.2			
HE12	1	4	7.9	1.2	−22.6	1.3	−20.2	2.0	2.1	2.0	3.4
MS3	1	4	7.8	0.9	−22.3	0.9	−19.6	1.2	1.5	0.0	0.3
MS6	1	4	8.6	1.1	−21.5	1.5	−19.0	1.4	0.0	−0.1	0.2
NS1	1	4	8.7	1.2	−22.4	1.0	−19.8	1.5	1.1	−1.0	−0.4
NWS4	1	4	8.8	1.1	−21.9	0.8	−19.3	1.0	1.5	−1.1	−1.1
OB1		3	7.9	1.0	−21.8	1.4	−19.6	1.7			
OB2		4	8.3	1.4	−21.4	0.9	−19.3	1.1			
PB1		2	7.8	0.2	−21.3	0.4	−19.2	0.4			
PV1		3	8.5	0.8	−21.7	1.2	−19.6	1.9			
PW1		4	8.2	0.7	−22.0	0.7	−19.7	0.8			
SEA11	1	4	8.8	0.6	−22.0	0.3	−19.4	0.8	−0.1	0.0	−0.2
SEA2	2		9.1	0.7	−22.8	0.8	−20.5	0.5			
SEA20	2		8.4	1.5	−22.4	0.2	−19.8	0.5			
SEA22	1	3	7.7	1.5	−21.5	1.3	−19.1	1.4	−2.7	−2.2	−2.0
SEA25	2	4	8.6	0.9	−22.0	0.7	−19.8	1.0	0.6	−0.5	−0.9
SEA26	2		8.7	0.2	−22.4	0.1	−20.7	0.5			
SEA27	1	4	8.5	0.8	−21.8	0.7	−19.2	1.0	0.8	−0.7	−1.5
SEA29	2		9.2	0.0	−21.9	0.4	−20.0	0.4			
SEA32	1	3	8.4	0.9	−22.1	0.5	−19.9	0.4	1.2	0.2	−0.2
SEA37	1	3	8.2	0.7	−22.5	1.5	−19.9	2.0	1.2	1.6	3.3
SEA39	2		8.9	0.2	−21.9	0.4	−20.2	0.2			
SEA4	8	3	7.9	1.1	−22.6	0.5	−19.8	0.4	−0.7	−0.4	−0.6
SEA8	2		7.4	2.0	−22.3	0.9	−20.2	0.8			
SEA9	2		8.3	0.4	−22.1	0.4	−19.7	0.2			
Mean[b]	38	78	8.3	0.9	−22.1	0.9	−19.7	1.0	0.6	−0.1	0.1
Water column (1995 only)											
CFOS13		4	9.0	1.4	−22.3	1.9	−19.8	1.6			
CS4		2	9.3	1.7	−21.4	1.5	−18.8	0.5			
CS9		4	8.9	1.3	−21.8	0.8	−19.4	1.0			
GOA6		2	7.2	1.8	−24.4	0.8	−22.0	1.4			
HE12		4	7.4	1.2	−22.6	1.1	−20.0	1.4			
HE13		3	8.3	1.8	−23.2	1.4	−20.1	1.3			
NWS4		4	8.7	0.3	−20.9	0.6	−18.6	0.8			
PB1		3	8.5	0.7	−21.2	0.8	−19.0	0.7			
PV1		3	8.2	0.7	−20.7	0.8	−18.7	0.8			
PW1		4	9.5	1.0	−21.9	0.4	−19.5	0.6			
SEA11		4	9.0	0.8	−21.5	0.4	−18.9	0.7			
SEA22		3[c]	9.9	0.9	−21.1	0.1	−18.6	0.8			
SEA25		3	9.2	0.8	−21.3	0.3	−18.5	0.7			
SEA27		3	8.3	0.5	−20.9	0.7	−18.5	0.9			
SEA4		4	9.1	0.8	−21.8	0.3	−19.3	0.3			
Mean[b]		50	8.7	1.1	−21.8	0.8	−19.3	0.9			

[a] N = number of times.
[b] Rounding performed after calculation.
[c] $N = 2$ for ^{13}C.

© 1999 NRC Canada

Table 2. Regression analyses: correlation coefficient, intercept, and slope values (significant relationships indicated by asterisks).

Data	Fixed parameter	*X* variable	*Y* variable	*N*	$P < 0.05$	r^2	Intercept	Slope
Zooplankton[a]								
Spring 1995	Upper 50 m	$\delta^{15}N$	$\delta^{13}C$	79	*	0.44	−28.3	0.78
Mar. 1995	Upper 50 m	$\delta^{15}N$	$\delta^{13}C$	16	*	0.57	−29.8	0.99
Apr. 1995	Upper 50 m	$\delta^{15}N$	$\delta^{13}C$	22	*	0.74	−28.5	0.84
May 1995	Upper 50 m	$\delta^{15}N$	$\delta^{13}C$	19		0.13	−25.1	0.43
June 1995	Upper 50 m	$\delta^{15}N$	$\delta^{13}C$	22		0.18	−29.6	0.89
Spring 1995	Upper 50 m	$\delta^{15}N$	$\delta^{13}C'$	79	*	0.49	−27.2	0.95
Mar. 1995	Upper 50 m	$\delta^{15}N$	$\delta^{13}C'$	16	*	0.54	−28.4	1.06
Apr. 1995	Upper 50 m	$\delta^{15}N$	$\delta^{13}C'$	22	*	0.55	−25.2	0.74
May 1995	Upper 50 m	$\delta^{15}N$	$\delta^{13}C'$	19		0.19	−22.4	0.47
June 1995	Upper 50 m	$\delta^{15}N$	$\delta^{13}C'$	22		0.17	−26.1	0.73
Temporal comparisons with Auke Bay, Alaska								
	Upper 50 m	Julian date[b]	$\delta^{15}N$[c]	6	*	0.87	4.6	0.03
	Upper 50 m	Julian date[b]	$\delta^{15}N$	82	*	0.59	0.4	0.07
	Upper 50 m	Julian date[b]	$\delta^{13}C$[c]	6	*	0.73	−26.9	0.05
	Upper 50 m	Julian date[b]	$\delta^{13}C$	82	*	0.36	−26.8	0.05
Zooplankton,[a] spring 1995								
	$\delta^{15}N$	Water column[d]	Upper 50 m[e]	44	*	0.10	5.5	0.30
	$\delta^{13}C$	Water column[d]	Upper 50 m[e]	43	*	0.33	−10.2	0.54
	$\delta^{13}C'$	Water column[d]	Upper 50 m[e]	43	*	0.51	−6.4	0.72
Neocalanus versus zooplankton[a]								
Upper 50 m[e]								
Spring 1995	$\delta^{15}N$	Zooplankton[a]	*Neocalanus cristatus*	18		0.00	7.9	0.07
Spring 1995	$\delta^{13}C$	Zooplankton[a]	*Neocalanus cristatus*	21	*	0.43	−1.6	0.89
Spring 1995	$\delta^{13}C'$	Zooplankton[a]	*Neocalanus cristatus*	21	*	0.51	−6.4	0.72
Water column[d]								
Spring 1995	$\delta^{15}N$	Zooplankton[a]	*Neocalanus cristatus*	31		0.11	5.7	0.28
Spring 1995	$\delta^{13}C$	Zooplankton[a]	*Neocalanus cristatus*	32		0.12	−15.6	0.27
Spring 1995	$\delta^{13}C'$	Zooplankton[a]	*Neocalanus cristatus*	32		0.04	−16.7	0.17
Neocalanus cristatus								
Spring 1995	Upper 50 m	$\delta^{15}N$	$\delta^{13}C$	124	*	0.26	−29.3	0.99
May 1995	Upper 50 m	$\delta^{15}N$	$\delta^{13}C$	72	*	0.21	−29.6	1.07
Spring 1995	Upper 50 m	$\delta^{15}N$	$\delta^{13}C'$	124	*	0.35	−28.0	0.91
May 1995	Upper 50 m	$\delta^{15}N$	$\delta^{13}C'$	72	*	0.34	−30.0	1.18
Spring 1995	Water column	$\delta^{15}N$	$\delta^{13}C$	420	*	0.08	−24.4	0.36
Spring 1995	Water column	$\delta^{15}N$	$\delta^{13}C'$	420		0.01	−20.9	0.09

[a]Bulk net zooplankton.
[b]Time period restricted to April and May to match the Goering et al. (1990) study.
[c]Data from Goering et al. (1990).
[d]Samples collected from the entire water column.
[e]Samples collected from the upper 50 m.

Bulk zooplankton

Isotopic values of bulk net zooplankton samples from individual stations sampled from 1994 to 1995 differed between years by as much as 3.4‰ (Table 1). Much of this variability was due to stations with only one observation for 1994 (many of these were from fall 1994; Appendix), since those stations sampled more than once in 1994 as well as in 1995 (CFOS13, SEA25, and SEA4) differed by <1‰ (Table 1). Contrasting with March–June 1995, which had $\delta^{15}N$ gradients <2‰, the fall 1994 zooplankton had an east–west $\delta^{15}N$ gradient of 4‰ with higher values to the east (Fig. 2), suggesting that eastern samples consisted of a proportion of higher trophic level zooplankters (Fig. 2).

The similarity of isotopic data for zooplankton collected at stations CFOS13, SEA11, SEA25, SEA32, and SEA4 in early 1994 to the data collected at these stations in 1995 suggested that using only the spring bloom data more effectively assessed consistency in pelagic productivity isotopic signature. For example, during the PWS phytoplankton (April) and zooplankton (May) biomass peak periods (Cooney 1997), the $\delta^{15}N$ values within PWS were uniform (within 1‰, although higher in May than in April) when compared with March and the previous fall (Fig. 2), consistent with a composition principally of herbivores at this time throughout the region.

Macrozooplankton

Variability (expressed as SD) (Table 3) of macrozooplanton isotopic composition was greater in the fall than in the spring (except the $\delta^{15}N$ values of interzonal copepods,

© 1999 NRC Canada

Table 3. $\delta^{15}N$, $\delta^{13}C$, and $\delta^{13}C'$ (mean and SD, ‰) and sample size (*N*) of individual macrozooplankters by taxon collected in PWS, Alaska, in 1994.

Taxon/season	$\delta^{15}N$	SD	$\delta^{13}C$	SD	$\delta^{13}C'$	SD	*N*
Amphipods							
Spring	11.58	0.79	–20.25	1.10	–18.46	0.81	23
Fall	10.58	2.02	–21.55	1.19	–18.94	1.14	85
Decapods							
Spring	11.39	1.52	–20.42	0.46	–19.53	0.28	38
Fall	11.22	1.92	–20.56	0.88	–19.04	0.67	20
Euphausiids							
Spring	10.53	0.57	–19.36	0.56	–18.71	0.53	55
Summer	9.36	0.28	–19.76	0.63	–19.34	0.62	20
Fall	10.72	1.90	–21.24	1.13	–19.70	0.81	95
Copepods (C)							
Spring	12.00	0.24	–21.38	0.40	–19.98	0.39	6
Fall	11.91	0.62	–22.43	0.67	–19.92	0.33	23
Copepods (I)							
Spring	8.64	1.20	–22.96	0.96	–19.81	1.18	59
Fall	8.33	1.07	–22.89	2.12	–20.95	1.75	20

Note: Copepod taxa were either the carnivorous *E. elongata* (C) or interzonal *Neocalanus* spp. (I). Fall 1994 interzonal copepods consisted of *N. cristatus* in diapause.

Neocalanus spp., which decreased slightly). The increase in SD of $\delta^{15}N$ values suggests a greater degree of omnivory (Kline and Pauly 1998) for zooplankton species during the late season.

Neocalanus cristatus

Neocalanus cristatus sample inventories from whole water column tows at particular stations varied with time (Table 5), suggesting greatest springtime abundance (in terms of number per unit area) in March at stations NWS4, PW1, SEA11, SEA22, and SEA27. These stations have depths >400 m, approximately the shallowest diapause habitat (Fig. 1). In May 1995, there were far fewer at the deepest station, SEA22 (depth = 720 m), with only 18 sampled compared with >100 found in March (note: only 33 of these were analyzed, while at other stations, all were analyzed, so the numbers in Table 5 reflect sample inventories). In May, however, *N. cristatus* were more broadly distributed than earlier, e.g., occurring in greater numbers at stations CS9, HE12, HE13, PV1, and SEA25, where only few had been collected before.

There was a gradual isotopic shift in water column collected *N. cristatus* to more positive $\delta^{13}C'$ values in May (Table 5). The isotopic values of *N. cristatus* sampled in March–April throughout PWS as well as those from station SEA22 ($\delta^{15}N = 8.7 \pm 1.6$‰, $\delta^{13}C = -21.7 \pm 2.1$‰, $\delta^{13}C' = -20.5 \pm 1.8$‰) were comparable with those of the 20 *N. cristatus* sampled with the Tucker trawl at SEA22 in the fall of 1994 ($\delta^{15}N = 8.3 \pm 1.1$‰, $\delta^{13}C = -22.9 \pm 2.1$‰, $\delta^{13}C' = -21.0 \pm 1.8$‰) (Tables 3 and 5). However, *N. cristatus* sampled with a closing net in the fall of 1995 differed considerably in ^{13}C ($\delta^{13}C = -24.0 \pm 1.6$‰, $\delta^{13}C' = -22.4 \pm 1.4$‰) from both the fall 1994 and spring 1995 water column samples. The mean $\delta^{13}C'$ of the fall 1995 copepods of –22.4‰ fell between the –23.2 and –20.6‰ mean $\delta^{13}C'$ values of *N. cristatus* feeding (i.e., upper 50 m samples) in the GOA and PWS, respectively, during the March–June period (Tables 5 and 6).

Zooplankton spatial variability

Time-averaged data from stations that were sampled more than once in the period 1994–1995 reveal a regional isotopic spatial pattern whereby zooplankton $\delta^{15}N$ values were relatively uniform at about +8 ± 1‰ (Fig. 3A), while ^{13}C gradients of about 3–4‰ were observed between the GOA and PWS (Fig. 3B). The ^{13}C gradient was independent of sampling method (bulk net zooplankton from the upper 50 m or entire water column or individual *N. cristatus* from the upper 50 m), although more distinct for *N. cristatus*, with more negative values occurring in the GOA.

The most ^{13}C-depleted signatures in bulk zooplankton occurred at station GOA6 in June (Fig. 2J) when peak zooplankton abundance occurred in the GOA (R.T. Cooney, University of Alaska Fairbanks, Fairbanks, Alaska, personal communication). Furthermore, $\delta^{13}C$ values throughout the 1995 spring sampling series were consistently more depleted at GOA6 than at PWS stations (Fig. 2). Unlike the spring, the spatial variability in fall 1994, although considerable, suggests no interpretable pattern in $\delta^{13}C$ (Fig. 2B). There was, however, a $\delta^{15}N$ gradient with more positive values to the east and south. In the spring of 1995, bulk zooplankton $\delta^{15}N$ values were about 1‰ lower in the GOA than in PWS (Figs. 2 and 3). This is much less than the concurrent approximately 3‰ difference in ^{13}C values.

Data for *N. cristatus* from the upper 50 m in PWS when compared with data from station GOA6 suggest differences in $\delta^{13}C'$ values of 3.5 and 3.6‰ over the season and in May, respectively, between PWS and GOA (Table 4). These same PWS versus GOA comparisons when made for $\delta^{13}C$ were similar, 4.1 and 3.9‰. However, $\delta^{15}N$ differed by only 1.3 and 0.8‰ over the season and in May, respectively. The $\delta^{15}N$ is suggested to be relatively uniform in the region (PWS versus the adjacent GOA) in May, since the difference was about 1 SD of the data from each area (Table 4). Thus, *N. cristatus* reflected the same regional isotopic spatial variability observed in bulk samples, although with a more distinctive $\delta^{13}C'$ gradient (Fig. 3B), i.e., *N. cristatus* from

© 1999 NRC Canada

Table 4. Isotopic composition (mean and SD, ‰) and sample size (*N*) of copepodite stage IV and V *N. cristatus* from upper 50 m at indicated oceanographic stations in PWS and northern GOA in March–June 1995.

	April									May								
Station	$\delta^{15}N$	SD	*N*	$\delta^{13}C$	SD	*N*	$\delta^{13}C'$	SD	*N*	$\delta^{15}N$	SD	*N*	$\delta^{13}C$	SD	*N*	$\delta^{13}C'$	SD	*N*
CFOS 13										8.7		1	−19.8		1	−19.3		1
CFOSBY										8.3	0.5	21	−19.7	0.3	21	−19.7	0.4	21
CS3										7.8	0.8	11	−20.0	0.3	11	−19.9	0.6	11
CS9																		0
HE12										8.2	0.3	2	−19.7	0.0	2	−19.4	0.5	2
NS1	7.9		1	−23.1		1	−20.8		1	8.6	0.2	2	−19.2	0.8	2	−18.8	0.7	2
NWS4										9.3	0.6	4	−20.2	0.5	4	−18.6	0.5	4
OB1	7.1		1	−20.8		1	−18.7		1									0
OB2	9.1		1	−22.9		1	−20.9		1									0
PV1										8.7	0.2	2	−19.2	0.9	2	−18.9	0.9	2
PW1				−20.2		1	−20.3		1									0
SEA11										8.4	1.1	10	−20.4	1.1	10	−19.4	0.6	10
SEA22	9.1		1	−20.3	1.5	3	−19.3	1.6	3									0
SEA25	8.8	1.5	8	−21.7	1.4	8	−19.4	1.3	8									0
SEA4										8.3	0.6	3	−20.5	0.5	3	−19.4	0.9	3
All PWS	8.6	1.4	12	−21.5	1.4	15	−19.6	1.2	15	8.3	0.8	56	−19.9	0.7	56	−19.5	0.6	56
GOA6			—			—			—	7.5	0.7	20	−23.8	1.4	20	−23.1	1.3	20
	June									March–June[a]								
	$\delta^{15}N$	SD	*N*	$\delta^{13}C$	SD	*N*	$\delta^{13}C'$	SD	*N*	$\delta^{15}N$	SD	*N*	$\delta^{13}C$	SD	*N*	$\delta^{13}C'$	SD	*N*
CFOS 13										8.7	1	−19.8		1	−19.3		1	
CFOSBY										8.3	0.5	21	−19.7	0.3	21	−19.7	0.4	21
CS3										7.8	0.8	9	−20.0	0.3	11	−19.9	0.6	11
CS9	8.7	0.5	14	−20.1	0.6	14	−20.3	0.6	14	8.7	0.5	14	−20.1	0.6	14	−20.3	0.6	14
HE12										8.2	0.3	2	−19.7	0.0	2	−19.4	0.5	2
NS1										8.4	0.4	3	−20.5	2.3	3	−19.5	1.3	3
NWS4										9.3	0.6	4	−20.7	1.1	5	−19.1	1.1	5
OB1													−20.8		1	−18.7		1
OB2	8.3	1.2	8	−19.4	0.6	8	−19.9	0.8	8	8.2	1.2	9	−19.8	1.3	9	−20.0	0.8	9
PV1										8.7	0.2	2	−19.2	0.9	2	−18.9	0.9	2
PW1										9.5	1.5	6	−20.3	2.1	7	−19.8	1.5	7
SEA11										8.8	1.9	11	−20.3	1.2	11	−19.4	0.6	11
SEA22										9.1		1	−20.3	1.5	3	−19.3	1.6	3
SEA25										8.8	1.5	8	−21.7	1.4	8	−19.4	1.3	8
SEA4										8.3	0.6	3	−20.5	0.5	3	−19.4	0.9	3
All PWS	8.6	0.8	22	−19.8	0.7	22	−20.2	0.7	22	8.6	1.1	94	−20.2	1.1	101	−19.7	0.9	101
GOA6	7.0	0.5	12	−25.1	0.9	12	−23.5	0.6	12	7.3	0.7	30	−24.3	1.4	32	−23.2	1.1	32

Note: Empty cells indicate that none were found or that the station was not sampled. Values of *N* for some $\delta^{15}N$ analyses are less than the station sample total; nitrogen mass of these copepods was insufficient for the analysis (B. Barnett, mass spectrometry technician, personal communication). The overall means for PWS stations are given just above station GOA6.

[a]No monthly table is given for March, since only eight copepods were found in total.

© 1999 NRC Canada

Table 5. Isotopic composition (mean and SD, ‰) and sample size (*N*) of copepodite stage V and VI *N. cristatus* sampled from the water column at indicated oceanographic stations in PWS and northern GOA where at least one individual was found in March, April, May, and September–October 1995.

	March									April								
Station	$\delta^{15}N$	SD	*N*	$\delta^{13}C$	SD	*N*	$\delta^{13}C'$	SD	*N*	$\delta^{15}N$	SD	*N*	$\delta^{13}C$	SD	*N*	$\delta^{13}C'$	SD	*N*
CFOS 13	10.6	0.8	7	–20.7	2.0	7	–20.0	1.9	7				–20.0	1.0	2	–17.6	0.4	2
CS4																		
CS9				–21.1	2.4	4	–19.6	2.4	4	8.1	0.6	2	–21.4	0.4	3	–20.0	1.1	3
HE11	6.8		1	–23.2		1	–21.4		1									
HE12																		
HE13	8.6	1.8	9	–20.3	1.4	9	–20.0	1.6	9	6.8		1						
NS2																		
NWS4	9.0	1.5	20	–21.5	2.3	20	–20.7	1.8	20	9.5	1.1	16	–21.6	1.8	16	–20.5	1.6	16
PB1										7.1	0.7	2	–21.2	1.2	3	–19.8	1.1	3
PV1										9.0		1	–22.1	1.2	3	–20.4	1.0	3
PW1	8.8	2.3	21	–22.0	2.3	21	–21.1	1.9	21	9.1	1.7	17	–21.4	2.1	17	–20.8	1.9	17
SEA11	8.9	1.5	20	–21.5	2.1	20	–20.6	1.9	20	8.0	0.9	15	–22.5	1.8	18	–20.5	1.8	18
SEA22	8.0	0.9	31	–21.6	2.4	33	–20.4	2.1	33	7.8	1.4	30	–22.2	2.4	33	–20.2	2.0	33
SEA25										8.7	2.3	8	–23.1	1.1	8	–21.6	1.2	8
SEA27	9.3	2.1	22	–22.1	2.1	26	–21.2	1.7	26	8.9	1.0	12	–21.2	1.6	17	–20.0	1.4	17
SEA4	9.4		1	–21.4	0.8	2	–21.2	1.9	2	8.3	1.0	11	–21.2	1.5	14	–19.7	1.3	14
All PWS	8.8	1.7	132	–21.6	2.2	143	–20.7	1.9	143	8.5	1.5	115	–21.8	1.9	134	–20.3	1.7	134
	May									September–October								
	$\delta^{15}N$	SD	*N*	$\delta^{13}C$	SD	*N*	$\delta^{13}C'$	SD	*N*	$\delta^{15}N$	SD	*N*	$\delta^{13}C$	SD	*N*	$\delta^{13}C'$	SD	*N*
CFOS 13	8.2	0.1	3	–20.9	0.1	3	–18.5	0.3	3	7.1	1.9	24	–24.4	1.6	24	–22.4	1.6	24
CS4	8.6	0.7	19	–20.2	0.5	20	–19.4	1.0	20									
CS9	8.9	1.0	12	–20.6	0.8	13	–19.6	0.8	13									
HE11																		
HE12	8.0	0.5	20	–20.1	0.3	21	–19.7	0.6	21									
HE13	8.0	0.9	18	–21.3	1.2	20	–21.1	1.2	20	8.5	2.6	12	–23.0	1.7	12	–21.7	1.7	12
NS2										8.9	3.0	25	–24.3	1.7	25	–22.6	1.7	25
NWS4	8.3	0.9	8	–20.8	1.2	12	–19.4	0.9	12	6.9	1.7	26	–23.6	1.1	26	–22.3	1.1	26
PB1																		
PV1	8.2	0.7	19	–20.4	1.1	19	–19.3	0.9	19									
PW1	7.5	1.2	13	–21.2	1.2	13	–19.5	0.8	13									
SEA11	7.6	1.1	13	–20.5	0.8	18	–19.0	0.4	18	7.9	1.7	25	–24.3	1.3	25	–22.5	1.3	25
SEA22	6.8	0.9	17	–22.0	1.8	18	–19.7	1.7	18	6.8	1.8	50	–24.5	1.2	50	–22.5	1.2	50
SEA25	7.6	1.0	10	–21.0	2.2	12	–19.7	1.8	12	7.1	1.9	25	–24.0	1.2	25	–22.3	1.2	25

© 1999 NRC Canada

Table 5 (*concluded*).

	May								September–October							
	$\delta^{15}N$	SD	*N*	$\delta^{13}C$	SD	*N*	$\delta^{13}C'$	SD	*N*	$\delta^{15}N$	SD	*N*	$\delta^{13}C$	SD	*N*	$\delta^{13}C'$	SD	*N*
SEA27	7.8	1.3	11	–20.9	0.5	11	–19.1	0.8	11	11.5	4.3	22	–23.0	1.2	22	–22.3	1.2	22
SEA4	8.0	0.7	11	–20.9	1.0	12	–19.6	0.6	12									
All PWS	7.9	1.0	174	–20.8	1.8	192	–19.6	1.1	192	7.8	2.8	209	–24.0	1.6	209	–22.4	1.4	209
	March–April									March–May								
	$\delta^{15}N$	SD	*N*	$\delta^{13}C$	SD	*N*	$\delta^{13}C'$	SD	*N*	$\delta^{15}N$	SD	*N*	$\delta^{13}C$	SD	*N*	$\delta^{13}C'$	SD	*N*
All PWS	8.7	1.6	247	–21.7	2.1	277	–20.5	1.8	277	8.4	1.4	421	–21.3	1.8	469	–20.1	1.6	469

Note: Number of copepods collected at each station each month is given. Empty cells indicate that none were found or that the station was not sampled. Values of *N* less than the station sample total reflect copepods containing insufficient nitrogen mass for the analysis (B. Barnett, mass spectrometry technician, personal communication). Data for the fall cruise, which started in September and ended in October, are given in the September–October block. Means for the March–April and March–May periods are given at the bottom.

PWS had $\delta^{13}C'$ values of about –19‰, while GOA *N. cristatus* $\delta^{13}C'$ was about –23‰.

Zooplankton bloom period spatial and temporal variability model

A large isotopic data set from bulk net zooplankton samples collected from March to June 1995 (Appendix) throughout PWS enabled an integrated assessment of spring bloom spatial and temporal variability in PWS using eq. 2. The resultant plots suggest that isotopic shifts were concordant, with their peak values occurring in May (Fig. 4), coinciding with the end of the 1995 PWS diatom-dominated phytoplankton bloom on Julian day 126 (Ward 1997). The 1995 phytoplankton bloom was followed by a 20-day postbloom period of very low biomass that was dominated by microflagellates (Ward 1997). Reduced zooplankton grazing and tidal pumping of nutrients from below the photic zone caused a slight phytoplankton recovery that was dominated in biomass (in terms of carbon) by a single diatom taxon, *Rhizosolenia fragilissima* (Ward 1997). The June isotopic shift to lower values, about 20 days into this recovery period, is consistent with increased nutrient supply.

Normalization of $\delta^{13}C$ to $\delta^{13}C'$ doubled the time dependency in the data to 40% (Fig. 4B versus Fig. 4C). The similarity in the $\delta^{15}N$ and $\delta^{13}C'$ correlations (Figs. 4A and 4C, both $r^2 \approx 0.4$) suggests that variance explained as temporal variability was 0.4 or 40%.

Diagnostic signatures for GOA and PWS production

Dual-isotope scatterplots and histograms (Fig. 5) revealed that $\delta^{13}C'$ values from *Neocalanus* were bimodal, whereas $\delta^{15}N$ values were unimodal. March and April 1995 water column samples (Fig. 5A) consisted principally of copepods in diapause phase from the 1994 year-class (the calendar year when they were actively feeding). Since the May 1995 water column copepods (Fig. 5B) were more similar to the upper 50 m copepods (Fig. 5D) than the March and April water column samples (Fig. 5A), they were most likely from the 1995 year-class, either feeding or just entering diapause, while the fall 1995 sample (Fig. 5C) was taken at depth and at the time of year when the population is in diapause. Reference lines approximating the mean GOA and PWS isotopic values of *N. cristatus* of $\delta^{15}N$ = 8‰, $\delta^{13}C'$ = –23‰, and –19‰ were drawn in each panel of Fig. 5 to aid the comparisons. There is a consistency in occurrence of values near the intersections of the lines. These "cross hairs" fall near the centers of the two clusters of diapausing copepods from the 1994 year-class (Fig. 5A) and the single dominant cluster of diapausing copepods from the 1995 year-class (Fig. 5C). This latter cluster departs from both the upper 50 m PWS copepods sampled throughout the spring of 1995 (Fig. 5D) and the May 1995 water column data (Fig. 5B) that were dominated by the $\delta^{13}C'$ values near –19‰. Based on the $\delta^{13}C'$ values of copepods during their terminal feeding stages in spring in the GOA and PWS (Table 4), the cross hairs in Fig. 5 approximate centers of the isotopic value distribution for GOA copepods on the left ($\delta^{13}C'$ = –23‰) and PWS copepods on the right ($\delta^{13}C'$ = –19‰) of each plot. Thus, a dichotomy is suggested for ^{13}C, with each isotopic signature corresponding to GOA or PWS production.

© 1999 NRC Canada

Fig. 2. Areal distribution of net zooplankton $\delta^{15}N$ and $\delta^{13}C$ (‰) during (A and B) September 1994, (C and D) March 1995, (E and F) April 1995, (G and H) May 1995, and (I and J) June 1995 from the upper 50 m in the PWS study area.

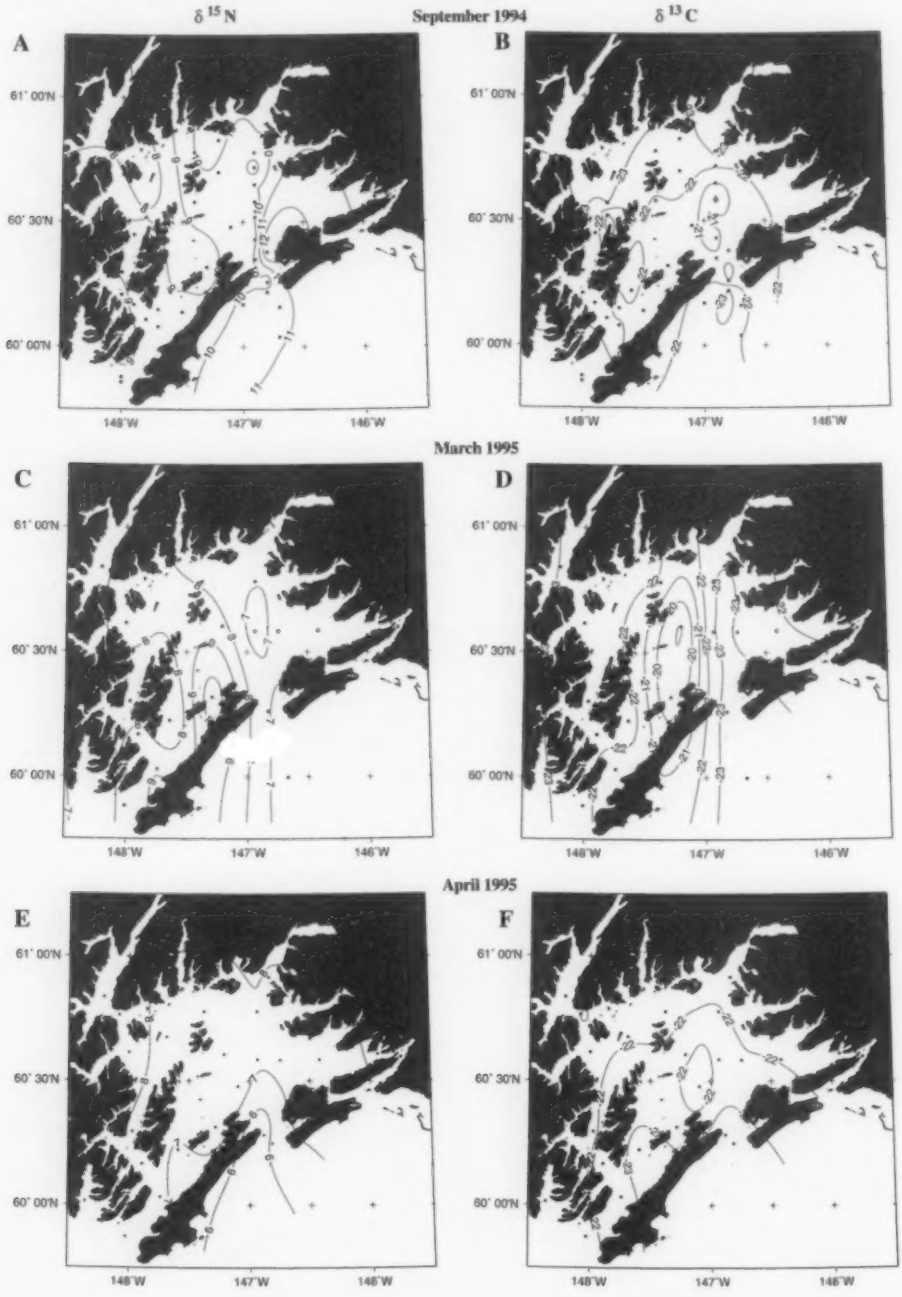

Juvenile Pacific herring and walleye pollock

There was a shift to lower ^{13}C values for juvenile fishes between 1994 and 1995. Age-0 and age-1 Pacific herring and age-0 walleye pollock were found at 10 and seven sites (Table 6), respectively, during the fall 1995 broadscale fish survey. Walleye pollock had higher $\delta^{15}N$ values than Pacific herring, with a difference of 0.4‰ corresponding to about 0.1 trophic level difference. Although trophic level normalization reduced the difference in $\delta^{13}C'_{TL}$ between the species in 1995 to 0.7‰, they differed by twice the SD, which was significant (t test, $P < 0.0001$). The $\delta^{13}C'_{TL}$ values of juvenile fishes in 1995 were quite different (t test, $P < 0.0001$)

© 1999 NRC Canada

Fig. 2 (*concluded*).

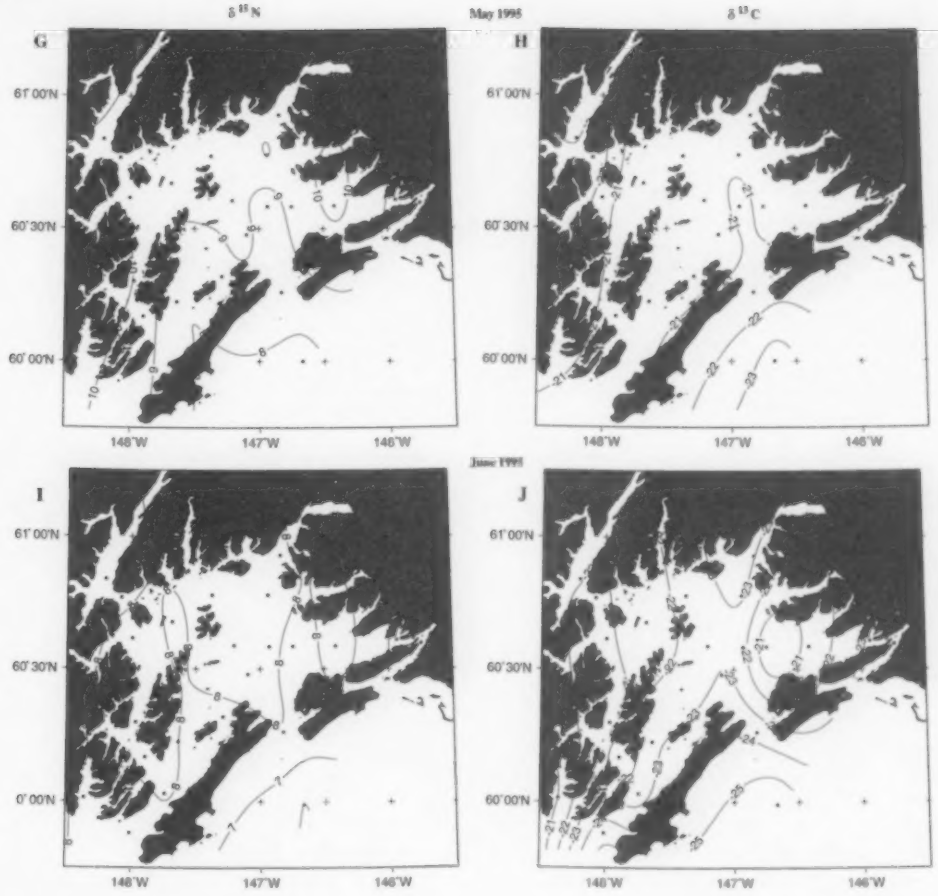

from those obtained in 1994 (Table 6). The differences between mean 1994 and 1995 $\delta^{13}C'_{TL}$ values of walleye pollock and Pacific herring of 1.4 and 2.0‰, respectively, were greater than the differences between species for each year.

Discussion

Diagnostic signatures for GOA and PWS production

The $\delta^{13}C'$ values of upper 50 m (i.e., feeding) GOA *N. cristatus* and GOA bulk net zooplankton consistently demonstrated higher levels of ^{13}C depletion than those in PWS, whether based on time-averaged data or on monthly spring bloom data. Furthermore, the variability model (eq. 2) analysis suggested that 60% of the total bloom period variability in bulk plankton samples could not explained by temporal variance. Based on the consistency in the observed isotopic signatures, it was conjectured for the period of this study, 1994–1995, that $\delta^{13}C'$ values less than about –22‰, when measured at the herbivore trophic level, were diagnostic of GOA carbon. PWS production in the form of herbivore carbon had $\delta^{13}C'$ values greater than about –21‰. This dichotomy in pelagic carbon source ^{13}C is similar to that observed in Atlantic Ocean mesopelagic shrimp (Rau et al. 1989). Pelagic ^{13}C gradients have also been observed across the continental shelf of New England (Fry 1988), across Drake Passage, Southern Ocean (Rau et al. 1991), and between the Beaufort, Chukchi, and Bering seas off Alaska (Saupe et al. 1989; Schell et al. 1998). The PWS zooplankton carbon isotope range observed here confirmed an isotope source effect postulated on $\delta^{13}C'_{TL}$ of about 1700 nekton collected from PWS (Kline 1997).

Sample-type effects

Plankton

Zooplankton in the Northeast Pacific shift in $\delta^{15}N$ value in concordance with the $\delta^{15}N$ value of their phytoplankton diet, which in turn is driven by NO_3^- depletion in the photic zone (Goering et al. 1990; Wu et al. 1997). PWS zooplankton $\delta^{15}N$ values were in the same range as those for zooplankton from Auke Bay (southeastern Alaska near Juneau) and for zooplankton from the Pacific Ocean off the British Columbia coast (Goering et al. 1990; Wu et al. 1997). All $\delta^{13}C$ versus $\delta^{15}N$ regressions were significant ($P < 0.05$) except for May. Zooplankton $\delta^{13}C$ was correlated with $\delta^{15}N$ from April to

© 1999 NRC Canada

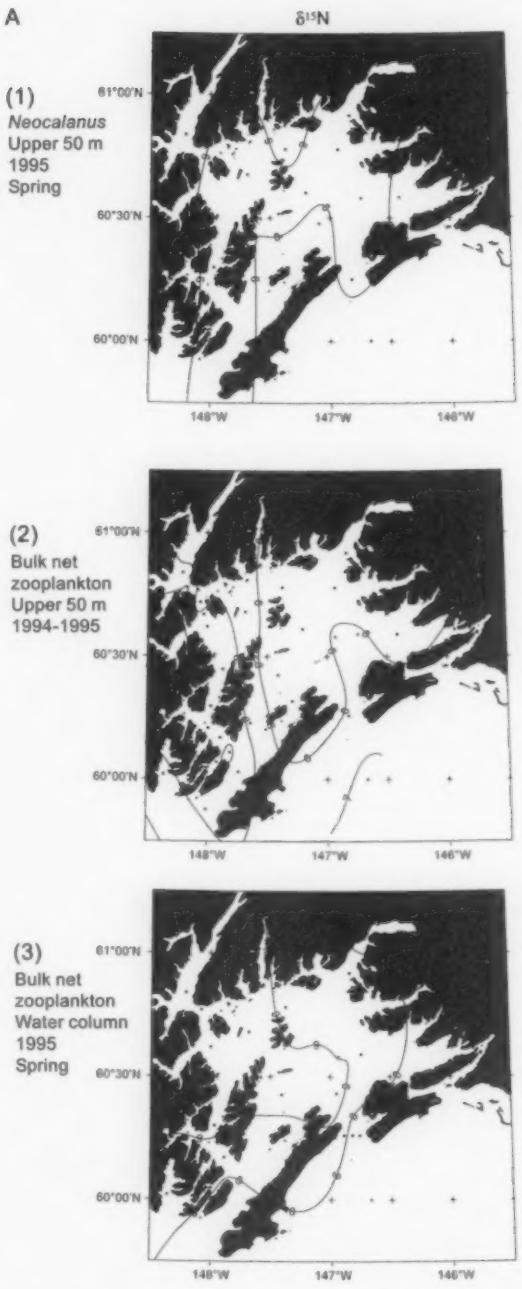

Fig. 3. Mean areal distribution of (A) $\delta^{15}N$ and $\delta^{13}C$ and $\delta^{13}C'$ (‰) in (1) upper 50 m (feeding) *N. Cristatus* (2) upper 50 m net zooplankton, and (3) water column net zooplankton in the PWS study during 1994–1995.

May in Auke Bay (Goering et al. 1990) but only in March and April in PWS (Table 2). Goering et al. (1990) found the following relationship for Auke Bay zooplankton: $\delta^{13}C = 1.8\delta^{15}N - 34.2$ ($r^2 = 0.46$), which is comparable with that found here for PWS zooplankton: $\delta^{13}C = 0.8\delta^{15}N - 28.3$ ($r^2 = 0.49$) (collectively over the spring bloom period). The reduced correlation in May and June suggests that phytoplankton isotopic fractionation effects on ^{15}N and ^{13}C become decoupled in zooplankton as the spring bloom winds down. Since zooplankton, and calanoid copepods in particular, build energy reserves by storing carbon, turnover rates of carbon and nitrogen within the organisms must differ. Additionally, zooplankton regenerate the nitrogen pool (Dugdale and Goering 1967) with ^{15}N-depleted nitrogen (Checkley and Miller 1989) serving to counteract the nitrogen uptake isotopic distillation process (e.g., Owens 1987). This nitrogen source became available as the zooplankton bloom developed, lagging about 1 month behind the phytoplankton.

The fall samples reflected secondary production long after the spring phytoplankton bloom that accounts for most of the pelagic productivity in PWS (Goering et al. 1973). Accordingly, the high variability may reflect where littoral carbon was pumped into the pelagic area by tidal action. This is a possibility in this tidally dominated system (Niebauer et al. 1994). Enriched ^{13}C is consistent with isotopic signatures of littoral carbon sources such as eelgrass (McConnaughey and McRoy 1979; Cooper 1989) and macroalgae (Stephenson et al. 1986; Dunton and Schell 1987).

Bulk zooplankton samples typically consist of a mixture of different species and life history stages, each feeding at potentially different trophic levels. Differences in trophic level (note that carnivorous copepods had the highest $\delta^{15}N$ values; Table 3) and lipid storage abilities (note that lipid normalization changed the ^{13}C values of copepods more than those of other taxa; Table 3) among the taxa comprising bulk zooplankton samples probably contributed to much of their isotopic variability. Trophic level differences among species found in bulk samples is conjectured to explain the poor correlation of 50-m and water column zooplankton $\delta^{15}N$ values, since higher trophic level taxa were more commonly collected in deep tows. The ^{13}C gradient takes on more significance when trophic isotopic fractionation factors are taken into account, e.g., if the ^{13}C difference between PWS and GOA was due to trophic level differences (i.e., about three or four trophic levels), a $\delta^{15}N$ gradient of about 10–14‰ would be expected. Since the observed $\delta^{15}N$ gradient was not of this magnitude, processes other than trophic fractionation had to explain the ^{13}C spatial variation.

Based on eq. 2, $V_t = 0.4$; therefore, spatial variance could explain as much as 60% of V_b if $V_o = 0$. This 60/40 split should differ among annual spring blooms depending on the influence of processes affecting isotopic composition such as strength of physical processes controlling horizontal and vertical mixing. Site factors (e.g., proximity to islands and eddies) that affect horizontal and vertical mixing which indirectly affects zooplankton isotopic composition by controlling photic zone nutrient fluxes, and thus isotopic fractionation by phytoplankton, may have contributed to the observed spatial variability. The lower correlation of $\delta^{13}C$ with time (compared with $\delta^{13}C'$), which implied a V_t of about 20% (Fig. 4B), suggested that variability due to lipids (carbon storage) was about 20% of V_b.

The complex nature of bulk net plankton samples may confound interpretations because of processes with varying

© 1999 NRC Canada

Fig. 3 (*concluded*).

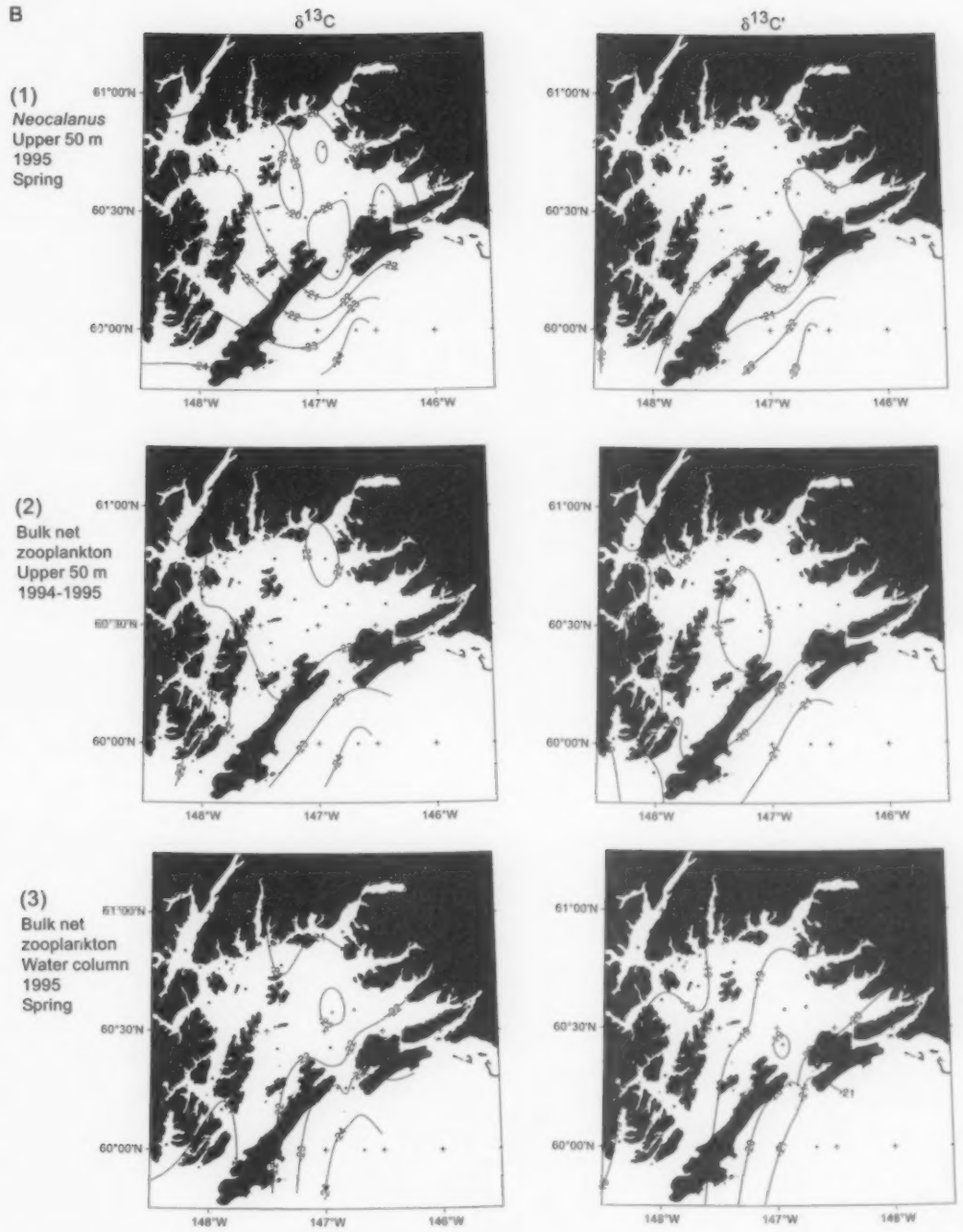

attendant isotopic effects. For example, history of vertical mixing, lateral movement, and nutrient depletion isotope effects, due to bloom dynamics, vary among the individual organisms comprising the samples. Extensive analyses were performed on individuals of a single copepod species as an alternative approach to reduce these confounding effects. This approach was directed at copepodite stage IV–VI *N. cristatus* for the following reasons: (*i*) they are large in size at about 7–10 mm in length, about 1–5 mg in weight, thus large enough for one animal per analysis, (*ii*) they are easy to identify at sea, (*iii*) they have a described life history pattern (Miller et al. 1984), thus known to be at the terminal feeding stage, and (*iv*) they are principally herbivorous (Gifford 1993), giving them a well-defined trophic level (herbivore, trophic level 2). Although these copepods are consumed by Pacific herring <150 mm in length (B. Foy,

© 1999 NRC Canada

Table 6. Isotope data (mean and SD, ‰) and sample size (*N*) of Pacific herring (ages 0 and 1) and walleye pollock (age 0) from PWS sampling sites (map codes refer to site location symbols in Fig. 1) sampled from 1994 to 1995.

			$\delta^{15}N$		$\delta^{13}C$		$\delta^{13}C'_{TL}$	
	Map code	*N*	Mean	SD	Mean	SD	Mean	SD
1994								
Pacific herring								
Apr., Wells Passage	A	20	12.1	1.86	−20.5	0.69	−19.9	0.54
June, Chenega Bay	B	9	13.1	0.21	−19.8	0.57	−20.8	0.50
Oct., Port Gravina	C	31	12.0	0.49	−22.0	0.76	−21.5	0.49
Oct., Knowles Head	D	13	13.1	0.18	−19.5	0.34	−20.8	0.35
Oct., Windy Bay	E	37	12.2	0.26	−20.9	0.90	−20.8	0.74
Total		110	12.3	0.93	−20.9	1.12	−20.8	0.80
Walleye pollock								
July, Knight Is.Pass.	F	59	10.6	0.20	−21.1	0.23	−20.8	0.15
Sept., Redhead/Gravina	C	20	11.4	0.15	−19.4	0.23	−20.3	0.22
Oct., Redhead/Gravina	C	11	12.4	0.64	−18.9	1.49	−20.3	1.33
Oct., Windy Bay	E	26	12.5	0.20	−19.7	0.41	−20.6	0.43
Total		116	11.3	0.88	−20.3	1.00	−20.7	0.51
Fall 1995								
Pacific herring								
Eaglek Bay	G	25	12.7	0.35	−22.9	0.73	−22.8	0.52
Green Island	H	25	12.7	0.22	−22.5	0.40	−22.6	0.23
Hogg Bay	I	25	12.7	0.32	−22.3	0.46	−22.7	0.18
Jack Bay	J	25	12.6	0.33	−22.5	0.51	−22.7	0.29
Knowles Head	D	25	12.7	0.36	−23.4	0.71	−22.9	0.58
Sawmill Bay	K	25	12.8	0.27	−22.9	0.39	−22.9	0.26
Simpson Bay	L	25	12.7	0.24	−22.6	0.67	−22.8	0.43
Snug Corner Cove	M	25	12.8	0.35	−22.5	0.59	−22.9	0.37
Whale Bay	N	25	12.3	0.22	−23.0	0.34	−23.2	0.20
Zaikof Bay	O	25	12.8	0.35	−22.3	0.40	−22.7	0.19
Total		250	12.7	0.34	−22.7	0.62	−22.8	0.37
Walleye pollock								
Eaglek Bay	G	25	12.9	0.20	−21.2	0.59	−22.0	0.48
Hogg Bay	I	25	13.0	0.25	−20.9	0.31	−22.1	0.26
Knowles Head	D	25	13.4	0.27	−20.6	0.38	−22.0	0.33
Sawmill Bay	K	25	13.1	0.36	−21.1	0.34	−22.2	0.30
Simpson Bay	L	25	13.2	0.35	−20.9	0.43	−22.1	0.41
Whale Bay	N	25	12.9	0.26	−20.9	0.44	−22.0	0.41
Zaikof Bay	O	21	13.1	0.28	−20.6	0.40	−22.1	0.33
Total		171	13.1	0.32	−20.9	0.45	−22.1	0.37

University of Alaska Fairbanks, Fairbanks, Alaska, personal communication, including age-1 fish) and other fishes (Willette et al. 1997) in PWS, they are probably not the prey of age-0 fish because of gape-size limitations. However, since *N. cristatus* and bulk net zooplankton $\delta^{13}C'$ values were correlated (Table 2) and had a similar ^{13}C spatial distribution (Fig. 3B), they appear to be a good proxy for each other and for carbon source.

Neocalanus cristatus ^{13}C was more strongly correlated with $\delta^{15}N$ in May than in bulk samples by a factor of about 2 and had *y*-intercept values (in the correlation analyses) more similar to those of earlier bulk plankton (Table 2), possibly because *N. cristatus* reflected a greater proportion of carbon that was previously assimilated. This is consistent with their storage of carbon, integrating longer time intervals. *Neocalanus cristatus* ^{13}C values thus reflected an averaging of the carbon isotopic variation of phytoplankton to a greater extent than nitrogen, consistent with decoupling of nitrogen and carbon cyles in zooplankton.

Seasonally, diapausing interzonal copepods form a large portion of the deep bulk zooplankton in PWS and thus should have been correlated at the time of sampling. There was a poor relationship between $\delta^{15}N$ of *N. cristatus* and that of bulk net zooplankton. This may have been due, in part, to the mixed-species assemblage and therefore mixed trophic level nature of bulk samples. Poor ^{13}C correlations (Table 2) could only be explained when the bimodal nature of the variability was revealed in dual-isotope plots, i.e., a portion of the diapausing samples had ^{13}C inconsistent with that of other zooplankton from the same location. This was probably the case for the fall 1994 interzonal copepod sample as well (Table 3). Bimodality also explained the greater SDs obtained for deep *N. cristatus* compared with 50-m samples, since the deep tows reflected a mixture of the two modes, while 50-m samples consisted of only one mode (i.e., the local carbon source).

Scatterplots with frequency histograms of *N. cristatus* isotopic data revealed a bimodal distribution of ^{13}C that was not

© 1999 NRC Canada

Fig. 4. Temporal shift in net zooplankton (A) $\delta^{15}N$, (B) $\delta^{13}C$, and (C) $\delta^{13}C'$ (‰) in the PWS study area during March–June 1995 assessed using third-order polynomial regressions as a function of Julian day (J, day of the year). In Fig. 4A, all regression P values <0.0001, in Fig. 4B, the regression P values for the J, J^2, and J^3 coefficients and y-intercept are 0.0068, 0.0029, 0.0013, and 0.959, respectively, and in Fig. 4C, the regression P values for the J, J^2, and J^3 coefficients and y-intercept are 0.0021, 0.0003, <0.0001, and 0.720, respectively.

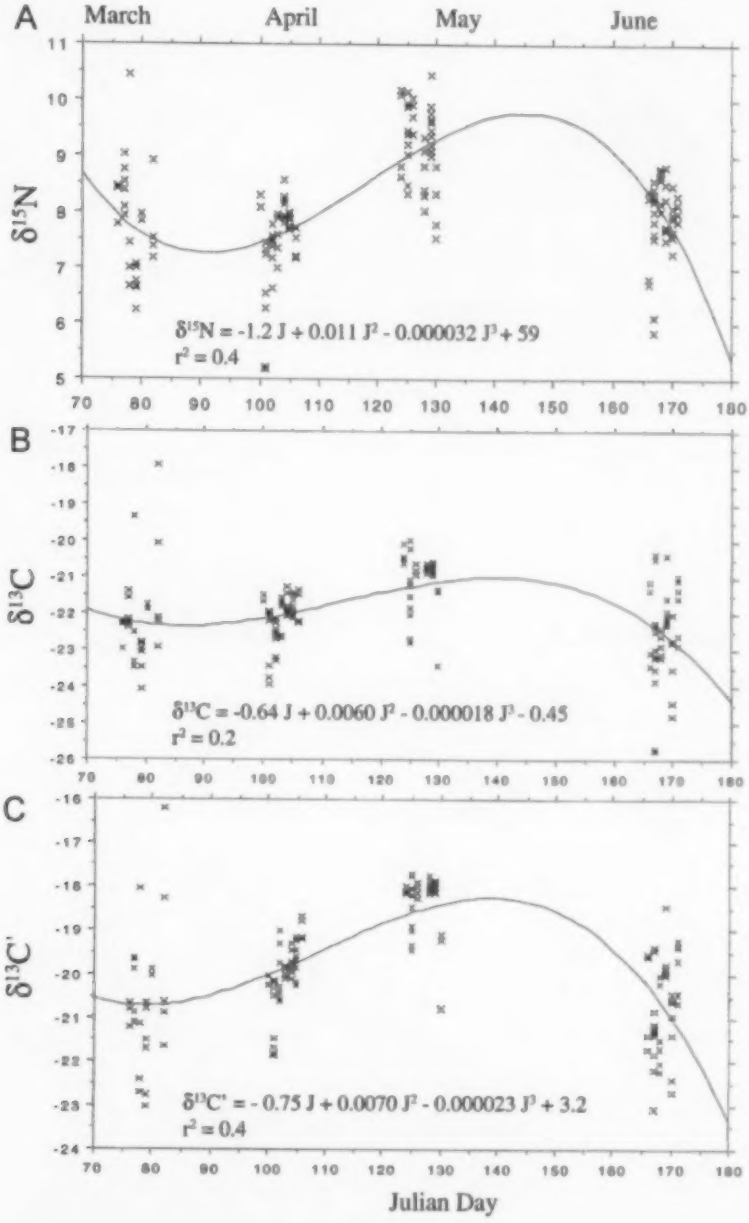

present in an analogous bulk net zooplankton analysis. The analyses of a large number of individual zooplankters, particularly during diapause, revealed the bimodality. However, since bulk net zooplankton sample analysis provided a single datum for each time and place, it was more practical for assessment of spatiotemporal factors. Thus, each sample type had a useful role.

Fishes

Juvenile fishes change isotopic composition rapidly, reflecting isotopic changes in diet at temporal scales of about 1 month (Hesslein et al. 1993), which was also seen here for zooplankton. Isotopic spatial variability of fishes may differ from zooplankton, since they have the potential to integrate food sources of varying isotopic composition from different

© 1999 NRC Canada

Fig. 5. Scatterplots with histograms for *N. cristatus* collected from the water column in (A) March–April 1995, (B) May 1995, (C) below 200 m in fall 1995, and (D) from the upper 50 m in spring 1995. "Cross-hairs" are positioned near the center of the distribution of inferred GOA and PWS isotopic signatures (‰) to aid in comparisons of the plots. Inferred life history stage is shown in parentheses. Figures 5A and 5C suggest large differences in the source of copepods in diapause each year. Diapaused copepods in late 1995 differed considerably from those completing feeding and entering diapause phase in spring (Fig. 5B), instead resembling copepods sampled in the GOA (left cluster in Fig. 5D).

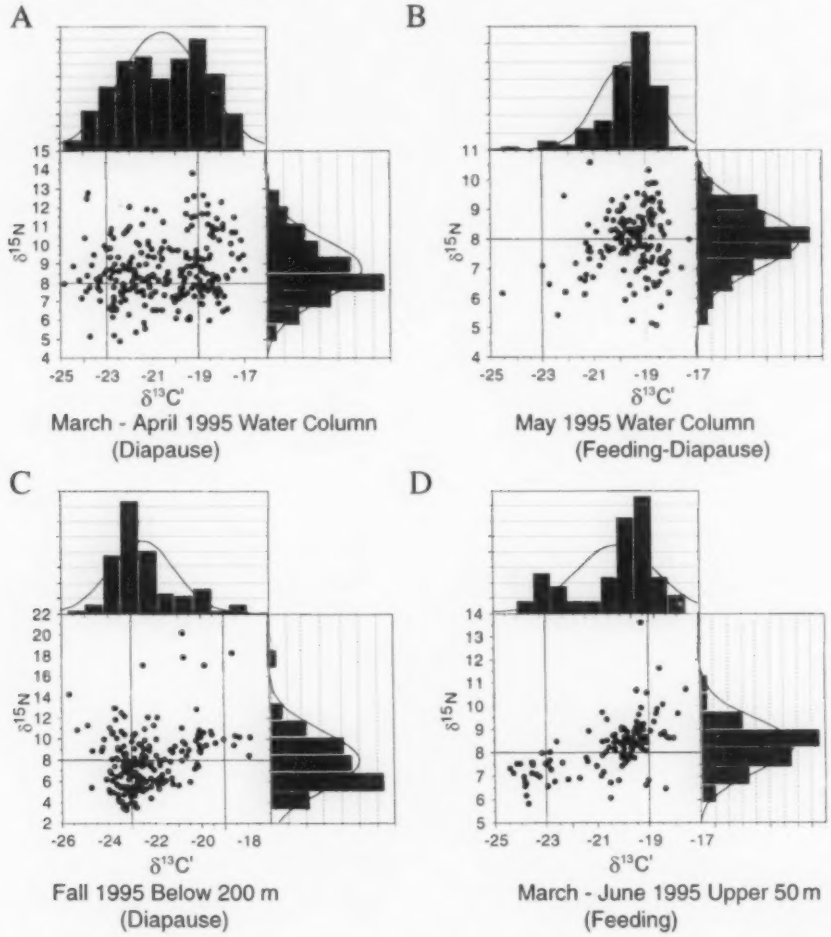

locations in proportion to their foraging range. This was revealed in the data (Table 6), as the differences in mean values among locations were small compared with bulk plankton samples during any one sampling period, suggesting that fishes reduced ^{13}C spatial variability by integrating available carbon. However, changes in carbon source occurring from year to year were revealed in juvenile fish ^{13}C, since they reflected temporal integration on time scales much shorter than 1 year.

Stable isotopes: an indicator of process

The variability and distinct patterns of isotopic data, when identified with an underlying process, can be used to trace that process in the ecosystem. Of particular interest here is the connection of isotopic signatures with oceanographic processes that have been postulated to control the strength of secondary production, which is important for planktivorous fishes in PWS (Cooney 1993, 1997). Bimodal $\delta^{13}C'$ in PWS is consistent with lateral movement of organic carbon from the GOA to PWS.

Diapausing interzonal copepods

The low $\delta^{13}C'$ values for *N. cristatus* diapausing in PWS in fall 1995 differed from those for feeding *N. cristatus* sampled there during the spring. Instead, fall 1995 diapausing *N. cristatus* in PWS were similar to *N. cristatus* sampled in the spring from the GOA. Copepods sampled in May in PWS had predominantly high values of $\delta^{13}C'$. Diapausing copepods in PWS that had low $\delta^{13}C'$ (less than –22‰) appeared to originate in the GOA. It is also apparent that 1995 had a greater proportion of GOA origin copepods than 1994. Most copepods (>90%) (Fig. 5B) collected in diapause in PWS during fall 1995 were from the GOA, whereas GOA *N. cristatus* appeared to represent about half of the 1994 co-

© 1999 NRC Canada

Table 7. Summary of differences between 1994 and 1995 in terms of sources of diapausing copepods and fish carbon in PWS, Alaska, and their conjectured causation.

Observations	1994	1995
Source of diapaused copepods in PWS	GOA and PWS	GOA
Carbon source in PWS juvenile fishes	GOA and PWS	GOA
Advection deduced to be	Moderate	Strong

hort. The few ($N = 20$) diapaused *N. cristatus* that were collected in fall 1994 were similar to those sampled in early spring 1995, with mean $\delta^{13}C' = -21‰$ and SD = 1.8‰. The timing of the collection in the diapause period (either fall or early spring) was therefore not important, confirming the differences between the 1994 and 1995 cohorts diapausing in PWS. A significant portion of the copepods diapausing in PWS appear to originate from the GOA, but the proportion varies from year to year.

Fish production dependencies

Year-to-year differences in the proportion of GOA copepods diapausing in PWS mirrored patterns observed in $\delta^{13}C'_{TL}$ of PWS juvenile Pacific herring and walleye pollock. In 1995, Pacific herring and walleye pollock had an isotopic signature similar to that of GOA zooplankton (potential food source). One explanation for these similarities in isotope signatures is that changes in advection affected each species each year to a similar extent. Cooney (1986, 1988) estimated that Ekman transport could move 1×10^6 t of zooplankton per year over the 1000-km northern GOA continental shelf from the GOA and then into the ACC and coastal waters during periods of relaxed downwelling in the late spring and summer. Late spring to summer is also the period of deep-water renewal for PWS (Niebauer et al. 1994) and is a period of spring tides. The isotopic shift suggests that these processes may vary markedly from year to year in their transport of zooplankton into PWS, supporting the SEA river–lake hypothesis.

Another possible explanation is that Pacific herring and walleye pollock immigrated into PWS from the GOA and thus contained the GOA signature. However, this explanation is inconsistent with what is known of Pacific herring populations in the Northeast Pacific (E. Brown, former regional Pacific herring biologist, Alaska Department of Fish and Game, presently at University of Alaska Fairbanks, Fairbanks, Alaska, personal communication). Alternatively, virtually all juvenile Pacific herring and walleye pollock may leave PWS, feed in the GOA, and then return as a group to explain the 1995 within-species isotopic uniformity. Such a mass migration has never been noted. They more likely acquired the GOA signature from a diet of allochthonous plankton. Since plankton are by definition drifters, their inflow into PWS is passive and thus dependent on physical processes, as were the diapausing copepods. Thus, year-to-year differences in advection provide the most consistent explanation for the isotopic shifts observed in this study (Table 7).

Isotopic variability modes

Two mesoscale modes of isotopic variability were found in the data: (*i*) spatial (e.g., about 100 km, the length dimension of PWS) and (*ii*) temporal (seasonal to annual). Zooplankton isotopic values had both spatial and temporal variability. Although there was a moderate seasonal shift in ^{15}N and ^{13}C, the spatial gradient occurring between the GOA and PWS was the principal mode of ^{13}C variability (Fig. 6). Year-to-year variability in physical processes that mediate the transfer of organic carbon in the form of zooplankton from the GOA to PWS (conjectured to cause the interannual differences in ^{13}C abundance in juvenile fishes and diapausing copepods in PWS) formed the second variability mode, while seasonal changes in availability of dissolved minerals for phytoplankton formed a third. Spatial variability in ^{13}C for fishes was negligible when the GOA transfer was great but was present when the GOA and PWS carbon inputs were balanced, as in 1994, thus forming a weak fourth mode in ^{13}C variability (Fig. 6).

Fig. 6. Scales of ^{13}C variability in the PWS pelagic system. The relative strength suggested by this study is ranked and reflected by the number of asterisks (the greater number of asterisks, the higher the rank). Physical forcing mediates the transfer of spatial variability on biota at annual scaling. Although not specifically addressed in this study, the 1994 data suggest that seasonal change in fishes was less than interannual change or spatial variability (Table 6).

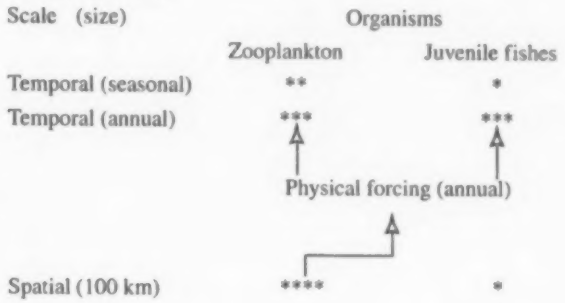

Proxy sampling for long-term studies

Year-to-year differences in ^{13}C measured in diapausing copepods and juvenile fishes (ascribed to the advective processes that transfer carbon in the form of zooplankton from the GOA to PWS) suggest using isotopic measurements as a carbon transport proxy for long-term studies. For example, an isotopic time series (when compared with upwelling indices and fishery statistics) could resolve relationships between oceanographic processes and fluctuations in marine populations and fisheries. Sampling would consist of confirming the isotopic gradient as well as diapaused copepods and fishes. The simplicity of single zooplankter species analysis appears to yield clearer results than bulk net sampling and may thus be the best sampling approach for long-term studies. *Neocalanus cristatus* consistently had low mean $\delta^{15}N$ values of about 8‰, confirming their herbivorous ecological role (Gifford 1993) and making them an ideal candidate. Although bulk net zooplankton samples are more likely to include the small zooplankton prey of early stage juvenile Pacific herring and walleye pollock, using *N. cristatus*, an herbivorous species, for the analysis eliminates sources of variability found in bulk samples such as species composi-

© 1999 NRC Canada

tion, life history stage, and trophic level. The PWS setting includes an area of deep water (>700 m near SEA22) (Fig. 1) that provides an isolated and well-defined diapausing habitat for *Neocalanus* spp., suggesting the feasibility for consistent sampling to determine if changes in source of diapausing copepods occur in cycles like those postulated for zooplankton abundance in the subarctic Pacific Ocean (Brodeur and Ware 1992).

PWS fishes dependent on GOA carbon are subject to vagaries of carbon flow, and are thus under the domain of physical oceanographic processes controlling advection between the GOA and PWS, while PWS fishes wholly dependent on PWS carbon are more directly affected by internal PWS processes. However, increased competition for PWS carbon by all species would occur if GOA carbon were less available to those that normally use it. Shifting to increased dependency on PWS carbon by species with normal affinity for GOA carbon during years of poor GOA carbon availability could provide evidence of competition for a limited carbon supply by the increasing overlap in their ^{13}C values. Alternatively, increased proportion of GOA carbon in organisms could reflect greater dilution of available carbon if PWS carbon were more concentrated or in a form more suitable as forage than GOA carbon.

Northeast Pacific marine population cycles are presumed to be caused by changes in zooplankton abundance that are driven by decadal-scale climatic regime shifts (Francis and Hare 1994), particularly in the region's perimeter (Brodeur and Ware 1992). This study suggests that GOA zooplankton stocks are transported further, beyond the northern perimeter (Ingraham et al. 1998), and into PWS, being detectable by changes in ^{13}C abundance. Time series measurements of natural stable isotope abundance in zooplankton and fishes in conjunction with population indices and physical oceanographic measurements could enable a new understanding of how climate-driven bottom-up processes affect fish recruitment and interaction.

Acknowledgments

This project was funded by the *Exxon Valdez* Oil Spill Trustee Council through the SEA project. However, the findings presented by the author are his own and not necessarily the Trustee Council's position. SEA colleagues collected fish specimens. Evelyn Brown oversaw aging of the fish. J.M. Paul and P. Shoemaker did the initial fish sample preparation. Captain Mike Gaegel and the crew of the R/V *Bering Explorer*, E. Stockmar, J. Murphy, B. Barnett, and T. Cooney assisted with *N. cristatus* sampling. Kim Antonucci did the laboratory processing of samples for stable isotope analysis. Bruce Barnett at the University of Alaska Fairbanks Stable Isotope Facility performed the stable isotope analysis. John Williams made the station map and contour plots. Paul Wessel and others in the GMT discussion group assisted with Fig. 1. Kate Williams assisted with editing the first draft. This paper was improved by the constructive suggestions made by two anonymous reviewers and Guest Editor Doran Mason.

References

Brodeur, R.D., and Ware, D.M. 1992. Long-term variability in zooplankton biomass in the subarctic Pacific Ocean. Fish. Oceanogr. **1**: 32–38.

Bunn, S.E., Loneragan, N.R., and Kempster, M.A. 1995. Effects of acid washing on stable isotope ratios of C and N in penaeid shrimp and seagrass: implications for food-web studies using multiple stable isotopes. Limnol. Oceanogr. **40**: 622–625.

Cabana, G., and Rasmussen, J.B. 1994. Modeling food chain structure and contaminant bioaccumulation using stable nitrogen isotopes. Nature (Lond.), **372**: 255–257.

Checkley, D.M., Jr., and Miller, C.A. 1989. Nitrogen isotopic fractionation by oceanic zooplankton. Deep-Sea Res. **36**: 1449–1456.

Cooney, R.T. 1986. The seasonal occurrence of *Neocalanus cristatus*, *Neocalanus plumchrus*, and *Eucalanus bungii* over the shelf of the northern Gulf of Alaska. Continental Shelf Res. **5**: 541–553.

Cooney, R.T. 1988. Distribution and ecology of zooplankton in the Gulf of Alaska: a synopsis. *In* The biology of the subarctic Pacific. Proceedings of the Japan – United States of America Seminar on the Biology of Micronekton of the Subarctic Pacific. Part I. *Edited by* T. Nemoto and W.G. Pearcy. Bull. Ocean Res. Inst. Univ. Tokyo, Tokyo, Japan. pp. 27–41.

Cooney, R.T. 1993. A theoretical evaluation of the carrying capacity of Prince William Sound, Alaska, for juvenile Pacific salmon. Fish. Res. **18**: 77–87.

Cooney, R.T. 1997. Sound Ecosystem Assessment (SEA): a science plan for the restoration of injured species in Prince William Sound, Alaska. *Exxon Valdez* Oil Spill Restoration Project Annual Report (Restoration Project 96320). Institute of Marine Science, University of Alaska Fairbanks, Fairbanks, Alaska.

Cooper, L.W. 1989. Patterns of carbon isotopic variability in eelgrass, *Zostera marina* L., from Izembek Lagoon, Alaska. Aquat. Bot. **34**: 329–339.

DeNiro, M.J., and Epstein, S. 1977. Mechanism of carbon isotope fractionation associated with lipid synthesis. Science (Washington, D.C.), **197**: 261–263.

DeNiro, M.J., and Epstein, S. 1978. Influence of diet on the distribution of carbon isotopes in animals. Geochim. Cosmochim. Acta, **42**: 495–506.

DeNiro, M.J., and Epstein, S. 1981. Influence of diet on the distribution of nitrogen isotopes in animals. Geochim. Cosmochim. Acta, **45**: 341–353.

Dugdale, R.C., and Goering, J.J. 1967. Uptake of new and regenerated forms of nitrogen in primary productivity. Limnol. Oceanogr. **12**: 196–206.

Dunton, K.H., and Schell, D.M. 1987. Dependence of consumers on macroalgal (*Laminaria solidungula*) carbon in an Arctic kelp community: $\delta^{13}C$ evidence. Mar. Biol. **93**: 615–625.

Dunton, K.H., Saupe, S.M., Golikov, A.N., Schell, D.M., and Schonberg, S.V. 1989. Trophic relationships and isotopic gradients among Arctic and subarctic marine fauna. Mar. Ecol. Prog. Ser. **56**: 89–97.

Francis, R.C., and Hare, S.R. 1994. Decadal-scale regime shifts in the large marine ecosystems of the northeast Pacific: a case for historical science. Fish. Oceanogr. **3**: 279–291.

Fry, B. 1988. Food web structure on Georges Bank from stable C, N, and S isotopic compositions. Limnol. Oceanogr. **33**: 1182–1190.

Fry, B., and Sherr, E.B. 1984. $\delta^{13}C$ measurements as indicators of carbon flow in marine and freshwater ecosystems. Contrib. Mar. Sci. **27**: 13–47.

Gifford, D.J. 1993. Protozoa in the diets of *Neocalanus* spp. in the oceanic subarctic Pacific. Prog. Oceanogr. **32**: 223–237.

Goering, J.J., Patton, C.J., and Shiels, W.E. 1973. Primary production. *In* Environmental studies of Port Valdez. *Edited by* D.W. Hood, W.E. Shiels, and E. Kelley. Inst. Mar. Sci. Occas. Publ. No. 3. University of Alaska Fairbanks, Fairbanks, Alaska. pp. 253–279.

Goering, J.J., Alexander, V., and N. Haubenstock. 1990. Seasonal

© 1999 NRC Canada

variability of stable carbon and nitrogen isotope ratios of organisms in a north Pacific bay. Estuarine Coastal Shelf Sci. **30**: 239–260.

Hesslein, R.H., Hallard, K.A., and Ramlal, P. 1993. Replacement of sulfur, carbon, and nitrogen in tissue of growing broad whitefish (*Coregonus nasus*) in response to a change in diet traced by $\delta^{34}S$, $\delta^{13}C$, and $\delta^{15}N$. Can. J. Fish. Aquat. Sci. **50**: 2071–2076.

Hobson, K.A., and Welch, H.E. 1992. Determination of trophic relationships within a high Arctic marine food web using $\delta^{13}C$ and $\delta^{15}N$ analysis. Mar. Ecol. Prog. Ser. **84**: 9–18.

Ingraham, W.J., Jr., Ebbesmeyer, C.C., and Hinrichsen, R.A. 1998. Imminent climate and circulation shift in northeast Pacific Ocean could have major impact on marine resources. EOS Trans. Am. Geophys. Union, **79**: 197–201.

Kline, T.C. 1997. Confirming forage fish food web dependencies in the Prince William Sound ecosystem using natural stable isotope tracers. Proceedings of the International Symposium on the Role of Forage Fishes in Marine Ecosystems. Alaska Sea Grant College Program Rep. No. 9701. University of Alaska Fairbanks, Fairbanks, Alaska. pp. 257–269.

Kline, T.C., and Pauly, D. 1998. Cross-validation of trophic level estimates from a mass-balance model of, and $^{15}N/^{14}N$ data from, Prince William Sound. *In* Fishery Stock Assessment Models. *Edited by* F. Funk, T.J. Quinn II, J. Heifetz, J.N. Ianelli, J.E. Powers, J.F. Schweigert, P.J. Sullivan, and C.-I. Zhang. Alaska Sea Grant College Program Rep. AKSG-98-01. University of Alaska-Fairbanks, Fairbanks, Alaska. pp. 693–702.

McConnaughey, T., and McRoy, C.P. 1979. Food-web structure and the fractionation of carbon isotopes in the Bering Sea. Mar. Biol. **53**: 257–262.

Miller, C.B., and Terazaki, M. 1989. The life histories of *Neocalanus flemingeri* and *Neocalanus plumchrus* in the Sea of Japan. Bull. Plankton Soc. Jpn. **36**: 27–41.

Miller, C.B., Frost, B.W., Batchelder, H.P., Clemons, M.J., and Conway, R.E. 1984. Life histories of large, grazing copepods in a subarctic ocean gyre: *Neocalanus plumchrus*, *Neocalanus cristatus*, and *Eucalanus bungii*. Prog. Oceanogr. **13**: 201–243.

Minagawa, M., and Wada, E. 1984. Stepwise enrichment of ^{15}N along food chains: further evidence and the relation between $\delta^{15}N$ and animal age. Geochim. Cosmochim. Acta, **48**: 1135–1140.

Niebauer, H.J., Royer, T.C., and Weingartner, T.J. 1994. Circulation of Prince William Sound, Alaska. J. Geophys. Res. **99**: 113–126.

Norcross, B.L., Brown, E.D., Stokesbury, K.D.E., and Frandsen, M. 1996. Juvenile Pacific herring growth and habitat. *Exxon Valdez* Oil Spill Restoration Project Annual Report (Restoration Project 95320T). Institute of Marine Science, University of Alaska Fairbanks, Fairbanks, Alaska.

Owens, N.J.P. 1987. Natural variations in ^{15}N in the marine environment. Adv. Mar. Biol. **24**: 389–451.

Paul, A.J., Paul, J.M., and Brown, E. 1998. Fall and spring somatic energy content for Alaskan Pacific herring (*Clupea pallasi* Valenciennes 1847) relative to age, size and sex. J. Exp. Mar. Biol. Ecol. **223**: 133–142.

Rau, G.H., Mearns, A.J., Young, D.R., Olson, R.J., Schafer, H.A., and Kaplan, I.R. 1983. Animal $^{13}C/^{12}C$ correlates with trophic level in epipelagic food webs. Ecology, **64**: 1314–1318.

Rau, G.H., Heyraud, M., and Cherry, R.D. 1989. $^{15}N/^{14}N$ and $^{13}C/^{12}C$ in mesopelagic shrimp from the northeast Atlantic Ocean: evidence for differences in diet. Deep-Sea Res. **36**: 1103–1110.

Rau, G.H., Takahasi, T., Des Marais, D.J., and Sullivan, C.W. 1991. Particulate organic matter $\delta^{13}C$ variations across the Drake Passage. J. Geophys. Res. **96**: 131–135.

Saupe, S.M., Schell, D.M., and Griffiths, E.W. 1989. Carbon isotope ratio gradients in western Arctic zooplankton. Mar. Biol. **103**: 427–433.

Schell, D.M., Barnett, B.A., and Vinette, K.A. 1998. Carbon and nitrogen isotope ratios in zooplankton of the Bering, Chukchi and Beaufort seas. Mar. Ecol. Prog. Ser. **162**: 11–23.

Smith, W.H.F., and Wessel, P. 1990. Gridding with continuous curvature splines in tension. Geophysics, **55**: 293–305.

Stephenson, R.L., Tan, F.C., and Mann, K.H. 1986. Use of stable carbon isotope ratios to compare plant material and potential consumers in a seagrass bed and kelp bed in Nova Scotia, Canada. Mar. Ecol. Prog. Ser. **30**: 1–7.

Vander Zanden, M.J., Cabana, G., and Rasmussen, J.B. 1997. Comparing trophic position of freshwater fish calculated using stable nitrogen isotope ratios ($\delta^{15}N$) and literature dietary data. Can. J. Fish. Aquat. Sci. **54**: 1142–1158.

Wada, E., Mizutani, H., and Minagawa, M. 1991. The use of stable isotopes for food web analysis. Crit. Rev. Food Sci. Nutr. **30**: 361–371.

Ward, A.E. 1997. A temporal study of the phytoplankton spring bloom in Prince William Sound, Alaska. M.S. thesis, University of Alaska Fairbanks, Fairbanks, Alaska.

Wessel, P., and Smith, W.H.F. 1995. New version of the Generic Mapping Tools released. EOS Trans. Am. Geophys. Union, **72**: 441, 445–446.

Willette, M., Clapsadl, M., Saddler, P., and Powell, M. 1997. Sound ecosystem assessment: salmon and Pacific herring integration. *Exxon Valdez* Oil Spill Restoration Project Annual Report (Restoration Project 96320E). Alaska Department of Fish and Game, Cordova, Alaska.

Wu, J., Calvert, S.E., and Wong, C.S. 1997. Nitrogen isotope variations in the subarctic Pacific: relationships to nitrate utilization and trophic structure. Deep-Sea Res. **44**: 287–314.

Appendix. Bulk net zooplankton isotopic (‰) and C/N data from PWS and the adjacent GOA oceanographic stations (Fig. 1) sampled from 1994 to 1995 by cast type (upper 50 m or entire water column).

Date (year-month-day)	Time	Station	$\delta^{15}N$	$\delta^{13}C$	C/N	$\delta^{13}C'$
Upper 50 m						
940421	19:58	CFOS13	6.42	–21.81	5.15	–20.79
940623	13:45	CFOS13	8.66	–21.90	6.30	–20.24
940927	17:08	CFOS13	9.42	–19.83	6.99	–17.89
950320	14:00	CFOS13	6.66	–22.91	9.07	–20.38
950416	13:38	CFOS13	7.20	–22.23	14.55	–18.96
950505	23:57	CFOS13	8.42	–21.11	13.80	–17.91
950616	4:13	CFOS13	8.33	–22.26	6.04	–20.72
950323	10:05	CFOSBY	8.24	–18.97	7.52	–16.84

© 1999 NRC Canada

Appendix (*continued*).

Date (year-month-day)	Time	Station	$\delta^{15}N$	$\delta^{13}C$	C/N	$\delta^{13}C'$
950412	20:13	CFOSBY	7.58	–22.19	14.39	–18.93
950509	01:00	CFOSBY	9.09	–20.82	11.87	–17.82
950616	06:42	CFOSBY	8.51	–22.82	7.50	–20.70
940924	22:01	CS1	9.44	–21.92	7.17	–19.91
940623	11:26	CS10	7.66	–21.89	5.33	–20.76
940925	23:29	CS13	10.20	–21.21	6.39	–19.51
940924	18:05	CS3	9.40	–21.17	32.70	–17.22
950416	17:43	CS3	7.65	–21.39	11.39	–18.46
950508	21:50	CS3	9.22	–20.68	10.64	–17.86
950616	09:19	CS3	8.24	–23.09	7.94	–20.84
940927	13:51	CS4	9.78	–20.71	6.24	–19.08
940925	21:52	CS5	12.81	–21.53	6.81	–19.65
950323	14:15	CS9	7.40	–22.89	6.45	–21.17
950411	05:45	CS9	7.35	–22.12	7.52	–19.99
950509	18:10	CS9	9.37	–20.85	13.87	–17.64
950616	01:40	CS9	7.60	–20.41	5.99	–18.90
940926	23:41	GOA2	10.40	–22.27	9.99	–19.56
940927	01:27	GOA5	10.84	–22.02	6.64	–20.21
950320	05:45	GOA6	6.50	–23.75	5.77	–22.35
950510	21:18	GOA6	7.67	–23.41	11.16	–20.51
950616	21:46	GOA6	5.98	–25.72	11.16	–22.82
940926	14:15	HE12	9.56	–21.02	17.70	–17.53
950319	22:35	HE12	7.05	–23.39	5.75	–22.00
950411	13:10	HE12	6.41	–23.56	8.12	–21.26
950510	15:20	HE12	8.58	–21.36	9.13	–18.81
950616	16:20	HE12	7.94	–23.68	7.40	–21.59
950411		HE13	5.19	–23.80	8.48	–21.41
940926	22:10	HE2	10.34	–23.03	8.06	–20.74
940926	18:25	HE5	10.20	–22.46	7.29	–20.41
940923	13:15	MS1	9.29	–22.11	7.43	–20.02
940923	19:11	MS2	9.59	–21.74	7.76	–19.55
940923	21:11	MS3	9.06	–22.35	11.34	–19.42
950319	09:20	MS3	7.00	–22.51	6.68	–20.69
950412	13:50	MS3	6.92	–23.23	12.72	–20.13
950508	14:31	MS3	8.16	–20.75	12.17	–17.71
950619	11:08	MS3	8.00	–22.75	9.19	–20.19
940923	17:30	MS5	9.37	–21.16	17.47	–17.68
940924	14:06	MS6	8.65	–21.57	10.08	–18.84
950319	14:40	MS6	10.44	–19.36	6.55	–17.59
950412	10:50	MS6	7.55	–22.66	8.63	–20.23
950508	18:55	MS6	8.61	–20.77	13.09	–17.63
950619	07:42	MS6	7.89	–23.13	8.90	–20.63
940927	21:30	NS1	9.55	–23.24	12.98	–20.12
950320	18:45	NS1	7.04	–22.93	6.67	–21.11
950415	18:25	NS1	7.92	–22.07	13.08	–18.93
950509	14:35	NS1	10.03	–20.87	12.72	–17.77
950617	10:19	NS1	8.77	–23.11	7.00	–21.16
940927	20:06	NS2	8.58	–22.08	7.63	–19.92
940927	18:30	NS3	9.96	–21.08	6.21	–19.46
940927	16:01	NS4	9.97	–21.15	6.47	–19.41
940928	21:21	NWS1	9.86	–22.77	9.21	–20.21
940928	23:52	NWS3	10.17	–22.71	9.20	–20.15
940929	01:45	NWS4	10.00	–22.83	9.89	–20.13
950321	00:15	NWS4	7.92	–21.82	7.90	–19.58
950415	06:52	NWS4	7.73	–21.72	9.03	–19.19
950509	04:45	NWS4	9.83	–20.74	12.51	–17.67
950617	22:01	NWS4	8.63	–22.51	9.89	–19.81

© 1999 NRC Canada

Appendix (*continued*).

Date (year-month-day)	Time	Station	$\delta^{15}N$	$\delta^{13}C$	C/N	$\delta^{13}C'$
950410	21:40	OB1	8.19	–21.55	6.78	–19.69
950504	14:40	OB1	8.73	–20.52	9.91	–17.82
950615	18:37	OB1	6.78	–23.25	7.46	–21.15
950323	16:45	OB2	7.17	–22.19	6.60	–20.40
950411	02:30	OB2	7.39	–21.96	7.78	–19.75
950504	19:02	OB2	10.14	–20.27	9.19	–17.71
950615	22:01	OB2	8.33	–21.23	7.35	–19.16
950413	00:00	PB1	7.62	–21.60	7.47	–19.49
950620	23:59	PB1	7.92	–21.01	7.54	–18.88
950415	15:26	PV1	7.96	–21.45	7.48	–19.34
950509	12:00	PV1	9.41	–20.58	10.43	–17.79
950617	13:07	PV1	8.11	–23.03	5.83	–21.60
950317	16:40	PW1	7.78	–22.96	7.69	–20.79
950414	16:50	PW1	8.24	–21.33	6.42	–19.62
950505	17:05	PW1	9.21	–21.92	13.68	–18.73
950618	14:03	PW1	7.74	–21.97	8.40	–19.59
940423	17:18	SEA11	8.72	–21.98	8.55	–19.57
950317	20:45	SEA11	8.44	–22.25	7.02	–20.30
950414	09:55	SEA11	8.39	–21.82	10.21	–19.07
950505	22:00	SEA11	9.92	–21.53	14.50	–18.26
950618	07:55	SEA11	8.68	–22.21	9.22	–19.64
940423	22:42	SEA14	7.52	–22.93	10.52	–20.12
940920	16:39	SEA15B	7.53	–23.05	20.95	–19.41
940424	08:55	SEA17	6.49	–22.60	12.55	–19.52
940920	17:53	SEA18	8.93	–20.97	7.75	–18.78
940422	14:27	SEA2	9.56	–23.39	9.35	–20.81
940602	10:30	SEA2	8.56	–22.27	7.45	–20.17
940424	12:55	SEA20	7.30	–22.30	10.47	–19.51
940920	20:02	SEA20	9.43	–22.55	8.35	–20.19
940421	23:46	SEA22	5.63	–23.18	9.28	–20.61
950415	22:50	SEA22	7.70	–21.93	7.51	–19.81
950505	09:00	SEA22	9.33	–20.10	9.79	–17.42
950618	02:17	SEA22	7.97	–20.97	7.99	–18.71
940613	12:32	SEA25	8.86	–21.80	5.84	–20.37
940921	00:07	SEA25	9.09	–22.90	8.88	–20.41
950323	14:00	SEA25	7.40	–22.10	6.90	–20.19
950414	22:50	SEA25	7.89	–21.86	8.17	–19.54
950506	15:34	SEA25	9.98	–20.90	11.67	–17.93
950620	19:24	SEA25	8.23	–22.73	8.98	–20.21
940613	17:37	SEA26	8.58	–22.36	6.19	–20.75
940921	11:34	SEA26	8.85	–22.52	6.83	–20.63
940921	14:54	SEA27	9.12	–22.40	7.17	–20.39
950318	16:30	SEA27	8.24	–22.21	10.82	–19.36
950412	18:00	SEA27	7.54	–22.46	11.72	–19.48
950506	18:25	SEA27	9.55	–20.72	12.02	–17.71
950620	15:31	SEA27	8.15	–21.43	8.17	–19.12
940613	19:52	SEA29	9.16	–21.66	6.85	–19.77
940921	17:02	SEA29	9.17	–22.18	6.79	–20.31
940614	11:34	SEA32	9.29	–21.98	6.96	–20.05
950318	19:10	SEA32	8.90	–21.47	7.53	–19.34
950413	10:15	SEA32	7.19	–22.63	10.90	–19.77
950619	14:06	SEA32	8.22	–22.39	7.28	–20.34
940613	13:41	SEA34	7.89	–22.71	6.84	–20.83
940922	16:22	SEA37	9.06	–21.28	26.38	–17.46
950318	23:20	SEA37	8.24	–22.28	6.54	–20.51
950413	05:20	SEA37	7.93	–21.74	7.80	–19.53
950619	18:54	SEA37	7.43	–24.60	8.48	–22.21

© 1999 NRC Canada

Appendix (*continued*).

Date (year-month-day)	Time	Station	$\delta^{15}N$	$\delta^{13}C$	C/N	$\delta^{13}C'$
940614	09:45	SEA39	8.80	–22.23	6.86	–20.33
940923	11:15	SEA39	9.10	–21.63	6.20	–20.01
940422	17:00	SEA4	7.59	–22.79	8.52	–20.39
940425	10:24	SEA4	6.40	–23.74	12.57	–20.66
940425	14:43	SEA4	7.36	–22.94	11.02	–20.06
940425	18:48	SEA4	5.73	–22.71	9.86	–20.02
940425	22:43	SEA4	8.47	–22.42	9.45	–19.81
940426	02:40	SEA4	8.89	–22.02	8.88	–19.53
940426	07:26	SEA4	8.23	–22.93	11.82	–19.94
940602	13:15	SEA4	8.85	–21.93	8.00	–19.66
950414	14:35	SEA4	8.03	–22.01	9.36	–19.42
950505	14:20	SEA4	9.59	–22.75	18.36	–19.23
950618	11:44	SEA4	7.61	–22.22	9.87	–19.53
940615	15:39	SEA40	7.98	–22.72	4.83	–21.93
940422	20:43	SEA6	9.18	–22.07	6.90	–20.16
940423	09:52	SEA8	6.00	–22.98	7.76	–20.78
940604	09:39	SEA8	8.77	–21.71	7.50	–19.59
940423	12:24	SEA9	8.07	–22.39	10.82	–19.54
940604	11:58	SEA9	8.63	–21.77	6.94	–19.84
Entire water column						
950315		CFOS13	11.10	–21.20	6.29	–19.54
950416		CFOS13	8.61	–21.62	7.48	–19.51
950505		CFOS13	8.11	–25.22	13.65	–22.03
950616		CFOS13	8.11	–21.34	12.37	–18.29
950509		CS4	10.52	–20.29	6.93	–18.37
950617		CS4	8.08	–22.43	14.79	–19.14
950323		CS9	10.71	–21.57	6.20	–19.95
950411		CS9	8.08	–22.35	8.04	–20.07
950509		CS9	9.14	–20.76	10.35	–17.99
950616		CS9	7.87	–22.55	12.24	–19.51
950510		GOA6	8.50	–23.87	11.18	–20.97
950616		GOA6	5.94	–25.00	7.21	–22.98
950319		HE11	7.19	–23.45	8.05	–21.17
950319		HE12	7.08	–23.08	7.76	–20.89
950411		HE12	6.02	–23.28	7.51	–21.16
950510		HE12	8.97	–20.99	11.46	–18.05
950615		HE12	7.59	–23.16	12.45	–20.09
950419		HE13	6.59	–24.76	13.96	–21.54
950510		HE13	10.15	–22.05	11.72	–19.07
950616		HE13	8.19	–22.70	11.15	–19.80
950321		NWS4	9.09	–21.50	7.42	–19.41
950415		NWS4	8.34	–21.19	7.29	–19.14
950509		NWS4	8.82	–20.02	8.12	–17.72
950617		NWS4	8.68	–21.01	10.67	–18.18
950413		PB1	8.71	–21.96	9.33	–19.37
950413		PB1	9.03	–20.33	5.10	–19.34
950620		PB1	7.71	–21.22	12.53	–18.14
950415		PV1	7.90	–21.15	6.46	–19.42
950509		PV1	9.05	–19.86	7.08	–17.89
950617		PV1	7.66	–21.23	8.91	–18.74
950317		PW1	10.47	–21.68	8.62	–19.25
950414		PW1	8.84	–21.70	6.19	–20.09
950505		PW1	10.32	–21.61	10.26	–18.85
950618		PW1	8.49	–22.50	9.98	–19.79
950317		SEA11	8.92	–21.74	7.30	–19.69
950414		SEA11	9.64	–21.81	8.58	–19.39
950505		SEA11	9.57	–21.10	10.55	–18.29

© 1999 NRC Canada

Appendix (*concluded*).

Date (year-month-day)	Time	Station	$\delta^{15}N$	$\delta^{13}C$	C/N	$\delta^{13}C'$
950618		SEA11	7.95	–21.16	10.37	–18.38
950317		SEA22	10.97	–20.97	6.50	–19.22
950414		SEA22	9.44	–21.87	8.11	–19.59
950505		SEA22	9.11	–21.15	12.58	–18.07
950618		SEA22	9.74		8.91	
950414		SEA25	9.62	–21.60	8.22	–19.27
950506		SEA25	9.76	–21.06	11.15	–18.16
950620		SEA25	8.37	–21.21	12.98	–18.09
950412		SEA27	8.36	–21.74	7.76	–19.54
950506		SEA27	8.65	–20.45	8.04	–18.17
950620		SEA27	7.76	–20.62	10.06	–17.90
950317		SEA4	9.77	–21.65	8.26	–19.31
950414		SEA4	8.76	–21.85	7.79	–19.64
950505		SEA4	9.70	–22.27	14.73	–18.99
950618		SEA4	8.10	–21.55	7.76	–19.36

© 1999 NRC Canada

Hyperaggregation of fish and fisheries: how catch-per-unit-effort increased as the northern cod (*Gadus morhua*) declined

G.A. Rose and D.W. Kulka

Abstract: Misinterpretations of elevated catch-per-unit-effort (CPUE) in the northern cod (*Gadus morhua*) fishery contributed to overestimations of stock size, inflated quotas, and unsustainable fishing mortality in the 1980s and early 1990s. We hypothesize that concentration of the fish and fishery led to extreme hyperstability in the CPUE–abundance relationship. In the late 1980s, migrant cod began to concentrate within the Bonavista corridor, their most southerly cross-shelf migration route. By the spring of 1990, approximately 450 000 t was concentrated within 7000 km^2 at densities quadruple those of the 1980s. Densities remained high through 1992, while abundance declined fivefold. During this period, cod hyperaggregated (local densities increased with decreasing biomass) in the Bonavista corridor and CPUE increased. To the north, no hyperaggregation occurred, and densities and CPUE declined with biomass. In the Bonavista corridor from 1990 to 1993, CPUE was hyperstable with local cod density. Areas of high cod densities (>0.1 fish·m^{-2}) shrunk as regional estimates of cod biomass declined. The spatial extent of the fishery contracted proportional to the shrinkage in area occupied by the fish. Hence, CPUE was related to abundance at the local scales of a fishing set (local acoustic density) but not to abundance at regional or stock scales.

Résumé : En raison d'interprétations erronées de l'indice élevé des captures par unité d'effort (CPUE) qui était observé dans la pêche à la morue franche (*Gadus morhua*) du Nord, on a surestimé la taille du stock, fixé des quotas exagérés et enregistré une mortalité par pêche non durable dans les années 80 et au début des années 90. Nous posons que la concentration des poissons et de la pêche a entraîné une hyperstabilité extrême du rapport CPUE–abondance. À la fin des années 80, la morue migrante a commencé à se concentrer dans le corridor de Bonavista, sa voie migratoire la plus méridionale en travers de la plate-forme continentale. Dès le printemps 1990, environ 450 000 t de morue étaient concentrées sur une superficie de 7000 km^2, avec des densités quatre fois supérieures à celles relevées dans les années 80. Les densités sont demeurées élevées jusqu'en 1992, tandis que l'abondance était cinq fois plus faible. Pendant cette période, on a noté une hyperagrégation de la morue (les densités augmentaient localement avec la baisse de la biomasse) dans le corridor de Bonavista, et l'indice CPUE a augmenté. Vers le nord, il n'y avait pas d'hyperconcentrations de morue, et les densités et l'indice CPUE diminuaient avec la biomasse. Dans la corrider de Bonavista, de 1990 à 1993, l'indice CPUE était hyperstable par rapport à la densité locale de la morue. Les aires à densité élevée (>0,1 poisson·m^{-2}) se sont resserrées à mesure que les estimations de la biomasse régionale de morue diminuaient. L'étendue spatiale de la pêche a diminué de façon proportionnelle au rétrécissement de l'aire occupée par les poissons. Donc, l'indice CPUE était lié à l'abondance à l'échelle locale d'un trait de pêche (densité acoustique locale) mais pas à l'échelle de la région ou du stock.

[Traduit par la Rédaction]

Introduction

The decline of the northern cod (*Gadus morhua*) stock off Newfoundland and Labrador was almost certainly precipitated by overfishing (deYoung and Rose 1993; Rose et al. 1994). However, the conclusion that overfishing acted in isolation from ecological factors, and without major changes in cod distribution (Hutchings and Myers 1994; Hutchings 1996), is questioned in this paper. We propose that changes in the spatial distribution of cod not only contributed to the overfishing but also to inappropriate interpretations of catch-per-unit-effort (CPUE) from the offshore trawler fishery.

Analytical assessments of the northern cod in the 1980s employed CPUE of the mobile winter trawler fisheries under the assumption that this index would be linearly related to stock size at the scale of the full stock. However, the assumption of linearity between catch rates and stock size has been questioned for over 30 years (Paloheimo and Dickie 1964). For pelagic shoaling fishes such as the clupeids, it is widely acknowledged that CPUE is unlikely to reflect abundance because local densities are behaviorally determined (reviewed by Winters and Wheeler 1985). Early in the development of the winter trawler fishery for cod in Newfoundland waters, which targeted prespawning and spawning

Received October 17, 1997. Accepted September 8, 1998. J14262

G.A. Rose.[1] Fisheries and Marine Institute, Memorial University of Newfoundland, St. John's, NF A1C 5R3, Canada.
D.W. Kulka. Department of Fisheries and Oceans, Science Branch, St. John's, NF A1C 5X1, Canada.

[1]Author to whom all correspondence should be addressed. e-mail: grose@caribou.mi.mun.ca

© 1999 NRC Canada

Fig. 1. Newfoundland region and Bonavista corridor study area.

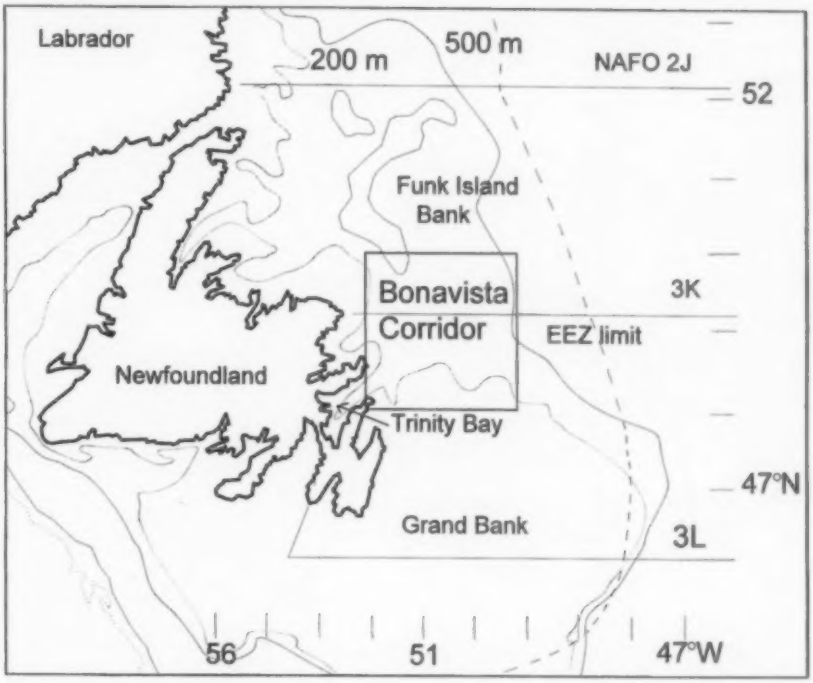

aggregations, Templeman (1966) recognized that CPUE was unlikely to track abundance changes for similar reasons. Two decades later, the lack of linearity between CPUE of cod fisheries employing moveable gear (gillnet) and fish abundance was demonstrated in experimental work by Rose and Leggett (1989, 1991). Nevertheless, attempts to use CPUE as a stock abundance index in analytical assessments continued well into the 1990s (e.g., Bishop et al. 1993).

We hypothesize that changes in spatial patterns of abundance of demersal fish can bring about changes in CPUE and catchability (ratio of CPUE to abundance). Catchability must be constant for CPUE to form a useful index of abundance. Changes in the spatial distribution of the northern cod have occurred since the late 1980s, coincident with the period of steepest stock decline (deYoung and Rose 1993; Kulka et al. 1995; Warren 1997). Rose et al. (1994) argued that these distribution changes may have played a role in the rate of decline of this stock. According to this argument, southward movements of cod increased their vulnerability to the inshore and offshore Canadian fisheries in the early 1990s (until the moratorium on fishing within the Canadian zone) and to the Spanish trawler fleet that began fishing adjacent waters outside the Canadian Exclusive Economic Zone in 1990 (Rose et al. 1994). Atkinson et al. (1997) concluded that beginning in the late 1980s, the extant stock may have aggregated in their southern range at densities well above historic norms. Accordingly, increased vulnerability to contemporary fishing practices (both legal and illegal, Canadian and foreign) could have brought about an abrupt decline of the stock both before and after the moratorium in Canadian waters (Rose et al. 1994). Alternatively, several workers have discounted the importance of widespread spatial change to the overfishing of the northern cod (Hutchings and Myers 1994; Hutchings 1996), and others have taken no account of it (Hilborn and Walters 1992; Walters and Maguire 1996).

The decline of the northern cod since the 1960s occurred progressively from north to south (Taggart et al. 1994). In the early 1990s, the last observed concentration on the northeast Newfoundland shelf was located in the "Bonavista corridor," which is the most southerly cross-shelf migration route for this stock (Rose 1993) (Fig. 1). Both inshore and offshore fisheries were concentrated in the Bonavista corridor and in the adjacent areas during this period of cod decline. Although the corridor was undoubtedly used by cod in their historic onshore migrations, as evidenced by a concentration of inshore fisheries at its shoreward reach (e.g., Lear et al. 1986), the corridor was utilized heavily from 1990 to 1992 (Rose 1993; Rose et al. 1995; Colbourne et al. 1997). However, by 1993, no migrating fish were located in this area (Rose 1996).

In the present paper, we use acoustic and trawl survey data and observer records from the offshore fishery to examine the changing spatial patterns of the northern cod from 1983 to 1993 and their relationship to CPUE from the offshore fishery. We test for hyperstability of CPUE (sensu Hilborn and Walters 1992) relative to biomass at several scales and to local density and also for hyperaggregation, defined as an inverse relationship between local densities and stock abundance. For the period 1990–1993, for which more detailed data are available for the Bonavista corridor, we investigate how biomass, densities, and range changed in

© 1999 NRC Canada

Fig. 2. Acoustic densities of the northern cod in the Bonavista corridor study area, 1990. Acoustic transects are shown as broken lines. Densities are shaded in three tones from light to dark (0.1–0.5, 0.5–2.5, and 2.5–5 fish·m^{-2}).

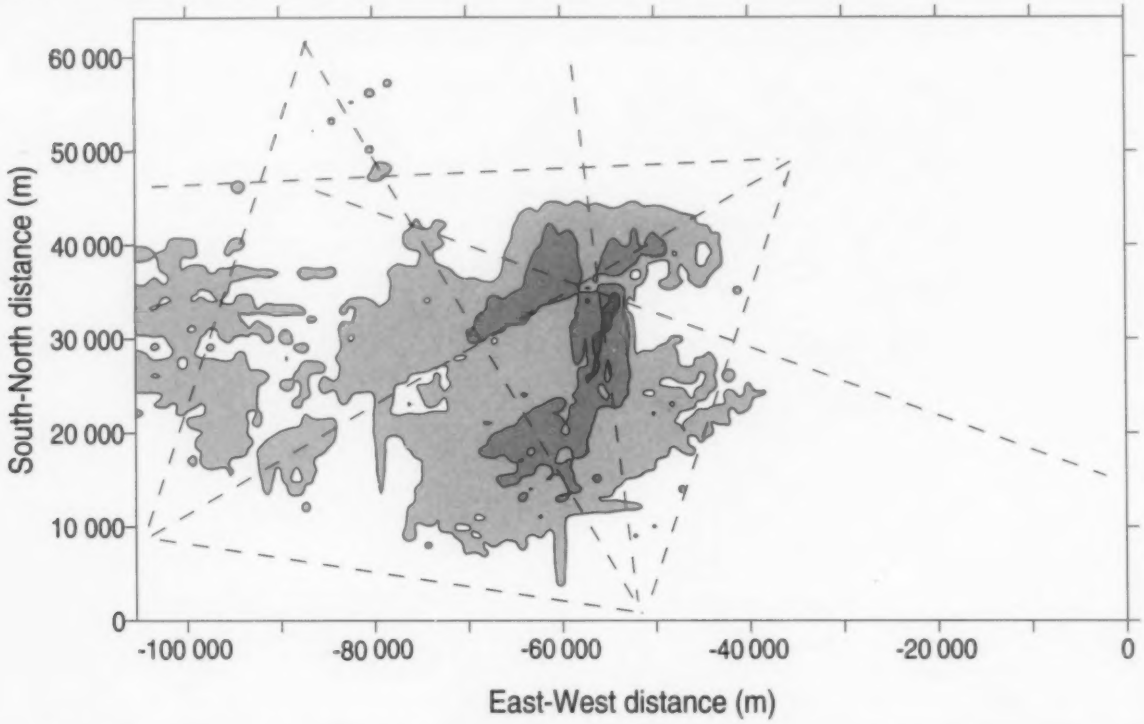

a rapidly declining cod population and how fishing patterns and CPUE were influenced by fish spatial distribution dynamics.

Methods

Acoustic searches for cod were conducted in springtime (May–July) annually from 1983 to 1994 in the area bounded by 48°00.0′–50°00.0′N and 050°00.0′–053°00.0′W (this region approximates the Bonavista corridor) (Fig. 1). The area comprises a deep (300–400 m) basin between the northern edge of the Grand Bank and the Funk Island Bank, which funnels into the deep waters off Trinity Bay. The Bonavista corridor forms part of Northwest Atlantic Fisheries Organization (NAFO) division 3L, which is the southernmost part of the range of this stock. The full stock range includes NAFO divisions 2J, 3K, and 3L, hereafter 2J3KL, commonly referred to, and managed, as the singular "northern" stock (there is ample evidence to suggest that several populations comprise the northern stock; see review in deYoung and Rose 1993). In all years, the acoustic searches were conducted from the 80-m RV *Gadus Atlantica* by staff of the Northwest Atlantic Fisheries Centre, St. John's, Nfld. Scientific echosounders (Simrad EK400 or BioSonics 102 with 49- or 38-kHz transducers deployed from a towed body) and an Engels high-rise bottom trawl were used. Although until 1990, acoustic search patterns did not cover the full study area each year, in all years, large cod aggregations were located, measured acoustically, and sampled with the bottom trawl in short-duration sets (5–15 min). From 1983 until 1989, the chief purpose of the work was to tag cod, whereas from 1990 until 1992, quantitative acoustic surveying and tagging were undertaken together, and in 1993 and 1994, only quantitative acoustics were undertaken because there was no fishery from which tags would be returned. The fisheries-independent research vessel data reported here are catch rates by weight standardized to a 30-min fishing duration.

The Bonavista corridor study area was surveyed comprehensively using scientific echosounders (BioSonics, Inc., model 102 dual-beam, 38 kHz) each June from 1990 to 1994 (Fig. 1). Echosounders were calibrated using tungsten carbide standard reference spheres (MacLennan and Simmonds 1992). Surveys were conducted from two vessels, the *Gadus Atlantica* and the 60-m *Petrel V.* Acoustic sampling was similar in all years. A randomized grid was run over the area. Located cod aggregations were crisscrossed (producing one plane of density data) as many times as possible before the aggregation shifted position. The number of transects varied as a consequence of migration behaviors (Rose et al. 1995). However, a minimum of four transects across the aggregation, and several others adjacent to it, were used to create a density map (e.g., Fig. 2). Note that very high densities of cod attributable to spawning behavior, especially the case in 1992, have not been included in this paper. In all years, cod were in their migratory phase and demonstrating similar behavior (e.g., Rose 1993). All acoustic work was supported by bottom and midwater trawling for species identification, size, reproductive condition, and other biological information (e.g., Rose and Porter 1996).

Data were integrated at 100- or 1000-m intervals and scaled to absolute biomass (fish per square metre) using the target strength model TS (decibels) = 20 log total length (centimetres) – 66 (Rose and Porter 1996). Density maps were created using the normal kriging algorithm of Surfer (Golden Software) and density centroids calculated. To produce biomass to area data from the density maps, biomass was calculated within increasing areas surrounding the density centroid.

Fishery data have been collected in an observer program on Canadian fishing vessels since 1981 (Kulka and Firth 1987). Prior to 1987, approximately 20% of vessel-days were monitored. Since

© 1999 NRC Canada

Fig. 3. Descriptive model of hyper- and hypo-aggregation. Density is measured within fish aggregations or at some scale small compared with the full range of the stock. Units are relative.

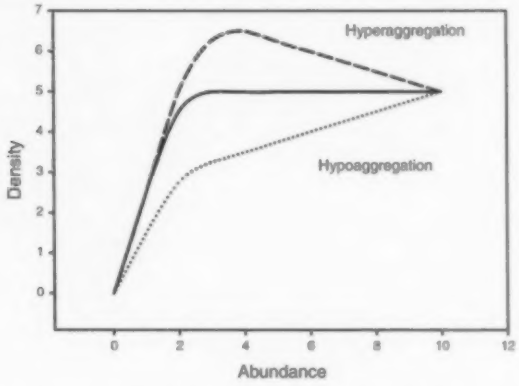

Fig. 4. Boxplot of mean latitude of sites fished by the commercial otter trawl fleet, weighted by standardized CPUE, for the years 1981–1992 within the area inhabited by the northern cod (NAFO 2J3KL). The box encompasses the interquartile range containing 50% of the values. Whiskers extend from the highest to lowest values excluding outliers.

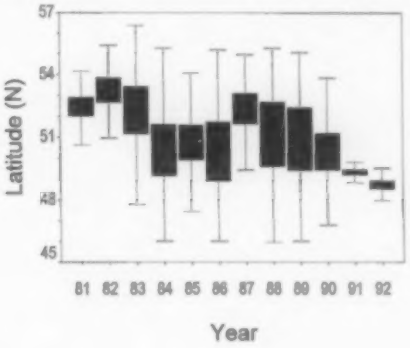

1987, there has been 90–100% coverage. The full data set used here includes a total of 275 488 otter trawl sets made during the winter–spring fishery (January–July 1981–1992) in NAFO 2J3KL (Fig. 1). The subset of the data for the Bonavista corridor comprises a total of 65 702 sets made from January to July 1981–1992. Each set was monitored as to location, duration, gear type, depth, and catch by species. Catch data were standardized by vessel, gear type, and duration prior to analyses and are presented as catch rates per hour of fishing time (for full details, see Kulka et al. 1996). No search or other time is included in effort.

Models of spatial decline

The behavior of nonsedentary fishes leads to two extremes in spatial distribution pattern dynamics (Hilborn and Walters 1992). One extreme is constant-density behavior, where range contracts and expands as abundance changes but local densities remain constant. This type of behavior is characteristic of shoaling species such as the herrings (e.g., Winters and Wheeler 1985). The other extreme exhibits relatively constant overall range but densities that increase and decrease proportional to abundance. Species that do not form shoals or show any type of aggregation behavior might display this type of behavior. These behavior types influence the likely relationship between CPUE and stock size. For example, the relationship between CPUE and abundance is said to be hyperstable if local densities tend to remain constant at the scale of the fishing (in the case of commercial otter trawls, approximately 0.1 km^2 or 2–3 linear nautical miles). Hyperstability is associated with constant-density behavior. At the other extreme, the CPUE – stock size relationship is hypostable if densities decline faster than abundance (associated with constant-range behavior). Stability can be tested for with the model CPUE = a biomass^b, where $b < 1$ indicates hyperstability and $b > 1$ indicates hypostability (Hilborn and Walters 1992). It follows that density can also be termed to be hyper- or hypo-stable and similarly tested.

We introduce the concept of hyperaggregation, which we define as a negative relationship between local density and stock abundance (fish aggregate with decreasing abundance) (Fig. 3). The opposite effect, hypoaggregation, would lead to local densities declining more rapidly than stock abundance (fish disperse when fewer). Hence, as stocks decline, a hyperaggregation response would be for local densities to increase.

Results

A full account of the shift in the spatial distribution of the northern cod in the early 1990s is beyond the scope of the present paper. However, it is important to note the southward changes in the fishery beginning in the late 1980s and the reduction in the range fished, especially after 1989 (Fig. 4). Until 1989, mean CPUE for the January–July fishing season generally increased in all zones within the historic range of the northern cod (NAFO 2J3KL) (Fig. 5). However, after 1989, CPUE within the Bonavista corridor continued to increase (Fig. 5*a*), while CPUE declined in areas to the north and south of the corridor (Figs. 5*b* and 5*c*).

Fisheries-independent measures of cod densities in the Bonavista corridor (research trawl CPUE) were relatively stable from their inception in the spring of 1982 until 1989 (Fig. 6). However, in 1990, densities increased abruptly to levels fourfold those recorded in the previous decade. Elevated densities continued through 1991 and 1992, but in 1993 the CPUE index suddenly declined to its lowest point in over a decade.

At the scale of the full stock (NAFO 2J3KL), commercial CPUE was weakly and negatively correlated with stock biomass as estimated from the Department of Fisheries and Oceans fall bottom trawl surveys ($r = -0.45$, $P < 0.05$) (Fig. 7). However, at the smaller scales of the NAFO divisions, spatial differences were apparent. CPUE and biomass were positively correlated in the northern area (2J) ($r = 0.58$, $P < 0.05$), not correlated in the middle area (3K) ($P > 0.05$), and negatively correlated in the southern area (3L) ($r = -0.52$, $P < 0.05$). However, trends of biomass and CPUE over time may confound these relationships. Hence, year and biomass were entered as independent variables in multiple regressions with CPUE as the dependent variable for each NAFO division. A selection criterion of $P < 0.05$ was used to exclude variables from the model. Similar to the single-factor correlations, the results differed by area. For the northern area (2J), biomass had a significant and positive effect on CPUE, but year did not (Table 1). In area 3K, time had a significant and positive effect on CPUE (CPUE increased over the years). In the southern zone (3L), both time and biomass were significant determinants of CPUE, with biomass having a negative effect on CPUE.

© 1999 NRC Canada

Fig. 5. Standardized mean CPUE and SE from the northern cod otter trawl fishery in NAFO 2J3KL, 1981–1992, (*a*) within the Bonavista corridor study area, (*b*) to the north of the study area, and (*c*) to the south of the study area.

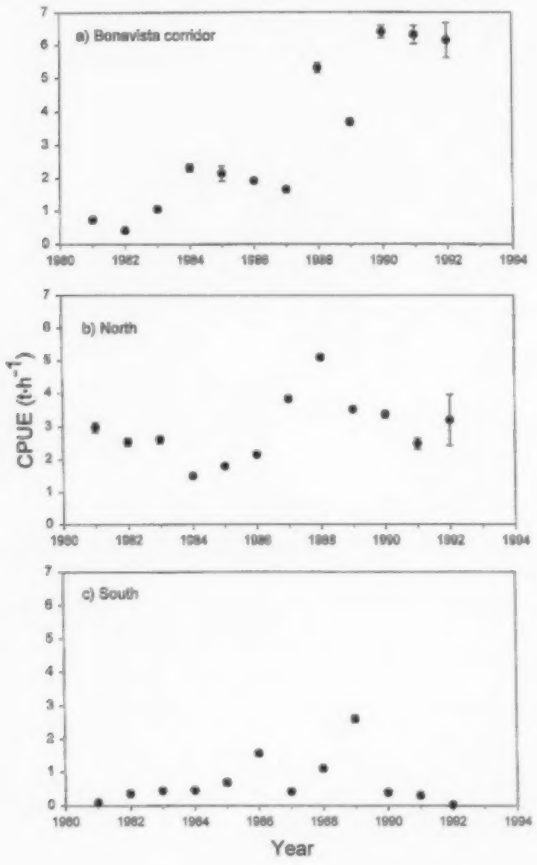

Fig. 6. Mean CPUE and SE, representing local northern cod density, from research trawls directed by echosoundings within the Bonavista corridor study area, 1983–1993.

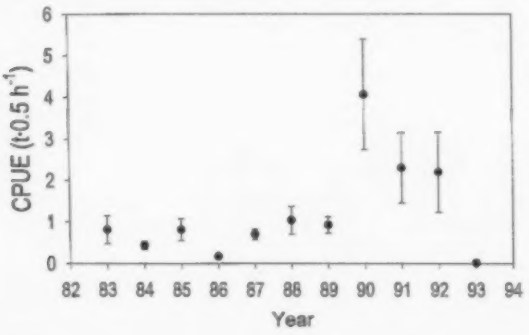

CPUE was hyperstable with respect to local cod density (not biomass) within the Bonavista corridor from 1983 to 1991 (Fig. 8). Under the model CPUE (tonnes per hour) = 0.13 × density$^{0.53}$ (R^2 = 0.89), b was significantly less than 1 ($P < 0.05$). The 1992 data were not included in this analysis because the fishery was under a full moratorium prior to the acoustic survey in that year from which the density data were derived.

Fig. 7. Mean CPUE and SE for the commercial otter trawl fishery against total trawlable biomass of the northern cod stock as determined from the Department of Fisheries and Oceans fall survey, 1981–1992. (*a*) Data for the full stock (NAFO 2J3K3L); (*b–d*) contain data for the smaller scales of the individual NAFO divisions.

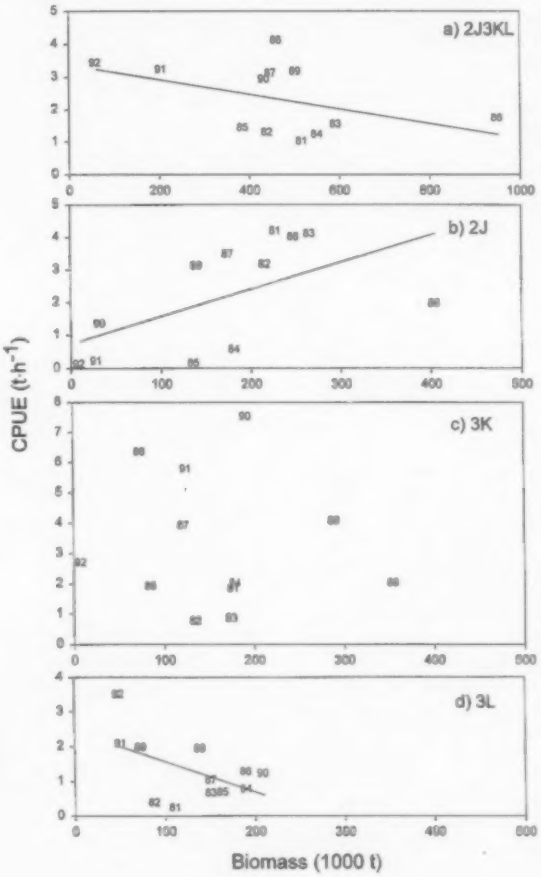

Biomass and area occupied in the corridor, as determined from volumetric analyses of kriged acoustic data, declined rapidly from 1990 to 1993 (Fig. 9). In June 1990, more than 450 000 t of cod was concentrated within 7000 km^2. The biomass–area curve suggests a high degree of aggregation, with 225 000 t (half of the biomass) located within 1500 km^2 (20% of the area). By 1991, total abundance had been reduced to less than 300 000 t, half of which was located within 3500 km^2 (40% of the area). By 1992, abundance had declined further to approximately 125 000 t, half of which occupied 30% of the range. By 1993, abundance had declined sharply to less than 25 000 t that was evenly

© 1999 NRC Canada

Table 1. Summary of backward selection regression of commercial fishery CPUE with independent variables time (year) and research vessel biomass for NAFO 2J3K3L for the years 1981–1992.

Area	Effect	Coefficient	Significance	Model R^2
2J	Year			0.34
	Biomass	0.0084	0.37	
	Constant	0.72	0.05	
3K	Year	0.44	0.01	0.72
	Biomass			
	Constant	–35.0	0.01	
3L	Year	0.21	0.01	0.85
	Biomass	–0.0047	0.05	
	Constant	–15.8	0.01	

Note: Empty cells indicate that the variable was deselected from the model ($P > 0.05$).

Fig. 8. Mean CPUE and SE for the commercial otter trawl fishery against relative acoustic density in the Bonavista corridor, 1982–1991. The best-fit power model is CPUE = 0.13 × density$^{0.53}$ (R^2 = 0.89).

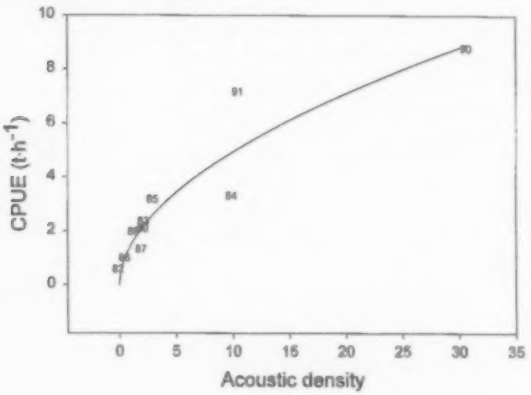

dispersed over 4500 km^2 (half the fish occupied 50% of the range). The high densities recorded in 1990 were sustained in 1991, but over a much reduced area (Fig. 9). For densities above 0.1 fish·m^{-2} (of interest to the commercial fisheries and present over an extended area only in 1990 and 1991), the cumulative biomass profiles did not differ between 1990 and 1991 (Table 2). However, considering all densities, there were declines each year from 1990 to 1993.

Total area holding high densities above 0.1 fish·m^{-2} was reduced from 1250 to 500 km^2 from 1990 to 1991 and to somewhat less than 100 km^2 by 1992 (the fishery terminated prior to these measures in 1992) (Fig. 10). At these densities, approximately 3–6 t of fish would have been available to a typical fishing set of the commercial fleet, assuming a swept area of 20 × 5600 m per commercial bottom trawl set (Kulka et al. 1996) and a range of distributions of cod up to 10–25 m from bottom (Rose 1993). The area fished was proportional to the area holding high densities of cod (>0.1 fish·m^{-2}) in each year by a constant factor of approximately 20 (Fig. 11).

Fig. 9. Cumulative density (biomass versus area) profiles for the northern cod in the Bonavista corridor study area, 1990–1993. Statistical analyses are given in Table 2.

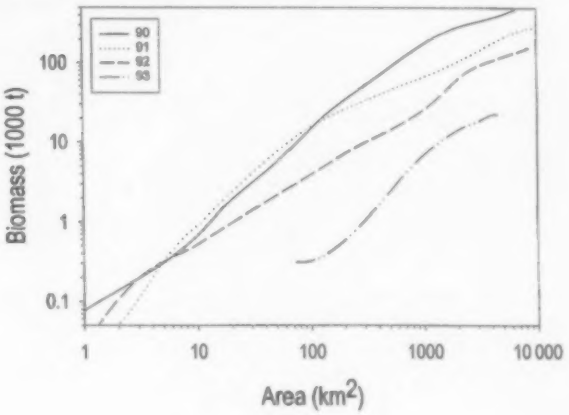

Discussion

The historical otter trawl fisheries for northern cod were designed to exploit cod at their highest densities and during their least migratory phase, which occurs in the winter–spring (January–June) period and spans the spawning season (Kulka et al. 1996). During winter the northern cod formed large aggregations that moved within a confined zone along the outer shelf (Kulka et al. 1995; Wroblewski et al. 1995). These aggregations persisted through the springtime spawning period and until some proportion of the fish approached coastal waters during the onshore migration in late June or early July (Rose 1993). CPUE from this fishery was used in attempts to "tune" population assessment models until the early 1990s (Bishop et al. 1993), under an assumption of linearity between CPUE and abundance.

The relationship between CPUE and abundance or biomass has long been debated (e.g., Baranov 1918, cited in Ricker 1975; Garrod 1964; Paloheimo and Dickie 1964). Our data indicate that CPUE did not closely reflect abundance (biomass) at any scale measured (full stock, NAFO divisions, study area). However, at smaller scales, some significant relationships were evident. In the northern zone (2J), CPUE was positively related to biomass. In the southern zone (3L), there was a negative relationship between CPUE and biomass, independent of the time trend in these data. Hence, the hyperaggregation hypothesis is supported for the southern region, but not for the middle (3K) or north region. Our data are insufficient to address the cause of such spatial variation. However, the spatial difference suggests that cod may aggregate differently with respect to abundance over their range. deYoung and Rose (1993) proposed a modified basin model for the northern cod (MacCall 1990) wherein the Bonavista corridor was the basin trough wherein fish aggregated at times of low abundance. Such a model could explain the differing relationship between CPUE and biomass between the northern and southern ranges. For example, densities may only increase with declines in biomass in the trough, but decrease elsewhere. However, by the

© 1999 NRC Canada

Table 2. Summary of statistics based on the model log(biomass) = B log (area) + K applied to acoustic data on biomass and distribution of cod in the Bonavista corridor study area in the springs of 1990–1993.

	1990		1991		1992		1993	
	K	*B*	*K*	*B*	*K*	*B*	*K*	*B*
All data	−1.69* (0.24)	1.09 (0.03)	−0.61* (0.04)	0.93 (0.05)	−0.32* (0.19)	0.86 (0.02)	−2.46* (0.38)	1.02 (0.04)
High density	−2.29 (0.14)	1.18 (0.02)	−2.54 (0.52)	1.21 (0.07)				

Note: High density is >0.1 fish·m^{-2}. SE is given in parentheses. Comparisons are made horizontally between parameters. *Difference ($P < 0.05$).

Fig. 10. Cumulative area occupied by the northern cod over the full density range encountered in the Bonavista corridor study area, determined using acoustic estimates, 1990–1993. Areas of commercial interest are >0.1 fish·m^{-2}.

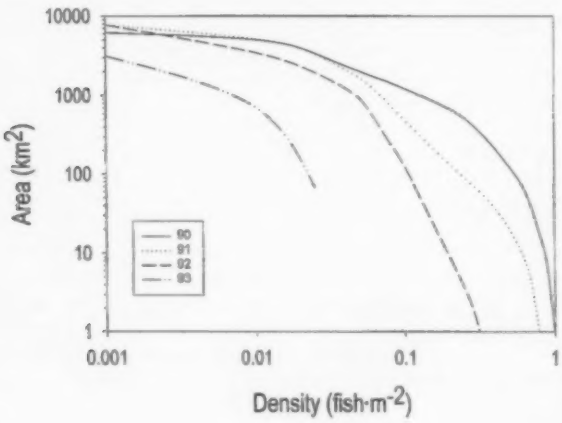

spring of 1993, the approximately 100 000 t of cod present in 1992 was not to be found in the Bonavista corridor or adjacent waters. Hence, the model does not fully account for the spatial demise of the northern cod.

Further evidence supporting hyperaggregation can be garnered from the fishery. The fishery moved southward quickly in the late 1980s to exploit the shifting cod concentrations, despite a management initiative that attempted to spread out the fishing effort (J. Kelly, commercial trawler fisherman, Marystown, Nfld., personal communication). Not only did vessels congregate to the south, but fishing set duration was shortened to reduce increasingly large catches, which in the opinion of fishers and observers were caused by increasing densities of cod (Kulka 1997). There is little doubt that the high cod densities in the Bonavista corridor led to the high catch rates in the late 1980s and until the moratorium on fishing in 1992. However, CPUE was hyperstable with respect to density and not to biomass (Hilborn and Walters 1992). Unfortunately, high cod densities were interpreted as indicative of high abundance in the late 1980s. In 1989, otter trawler skippers and their company stated "our captains are convinced that northern cod are as plentiful as ever offshore and our vessels have few problems catching their trip allotments throughout the year" (memorandum to the Department of Fisheries and Oceans from National Sea Products, Lunenburg, N.S.). Two years later, this fishery had collapsed.

The spatial decline of the northern cod appears to be complex, and as yet only partially understood. As the north to south shift in distribution was occurring, local densities of the extant aggregations were being maintained or even increasing. This situation continued until the spring of 1992, after the imposition of a moratorium on all fishing in Canadian waters (Rose et al. 1995). After 1992, the distribution pattern of the northern cod shifted again (there can be no argument that these fish were simply fished out because there was no fishery at all in the Canadian zone at this time). By 1993, few fish remained in the Bonavista corridor, the area in which the last large aggregations were observed. These findings are inconsistent with the notion that the spatial decline of the northern cod was a simple fishing-down from north to south, as suggested by Hutchings and Myers (1994) and Hutchings (1996). However, the data are consistent with the alternative hypothesis that distribution and aggregation changes increased the availability of the fish to the fisheries. Increased availability to the fisheries could have greatly hastened the decline of this stock and may help explain its quick demise (Rose et al. 1994). We cannot rule out other potential sources of mortality. Nevertheless, distribution changes also offer an explanation of how the foreign fishery, located in the relatively small area of the Grand Bank outside the Canadian Exclusive Economic Zone, continued to increase their catches of cod until 1991 (approximately 50 000 t reported) and why the fishable stock continued to decline after 1992 and a full moratorium on fishing within the Canadian zone. It is important for future interpretations of stock status that the spatial aspects of this stock and its fisheries be explicitly addressed.

We believe that our results may be applicable to other gadoid fisheries. Our analyses indicate that local densities can not only remain relatively stable as biomass changes (resulting in hyperstability in the CPUE–biomass relationship), but can increase as biomass declines. We have termed such behavior "hyperaggregation." Hyperaggregation may be viewed as an extreme form of hyperstability that resulted from the coincidence of distribution changes and severe overfishing. However, less severe forms of hyperstability may be commonplace. There is a growing literature suggesting that CPUE from mobile fisheries for groundfish does not relate linearly to abundance (e.g., Houghton and Flatman 1981; Rose and Leggett 1989, 1991; Crecco and Overholtz 1990; Gordoa and Hightower 1991; Swain and Wade 1993; Swain et al. 1994). Moreover, most gadoids are shoaling fishes whose local densities are behaviorally determined (e.g., Rose 1993). Hence, a linear and constant catchability (the relationship between CPUE and biomass) should not be expected (O.R. Godo, Institute of Marine Research, Bergen, Norway, personal communication). We suggest that CPUE

© 1999 NRC Canada

Fig. 11. Fishing by the commercial otter trawler fleet (left panels) and the distribution of the northern cod from acoustic surveys (right panels), May–July 1990–1992, within the Bonavista corridor study area. Commercial CPUE is shown in five categories representing 0–0.5, 0.5–2.5, 2.5–5, 5–10, and >10 $t \cdot h^{-1}$. Acoustic survey densities are shown in three categories representing 0.01–0.1, 0.1–1, and >1 $fish \cdot m^{-2}$. The total areas fished were approximately 24 740 km^2 (1990), 10 840 km^2 (1991), and 3450 km^2 (1992). Areas occupied by densities of >0.1 $fish \cdot m^{-2}$ were approximately 1250, 500, and 100 km^2 for 1990, 1991, and 1992, respectively.

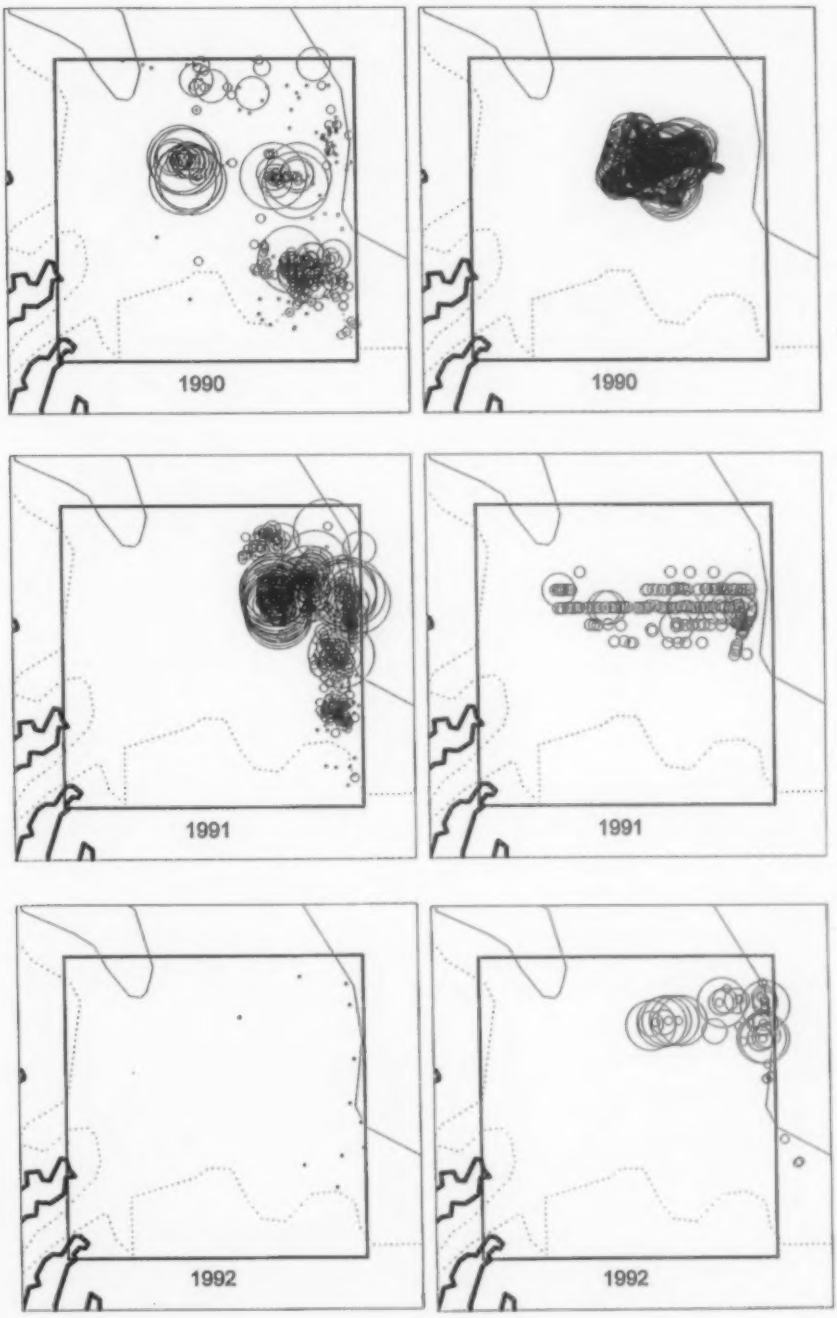

© 1999 NRC Canada

should not be used as an index of abundance for groundfish species without careful examination of the spatial characteristics of both the fish and the fisheries.

In conclusion, we have shown how CPUE of the mobile fishery became elevated during a major decline of the northern cod. Increased CPUE can be attributed to hyperaggregation in the southern extremeties of the stock's range. As a direct consequence, CPUE did not reflect stock abundance (but did reflect local densities). Hyperaggregation resulted in the fish being more vulnerable to contemporary fishing practices (legal and illegal with attendant high-grading and discarding) and led many in industry, science, and management to believe that the stock was still healthy whereas in reality, it was being overfished and declining rapidly.

Acknowledgments

We thank the crews of the RV *Gadus Atlantica* and *Petrel V* and groundfish and acoustics staff from the Northwest Atlantic Fisheries Centre, in particular D. Porter, C. Lang, and C. Stevens, for assistance at sea and the many fisheries observers. Funding was provided by the Natural Sciences and Engineering Research Council of Canada Fisheries Conservation Chair at Memorial University, the Northern Cod Science Program (Department of Fisheries and Oceans), and the Ocean Production Enhancement Network (a Natural Sciences and Engineering Research Council of Canada Network Centre of Excellence).

References

Atkinson, B.A., Rose, G.A., Murphy, E., and Bishop, C.A. 1997. Distribution changes and abundance of northern cod (*Gadus morhua*): 1981–1993. Can. J. Fish. Aquat. Sci. **54**(Suppl.1): 132–138.

Baranov, F.I. 1918. On the question of the biological basis of fisheries. Nauchn. Issled. Ikhtiol. Inst. Izv. **1**: 81–128.

Bishop, C.A., Murphy, E.F., Davis, M..B., Baird, J.W., and Rose, G.A. 1993. An assessment of the cod stock in NAFO divisions 2J+3KL. NAFO SCR Doc. 93/86.

Colbourne, E.B., deYoung, B., and Rose, G.A. 1997. Environmental analysis of cod (*Gadus morhua*) migration in relation to the seasonal variations on the Northeast Newfoundland Shelf. Can. J. Fish. Aquat. Sci. **54**(Suppl.1): 149–157.

Crecco, V., and Overholtz, W.J. 1990. Causes of density-dependent catchability for Georges Bank haddock *Melanogrammus aeglefinus*. Can. J. Fish. Aquat. Sci. **47**: 385–394.

deYoung, B., and Rose, G.A. 1993. On recruitment and distribution of Atlantic cod (*Gadus morhua*) off Newfoundland. Can. J. Fish. Aquat. Sci. **50**: 2729–2741.

Garrod, D.J. 1964. Effective fishing effort and catchability coefficient. Rapp. P.-v. Réun. Cons. Int. Explor. Mer, **155**: 66–70.

Gordoa, A., and Hightower, J.E. 1991. Changes in catchability in a bottom-trawl fishery for cape hake (*Merluccius capensis*). Can. J. Fish. Aquat. Sci. **48**: 1887–1895.

Hilborn, R., and Walters, C.J. 1992. Quantitative fisheries stock assessment: choice, dynamics and uncertainty. Chapman and Hall, New York.

Houghton, R.G., and Flatman, S. 1981. The exploitation pattern, density-dependent catchability, and growth of cod (*Gadus morhua*) in the west-central North Sea. J. Cons. Cons. Int. Explor. Mer, **39**: 271–287.

Hutchings, J.A. 1996. Spatial and temporal variation in the density of northern cod and a review of hypotheses for the stock's collapse. Can. J. Fish. Aquat. Sci. **53**: 943–962.

Hutchings, J.A., and Myers, R.A. 1994. What can be learned from the collapse of a renewable resource? Atlantic cod, *Gadus morhua*, of Newfoundland and Labrador. Can. J. Fish. Aquat. Sci. **51**: 2126–2146.

Kulka, D.W. 1997. Discarding of cod (*Gadus morhua*) in the northern cod and northern shrimp directed trawl fisheries, 1980–94. NAFO Sci. Counc. Stud. **29**: 67–79.

Kulka, D.W., and Firth, J.R. 1987. Observer program training manual — Newfoundland region. Can. Tech. Rep. Fish. Aquat. Sci. No. 1355 (rev.).

Kulka, D.W., Wroblewski, J.S., and Narayanan, S. 1995. Recent changes in the winter distribution and movements of northern Atlantic cod (*Gadus morhua*) on the Newfoundland–Labrador shelf. ICES J. Mar. Sci. **52**: 889–902.

Kulka, D.W., Pinhorn, A.T., Halliday, R.G., Pitcher, D., and Stansbury, D. 1996. Accounting for changes in spatial distribution of groundfish when estimating abundance from commercial fishing data. Fish. Res. **28**: 321–342.

Lear, W.H., Baird, J.W., Rice, J.C., Carscadden, J.E., Lilly, G.R., and Akenhead, S.A. 1986. An examination of factors affecting the inshore cod fishery of Labrador and eastern Newfoundland. Can. Tech. Rep. Fish. Aquat. Sci. No. 1469.

MacCall, A.D. 1990. Dynamic geography of marine fish populations. University of Washington Press, Seattle, Wash.

MacLennan, D.W., and Simmonds, E.J. 1992. Fisheries acoustics. Chapman and Hall, London, U.K.

Paloheimo, J.E., and Dickie, L.M. 1964. Abundance and fishing success. Rapp. P.-v. Réun. Cons. Int. Explor. Mer, **155**: 152–163.

Ricker, W.E. 1975. Computation and interpretation of biological statistics of fish populations. Bull. Fish. Res. Board Can. No. 191.

Rose, G.A. 1993. Cod spawning on a migration highway in the north-west Atlantic. Nature (Lond.), **366**: 458–461.

Rose, G.A. 1996. Cross-shelf distributions of cod in NAFO division 2J3KL in May and June 1995: some preliminary findings of a longer term study. Can. Stock Assess. Secr. WP 96/10.

Rose, G.A., and Leggett, W.C. 1989. Predicting variability in catch-per-effort in Atlantic cod, *Gadus morhua*, trap and gillnet fisheries. J. Fish Biol. **35**(Suppl. A): 155–161.

Rose, G.A., and Leggett, W.C. 1991. Effects of biomass–range interactions on catchability of migratory demersal fish by mobile fisheries: an example of Atlantic cod (*Gadus morhua*). Can. J. Fish. Aquat. Sci. **48**: 843–848.

Rose, G.A., and Porter, D.R. 1996. Target strength studies on Atlantic cod (*Gadus morhua*) in Newfoundland waters. ICES J. Mar. Sci. **53**: 259–265.

Rose, G.A., Atkinson, B., Baird, J., Bishop, C.A., and Kulka, D.W. 1994. Atlantic cod distribution changes and thermal variations in Newfoundland waters, 1980–1992. ICES Mar. Sci. Symp. **198**: 542–552.

Rose, G.A., deYoung, B., and Colbourne, E.B. 1995. Cod (*Gadus morhua*) migration speeds and transport relative to currents on the north-east Newfoundland Shelf. ICES J. Mar. Sci. **52**: 903–914.

Swain, D.P., and Wade, E.J. 1993. Density-dependent geographic distribution of Atlantic cod (*Gadus morhua*) in the southern Gulf of St. Lawrence. Can. J. Fish. Aquat. Sci. **50**: 725–733.

Swain, D.P., Nielsen, G.A., Sinclair, A.F., and Chouinard, G.A. 1994. Changes in catchability of Atlantic cod (*Gadus morhua*)

© 1999 NRC Canada

to an otter-trawl fishery and research survey in the southern Gulf of St. Lawrence. ICES J. Mar. Sci. **51**: 493–504.

Taggart, C.T., Anderson, J., Bishop, C., Colbourne, E., Hutchings, J., Lilly, G., Morgan, J., Murphy, E., Myers, R., Rose, G., and Shelton, P. 1994. Overview of cod stocks, biology, and environment in the Northwest Atlantic region of Newfoundland, with emphasis on northern cod. ICES Mar. Sci. Symp. **198**: 140–157.

Templeman, W. 1966. Marine resources of Newfoundland. Bull. Fish. Res. Board Can. No. 154.

Walters, C., and Maguire, J.-J. 1996. Lessons for stock assessment from the northern cod collapse. Rev. Fish Biol. Fish. **6**: 125–138.

Warren, W.G. 1997. Changes in the within-survey spatio-temporal structure of the northern cod (*Gadus morhua*) population, 1985–1992. Can. J. Fish. Aquat. Sci. **54**(Suppl. 1): 139–148.

Winters, G.H., and Wheeler, J.P. 1985. Interaction between stock area, abundance, and catchability coefficient. Can. J. Fish. Aquat. Sci. **42**: 989–998.

Wroblewski, J.S., Kulka, D.W., Narayanan, S., Oake, A.M., Collier, A.G., and McGrath, B.D. 1995. Winter distribution and movements of northern Atlantic cod *(Gadus morhua)* along the Newfoundland–Labrador continental shelf edge derived from observations on commercial trawlers. Fish. Oceanogr. **4**: 128–146.

© 1999 NRC Canada

Estimating diel, depth-specific foraging opportunities with a visual encounter rate model for pelagic piscivores

David A. Beauchamp, Casey M. Baldwin, Jason L. Vogel, and Chad P. Gubala

Abstract: We developed a visual foraging model for piscivores that predicts search volume as a function of light and turbidity. We combined this model with diel hydroacoustic measurements of depth-specific prey fish densities during summer stratification in Lake Tahoe, Lake Washington, and Strawberry Reservoir to examine differences in diel, depth-specific visual encounter rates of prey. These study sites were selected to represent gradients of increasing limnetic prey fish density and declining transparency. The model predicted over a 30-fold difference in maximum depth-specific diel encounter rates among the three lakes. Lake Washington, which was characterized by intermediate transparency and moderate limnetic prey density, had the highest predicted prey encounter rates. The pattern of prey encounter rates among the three lakes was similar to the proportional contribution of limnetic prey fishes observed in the diet of piscivores from these waters. This approach may be used to construct temporally and spatially explicit trophic interaction models for examining mechanisms underlying predator and prey distributions or to predict the response of existing or introduced predators to changing environmental conditions, prey abundance, or distribution.

Résumé : Nous avons élaboré un modèle de recherche visuelle de nourriture pour les piscivores qui prévoit que le volume de recherche est fonction de la lumière et de la turbidité. Nous avons combiné ce modèle avec des mesures hydroacoustiques nycthémérales des densités de poissons proies à des profondeurs spécifiques durant la période de stratification estivale dans le lac Tahoe, le lac Washington et le réservoir Strawberry pour étudier les différences dans les taux nycthéméraux de rencontre visuelle de proies à des profondeurs spécifiques. Nous avons choisi ces sites d'étude parce qu'ils présentaient un gradient croissant de densité des poissons proies limnétiques et un gradient décroissant de transparence. La modèle a prévu une différence d'un facteur de plus de 30 dans les taux maximaux de rencontre nycthémérale aux profondeurs spécifiques entre les trois lacs. C'est dans le lac Washington, caractérisé par une transparence intermédiaire et une densité modérée de proies limnétiques, que le modèle a prévu le plus haut taux de rencontre de proies. Le profil des taux de rencontre de proies parmi les trois lacs reflétait la contribution proportionnelle des poissons proies limnétiques observée dans le régime alimentaire des piscivores de ces eaux. Cette approche peut être utilisée pour construire des modèles d'interaction trophique temporellement et spatialement explicites permettant d'examiner les mécanismes qui régissent les distributions de prédateurs et de proies ou de prévoir la réponse des prédateurs en place ou introduits au changement dans les conditions environnementales et dans l'abondance ou la distribution des proies.

[Traduit par la Rédaction]

Introduction

In lakes and reservoirs, large pelagic piscivores are typically the target of recreational fisheries and are often manipulated through introductions to new waters, supplementary stocking, and regulated harvest. The influence of these top predators on the structure and function of aquatic communities has been recognized for over a decade (e.g., Carpenter et al. 1985; Northcote 1988). However, the mechanisms that determine the magnitude of top-down control in systems of varying environmental characteristics, basin morphometries, and trophic status are less well understood. Given the uncer-

Received October 8, 1997. Accepted October 14, 1998.
J14236

D.A. Beauchamp,[1,2] C.M. Baldwin, and J.L. Vogel. Utah Cooperative Fisheries and Wildlife Research Unit,[3] Department of Fisheries and Wildlife/Ecology Center, Utah State University, Logan, UT 84322-5255, U.S.A.
C.P. Gubala.[4] Institute of Natural Systems Engineering, Department of Civil and Environmental Engineering, Utah Water Research Laboratory, Utah State University, Logan, UT 84322-4910, U.S.A.

[1]Author to whom all correspondence should be addressed. e-mail: daveb@fish.washington.edu
[2]Present address: Washington Cooperative Fisheries and Wildlife Research Unit, School of Fisheries, Box 357980, University of Washington, Seattle, WA 98195, U.S.A.
[3]The Unit is jointly sponsored by the Biological Resources Division of the U.S. Geological Survey, Utah State University, Utah Division of Wildlife Resources, and the Wildlife Management Institute.
[4]Present address: Department of Geography, University of Toronto at Mississauga, 3359 Mississauga Road North, Mississauga, ON L5L 1C6, Canada.

© 1999 NRC Canada

Fig. 1. Ultraoligotrophic Lake Tahoe, mesooligotrophic Lake Washington, and mesoeutrophic Strawberry Reservoir represent a gradient of increasing productivity illustrated by increasing prey fish density and declining transparency. Fish densities were estimated from hydroacoustic surveys in Lake Tahoe (August 1993), Lake Washington (July 1992), and Strawberry Reservoir (June 1996). Secchi disk transparencies represent average values during summer stratification.

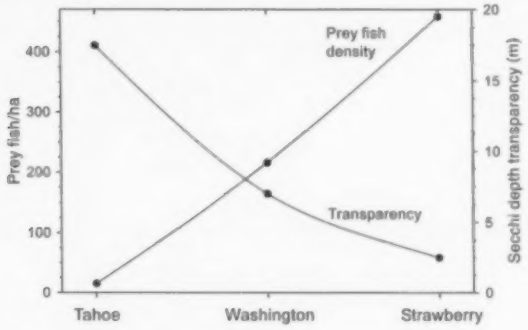

tainty about community-level responses to these frequent manipulations of piscivores, we need to develop tools for predicting responses to these changes to enable careful evaluation of potential impacts from proposed manipulations before irreversible actions are taken.

The distribution and behavior of predators and prey in limnetic communities are largely determined by vertical or horizontal gradients of biotic and abiotic factors (e.g., light, transparency, temperature, water chemistry). Brandt et al. (1992) described a spatially explicit model that integrated the effects of environmental conditions and food supply to estimate the volume of different habitat zones offering specific growth potentials for predators during different seasons. A visual foraging model converted prey biomass and density into a daily ration size using a simple, static prey encounter rate model. Daily ration was then converted to growth rate potential of the predator using a bioenergetics model (Hewett and Johnson 1992). For simplicity, the initial foraging model in Brandt et al. (1992) estimated prey encounters assuming a constant search volume, independent of the change in optical qualities of the waters by depth or diel period. Mason and Patrick (1993) elaborated on this approach by explicitly modeling temporal and depth-specific changes in search volume for planktivorous alewife (*Alosa pseudoharengus*). Piscivory in pelagic waters often occurs during crepuscular periods (Beauchamp 1990; Beauchamp et al. 1992) when prey distributions and light intensity are dynamic functions of depth and time (Clark and Levy 1988; Luecke and Wurtsbaugh 1993; Appenzeller and Leggett 1995). As light intensity decreases at dusk, piscivores react to prey at rapidly declining distances (reaction distance); this pattern is reversed at dawn. Thus, prey densities and search volumes can change simultaneously in complex patterns that result in dynamic probabilities of encounter. By modeling prey encounters at appropriate temporal and spatial scales, we should gain new insights regarding the ability of pelagic piscivores to influence the behavior and population dynamics of lower trophic levels in different limnetic communities. However, for a model to be a useful management tool, inputs should be minimal and their acquisition timely and affordable. The model proposed here requires information on water transparency and diel distributions of limnetic predators and prey.

Hydroacoustic measurement of temporal, spatial, and size-specific prey fish densities enables an assessment of diel prey availability patterns (Brandt 1996) experienced by piscivores, based on the predator's depth and foraging path in the water column. By linking a visual foraging model with diel prey distribution patterns, we can estimate diel changes in encounter rates by predators for various prey. By comparing encounter rates at different prey densities, or between prey species, or under different conditions of light and transparency, we can predict which species, or which life stage of a species, is most vulnerable to predation and under what conditions we might expect piscivores to switch to alternative prey. This approach can therefore make predictions about the effect of predation among or within systems representing a wide range of environmental conditions and prey densities.

The purpose of this paper was to briefly summarize the visual encounter rate model and then describe its application for estimating depth-specific diel prey encounters in Lake Tahoe (California–Nevada, U.S.A.), Lake Washington (Washington State, U.S.A.), and Strawberry Reservoir (Utah, U.S.A.). These waters represent opposing gradients of increasing limnetic prey fish densities and declining transparencies (Fig. 1); therefore, application of the model to these waters serves to demonstrate how foraging opportunities of piscivores, and conversely, predation risk to prey fishes, vary among waters across a representative range of prey densities and transparencies. The piscivore–prey assemblages examined in this study were lake trout (*Salvelinus namaycush*) foraging on kokanee (*Oncorhynchus nerka*) in Lake Tahoe, rainbow (*Oncorhynchus mykiss*) and cutthroat trout (*Oncorhynchus clarki*) foraging on juvenile sockeye salmon (*O. nerka*) and longfin smelt (*Spirinchus thaleichthys*) in Lake Washington, and cutthroat trout foraging on juvenile cutthroat trout and kokanee in Strawberry Reservoir.

Methods

Visual foraging rate model

We modeled prey encounter rates $ER_{z,t}$ (prey per hour at depth z and diel time period t) as the product of spatially and temporally explicit search volumes $SV_{z,t}$ and the vertical density distribution of prey fishes $PD_{z,t}$:

$$(1) \qquad ER_{z,t} = SV_{z,t} PD_{z,t}.$$

Search volume varied with diel changes in piscivore swimming speeds SS_t (centimetres per second) (Henderson and Northcote 1985; Warner and Quinn 1995) (Table 1) and reaction distances $RD_{z,t}$ (centimetres) to prey in response to diel shifts in the photic environment:

$$(2) \qquad SV_{z,t} = \pi RD_{z,t}^2 SS_t.$$

Swimming speeds (body lengths per second) were computed from the laboratory data of Henderson and Northcote (1985) for cutthroat trout and Dolly Varden (*Salvelinus malma*) and from in situ telemetry data from rainbow trout in Lake Washington (Warner and Quinn 1995) and cutthroat trout in Strawberry Reservoir

© 1999 NRC Canada

Table 1. Diel swimming speeds, as a percentage of fork length (FL), applied to piscivores in Lake Tahoe (50-cm lake trout), Lake Washington (42-cm rainbow trout and cutthroat trout), and Strawberry Reservoir (42-cm cutthroat trout).

	Day		Crepuscular		Night	
Piscivore	Mean	SD	Mean	SD	Mean	SD
Lake trout (50 cm)[a]						
% FL/s	59	0	47	14	8	—
cm/s	29.5	0.0	23.5	7.0	4.0	—
Rainbow trout (42 cm)[b]						
% FL/s	41	24	39	29	20	19
cm/s	17.2	10.1	16.4	12.2	8.4	8.0
Cutthroat trout (42 cm)[c]						
% FL/s	79	51	29	16	38	21
cm/s	33.2	21.4	12.2	6.7	16.0	8.8
Cutthroat trout (42 cm)[d]						
% FL/s	78	1	26	32	0	—
cm/s	32.8	0.4	10.9	13.4	0.0	—

Note: Dolly Varden data from Henderson and Northcote (1985) were applied to lake trout in Lake Tahoe. Cutthroat trout data from Henderson and Northcote (1985) are presented for comparison with the estimates derived from in situ telemetry data from cutthroat trout in Strawberry Reservoir.

[a]Henderson and Northcote (1985) data on Dolly Varden.
[b]Warner and Quinn (1995).
[c]C.M. Baldwin (unpublished data).
[d]Henderson and Northcote (1985).

(C. Baldwin, unpublished data) (Table 1). Although telemetry-based estimates of swimming speed are generally assumed to underestimate actual swimming speeds, the laboratory and telemetry-based estimates for diel swimming speeds by cutthroat trout were similar (Table 1). Diel swimming speeds were applied to piscivorous (mean fork length = 42 cm in June–July) cutthroat trout and rainbow trout in Lake Washington and Strawberry Reservoir. Diel swimming speeds for Dolly Varden (Henderson and Northcote 1985) were applied to lake trout (mean fork length = 50 cm) in Lake Tahoe (Table 1).

The $RD_{z,t}$s (centimetres) were determined as a function of light level and prey size from the experimental data of Howick and O'Brien (1983) on largemouth bass (*Micropterus salmoides*) foraging on bluegill (*Lepomis macrochirus*):

$$(3) \qquad RD_{z,t} = 24.5 I_{z,t}^{0.4747} TL^{0.9463} \quad (r^2 = 0.986)$$

where TL is total length (centimetres) of prey, $I_{z,t}$ is ambient light intensity (microeinsteins per square metre per second, lux, foot-candles, etc.), and the subscripts z and t represent depth (metres) and time (diel period), respectively. The intercept of 24.5, used for light in microeinsteins per square metre per second, would be converted to 3.787 when using lux or to 11.7 when using foot-candles.

We compared eq. 3 with experimentally measured RD for lake trout foraging on salmonid prey (Vogel and Beauchamp 1999). Equation 3 compared well with experimental data for $I < 17.8$ lx but overestimated RD for $I > 17.8$ lx and was overly sensitive to changes in prey size (Fig. 2). Howick and O'Brien (1983) reported that RD for largemouth bass to bluegill (2.9–9.9 cm TL) and redfin shiner (*Lythrurus umbratilis*, 3.1–7.5 cm TL) showed a strong prey-size effect and greater maximum RD (about 200 cm) than was observed for salmonids. Prey size had no effect on RD by lake trout to salmonid prey (5.5–13.8 cm TL; Vogel and Beauchamp 1999). For $I_{z,t} < 17$ lx and prey size of 7.5 cm TL, eq. 3 compared well with experimentally measured RD for lake trout responding to 5.5- or 13.8-cm cutthroat trout (Fig. 2). Therefore, since the model was applied to salmonid predators and salmoniform prey, the effect of prey size was removed by setting TL = 7.5 cm. Thus, eq. 3 becomes

$$(4) \qquad RD = 164.9 I_{z,t}^{0.4747}$$

when used for light in microeinsteins per square metre per second. The intercept would be converted to 25.490 when using lux or to 78.8 when using foot-candles. The effect of prey size on RD may be specific for different taxonomic groups and represents a hypothesis requiring further experimentation over a broader range of taxa, prey sizes, and light levels.

At higher light levels ($I_{z,t} \geq 17.8$ lx), RD generated from eq. 3 continued to increase, whereas experimentally measured RD for lake trout remained relatively constant at 94.5 cm (2 SE = 6.7 cm) over 17.8–1103 lx (Vogel and Beauchamp 1999). This threshold effect was termed the saturation intensity threshold (SIT) by Henderson and Northcote (1985), which they demonstrated for salmonids (cutthroat trout and Dolly Varden), and has also been reported for centrarchids (largemouth bass and bluegill, Howick and O'Brien 1983). Thus, when $I_{z,t} > 17.8$ lx (SIT), eq. 3 was modified to set $RD = RD_{max}$ = (mean + 2 SE) = 94.5 + 6.7 = 101.2 cm:

$$(5) \qquad RD = 164.9 I_{z,t}^{0.4747} \text{ for } I_{z,t} \leq 17.8 \text{ lx}$$

$$RD = RD_{max} = 101.2 \text{ cm for } I_{z,t} > 17.8 \text{ lx}.$$

RD also declines with increasing turbidity at a given light level (Miner and Stein 1996). We modeled turbidity as a proportional reduction of RD referenced to RD under clear water conditions at the same light level (i.e., no interaction with light or prey size). From Miner and Stein (1996), RD declined with increasing turbidity as a proportion of the observed maximum RD = 208 cm in clear water (0.3 NTU for a 24-cm largemouth bass at 135 lx) compared to RD at higher turbidity levels:

$$(6) \qquad RD_{NTU}/RD_{clear} = 98.2 NTU^{-0.624}/208 = 0.472 NTU^{-0.624}.$$

Combining eqs. 5 and 6 for light measured in microeinsteins per square metre per second yields

$$(7) \qquad RD = 77.9 I_{z,t}^{0.4747} NTU^{-0.624} \text{ for } I_{z,t} \leq 17.8 \text{ lx}$$

$$RD = RD_{max} = 47.8 NTU^{-0.624} \text{ for } I_{z,t} > 17.8 \text{ lx}$$

© 1999 NRC Canada

Fig. 2. Visual foraging model predictions of piscivore RD as a function of light for two prey sizes (5.5 and 7.5 cm). RD reached a constant maximum value above the SIT at light levels ≥17.8 lx (broken line). Model estimates were compared with laboratory measurements of lake trout responding to 5.5- to 13.9-cm cutthroat trout (Vogel and Beauchamp 1999) and bluegill responding to 29-cm largemouth bass (Howick and O'Brien 1983).

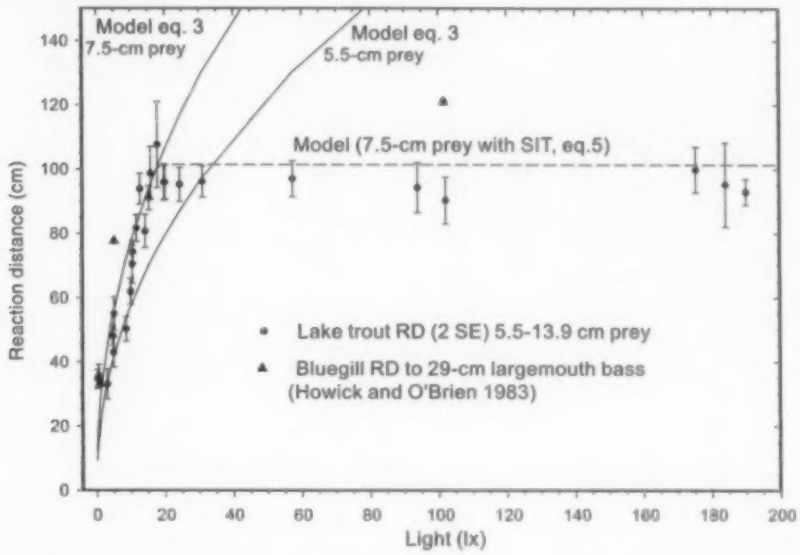

where "clear water" has a minimum turbidity of 0.3 NTU. When $I_{z,t} \leq 17.8$ lx, the intercept 77.9 would be converted to 12.034 for lux and to 37.2 for foot-candles.

Depth- and temporally specific search volumes were computed from estimates of ambient light and turbidity for each lake and reservoir corresponding to the dates and times of the diel hydroacoustic surveys of prey density and distribution during summer stratification. Surface light intensity $I_{0,t}$ varied as a function of time (date and diel period), cloud cover, and location (latitude, longitude, surrounding topography) and was estimated by supplying these data to a computer program by Janiczcek and Young (1987). The diel change in ambient light $I_{z,t}$ experienced by a predator at a given depth, date, and time was computed as

$$(8) \qquad I_{z,t} = I_{0,t}e^{zk}.$$

We set $k = -0.0677$ (Tahoe Research Group, unpublished data) and NTU = 0.30 (the minimum turbidity allowed in this formulation of the model) for Lake Tahoe, $k = -0.3500$ (Eggers 1978; and computed from Lehman 1988) and NTU = 0.35 for Lake Washington, and $k = -0.3778$ and NTU = 5.00 for Strawberry Reservoir (C.M. Baldwin, unpublished data).

Hydroacoustic measurements

Prey fish densities ($PD_{z,t}$) were estimated from diel hydroacoustic and net surveys (Brandt 1996) during summer stratification to obtain species- and size-specific densities of prey fishes in each depth interval and diel period. We measured size-specific diel vertical distributions of fish density along limnetic transects perpendicular to shore using a dual-beam echo sounder. Data from Lake Washington (July 17–18, 1992), Lake Tahoe (August 19–20, 1993), and Strawberry Reservoir (June 26–28, 1996) were collected using a BioSonics model 105 echo sounder with a 420-kHz dual-beam (6 × 15°) transducer and ESP 2.0 signal-processing software. The transducer was towed 0.5 m deep off the port bow of a planing-hull boat at an average speed of 2.5 m/s. We acquired data at 2 pings/s with a 0.4-ms pulse width. Only echoes within 3° (–6 dB off-axis) of the acoustic axis were included in the analyses. Echo counting was employed to measure density of single targets (fish per 1000 m^3). Ordinarily, echo integration would have been used to detect fish schools; however, problems with operating the echo integrator forced us to use paper chart recordings. These paper charts provided information on the vertical and temporal distribution of fish schools but could not be used to quantify biomass or numbers of fish in schools. Since target densities increased toward the surface in Strawberry Reservoir, transducers were alternately oriented vertically and horizontally on transects. The side-facing transects measured relative densities of the near-surface targets that would not have been detected by the conventional down-looking transducer due to near-field effects, small diameter of the acoustic beam, and potential boat avoidance. Transects were repeated during day, dusk, and night periods within the same region of each lake to characterize size-specific depth distribution and density in offshore regions. The sizes of prey fishes available to piscivores varied among lakes. Kokanee were 7–30 cm (fork length) with mean weight = 46.3 g during August in Lake Tahoe, juvenile sockeye salmon and longfin smelt were 5–10 cm with mean weight = 3.3 g during July in Lake Washington, and juvenile kokanee and cutthroat trout were 7–12 cm with mean weight = 13 g during June in Strawberry Reservoir. In each lake, identification of acoustic targets was determined by depth-specific midwater trawling and vertical gill nets. Based on these samples, we assumed that all limnetic targets greater than –35 dB in Lake Tahoe were lake trout.

The horizontal patchiness of nonschooling prey fishes was examined by computing the density (fish per cubic metre) of prey-sized targets in 20-ping (25-m-long) "patches" within each depth interval (3-m intervals in Strawberry Reservoir, 5-m intervals in Lake Washington, and 10-m intervals in Lake Tahoe) for each transect during daylight and crepuscular periods. The proportion of empty patches and frequency of different patch densities were compared graphically between diel periods and among waters.

Diel depth distributions of the piscivores were estimated from their depth-specific relative abundance using a combination of net sampling (vertical and sinking horizontal gill nets, midwater trawls, purse seines, Beauchamp et al. 1992), ultrasonic telemetry

© 1999 NRC Canada

Fig. 3. Diel depth distribution of prey fish (18–30 cm) in Lake Tahoe in August 1993 during the day, dusk, and night. Densities of individual targets are indicated by solid bars, and schooling kokanee are represented on a relative scale by cross-hatched bars. The line represents the decline in RD of piscivores to prey with depth for each diel period. The vertical temperature during this period is also shown.

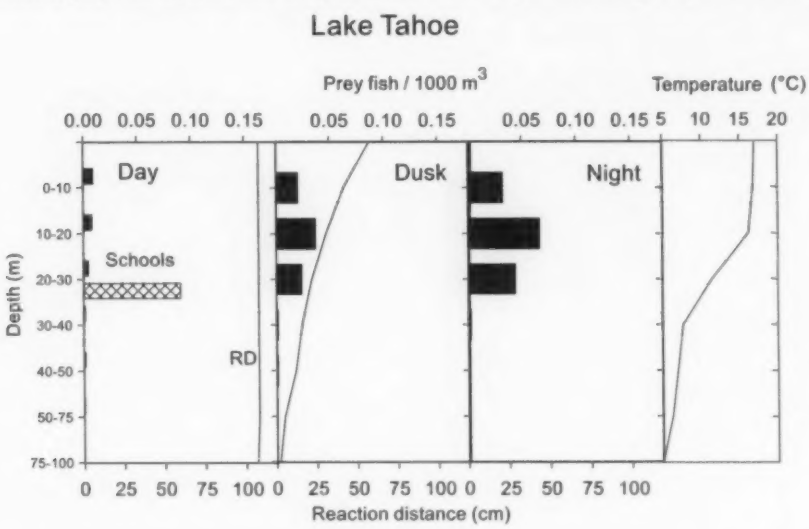

(Warner and Quinn 1995; C.M. Baldwin and C.P. Gubala, unpublished data), and hydroacoustics.

Model evaluation

Prey encounter rates predicted from the visual foraging model were compared with predation rates that were estimated independently from field samples and bioenergetics modeling in Lake Tahoe (Thiede 1997), Lake Washington (Beauchamp 1994), and Strawberry Reservoir (Baldwin 1998). Daily numerical encounter rates were converted to the biomass of prey fish encountered, based on the size distribution of prey fishes available. To standardize for differences in predator and prey sizes among these waters, the prey biomasses that were encountered or consumed were presented as percentages of predator body weight.

We performed several sensitivity analyses on the model. An individual parameter perturbation analysis (e.g., Bartell et al. 1986) was performed on the variables and parameters in eq. 7 for light levels below SIT. Variables (light, turbidity) and parameters (intercept, light dependence coefficient, and turbidity-dependence coefficient) were varied by ±10% and the resulting RD was compared with the nominal RD. A Monte Carlo simulation of eq. 8 was also performed across a range of seven turbidities (0.3, 0.5, 1.0, 3.0, 5.0, 7.0, and 9.0 NTU) and five light levels below SIT (0.2, 5.0, 10.0, 15.0, and 17.8 lx) to estimate the collective propagation of error in estimates of RD. Each parameter was assumed to be normally distributed with means equal to the values in eq. 8 and SD = 10% of each mean. For each combination of light and turbidity, RD was estimated 30 times to generate a mean, SD, and coefficient of variation (CV). Since SD for the three parameters was set at 10% of the mean, CV < 10% for RD from the Monte Carlo simulation would suggest that parameter errors were dampened in the model, whereas CV > 10% would indicate that the model was relatively volatile to parameter error.

Results

Diel distribution of prey fish and depth-specific RDs

Diel vertical distributions of piscivores, prey fishes, and RD varied among the three lakes. In Lake Tahoe, kokanee primarily remained in 0–30 m depths throughout the diel cycle (Fig. 3). Kokanee formed aggregations (seen on chart recordings) in and below the thermocline (20–30 m) during daylight, whereas extremely low densities of individual targets (<0.01 target/1000 m^3) were found from the surface down to 50 m. Due to the high light intensity and extremely low turbidity, depth-specific RDs remained at maximum saturation levels (RD_z = 101.2 cm) over 0–75 m and just started declining at 100 m (RD_z = 100 cm). Any kokanee occupying depths below 120 m would not have been detected with our hydroacoustic surveys due to degradation of the signal-to-noise ratio. However, no measurable density of targets ascending from below 100 m was evident at dusk or dawn, so we concluded that kokanee remained in the upper 50 m throughout the diel cycle. Schools dispersed at dusk, and the density of single (nonaggregated) targets increased to 0.021–0.037 target/1000 m^3 in 0–30 m depths. RDs declined rapidly at all depths during dusk, but RD_z (midway between sunset and astronomic twilight) declined from 58 cm at the surface to 2 cm at 100 m. At night, individual targets were more abundant (0.033–0.066 target/1000 m^3) but were still concentrated in depths of 0–30 m. Piscivores' nocturnal RD_z declined from 2 cm at the surface to 0 cm below 50 m. The vertical distribution of piscivores in Lake Tahoe was similar among diel periods. Piscivore-sized acoustic targets (target strength greater than or equal to –35 dB) remained in 10–50 m depths throughout the diel period, and the modal depth of piscivorous lake trout from both overnight gillnet catches and large acoustic targets was 30 m (Fig. 4).

In Lake Washington during July 1992, juvenile sockeye salmon and longfin smelt formed schools in and below the thermocline during daylight, whereas individual targets were bimodally distributed with peak densities at 15–18 m (0.45 target/1000 m^3) and 39–45 m (0.62 target/1000 m^3) (Fig. 5). During daylight, RD_z remained high at 97 cm from the

© 1999 NRC Canada

Fig. 4. Vertical distribution of predatory lake trout in Lake Tahoe during August 1993 as determined from mean catch per unit effort in sinking horizontal gill nets set overnight down the shore slope and from the vertical density of acoustic targets greater than –35 dB. The acoustic depth distribution patterns were similar between day and night transects, so they were averaged together. Error bars represent ±1 SE.

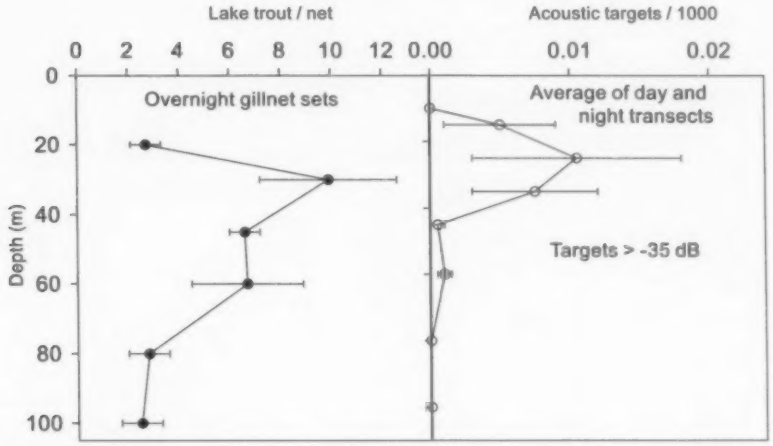
Lake trout / net
Acoustic targets / 1000
0 2 4 6 8 10 12
0.00 0.01 0.02
Overnight gillnet sets
Average of day and night transects
Targets > -35 dB
Depth (m)
0 20 40 60 80 100

Fig. 5. Diel depth distribution of prey fish (5–10 cm) in Lake Washington in July 1992 during the day, dusk, and night. Densities of individual targets are indicated by solid bars, and schooling longfin smelt and juvenile sockeye salmon are represented on a relative scale by cross-hatched bars. The line represents the decline in RD of piscivores to prey with depth during each diel period. The vertical temperature during this period is also shown.

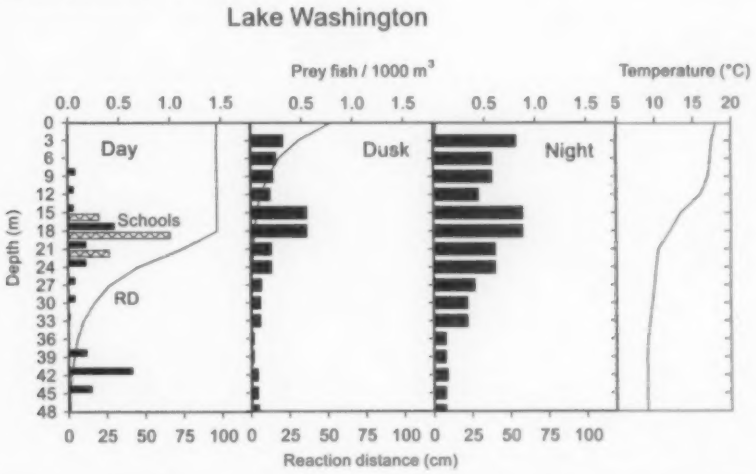

surface to 18 m and then declined rapidly to 1 cm at 48 m. Schools dispersed at dusk, with peaks in target density (0.13–0.27 target/1000 m^3, longfin smelt) occurring at 0–3 and 15–18 m depths (0.55 targets/1000 m^3; predominantly juvenile sockeye salmon mixed with some longfin smelt, Beauchamp et al. 1992). Midcrepuscular RD_z declined exponentially from 53 cm at the surface to 0 cm at 30 m. At night, targets were more abundant (0.10–0.86 target/1000 m^3) but maintained the bimodal depth distribution observed during dusk. The nocturnal RD_z ranged from 2 to 0 cm from the surface to 9 m. The modal depth of piscivorous rainbow trout was 1 m throughout the diel cycle but ranged from 0 to 13 m (Warner and Quinn 1995). Piscivorous cutthroat trout occupied 5–25 m with a modal depth at 15 m (Beauchamp et al. 1992; Beauchamp 1994).

In Strawberry Reservoir during late June 1996, no schools of prey fishes (juvenile cutthroat trout or kokanee) were detected in limnetic regions during daylight, and relatively low densities of individual fishes (0.5 target/1000 m^3) were concentrated in 0–2 m (Fig. 6). During daylight, RD_z was only 18 cm from the surface to 17 m and then declined to 10 cm at 23 m. Fish densities increased at dusk with peak densities of 1.4 targets/1000 m^3 and at night with peak densities of 2.4 targets/1000 m^3 in the 2–5 m depth stratum. The midcrepuscular RD_z declined from 10 cm at the surface to 0 cm at 20 m. The nocturnal RD_z for piscivores declined gradually from 6 cm at the surface to 2 cm at 23 m. Predatory-sized cutthroat trout ranged from 0 to 11 m throughout epi- and meta-limnetic waters but were most concentrated in 0–2 m during this period (Baldwin 1998).

© 1999 NRC Canada

Fig. 6. Diel depth distribution of prey fish (5–12 cm) in Strawberry Reservoir in June 1996 during the day, dusk, and night. Densities of individual targets are indicated by solid bars. No schooling was evident during daylight. The line represents the decline in RD of piscivores to prey with depth during each diel period. The vertical temperature during this period is also shown.

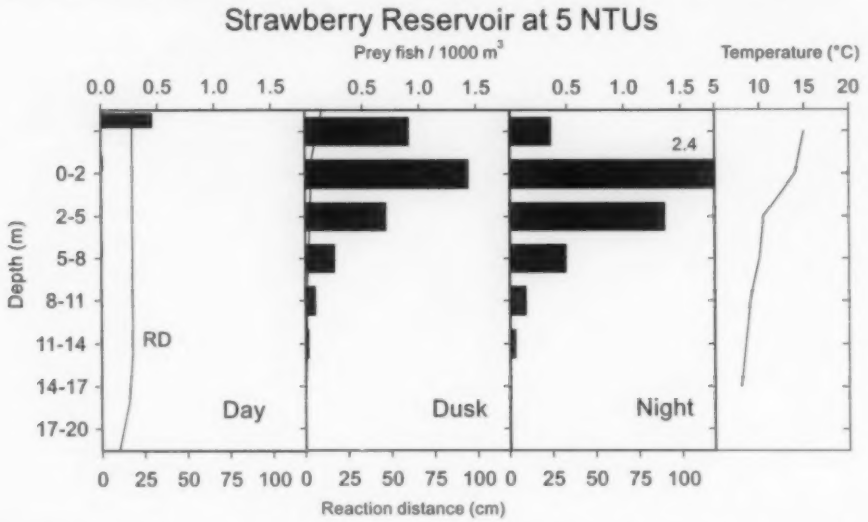

Fig. 7. Percentage of patches containing different densities of prey fish during daylight and crepuscular hydroacoustic transects in each lake. The patches represent 25-m segments of the transects. Total number of patches and the percentage of empty patches are displayed for day and crepuscular periods in each lake. Note that the vertical scale is 10 times larger for Lake Washington than for Lake Tahoe and Strawberry Reservoir.

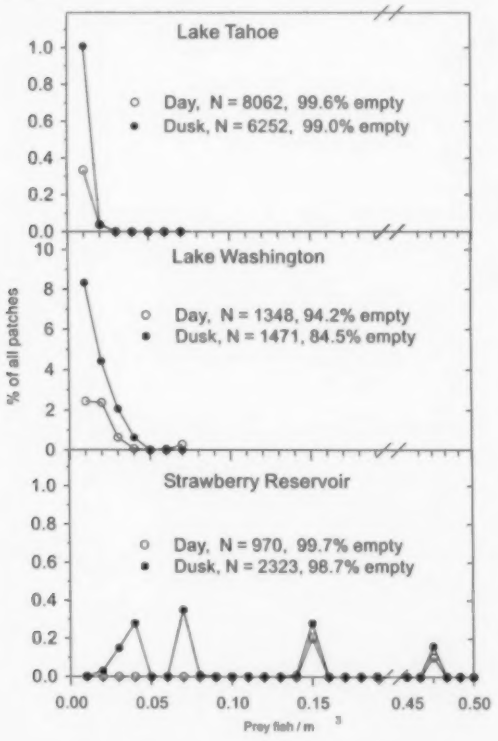
Lake Tahoe
Day, N = 8062, 99.6% empty
Dusk, N = 6252, 99.0% empty
Lake Washington
Day, N = 1348, 94.2% empty
Dusk, N = 1471, 84.5% empty
Strawberry Reservoir
Day, N = 970, 99.7% empty
Dusk, N = 2323, 98.7% empty
% of all patches
0.0 0.2 0.4 0.6 0.8 1.0
0 2 4 6 8 10
0.00 0.05 0.10 0.15 0.45 0.50
Prey fish / m3

The horizontal distribution of prey fishes was extremely patchy in all three systems. The majority (84.5–99.7%) of 25-m-long patches were empty, but the frequency of nonempty patches was consistently higher during crepuscular periods than during daylight (Fig. 7). Lake Washington showed both a larger percentage of nonempty patches and higher patch densities than Lake Tahoe. Higher-density patches were found in Strawberry Reservoir but at much lower frequencies than in Lake Washington. The maximum patch density of prey fishes was 500–2000 times greater than the mean density at their modal depth for all daytime and crepuscular transects in Lake Tahoe, 100–150 times greater in Lake Washington, and 1000–3000 times greater in Strawberry Reservoir.

Diel changes in depth-specific prey encounter rates

Diel foraging opportunities differed considerably in magnitude and by depth among the three lakes. In all waters, prey encounters were relatively rare, with maximum rates ranging from 0.035/h in Lake Tahoe to 0.833/h in Lake Washington and 0.116/h in Strawberry Reservoir (Fig. 8). Piscivores could encounter prey fishes for longer periods over a greater range of depths in waters with higher transparency. During summer stratification in Lake Tahoe, piscivores should encounter the most prey fish in 0–30 m depths during daylight (0.016–0.035 prey fish/h), with much reduced encounters during crepuscular periods (0.003–0.010 prey fish/h) and no measurable visual encounters at night (<0.001 prey fish/h). When considering the horizontal patchiness of prey, piscivores would randomly encounter 0.16 nonempty patches/h during daylight, 0.35/h during crepuscular periods, and 0.1/h at night.

In Lake Washington, piscivores could encounter 5- to 10-cm prey fish in 9–30 m depths during daylight, with maximum encounter rates of 0.833 prey fish/h in 15–18 m (Fig. 8). Encounter rates declined at dusk, with peak encounter rates at 0–6 m (0.014–0.056 prey fish/h). Encounter rates

© 1999 NRC Canada

Fig. 8. Diel encounter rates predicted for piscivores foraging at depth in Lake Tahoe, Lake Washington, and Strawberry Reservoir. Daylight encounter rates extend to 0.833 prey/h at 15–18 m in Lake Washington.

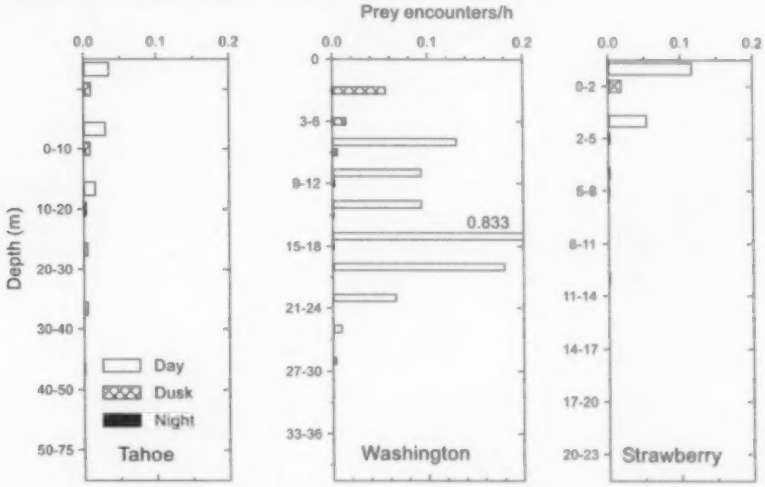

were negligible at night. When considering the horizontal patchiness of prey, piscivores would encounter 1.4 nonempty patches/h during daylight, 3.6/h during crepuscular periods, and 1.8/h at night.

In Strawberry Reservoir, piscivores could encounter 5- to 12-cm prey fish (juvenile cutthroat trout and kokanee) during daylight, with maximum encounter rates of 0.116 prey fish/h in 0–2 m, declining to 0.001 prey fish/h at 14 m (Fig. 8). Encounter rates declined at dusk, with peak encounter rates of 0.018 prey fish/h in 0–2 m, declining to 0.001 prey fish/h at 8 m. Encounter rates were negligible at night over all depths. When considering the horizontal patchiness of prey, piscivores would encounter 0.15 nonempty patches/h during daylight, 0.22/h during crepuscular periods, and 0.50/h at night.

Comparison of model predictions with independent estimates of piscivory

The model predicted that piscivores would encounter more than enough prey fish biomass to satisfy the growth rates and diet compositions observed in each of the systems. Despite the increasing density of prey fishes from Lake Tahoe to Lake Washington to Strawberry Reservoir, we predicted that piscivory should be low in Lake Tahoe and Strawberry Reservoir but higher in Lake Washington. These predictions agreed qualitatively with the estimated consumption of fish prey (grams prey fish per gram predator) by piscivores from these waters during the summer (Beauchamp 1990; Beauchamp et al. 1992; Thiede 1997; Baldwin 1998) (Fig. 9). The estimated daily consumption of fish prey represented 2% of the prey fish biomass encountered in Lake Tahoe, 24% in Lake Washington, and 2% in Strawberry Reservoir. Invertebrates supplemented the diets in all cases, representing 90% of the diet by weight for lake trout in Lake Tahoe, only 29% of the diet for rainbow and cutthroat trout in Lake Washington, and 95% of the diet for cutthroat trout in Strawberry Reservoir.

Sensitivity analysis

Since encounter rates are estimated by overlaying time- and depth-specific search volumes on corresponding ambient prey densities, the relative sensitivity of the model to each of the lake-specific inputs can be evaluated analytically. Encounter rates at any depth or time will vary as a 1:1 correspondence to changes in swimming speed or prey density (e.g., a 10% increase in either variable will result in a 10% increase in encounter rate). The model is much more sensitive to changes in RD, since search volume is proportional to RD^2. Moreover, RD varies as complex functions of light and turbidity. RD increases rapidly with increasing light to a threshold and then remains constant at all light levels above SIT (Henderson and Northcote 1985; Vogel and Beauchamp 1999). Sensitivity analysis indicated that search volume was more sensitive than RD to changes in light and turbidity, and both search volume and RD were more sensitive to changes in turbidity than to changes in light. A 10% reduction or increase in light level changed RD by –4.9 or 4.6%, respectively, and changed search volume by ±9.5%. Whether above or below SIT, a 10% reduction or increase in turbidity changed RD by 7.0% or –5.9%, respectively, and changed search volume by 14.5 or –11.5%, respectively. A ±10% variation in the constant 12.034 lx (77.9 μeinsteins·m^{-2}·s^{-1}) resulted in an equal ±10% variation in RD. A ±10% variation in the light dependence coefficient (0.4747) resulted in a –10 or 12% change in RD, whereas a ±10% change in the turbidity dependence coefficient (–0.624) resulted in changes in the opposite direction of ±4%. Results of the Monte Carlo simulations for the collective error propagation of eq. 8 resulted in an overall average CV of 17.2% across all light and turbidity levels with no trends in CV related to either factor. The results of the individual parameter perturbation and Monte Carlo simulations indicated that RD was moderately sensitive to parameter error and somewhat less sensitive to measurement errors for the input variables light and turbidity.

Discussion

The visual foraging model predicted that piscivory should

© 1999 NRC Canada

Fig. 9. Comparison of predicted daily biomass of prey fish encountered by piscivores, with estimates of biomass of prey consumed in Lake Tahoe (Thiede 1997), Lake Washington (Beauchamp 1994), and Strawberry Reservoir (Baldwin 1998). Prey biomasses were reported as percentages of predator body weight to adjust for differences in predator and prey sizes among the lakes.

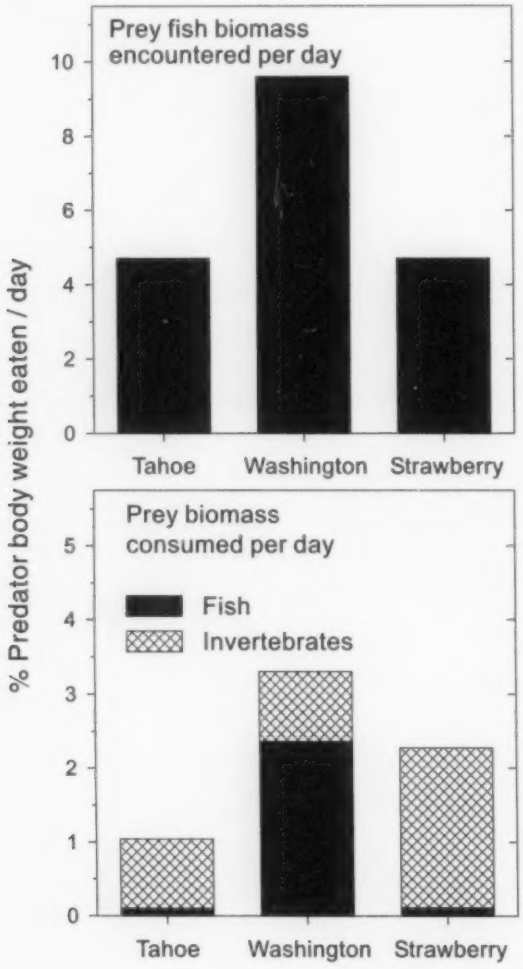

be low in Lake Tahoe and Strawberry Reservoir but much higher in Lake Washington, despite the increasing density of prey fishes from Lake Tahoe to Lake Washington to Strawberry Reservoir. The predicted encounter rates were sufficient to satisfy the observed growth rates of piscivores in all three systems, and our predictions qualitatively agreed with the biomass of prey fish observed in the diet of piscivores during the summer in all three lakes. Whether estimating encounter rates from average depth-specific prey densities or from the frequency of nonempty patches, the same pattern emerged: the opportunity and importance of piscivory were greatest in Lake Washington and considerably less in both Lake Tahoe and Strawberry Reservoir.

A general prediction of this model was that fish consumption should be highest for pelagic piscivores in waters of intermediate productivity. Encounter rates are determined by the product of search volume and prey density. When transparency is caused by organic rather than mineral turbidity, transparency will decline with increasing productivity, whereas prey fish production should increase. In low-productivity lakes, transparency and light penetration are high, search volumes are at or near maximum, but prey fish densities are low. Since RDs are asymptotic, search volumes do not increase in proportion to increased transparency once light exceeds SIT. Thus, prey encounters should be low because search volumes cannot increase enough to compensate for the low prey densities. Pelagic prey encounters should be maximized in lakes of intermediate productivity because search volumes remain near maximum, while prey densities increase. As lakes become more productive, prey densities do not increase fast enough to compensate for the rapid decline in search volume. This interaction between prey density and search volume could explain some of the shifts in fish communities along productivity gradients that were reported by Persson et al. (1991); they reported that the proportion of pelagic piscivores in the total fish biomass peaked in systems of intermediate productivity.

This approach provides a framework for examining ecological trade-offs confronting both predator and prey species. When temporally and spatially explicit encounter rates are combined with predator abundance and distribution data, the foraging opportunity (prey encounter rate in numbers or grams of prey per hour) and predation risk (number of encounters with predators per hour) associated with specific time and depth cells could be quantified. Predator abundance or distribution data are often lacking, in which case the model would only estimate the relative risk or foraging opportunity associated with each time and depth cell as hourly encounters per predator in each cell. Therefore, this model can be used to make predictions about diel vertical migration or horizontal distribution patterns of prey, based solely on predation risk, or it could be linked with data or predictions from other models (e.g., Stockwell and Johnson 1997) regarding the distribution or foraging opportunity of prey.

Earlier works on planktivorous fish distributions assumed that predation risk helped determine diel distribution patterns of prey (Eggers 1978; Wurtsbaugh and Li 1985; Clark and Levy 1988; Levy 1990, 1991; Appenzeller and Leggett 1995) but rarely provided data on the diet, distribution, or density of predators or a quantitative measure of predation risk as a function of time and space (but see Clark and Levy 1988). By linking a mechanistic foraging model with empirical data on diel distribution and density from hydroacoustic transects, the approach described here provides a framework for integrating the effects of biotic and abiotic factors into predictions of the trophic dynamics of a limnetic community under a variety of conditions. The foraging model could be integrated into spatially explicit models for fish growth (e.g., Brandt et al. 1992) to examine the implications of various spatial and temporal changes in foraging opportunities and predator distribution for its growth potential.

This work represents the first known development, application, and initial test of a visual foraging model for pelagic piscivores. Eggers (1977) and Aksnes and Giske (1993) presented theoretical models for visually feeding zooplank-

© 1999 NRC Canada

tivorous fish and more general visual foragers, respectively. These models required numerous parameters that would not be routinely available, and they primarily focused on zooplanktivore–zooplankton systems (Gerritsen and Strickler 1977; Confer et al. 1978; Hairston et al. 1983; Wright and O'Brien 1984). Breck (1993) described important differences between the visual systems required by fish feeding on zooplankton versus those feeding on larger, more mobile prey fishes, which occur at much lower densities than zooplankton (e.g., 0.000 001–10 fish/m^3 compared with 0.1–100 000 crustacean zooplankton/m^3). He warned against extrapolating from acuity-based zooplanktivore foraging models to piscivore systems because gross overestimates of RD would result. RDs required of piscivores are great enough that increased backscattering over these distances and the consequent declining contrast between the prey, and its background (Loew and McFarland 1990; Guthrie and Muntz 1993), cause RDs to asymptote much sooner than would be predicted from an acuity-based model. Our goal was to develop a piscivore model constructed from a much reduced set of parameters that subsumed many of the mechanisms modeled explicitly by the theoretically derived models of Eggers (1977) and Aksnes and Giske (1993). Furthermore, for the model to be readily applicable to new waters, lake-specific inputs (e.g., light extinction, turbidity, diel prey fish density distributions) needed to be acquired either with relative ease, economy, and timeliness or from reasonable values inferred from behavioral or physiological principles. Previous models of this sort have rarely been tested against field observations (but see Wright and O'Brien 1984).

By estimating temporally and spatially explicit search volumes, we can gain insight into the scale at which piscivores experience patchiness. For example, we estimated that a lake trout in Lake Tahoe could swim 1062 m/h and search 3863 m^3/h at midday but swim 846 m/h and search only 100–500 m^3/h at dusk. This has implications for how we measure prey density so that these estimates and their variability correspond to the foraging capabilities of predators. Hydroacoustics and ultrasonic telemetry will play important roles in this area. With current hydroacoustic technology, the spatial resolution of prey densities can be acquired at a precision of ≤ 1 m in the vertical dimension and by individual or fixed numbers of pings to achieve the desired precision in the lateral dimension (e.g., Nero and Magnuson 1989; Schael et al. 1995). Seasonal and diel movement and distribution patterns of piscivores can be obtained by ultrasonic telemetry to examine factors that influence how piscivores perceive and operate in their environment.

The estimates for search volume are based on several critical assumptions. The model assumes that RD represents the radius of a piscivore's visual field; however, prey might be detected at greater distances than RD measured in laboratory experiments. If prey detection distances DD exceed RD, then search volumes would be underestimated by the model, biased in proportion to $(RD^2 - DD^2)/DD^2$. Since the encounter rate predictions exceeded observed consumption rates, we assume that differences between DD and RD are probably less important than changes in capture success as a function of prey size (Juanes 1994; Christensen 1996; Mason et al. 1998), light (Petersen and Gadomski 1994), turbidity, or other factors. Diel swimming speed estimates were obtained from both laboratory and telemetry studies. Swimming speed is typically underestimated by telemetry studies due to the inability to record continuous fine-scale movements. Laboratory estimates might not represent natural swimming speeds due to influences imposed by the experimental arena. However, the reasonably close agreement between the laboratory and telemetry estimates enhanced our confidence in the values that we used in the model.

The predicted biomass of prey fish encountered exceeded the consumption rates required to satisfy the summer growth rates observed for predators in all three lakes. Encounter rates do not necessarily equate to consumption rates (Savitz and Bardygula 1989; Christensen 1996). Therefore, when translating encounter rates into predation rates, encounters will need to be discounted by varying probabilities of attack and capture success as a function of diel period, light intensity (Petersen and Gadomski 1994), size (Juanes 1994; Christensen 1996), or schooling/nonschooling status (Magurran and Pitcher 1987; Pitcher and Parrish 1993). Therefore, one of the next logical steps will be to develop capture success relationships, probably from experiments in large laboratory tanks or enclosures in lakes. Spatial and temporal changes in prey encounter rates form the basis for hypotheses regarding the expected distribution and movement patterns of predators and for whether predators could or should switch to alternative prey as prey availability or environmental conditions change. Moreover, deviations from predicted movement and distribution patterns could reveal additional factors that contribute significantly to the diet and distribution patterns of predators and prey (e.g., temperature, dissolved oxygen).

The performance of this model over a relatively broad range of trophic conditions should encourage refinement and application of this approach to more waters and to a wider range of species where interactions between cruising piscivores and prey fishes would be expected in limnetic regions. The current model represents an early version of work in progress. Considerable refinement is expected, and this will be driven by the types of questions posed and the accuracy and precision required by new objectives.

As more species-specific parameters are generated for this model, we can begin to evaluate interspecific differences in the abilities of predators to exploit different prey species under varying environmental conditions. Of particular interest will be the generality of the model parameters among taxa. Will a generic model suffice for all pelagic piscivores, or will we need to generate unique parameters for each order, family, genus, or species? Despite its development from laboratory experiments on largemouth bass, a predominantly littoral, sit-and-wait predator, the model performed reasonably well against data from laboratory trials with lake trout, except that prey size had no effect on RD by salmonid predators, and maximum RD was shorter for salmonid predators (Vogel and Beauchamp 1999).

As the demand to manipulate predator or prey populations increases, so does the need to predict the effects of these changes on the structure and function of existing aquatic communities. As environmental conditions in a watershed change, the trophic dynamics of the food web could change significantly due to shifts in productivity and transparency of

© 1999 NRC Canada

the lake or reservoir. A visual foraging model for top predators should improve our predictive capability by providing a tool for estimating the expected proportional contribution of fish prey to the diet, based on temporal changes in prey fish density distributions and the optical conditions of the water body.

Acknowledgments

Funding was provided by the Vice President for Research at Utah State University. The Utah Water Research Laboratory and Utah Cooperative Fisheries Research Unit provided facilities. We thank the University of California-Davis Tahoe Research Group for supplying unpublished data. Jeff Godfrey, Rick Orme, and Jason Van Tassell assisted with field sampling. Jason Stockwell, Peter Rand, and Doran Mason provided constructive and insightful reviews of this manuscript. We appreciate the invitation from Gary Thomas and Jay Kirsch to present these results at the Hydroacoustics Symposium at the 1997 American Fisheries Society meeting.

References

Aksnes, D.L., and Giske, J. 1993. A theoretical model of aquatic visual feeding. Ecol. Modell. **67**: 233–250.

Appenzeller, A.R., and Leggett, W.C. 1995. An evaluation of light-mediated vertical migration of fish based on hydroacoustic analysis of the diel vertical rainbow smelt (*Osmerus mordax*). Can. J. Fish. Aquat. Sci. **52**: 504–511.

Baldwin, C.M. 1998. Strawberry Reservoir food web interactions: a bioenergetic assessment of salmonid diet and predator–prey supply and demand. M.S. thesis, Utah State University, Logan, Utah.

Bartell, S.M., Breck, J.E., Gardner, R.H., and Brenkart, A.L. 1986. Individual parameter perturbation and error analysis of fish bioenergetics models. Can. J. Fish. Aquat. Sci. **43**: 160–168.

Beauchamp, D.A. 1990. The seasonal and diel food habits of rainbow trout stocked as juveniles in Lake Washington. Trans. Am. Fish. Soc. **119**: 475–482.

Beauchamp, D.A. 1994. Spatial and temporal dynamics of piscivory: implications for food web stability and the transparency of Lake Washington. Lake Reservoir Manage. **9**: 151–154.

Beauchamp, D.A., Vecht, S.A., and Thomas, G.L. 1992. Temporal, spatial, and size-related foraging of wild cutthroat trout in Lake Washington. Northwest Sci. **66**: 149–159.

Brandt, S.B. 1996. Acoustic assessment of fish abundance and distribution. *In* Fisheries techniqes. 2nd ed. *Edited by* B.R. Murphy and D.W. Willis. American Fisheries Society, Bethesda, Md. pp. 385–432.

Brandt, S.B., Mason, D.M., and Patrick, E.V. 1992. Spatially explicit models of fish growth rate. Fisheries (Bethesda), **17**: 23–31, 34–35.

Breck, J.E. 1993. Foraging theory and piscivorous fish: are forage fish just big zooplankton? Trans. Am. Fish. Soc. **122**: 902–911.

Carpenter, S.R., Kitchell, J.F., and Hodgson, J.R. 1985. Cascading trophic interactions and lake productivity. BioScience, **35**: 634–639.

Christensen, B. 1996. Predator foraging capabilities and prey antipredator behaviours: pre- versus postcapture constraints on size-dependent predator–prey interactions. Oikos, **76**: 368–380.

Clark, C.W., and Levy, D.A. 1988. Diel vertical migrations by juvenile sockeye salmon and the antipredation window. Am. Nat. **131**: 271–290.

Confer, J.L., Howick, G.L., Corzette, M.H., Framer, S.L., Fitzgibbon, F., and Landesberg, R. 1978. Visual predation by planktivores. Oikos, **31**: 27–37.

Eggers, D.M. 1977. The nature of prey selection by planktivorous fish. Ecology, **58**: 46–59.

Eggers, D.M. 1978. Limnetic feeding behavior of juvenile sockeye salmon in Lake Washington and predator avoidance. Limnol. Oceanogr. **23**: 1114–1125.

Gerritsen, J., and Strickler, J.R. 1977. Encounter probabilities and community structure in zooplankton: a mathematical model. J. Fish. Res. Board Can. **34**: 73–82.

Guthrie, D.M., and Muntz W.R.A. 1993. Role of vision in fish behavior. *In* Behaviour of teleost fishes. 2nd ed. *Edited by* T.J. Pitcher. Chapman and Hall, London, U.K. pp. 89–121.

Hairston, N.G., Li, K.T., and Easter, S.S. 1983. Fish vision and the detection of planktonic prey. Science (Washington, D.C.), **218**: 1240–1242.

Henderson, M.A., and Northcote, T.G. 1985. Visual prey detection and foraging in sympatric cutthroat trout (*Salmo clarki*) and Dolly Varden (*Salvelinus malma*). Can. J. Fish. Aquat. Sci. **42**: 785–790.

Hewett, S.J., and Johnson, B.L. 1992. Fish bioenergetics model 2: an update of a generalized bioenergetics model of fish growth for microcomputers. Tech. Rep. WIS-SG-92-250. University of Wisconsin Sea Grant Institute, Madison, Wis.

Howick, G.L., and O'Brien, W.J. 1983. Piscivorous feeding behavior of largemouth bass: an experimental analysis. Trans. Am. Fish. Soc. **112**: 508–516.

Janiczcek, P.M.J., and Young, A.J. 1987. Computer programs for sun and moon illuminance with contingent table and diagram. U.S. Nav. Observ. Circ. **171**: 1–32.

Juanes, F. 1994. What determines prey size selectivity in piscivorous fishes? *In* Theory and application in fish feeding ecology. *Edited by* D.J. Stouder, K.L. Fresh, and R.J. Feller. The Belle W. Baruch Library in Marine Science Number 18. pp. 79–100.

Lehman, J.T. 1988. Hypolimnetic metabolism in Lake Washington: relative effects of nutrient load and food web structure on lake productivity. Limnol. Oceanogr. **33**: 1334–1347.

Levy, D.A. 1990. Sensory mechanism and selective advantage for diel vertical migration behavior in juvenile sockeye salmon (*Oncorhynchus nerka*). Can. J. Fish. Aquat. Sci. **47**: 1796–1802.

Levy, D.A. 1991. Acoustic analysis of diel vertical migration behavior of *Mysis relicta* and kokanee (*Oncorhynchus nerka*) within Okanagan Lake, British Columbia. Can. J. Fish. Aquat. Sci. **48**: 67–72.

Loew, E.W., and McFarland, W.N. 1990. The underwater visual environment. *In* The visual system of fish. *Edited by* R.H. Douglas and M.B.A. Djamgoz. Chapman and Hall, London, U.K. pp. 1–44.

Luecke, C., and Wurtsbaugh, W.A. 1993. Effects of moonlight and daylight on hydroacoustic estimates of pelagic fish abundance. Trans. Am. Fish. Soc. **122**: 112–120.

Magurran, A.E., and Pitcher, T.J. 1987. Provenance, shoal size and the sociobiology of predator evasion behaviour in minnow shoals. Proc. R. Soc. Lond. Ser. B, Biol. Sci. **229**: 439–465.

Mason, D.M., and Patrick, E.V. 1993. A model for the time–space dependence of feeding for pelagic fish populations. Trans. Am. Fish. Soc. **122**: 884–901.

Mason, D.M., Johnson, T.B., and Kitchell, J.F. 1998. Consequences of prey fish community dynamics on lake trout (*Salvelinus namaycush*) foraging efficiency in Lake Superior. Can. J. Fish. Aquat. Sci. **55**: 1273–1284.

Miner, J.G., and Stein, R.A. 1996. Detection of predators and habitat choice by small bluegills: effect of turbidity and alternative prey. Trans. Am. Fish. Soc. **125**: 97–103.

Nero, R.W., and Magnuson, J.J. 1989. Characterization of patches along transects using high-resolution 70-kHz integrated acoustic data. Can. J. Fish. Aquat. Sci. **46**: 2056–2064.

© 1999 NRC Canada

Northcote, T.G. 1988. Fish in the structure and function of freshwater ecosystems: a "top down" view. Can. J. Fish. Aquat. Sci. **45**: 361–379.

Persson, L., Diehl, S., Johansson, L., Andersson, G., and Hamrin, S.F. 1991. Shifts in fish communities along a productivity gradient of temperate lakes — patterns and the importance of size-structured interactions. J. Fish Biol. **38**: 281–293.

Petersen, J.M., and Gadomski, D.M. 1994. Light-mediated predation by northern squawfish on juvenile chinook salmon. J. Fish Biol. **45**(Suppl. A): 227–242.

Pitcher, T.J., and Parrish, J.K. 1993. Functions of shoaling behaviour in teleosts. *In* Behaviour of teleost fishes. 2nd ed. *Edited by* T.J. Pitcher. Chapman and Hall, London, U.K. pp. 363–440.

Savitz, J., and Bardygula, L. 1989. Analysis of the behavioral basis for changes in salmon diets. Illinois–Indiana Sea Grant Rep. IL-IN-SG-R-89-3.

Schael, D.M., Rice, J.A., and Degan, D.J. 1995. Spatial and temporal distribution of threadfin shad in a southeastern reservoir. Trans. Am. Fish. Soc. **124**: 804–812.

Stockwell, J.D., and Johnson, B.M. 1997. Refinement and calibration of a bioenergetics-based foraging model for kokanee (*Oncorhynchus nerka*). Can. J. Fish. Aquat. Sci. **54**: 2659–2676.

Thiede, G.P. 1997. Impact of lake trout predation on prey populations in Lake Tahoe: a bioenergetics assessment. M.S. thesis, Utah State University, Logan, Utah.

Vogel, J.L., and Beauchamp, D.A. 1999. Effects of light, prey size, and turbidity on reaction distances of lake trout (*Salvelinus namaycush*) to salmonid prey. Can. J. Fish. Aquat. Sci. **56**: 1293–1297.

Warner, E.J., and Quinn, T.P. 1995. Horizontal and vertical movements of telemetered rainbow trout (*Oncorhynchus mykiss*) in Lake Washington. Can. J. Zool. **73**: 146–153.

Wright, D.I., and O'Brien, W.J. 1984. The development and field test of a tactical model of the planktivorous feeding of white crappie (*Pomoxis annularis*). Ecol. Monogr. **54**: 65–98.

Wurtsbaugh, W.A., and Li, H.W. 1985. Diel migrations of a zooplanktivorous fish (*Menidia beryllina*) in relation to the distribution of its prey in a large eutrophic lake. Limnol. Oceanogr. **30**: 565–576.

© 1999 NRC Canada

Field evaluation of a bioenergetics-based foraging model for kokanee (*Oncorhynchus nerka*)

Jason D. Stockwell and Brett M. Johnson

Abstract: We used a bioenergetics-based foraging model to determine if bioenergetic and foraging constraints could explain kokanee (*Oncorhynchus nerka*) diel vertical migration in Blue Mesa Reservoir, Colorado. We compared model predictions of daily growth and migration strategies with observed growth and diel vertical distributions on three dates during the summer. Results suggest that bioenergetic and foraging constraints were not sufficient to explain diel vertical migration early in the summer, when thermal stratification was weak. However, these constraints could explain observed patterns later in the summer, when optimal thermal habitat for kokanee was spatially segregated from food-rich surface waters. The onset of a strong thermocline, and its exclusion of piscivorous lake trout (*Salvelinus namaycush*) from surface waters, appeared to determine the relative importance of predation risk for kokanee diel vertical migration patterns. Our observations and modeling results suggest that the relative importance of various factors driving diel vertical migration changes seasonally. Furthermore, the relative importance of each factor likely varies from system to system and may have caused the variety of single-factor hypotheses proposed to explain kokanee diel vertical migration. The model provides a framework for studying diel vertical migration across systems of differing thermal regimes, productivity, and predation pressures.

Résumé : Nous avons utilisé un modèle bioénergétique de recherche de nourriture pour déterminer si les contraintes bioénergétiques et alimentaires pouvaient expliquer la migration verticale nycthémérale du kokani (*Oncorhynchus nerka*) dans le réservoir Blue Mesa, au Colorado. Nous avons comparé les prévisions du modèle concernant la croissance quotidienne et les stratégies de migration avec la croissance et les distributions verticales nycthémérales observées à trois dates durant l'été. Les résultats laissent entendre que les contraintes bioénergétiques et alimentaires n'étaient pas suffisantes pour expliquer la migration nycthémérale verticale au début de l'été, quand la stratification thermique était peu marquée. Cependant, ces contraintes pourraient expliquer les observations faites plus tard dans l'été, quand l'habitat thermique optimal du kokani était spatialement séparé des eaux de surface riches en aliments. L'apparition d'une thermocline marquée, qui a chassé les touladis (*Salvelinus namaycush*) piscivores des eaux de surface, semble avoir déterminé l'importance relative du risque de prédation que présentent pour le kokani ses migrations verticales nycthémérales. Nos observations et les résultats de la modélisation laissent penser que l'importance relative des divers facteurs qui déterminent la migration verticale nycthémérales change avec les saisons. De plus, l'importance relative de chaque facteur varie d'un système à l'autre, d'où peut-être les diverses hypothèses proposées faisant appel à un seul facteur pour expliquer la migration verticale nycthémérale du kokani. Notre modèle fournit un cadre pour l'étude de la migration verticale nycthémérale dans divers systèmes caractérisés par des régimes thermiques, une productivité et des pressions de prédation différents.

[Traduit par la Rédaction]

Introduction

Vertical spatial structure is an important feature of many lentic systems. Depth gradients in light, temperature, and food are generally sharper and more heterogeneous than horizontal gradients (Legendre and Demers 1984). Many organisms exhibit diel vertical migrations, presumably to take advantage of or cope with these vertical features. However, assuming that predators also respond to vertical structure, then such diel migrations also likely affect the migrators' encounter rates with their predators. The fittest organisms will be those that optimize energetic and mortality tradeoffs. Understanding the factors driving diel vertical migration and their relative importance is an important step for developing more realistic models of predator–prey interactions, as well as developing predictive models that can be used to forecast impacts of environmental perturbations that alter the spatial structure of ecosystems.

Kokanee (*Onchorynchus nerka*), and their anadromous form sockeye salmon, exhibit strong diel vertical migration (e.g., Finnell and Reed 1969; Narver 1970; Levy 1987). Several hypotheses have been proposed to explain this behavior, including maximization of food consumption (Janssen and

Received October 23, 1997. Accepted January 20, 1999. J14273

J.D. Stockwell[1] and B.M. Johnson. Department of Fishery and Wildlife Biology, Colorado State University, Fort Collins, CO 80523, U.S.A.

[1]Author to whom all correspondence should be sent at the following address: Massachusetts Division of Marine Fisheries, Annisquam River Marine Fisheries Station, 30 Emerson Avenue, Gloucester, MA 01930, U.S.A. e-mail: jason.stockwell@state.ma.us

© 1999 NRC Canada

Brandt 1980; Wurtsbaugh and Neverman 1988), minimization of energetic costs (Brett 1971), and minimization of predation risk (Eggers 1978; Clark and Levy 1988). There appears to be no general consensus on which of these factors is most important for kokanee and sockeye. For example, Johnston (1990) rejected the bioenergetic efficiency hypothesis (Brett 1971, 1983) through field experiments, while Bevelhimer and Adams (1993) established the theoretical validity of the same hypothesis using a model and field observations. Levy (1990) suggested diel vertical migration in kokanee and sockeye might reflect an optimization of tradeoffs among energy intake, physiological costs, and predation risk.

It is probable that the relative importance of each factor varies from system to system. For example, in the Pacific northwest, thermal stratification may not be as pronounced, and therefore less important, than at lower latitudes. Consequently, bioenergetic arguments may not be as important as predation in the northwest. Additionally, predation risk may vary greatly from system to system both within and among age-classes.

The model of Bevelhimer and Adams (1993) is one approach that can be used to evaluate the relative importance of bioenergetic constraints. Their model is based on an energy budget and a functional response, and therefore can directly evaluate the interplay between energy intake and physiological costs in relation to diel vertical migration (i.e., the growth maximization hypothesis; Bevelhimer and Adams 1993). If kokanee behave optimally with regard to thermal and resource gradients, then we would expect model predictions to be similar to field observations. If predictions deviate from observations, then other factors such as predation are probably more important than energetic constraints and deserve further evaluation. An attraction of the modeling approach is that it could be readily applied to a range of systems exhibiting different thermal, resource, and predation conditions. Thus the model provides a framework for evaluating how kokanee respond to different spatial configurations of their environment.

In this study, we use the bioenergetics-based foraging model of Stockwell and Johnson (1997) to predict daily growth and vertical distribution of kokanee in Blue Mesa Reservoir, Colorado, in June, July, and August 1997. The model is a modified version of the one developed by Bevelhimer and Adams (1993). It operates on a 30-min time step and uses inputs of temperature and prey density profiles, and fish mass, to evaluate kokanee growth as a function of migration strategies, feeding durations, and prey handling times. We used diel survey data to evaluate model predictions and examine whether bioenergetic arguments are sufficient to explain kokanee growth and migration behavior in Blue Mesa Reservoir.

Methods

Model inputs

Field data on temperature, zooplankton densities, and fish size were collected from Blue Mesa Reservoir for input to the model. All sampling occurred in early June, July, and August 1997 during the new moon. Blue Mesa Resevoir is a 3700-ha mesotrophic reservoir located near Gunnison, Colorado. It is characterized by high abundances of large (≥1.0 mm) *Daphnia* and some of the highest kokanee growth rates in North America (Stockwell and Johnson 1997). Blue Mesa Resevoir supports a fish assemblage of kokanee, rainbow trout (*Oncorhynchus mykiss*), lake trout (*Salvelinus namaycush*), brown trout (*Salmo trutta*), cutthroat trout (*Oncorhynchus clarki*), white sucker (*Catostomus commersoni*), and longnose sucker (*Catostomus catostomus*). Kokanee is the dominant pelagic fish species, comprising an average of 83% of all fish caught in experimental vertical gill nets from 1994 to 1996 (Johnson et al. 1995, 1996, 1997).

We used a YSI model 58 digital meter to measure temperature and dissolved oxygen during midmorning from a reference station in Blue Mesa Reservoir on 31 May, 8 July, and 4 August 1997. Measurements were taken at 1-m intervals from 0 to 20 m and at 5-m intervals from 20 to 55 m. Temperature data were then averaged into seven depth strata (0–5, 5–10, 10–15, 15–20, 20–25, 25–30, and 30–50 m) for model input. Dissolved oxygen always exceeded 3.2 $mg \cdot L^{-1}$ down to 60 m.

To determine prey densities to input to the model, we collected zooplankton samples at the same time as temperature measurements. We used a Wildco model 37-315 Clarke–Bumpus sampler with a 13-cm-diameter opening and a 500-μm-mesh net to collect samples from each of the 0–5, 5–10, and 10–15 m depth strata. In Blue Mesa Reservoir, *Daphnia* >1.0 mm (the dominant prey item found in kokanee stomachs) are found primarily in the upper 10 m of the water column (Stockwell and Johnson 1997) and do not perform diel vertical migration (Johnson et al. 1995). Samples were preserved in 4% sugared, buffered formalin. Samples were enumerated and identified as *Daphnia* or copepods (the only two taxonomic groups sampled) under a compound microscope. Lengths of 50 *Daphnia* in each sample were measured to the nearest 0.01 mm using an ocular micrometer. Densities of *Daphnia* ≥1.0 mm in each of the three depth strata were input to model simulations (Stockwell and Johnson 1997).

Kokanee were collected with vertical gill nets (mesh size range 1.25–5.1 cm) during each sampling trip. We measured length and mass and extracted otoliths (a subset of kokanee on each date) and stomachs (July and August). Ages were determined from otoliths and validated by length–frequency analysis. Kokanee growth for each age-class was estimated by assuming exponential growth (mean mass) between sampling dates (Stockwell and Johnson 1997).

Model digestion function

The original digestion function used in the model is based on the evacuation rate of dry pellets by sockeye (Brett and Higgs 1970). We extracted kokanee stomachs in July and August to evaluate the validity of this digestion function for use with natural prey (e.g., Ruohonen et al. 1997).

Extracted stomachs were immediately placed on dry ice and were kept frozen until contents were removed from the frozen stomachs (Brett and Higgs 1970). Stomach contents were then weighed to the nearest 0.0001 g using an analytical balance. For each age-class/month, we plotted mean stomach content mass against time of day. Time of day included dusk to dawn because kokanee were only vulnerable to our sampling gear during this time. Using thermal profiles and observed nighttime distributions of kokanee (based on sonar) to estimate digestion temperature, we found that the original digestion function consistently underestimated the observed stomach evacuation rate. This discrepancy has also been noted for evacuation rates of rainbow trout fed both dry pellets and natural prey (Ruohonen et al. 1997). We therefore modified the temperature-dependent function for the gastric evacuation rate (r, per hour) from Brett and Higgs (1970):

$$(1) \qquad r = 0.0140T - 0.0154$$

© 1999 NRC Canada

Table 1. Modifications to the kokanee model from Stockwell and Johnson (1997) (see text for justification of changes).

Parameter	Value	Source
h, handling time (s·*Daphnia*$^{-1}$)	1.2–0.16	Hyatt 1980; Janssen 1976
L_d, *Daphnia* length (mm)	1.84	Stockwell et al. 1999
m, *Daphnia* mass (wet mg)	$0.5(0.052L_d^{3.012})$ in July and August	Stockwell et al. 1999
r, digestion coefficient	$0.0140T + 0.1135$	This study
E_{dap}, (kJ·wet g *Daphnia*$^{-1}$)	2.42	Snow 1972; Stockwell et al. 1999

where T is temperature (degrees Celsius). We assumed that the slope of the relationship remained constant but the intercept increased. We iteratively increased the intercept until we minimized the total sums of squares for observed and expected mean stomach content mass through time, for all age-class/month combinations, using the digestion function of Elliot and Persson (1978):

$$(2) \qquad D = (M_0 - Cm/r)(1 - e^{-rt}) + Cmt$$

where D is the amount of food digested in t hours, M_0 is the initial stomach content mass (wet grams), C is the number of prey consumed in t hours, and m is the mean mass of an individual prey item (wet grams). We then incorporated the new temperature-dependent gastric evacuation rate into the digestion function for model simulations.

For this analysis, we excluded one stomach from each age-class during the time period of 04:45–08:00 in July. These stomachs had much greater amounts of food (1.62 g for age 1, 2.90 g for age 2, 3.03 g for age 3) compared with other stomachs collected at this time (mean of 0.00 g for age 1 (n = 3), mean of 0.48 g for age 2 (n = 5), mean of 0.10 g for age 3 (n = 4)). We assumed that these fish were caught late in the sampling period and had begun to feed after dawn but prior to capture.

Single versus multiple migrations

Observations from creel surveys from 1993 to 1996 indicated that kokanee had relatively full stomachs during late morning (B.M. Johnson, personal observation). Stomach samples from fish caught in gill nets in 1997 also indicated relatively full stomachs at dusk. Furthermore, gut evacuation data showed that kokanee must empty their stomachs between late morning and early evening. This suggests that kokanee had at least two foraging bouts (migrations) per day. We therefore allowed model kokanee to migrate twice per day in all simulations.

Daphnia energy content

Kokanee from Blue Mesa Reservoir reduced the water content of their daphnid prey by 50%, compared with ambient prey, in July and August 1997 (Stockwell et al. 1999). We therefore reduced the mass of each individual *Daphnia* consumed by a factor of 0.5 on these simulation days (Table 1). This effectively allowed kokanee to pack twice as many prey into the same stomach volume if feeding duration and handling time were not limiting. However, percent dry matter of stomach contents was similar in June (when *Daphnia* egg production was high), July, and August (mean 10.8%, range 10.0–11.8%; Stockwell et al. 1999). Using a mean dry mass energy density of 22.4 kJ·g^{-1} (based on 1.6- to 2.0-mm *Daphnia pulicaria* from May to August, West Blue Lake, Manitoba; Snow 1972), we converted mass of *Daphnia* consumed to energy using a wet mass energy density of 2.42 kJ·g^{-1} (22.4 kJ·g^{-1} multiplied by 10.8%) on all simulation days (Table 1).

Model simulations

Simulations were run according to Stockwell and Johnson (1997), incorporating the modifications outlined above (Table 1). Briefly, model fish were allowed to locate at two depths (a feeding depth and a nonfeeding depth) during each 24-h simulation. Depths were midpoints of the seven strata identified above (2.5, 7.5, 12.5, 17.5, 22.5, 27.5, and 40 m). All possible combinations of migration strategies were evaluated (e.g., fixed at 2.5 m, 2.5–7.5 m, 2.5–12.5 m, etc.). However, we did restrict feeding depths to the top three strata (2.5, 7.5, and 12.5 m) because kokanee diet in Blue Mesa Reservoir consists almost entirely of large *Daphnia* (e.g., mean size of 1.84 mm in 1997; Stockwell et al. 1999), and most *Daphnia* ≥ 1.0 mm in length are found in the 0–10 m stratum (Stockwell and Johnson 1997). Simulations were referenced to day length on each simulation day. Model kokanee remained at nonfeeding depth during the night, feeding depth for half of the feeding duration during dawn and early morning, nonfeeding depth for the middle portion of the day (24 h minus night length minus feeding duration), and then feeding depth for the remainder of the feeding duration (late afternoon and dusk). The start of dawn and end of dusk were based on local times for the beginning and ending of nautical twilight (when the sun is 12° below the horizon). We used a range of prey handling times (1.2, 0.67, 0.33, and 0.16 s·Daph*nia*$^{-1}$) and feeding durations (4–12 h) for each simulation to bound the range of plausible values. The highest handling time was based on particulate-feeding age-0 kokanee (Hyatt 1980), and the lowest value was based on an intermediate value estimated from gulp- and filter-feeding alewife (*Alosa pseudoharengus*) (Janssen 1976) (Table 1).

Model evaluation

We monitored kokanee vertical distribution over the diel cycle during each of the three sampling trips using vertical gill nets and sonar. Vertical gill nets were set and lifted as follows: 1–2 June during 11:30–19:00, 19:00–00:00, 00:00–08:00, and 08:00–13:00; 8–9 July during 19:30–22:30, 22:30–02:00, 02:00–04:45, and 04:45–08:00; and 4–5 August during 18:45–19:30, 21:30–01:00, 01:00–04:30, and 04:30–08:15. Nets were set at the same reference station used for temperature measurements and zooplankton sampling. In addition to information taken from fish outlined above, we also recorded depth of capture.

Vertical distribution of fish was monitored acoustically using an HTI model 240 split-beam 200-kHz echo sounder. During each diel survey, we repeatedly traversed a 3.2-km transect for 3–4 h at sunrise (~03:30–07:00) and sunset (~19:00–22:00), 1 h during midday (~11:00–12:00), 1 h during the middle of the night in June (01:00–02:00), and 1 h during midmorning in July and August (~09:00–10:00). Sonar data were processed using HTI software. Fish densities were calculated by echocounting. Volume sampled was determined by cone area and distance traveled. Analyses were limited to those parts of the transect ≥ 60 m (June) or ≥ 70 m depth (July and August), typically from 1.5 to 2.8 km of the original transect. Due to weather and technical difficulties, we were not able to obtain a complete diel cycle of sonar data on any of the sampling dates.

Using Love's (1971) equation, we converted length–frequency distributions (millimetres) of all fish caught in the vertical gill nets to target strength (decibels) for each of the three sampling trips. We then used these distributions to parse target strengths from sonar into age-1 or ages-2 and -3 size-classes. Vertical distributions of each age-class from sonar were used to infer feeding (within 0–15 m depth) and nonfeeding depths.

© 1999 NRC Canada

We compared sonar observations with model predictions of depth distributions. Because several migration strategies in model simulations often resulted in model daily growth estimates close to the optimum growth estimate, we report the range in feeding and nonfeeding depths that produced model growth rates within 10% of optimum. We also compared observed daily growth with optimum model daily growth.

Results

Model inputs

On 31 May, water temperature decreased gradually from 12°C near the surface to <5°C at depth (Fig. 1). Surface waters warmed to >16 and >19°C in July and August, with the thermocline beginning at about 10 and 5 m depths, respectively (Fig. 1). Abundances of large *Daphnia* in the top 15 m of Blue Mesa Reservoir were uniformly low (~1·L^{-1}) early in the season (Fig. 1). In July and August, abundances peaked in the 0–5 m stratum (~13 and 8·L^{-1}, respectively) and decreased sharply in the 10–15 m stratum (2 and <1·L^{-1}, respectively) (Fig. 1).

Mean masses of kokanee on the three sampling dates (1 June, 8–9 July, and 4–5 August) were as follows: age 1, 58.4, 90.9, and 115.8 g; age 2, 241.8, 315.7, and 330.1 g; age 3, 525.5, 608.4, and 698.9 g (Fig. 2). Assuming exponential growth between sampling dates (Stockwell and Johnson 1997), daily growth rates of each age-class for each sampling date were as follows: age 1, 0.68, 1.06, and 1.03 g·day^{-1}; age 2, 1.77, 2.22, and 0.48 g·day^{-1}; age 3, 2.03, 2.35, and 3.63 g·day^{-1}.

Model digestion function

The mean mass of kokanee stomach contents decreased through the night to near empty by early morning in July (Fig. 3) and August (Fig. 4), indicating that age-1 to age-3 kokanee do not feed during the night. Northcote and Lorz (1966) and Finnell and Reed (1969) found similar results for kokanee populations in British Columbia and Colorado, respectively. We found that the digestion function of Elliot and Persson (1978) (eq. 2) underestimated the amount of food digested, when using the gastric evacuation rate based on dry pellets (Brett and Higgs 1970) (eq. 1; Figs. 3 and 4). We found that the relationship

$$(3) \qquad r = 0.0140T + 0.1135$$

minimized the total sums of squares for observed and expected mean stomach content mass through time (eq. 2; Figs. 3 and 4). Consequently, we used eq. 3 for all simulations (Table 1).

We do not advocate the use of eq. 3 as a generalized relationship suitable for other studies because of the very limited range in our inferred digestion temperatures (9.8–11.4°C, based on thermal profiles and sonar observations) (Fig. 1) and lack of control associated with field observations. More work is needed to establish a general relationship between temperature and kokanee digestion of natural prey, especially when these data are used to establish maximum daily consumption (C_{max}) values in bioenergetics models (e.g., Beauchamp et al. 1989).

Model predictions and field observations

For all three simulation dates, model daily growth bounded or approached the observed growth for each age-class (Figs. 5–7). In June, a wide range of prey handling times and feeding durations could account for the observed growth. Model daily growth for an age-1 kokanee with 4 h of feeding and a prey handling time of 1.2 s·*Daphnia*$^{-1}$ was 0.66 g·day^{-1}, compared with observed growth of 0.68 g·day^{-1}. All other model growth estimates were ≥1.27 g·day^{-1} (Fig. 5A). Model growth estimates for age-2 fish with prey handling times between 0.16 and 0.33 s·*Daphnia*$^{-1}$ for 4 h of feeding, 0.67 s·*Daphnia*$^{-1}$ for 8 h, and 1.2 s·*Daphnia*$^{-1}$ for 12 h approached the observed growth of 1.77 g·day^{-1} (Fig. 5B). Observed growth for age-3 kokanee in June was 2.03 g·day^{-1} and was approximated by model predictions using prey handling times of 0.16 s·*Daphnia*$^{-1}$ for 4 h of feeding, between 0.33 and 0.67 s·*Daphnia*$^{-1}$ for 8 h, and 0.67 s·*Daphnia*$^{-1}$ for 12 h (Fig. 5C).

In July simulations, model growth estimates from a combination of prey handling times and feeding durations were close to the observed growth for age-1 and -2 fish (Figs. 6A and 6B). Model growth for age-1 kokanee approached their observed growth of 1.06 g·day^{-1} using 0.33, 0.67, or 1.2 s·*Daphnia*$^{-1}$ for 4, 8, or 12 h of feeding, respectively (Fig. 6A). Model predictions for age-2 fish approached their observed growth when allowed to feed at 0.16 s·*Daphnia*$^{-1}$ for 4 h, between 0.16 and 0.33 s·*Daphnia*$^{-1}$ for 8 h, or slightly greater than 0.33 s·*Daphnia*$^{-1}$ for 12 h (Fig. 6B). For age-3 kokanee, model simulations indicate that they can approach their observed growth with a prey handling time slightly greater than 0.16 s·*Daphnia*$^{-1}$ for 8 h of feeding or between 0.16 and 0.33 s·*Daphnia*$^{-1}$ for 12 h (Fig. 6C).

In August, model age-1 kokanee approached their observed growth using prey handling times of 0.33, 0.67, or between 0.67 and 1.2 s·*Daphnia*$^{-1}$ while feeding for 4, 8, or 12 h, respectively (Fig. 7A). Age-2 kokanee required between 0.16 and 0.33 s·*Daphnia*$^{-1}$ with 4 h of feeding and between 0.33 and 0.67 s·*Daphnia*$^{-1}$ with 8 or 12 h, respectively (Fig. 7B). Age-3 kokanee had to feed for 12 h with a prey handling time of 0.16 s·*Daphnia*$^{-1}$ to reach their observed growth of 3.63 g·day^{-1} (Fig. 7C).

There was a wide range of patterns in kokanee vertical distribution over the course of the field season (Fig. 1). In June, age-1 fish were primarily concentrated between 15 and 25 m depth during daylight hours, although they were also present between the 5–15 and 25–45 m depth strata (Fig. 1). Ages-2 and -3 kokanee showed a bimodal distribution at this time, with peaks in the 0–5 and 15–25 m depth strata (Fig. 1). Kokanee from all three age-classes appeared to ascend at dusk, forming a thick layer between 5 and 10 m during the night (Fig. 1).

The same general pattern occurred in July (Fig. 1). During darkness, kokanee were concentrated between 10 and 20 m depth. At dawn, kokanee were somewhat more dispersed but primarily located between 5 and 20 m depth (Fig. 1). During morning and midday, age-1 fish were concentrated between the 5–10 and 15–25 m depth strata, while ages-2 and -3 fish were scattered throughout the water column (Fig. 1).

In August, the migration patterns reversed (Fig. 1). Mid-morning distributions were located between 5 and 15 m for all ages. At dusk, kokanee occupied a much broader and

© 1999 NRC Canada

Fig. 1. Vertical profiles (first column of panels) of prey densities (circles) and temperature (solid lines) from Blue Mesa Reservoir in June (top panel), July (middle panel), and August (bottom panel) used in model simulations, and vertical distributions (second, third, and fourth columns of panels) of age-1 and ages-2 and -3 kokanee in Blue Mesa Reservoir as observed using sonar on 1 June (top panels), 8–9 July (middle panels), and 4–5 August 1997 (bottom panels).

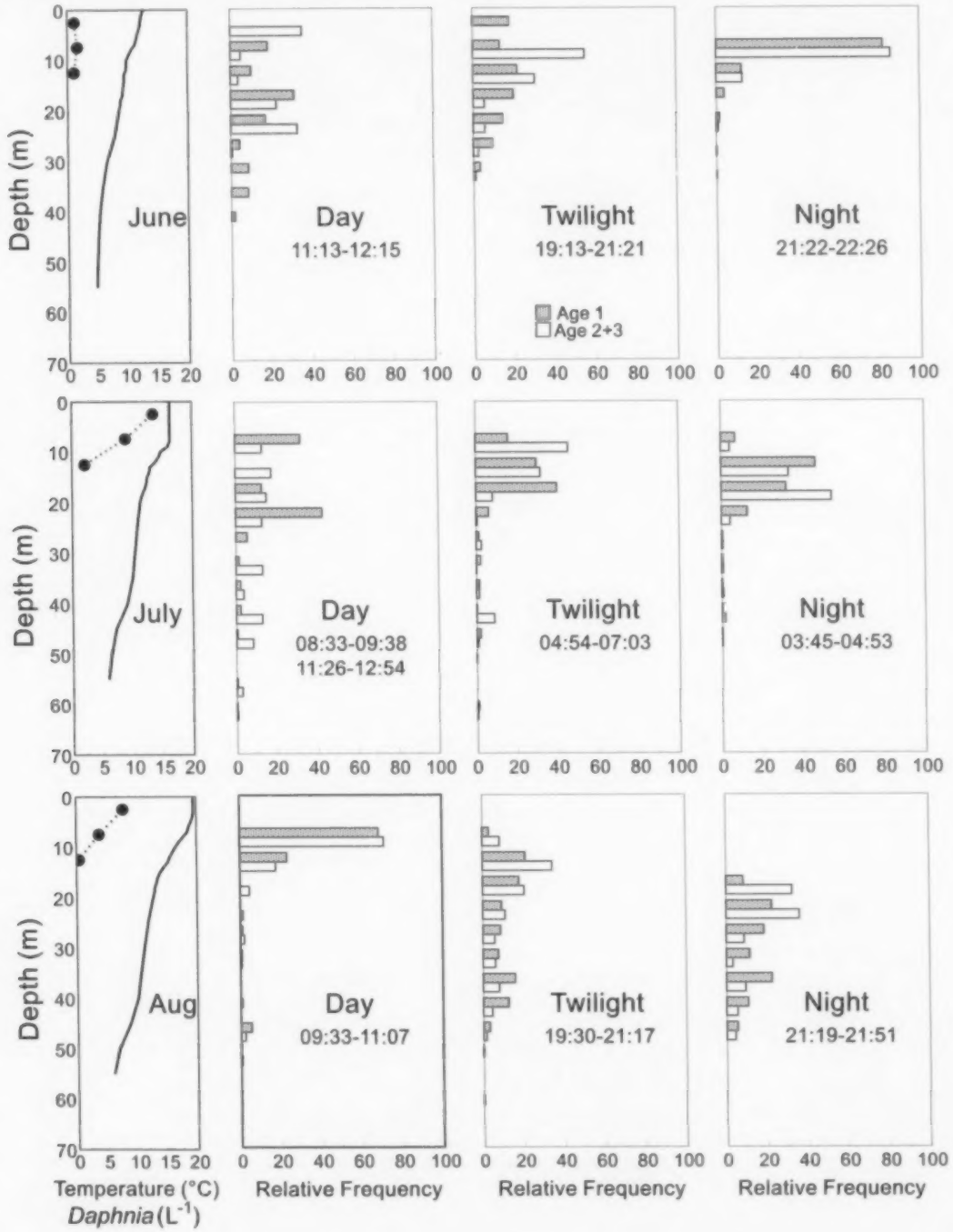

© 1999 NRC Canada

Fig. 2. Mean mass (±95% confidence intervals) of (A) age-1, (B) age-2, and (C) age-3 kokanee from Blue Mesa Reservoir during 1997. Sample sizes are indicated in parentheses. Note the different scales of the *y*-axes.

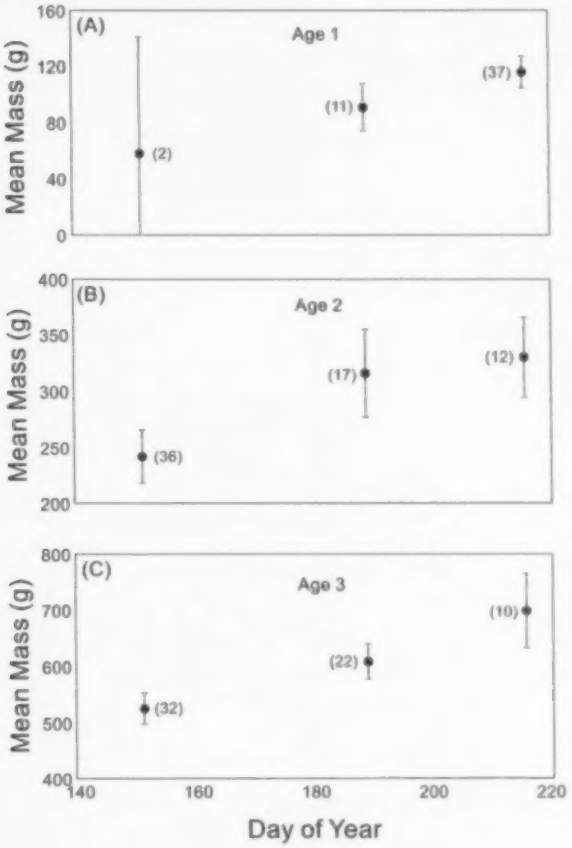

Fig. 3. Mean mass (±95% confidence intervals) of observed stomach contents (solid circles) through the night for (A) age-1, (B) age-2, and (C) age-3 kokanee from Blue Mesa Reservoir on 8–9 July 1997. The broken line indicates simulated digestion (eq. 2) based on the gastric evacuation rate of Brett and Higgs (1970) (eq. 1) and used in the original application of the kokanee model (Bevelhimer and Adams 1993; Stockwell and Johnson 1997). The solid line indicates simulated digestion based on the modified function for gastric evacuation rate (eq. 3). Sample sizes are indicated in parentheses. Temperatures used in simulations were 11.2°C for age-1 kokanee and 9.8°C for ages-2 and -3 kokanee and were based on thermal profiles and observed nighttime distributions of kokanee using sonar (Fig. 1).

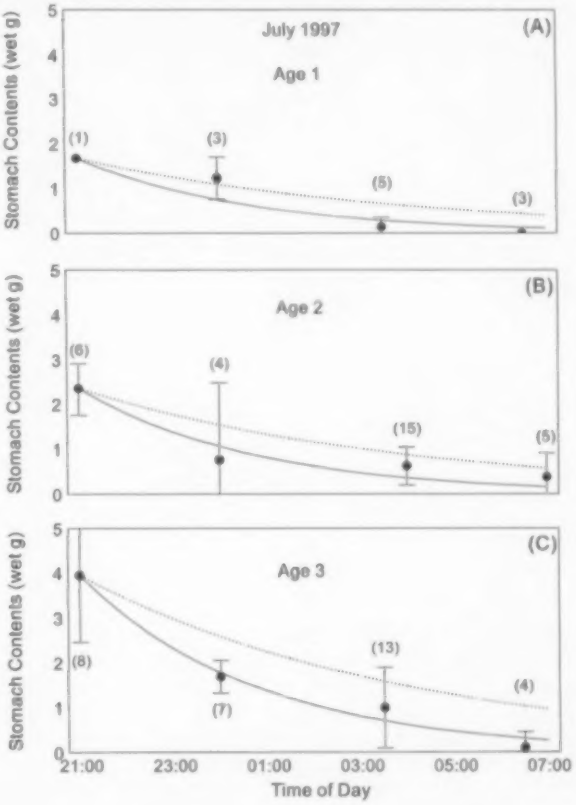

deeper range of depths (Fig. 1). At dark, vertical distributions were concentrated between 15 and 50 m for age-1 fish and primarily between 15 and 30 m for ages-2 and -3 fish (Fig. 1).

Comparisons between model predictions and observed vertical distributions show qualitative agreement, although discrepancies do exist. In June, the migration strategy for the only matching model growth estimate (at 1.2 s·*Daphnia*$^{-1}$ and 4 h) for age-1 fish was to migrate from 0–15 m (feeding) to 15–50 m (nonfeeding) (Fig. 5A). This agrees with inferred feeding and nonfeeding depths during daylight and dusk but does not overlap with the nighttime distribution of 5–10 m (Figs. 1 and 5A). Similar results were found for ages-2 and -3 fish (Figs. 1, 5B, and 5C).

Predicted and observed migration strategies overlap for age-1 kokanee in July for those feeding durations and handling times that generate model growth similar to observed growth (Fig. 6A). July comparisons are slightly different for ages-2 and -3 kokanee. For age-2 fish, model predictions of nonfeeding depths differed from observed nighttime distributions for two of the three matching growth estimates (4 and 8 h of feeding) (Fig. 6B). The predicted range for nonfeeding depths for an age-2 kokanee feeding for 12 h (0.33 s·*Daphnia*$^{-1}$) overlaps observed nonfeeding depths (Fig. 6B). Nonfeeding depths for age-3 fish overlap the observed depths for daytime distributions but were also too deep for nighttime distributions (Fig. 6C).

The predicted vertical distributions in August were similar to the observed ones for all age-classes (Fig. 7), although we did not observe a midday descent (Fig. 1) because of incomplete sonar sampling.

Discussion

Our diel observations show several interesting patterns in kokanee diel vertical migration behavior. First, it appears that in June and July, during the day, kokanee are distributed

© 1999 NRC Canada

Fig. 4. Same as Fig. 3 but for 4–5 August 1997. Temperatures used in simulations were 10.3°C for age-1 kokanee and 11.4°C for ages-2 and -3 kokanee and were based on thermal profiles and observed nighttime distributions of kokanee using sonar (Fig. 1).

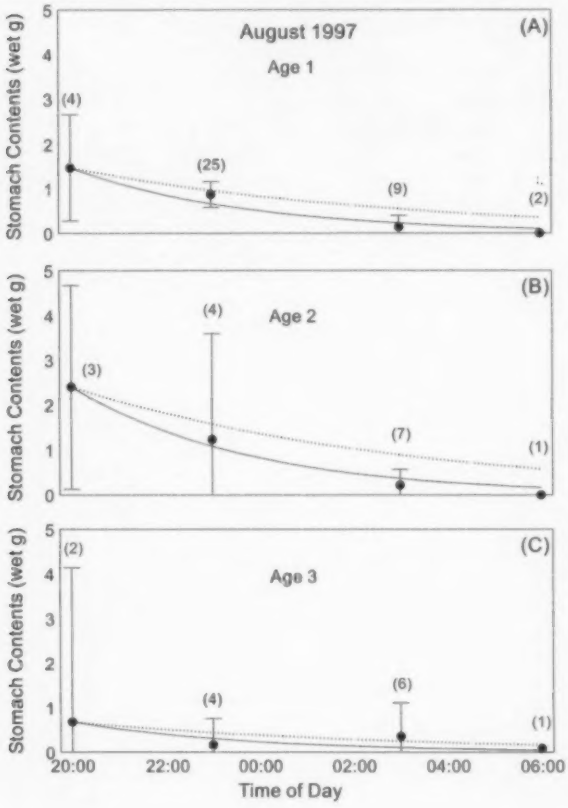

either bimodally or uniformly throughout the water column, indicating asynchronous migration behavior at this time. A portion of the population is near the surface, presumably feeding, while the remainder of the population is deeper where metabolic costs and (or) predation risk are lower. During crepuscular periods most of the population moves shallower; the kokanee form a relatively concentrated layer near surface waters at night. This same pattern was observed in Blue Mesa Reservoir during June and July 1995 using vertical gill nets and a Lowrance X-16 fish finder (Johnson et al. 1996), indicating that this "normal" diel cycle (sensu Levy 1990) may be consistent from year to year during these months. In August 1997, this pattern was reversed. Kokanee appeared highly concentrated in the 5–15 m depth stratum during daylight, and dispersed and descended during dusk and into the night. These results suggest a seasonal ontogeny in diel vertical migration behavior of kokanee.

The ranges in August feeding and nonfeeding depths predicted by the model overlap the observed distributions, indicating that the growth maximization hypothesis is sufficient to explain kokanee diel vertical migration at this time. The spatial segregation of maximum food densities and optimal thermal habitat in Blue Mesa Reservoir is greatest in August, environmental conditions under which diel vertical migration confers the greatest bioenergetic advantage (Bevelhimer and Adams 1993). For example, an age-1 kokanee would experience a 79% decrease in daily growth (from 0.84 to 0.18 g·day^{-1}) if it did not migrate out of the 5–10 m depth stratum into colder water (based on simulations with 8 h of feeding and a prey handling time of 0.67 s·*Daphnia*$^{-1}$). However, although daytime and twilight vertical distributions in June and July were predicted by the model for those model growth estimates that *matched* observed growth, nighttime vertical distributions were not (all age-classes in June, age 3 in July). Thus, the growth maximization hypothesis is not sufficient to explain kokanee diel vertical migration earlier in the summer.

We examined the hypothesis that kokanee may thermoregulate for digestion rate (Wurtsbaugh and Neverman 1988) in June (i.e., they may choose different day and night nonfeeding temperatures to regulate digestion rate to ensure an empty gut by the time of next feeding). Several simulations using the observed vertical distributions from this time period (7.5 m for feeding and nighttime nonfeeding depths and 22.5 m for daytime nonfeeding depths), and model feeding durations and prey handling times that closely matched observed growth (age 1, 4 h and 1.2 s·*Daphnia*$^{-1}$; age 2, 4 h and 0.33 s·*Daphnia*$^{-1}$; age 3, 8 h and 0.33 s·*Daphnia*$^{-1}$), showed decreases of 12, 15, and 14% from maximum growth for each age-class, respectively. Therefore, thermoregulation of digestion rate does not appear to confer a substantial advantage over constant nonfeeding depths. It also demonstrates that a wide range of diel vertical migration strategies can generate model growth estimates within 15% of maximum growth when strong environmental gradients are not present, suggesting that kokanee behavior in June is not constrained by temperature.

Predation risk is another factor that might explain the observed depth distributions of kokanee early in the summer. In Blue Mesa Reservoir, lake trout is the primary predator. Because of relatively low water temperatures in June and July, these predators have access to the entire water column (e.g., 80% of all piscivorous lake trout sized targets from June and July sonar surveys were at <10 m depth; B.M. Johnson, unpublished data). We therefore might expect kokanee to disperse to deeper depths during the day, when not feeding, to avoid predators under decreased light levels. At night, kokanee could concentrate near surface waters with lower risk of predation. Although predation risk explains these diel vertical migration patterns, it also assumes that kokanee would prefer to locate exclusively in the 5–10 m stratum (>80% of all kokanee were located in this stratum at night in June) when not feeding but are restricted from this depth stratum during the day because of predation risk. Our modeling suggests that there is no energetic advantage to this observed nighttime distribution. Based on the above simulations to evaluate thermoregulation of digestion rate, there also appears to be relatively little disadvantage to this behavior. Remaining in surface waters through the night may minimize migration costs while allowing kokanee to be in close spatial proximity to prey to take advantage of the antipredation window at dusk and dawn (Clark and Levy 1988).

In July, model predictions for growth and corresponding depth distributions for age-1 kokanee match observations,

© 1999 NRC Canada

Fig. 5. Maximum model daily growth and observed growth for (A) age-1, (B) age-2, and (C) age-3 kokanee in Blue Mesa Reservoir. Model growth was estimated using vertical profiles of prey densities and temperature from 31 May 1997, prey handling times ranging from 0.16 to 1.2 s·*Daphnia*$^{-1}$, and feeding durations of 4–12 h. Starting mass of each age-class for model simulations, as determined from field observations, was 58.4 g for age-1 kokanee, 241.8 g for age-2 kokanee, and 525.5 g for age-3 kokanee. The horizontal broken line represents the observed growth and facilitates comparisons with model results. Vertical bars indicate the ranges in feeding (solid) and nonfeeding (broken) migration depths producing model growth rates within 10% of maximum and inferred from sonar observations. The observed upper nonfeeding depth ranges indicate the nighttime vertical distributions of kokanee, while the bottom ranges indicate daytime and twilight nonfeeding depths (see Fig. 1).

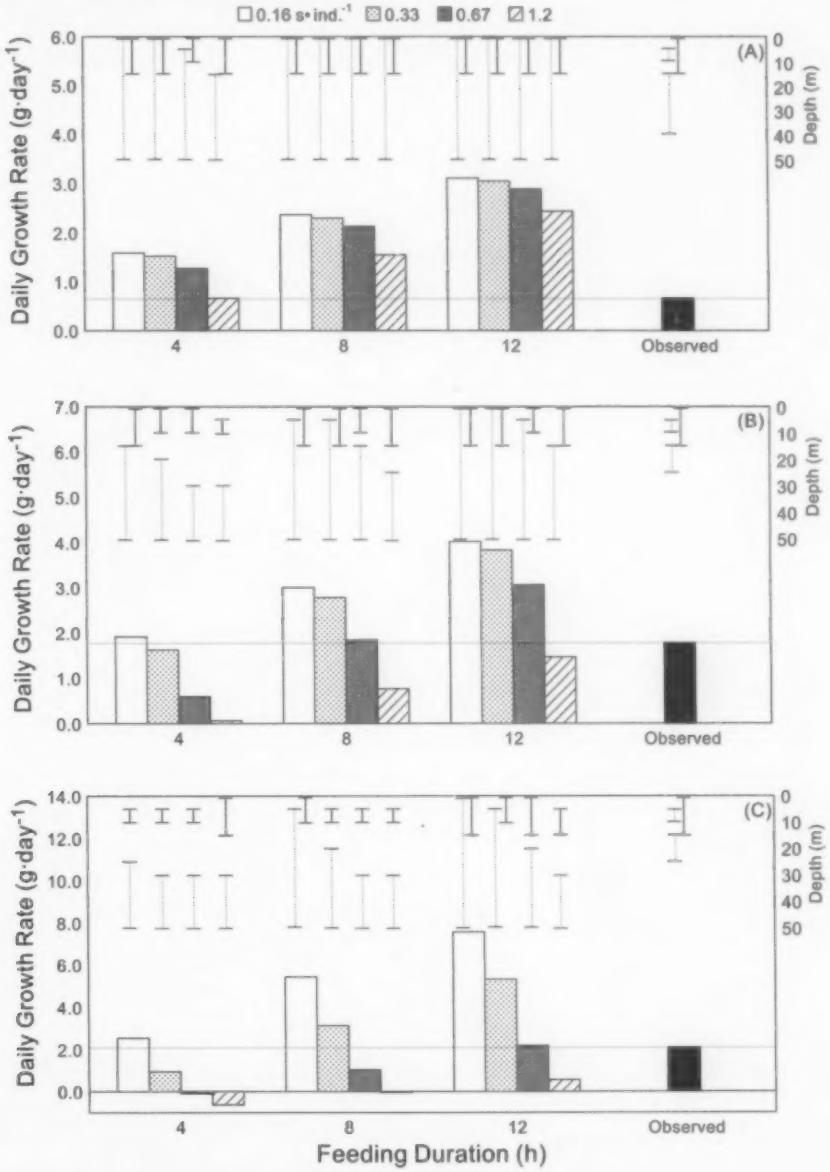

suggesting that bioenergetics is sufficient to explain their diel vertical migration at this time. Age-2 distributions are also explained by the model for feeding durations of 8 and 12 h. Model predictions for age-3 kokanee do not match observed nighttime distributions (for the model growth estimate that most closely matches observed growth). Using their observed depth distributions (7.5 m for feeding, 40 m for daytime nonfeeding, and 17.5 m for nighttime) with a feeding duration of 8 h and a prey handling time of 0.16 s·*Daphnia*$^{-1}$, growth was reduced by only 12% from the maximum (from 3.31 to 2.92 g·day^{-1}). This suggests that age-3 kokanee may minimize migration costs while taking

© 1999 NRC Canada

Fig. 6. Same as Fig. 5 but for 8 July 1997. Starting mass of each age-class for model simulations, as determined from field observations, was 90.9 g for age-1 kokanee, 315.7 g for age-2 kokanee, and 608.4 g for age-3 kokanee.

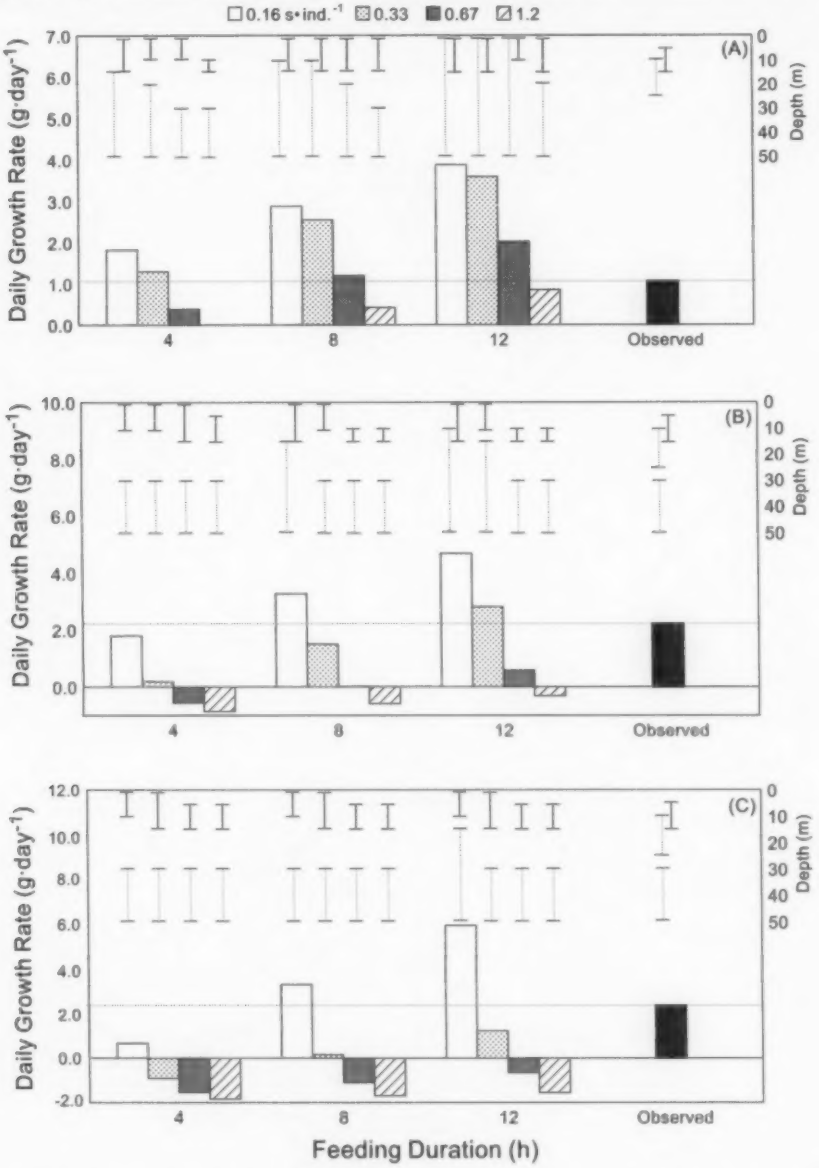

advantage of the antipredation window in July. However, these results appear to be counterintuitive based on what we would expect from size-selective predation and preliminary diet analyses of piscivores in Colorado reservoirs. Intact kokanee found in lake trout stomachs collected from Blue Mesa Reservoir in 1997 averaged 30% of their predator's length (n = 7 stomachs, kokanee ranged from 71 to 151 mm, lake trout ranged from 312 to 534 mm; B.M. Johnson, unpublished data). If we linearly extrapolate this relationship to the largest lake trout in Blue Mesa Reservoir (1000 mm), the largest kokanee that we would expect lake trout to consume would be age-2 fish. Although the sample size is low, these data provide preliminary evidence that age-3 kokanee are probably not targeted by the main piscivore in Blue Mesa Reservoir.

The validity of comparing observed and modeled growth and subsequent comparisons of migration behavior relies on how well we measure growth. The wide confidence intervals for age-1 kokanee in June is an artifact of small sample size (n = 2) (Fig. 2A). We believe that our estimate of mean mass for this age-class (58.4 g) is realistic for this time of year. The other potentially troubling growth estimate is for age-2

© 1999 NRC Canada

Fig. 7. Same as Fig. 5 but for 4 August 1997. Starting mass of each age-class for model simulations, as determined from field observations, was 115.8 g for age-1 kokanee, 330.1 g for age-2 kokanee, and 698.9 g for age-3 kokanee.

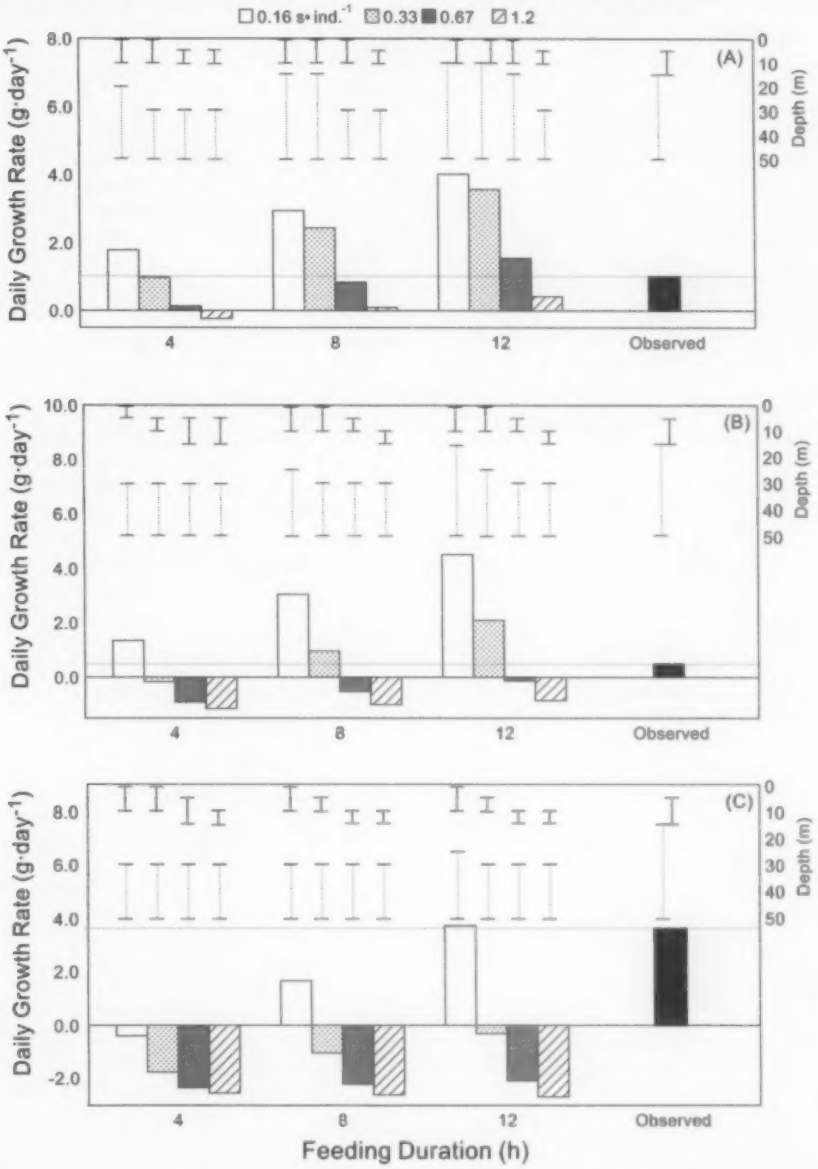

kokanee. According to our measurements, these fish only grew from 315.7 to 330.1 g between July and August (0.48 g·day^{-1}). We observed a similar low growth rate (0.5 g·day^{-1}) for age-2 fish during the late summer of 1995 (Stockwell and Johnson 1997). Based on the results of the present study and the results from Stockwell and Johnson (1997), we can only conclude that age-2 fish in Blue Mesa Reservoir, for reasons that are not apparent, are subject to a large decrease in growth during late summer.

Measuring feeding durations in the field is also difficult because gill nets offer only rather coarse temporal resolution, and kokanee are nearly invulnerable to gill nets during daylight. Because of these challenges, feeding duration remains an uncertain parameter in our simulations. However, regardless of unknown feeding durations, the model does indicate that ages-2 and -3 kokanee, at least in July and August, need to feed at a rate of 3–6 *Daphnia*·s^{-1} to approach their observed growth. This estimate is higher than predicted by Stockwell and Johnson (1997) and is a result of reducing the mass of each *Daphnia* consumed by 50% during these months (Stockwell et al. 1999). Modeling results from Stockwell and Johnson (1997) suggested that kokanee might

© 1999 NRC Canada

have the ability to gulp- or filter-feed. Results from the present study further support this hypothesis. Laboratory feeding trials using densities of large *Daphnia* observed in this study are required to conclusively test this hypothesis.

Despite uncertainties in growth and feeding rates, application of the model to other systems provides a useful framework for evaluating diel vertical migration with respect to the growth maximization hypothesis (Bevelhimer and Adams 1993). Deviations of model predictions from observations should point to other possible causal mechanisms. For example, Johnston (1990) evaluated the bioenergetics efficiency hypothesis (Brett 1971, 1983) for kokanee fry in Kootenay Lake, British Columbia. He showed that fry restricted to epilimnetic habitat grew better than ambient fry that performed diel vertical migration, thus negating the bioenergetics hypothesis as a causal mechanism for diel vertical migration in this system. We ran simulations using August field conditions from Blue Mesa Reservoir for a 3-g kokanee to evaluate the growth maximization hypothesis for the same-sized fish used in Johnston's (1990) study. We used prey handling time (1.2 s·*Daphnia*$^{-1}$) and feeding duration (4 h) that typically resulted in the most distinct migration strategies (e.g., see Figs. 5–7). The model predicted daily growth in the range of 0.17 (remaining in the 0–5 m depth stratum) to 0.21 g·day^{-1} (migrating from 20–50 to 5–10 m). Our model has no built-in cost for migration, other than that associated with changes in respiration rate as a function of temperature and swimming speed. Estimated energetic costs of migration, based on the work of Alexander (1972), range from 20% (Bevelhimer and Adams 1993) to 50% (Clark and Levy 1988) of daily growth. Additionally, if fry remained in surface waters for 24 h, they might likely feed for >4 h. The model estimate for daily growth, when fry are kept at 0–5 m and allowed to feed for 12 h, is 0.40 g·day^{-1}. These modeling results suggest that it is more advantageous for kokanee fry to remain in surface waters than to migrate, consistent with the findings of Johnston (1990). The presence of diel vertical migration for kokanee fry in Kootenay Lake suggests that another factor(s), such as predation risk, is driving their behavior (Johnston 1990). We have no field data for kokanee fry in Blue Mesa Reservoir to compare with model results. Nevertheless, the simulations illustrate how the modeling framework can be used to examine the sufficiency of the growth maximization hypothesis to explain kokanee diel vertical migration in Blue Mesa Reservoir, as well as in other systems.

Results from the model also make predictions about kokanee diel vertical migration across latitudinal and productivity gradients. From the simulations, it appears that migration behavior becomes more flexible as acquisition of food becomes less limiting (increased time spent feeding or decreased prey handling time) and (or) as thermoclines become less pronounced. From a bioenergetics perspective, we would therefore expect to see stronger diel vertical migration patterns in systems with low productivity and (or) sharper thermoclines. Application of the model across a range of lakes of differing trophic status and (or) latitudes would provide a baseline test of this hypothesis. Deviations of observations from model predictions would indicate that other processes might be driving diel vertical migration at a regional scale.

We propose that seasonal variation of environmental conditions within lakes, as well as environmental variability among lakes, has led to the development of a variety of single-factor hypotheses to explain diel vertical migration. Results from this study, as well as from other recent studies (e.g., Clark and Levy 1988; Johnston 1990; Levy 1990; Bevelhimer and Adams 1993), provide strong evidence that kokanee diel vertical migration is likely the product of several factors. In Blue Mesa Reservoir, it appears that tradeoffs between bioenergetic constraints and predation risk can explain kokanee diel vertical migration. Moreover, our results suggest that the relative importance of each factor changes seasonally, as hypothesized by Bevelhimer and Adams (1993). The shift in diel vertical migration behavior in Blue Mesa Reservoir appears to be directly related to abiotic conditions: the strength of the thermocline determines the extent to which kokanee are susceptible to piscivorous lake trout in plankton-rich surface waters and therefore the extent to which predation risk influences behavior. It is therefore likely that the relative importance of factors driving kokanee diel vertical migration in other systems will vary from lake to lake and through time. The modeling approach demonstrated in this study is relatively easy to apply and can be used as a baseline reference given the environmental conditions of any lake. Supplementing model results with information on kokanee and predator depth distributions, or predator characteristics (e.g., thermal preference), can help in evaluating the relative importance of the different hypotheses. In the future, explicit incorporation of other spatial variables like predation risk will be important to refine the model's ability to predict kokanee diel vertical migration.

Acknowledgments

We thank Brady Allen, Kathleen Apakupakul, Krista Bonfantine, Dan Brauch, Tom Cady, Daren Carlisle, Daren Chacon, Gregg Chenu, Jason Garner, Sture Hansson, Steve Johnson, Shawndra Mawhorter, Ron Sutton, and Joe Zendt for their tireless help in the field. Patrick Martinez, Dan Brauch, and the Colorado Division of Wildlife graciously provided the use of their boats and sonar equipment. Steve Johnson and Doran Mason provided valuable guidance with processing of sonar data. Krista Bonfantine processed zooplankton samples and aged fish. We also thank Rick Harris and the National Park Service for their logistical support. This study was supported by funds from the U.S. Department of the Interior, Bureau of Reclamation, Grand Junction Projects Office.

References

Alexander, R.M. 1972. The energetics of vertical migration by fishes. Symp. Soc. Exp. Biol. **26**: 273–294.

Beauchamp, D.A., Stewart, D.J., and Thomas, G.L. 1989. Corroboration of a bioenergetics model for sockeye salmon. Trans. Am. Fish. Soc. **118**: 597–607.

Bevelhimer, M.S., and Adams, S.M. 1993. A bioenergetic analysis of diel vertical migration by kokanee salmon, *Oncorhynchus nerka*. Can. J. Fish. Aquat. Sci. **50**: 2336–2349.

Brett, J.R. 1971. Energetic responses of salmon to temperature. A study of some thermal relations in the physiology and freshwater

© 1999 NRC Canada

ecology of sockeye salmon (*Oncorhynchus nerka*). Am. Zool. **11**: 99–113.

Brett, J.R. 1983. Life energetics of sockeye salmon, *Oncorhynchus nerka*. *In* Behavioral energetics: the cost of survival in vertebrates. *Edited by* W.P. Aspey and S.I. Lustick. Ohio State University Press, Columbus, Ohio. pp. 29–63.

Brett, J.R., and Higgs, D.A. 1970. Effect of temperature on the rate of gastric digestion in fingerling sockeye salmon, *Oncorhynchus nerka*. J. Fish. Res. Board Can. **27**: 1767–1779.

Clark, C.W., and Levy, D.A. 1988. Diel vertical migrations by juvenile sockeye salmon and the antipredation window. Am. Nat. **131**: 271–290.

Eggers, D.M. 1978. Limnetic feeding behavior of juvenile sockeye salmon in Lake Washington and predator avoidance. Limnol. Oceanogr. **23**: 1114–1125.

Elliot, J.M., and Persson, L. 1978. The estimation of daily rates of food consumption for fish. J. Anim. Ecol. **47**: 977–991.

Finnell, L.M., and Reed, E.B. 1969. The diel vertical movements of kokanee salmon, *Oncorhynchus nerka*, in Granby Reservoir, Colorado. Trans. Am. Fish. Soc. **98**: 245–252.

Hyatt, K.D. 1980. Mechanisms of food resource partitioning and the foraging strategies of rainbow trout (*Salmo gairdneri*) and kokanee (*Oncorhynchus nerka*) in Marion Lake, British Columbia. Ph.D. thesis, University of British Columbia, Vancouver, B.C.

Janssen, J. 1976. Feeding modes and prey size selection in the alewife (*Alosa pseudoharengus*). J. Fish. Res. Board Can. **33**: 1972–1975.

Janssen, J., and Brandt, S.B. 1980. Feeding ecology and vertical migration of adult alewives (*Alosa pseudoharengus*) in Lake Michigan. Can. J. Fish. Aquat. Sci. **37**: 177–184.

Johnson, B.M., Wise, M.J., Counard, C.J., and Szerlong G. 1995. Ecological effects of reservoir operations on Blue Mesa Reservoir. Annual Progress Report to U.S. Bureau of Reclamation. U.S. Bureau of Reclamation, Grand Junction.

Johnson, B.M.,Wise, M.J., Herwig, B., Szerlong, G., Faber, D., and Byall, B. 1996. Ecological effects of reservoir operations on Blue Mesa Reservoir. Annual Progress Report to U.S. Bureau of Reclamation. U.S. Bureau of Reclamation, Grand Junction.

Johnson, B.M., Stockwell, J.D., and Bonfantine, K. 1997. Ecological effects of reservoir operations on Blue Mesa Reservoir. Annual Progress Report to U.S. Bureau of Reclamation. U.S. Bureau of Reclamation, Grand Junction.

Johnston, N.T. 1990. A comparison of the growth of vertically-migrating and nonmigrating kokanee (*Oncorhynchus nerka*) fry. Can. J. Fish. Aquat. Sci. **47**: 486–491.

Legendre, L., and Demers, S. 1984. Towards dynamic biological oceanography and limnology. Can. J. Fish. Aquat. Sci. **41**: 2–19.

Levy, D.A. 1987. Review of the ecological significance of diel vertical migrations by juvenile sockeye salmon (*Oncorhynchus nerka*). *In* Sockeye salmon (*Oncorhynchus nerka*) population biology and future management. *Edited by* H.D. Smith, L. Margolis, and C.C. Wood. Can. Spec. Publ. Fish. Aquat. Sci. No. 96. pp. 44–52.

Levy, D.A. 1990. Reciprocal diel vertical migration behavior in planktivores and zooplankton in British Columbia lakes. Can. J. Fish. Aquat. Sci. **47**: 1755–1764.

Love, R.H. 1971. Dorsal-aspect target strength of an individual fish. J. Acoust. Soc. Am. **49**: 816–823.

Narver, D.W. 1970. Diel vertical movements and feeding of underyearling sockeye salmon and the limnetic zooplankton in Babine Lake, British Columbia. J. Fish. Res. Board Can. **27**: 281–316.

Northcote, T.G., and Lorz, H.W. 1966. Seasonal and diel changes in food of adult kokanee (*Oncorhynchus nerka*) in Nicola Lake, British Columbia. J. Fish. Res. Board Can. **23**: 1259–1263.

Ruohonen, K., Grove, D.J., and McIlroy, J.T. 1997. The amount of food ingested in a single meal by rainbow trout offered chopped herring, dry and wet diets. J. Fish Biol. **51**: 93–105.

Snow, N.B. 1972. The effect of season and animal size on the caloric content of *Daphnia pulicaria* Forbes. Limnol. Oceanogr. **17**: 909–913.

Stockwell, J.D., and Johnson, B.M. 1997. Refinement and calibration of a bioenergetics-based foraging model for kokanee (*Oncorhynchus nerka*). Can. J. Fish. Aquat. Sci. **54**: 2659–2676.

Stockwell, J.D., Bonfantine, K.L., and Johnson, B.M. 1999. Kokanee foraging: a *Daphnia* in the stomach is worth two in the lake. Trans. Am. Fish. Soc. **128**: 169–174.

Wurtsbaugh, W.A., and Neverman, D. 1988. Post-feeding thermotaxis and daily vertical migration in a larval fish. Nature (Lond.), **333**: 846–848.

© 1999 NRC Canada

Under-ice diel vertical migrations of *Oncorhynchus nerka* and their zooplankton prey

Geoffrey B. Steinhart and Wayne A. Wurtsbaugh

Abstract: We used stationary hydroacoustics and measures of environmental conditions (water temperature, dissolved oxygen, light levels, and zooplankton) to determine what factors, foraging or predation risk, influenced diel vertical migrations of *Oncorhynchus nerka* during winter in three high-mountain lakes. The Sawtooth Valley lakes are deep, oligotrophic, glacial lakes located in central Idaho, U.S.A., and historically contained populations of anadromous *O. nerka*. In general, low light intensities limited foraging opportunities of *O. nerka* under ice, especially at night. In Stanley Lake, *O. nerka* underwent diel vertical migrations to exploit available light to feed. *Oncorhynchus nerka* occupied shallow water at night, where there was still sufficient light to feed, but were found in deep water during the day. It is unknown whether *O. nerka* occupied deep depths during the day to feed on high densities of zooplankton or to avoid predators. In Alturas Lake, *O. nerka* remained in the top 25 m both day and night to feed high densities of zooplankton found near the surface. In Redfish Lake, *O. nerka* also showed little migration: *O. nerka* stayed in shallow water both day and night and occupied the same depths with the highest zooplankton densities. The vertical distribution of *O. nerka* during the winter appears to be determined by available food and light, but the deep daytime distribution found in Stanley Lake is still unexplained.

Résumé : Les auteurs ont utilisé des senseurs hydroacoustiques stationnaires et mesuré divers paramètres environnementaux (température de l'eau, oxygène dissous, luminosité et zooplancton) pour déterminer quels facteurs, à savoir la quête de nourriture ou le risque de prédation, expliquaient les migrations verticales journalières d'*Oncorhynchus nerka* en hiver dans trois lacs alpins de la vallée Sawtooth, en Idaho (États-Unis). Ces lacs glaciaires, profonds et oligotrophes, abritent depuis des temps immémoriaux des populations anadromes d'*O. nerka*. En général, la quête de nourriture était inhibée par la faible luminosité, en particulier la nuit. Dans le lac Stanley, *O. nerka* effectuait des migrations journalières afin d'exploiter la lumière disponible pour se nourrir. Il demeurait en eau peu profonde durant la nuit, y trouvant suffisamment de lumière pour se nourrir, mais regagnait les eaux plus profondes durant la journée. Les auteurs n'ont pas été en mesure de déterminer si *O. nerka* migrait vers les eaux profondes durant le jour pour exploiter les fortes densités de zooplancton ou pour échapper à ses prédateurs. Dans le lac Alturas, *O. nerka* demeurait tant le jour que la nuit dans la couche superficielle formée par les premiers 25 m d'eau afin de se nourrir des fortes densités de zooplancton observées près de la surface. Dans le lac Redfish, *O. nerka* effectuait des migrations limitées, demeurant en eaux peu profondes tant la nuit que le jour et occupant les strates les plus riches en zooplancton. La distribution verticale de *O. nerka* en hiver semble dictée par la disponibilité de la nourriture et de la lumière. Toutefois, dans le lac Stanley, la présence de *O. nerka* en eaux profondes durant le jour demeure inexpliquée.

[Traduit par la Rédaction]

Introduction

Diel vertical migrations (DVM) are common behavior for many species of aquatic organisms (Cunningham 1972; Levy 1987; Wurtsbaugh and Neverman 1988; Lampert 1989). Among fish, much attention has been focused on the migrations of sockeye (Narver 1970; Eggers 1978; Levy 1990*a*) and kokanee salmon (Johnston 1990; Levy 1991; Bevelhimer and Adams 1993), both *Oncorhynchus nerka*. While many researchers have studied diel migratory behavior of *O. nerka*, the explanations for the observed migrations are still under debate.

There are three major hypotheses for the adaptive significance of DVM in fish: foraging, bioenergetics, and predator avoidance (Levy 1987, 1990*b*; Clark and Levy 1988; Bevelhimer and Adams 1993). The foraging hypothesis predicts that fish will track the movements of their prey, resulting in increased foraging opportunities and higher growth rates (Narver 1970; Levy 1990*a*, 1990*b*). Bioenergetics hypotheses predict that fish will select temperatures that either increase digestion rates (Wurtsbaugh and Neverman 1988; Neverman and Wurtsbaugh 1994) or maximize net growth efficiency (Brett 1971; Brett and Groves 1979), both resulting in higher growth rates (Bevelhimer and Adams 1993). Predator avoidance theory states that by minimizing exposure to predators, fish will increase survival, even though growth may be depressed (Levy 1987, 1990*b*; Clark and Levy 1988).

It is likely that the migratory behaviors of many *O. nerka* populations are a combination of these factors; for example,

Received November 21, 1997. Accepted December 9, 1998. J14317

G.B. Steinhart[1] and W.A. Wurtsbaugh. Department of Fisheries and Wildlife, and the Ecology Center, Utah State University, Logan, UT 84322-5210, U.S.A.

[1]Author to whom all correspondence should be sent at the following address: Aquatic Ecology Laboratory, The Ohio State University, 227 Research Center, 1314 Kinnear Road, Columbus, OH 43212-1194, U.S.A.

© 1999 NRC Canada

Table 1. Physical and biological characteristics of the Sawtooth Valley lakes during ice cover from December 1993 to March 1995.

Lake	Surface area (km^2)	Maximum depth (m)	Mean chlorophyll *a* (mg/m^3)	Mean zooplankton biomass (μg/L)
Redfish	6.17	91	0.58	1.8
Alturas	3.38	53	0.74	3.5
Stanley	0.73	26	0.96	6.1

Note: Chlorophyll *a* values are from surface samples (0–6 m). Zooplankton biomass is a whole-lake average of crustacean zooplankton except nauplii.

Table 2. Gillnet catch-per-net-hour (CPUE) for piscivorous fish in the Sawtooth Valley lakes.

		CPUE[a]			Predation index		
Predator (weight)	*O. nerka* in diet (%)	Redfish Lake	Alturas Lake	Stanley Lake	Redfish Lake	Alturas Lake	Stanley Lake
Bull trout (0.45 kg)	77	0.1	0.07	0.0	3.5	2.4	0.0
Lake trout (1.2 kg)	66	0.0	0.0	0.19	0.0	0.0	15.0
Northern squawfish (0.27 kg)	14	0.15	1.20	0.0	0.6	4.5	0.0
Total		0.25	1.27	0.19	4.1	6.9	15.0

Note: To better assess predation pressure, we multiplied CPUE by mean predator weight (kg) and the percentage of *O. nerka* in the predator's diet to create a predation index.

[a]Data from Spaulding (1993), Kline (1994), and Teuscher and Taki (1994).

the growth to mortality ratio or the foraging to survival ratio (Levy 1987, 1990*a*, 1990*b*; Bevelhimer and Adams 1993). It is difficult, however, to determine which factors are most important in determining migration patterns because of confounding elements in many studies. For example, most studies have been done when lakes are thermally stratified, so it has been difficult to distinguish between bioenergetic advantages and the effects of prey and predators on the diel vertical distributions of fish (Beauchamp et al. 1997).

Here, we describe the patterns of DVM during winter for *O. nerka* in three high-mountain, oligotrophic lakes. The results of this study allow closer examination of the current hypotheses on what drives *O. nerka* vertical migrations. Nearly constant temperature profiles during winter eliminate possible physiological benefits of migration, while different predator densities between lakes demonstrate the influence of the predator avoidance hypothesis. Winter zooplankton abundance in these lakes can be extremely low, and *O. nerka* may have trouble meeting their maintenance ration (Teuscher and Taki 1995; Steinhart 1997), so we hypothesized that the foraging hypothesis played a major role in structuring the vertical distribution of *O. nerka*. In addition, we examined how low light penetration may limit feeding and influence the observed patterns of DVM for visually foraging *O. nerka*. Finally, describing DVM patterns of *O. nerka* in winter will better our understanding of how *O. nerka* populations use available resources and what might limit their populations in winter.

Methods

Study site

Redfish, Stanley, and Alturas lakes are glacially formed, high-altitude lakes (1985–2138 m) located in the Sawtooth Valley of central Idaho, U.S.A. (44°N, 115°W). In general, all three lakes are oligotrophic, with little macrophyte growth, low chlorophyll levels, and low zooplankton biomass, but differ in size and depth (Table 1). The Sawtooth Valley lakes are typically ice covered for at least 5 months each year, and during this study, snow and ice thickness varied from 30 to 75 cm.

All three lakes contain kokanee, a type of sockeye salmon that do not migrate to the ocean as adults, but only Redfish Lake is known to contain both kokanee and sockeye salmon. As juveniles, the two types are functionally similar (from here on, we will refer to sockeye and kokanee collectively as *O. nerka*). Data from summer and fall nearshore gillnet studies and winter under-ice gillnet surveys (for methods, see Spaulding 1993; Kline 1994; Teuscher and Taki 1994) were used to estimate predator abundance and diet to calculate relative indices of predation risk for the lakes (Table 2). Stanley Lake appeared to have the highest predation risk due to a large population of predaceous lake trout (*Salvelinus namaycush*). Redfish Lake contains some piscivorous bull trout (*Salvelinus confluentus*) and northern squawfish (*Ptychocheilus oregonensis*). Alturas Lake has a low density of bull trout but a large population of northern squawfish. Other fish species present in the lakes include rainbow trout (*Oncorhynchus mykiss*), brook trout (*Salvelinus fontinalis*), suckers (*Catastomus* spp.), redside shiner (*Richardsonius balteatus*), dace (*Rhinichthys* spp.), and sculpin (*Cottus* spp.). Rainbow trout found in these lakes are hatchery-stocked fish, and few survive overwinter, and while both the rainbow and brook trout eat juvenile salmon, no salmon were found in their diets during the course of this study (Teuscher and Taki 1995).

Data collection

On each sampling date, samples were collected near the deepest section of each lake. A hole was cut through the ice using either an ice auger or a chainsaw. The depths of snow and of the different ice layers were recorded, as was light intensity. Temperature and dissolved oxygen profiles were measured using a YSI model 58 dissolved oxygen meter. For a complete description of limnological methods, see Budy et al. (1995).

Light intensity was measured using a submersible Li-Cor model LI-188B radiometer through a hole about 0.75 m^2 cut by chainsaw. The spherical light sensor measured light between 400 and 700 nm. To avoid increased light intensity surrounding the hole, the sensor was extended about 3 m away from the hole using a plastic pipe equipped with floatation to keep the pipe near the surface. A metered cable and line were passed through the plastic pipe and attached to a weighted and self-righting arm that held the sensor (Fig. 1). Snow and ice were piled back into the hole to reduce light penetration from the hole. The probe was slowly lowered at 1-m intervals to 36 m, or until light was undetectable (<0.1 μeinsteins·m^{-2}·s^{-1}). During the sampling period, a deck cell

© 1999 NRC Canada

Fig. 1. Diagram of gear deployment during periods of ice cover on the Sawtooth Valley lakes. Holes were cut using either an auger or a chainsaw. Hydroacoustics and gill nets were used to measure the vertical distributions of fish. Note the construction of the flexible plastic pole used to extend the underwater light sensor away from the light surrounding the hole, but keeping the sensor near the surface of the ice.

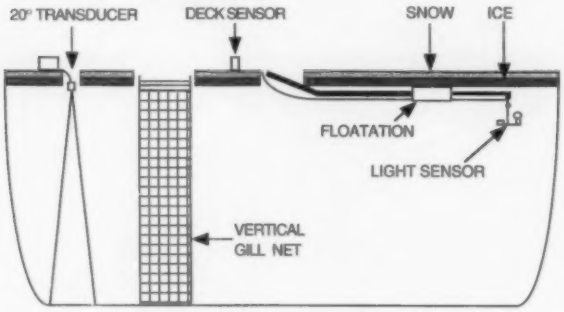

measuring incident light intensities was used to correct for changes in light intensity from clouds passing overhead.

To examine the extent of light-limited foraging, under-ice light intensities for a diel period were calculated using the percent light blocked by ice and snow, extinction coefficients, and a computer program that predicts surface intensity based on location, percent cloud cover (estimated during field sampling), and sunlight and moonlight (Janiczek and Young 1987). The percent light blocked by ice and snow was calculated for each sample date by dividing the light intensity immediately beneath the ice by the light intensity measured just below the surface of the water in the open hole. We calculated extinction coefficients as the slope of the regression of the natural log of percent surface intensity against depth (Wetzel and Likens 1991). Light intensities measured in einsteins were converted to units of lux or foot-candles for consistency with available literature on sockeye feeding (1 lx ≅ 1.95×10^{-2} μeinsteins/m^2-s ≅ 0.093 ft-candle).

Zooplankton samples were collected using a closing conical net 35 cm in diameter and 80 cm long with 80-μm mesh. The net was equipped with a flowmeter to calculate net efficiencies. In each lake, zooplankton samples were collected at two stations separated by at least 50 m and over several discrete depth strata, depending on sample protocol (diel or routine sampling) and the lake. Diel zooplankton sampling in Stanley Lake occurred between 12:15 and 12:45 and between 00:00 and 00:30 on 17–18 March 1995 (strata: 0–2, 2–5, 5–10, and 10–17 m and 17 m to the bottom). Diel zooplankton sampling in Redfish Lake was from 12:00 to 13:30 and from 00:00 to 01:30 on 22–23 January 1995 (strata: 0–2, 2–5, 5–10, 10–20, 20–40, and 60 m to the bottom). Daytime-only depth-stratified samples were collected in Alturas Lake on 23 February 1995 (strata: 0–10 and 10–20 m and 20 m to the bottom) and in Stanley Lake on 22 March 1994 (strata: 0–10 m and 10 m to the bottom). Zooplankton samples were preserved in 10% neutralized formalin solution and were enumerated and measured in the laboratory. Dry biomass was calculated by length–weight regressions from McCauley (1984) and Koenings et al. (1987). Copepod nauplii are not included in the zooplankton data reported here, as nauplii rarely appeared in *O. nerka* diets.

A two-way repeated measures analysis of variance (ANOVA) was used to test for DVM for all zooplankton combined and by individual species. For all zooplankton, time and depth were factors and zooplankton biomass (micrograms per litre) was the independent variable. For individual taxa, the independent variable was the percentage of the total taxa population in each stratum (arcsine transformed; Sokal and Rohlf 1981). Since the abundance of some taxa was low, and was variable between night and day, percentages were used to avoid any confounding results due to different catch rates at different times. A significant interaction between time and depth indicated that the two distributions were not similar and a diel migration did occur.

Hydroacoustic sampling of fish distributions was conducted concurrently with the limnological and zooplankton diel sampling using a Lowrance X-16 chart recorder. Data on fish distributions were collected for a 24-h period using a stationary transducer deployed through the ice. The downward-facing transducer (20° beam angle, 200 kHz) was placed at the bottom edge of the ice through an auger-cut hole (Fig. 1). The hole was subsequently filled with snow to prevent excess light penetration. The gain was adjusted to the maximum setting that did not result in noise levels that would prevent detection of fish in the top 5 m.

The time and depth of each fish target on the chart paper were recorded. To determine the time of occurrence for each target, the distance from the start of the roll was measured and converted to minutes elapsed using a regression between distance and time. Only targets deeper than 2 m were recorded because the transducer was not able to discern targets closer than 2 m. To separate daytime and nighttime targets, data from 1 h before until 1 h after sunrise and sunset are excluded from the analyses. The data were corrected for transducer beam spread by calculating the density of targets in each depth stratum based on the volume sampled. We did not correct for small *O. nerka* near the edge of the beam, or far away from the transducer, that may not have been detected due to spreading losses. However, summer acoustic surveys collected with a scientific-grade echosounder suggest that *O. nerka* were typically found shallower than 30 m (Teuscher and Taki 1994; Beauchamp et al. 1997), so we do not think that this shortcoming would affect our results. Since there was no replication of the acoustic data, we used a χ^2 test to test for differences between day and night vertical distributions of *O. nerka*. In addition, each distribution (day and night) was compared with a random distribution of fish using a χ^2 test.

Vertical gill nets were used to provide target identification to supplement the hydroacoustic sampling. Three vertical gill nets (3 m wide by 25 m deep, 19-, 25-, and 38-mm^2 square mesh) were marked in 2.5-m increments and were set so that they stretched from the surface to the bottom in Stanley Lake and from the surface to 25 m in Alturas Lake. Preliminary sampling indicated that nets did not capture fish during the day, so they were only checked in the morning, between 08:00 and 10:00. We assumed that all fish in the nets were captured between dusk and dawn. Redfish Lake was not sampled with gill nets because it contains endangered sockeye salmon. In Alturas Lake, two bull trout were captured by vertical gill nets set under the ice, but in general, under-ice gillnetting was ineffective (10 *O. nerka* captured in 225 net-hours). For these lakes, we used previous data from midwater trawls (summer 1993, 1994, and 1995, November 1993 and 1994, and May 1994 and 1995) that showed that *O. nerka* make up nearly 100% of the pelagic fish population (where our acoustic sampling occurred). Previous gillnet surveys have found that predators were typically found in littoral and benthic areas (Kline 1994; Steinhart 1997).

To test the hypothesis that *O. nerka* migrate to maximize food intake (a combination of both prey density and foraging ability), a simple model of feeding rates was created. Instantaneous clearance rates at different light intensities were calculated using the equation from Dodson (1975):

$$(1) \qquad k = -\log_e \frac{(P_f/P_i)}{Xt}$$

where k is clearance rate (litres per hour), P_f is the final number of prey in the tank, P_i is the initial number of prey, X is the number of

© 1999 NRC Canada

Fig. 2. Thickness of snow, slush, and ice and the depth of 1% surface light intensity (compensation point) for (A) Stanley, (B) Redfish, and (C) Alturas lakes during 1993–1995.

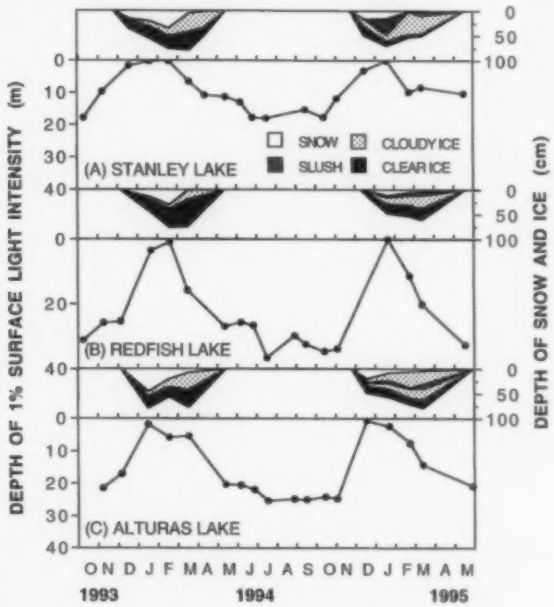

predators in the tank, and t is time (hours). Data from Ali's (1959) work on *O. nerka* capture success in laboratory experiments were used to calculate k at different light intensities. We multiplied our estimate of clearance rate (k) by the ambient zooplankton density to calculate the maximum consumption of zooplankton by *O. nerka* at observed light intensities. Three different DVM strategies were tested using this model: (*i*) remain shallow throughout the day and night, (*ii*) remain deep, and (*iii*) remain deep during the day and shallow at night.

Results

Under-ice light intensities varied among the lakes. Stanley Lake had the lowest mean light penetration (Fig. 2A) because it froze over earlier in the year, was covered by thick ice, and its small fetch resulted in more snow accumulation. Light penetration was often highest in Redfish and Alturas lakes (Figs. 2B and 2C). Since these lakes are deeper than Stanley Lake, a larger proportion of the water column was not sufficiently illuminated for foraging.

Winter zooplankton abundance and species composition differed among lakes but were generally dominated by *Bosmina longirostris*, *Daphnia rosea*, and an unidentified cyclopoid copepod. In general, there was little DVM of zooplankton under ice during this study. For Stanley Lake, in March 1995, zooplankton biomass was <3 µg/L in most of the water column, with a higher biomass (>6 µg/L) found near the bottom of the lake (Fig. 3A). As a whole, there was no DVM of the zooplankton; however, *Bosmina* sp. showed a slight migration toward the surface at night (Table 3). Nearly all cyclopoids were located between 17 and 24 m throughout the sampling period. During March 1994, the daytime zooplankton abundance was extremely low

Fig. 3. Diel vertical distribution of (A) crustacean zooplankton (not including copepod nauplii) (±1 SE) and (B) *O. nerka* in Stanley Lake on 17 March 1995. Also shown are temperature (solid line), dissolved oxygen (broken line), predicted *O. nerka* depths of foraging success (arrows and % success), and the number of targets from the hydroacoustic data (N).

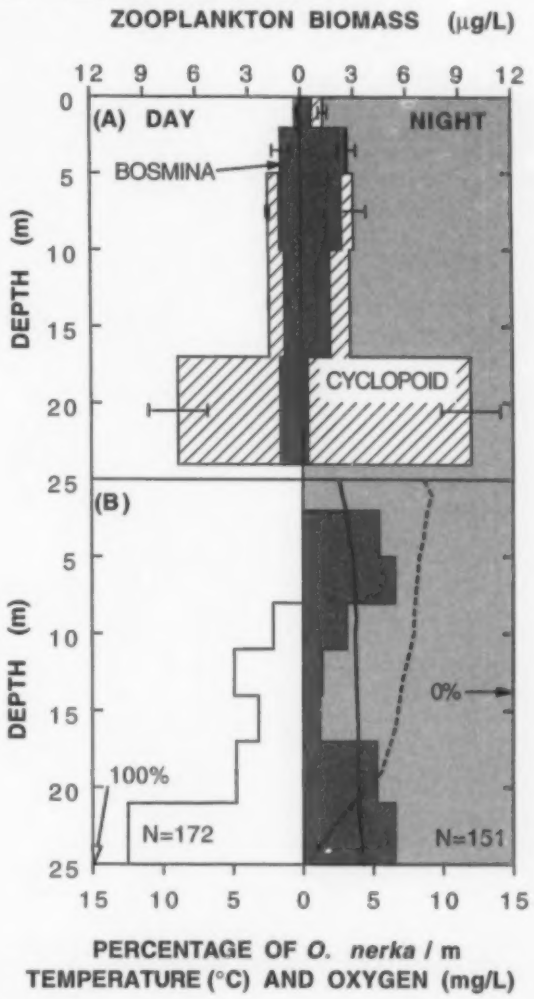

(0.6 µg/L) in Stanley Lake (Fig. 4A). For Redfish Lake, the highest biomass of zooplankton was in the 0- to 2-m stratum (>1 µg/L) (Fig. 5A), but the mean biomass was only 0.4 µg/L. Overall, DVM by all zooplankton in Redfish Lake was insignificant; however, *Bosmina* sp. showed a significant upward migration at night (Table 3). Zooplankton densities in Alturas Lake were low (0.7 µg/L) throughout the water column, but biomass was higher near the surface than below 10 m (Fig. 6A). We assumed that this daytime sample was representative of the nighttime distribution because diel sampling of the zooplankton distribution in Alturas Lake was conducted in February 1994 and found no significant diel migration of plankton (G.B. Steinhart, unpublished data).

© 1999 NRC Canada

Table 3. Results of ANOVA of zooplankton DVM in Stanley and Redfish lakes.

		ANOVA p values		
Lake	Zooplankton	Depth	Time	Depth × time
Stanley, 17 Mar. 1995	All	0.007	0.003	0.59
	Bosmina	0.03	0.29	0.03
	Cyclopoid copepods	<0.0001	0.93	0.10
Redfish, 22 Jan. 1995	All	0.001	0.37	0.08
	Bosmina	<0.0001	0.16	0.04
	Daphnia	<0.0001	0.60	0.40
	Cyclopoid copepods	0.0002	0.70	0.94

Note: We tested the migration of the total crustacean zooplankton population by comparing total zooplankton density at different depths and times. Migrations of each zooplankton group were analyzed by comparing the arcsine-transformed percentage of individuals per metre at different depths and times. A significant depth × time interaction indicates that the day and night distributions were different.

Under the ice, *O. nerka* in Stanley Lake migrated toward the surface at night but remained deep during the day in March 1994 and 1995 (Figs. 3B and 4B). In March 1995, nearly 50% of the targets were detected below 21 m during the day; however, at night, <20% were deeper than 21 m and over 30% of the targets were shallower than 8 m (Fig. 3B). The distribution of *O. nerka* during the day was significantly different than at night, and both distributions were significantly different from random (Table 4). On 22 March 1994, daytime and nighttime distributions of *O. nerka* were significantly different from each other, but only the daytime distribution was significantly different from random (Fig. 4B; Table 4).

In Stanley Lake, only *O. nerka* were captured in vertical gill nets during this study, and only *O. nerka* and lake trout have been captured in previous studies (some lake trout were captured in other areas of the lake and on other winter sampling dates (Steinhart 1997)). We therefore assume that all of the hydroacoustic targets were *O. nerka* salmon. *Oncorhynchus nerka* were captured at depths ranging from 7 to 19 m (Fig. 7).

Oncorhynchus nerka in Redfish and Alturas lakes remained near the surface throughout the day and night (Figs. 5B and 6B). In Redfish Lake, *O. nerka* did not show any significant change in vertical distribution from day to night (Table 4). The distribution was highly skewed, with all the targets detected above 20 m and the highest proportion of fish in the 2- to 5-m stratum (Fig. 5B). Both these distributions were significantly different from random (Table 4). *Oncorhynchus nerka* in Alturas Lake had a significant upwards vertical migration at night (Table 4), but the magnitude of this migration was small: *O. nerka* were concentrated closer to the surface at night, but during day and night, few *O. nerka* were detected below 14 m (Fig. 6B). In general, fewer *O. nerka* were detected in Redfish and Alturas lakes than in Stanley Lake in March 1995.

The greatest *O. nerka* capture rates of zooplankton were usually shallow (<30 m) in the lakes, due to the decreased light penetration (Fig. 8). This was especially evident in Redfish and Alturas lakes, where zooplankton density varied little with depth, and changes in capture rates reflected changes in light levels. In Redfish Lake, consumption was highest near the surface during the day, with a small peak around 20–30 m due to a slight increase in zooplankton density. Relatively high light penetration into Alturas Lake resulted in the highest predation rates in the top 35 m during the day, but there was little or no feeding at night. In 1995 in Stanley Lake, the high zooplankton abundance near the bottom resulted in a huge increase in capture rates. However, in 1994 and during the night in 1995, capture rates were highest in the illuminated surface waters. Low light intensities and little light penetration through the snow and ice limited nighttime feeding opportunities in all three lakes.

The results of our feeding rate model for Stanley Lake demonstrate the importance of light for maximizing food intake. *Oncorhynchus nerka* that migrated toward the surface at night could increase their consumption by at least 12% over nonmigrating fish (Table 5). This increase in consumption was caused by higher clearance rates in the illuminated surface waters than at the dark bottom at night. These results are especially important at low zooplankton densities but may not be important when food is more abundant.

Discussion

Oncorhynchus nerka in the Sawtooth Valley lakes migrated on a diel cycle under the ice on some occasions. The ecological significance of these migrations appeared to be a combination of foraging success and possibly predator avoidance. Spatially variable prey abundance and limited foraging ability due to low light intensities limited the feeding opportunities for *O. nerka*. As a result, the salmon migrated to make use of available light and to exploit areas of highest zooplankton abundance. Predator avoidance may have played a role in structuring the migrations in Stanley Lake. Physiological benefits due to differences in temperature should not have been a factor during winter in any of these lakes.

The foraging hypothesis predicts that *O. nerka* will migrate to depths where food is more abundant, or where feeding is more efficient. Due to low light intensities under the ice, it was common for only the surface portion of the water column to be available for visual prey detection by *O. nerka*. Consequently, fish would have been near the surface to see and, therefore, to feed. In Stanley Lake, *O. nerka* feeding was not inhibited by light levels during the day; however, at night, only the surface waters were available for visual feeding. Even though higher zooplankton densities were present at the bottom of the lake, *O. nerka* in Stanley Lake migrated up at night to depths where there was sufficient light to permit foraging. In Redfish and Alturas lakes, *O. nerka* remained in the surface waters where light levels and zoo-

© 1999 NRC Canada

Fig. 4. (A) Noon vertical distribution of crustacean zooplankton (not including copepod nauplii) (±1 SE) and (B) diel vertical distribution of *O. nerka* in Stanley Lake on 22 March 1994. BOS, *Bosmina*; CYC, cyclopoid copepods. Also shown are temperature (solid line), dissolved oxygen (broken line), predicted *O. nerka* depths of foraging success (arrows and % success), and the number of targets from the hydroacoustic data (*N*).

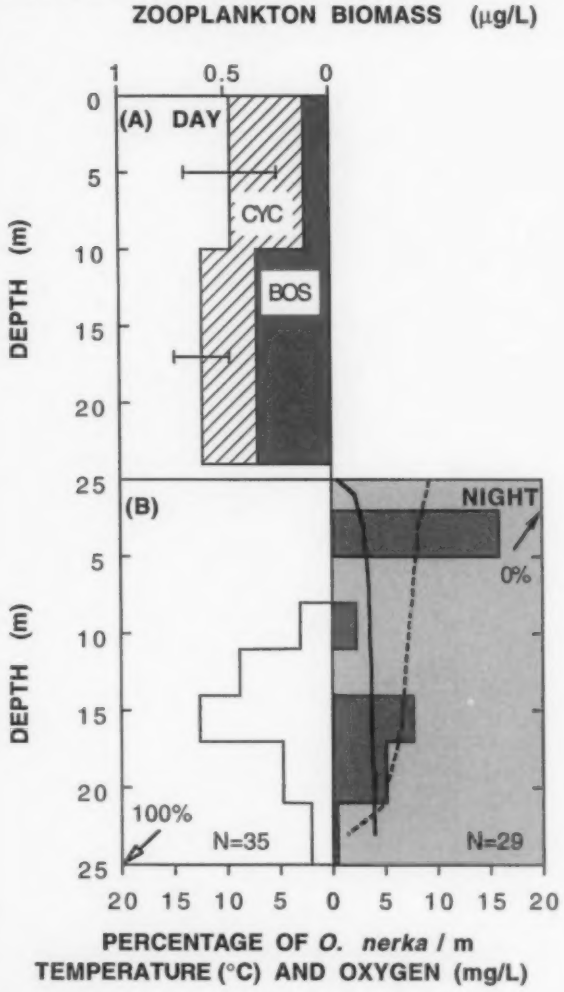

Fig. 5. Diel vertical distribution of (A) crustacean zooplankton (not including copepod nauplii) (±1 SE) and (B) *O. nerka* in Redfish Lake on 22 January 1995. Also shown are temperature (solid line), dissolved oxygen (broken line), predicted *O. nerka* depths of foraging success (arrows and % success), and the number of targets from the hydroacoustic data (*N*).

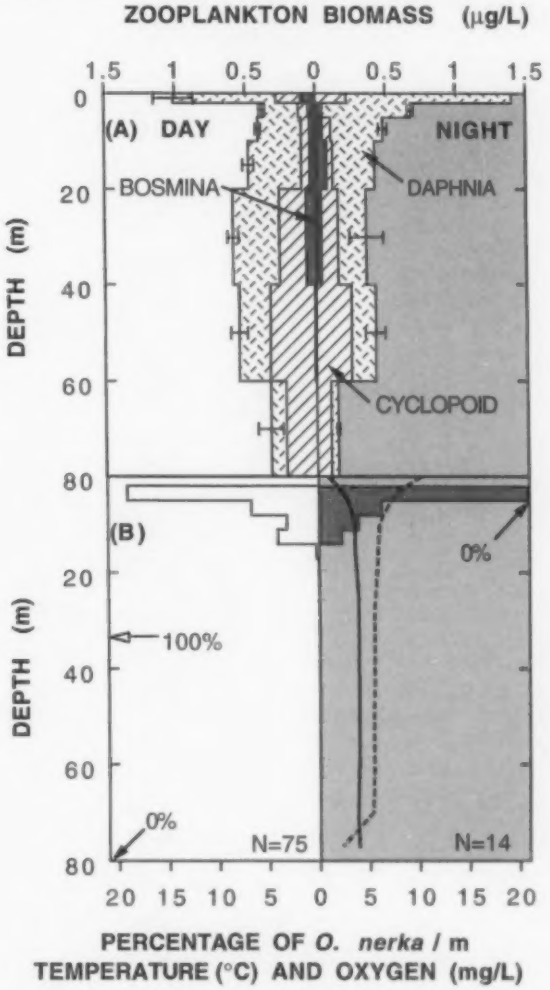

plankton density and biomass were highest. This suggests that *O. nerka* inhabit waters where they can capture the most prey, a combination of prey density and foraging success, and not necessarily where prey numbers are highest.

Low light intensities may have prevented *O. nerka* from meeting their metabolic demands during the winter. Even with DVM, *O. nerka* consumption in Stanley Lake was extremely low, necessitating nearly continual feeding to maintain growth. At 4°C, juvenile sockeye need to consume about 0.4% of their dry weight per day to sustain positive growth (Brett 1983). Consumption by vertically migrating *O. nerka* would be 0.095% of dry weight per day in March 1994 and 1.25% per day in March 1995. To meet basic metabolic costs, *O. nerka* may have migrated into higher concentrations of prey to feed. Although low dissolved oxygen levels were found deep in Stanley Lake (<4 mg/L) (Figs. 3B and 4B), many acoustic targets were detected below 21 m, suggesting that *O. nerka* tolerated the low oxygen levels, possibly in order to feed on the high abundance of zooplankton near the bottom.

Light levels were sufficient to allow foraging in the top 10–20 m in Stanley Lake during this study, but on other dates, light-limited feeding may be more important. Our sampling took place on cloudless nights with nearly a full moon (in 1995) or a partial moon (in 1994): on moonless or cloudy nights, *O. nerka* feeding may be more limited than under the conditions we sampled. Indeed, *O. nerka* in Stanley and Alturas lakes lost lipid over the winter and may have experienced mortality of smaller size-classes (Steinhart

© 1999 NRC Canada

Fig. 6. (A) Noon vertical distribution of crustacean zooplankton (not including copepod nauplii) (±1 SE) and (B) diel vertical distribution of *O. nerka* in Alturas Lake on 23 February 1995. Also shown are temperature (solid line), dissolved oxygen (broken line), predicted *O. nerka* depths of foraging success (arrows and % success), and the number of targets from the hydroacoustic data (*N*).

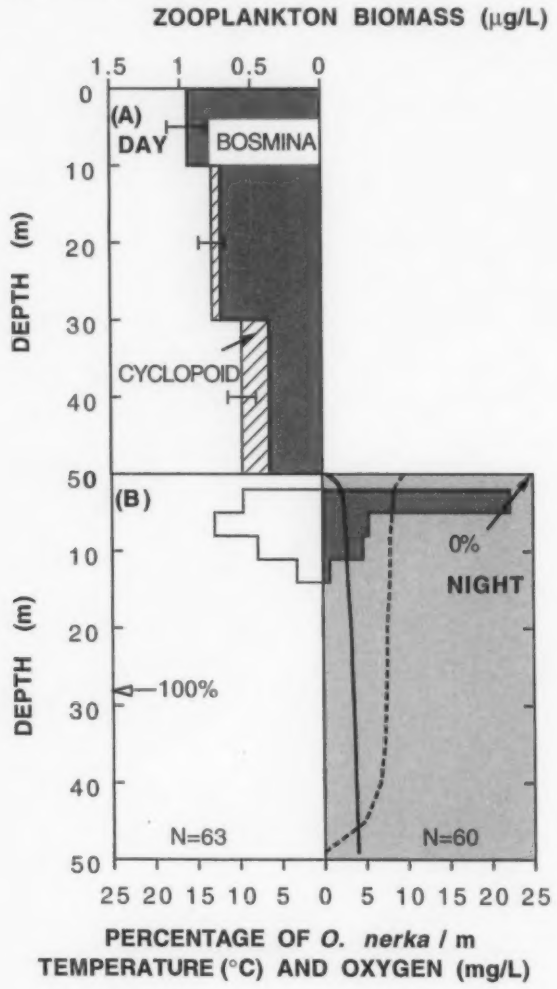

1997). Furthermore, in Alturas Lake, benthic zooplankton and insects such as *Alona* spp. and chironomid larvae were found in the diets of *O. nerka*, suggesting that *O. nerka* may move to nearshore slopes or benthic areas to look for alternative prey when foraging is limited by low light or low zooplankton densities.

Oncorhynchus nerka depth distribution from the gill nets and hydroacoustics were similar in Stanley Lake, but we may have missed a portion of the *O. nerka* population that moved into benthic or nearshore areas. Furthermore, in the deeper Redfish and Alturas lakes, we may have failed to detect some deep (>30 m) targets. The Lowrance X-16 does not have a time-varied gain, so deep targets in these lakes may not have been detected due to attenuation of the acoustic signal. Summer acoustic surveys using scientific echosounders equipped with time-varied gain, however, have found that much of the fish population in Redfish Lake was shallower than 30 m both day and night. In Alturas Lake, the salmon were shown to move from bottom and perimeter zones during the day to the limnetic zone (above 30 m) at night (Teuscher and Taki 1995; Beauchamp et al. 1997). Since our stationary transducers were located in the deepest area of the lake, also near the middle of the lake, we did not sample nearshore areas where fish may have moved to feed

Table 4. Results of χ^2 tests of *O. nerka* vertical distributions.

			χ^2 test p values	
Lake	Date	Time	Night	Random
Stanley	22 Mar. 1994	Day	<0.001	<0.001
		Night	na	<0.001
Stanley	18 Mar. 1995	Day	<0.001	<0.001
		Night	na	0.23
Redfish	22 Jan. 1995	Day	0.99	<0.001
		Night	na	<0.001
Alturas	23 Feb. 1995	Day	<0.001	<0.001
		Night	na	<0.001

Note: A significant p value represents a significant difference between day and night distributions of *O. nerka* or a difference of day or night vertical distribution from a random distribution (i.e., evenly distributed population).

Fig. 7. Vertical distribution of *O. nerka* captured in vertical gill nets in Stanley Lake during March 1994 and March 1995. Preliminary work showed that no fish were captured during the day, so it was assumed that all fish were caught during night or crepuscular periods.

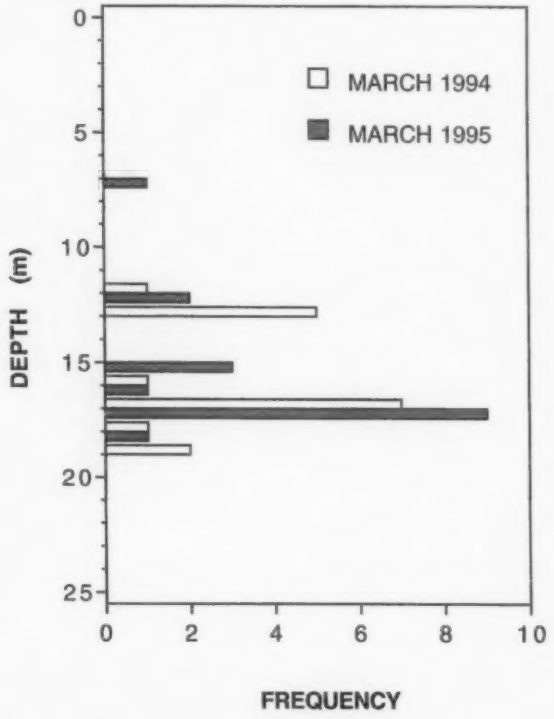

© 1999 NRC Canada

Fig. 8. Theoretical *O. nerka* predation rate on zooplankton in (A and B) Stanley, (C) Redfish, and (D) Alturas lakes. Predation rate was calculated as a function of light intensity and zooplankton density (see text for complete details). Note the different bottom depths in each lake.

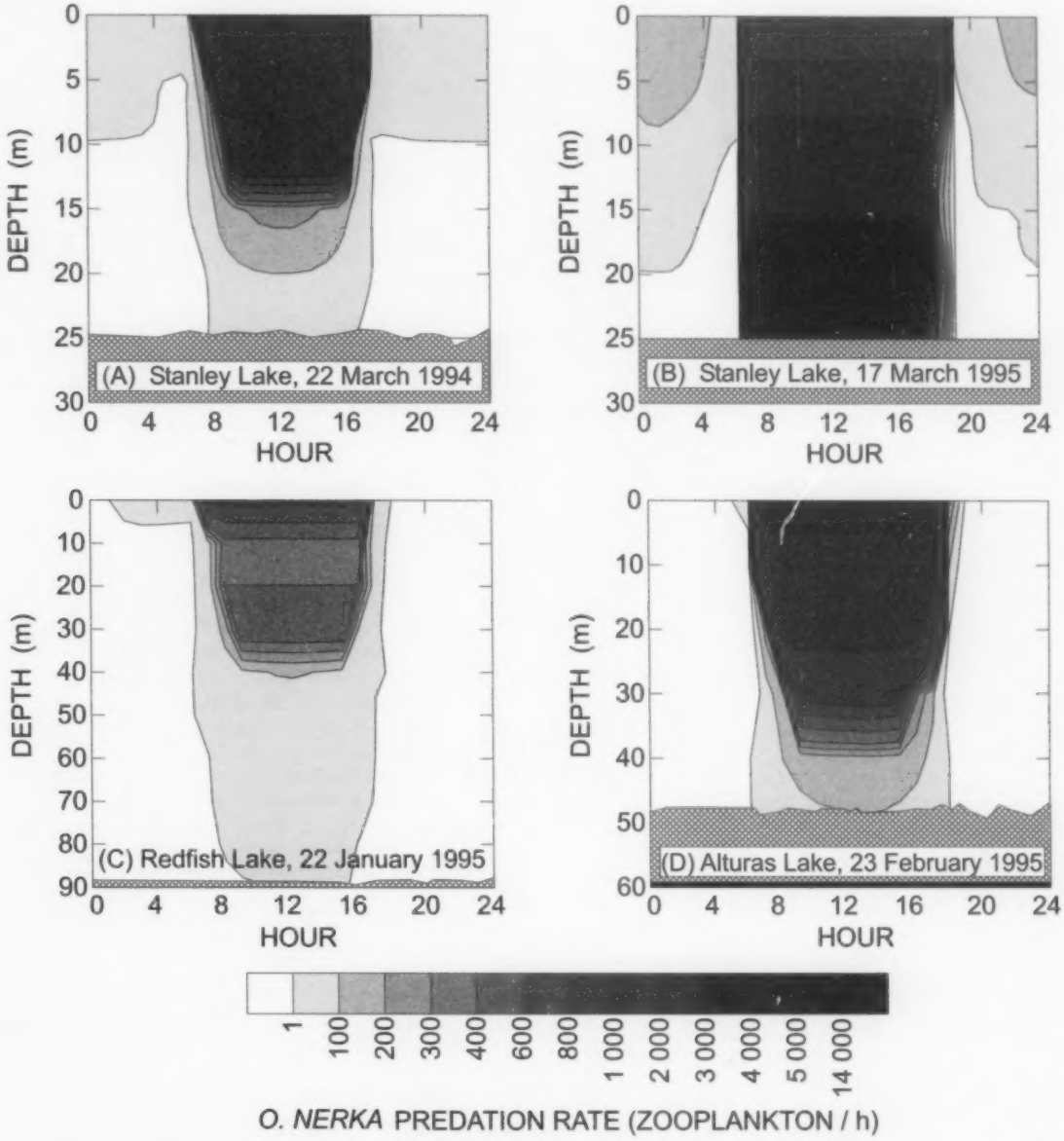

or seek refuge. In addition, *O. nerka* on the bottom would not have been detected by our transducers. Therefore, we were not able to fully describe nearshore fish populations or detect some deep or benthically oriented fish. Future studies should address the possibility of a diel onshore–offshore migration, especially since it may be more prominent during the winter when food may be limiting salmon growth and survival.

The predator avoidance hypothesis may cause diel changes in salmon distribution in these lakes during summer (Beauchamp et al. 1997) and may explain some of the migratory behavior seen in this study. Stanley Lake had the highest predation index (Table 2). As visual predators, lake trout also experience changes in foraging success based on light intensity. Data on lake trout foraging ability were not available, but Dolly Varden (*Salvelinus malma*), a closely related species, maintain maximum capture success to 0.6 lx and experience no capture success below 0.01 lx (Henderson and Northcote 1985). This suggests that lake trout foraging may be more light limited than *O. nerka* foraging; however, these data are for fish up to 30 cm, and larger fish may have better vision (Ali 1959). During the day, high light intensi-

© 1999 NRC Canada

Table 5. Foraging model predictions of consumption for different *O. nerka* migratory patterns in Stanley Lake.

	Consumption (% dry weight/day)	
Pattern of migration	March 1994	March 1995
No migration/remain shallow	0.075	0.26
No migration/remain deep	0.085	1.19
DVM	0.095	1.25
Increase in consumption due to DVM (%)	12	5

Note: The increase in consumption was calculated from the difference between no migration/remain deep and the observed pattern of DVM (shallow at night, deep during the day). For details of the model, see text.

ties in Stanley Lake would not provide any refuge from lake trout predation. At night, however, *O. nerka* migrated to the surface where light levels permitted their feeding but may have reduced the reactive distance of lake trout, or even prohibited their feeding. Unless more accurate information on lake trout foraging is available, the predator avoidance hypothesis cannot be ruled out.

Predator avoidance likely did not play a role in structuring the observed fish distribution in Redfish and Alturas lakes. There was no vertical migration of salmon seen in Redfish Lake, which had the lowest predation index (Table 2). Although we have few data on predator behavior during winter in Redfish Lake, observations from Stanley and Alturas lakes suggest that even in winter, there is some risk of predation (Teuscher and Taki 1995). In Alturas Lake, there was a slight downward migration of *O. nerka* during the day, and gillnetting indicated that bull trout were at least occasionally in the pelagic zone (G.B. Steinhart, unpublished data). Consequently, bull trout present a predation risk for *O. nerka*, as do northern squawfish (Kline 1994; Teuscher and Taki 1995). The short migration in Alturas Lake, however, would not have significantly reduced fish predation on *O. nerka*; according to the light data, intensities would still have allowed visually feeding bull trout to prey on them. Predator avoidance may have contributed to the DVM in Stanley Lake, but the lack of significant migrations in Alturas and Redfish lakes suggests that predation risk does not always influence fish migrations.

In winter, temperature was not likely a factor influencing vertical migrations of *O. nerka*. Only a small temperature gradient existed under the ice and should not have significantly affected growth. Bioenergetics simulations showed that juvenile *O. nerka* growth at 2.7°C is only 2% less than growth experienced at 4°C (G.B. Steinhart, unpublished data). During winter, it is reasonable to assume that changes in temperature are not a factor in determining the patterns of DVM of *O. nerka* in these lakes.

Given these results, it appears that feeding ability (a combination of foraging success and zooplankton density) best describes the patterns of *O. nerka* DVM in two of the three lakes during winter. Specifically, low light penetration through accumulated snow and ice limited foraging success of visually feeding salmon. Predator avoidance may stimulate salmon migrations in some other systems (Levy 1987, 1990*b*; Clark and Levy 1988; Bevelhimer and Adams 1993), but we did not see any vertical migrations to avoid predators in either Redfish Lake or Alturas Lake, but the cause of DVM in Stanley Lake is still undetermined. Low zooplankton densities and light-limited foraging success may have outweighed the risk of predation during these surveys. We suggest that in order to obtain adequate food in winter, *O. nerka* must be able to feed throughout the day and night. The advantages of continual feeding may outweigh the possible risks of predator avoidance in these systems. In summer, when zooplankton are more abundant, temperature effects and (or) predator density may alter these observed migration patterns. In fact, during summer, *O. nerka* in Redfish and Alturas lakes were typically found near the bottom during the day and in the metalimnion at night, while *O. nerka* in Stanley Lake stayed in shallow water to avoid the anoxic hypolimnion (Teuscher and Taki 1994; Beauchamp et al. 1997).

This study does not dispute any of the current hypotheses on *O. nerka* DVM; however, it does demonstrate that during periods of low zooplankton densities and low light intensities, foraging success may be the dominant factor in sculpting vertical migrations. This work also shows that *O. nerka* migrations vary significantly, both in similar systems and even within the same system during different times of year. This suggests that the behavior is very plastic and changes in response to the ambient conditions. Bevelhimer and Adams (1993) also emphasized that there is no set pattern for DVMs: they are a function of temperature, feeding ability, and predator density. As these variables change among lakes or seasons, the migratory behavior of fishes will also change.

Acknowledgments

Funding for this project came from the Ecology Center, Utah State University, and the Shoshonne-Bannock Indian Tribes (through the Bonneville Power Administration); however, the findings and conclusions presented by the authors are their own. We would also like to acknowledge all those people who helped collect the data necessary for this project: Odette Brandt, Phaedra Budy, Michelle Gregg, Howard Gross, Chad Mellison, Fredrick Norrsell, Rick Orme, John Ossowski, Mike Slater, and Darek Staab were all generous enough to help during rough field conditions. A special thank you goes to Doug Taki, David Teuscher, and Paul Kline for help in the field and sharing of data. We would also like to thank David Beauchamp, Dana Vaughan, Doran Mason, and two anonymous reviewers for comments on earlier drafts of this manuscript.

References

Ali, M.A. 1959. The ocular structure, retinomotor and photo-behavioral responses of juvenile pacific salmon. Can. J. Zool. **37**: 965–998.

© 1999 NRC Canada

Beauchamp, D.A., Luecke, C., Wurtsbaugh, W.A., Gross, H.G., Budy, P., Spaulding, S., Dillenger, R., and Gubala, C.P. 1997. Hydroacoustic assessment of abundance and diel distribution of sockeye salmon and kokanee in the Sawtooth Valley lakes, Idaho. N. Am. J. Fish. Manage. **17**: 253–267.

Bevelhimer, M.S., and Adams, S.M. 1993. A bioenergetics analysis of diel vertical migration by kokanee salmon, *Oncorhynchus nerka*. Can. J. Fish. Aquat. Sci. **50**: 2336–2349.

Brett, J.R. 1971. Energetic responses of salmon to temperature. A study of some thermal relations in the physiology and freshwater ecology of sockeye salmon (*Oncorhynchus nerka*). Am. Zool. **11**: 99–113.

Brett, J.R. 1983. Life energetics of sockeye salmon, *Oncorhynchus nerka*. *In* Behavioral energetics: the cost of survival in vertebrates. *Edited by* W.P. Aspey and I. Lustic. Ohio State University Press, Columbus, Ohio. pp. 29–63.

Brett, J.R., and Groves, T.D.D. 1979. Physiological energetics. *In* Fish physiology. Vol. 8. *Edited by* W.S. Hoar, D.J. Randall, and J.R. Brett. Academic Press, New York. pp 279–352.

Budy, P., Luecke, C., Wurtsbaugh, W.A., Gross, H.P., and Gubala, C. 1995. Limnology of the Sawtooth Valley lakes with respect to potential growth of juvenile Snake River sockeye salmon. Northwest Sci. **69**: 133–150.

Clark, A.N.W., and Levy, D.A. 1988. Diel vertical migrations by juvenile sockeye salmon and the antipredation window. Am. Nat. **131**: 271–290.

Cunningham, L. 1972. Vertical migrations of *Daphnia* and copepods under the ice. Limnol. Oceanogr. **17**: 301–303.

Dodson, S.I. 1975. Predation rates of zooplankton in arctic ponds. Limnol. Oceanogr. **20**: 426–433.

Eggers, D.M. 1978. Limnetic feeding behavior of juvenile sockeye salmon in Lake Washington and predator avoidance. Limnol. Oceanogr. **23**: 1114–1125.

Henderson, M.A., and Northcote, T.G. 1985. Visual prey detection and foraging in sympatric cutthroat trout (*Salmo clarki clarki*) and dolly varden (*Salvelinus malma*). Can. J. Fish. Aquat. Sci. **42**: 785–790.

Janiczek, P.M., and Young, A.J. 1987. Computer program for sun and moon illuminance with contingent tables and diagram. Circ. U.S. Nav. Observatory No. 171.

Johnston, N.T. 1990. A comparison of the growth of vertically-migrating and non migrating kokanee (*Oncorhynchus nerka*) fry. Can. J. Fish. Aquat. Sci. **47**: 486–491.

Kline, P. 1994. Research and recovery of Snake River sockeye salmon. Annu. Rep. 1993. Project No. 91-72. U.S. Department of Energy, Bonneville Power Administration, Portland, Oreg.

Koenings, J.P., Edmundson, J.E., Kyle, G.B., and Edmundson, J.M. 1987. Limnological field and laboratory manual: methods for assessing aquatic production. Alaska Dep. Fish Game FRED Div. Rep. Ser. No. 71.

Lampert, W. 1989. The adaptive significance of diel vertical migration of zooplankton. Funct. Ecol. **3**: 21–27.

Levy, D.A. 1987. Review of the ecological significance of diel vertical migrations by juvenile sockeye salmon (*Oncorhynchus nerka*). *In* Sockeye salmon (*Oncorhynchus nerka*) population biology and future management. *Edited by* H.D. Smith, L. Margolis, and C.C. Wood. Can. Spec. Publ. Fish. Aquat. Sci. No. 96. pp. 44–52.

Levy, D.A. 1990*a*. Reciprocal diel vertical migration behavior in planktivores and zooplankton in British Columbia lakes. Can. J. Fish. Aquat. Sci. **47**: 1755–1764.

Levy, D.A. 1990*b*. Sensory mechanism and selective advantage for diel vertical migration in juvenile sockeye salmon, *Oncorhynchus nerka*. Can. J. Fish. Aquat. Sci. **47**: 1796–1802.

Levy, D.A. 1991. Acoustic analysis of diel vertical migration behavior of *Mysis relicta* and kokanee (*Oncorhynchus nerka*) within Okanagan Lake, British Columbia. Can. J. Fish. Aquat. Sci. **48**: 67–72.

McCauley, E. 1984. The estimation of the abundance and biomass of zooplankton in samples. *In* A manual on methods of secondary productivity in freshwaters. 2nd ed. *Edited by* J.A. Downing and F. Rigler. Blackwell Scientific Publications, Cambridge, Mass. pp. 228–265.

Narver, D.W. 1970. Diel vertical movements and feeding of underyearling sockeye salmon and the limnetic zooplankton in Babine Lake, British Columbia. J. Fish. Res. Board Can. **27**: 281–316.

Neverman, D., and Wurtsbaugh, W.A. 1994. The thermoregulatory function of diel vertical migration for a juvenile fish, *Cottus extensus*. Oecologia, **98**: 247–256.

Sokal, R.R., and Rohlf, F.J. 1981. Biometry. W.H. Freeman and Company, New York.

Spaulding, S. 1993. Snake River sockeye salmon (*Oncorhynchus nerka*) habitat/limnology research. Annu. Rep. 1992. DOE/BP 22548-1. U.S. Department of Energy, Bonneville Power Administration, Portland, Oreg.

Steinhart, G.B. 1997. Winter limnology and the ecology of *Oncorhynchus nerka* in high-mountain lakes of Idaho. Master's thesis, Utah State University, Logan, Utah.

Teuscher, D.M., and Taki, D. 1994. Snake River sockeye salmon habitat and limnological research. Annu. Rep. 1993. DOE/BP 22548-2. U.S. Department of Energy, Bonneville Power Administration, Portland, Oreg.

Teuscher, D., and Taki, D. 1995. Snake River sockeye salmon habitat and limnological research. Annu. Rep 1994. DOE/BP 22548-3. U.S. Department of Energy, Bonneville Power Administration, Portland, Oreg.

Wetzel, R.G., and Likens, G.E. 1991. Limnological analyses. Springer-Verlag, New York.

Wurtsbaugh, W.A., and Neverman, D. 1988. Post-feeding thermotaxis and daily vertical migration in a larval fish. Nature (Lond.), **33**: 846–848.

© 1999 NRC Canada

Comparing results of a spatially explicit growth model with changes in the length–weight relationship of lake trout (*Salvelinus namaycush*) in Flaming Gorge Reservoir

Chris Luecke, M. William Wengert, and Roger W. Schneidervin

Abstract: We employed a spatially explicit simulation model to assess growth rate potential for lake trout (*Salvelinus namaycush*) in Flaming Gorge Reservoir, Utah–Wyoming. Late-summer water temperatures and forage fish densities in 168 habitat cells were collected from 1989 to 1996 and were used to estimate the potential growth of lake trout inhabiting each cell. Results of model simulations indicated that habitat quality for lake trout growth had decreased from 1990 to 1993. This decrease in lake trout growth rate potential was related to decreased forage fish densities during this period. Lake trout condition, as measured using length–weight analyses of individuals captured in spring gillnetting surveys, also decreased from the early 1990s to the mid-1990s. The change in the slope of the length–weight relationship was correlated with the proportion of habitat cells containing positive simulated growth rate potentials (r^2 = 0.60, p = 0.024). No significant correlation between the sum of growth rate potentials in habitat cells and changes in the slope of the length–weight relationship was apparent. These correlations suggest that spatially explicit models of habitat quality have relevance to the performance of individual organisms functioning in field environments.

Résumé : Nous avons utilisé un modèle de simulation spatialement explicite pour évaluer le taux potentiel de croissance du touladi (*Salvelinus namaycush*) dans le réservoir Flaming Gorge, qui chevauche la frontière entre l'Utah et le Wyoming. Nous avons mesuré dans la période 1989–1996 les températures de l'eau à la fin de l'été et les densités des poissons fourrage dans 168 cellules d'habitat; ces mesures ont été utilisées pour estimer la croissance potentielle des touladis de chacune de ces cellules. Les résultats des simulations réalisées au moyen du modèle ont montré que la qualité de l'habitat pour le touladi a diminué de 1990 à 1993. La diminution du taux potentiel de croissance du touladi ainsi observée était reliée à une baisse des densités de poissons fourrage durant cette période. La condition des touladis, établie au moyen d'analyses longueur–poids appliquées à des poissons capturés lors d'échantillonnages printaniers au filet maillant, a aissi diminué entre le début et le milieu des années 1990. Le changement dans la pente de la relation longueur–poids était corrélé avec la proportion de cellules d'habitat où on a obtenu à la simulation des taux potentiels de croissance positifs (r^2 = 0,60, p = 0,024). Nous n'avons observé aucune corrélation significative entre la somme des taux de croissance potentiels dans les cellules d'habitat et les changements dans la pente de la relation longueur–poids. Ces corrélations laissent penser que les modèles spatialement explicites de la qualité de l'habitat donnent une bonne indication de la performance des organismes en milieu natural.

[Traduit par la Rédaction]

Introduction

Spatially explicit models of potential growth rate of fishes have been proposed for numerous species occupying a variety of habitats (Brandt et al. 1992). These models have been used extensively to assess issues of habitat quality (Brandt and Kirsch 1993), fish behavior (Bevelheimer 1990), predator–prey interactions (Mason and Patrick 1993), and fisheries management (Luecke et al. 1996).

Although several different models have been proposed, all are similar in that they combine a foraging module with an energetics module to estimate the potential growth of an individual fish occupying a single habitat (Brandt et al. 1992; Luecke and Teuscher 1994; Mittelbach and Osenberg 1994). The foraging modules are based on a functional response or encounter rate model (Stockwell and Johnson 1997), and the energetics modules generally derive from published bioenergetics models (Hewett and Johnson 1992). The foraging module dictates how environmental conditions of food availability, physical habitat structure, and temperature determine the amount of food consumed by an individual fish. The energetics module dictates how this consumed energy is allocated to metabolic costs and growth (Brandt et al. 1992).

This type of model has been used extensively for salmonine fishes occupying a variety of habitats. The growth

Received October 14, 1997. Accepted October 30, 1998.
J14254

C. Luecke.[1] Department of Fisheries and Wildlife, Utah State University, Logan, UT 84322, U.S.A.
M.W. Wengert, Jr. Wyoming Game and Fish Department, Green River, WY 82935, U.S.A.
R.W. Schneidervin. Utah Division of Wildlife Resources, Dutch John, UT 84023, U.S.A.

[1]Author to whom all correspondence should be addressed.
e-mail: luecke@cc.usu.edu

© 1999 NRC Canada

Fig. 1. Maximum consumption of forage fish for a 2-kg lake trout. The solid line represents the temperature-dependent function present in Stewart et al. (1983). The broken line represents the changes to the maximum consumption used in our simulations.

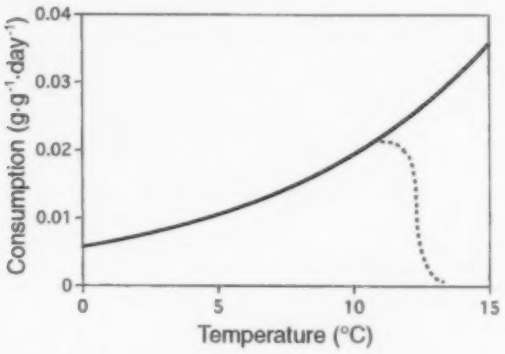

rate potential of salmonids in the Laurentian Great Lakes has been mapped using fine-scale acoustic estimates of forage fish abundance and temperature as habitat inputs (Mason et al. 1995). In smaller lakes the diel and seasonal shifts in salmonid behavior have been examined by estimating potential growth rate of planktivorous salmonids given changes in thermal structure and food availability (Bevelheimer 1990; Luecke and Teuscher 1994; Stockwell and Johnson 1997). In streams, potential growth rate has been used to assess habitat quality for salmonids (Hughes and Dill 1990; Hill and Grossman 1993; Addley 1993).

In spite of the extensive development and use of these models, few researchers have attempted to determine whether realized fish growth changes in ways similar to model predictions. In this paper, we compare the predictions of a previously developed model of lake trout (*Salvelinus namaycush*) growth potential with changes in the length–weight structure of lake trout in Flaming Gorge Reservoir in Utah–Wyoming. We demonstrate that significant changes have occurred in lake trout length–weight relationships from 1989 to 1997 and examine how changes in pelagic habitats can account for these growth differences. This type of comparison provides evidence of the relationship between estimates of habitat quality and salmonine performance in lacustrine habitats.

Methods

Potential growth rate simulations

We developed a model to simulate the growth rate potential of lake trout following the general procedures of Goyke and Brandt (1993). We estimated the potential growth rate of a 2-kg lake trout in Flaming Gorge Reservoir during the late summers of 1989–1996. The simulation model is based on a balanced energy budget given the biomass of forage fish consumed (C) and the allocation of this ingested energy into costs of standard metabolism (R), activity (A), wastes (urine (U) and feces (F)), and somatic growth (G):

$$(1) \qquad C = R + A + U + F + G.$$

The allocation of ingested energy derives from a bioenergetics model of lake trout growth processes (Stewart et al. 1983). We used the same functions and parameter values for metabolic costs as Stewart et al. (1983); however, we modified the original maximum consumption equations. Stewart et al. (1983) estimated maximum consumption as an exponential function of temperature and assumed that lake trout would not inhabit waters in which temperature exceeded 10.9°C. We modified Stewart et al.'s (1983) model to allow for consumption in water warmer than 10.9°C using Thornton and Lessem's (1978) temperature-dependent relationship for maximum consumption (C_{max}). Following the notation of Hewett and Johnson (1992),

$$(2) \qquad C_{max} = 0.0589W^{-0.307}f(T)$$

where W is the mass of an individual lake trout and $f(T)$ is the temperature-dependent function. For temperatures >12°C,

$$(3) \qquad f(T) = 0.01\ e^{4.243(15-T)}/1 + 0.01(e^{4.243(15-T)} - 1)$$

and for temperature <12°C,

$$(4) \qquad f(T) = 0.36\ e^{0.7445\ (T-5)}/1 + 0.36(e^{0.7445\ (T-5)} - 1)$$

where T is temperature (degrees Celsius). This algorithm allows maximum consumption to increase exponentially from 1 to 11°C, as in Goyke and Brandt (1993). Temperatures between 11 and 13°C provide >95% of maximum consumption. Maximum consumption decreases rapidly from 13 to 15°C (Fig. 1). This value for maximum consumption was used to truncate foraging by individual lake trout such that no individual could consume more food per day than was physiologically possible. In model simulations, wet mass energy density of a 2-kg lake trout was assumed to be 10.6 kJ·g^{-1} (Stewart et al. 1983) and energy density of forage fish 8.82 kJ·g^{-1} (Yule and Luecke 1993).

We also simplified the encounter rate function of Goyke and Brandt (1993) by assuming that lake trout swim through a field of stationary prey and encounter prey based on the volume of water scanned by a lake trout with a reaction distance of 0.5 m. We assumed that lake trout swam at an optimal rate (Stewart et al. 1983), searched for prey during nighttime hours only, and successfully captured all prey encountered. Our encounter rate function for a 2-kg lake trout searching for prey in Flaming Gorge Reservoir was

$$(5) \qquad E = \pi r^2 V$$

where r is the reaction distance and V is velocity (centimetres per second). The V is a function of lake trout body mass and water temperature (T) based on Stewart et al. (1983). For a 2-kg lake trout, $V = 17.1\ e^{0.0405T}$.

Forage fish spatial distribution

Inputs to the simulation model were forage fish biomass and water temperature in 10-m depth strata along 42 cross-reservoir transects. Previous midwater trawling surveys indicated that >90% of pelagic forage fish biomass consisted of kokanee (*Oncorhynchus nerka*) and Utah chub (*Gila atraria*). Hydroacoustic surveys were conducted in late summer along each transect using a BioSonics dual-beam (6 and 15°) echosounder (model 105). Samples were collected at night using a 420-kHz transducer towed near the front of the boat about 0.5 m below the surface. Acoustic samples were not collected in the bottom 1 m of the water column. Boat speed varied from 1 to 3 m·s^{-1}. The transducer and echosounder were calibrated approximately annually. A ping-pong ball was used as a field standard before each survey collection. During the years of our study, the source level varied from 216.64 to 217.05 dB and beam pattern factor ranged from 0.001 160 to 0.001 149. The pulse width for each survey was 0.4 ms. Acoustic samples were stored on DAT audiocassette tape and analyzed in four depth strata along each transect.

Initial analyses indicated that acoustic targets were dispersed enough to allow for counting of individual echoes. The target strength of each return echo was estimated using the BioSonics

© 1999 NRC Canada

dual-beam echo-counting software. Only acoustic targets between –51 and –37 dB were counted as forage fish (about 8–35 cm total length). Data were grouped within each of four depth strata (epilimnion (0–10 m), upper metalimnion (10–20 m), lower metalimnion (20–30 m), and hypolimnion (30–40 m)). The density and mean target strength of fish in each depth stratum of each transect were estimated, and the biomass of forage fish was calculated using Love's (1971) relationship between target strength and fish length:

$$(6) \quad \log(TL) = (TS + 64.1)/19.1$$

where TL is fish total length (millimetres) and TS is acoustic target strength (decibels).

Mass of individual forage fish was estimated from a length–weight relationship derived from Yule and Luecke (1993):

$$(7) \quad B = 0.000\,009\,11\ TL^{3.07}$$

where B is mass (grams) and TL is total length (millimetres). Forage fish density and lake trout catches in gill nets declined precipitously in waters deeper than 40 m, and thus, these waters were not used in the growth potential model.

Water temperatures

Profiles of water temperature were recorded at three stations on the reservoir corresponding to transects 4, 25, and 39. Mean temperature from 1-m depth intervals was estimated for each of the four depth strata and used as an input for the simulation model. The closest temperature site was used to estimate water temperatures of each transect.

Lake trout length–weight relationships

The length and weight of lake trout gillnetted during annual spring surveys of 1983–1997 were used to assess condition and growth relationships of lake trout in the reservoir (Cone 1989). Sinking monofilament gill nets (61 m long by 2.4 m high with 45-mm mesh) were set at six sites along the reservoir during the spring of each year from 1983 to 1997. Nets were set for 1 h at dawn. Netting began in late April and ended in early June of each year. At least six net-nights per year were sampled at each of the six sites during the survey period. More than 4000 lake trout were captured during this period. Lengths and weights were $\log_{10}$ transformed. Linear regression of transformed weights on transformed lengths was performed on data from each year.

We compared the annual variation in lake trout growth potential from model simulations with realized annual variation in lake trout growth as measured by the slope of the length–weight relationship (a measure of condition suggested by Cone 1989). Model simulations derived from environmental data collected in late summer, whereas the length–weight relationship was estimated from lake trout caught the following spring. This lag in the data comparison assumes that the length–weight relationship integrates growth conditions of the previous year. To complete this comparison, we integrated the growth rate potential from all habitat cells in the reservoir in two ways. First, we calculated the percentage of habitat cells that possessed positive growth potentials for each year. Second, we summed the value of potential growth rate in all of the positive cells in the reservoir for each year. We then correlated each of these indices of growth rate potential for lake trout in the reservoir with the slope of the realized length–weight relationship for the following spring to determine whether either of these indices of modeled growth reflected the interannual pattern in actualized growth.

Results

Forage fish spatial distribution

Densities of forage fish were greater in the upper reaches of the reservoir and in the 0–10 m stratum in most years of the survey (Fig. 2). The exception occurred in 1992 when high densities of fish targets were found in the lower portion of the reservoir (transects 1–22). Increase in forage fish abundance from the dam to the inflow of the reservoir corresponded to a general productivity (Yule and Luecke 1993).

Water temperatures

Water temperatures were similar among years (Table 1). The range in mean temperature within the 0–10 and 10–20 depth strata was <1.2°C among the sites Water temperatures in the 30–40 m depth stratum were higher in the upper portions of the reservoir because the depth of water in transects 36–42 ranged from 39 to 32 m.

Potential growth rate simulations

Results from the simulation model of lake trout potential growth rate indicated significant differences among years. The frequency of potential growth rates in each habitat cell indicated that 1989 and 1990 exhibited the highest growth conditions for lake trout,and that 1993 was the poorest year for potential growth rate (Fig. 3). An overall decline in growth rate potential was evident from 1989 to 1996. Years of the highest growth rate potential were 1989 and 1990, and years of the lowest growth rate potential were 1993 and 1995. A Kolmogorov–Smirnoff test indicated that differences in frequency distributions of potential growth between 1990 and 1993 were significant ($D_{max} = 21$, $p < 0.01$).

A plot of the spatial distribution of potential growth rate (Fig. 4) indicated that the metalimnetic region of the reservoir provided the best conditions for lake trout growth. Both epilimnetic (0–10 m) and hypolimnetic (30–40 m) regions showed generally negative growth rate potential. The 0–10 m stratum had low growth rate potential because temperatures were greater than those that support lake trout digestion. The 30–40 m stratum exhibited negative growth rate potential because of low forage fish abundances.

In the 10–20 and 20–30 m strata, growth rate potential was greatest in the inflow area (transects 36–42) and lowest in the canyon area (transects 1–20). General decrease in growth rate potential from the inflow to canyon area reflected the similar gradient in forage fish abundance.

Lake trout length–weight relationships

Linear regression of $\log_{10}$-transformed weight on $\log_{10}$-transformed length of individual lake trout captured in spring gillnet sets resulted in highly significant relationships for each year of the survey (r^2 values ranged from 0.967 to 0.988). A comparison of slopes indicated that significant differences in weight at length occurred among years ($F_{8,2113} = 8.92$, $p < 0.001$). The slope of the $\log_{10}$ length–weight relationship varied from a high of 3.81 in 1990 to a low of 3.38 in 1994 (Fig. 5). A von Bertalanffy multiple comparison of means indicated that the slopes of the $\log_{10}$ length–weight relationship were significantly different when comparing the 1983–1993 data with the 1994–1997 data. These slopes re-

© 1999 NRC Canada

Fig. 2. Spatial distribution of forage fish density in Flaming Gorge Reservoir from late-summer acoustic surveys, 1989–1996. Darker areas represent habitats with higher densities of forage fish. Data from 42 transects from the dam to the inflow are presented along the horizontal axis. Four depth strata are represented, with the surface of the reservoir at the top of each panel and 40 m at the bottom.

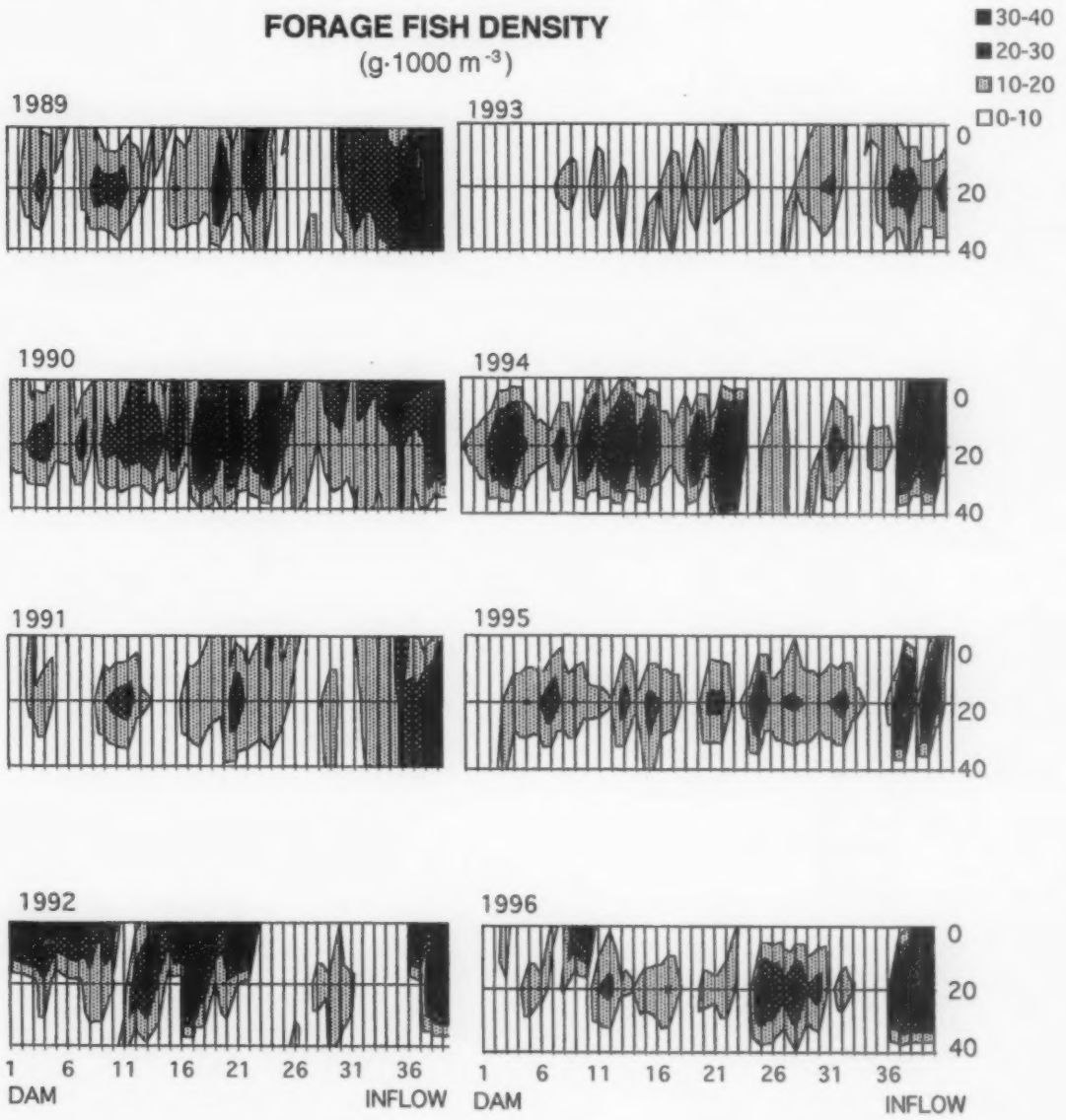

mained >3.6 during the early period and were reduced to <3.5 after 1993.

The *y*-intercepts of the $\log_{10}$ length–weight relationships negatively covaried with the slope (r^2 = 0.968). This negative relationship occurred because of a convergence of the length–weight relationships at about 600 mm. The similar weight of 600-mm lake trout captured in different years suggests that growing conditions for smaller lake trout varied little throughout the period of this research. The large differences in mean weight of 1000-mm lake trout among years (Fig. 6) indicated that growing conditions for these larger lake trout varied substantially among years.

The sum of growth rate potential from positive habitat cells was not significantly correlated with the slope of the length–weight relationship ($F_{1,6}$ = 1.22, p = 0.311) and explained only 16.9% of the variation in this slope (Fig. 7). These results suggest that this index of integrated lake trout growth potential was not a reliable measure of the performance of the fish. A significant correlation, however, between the percentage of habitat cells that contain positive

© 1999 NRC Canada

Table 1. Mean water temperatures (°C) along transect 4 during the late-summer acoustic surveys of 1989–1996.

	Depth (m)			
Year	0–10	10–20	20–30	30–40
1989	19.4	10.7	8.2	4.6
1990	19.8	10.7	8.0	4.8
1991	19.6	11.0	8.1	4.9
1992	19.6	11.2	8.4	5.1
1993	19.1	11.3	8.9	4.8
1994	19.9	10.2	8.3	4.2
1995	19.1	10.7	8.7	4.4
1996	19.8	10.9	8.9	5.4

Note: Mean water temperature in each of four depth strata was calculated by averaging water temperatures at 1-m intervals collected with a YSI thermistor.

potential growth rates and the slope of the length–weight relationship was observed ($F_{1,6} = 8.96$, $p = 0.024$) and explained 60% of the annual variation in this index of condition (Fig. 7).

Discussion

The spatially explicit simulation model of lake trout growth indicated that habitat quality (sensu Brandt et al. 1992) of Flaming Gorge Reservoir had decreased for lake trout from 1990 to 1996. This decrease was associated with a decline in the abundance of forage fish. Growth of individual lake trout, as measured by changes in the length–weight relationship, also declined during this period. This agreement between simulation model estimates of habitat quality and at least one measure of lake trout performance suggests that these relatively complex spatial models have heuristic value as predictors of effects of environmental change on the species of interest.

More detailed analyses of annual changes in modeled potential growth rate and actualized lake trout performance indicated that different measures of habitat quality had different degrees of relatedness to lake trout condition in the reservoir. Surprisingly, lake trout condition was not statistically related to total lake trout growth potential for the reservoir (as measured by summing the positive growth potential in each habitat cell) but rather was positively correlated with the amount of adequate habitat present (the proportion of habitat cells with positive growth potential).

A variety of other factors that were not accounted for in the simulation model could have influenced the growth of lake trout and weakened the correlation between actual and modeled lake trout growth characteristics. Annual variation in the density of lake trout and other piscivores in the reservoir could influence the behavior and feeding efficiency of individual lake trout. Smallmouth bass (*Micropterus dolomieu*), brown trout (*Salmo trutta*), and piscivorous rainbow trout were captured in the reservoir during the period of our study. Also, we estimated lake trout growth potential only during late summer but used an index of actual lake trout growth conditions that integrated environmental conditions present throughout the year. Goyke and Brandt (1993) documented varied lake trout growth potentials among different

Fig. 3. Frequency distribution of potential growth rates (1989–1996) from the spatially explicit simulation model for lake trout. The broken line represents a potential growth rate of zero.

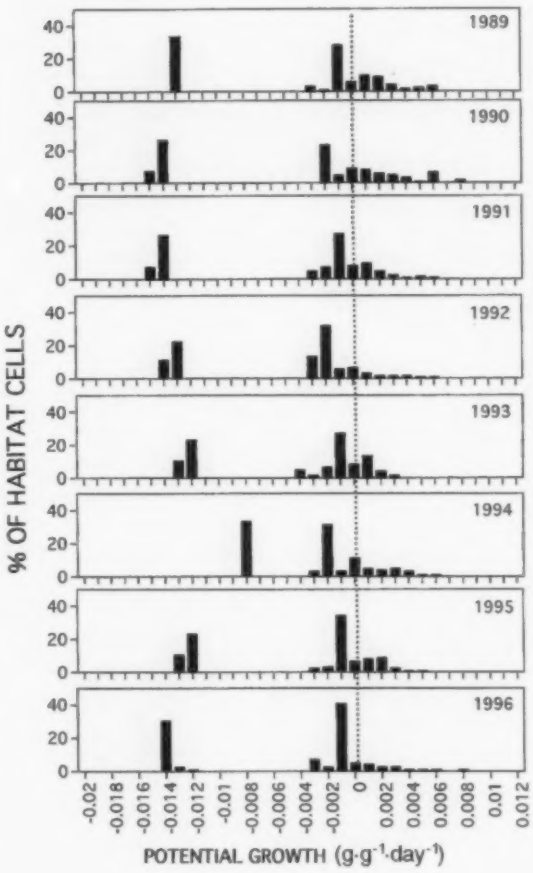

seasons in Lake Michigan. Lake trout growth potentials for Flaming Gorge Reservoir were estimated for May, July, and late August 1994 (Luecke and Canning 1996). Mean lake trout growth potential associated with these 1994 acoustic surveys indicated that May exhibited the highest growth potential. Lower water temperatures during spring reduce the metabolic costs associated with habitat cells with low forage fish densities. Estimates of growth rate potential for late August 1994 were similar to estimates for July of that year. High epilimnetic temperatures during summer reduced the volume of the reservoir that was suitable for lake trout growth. Our attempt to correlate late summer habitat conditions with annual lake trout growth may be flawed if this season accounts for only a small portion of annual lake trout energy gains. Another view, however, is that periods of energy scarcity (like late summer) may be most important to the performance of individual taxa.

One of the values of using spatially explicit habitat simulation models is that these models closely match the per-

© 1999 NRC Canada

Fig. 4. Spatial distribution of potential growth rates (1989–1996) from the simulation model for lake trout. Dark areas of the graph represent habitats with high growth rate potential. The horizontal axis depicts the 42 cross-reservoir transects conducted from the dam to the inflow area of the reservoir. The vertical axis represents depth from 0 m at the top of each panel to 40 m at the bottom.

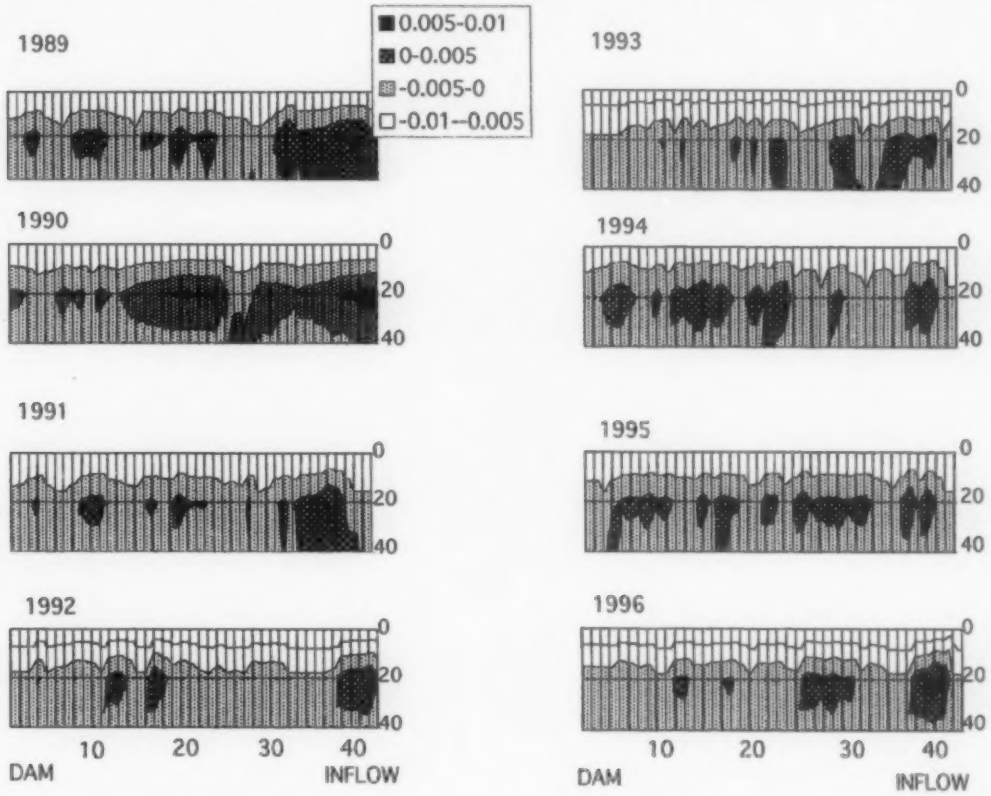

spective of an individual fish living in the environment. We chose to model the lake trout habitat at Flaming Gorge Reservoir at a spatial scale that resembles the daily home range of an individual lake trout. At that scale, most of the habitat cells cannot support positive lake trout growth. In all years of our study, the slope of the length–weight relationship exceeded the mean slope of 58 populations of lake trout throughout North America (Hubert et al. 1994). In order to grow at the rate suggested by the relatively steep slopes associated with the length–weight relationships present in Flaming Gorge Reservoir, individual lake trout must be very efficient at finding suitable habitat. In fact, catch of lake trout in gill nets was usually greatest in nets set on the bottom near the 20-m depth contour (R.W. Schneidervin, unpublished data).

The value of these types of models is also evident in the way in which complex, nonlinear relationships between fish growth and temperature, prey density, prey spatial distribution, and prey size can be integrated. In Flaming Gorge Reservoir, total forage fish abundance decreased by more than a factor of 2 from 1990 to 1996, yet modeled lake trout growth potential (the sum of all habitat cells) decreased by only 28%. This relatively small difference in growth potential appears consistent with the observed changes in the slope of the length–weight relationship and likely relates to changes in the species composition and spatial distribution of forage fish in the reservoir. During 1989–1990, catches of fish in vertical gill nets and purse seines indicated that Utah chub dominated the 0–10 m depth stratum whereas kokanee dominated the deeper strata (Yule and Luecke 1993). Catch of Utah chub has declined dramatically from 1990 to 1996, such that this species comprised <5% of the forage fish present in 1996 (Luecke and Canning 1996). The kokanee population size fluctuated, but no overall trend was apparent. The decline in Utah chub, an epilimnetic species, had only small effects on lake trout growth potential because modeled growth potential was limited by water temperatures in the upper strata during this time of year. The model's integration of temperature and forage fish spatial distributions resulted in this somewhat unexpected decoupling of lake trout

© 1999 NRC Canada

Fig. 5. Interannual variation in the slope and intercept of $\log_{10}$-transformed length–weight relationships for lake trout captured in spring gillnet surveys during 1983–1997. Error bars represent ±1 SE.

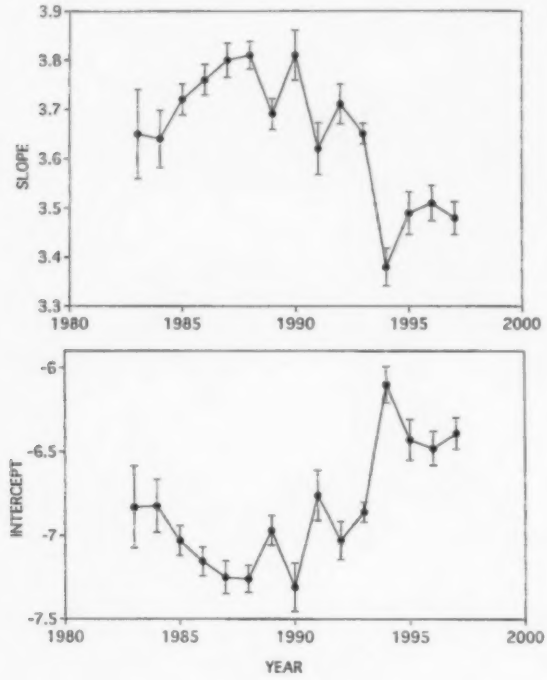

Fig. 6. Weight of 600- and 1000-mm lake trout from length–weight regressions, 1989–1996.

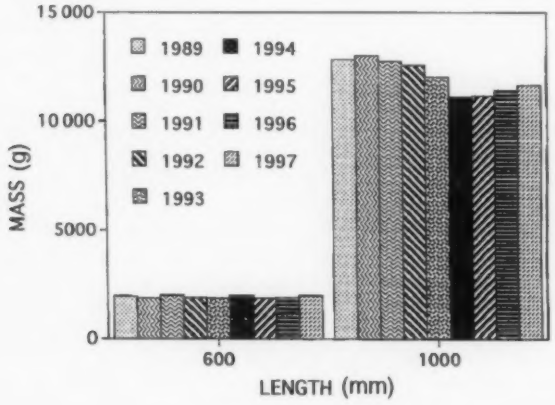

growth potential and abundance of Utah chub. This decoupling of piscivore growth and forage abundance has been observed in other analyses that combined bioenergetic processes and foraging theory (Mason et al. 1998).

Some attempt to relate the output of habitat quality models to the performance of organisms in these habitats is worthwhile. In this paper, we present one such attempt by relating the output from a spatially explicit growth potential

Fig. 7. Relationship between the slope of the length–weight relationship and the sum of potential growth rate of habitat cells with positive growth rate potentials (top panel) and the proportion of habitat cells with positive growth rate potentials (bottom panel).

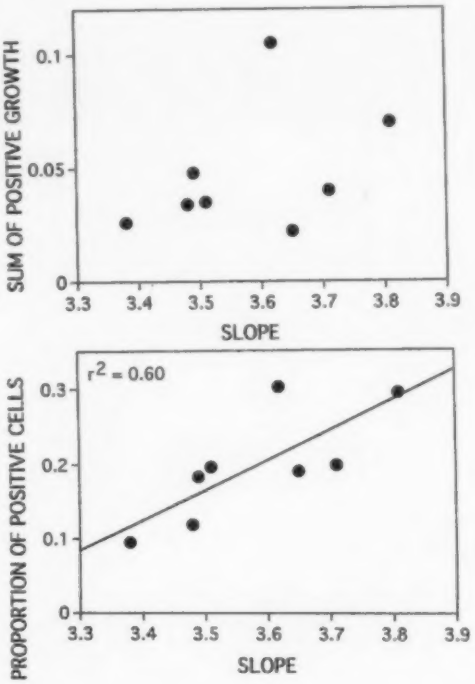

model to one index of the growth of lake trout. Our results lend support to the value of these types of models in that model results were correlated with performance characteristics of the fish population. Additional validation tests of these models are needed, however. Future experiments in which the growth rates of individual fish under specific habitat conditions are used to test predictions of spatially explicit habitat models would enhance our understanding of their scope and accuracy and lend credence to their value as tools for fisheries management.

Acknowledgments

We thank Steve Brayton and Ron Remick for assistance with data collection and data management. Dan Yule, Dave Teuscher, Mike Canning, and Michelle Gregg conducted some of the field sampling. The research was funded by the Utah Division of Wildlife Resources and the Ecology Center at Utah State University.

References

Addley, R.C. 1993. A mechanistic approach to modeling habitat needs of drift-feeding salmonids. M.S. thesis, Utah State University, Logan, Utah.

Bevelheimer, M.S. 1990. Habitat selection by kokanee salmon and smallmouth bass in thermally heterogeneous environments: the

© 1999 NRC Canada

importance of growth maximization to diel habitat shifts. Ph.D. dissertation, University of Tennessee, Knoxville, Tenn.

Brandt, S.B., and Kirsch, J. 1993. Spatially explicit models of striped bass growth potential in the Chesapeake Bay. Trans. Am. Fish. Soc. **122**: 845–869.

Brandt, S.B., Mason, D.M., and Patrick, E.V. 1992. Spatially-explicit models of fish growth rate. Fisheries (Bethesda), **17**: 23–31.

Cone, R.S. 1989. The need to reconsider the use of condition indices in fishery science. Trans. Am. Fish. Soc. **118**: 510–514.

Goyke, A., and Brandt, S.B. 1993. Spatial models of salmonine growth rate in Lake Ontario. Trans. Am. Fish. Soc. **122**: 870–883.

Hewett, S.W., and Johnson, B.L. 1992. Fish bioenergetics 2: a generalized bioenergetics model of fish growth for microcomputers. Univ. Wis. Sea Grant Tech. Rep. WIS-SG-92-250.

Hill, J., and Grossman, G.H. 1993. An energetic model of microhabitat use for rainbow trout and rosyside dace. Ecology, **74**: 685–698.

Hubert, W.A., Gipson, R.D., and Whaley, R.A. 1994. Interpreting relative weights of lake trout stocks. N. Am. J. Fish. Manage. **14**: 212–215.

Hughes, N.F., and Dill, L.M. 1990. Position choice by drift-feeding salmonids: model and tests for Arctic grayling in subarctic mountain streams, interior Alaska. Can. J. Fish. Aquat. Sci. **47**: 2039–2048.

Love, R.H. 1971. Dorsal-aspect target strength of an individual fish. J. Acoust. Soc. Am. **49**: 816–823.

Luecke, C., and Canning, M. 1996. Limnological and fisheries investigations of Flaming Gorge Reservoir. Utah. Div. Wildl. Res. Rep. 96-F-47-R,V.

Luecke, C., and Teuscher, D. 1994. Habitat selection by lacustrine rainbow trout within gradients of temperature, oxygen and food availability. *In* Theory and application in fish feeding ecology. *Edited by* D.J. Stouder, K.L. Fresh, and R.J. Feller. University of South Carolina Press, Columbia, S.C. pp. 133–150.

Luecke, C., Wurtsbaugh, W.A., Budy, P., Gross, H.P., and Steinhart, G. 1996. Simulated growth and production of endangered Snake River sockeye salmon: assessing management strategies for the nursery lakes. Fisheries (Bethesda), **21**: 18–25.

Mason, D.M., and Patrick, E.V. 1993. A model for the space–time dependence of feeding for pelagic fish populations. Trans. Am. Fish. Soc. **122**: 884–901.

Mason, D.M., Goyke, A., and Brandt, S.B. 1995. A spatially explicit bioenergetics measure of habitat quality for adult salmonines: comparison between Lakes Michigan and Ontario. Can. J. Fish. Aquat. Sci. **52**: 1572–1583.

Mason, D.M., Johnson, T.B., and Kitchell, J.F. 1998. Consequences of prey fish community dynamics on lake trout, *Salvelinus namaycush*, foraging efficiency in Lake Superior. Can. J. Fish. Aquat. Sci. **55**: 1273–1284.

Mittelbach, G.G., and Osenberg, C.W. 1994. Using foraging theory to study trophic interactions. *In* Theory and application in fish feeding ecology. *Edited by* D.J. Stouder, K.L. Fresh, and R.J. Feller. University of South Carolina Press, Columbia, S.C. pp. 45–60.

Stewart, D.J., Weininger, D.W., Rottiers, D.V., and Edsall, T.A. 1983. An energetics model for lake trout: application to the Lake Michigan population. Can. J. Fish. Aquat. Sci. **40**: 681–698.

Stockwell, J.D., and Johnson, B.M. 1997. Refinement and calibration of a bioenergetics-based foraging model for kokanee. Can. J. Fish. Aquat. Sci. **54**: 2659–2676.

Thornton, K.W., and Lessem, A.S. 1978. A temperature algorithm for modifying biological rates. Trans. Am. Fish. Soc. **107**: 284–287.

Yule, D.L., and Luecke, C. 1993. Lake trout consumption and recent changes in the forage fish assemblage of Flaming Gorge Reservoir. Trans. Am. Fish. Soc. **122**: 1058–1069.

© 1999 NRC Canada

Comparative examination of scale-explicit biological and physical processes: recruitment of Pacific hake (*Merluccius productus*)

John K. Horne, Paul E. Smith, and David C. Schneider

Abstract: The creation, maintenance, and destruction of aquatic organism distributions result from biological and physical processes that operate at different spatial and temporal scales. Rate diagrams plot and contour ratios of process rates as a function of spatial and temporal scale to summarize the relative importance of demographics, growth, and kinematics. We demonstrate the utility of this approach by examining physical and biological processes that influence the distribution and survival of larval and juvenile Pacific hake (*Merluccius productus*) in the California Current region. Processes that influence changes in hake biomass switch from mortality and drift among larvae to somatic growth and active locomotion among juveniles. Comparison of hake rate diagrams with those of capelin (*Mallotus villosus*) and Atlantic cod (*Gadus morhua*) show that dominant processes differ across scales, across life history stages, and across species.

Résumé : La création, le maintien et la disparition des aires de répartition des organismes aquatiques résultent de processus biologiques et physiques qui agissent à des échelles spatiales et temporelles différentes. Des diagrammes de taux et des rapports d'isolignes des taux des processus en fonction de l'échelle spatiale et temporelle sont présentés pour résumer l'importance relative des facteurs liés à la démographie, à la croissance et à la cinématique. Nous démontrons l'utilité de cette approche de par un examen des processus physiques et biologiques qui influent sur la répartition et la survie des larves et des juvéniles du merlu du Pacifique (*Merluccius productus*) dans la région du courant de Californie. Les processus qui influent sur la variation de la biomasse du merlu vont de la mortalité et de la dérive chez les larves à la croissance somatique et au déplacement actif chez les juvéniles. La comparaison des diagrammes du merlu avec ceux du capelan (*Mallotus villosus*) et de la morue franche (*Gadus morhua*) montre que les processus dominants varient selon l'échelle, l'étape du cycle vital et l'espèce.

[Traduit par la Rédaction]

Introduction

An ongoing challenge to aquatic scientists is applying results from process-oriented investigations to ecosystem conservation and management. Successful ecosystem management depends, in part, on scaling local results to regional or global scales. Unfortunately, direct extrapolation of results across scales is not always possible (Dayton and Tegner 1984; Carpenter et al. 1995; Thrush et al. 1997). "Scaling up" is particularly relevant to the design of aquatic studies where shiptime is limited and geographical areas of interest are extensive. One germane example is identifying the influence of biological and physical processes on the distribution, survival, and eventual recruitment of larval fish cohorts. Death of a single larva occurs at scales of centimetres and seconds, but the subsequent death of the adult cohort potentially spans thousands of kilometres and many years.

A factor that confounds identification of relevant biological and physical processes influencing biological quantities such as population abundance is the dependence of observed pattern on the scale of observation (e.g., Stommel 1963; Haury et al. 1978). Distributional patterns that are evident at one scale may not be evident when the measurement resolution is altered (e.g., Schneider and Piatt 1986). In aquatic environments, efforts to quantify scale-dependent pattern and process have traditionally focused on populations of particles or organisms that drift with water motion (e.g., Platt and Denman 1975; Powell et al. 1975; Horwood 1978). Parallel examinations of mobile organism distributions are not as common (e.g., Horwood and Cushing 1978) but are increasing in number (e.g., Weber et al. 1986; Schneider 1994*a*; Horne and Schneider 1997). Explicit treatment of scale is rapidly becoming standard practice (e.g., Giller et al. 1994; Schneider 1994*b*; Peterson and Parker 1998) when quantifying distribution patterns and the relevance of biological and physical processes.

One approach used to quantify the relative importance of biological and physical processes to distributions of biological quantities such as changes in fish biomass compares ratios of rates. To illustrate through example, Platt (1981) analyzed the relative contributions of phytoplankton growth

Received December 18, 1997. Accepted July 15, 1999.
J14351

J.K. Horne.[1] Cooperative Institute for Limnology and Ecosystems Research, 2205 Commonwealth Bouelvard, Ann Arbor, MI 48105, U.S.A.
P.E. Smith. Southwest Fisheries Center, National Marine Fisheries Service, 8604 La Jolla Shores Drive, La Jolla, CA 92038, U.S.A.
D.C. Schneider. Ocean Sciences Centre, Memorial University of Newfoundland, St. John's, NF A1C 5S7, Canada.

[1]Author to whom all correspondence should be addressed.
e-mail: horne@glerl.noaa.gov

© 1999 NRC Canada

and particle diffusion to the formation of a characteristic phytoplankton patch size using a dimensionless ratio (Bridgman 1922). When values of dimensionless ratios equal 1, they indicate time and space scales where biological and physical rates are similar in magnitude and processes potentially interact. Schneider et al. (1997) labeled these as "critical" time and space scales. For phytoplankton patches, this is the predicted scale where horizontal diffusion is balanced by phytoplankton production. The application of dimensional analysis to evaluate the relative importance of biological and physical processes can be extended to include demographic (i.e., natality, mortality), growth, and kinematic (i.e., locomotion, drift) terms (e.g., Horne and Schneider 1994; Schneider et al. 1997).

Dimensionless ratios computed in these two examples were based on the few biological and physical rates that can be extracted from the literature. The extent of critical scales was obtained by drawing contour lines using biological knowledge of the organisms of interest. An alternate approach (Schneider et al. 1999) extracts dimensionless rates of biological and physical processes from the literature and then uses extensive computation to calculate ratio values at all possible scales. Collectively, these three studies show that ratio values are not constant over all spatial and temporal scales and that critical scales are not limited to a single spatial and temporal scale. Neither the literature extraction nor the computation methods use extensive data or incorporate variability in biological processes such as natality or age-dependent mortality when computing dimensionless ratios.

In this paper, we use an extensive data set with a 45-year biological history to examine how biological and physical processes influence the distribution and survival of larval and juvenile fish. Pacific hake (*Merluccius productus*) is used as an illustrative example, as the genus is present in all of the world's eastern and some western boundary current regions, it has the largest biomass of any demersal species within its latitudinal range (25–55°N), and recruitment rates can vary over two orders of magnitude in adjacent years (Hollowed 1992; Dorn et al. 1993). We then compare dimensionless ratio values from hake with those for other fish species derived using literature values or extensive computations.

Forming dimensionless ratios

Rate diagrams use dimensionless ratios to summarize knowledge of biological and physical processes across spatial and temporal scales. The derivation of ratios used in rate diagrams is detailed in Schneider (1991) and Horne and Schneider (1994). A brief outline will be provided here. There are five steps when generating rate diagrams: (*i*) state the quantity of interest, (*ii*) choose an analytic perspective, (*iii*) write an equation incorporating all potential sources of variability, (*iv*) calculate dimensionless ratios, and (*v*) plot and contour ratio values using all available data.

Quantities of interest in this study are concentrations of larval B_l and juvenile B_j Pacific hake biomass in the eastern Pacific. Biomass concentration B is defined as the number of organisms N multiplied by the average mass of an individual M per unit volume V. We chose a Eulerian or fixed grid perspective to encompass the offshore spawning and nearshore nursery area of hake along the southern coast of California. Schneider et al. (1997) compared Eulerian with Lagrangian derivation of rates used when forming dimensionless ratios.

Proportional changes in the distribution of aquatic biomass B_0, in this case larval and juvenile hake biomass, are a net result of the expansion or contraction of the volume occupied $\dot{V}$, the flux F of organisms through boundaries of the volume, the net reproductive rate r, and the somatic growth rate m:

$$(1)\quad \underset{\text{Biomass distribution}}{B_0} = \underset{\text{Volume occupied}}{-\dot{V}} + \underset{\text{Flux}}{F} + \underset{\text{Demo - graphics}}{r} + \underset{\text{Growth}}{m}$$

All terms in eq. 1 have units percent per unit time. The two kinematic terms $\dot{V}$ and F can be further partitioned by separating changes in biomass due to passive drift with the surrounding fluid (fl) and from those due to active locomotion (loc):

$$(2)\quad -\dot{V} + F = -\dot{V}_{fl} - \dot{V}_{loc} + F_{fl} + F_{loc}.$$

The demographic term r can be categorized into the per capita birth rate r_b and the per capita death rate r_d. If data are available, then the per capita death rate can be further partitioned into natural r_n (e.g., starvation or predation) and harvesting r_h mortality:

$$(3)\quad r = r_b - r_d = r_b - r_n - r_h.$$

To determine the relative importance of these biological and physical sources of variation, dimensionless ratios (cf. Taylor 1974; Langhaar 1980) were formed using terms in eqs. 1–3. All terms must have the same units, which allows ratios to be formed in any combination relative to a process of interest such as mortality (e.g., Schneider 1992). Alternatively, dimensionless ratios can be formed using functional groups (Fischer et al. 1979) or can be combined in biologically reasonable groups.

The first ratio of interest is changes in biomass due to somatic growth m compared with biomass changes due to population dynamics. The population dynamics label is applied to demographic (i.e., r) and kinematic (i.e., $\dot{V}$ and F) terms. Because the range of observation is set to encompass all spawning and brood areas used by hake in the eastern Pacific over the last three decades, there is no change in biomass concentration due to changes in volume occupied. The resulting population dynamics term is a combination of net recruitment r and flux F of individuals in or out of the population:

$$(4)\quad \frac{m}{r+F}.$$

The second ratio evaluates the relative importance of population dynamics terms by comparing changes in biomass due to demographic r and kinematic F terms:

$$(5)\quad \frac{r}{F}.$$

A demographic ratio compares changes in biomass due to recruitment with those due to mortality:

© 1999 NRC Canada

(6) $\frac{r_b}{r_d}$.

Because the quantities of interest are larval and juvenile hake biomass, sources of mortality will not be partitioned to natural and harvesting mortality in this study. The fourth dimensionless ratio examines the relative importance of kinematic terms. Flux in biomass due to organism locomotion is compared with that due to passive drift with the fluid:

(7) $\frac{F_{loc}}{F_{fl}}$.

Methods

Data for estimating mortality and growth rates of larval and juvenile Pacific hake were extracted from the California Cooperative Oceanic Fisheries Investigations (CalCOFI) database from 1951 through 1995 (see Hewitt 1988 for a review of the program). Larval fish surveys were not conducted in 1967–1968, 1970–1971, 1973–1974, 1976–1977, 1979–1980, and 1982–1983. The latitudinal extent of quarterly larval surveys was reduced during 1985–1994.

Hake spawning and movement

Hake, the most abundant ichthyoplankton species in the eastern Pacific, is commercially valuable and important to the biological oceanography of western North America (Francis 1983; Smith 1995). Adult hake occupy a narrow feeding habitat near the continental shelf break for 6–8 months in an area extending from California in the south to British Columbia in the north (Alverson and Larkins 1969; Francis 1983; Methot and Dorn 1995). Following a southern migration in winter (Alverson and Larkins 1969; Alheit and Pitcher 1995), 95% of adult hake spawning occurs between December 19 and March 6 in a 300 000-km^2 area offshore of California and the Baja Peninsula (Ahlstrom and Counts 1955; Hollowed 1992; Smith 1995). Embryos and larvae remain offshore for 4–6 months. Juveniles are found on the Californian continental shelf in an ill-defined brood area (Berry and Perkins 1965; Bailey et al. 1986; Woodbury et al. 1995). Most of the interannual per capita recruitment variability occurs during the first 4 months of life (Hollowed 1992), but the relative importance of biological and physical mechanisms influencing recruitment has not been clearly demonstrated. Bailey and Francis (1985) found that recruitment exceeded the average in 11 of 18 warmer than average years (>14.8°C at the surface) during 1960–1977. Recruitment, indexed by the abundance of 2-year-old fish, did not exceed the average in all seven of the colder than average years (<14. 8°C at the surface) during the same period. Previous studies (Smith 1975; Bailey 1980) showed that cold water temperatures coincided with southern and offshore shifts in adult hake spawning locations, but it has not been proven whether the absence of large cohorts born during "cold years" is a direct or indirect result of water temperature.

In this study, we arbitrarily define the spawning and brood areas using the CalCOFI grid system: the southern boundary is set at Punta Eugenia (line 120), the northern boundary at San Francisco (line 60), the seaward boundary at station 120, and the spawning–brood boundary at station 60 (Fig. 1). We apportion the annual adult migration as 50% of the year (183 days) spent in the northern feeding area, 18% (66 days) spent in transit to the spawning grounds, 21% (76 days) resident in the spawning area, and 11% (40 days) spent in transit to the adult feeding area. All spawning is assumed to occur within the delineated spawning area. Spawning rates per adult female and survival rates of eggs and larvae are also assumed constant. Larvae are defined as fish less than 20 mm (Smith 1995; Ambrose 1996). We have further assumed that active swimming by adults and passive transport of eggs and larvae with water currents are uniform. We estimate that the linear distance traveled by adults to the spawning area is 1100 km (cf. Alverson and Larkins 1969; Wilson et al. 1997) and that the rate of progress is 20 cm·s^{-1} or nominally 0.4 body length (bl)·s^{-1} (cf. Alheit and Pitcher 1995). Neither the stimuli to which the adult hake respond while migrating nor the stimuli that cause them to stop and spawn are known. Larvae begin to appear in mid-December and smaller larvae are not readily found after the first week of March (Smith 1995). Northerly movement by adults continues through the feeding season (Dorn 1996).

Hake population models

Mortality and growth rates used in dimensionless calculations are derived from Lefkovitch stage-based models (Lefkovitch 1965) of hake abundance, survival, and growth in the California Current region (Smith 1995). Nine life history stages were collapsed by summation into embryo, larval, juvenile, and adult stages. The models use rates of adult maternity and mortality, larval mortality and stage duration, and juvenile stage duration. Adult maternity is defined as the number of fertilized eggs that survive one time step (i.e., day) per female adult. We have assumed that mortality is identical throughout the embryonic period, as little is known about survival postfertilization in open water. Adult natural mortality is assumed equal to that used in virtual population methods (Francis 1983). An equilibrium model of the population is fitted by tuning the juvenile mortality rate (Smith 1985, 1995). Juvenile mortality was adjusted using the size-based mortality rate of Peterson and Wroblewski (Peterson and Wroblewski 1984; Butler et al. 1993). Stage mortalities and adult fecundities are considered representative of demographic and somatic growth rates. The demographic output from the model summarizes the production at the beginning of each stage (i.e., natality and growth) and losses during the stage (i.e., mortality). Somatic growth rates for each stage are estimated using the initial weight-at-stage and duration-within-stage from model output (Smith 1995).

Larval hake production and mortality rates across the continental shelf were characterized using a series of exponential regression models fitted to hake catch-at-size data. Data used in the regressions are taken from CalCOFI cruises conducted from 1951 to 1995. Geographic coverage and seasonal sampling intensity have varied over this time span. Stations were grouped into 74-km (40 nautical miles) distance intervals i from shore. Hake larvae were divided into nine length-classes starting at 2.75 mm and incremented by 2 mm to a maximum length of 18.75 mm. The mean abundance of hake larvae in each size-class was tabulated for each station interval i. The density of larvae was then plotted as a function of size-class for each distance interval. The slope of the resulting z_i curve is proportional to the instantaneous mortality z_i (percent per day) across size-classes. The intercept of the curve with the ordinate is proportionate to the instantaneous production $\hat{n}_0$. The number of larvae n_i at any distance interval can then be modeled as a function of instantaneous production $\hat{n}_0$ in each interval and mortality z_i across size-classes:

(8) $n_i = \hat{n}_{0_i} e^{-z_i}$.

Instantaneous production and mortality indices were compared across the continental slope by plotting intercepts and slopes for each distance interval.

Rate diagrams

Rate diagrams provide a framework to evaluate the relative importance of processes that potentially influence the distribution of any biological quantity of interest. In this example, we qualitatively summarize the relative importance of biological and physical processes to changes in larval and juvenile hake biomass as a function of spatial and temporal scale. Where possible, values for each

© 1999 NRC Canada

Fig. 1. Pacific hake larval and juvenile habitat within the CalCOFI sampling area. The arbitrary spawning area is shaded and extends from San Francisco (line 60) in the north to Punta Eugenia (line 120) in the south. The seaward boundary is set at station 120. The unshaded zone represents the brood area of older larvae and juveniles at the time of recruiting to the coastal slope and shelf habitat. The brood area boundary is set at station 60. See Hewitt (1988) for a summary of the CalCOFI sampling program.

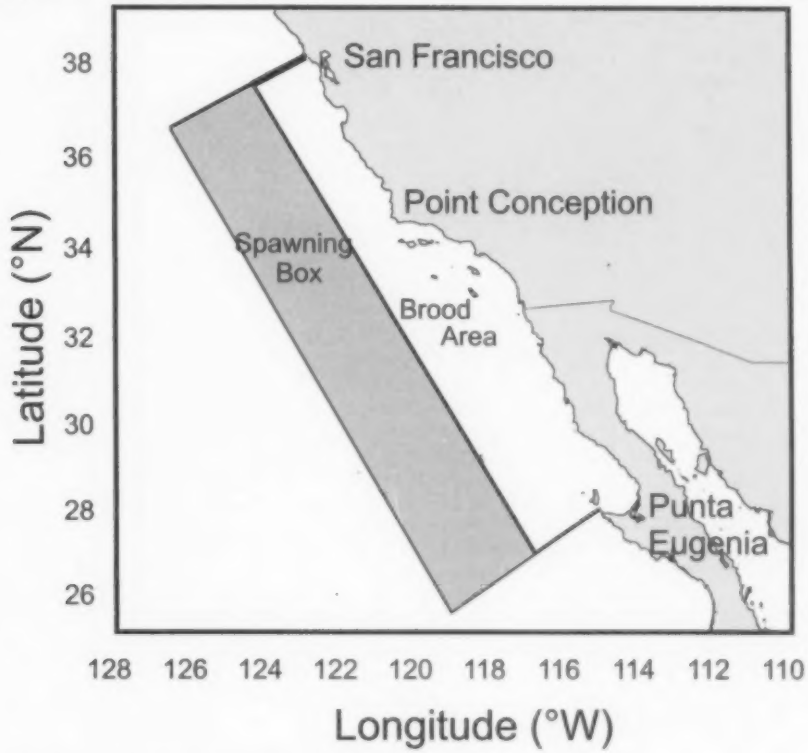

Table 1. Pacific hake life history parameters from the Lefkovitch matrix model.

Stage	Fecundity (no. embryos·day^{-1})	Mortality (day^{-1})	Duration (days)	Initial weight (g)	Length range (cm)
Embryo	0	0.135	16	9.05×10^{-4}	Egg–0.4
Larva	0	0.076	100	3.05×10^{-4}	0.4–2.0
Juvenile	0	0.0042	602	1.21×10^{-2}	2.0–33.3
Adult	120	0.0005	6570	26.3	33.3–62

ratio were calculated at discrete spatiotemporal scales for larval and juvenile hake using CalCOFI hake data, output from Lefkovitch population models, and velocities of the California Current system. Current vector velocities for the California Current, the California Current Extension, and the Coastal Jet were measured from average annual surface current charts (U.S. Hydrographics Office 1947). Dimensions of all terms in ratios are percent per unit time. Order of magnitude calculations show whether the absolute value of any dimensionless ratio was less than, equal to, or greater than 1 at a specified scale. Nominal values (>1, =1, <1) for each ratio were then plotted as a function of spatial and temporal scale for larval and juvenile hake. Ratio values >1 indicate the predominance of processes in the numerator, values =1 indicate a potential coupling between processes in the numerator and denominator, and values <1 indicate that processes in the denominator dominate over those in the numerator. Contour lines drawn on rate diagrams indicate spatial and temporal scales where dimensionless ratios change value. If data at all scales were not available, ratio values were extended across all scales in the plane. The construction of a rate diagram is an iterative process. Ratio values and contour locations should be adjusted as additional data and knowledge become available. No contours were added to hake rate diagrams.

Results

Matrix growth parameters

The Lefkovitch matrix model produces growth parameters for embryonic, larval, juvenile, and adult Pacific hake life history stages. The model assumes population stationarity and stable age distributions and that juvenile parameters can be tuned to comply with other life history stages. The CalCOFI database and the Lefkovitch matrix model combine to provide realistic estimates of adult fecundity, instantaneous mortality, stage duration, weight-at-stage, and length range during each stage (Table 1). Fecundity is restricted to the adult life stage. Instantaneous mortality decreases with age, while stage duration, weight, and length all increase with life history stage. Parameter values from the model are

© 1999 NRC Canada

Fig. 2. Dimensionless ratio values of larval (circles) and juvenile (squares) Pacific hake biomass distribution in the eastern Pacific. (*a*) Somatic growth to population dynamics (demographics minus kinematic fluxes), $m/r - F$; (*b*) demographic (natality, mortality) to kinematic fluxes (passive drift, active locomotion), r/F; (*c*) demographics, r_b/r_d; (*d*) kinematic fluxes, F_{loc}/F_{fl}. Symbol shading indicates value of dimensionless ratio calculations: open, <1; half solid, =1; solid, >1.

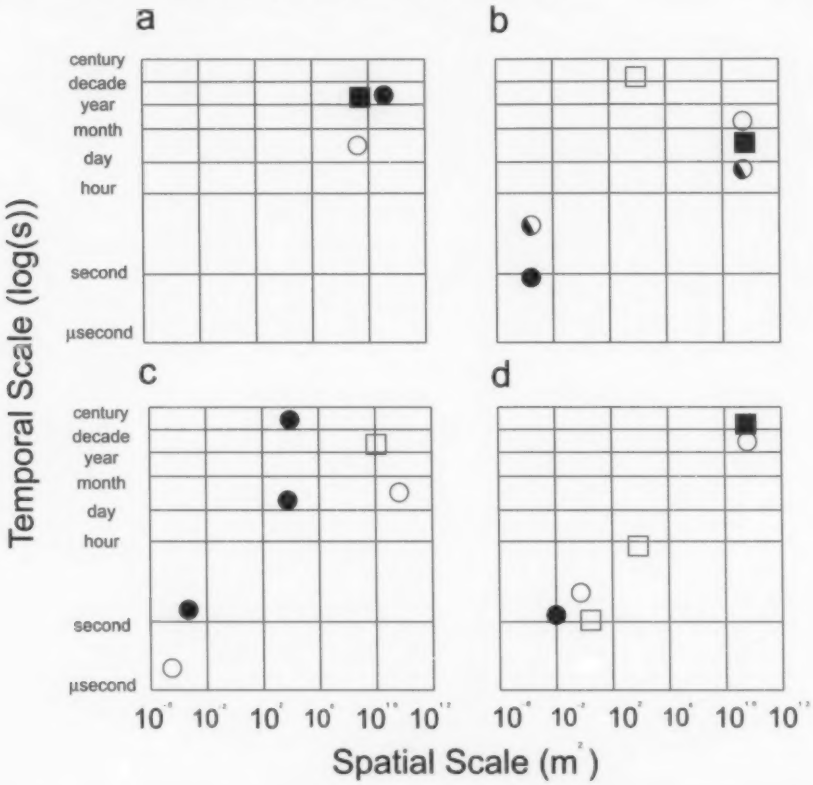

used to compute mortality and somatic growth rates in dimensionless ratios at specific spatial and temporal scales.

Rate diagrams

The rate diagram of the somatic growth to population dynamics ratio (Fig. 2*a*) indicates that changes in hake larval biomass concentration due to somatic growth exceed those due to demographic and flux processes at the scale of a spawning season. From the time that eggs are first laid until larvae are transported out of the spawning area, individual fish biomass increases from about 5×10^{-4} to 7×10^{-2} g or 140% of the birth weight (Smith 1995). Annual recruitment is 100% of the cohort, and virtually all of the biomass fluxes out of the spawning area. The resulting value of the somatic growth to population dynamics ratio is >1 (140%·season^{-1}/100%·season^{-1}). At daily scales, changes in biomass due to somatic growth are less than those due to demographics and the flux of larvae out of the spawning area and the ratio is <1 (1.84%·day^{-1}/–13.91%·day^{-1}).

Four values were calculated for the larval demographics to kinematics dimensionless ratio (Fig. 2*b*). Changes in larval hake biomass due to demographics at temporal scales larger than an annual cycle are balanced by those due to kinematics in the spawning area (100%·season^{-1}/100%·season^{-1}). Over an annual cycle, changes in biomass due to active and passive flux (≈100%·year^{-1}) greatly exceed those due to net recruitment (≈2.21%·year^{-1}) (see below). On a daily basis during an average spawning season of 76 days, the ratio of recruitment to kinematics is approximately equal, as follows. The spawning rate of hake averages 1.3% of eggs·day^{-1} and larval mortality averages 13%·day^{-1} (Smith 1995), which results in a net recruitment rate of 1.13%·day^{-1}. Passive flux of larvae from the midline of the spawning box to the eastern boundary (222 km), based on a net eastern transport by the Coastal Jet (1 cm·s^{-1} south) and the California Current (4 cm·s^{-1} southeast), is 1.48%·day^{-1}. Consequently, the ratio of net recruitment to kinematics will be 1.13%·day^{-1}/1.5%·day^{-1}. If all surviving larvae leave the spawning area, the flux of eggs averaged over the spawning season is 2.21% of egg production per day out of the spawning area. At the scale of the 76-day spawning season, biomass changes due to egg deposition exceed those due to flux of eggs with water currents.

Persistence of a population requires that biomass changes due to natality and somatic growth must equal or exceed those due to mortality at the largest temporal and spatial scales. Since there is a net flux out of the spawning area, the demographics ratio will exceed a value of 1 (Fig. 2*c*). At the scale of a spawning season (76 days), natality does not exceed 14%·week^{-1} and larval mortality is estimated at

© 1999 NRC Canada

13%·day^{-1} (Smith 1995). The resulting value of the demographic ratio is <1. At the scale of a spawning event by an aggregation (≈10^6 m^2 over a 24-h cycle) or a spawning pair (≈10^{-1} m^2, minutes), natality exceeds mortality and the value of the ratio exceeds 1. Ratio values are <1 at spatiotemporal scales of an individual organism dying (square millimetres, seconds).

The rate diagram of the kinematics ratio (Fig. 2*d*) indicates the dominance of passive flux over active locomotion across most spatiotemporal scales. Fluxes of larvae due to drift with tides, currents, and upwellings exceed fluxes due to active locomotion except over very short time scales. If an egg is released at the midpoint in the northern half of the spawning area, the net drift is 3.8 cm·s^{-1} eastward. About 68 days would elapse for these larvae to drift 222 km to the boundary of the juvenile brood area. Residence times in the spawning area average 102 days (Smith 1995), so an additional 34 days can be attributed to active locomotion. There is a net 1%·day^{-1} movement from the midline of the spawning area to the boundary of the juvenile brood area. At the scale of a day, drift of larvae out of the spawning box (3.28 km·day^{-1}) exceeds that due to average locomotion to remain within the spawning box (1.67 km·day^{-1}). The resulting value of the ratio (0.51) is <1. The kinematic ratio will only exceed a value of 1 at the time and space scale of a larval swimming burst.

In the juvenile hake rate diagrams, the growth to population dynamics ratio (Fig. 2*a*) is >1 at the scale of the coastal brood area. Changes in biomass due to somatic growth rate (500% over a 2-year residence period, Smith 1995) exceed those due to changes in recruitment (58% mortality) and changes due to active flux (100%) of 2-year-old fish to the adult population. Since growth is a continuous process and juvenile fish remain in the brood area, all other values of the ratio were set at >1.

At spatiotemporal scales greater than a brood cycle (about 2 years), the rate diagram of the demographic to flux ratio (Fig. 2*b*) indicates that changes in biomass due to the flux of juveniles into and out of the brood area (100% in 2 years) exceed those due to recruitment (58% mortality by age 2, Smith 1995). Even if the flux of larvae into the brood area is considered juvenile "natality," changes in biomass due to natality and mortality do not exceed the net flux of biomass out of the brood area. A newly recruited juvenile hake weighs 7 × 10^{-2} g when leaving the spawning area and 0.155 kg at the end of the second year of life (Smith 1995). At temporal scales of a year or less, biomass changes due to juvenile natality (100%·year^{-1}) and mortality (41%·year^{-1}) exceed those due to active (41.3% of age-2 fish survive and leave) or passive flux (0%) out of the brood box. The value of the ratio is >1 (59%·year^{-1}/41.3%·year^{-1}).

The demographics rate diagram (Fig. 2*c*) depicts a ratio <1 at the scale of a juvenile brood cycle (i.e., 2 years). Changes in biomass due to mortality over a biannual residence period will exceed those due to natality of juveniles from the spawning area.

The continuous presence of juvenile hake in the brood area over year to decade scales implies that absolute changes in biomass due to active flux exceed those due to drift out of the area with the California Current (Fig. 2*d*). Episodic events (e.g., upwellings) and large-scale water movements (e.g., currents) can change the value of the ratio to <1 over shorter temporal scales throughout the brood area.

The computation of rate diagrams for larval and juvenile hake qualitatively summarizes the relative importance of biological and physical processes influencing survival and distribution of early life history stages. Processes that influence changes in hake biomass switch between the spawning and brood areas at the scale of a spawning season. Changes in larval hake biomass are dominated by mortality and drift with prevailing currents.

Hake survival analyses

The distribution of larval hake densities across the spawning area illustrates the influence of mortality, growth, and drift on spatial and temporal changes in hake biomass. All catches-at-length from all years sampled during CalCOFI cruises are grouped by length and contoured. Larval fish (2.75 mm) are concentrated within the spawning area centered at station 5 (about 80 km offshore) from mid-January to mid February (Fig. 3*a*). Larvae are also present further offshore of the primary patch at lower concentrations centered at station 10 (about 400 km offshore) during February. At 6.75 mm total length the primary patch remains centered on station 5, but densities have dropped by an order of magnitude (Fig. 3*b*). Larvae isolated from the primary group are moving further offshore during March along with remnants of the offshore patch. Diffuse concentrations of 12.75-mm hake larvae remain within the spawning area (Fig. 3*c*). Concentrations of hake are no longer present beyond 200 km from shore.

Survival of hake larvae is maximized within the spawning box, 200–400 km offshore. Indices of production and mortality are plotted in Fig. 4 at the midpoint of each distance interval. The cross-shelf production index increases with distance offshore, peaking at a distance of 260 km, and then decreasing further seaward. The mortality index is around –0.91 up to 186 km offshore and then increases to around –1.04 in distance intervals beyond 260 km.

Discussion

Rate diagrams enable the relative importance of competing processes to be evaluated at any scale of interest. Rate diagrams are thus useful in identifying relevant sampling scales for process-oriented research. Prior to designing an early life history survey of Pacific hake, it is logical to ask "is drift with currents important to recruitment, and if so, over what scales should the California Current be examined?" From hake life history, we know that the adult spawning season lasts about 76 days each year and occurs offshore from the San Francisco area in the north to Baja, Mexico, in the south. The northern and southern limits of spawning shift among years due to water temperature (Horne and Smith 1997), but suitable spawning "habitat" is assumed to exist along the length of the coast. If we assume that all initial larval movement inshore is net drift with currents, then potential larval transport is 3.87 cm·s^{-1} or 3.34 km·day^{-1}. The spawning box (Fig. 1) covers an area of about 600 000 km^2. At the spatiotemporal scale of a spawning season, the rate diagram for the ratio of larval growth to population dynamics (Fig. 2*a*) indicates that demographic

© 1999 NRC Canada

Fig. 3. Areal density of larval Pacific hake at (*a*) 2.75 mm, (*b*) 6.75 mm, and (*c*) 12.75 mm total length, contoured as a function of month and distance offshore. All hake catches from all years are used in contour plots. Size-classes are not directly related to age.

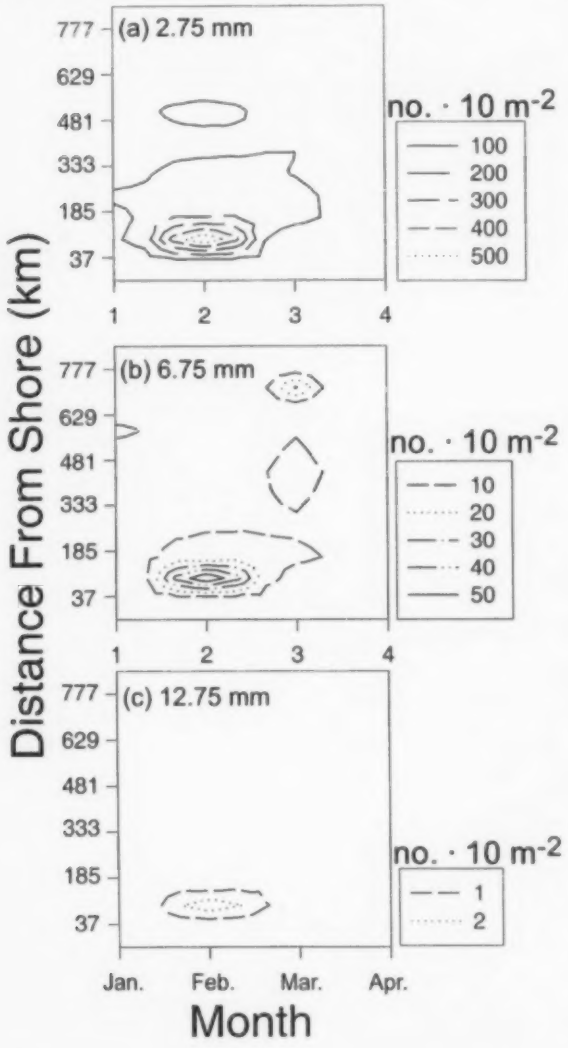

and kinematic processes are more important than growth processes. The ratio of demographic to kinematic rates (Fig. 2*b*) is <1, although at smaller temporal scales, demographic and kinematic processes may be important to the recruitment of hake. Further comparison shows that kinematic processes are dominated by flux out of the spawning area (Fig. 2*d*) and that mortality exceeds changes in biomass due to natality (Fig. 2*c*). When the focus is shifted to juvenile hake, changes in biomass due to somatic growth exceed those due to drift with currents (Fig. 2*a*). Over the course of a spawning season, larval research effort should focus on drift and mortality at a scale of days to months and kilometres.

The anticipated importance of drift and mortality to larval

Fig. 4. Production and mortality indices of catch-at-length curves for 74-km distance intervals offshore within the CalCOFI sampling grid. Slopes are proportional to instantaneous mortality rates estimated using an exponential model. Intercepts of the exponential curve with the ordinate are proportional to instantaneous production.

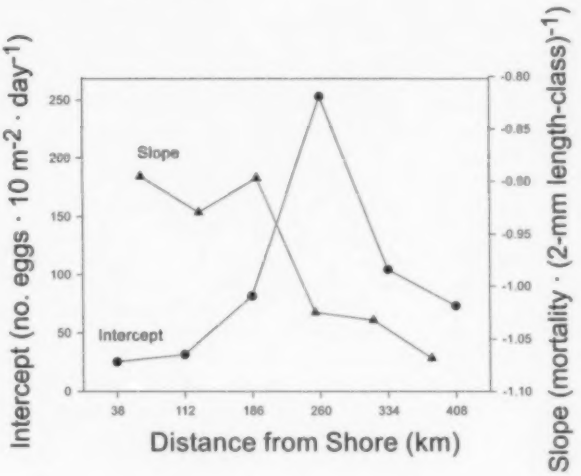

hake survival (Fig. 2) was then examined by drawing contour plots of larval density (Fig. 3) and then plotting production and mortality indices as a function of distance from shore (Fig. 4). Larval hake that are spawned or drift offshore survive through March at 6.75 mm but are not present in larger length-classes. Increased survival of larval hake is associated with high spawn production. A plateau in larval hake instantaneous mortality occurs just inshore of the peak in hake production. This result suggests inshore transport of surviving older hake larvae and indicates a potential offshore limit for increased hake survival. The coincidence of increased production and decreased mortality in hake starkly contrasts with patterns observed in two co-occurring fish species with coincident spawning and brood areas: northern anchovy (*Engraulis mordax*) and Pacific sardine (*Sardinops sagax*). Anchovy and sardine spawn is concentrated well inshore of hake production, and mortality generally increases with distance from shore (see fig. 7 in Smith et al. 2000). Despite differences in peak adult spawning location, critical spatial and temporal scales for passive kinematics (i.e., drift) and mortality are similar among these three co-occurring species.

Rate diagrams for larval and juvenile hake share some features included in rate diagrams for capelin (*Mallotus villosus*) (Horne and Schneider 1994) and Atlantic cod (*Gadus morhua*) (Schneider et al. 1999). The "critical scale" envelope observed in the larval hake rate diagram is not identical to that in juveniles. The critical scale envelope observed in mortality to movement rate diagrams for all life history stages of cod was also present in the larval and juvenile hake demographic to kinematic rate diagrams. A comparable envelope may exist in the capelin demographics to kinematic rate diagram (cf. fig. 1*b* in Horne and Schneider 1994), although the data are too sparse to be certain. It is worth noting that computation of ratios used in rate dia-

© 1999 NRC Canada

grams for capelin (Horne and Schneider 1994), cod (Schneider et al. this volume), and hake differs in the amount of data used to calculate dimensionless rates. Capelin rate diagrams were based on published literature values, which were few in number. Cod rate diagrams were based again on published values from the literature, augmented by extensive computation based on rough estimates of movement rates. Hake diagrams were based on extensive and relatively detailed spatial data from the CalCOFI program, augmented by computations from a population model that has been verified against survey data. A critical scale envelope (Schneider et al. 1999) is consistent with the results of capelin and hake diagrams, but further applications are needed to test the generality of these envelopes.

The approach used to identify important processes that generate spatial variance in fish density differs from the approach used to identify characteristic phytoplankton patch scales. The application of classical dimensional analysis (Bridgman 1922) to the analysis of phytoplankton patches balances the dissipating force of horizontal diffusion with the concentrating force of phytoplankton reproductive rates. The two processes converge at a critical scale where cell production equals export because of the reduction in patch perimeter relative to patch area (Skellam 1951; Kierstead and Slobodkin 1953). This approach assumes that discrete patches exist, and the objective was to determine the critical patch size. But discrete patches do not persist in the ocean, and mixing will import as well as export phytoplankton from a patch. In contrast, the approach used to evaluate biological and physical processes influencing changes in fish distribution and critical scales nests small compartments within larger compartments and can be termed "coarse graining." With this method, the resolution of measurement is arbitrarily set and multiscale analysis is accomplished by examining the ratio of two rates at multiple resolutions. The analytic procedure is analogous to removing walls of contiguous compartments to create larger compartments within the same area, so that the distance over which averages are computed increases. Coarse graining examines how the dynamics of a quantity of interest change over a continuous range of measurement resolution scales. It is interesting to note that a single critical scale is obtained when just two values are used to compare rates (as in the classical work on critical patch size). More complex dynamics emerge when values reported at several scales are combined, whether by drawing contour lines by hand (Horne and Schneider 1994; Schneider et al. 1997) or by coarse graining (Schneider et al. 1999).

It is not yet clear whether an Eulerian (i.e., fixed) perspective or a Lagrangian (i.e., moving) perspective is more appropriate for examining the relative importance of competing rates. The hake and cod studies in this volume use an Eulerian perspective, in contrast with earlier Lagrangian studies (Schneider 1991, 1993; Horne and Schneider 1994; Schneider et al. 1997). These Lagrangian formulations omitted a kinematic term, the expansion and contraction of the boundaries drawn around finite areas (Schneider et al. 1997). Computation of this kinematic term would require enough information on the location of marked individuals or groups to be able to plot and then measure boundaries at several points in time. This is rarely possible for marine organisms, and hence, the Lagrangian approach requires the assumption that boundaries drawn around finite areas do not expand and contract to a great degree.

Rate diagrams make explicit the relative importance of concomitant processes, which act to generate, maintain, or reduce spatial variance in population density. Rate diagrams constructed to date make it evident that there is no single critical scale at which one rate prevails over another. Instead, populations of marine organisms exhibit more complex dynamics, where the relative importance of concomitant process will vary, depending on spatial and temporal scale. The multiscale approach differs from more traditional approaches to population dynamics of exploited species, for which surveys and assessments are carried out at a single spatial scale (that of the stock) and a single temporal resolution (typically an annual survey). Our results, for the analysis of hake, show that it is possible to combine multiscale analysis with traditional methods for analyzing exploited species. Rate diagrams (Fig. 2), with their capacity to reveal complex dynamics at multiple scales, proved useful in guiding analysis of the spatial dynamics of hake (Figs. 3 and 4). Better integration of multiscale analysis with traditional population analysis remains, however, a major challenge.

Acknowledgments

This work was supported in part by the National Science Foundation (OCE-9415740 to S.B. Brandt), the New York Sea Grant Institute (NA46RG0090 to S.B. Brandt, J.K.H., J. Tyler, and G. Sprules), the Fisheries Society of the British Isles (travel grant to J.K.H.), and the Natural Sciences and Engineering Research Council of Canada (fellowship support to J.K.H. and long-term research funding to D.C.S.). We thank Drs. R.A. Neal, S.B. Brandt, and two anonymous reviewers for comments that improved the manuscript. This is GLERL contribution No. 1134.

References

Ahlstrom, E.H., and Counts, R.C. 1955. Eggs and larvae of the Pacific hake, *Merluccius productus*. Fish Bull. U.S. **56**: 295–329.

Alheit, J., and Pitcher, T.J. 1995. Hake: biology, fisheries and markets. Chapman and Hall, London, U.K.

Alverson, D.L., and Larkins, H.A. 1969. Status of the knowledge of the Pacific hake resource. Calif. Coop. Oceanic Fish. Invest. Rep. **13**: 24–31.

Ambrose, D.A. 1996. Merlucciidae: hakes. *In* The early stages of fishes in the California Current region. *Edited by* H.G. Moser. Calif. Coop. Oceanic Fish. Invest. Atlas, **33**: 508–509.

Bailey, K.M. 1980. Recent changes in the distribution of hake larvae: causes and consequences. Calif. Coop. Oceanic Fish. Invest. Rep. **21**: 167–171.

Bailey, K.M., and Francis, R.C. 1985. Recruitment of Pacific whiting, *Merluccius productus*, and the ocean environment. Mar. Fish. Rev. **47**: 8–15.

Bailey, K.M., Francis, R.C., and Mais, K.F. 1986. Evaluating incidental catches of 0-age Pacific hake to forecast recruitment. Calif. Coop. Oceanic Fish. Invest. Rep. **27**: 109–112.

Berry, F.H., and Perkins, H.C. 1965. Survey of pelagic fishes of the California Current area. Fish. Bull. U.S. **65**: 625–682.

Bridgman, P.W. 1922. Dimensional analysis. Yale University Press, New Haven, Conn.

Butler, J.L., Smith, P.E., and Lo, N.C.H. 1993. The effect of natural variability of life-history parameters on anchovy and sardine

© 1999 NRC Canada

population growth. Calif. Coop. Oceanic Fish. Invest. Rep. **3**: 104–111.

Carpenter, S.J., Chisholm, S.W., Krebs, C.J., Schindler, D.W., and Wright, R.F. 1995. Ecosystem experiments. Science (Washington, D.C.), **269**: 324–327.

Dayton, P.K., and Tegner, M.J. 1984. The importance of scale in community ecology: a kelp forest example with terrestrial analogs. *In* A new ecology: novel approaches to interactive systems. *Edited by* P.W. Price, C.N. Slobodchikof, and C.N. Gaud. Wiley, New York. pp. 457–481.

Dorn, M.W. 1996. Status of the coastal Pacific whiting resource in 1995. *In* Pacific Fishery Management Council, status of the Pacific groundfish fishery through 1995 and recommended acceptable biological catches in 1996. Pacific Fishery Management Council, Metro Center, Suite 420, 2000 SW First Ave, Portland, OR 97201, U.S.A. pp. A1–A52.

Dorn, M.W., Nunnallee, E.P., Wilson, C.D., and Wilkins, M.E. 1993. Status of the coastal Pacific whiting resource in 1993. NOAA Tech. Memo. F/AFSC-47.

Fischer, H., List, E.J., Koh, R.C.Y., Imberger, J., and Brooks, N.H. 1979. Dimensional analysis. *In* Mixing in inland and coastal waters. Academic Press, New York. pp. 23–29.

Francis, R.C. 1983. Population and trophic dynamics of Pacific hake (*Merluccius productus*). Can. J. Fish. Aquat. Sci. **40**: 1925–1943.

Giller, P.S., Hildrew, A.G., and Rafaelli, E. (*Editors*). 1994. Aquatic ecology: scale, pattern and process. Blackwell, Oxford, U.K.

Haury, L.R., McGowan, J.A., and Wiebe, P.H. 1978. Patterns and processes in the time–space scales of plankton distributions. *In* Spatial pattern in plankton communities. *Edited by* J.H. Steele. Plenum Press, New York. pp. 277–327.

Hewitt, R.P. 1988. Historical review of the oceanographic approach to fishery research. Calif. Coop. Oceanic Fish. Invest. Rep. **29**: 27–41.

Hollowed, A.B. 1992. Spatial and temporal distribution of Pacific hake larvae *Merluccius productus*, and estimates of survival during early life stages. Calif. Coop. Oceanic Fish. Invest. Rep. **33**: 100–123.

Horne, J.K., and Schneider, D.C. 1994. Analysis of scale-dependent processes with dimensionless ratios. Oikos, **70**: 201–211.

Horne, J.K., and Schneider, D.C. 1997. Spatial variance of mobile aquatic organisms: capelin and cod in Newfoundland coastal waters. Philos. Trans. R. Soc. Lond. B. Biol. Sci. **352**: 633–642.

Horne, J.K., and Smith, P.E. 1997. Space and time scales in Pacific hake recruitment processes: latitudinal variation over annual cycles. Calif. Coop. Oceanic Fish. Invest. Rep. **38**: 90–102.

Horwood, J.W. 1978. Observations on spatial heterogeneity of surface chlorophyll in one and two dimensions. J. Mar. Biol. Assoc. U.K. **58**: 487–502.

Horwood, J.W., and Cushing, D.H. 1978. Spatial distributions and ecology of pelagic fish. *In* Spatial pattern in plankton communities. *Edited by* J.H. Steele. Plenum Press, New York. pp. 355–382.

Kierstead, H., and Slobodkin, L.B. 1953.The size of water masses containing plankton blooms. J. Mar. Res. **12**: 141–147.

Langhaar, H.L. 1980. Dimensional analysis and the theory of models. Krieger Publishing, Huntington, N.Y.

Lefkovitch, L.P. 1965. The study of population growth in organisms grouped by stages. Biometrics, **21**: 1–18.

Methot, R.D., and Dorn, M.W. 1995. Biology and fisheries of north Pacific hake (*M. productus*). *In* Hake: biology, fisheries and markets. *Edited by* J. Alheit and T.J. Pitcher. Chapman and Hall, London, U.K. pp. 389–414.

Peterson, D., and Parker, T. (*Editors*). 1998. Scale issues in ecology. Columbia University Press, New York.

Peterson, I., and Wroblewski, J.S. 1984. Mortality rate of fishes in the pelagic ecosystem. Can. J. Fish. Aquat. Sci. **41**: 1117–1120.

Platt, T. 1981. Thinking in terms of scale: introduction to dimensional analysis. *In* Mathematical models in biological oceanography. *Edited by* T. Platt, K.H. Mann, and R.E. Ulanowicz. UNESCO Press, Paris. pp. 112–121.

Platt, T., and Denman, K.L. 1975. Spectral analysis in ecology. Annu. Rev. Ecol. Syst. **6**: 189–210.

Powell, T.M., Richerson, P.J., Dillon, T.M., Agee, B.A., Dozier, B.J., Godden, D.A., and Myrup, L.O. 1975. Spatial scales of current speed and phytoplankton biomass fluctuations in Lake Tahoe. Science (Washington, D.C.), **189**: 1088–1090.

Schneider, D.C. 1991. The role of fluid dynamics in the ecology of marine birds. Oceanogr. Mar. Biol. Annu. Rev. **29**: 487–521.

Schneider, D.C. 1992. Thinning and clearing of prey by predators. Am. Nat. **139**: 148–160.

Schneider, D.C. 1993. Scale-dependent spatial dynamics: marine birds in the Bering Sea. Biol. Rev. Camb. Philos. Soc. **68**: 579–598.

Schneider, D.C. 1994*a*. Scale-dependent patterns and species interactions in marine nekton. *In* aquatic ecology: scale, pattern and process. *Edited by* P.S. Giller, A.G. Hildrew, and E. Rafaelli. Blackwell, Oxford, U.K. pp. 441–467.

Schneider, D.C. 1994*b*. Quantitative ecology. Academic Press, San Diego, Calif.

Schneider, D.C., and Piatt, J.F. 1986. Scale-dependent correlation of seabirds with schooling fish in a coastal ecosystem. Mar. Ecol. Prog. Ser. **32**: 237–246.

Schneider, D.C., Walters, R., Thrush, S., and Dayton, P. 1997. Scale-up of ecological experiments: density variation in the mobile bivalve *Macomona liliana*. J. Exp. Mar. Biol. Ecol. **216**: 129–152.

Schneider, D.C., Bult, T., Gregory, R.S., Methven, D.A., Ings, D.W., and Gotceitas, V. 1999. Mortality, movement, and body size: critical scales for Atlantic cod (*Gadus morhua*) in the Northwest Atlantic. Can. J. Fish. Aquat. Sci. **56**(Suppl. 1). This issue.

Skellam, J.G. 1951. Random dispersal in theoretical populations. Biometrika, **78**: 196–218.

Smith, P.E. 1975. Pacific hake larval distribution and abundance. SWFC Admin. Rep. LJ-75-83. Southwest Fisheries Center, National Marine Fisheries Service, La Jolla, Calif.

Smith, P.E. 1985. Year-class strength and survival of 0-group clupeoids. Can. J. Fish. Aquat. Sci. **42**(Suppl. 1): 69–82.

Smith, P.E. 1995. Development of the population biology of the Pacific hake, *Merluccius productus*. Calif. Coop. Oceanic Fish. Invest. Rep. **36**: 144–152.

Smith, P.E., Horne, J.K., and Schneider, D.C. 2000. Life history strategies of anchovy, sardine and hake in the California Current: comparison of spatial dynamics of the pre-recruit stages. ICES J. Mar. Sci. In press.

Stommel, H. 1963. Varieties of oceanographic experience. Science (Washington, D.C.), **139**: 572–576.

Taylor, E.S. 1974. Dimensional analysis for engineers. Clarendon Press, Oxford, U.K.

Thrush, S.F., Pridmore, R.D., Bell, R.G., Cummings, V.J., Dayton, P.K., Ford, R., Grant, J., Green, M.O., Hewitt, J.E., Hines, A.H., Hume, T.M., Lawrie, S.M., Legendre, P., McArdle, B.H., Morrisey, D., Schneider, D.C., Turner, S.J., Walters, R.J., Whitlatch, R.B., and Wilkinson, M.R. 1997. The sandflat habitat: scaling from experiments to conclusions. J. Exp. Mar. Biol. Ecol. **216**: 1–9.

U.S. Hydrographics Office. 1947. Atlas of surface currents, northeastern Pacific Ocean. Publ. No. 570. U.S. Hydrographics Office, Washington, D.C.

Weber, L.H., El-Sayed, S.Z., and Hampton, I. 1986. The variance

© 1999 NRC Canada

spectra of phytoplankton, krill and water temperature in the Antarctic Ocean south of Africa. Deep-Sea Res. **33**: 1327–1343.

Wilson, C., Pierce, S., Kosro, P.M., Dorn, M., and Smith, R. 1997. Ocean currents and the distribution of Pacific whiting (*Merluccius productus*) along the Pacific coast during summer 1995. *In* Changing oceans and changing fisheries: environmental data for fisheries research and management. *Edited by* G.W. Boehlert and J.D. Schumacher. NOAA-TM-NMFS-SWFSC No. 239.

Woodbury, D., Hollowed, A.B., and Pearce, J.A. 1995. Interannual variation in growth rates and back-calculated spawn dates of juvenile Pacific hake, *Merluccius productus*. *In* Recent developments in fish otolith research. *Edited by* D.H. Secor, J.M. Dean, and S.E. Campana. University of South Carolina Press, Columbia, S.C. pp. 481–497.

© 1999 NRC Canada

Mortality, movement, and body size: critical scales for Atlantic cod (*Gadus morhua*) in the Northwest Atlantic

David C. Schneider, Tammo Bult, Robert S. Gregory, David A. Methven, Danny W. Ings, and Vytenis Gotceitas

Abstract: The problem of scaling spatially and temporally limited data to larger scale questions can no longer be ignored as evidence accumulates that the importance of any given process, relative to another, depends on spatial and temporal scale. A recently developed graphical technique allows identification of critical space and time scales, which separate scales at which one rate prevails from scales at which another rate prevails. We used data from the literature to test a series of hypotheses concerning change in critical scales with change with life history stage in Atlantic cod (*Gadus morhua*). The critical scales for mortality relative to kinematics increased slightly for pelagic juveniles relative to drifting eggs, decreased substantially for demersal juveniles relative to pelagic juveniles, increased again in adults, and, contrary to expectation, remained high in large adults ("mother fish"). Critical time and space scales were found to be linked and cannot be taken as constants.

Résumé : Nous ne pouvons plus ne pas tenir compte du problème de la mise à l'échelle des données limitées dans le temps et l'espace, car il ressort de plus en plus que l'importance de tout processus, par rapport à un autre, dépend de l'échelle spatio-temporelle. Une technique graphique mise au point dernièrement permet l'identification d'échelles spatio-temporelles critiques qui départagent les échelles auxquelles un taux prévaut des échelles auxquelles un autre taux prévaut. Nous avons utilisé des données tirées de la documentation pour vérifier une série d'hypothèses sur le changement des échelles critiques en fonction du changement selon le stade du cycle biologique chez la morue franche (*Gadus morhua*). Les échelles critiques de la mortalité en fonction de la kinématique ont augmenté légèrement chez les juvéniles pélagiques par rapport aux oeufs en dérive, ont diminué de façon importante chez les juvéniles démersaux par rapport aux juvéniles pélagiques, ont augmenté de nouveau chez les adultes et, contrairement à toute attente, sont demeurées élevées chez les adultes de grande taille. Nous avons constaté que les échelles spatio-temporelles critiques étaient liées et qu'elles ne pouvaient pas être considérées comme des constantes.

[Traduit par la Rédaction]

Introduction

One of the characteristics of the environmental sciences, including ecology, is the large spatial scope of the questions addressed. Spatial scope is defined as the area to which the question applies, divided by the area of the sampling unit. Marine fisheries supply good examples where the scope of the question is large relative to the area directly measured. The question of processes responsible for changes in stock size of Atlantic cod (*Gadus morhua*) in the Northwest Atlantic (NAFO zones 2J and 3KL) applies to an area of 570 000 km^2; within that area, a typical survey will cover 200 000 km^2, of which 22 km^2 will be measured directly in 900 trawls, each 0.0244 km^2 in area (Walsh and McCallum 1997). The scale-up from survey coverage to stock area is 570 000 km^2/200 000 km^2 = 2.8; the scale-up from area measured directly is 200 000 km^2/22 km^2 = 9000. The scale-up from area measured in two successive years, for randomly placed units, will be 200 000 km^2/44 km^2 = 4500. The question of annual change in stock size then has a scope of 2.8 × 4500 = 12 600 times the area actually measured, or 12 600 × 900 × 2 = 23 million times the area of one sampling unit.

Until the 1980s, environmental research largely ignored the problem of scale, i.e., the disparity between the dynamics at the large scale of questions and the dynamics at the small scale of areas measured directly. The disparity goes unmentioned in most reports of ecological research, the implication being that a result at the manageable spatial scale of field research applies directly at larger scales. An exception to this implicit approach comes from fisheries research, where the problem of scaling from local data to a larger scale question was recognized nearly a century ago (Johnstone 1908). In fisheries, the solution to this problem has been to identify a stock (closed to migration) and then examine demographic rates (recruitment and mortality) only at

Received December 4, 1997. Accepted March 17, 1999.
J14336

D.C. Schneider,[1] R.S. Gregory, and D.W. Ings. Ocean Sciences Centre, Memorial University of Newfoundland, St. John's, NF A1C 5S7, Canada.
T. Bult and D.A. Methven. Department of Biology, Memorial University of Newfoundland, St. John's, NF A1C 5S7, Canada.
V. Gotceitas. Department of Environmental Sciences, Lakeland College, 5707 47 Avenue, West Vermillion, AB T9X 1X5, Canada.

[1]Author to whom all correspondence should be addressed.
e-mail: a84dcs@morgan.ucs.mun.ca

© 1999 NRC Canada

Fig. 1. Scaled rate plot comparing mortality rate M with kinematic change F as a dimensionless ratio ($R = M/F$) for the bivalve *M. liliana*. The ratio is less than unity (kinematics prevail) at the lower left, within the contour line. The solid line was obtained by exhaustive computation. The dotted line was drawn by hand from benchmark values. Figure redrawn from Schneider et al. (1997).

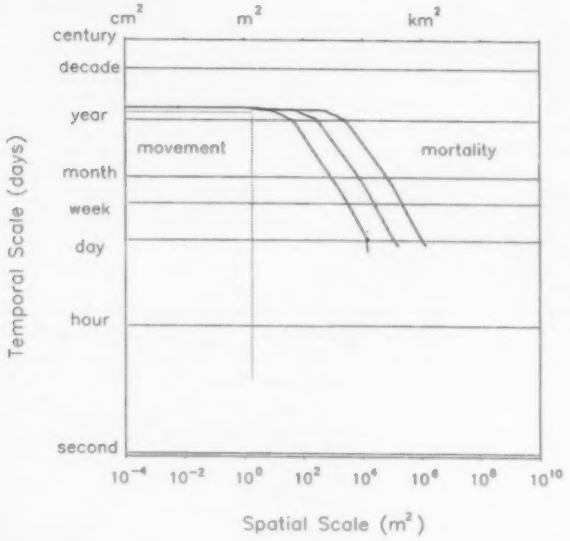

the larger scale of the stock. This is accomplished by statistical scale-up using random designs, stratified random designs, or optimal interpolation (Simard et al. 1993) to estimate a large scale quantity, all fish in the survey area at one point in time. The spatial scale is set as that of the entire stock, and hence, the survey must be carried out at this scale to allow estimation of change in stock size, free of the effects of movements.

In oceanography, the solution has been to compute "critical scales," which separate the time and space scales at which one rate (e.g., population growth) prevails over another (e.g., diffusive movement). Once computed, critical scales can be used in theoretical studies to simplify equations, in process-oriented studies to match data to theory, in surveys to identify sources of variance at small relative to large scales (Horne and Schneider 1994), and in design of field research (Hatcher et al. 1987). Critical scales have been traditionally identified by dimensional methods. Platt (1981) presented a simple example for phytoplankton patch size. For three parameters (phytoplankton growth r = %/time, phytoplankton diffusion K_H = distance^2/time, critical patch scale ζ = distance) taken to be similar to two dimensions (L = length and T = time), there is a single dimensionless Π ratio (Buckingham 1914). Any of several analytical methods (Massey 1986) produce the same ratio, $\Pi = \zeta^2 r/K_H$. At the critical scale, the rates are equal, $\Pi = 1$, and hence, the critical patch scale is $\zeta = (K_H/r)^{1/2}$.

Are critical scales fixed values? Conventional treatments based on dimensionless Π ratios imply this. Horne and Schneider (1994) used available data on capelin (*Mallotus villosus*) to calculate dimensionless ratios at several time and space scales then drew by hand a contour line surrounding the space and time scales where one rate (e.g., somatic growth) prevailed over another (e.g., demographic rates). They found that critical scales were not constant for Π ratios comparing somatic growth relative to population dynamics, demographics relative to kinematics (movements), locomotory relative to passive movement with currents, and recruitment relative to harvesting mortality. Nonconstant critical scales were also found for zooplankton (Horne and Schneider 1994, their fig. 2) and for an infaunal bivalve, *Macomona liliana*, a species with demographic and locomotory characteristics that differ substantially from those of zooplankton or pelagic fish (Schneider et al. 1997). The results for *M. liliana*, based on hand-drawn contours, were then examined by exhaustive computation (T. Bult, unpublished). In this bivalve species, both hand-drawn and exhaustively computed contours for critical time scales ran horizontally over small to intermediate spatial scales and then dropped at larger scales for demographics relative to kinematics (Fig. 1). The rate of drop was found to be gradual, not sudden, as was assumed for hand-drawn contours. These studies suggest that the critical scale (demographics relative to kinematics) forms an envelope, rather than being a constant.

Hand-drawn contours require a few minutes to construct, while exhaustive computation (T. Bult, unpublished) required more than a week of cpu time, after investing the time to write the computer code. Large amounts of cpu time are required because the dimensionless ratio is computed at thousands of points in the figure. It was thus of interest to determine whether the shape of the envelope (Fig. 1) is a general result or applies only to this bivalve species. It was also of interest to examine whether the location of the envelope (Fig. 1) can be predicted across a sequence of life history stages known to differ in demographic and kinematic characteristics.

The purpose of this paper is to determine whether (*i*) the critical scale envelope in Fig. 1 is a general result, (*ii*) the shape of the envelope in Fig. 1 is a general result, and (*iii*) knowledge of demographic and locomotory characteristics can be used to make qualitative predictions concerning critical scales. For Atlantic cod, we expected that the importance of mortality relative to kinematics would change markedly with body size as fish grow from drifting eggs, begin swimming as pelagic juveniles, settle into nursery areas, reach maturity, and grow to sizes greater then 1 m in length. Mortality tends to decrease with increasing body size, while swimming speed tends to increase with body size. More specifically, we expected that kinematics due to passive drift would be important at all but very large scales for planktonic stages and that the scales at which kinematics prevail would shrink upon settlement into nursery areas and then gradually expand as fish became mobile and undertook annual spawning migrations. Finally, we expected that kinematics would prevail only at small scales for very large fish, or "mother fish," for which there is no evidence of extensive migration.

Methods

Scaled rate plots were constructed for five stages of Atlantic cod defined by body size: drifting eggs and early larvae (<15 mm in length), later stage pelagic juveniles (15–40 mm), demersal juveniles (40–100 mm), mature fish (50–100 cm), and large mother fish (>100 cm). Estimates of stage-specific mortality rates were assem-

© 1999 NRC Canada

Fig. 2. Scaled rate plot comparing mortality rate M with kinematic change F as a dimensionless ratio ($R = M/F$) in eggs and early larvae of Atlantic cod. The ratio is less than unity (kinematics prevail) at the lower left. Lines show critical scales ($R = 1$) for the low-mortality (lower line) and high-mortality (upper line) cases. The ratio exceeds 1 (mortality rate prevails) above and to the right of the upper line.

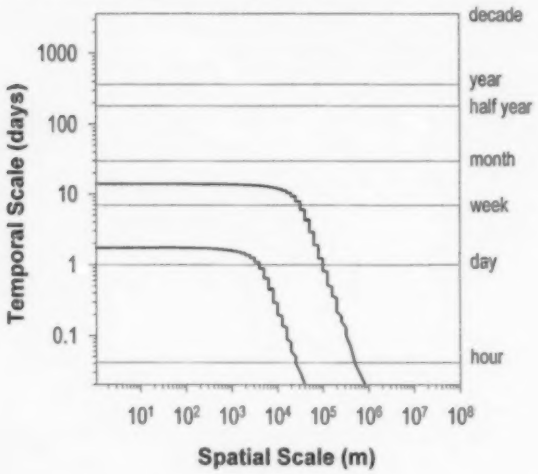

bled from the published literature on Atlantic cod (Appendix). No estimates were available for demersal juvenile fish, so we used values intermediate between pelagic juveniles and later stages. No estimates were available for mother fish, so we used a mortality rate of half that for smaller adult fish. We then assembled published information on seasonal movements and swimming speeds (Appendix). Lateral movement of eggs and larvae, living in the mixed surface layer, was computed from eddy diffusivity of the surrounding water. Lateral movements of vertically migrating pelagic juveniles were computed from eddy diffusivity plus net advection of the water column. Lateral movement during the first year of demersal life was computed so as to be consistent with unpublished data on percent straying of marked fish from point of release. Data collected in 1996 field studies on the northeast coast of Newfoundland (Terra Nova Park at 48°35′ N, 53°55′ W) were used to compute movements (time between mark and recapture) after settlement. Lateral movements during later (adult) demersal stages were computed from data on migration rates (DeBlois and Rose 1995) for an annual cycle with a 2-month migration from offshore spawning to coastal feeding grounds, a 3-month residence on coastal feeding grounds, a 2-month migration back to the spawning grounds, and a 5-month period on the spawning grounds. Movement while on the spawning or feeding grounds was computed as a random walk within a defined range. Lateral movement of large (>1 m) fish was computed under the assumption of no large-scale migration between spawning and feeding grounds.

The computational procedure, adapted from a program described in detail elsewhere (Bult et al. 1998), was as follows. For each stage, a cohort of 1000 fish was distributed randomly along a transect subdivided into 10 000 bins. At each time step, fish were subjected to a stage-specific mortality (Appendix), and then the proportion staying or moving from the bin was computed, based on distance traveled, as calculated from stage-specific rates of diffusion, advection, and swimming (Appendix). In the case of demersal juveniles, movement schedules were established so as to be consistent with unpublished data from mark–recapture experiments (R.S. Gregory, unpublished data). For periods >6 weeks, random numbers from a uniform distribution were used to assign distance traveled by these juveniles, within fixed ranges (20% of fish remaining within 8 m of start location, 79% in the range of 8–350 m, 1% in the range of 350 m or more). For periods <6 weeks, the distance traveled was again assigned within fixed ranges (Appendix), but to achieve realistic movement rates, the proportion assigned to each range was adjusted for time. The adjustment ranged from none (100%) at 42-day intervals down to 1/42 = 2.4% at 1-day intervals.

The percent changes due to mortality and to movement were then taken as a ratio for bin sizes corresponding to distances over the range $L = 10^1$–10^6 m. This was repeated for time periods over the range $T = 0.01$–30 days for drifting eggs and larvae, $T = 0.5$–60 days for pelagic larvae, $T = 1$–1000 days for demersal juveniles, and 1 – 10 000 days for the two adult stages. Within each stage, the average ratio of mortality to movement at each space and time scale was then computed from 100 runs, each with a randomly chosen starting point in space and time. If 100 runs proved too small to average out initial conditions, the number of runs was increased, to a maximum (2000) set by a computational limit of 12 cpu days. Contour lines were drawn to delineate those space and time scales where mortality prevails over kinematics. When several estimates were available from the literature, two contour lines were computed, one for the highest mortality relative to the lowest kinematic estimate and one for the lowest kinematic relative to the highest mortality estimate. The greater the range in reported rates (e.g., mortality), the greater the separation between the lines. Separation is thus a rough measure of uncertainty in the estimate of critical scale.

Results

The contoured rate diagrams showed that, as expected, kinematics prevailed at small space and time scales, while mortality prevailed at larger scales (Figs. 2–6). The two contour lines in these plots bracket the critical scale, defined as the scale at which the two rates were equal in importance. In all five life history stages, the critical scales for mortality relative to kinematics formed an envelope. In general, the critical time scales remained constant through a range of small spatial scales and then dropped at larger space scales. The turning point was often near a diagonal line drawn through the plot, but not always on this line. The shape was similar in all the stages except migratory adults (Fig. 5). In stages without migration (Figs. 2, 4, and 6), the shape of the envelope was similar to that in *M. liliana* (Fig. 1). At larger spatial scales, the decrease in critical time scale with increasing spatial scale was gradual when movement was random (Figs. 1, 2, and 6) and more rapid when advective movements were present (Figs. 3 and 5). Strongly seasonal migration resulted in complexly shaped contour lines (Fig. 5).

Eggs and larvae (Fig. 2) were assumed to drift randomly in a mixed surface layer, while pelagic juveniles (Fig. 3) were assumed to have an advective component in addition to random movement. As expected, the time and space scales at which movement prevailed in pelagic juveniles (Fig. 3) expanded relative to those for eggs and larvae (Fig. 2). The minimum and maximum critical scales (inner and outer contours in the figures) expanded, shifting toward larger space and time scales in Fig. 3 than in Fig. 2. The distance between the two contours also expanded in Fig. 3, reflecting greater uncertainty in the estimate of critical scales.

Demersal juveniles cease moving with the current as they make the transition to cryptically coloured individuals with

© 1999 NRC Canada

Fig. 3. Scaled rate plot comparing mortality rate M with kinematic change F as a ratio ($R = M/F$) in pelagic juvenile Atlantic cod. Lines show critical scales ($R = 1$) as in Fig. 1; $R < 1$ at the lower left.

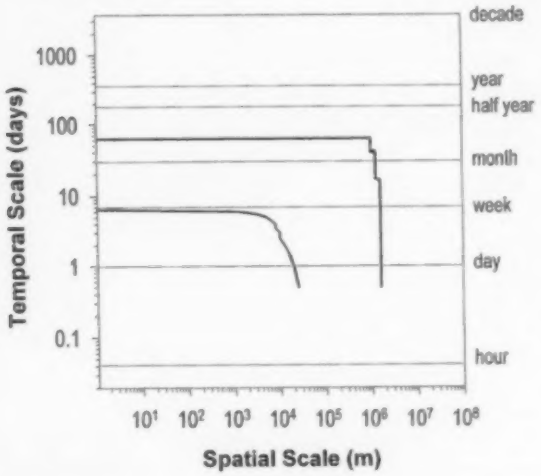

Fig. 4. Scaled rate plot comparing mortality rate M with kinematic change F as a ratio ($R = M/F$) in demersal juvenile Atlantic cod <1 year old. Lines show critical scales ($R = 1$) as in Fig. 1; $R < 1$ at the lower left.

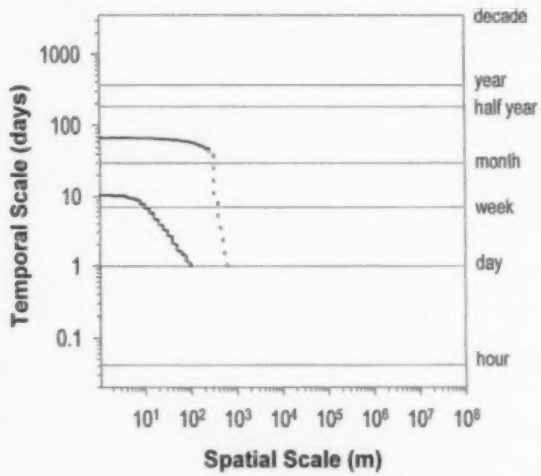

Fig. 5. Scaled rate plot comparing mortality rate M with kinematic change F as a ratio ($R = M/F$) in mature Atlantic cod. Lines show critical scales ($R = 1$) as in Fig. 1; $R < 1$ at the lower left.

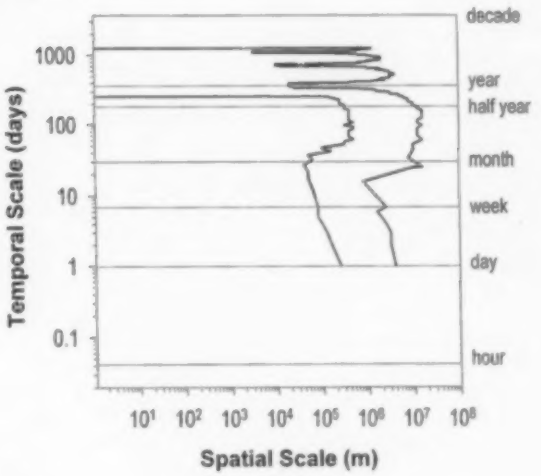

Fig. 6. Scaled rate plot comparing mortality rate M with kinematic change F as a ratio ($R = M/F$) in large (mother) Atlantic cod (length >100 cm). Lines show critical scales ($R = 1$) as in Fig. 1; $R < 1$ at the lower left.

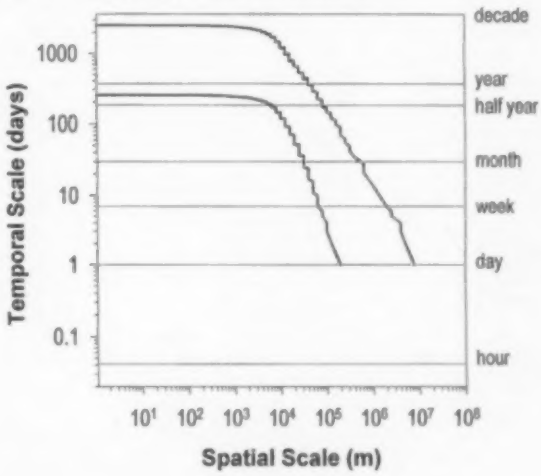

reduced movements to lower the risk of predation (Gotceitas et al. 1995). Under some conditions, these fish may show territorial behaviour (Tupper and Boutilier 1995). As expected, the time and space scales at which movement prevails contracted (Fig. 4) relative to earlier pelagic stages (Figs. 2 and 3). The solid lines in Fig. 4 are based only on data for movement over a 6-week period. The dotted line is based on daily movement calculated from the 6-week rate. Direct estimates of mortality and better data on short-term movements are needed to validate these plots.

Prior to stock collapse, adult Atlantic cod migrated across the shelf between spawning and feeding grounds. As expected, the time and space scales at which movement prevails in adult fish (Fig. 5) expanded relative to newly settled juveniles (Fig. 4). The seasonal migratory cycle is evident in the rightward bulge, toward large spatial scales, at time scales from 1 month (half the migration period) to a year. The oscillatory boundary at time scales of 1–5 years aliases the annual cycle because of random sampling during the year. Analysis on a fixed date should reduce the oscillatory shifts in Fig. 5.

There is no evidence that very large, or mother, fish migrate as extensively as spawning fish of smaller size, based on the published literature and on interviews with retired fishers (Neis et al. 1999). Critical scales were expected to contract when migration was reduced to zero and mortality

© 1999 NRC Canada

reduced by half. Contrary to expectation, the critical scales did not contract (Fig. 6) relative to fish with extensive migration (Fig. 5). The effect of reducing the mortality rate exceeded the effect of decreasing the seasonal migration rate, a result that was not anticipated. At time scales of less than a month or two, even limited feeding movements will prevail over mortality on the order of 10%/year (Fig. 6).

Discussion

As expected, mortality prevailed over movement at large scales, while movement was more important at smaller scales in all five stages. The critical scale (R = mortality/kinematics = 1) formed an envelope, rather than being a constant. These results, based on intensive computation, confirm earlier work using benchmark values (Horne and Schneider 1994) to evaluate concomitant effects of mortality and movement at multiple space and time scales.

The shape of the rightward boundary of the envelope varied. It sloped downward when movement was random (Figs. 1, 2, and 6), became vertical when large-scale advective motion was added (Fig. 3), and assumed a complex shape when seasonal migration was added (Fig. 5). The upper boundary of the envelope was fixed (horizontal), matching the duration of the life history stage.

The envelope expanded and contracted in a sequence of life history stages differing in mortality and movement. Expansion (or contraction) could often, but not always, be predicted. A simple prediction, based on the increase in mobility and decrease in mortality with increasing body size, is that the critical scale should increase with body size. In Atlantic cod, however, lateral movement decreases sharply at the point where fish settle to the bottom, seeking shelter from predation (Gotceitas et al. 1995). Lateral movement then increases as Atlantic cod approach maturity and adopt an annual migration between feeding and spawning grounds. Very large fish are not reported from migratory aggregations (Neis et al. 1999). From this information, we expected the critical scale to expand in pelagic juveniles relative to eggs and larvae, contract in demersal juveniles, expand in mature fish, and contract again in very large fish. When the available data from the literature were assimilated in scaled rate plots, we found that critical scales expanded in pelagic juveniles relative to drifting eggs, contracted in demersal juveniles, and then expanded in fish of mature size, as anticipated. Unexpectedly, the critical scale expanded in very large fish, with restricted feeding movements and no migration.

One criticism of this analysis is that it is already known that demographics prevail at large scales, while movements prevail at small scales. This is correct, but until the critical scale is calculated, it provides no guidance in applying this knowledge. Our results show that the critical scales for demographics relative to kinematics form an envelope, rather than being a constant, and that the size of this envelope cannot be drawn on intuitive grounds. A related criticism is that the analysis of critical scales can provide no assistance in survey design, where scale-up is achieved by random placement of sampling units. This again is correct, provided the survey encompasses all of the area occupied by the species of interest. When this is not possible, as is often the case, then computing the critical scales becomes useful in judging whether the area covered was large enough to meet the assumption of a closed population.

Scaled rate plots for Atlantic cod (Figs. 2–6) were constructed by intensive computation, in contrast with plots of critical scales constructed from the few available benchmarks. The principal advantage of the benchmark technique is that it is quick, requiring no more than a hand calculator once literature values are assembled. The contour lines are only approximate. Intensive computation produced more detailed contour lines, and it allowed upper and lower limits on critical scales to be contoured. A range in parameter values can be included in these plots, permitting the degree of uncertainty in critical scales to be judged. Intensive computation uncovered several features not detectable by benchmark contours. An example is the shape of the rightward boundary of the critical scale envelope for mortality relative to kinematics.

Our results were based on simulations computed from available estimates of movement and mortality, and as such are subject to several limitations. The computations assumed that rates act independently (e.g., mortality is independent of migration rate). Mortality rates were assumed to scale as L^0, i.e., that doubling the area does not change the mortality estimate. Mortality rates were assumed to scale as T^{-1}, i.e., that halving the time halves the estimated crude mortality (fish per year). Different results can be expected if these assumptions prove unfounded. Another limitation is that recruitment was not included in the analysis.

The results have a number of implications for surveys to monitor recovery rates of Atlantic cod. One is that estimates of population recovery will require less extensive effort in demersal juveniles than in other stages, where movement prevails at larger scales. Another is that the seasonal and local rates of movement need to be quantified if rates of recovery of very large fish, which have high reproductive potential, are to be monitored. Only at very large spatial scales can movement be ignored in pelagic juveniles (Fig. 2) or large adults (Fig. 6).

Construction of scaled rate plots by intensive computation confirmed earlier findings from benchmarks (Horne and Schneider 1994; Schneider et al. 1997) showing that critical space and time scales were not constants. For mortality relative to movement in Atlantic cod, the critical scale formed an envelope: the critical time scale held constant through some range of small spatial scales and then decreased at larger spatial scales. The decrease can be either rapid or slow. Critical time and space scales cannot be assumed to be constants, independent of the area (spatial scale) or duration (time scale).

Acknowledgements

Funding for this research came from the Natural Sciences and Engineering Research Council of Canada, the Department of Fisheries and Oceans (Northern Cod Science Program), and the Environmental Innovations Program (Canada Green Plan), with logistical support from Canadian Heritage-Parks Canada. The manuscript was improved by comments from two anonymous reviewers, whose efforts we appreciate.

© 1999 NRC Canada

References

Buckingham, E. 1914. On physically similar systems. Phys. Rev. **4**: 345–376.

Bult, T.P., Haedrich, R.L., and Schneider, D.C. 1998. New technique describing spatial scaling and habitat selection in riverine habitats. Regul. Rivers, **14**: 107–118.

DeBlois, E.M., and Rose, G.A. 1995. Effect of foraging activity on the shoal structure of cod (*Gadus morhua*). Can. J. Fish. Aquat. Sci. **52**: 2377–2387.

Gotceitas, V., Fraser, S., and Brown, J.A. 1995. Habitat use by juvenile Atlantic cod (*Gadus morhua*) in the presence of an actively foraging and non-foraging predator. Mar. Biol. **123**: 421–430.

Hatcher, B.G., Imberger, J., and Smith, S.V. 1987. Scaling analysis of coral reef systems: an approach to problems of scale. Coral Reefs, **5**: 171–181.

Horne, J.K., and Schneider, D.C. 1994. Analysis of scale-dependent processes with dimensionless ratios. Oikos, **70**: 201–211.

Johnstone, J. 1908. Conditions of life in the sea: a short account of quantitative marine biological research. Cambridge University Press, Cambridge, U.K. Reprinted by Arno Press, New York, in 1977.

Massey, B.S. 1986. Measures in science and engineering. Halstead (John Wiley), New York.

Neis, B., Felt, L., Haedrich, R.L., and Schneider, D.C. 1999. An interdisciplinary methodology for collecting and integrating fisher's ecological knowledge into resource management. Chap. 16. *In* Fishing places, fishing people: issues in Canadian small-scale fisheries. *Edited by* D. Newell and R. Ommer. University of Toronto Press, Toronto, Ont. In press.

Platt, T.R. 1981. Thinking in terms of scale: introduction to dimensional analysis. *In* Mathematical models in biological oceanography. *Edited by* T. Platt, K.H. Mann, and R.E. Ulanowicz. UNESCO Press, Paris. pp. 112–121.

Schneider, D.C., Walters, R., Thrush, S., and Dayton, P. 1997. Scale-up of ecological experiments: density variation in the mobile bivalve *Macomona liliana*. J. Exp. Mar. Biol. Ecol. **216**: 129–152.

Simard, Y., Marcotte, D., and Bourgault, G. 1993. Exploration of geostatistical methods for mapping and estimating acoustic biomass of pelagic fish in the Gulf of St. Lawrence: size of the echo-integration unit and auxiliary environmental variables. Aquat. Living Resour. **6**: 185–199.

Tupper, M., and Boutilier, R.G. 1995. Effects of habitat on settlement, growth, and postsettlement survival of Atlantic cod (*Gadus morhua*). Can. J. Fish. Aquat. Sci. **52**: 1834–1841.

Walsh, S.J., and McCallum, B.R. 1997. Performance of the campelen 1800 shrimp trawl during the 1995 northwest Atlantic fisheries centre autumn groundfish survey. NAFO Sci. Counc. Stud. **29**: 105–114.

Appendix. Atlantic cod life history stages, sizes, and parameter estimates for mortality and movement

Eggs and early larvae (<15 mm)

Description
— no swimming; movement due to diffusion only
— stage lasts 1 month

Scenario 1 (mortality high, movement low)
— mortality = 0.40/day (Houde 1987; Campana et al. 1989; Heessen and Rijnsdorp 1989)
— movement: diffusion = 50 m^2/s (Csanady 1982, Helbig et al. 1992)

Scenario 2 (mortality low, movement high)
— mortality = 0.05/day (Houde 1987; Campana et al. 1989; Heessen and Rijnsdorp 1989)
— movement: diffusion = 300 m^2/s (Lough and Bolz 1989)

Pelagic juveniles (15–40 mm)

Description
— ability to swim
— advection, the net result of passive movement with current plus diffusive movement
— stage lasts 2 months

Scenario 1 (mortality high, movement low)
— mortality = 40/year (Campana et al. 1989; Sundby et al. 1989)
— movement due to advection (0.0065 m/s; Lough and Bolz 1989) and diffusion (50 m^2/s; Csanady 1982; Helbig et al. 1992) same as with eggs and early larvae

Scenario 2 (mortality low, movement high)
— mortality: 4/year (Campana et al. 1989; Sundby et al. 1989)
— movement due to advection (0.20 m/s; De Young and Davidson 1994) and diffusion (300 m^2/s; Lough and Bolz 1989) same as with eggs and early larvae

© 1999 NRC Canada

Early juveniles, demersal (40–100 mm)

Description
— swimming within ranges
— distance moved, after time *T*, assigned within a range by a uniform random distribution
— stage lasts 1 year

Scenario 1 (mortality high, movement low)
— mortality = 0.05/day
— movement for periods >6 weeks:
  20% within 0–8 m range
  79% within 8–350 m range
  1% within 350–4500 m range
— movement for periods <6 weeks:
  0% within 350–4500 m range
  79% *T* within 8–350 m range where *T* = time period/42
  remaining fish within 0–8 m range

Scenario 2 (mortality low, movement high)
— mortality = 0.01/day
— movement for periods >6 weeks:
  6% within 0–8 m range
  93% within 8–350 m range
  1% within 350–4500 m range
— movement for periods <6 weeks:
  0% within 350–4500 m range
  93% *T* within 8–350 m range where *T* = time period/42
  remaining fish within 0–8 m range

Adults

Description
— stage lasts 20 years
— swimming to and from spawning and feeding areas; four different movement periods: (*i*) from feeding to spawning area, (*ii*) at spawning area, (*iii*) to feeding from spawning area, (*iv*) within feeding area

Scenario 1 (mortality high, movement low)
— mortality = 1.0/year (Campana et al. 1989)
— from spawning to feeding area:
  start: 1 April
  duration: 60 days (2 months)
  migration rate: –4 km/day (DeBlois and Rose 1995)
— at feeding area:
  start: 1 June
  duration: 90 days (3 months)
  movement rate: random at 1 km/day in 10-km home range
— from feeding to spawning area:
  start: 1 September
  duration: 60 days (2 months)
  movement rate: 4 km/day (DeBlois and Rose 1995)
— at spawning area:
  start: 1 November
  duration: 150 days (5 months)
  movement rate: random at 1 km/day in 10-km home range

Scenario 2 (mortality low, movement high)
— mortality = 0.2/year (Campana et al. 1989)
— from spawning to feeding area:
  start: 1 April
  duration: 75 days (2.5 months)
  movement rate: –20 km/day (DeBlois and Rose 1995)

© 1999 NRC Canada

— at feeding area:
start: 15 June
duration: 75 days (2.5 months)
movement rate: random at 4 km/day in 10-km home range
— from feeding to spawning area:
start: 1 September
duration: 75 days (2.5 months)
movement rate: 20 km/day (DeBlois and Rose 1995)
— at spawning area:
start: 15 November
duration: 135 days (4.5 months)
movement rate: random at 4 km/day in 10-km home range

Mother fish

Description
— stage lasts indefinite time
— swimming within home range; no long distance spawning/feeding migrations

Scenario 1 (mortality high, movement low)
— mortality = 1.0/year (Campana et al. 1989)
— movement within home range, modeled similar to period 2 or period 4 of mature adult stage (see above), with:
movement rate: random at 1 km/day in 10-km home range

Scenario 2 (mortality low, movement high)
— mortality = 0.1/year (Campana et al. 1989)
— movement within home range, modeled similar to period 2 or period 4 of mature adult stage (see above), with:
movement rate: random at 4 km/day in 10-km home range

Appendix references

Campana, S.E., Frank, K.T., Hurley, C.F., Koeller, P.A., Page, F.H., and Smith, P.C. 1989. Survival and abundance of young Atlantic cod (*Gadus morhua*) and haddock (*Melanogrammus aeglefinus*) as indicators of year-class strength. Can. J. Fish. Aquat. Sci. **46**(Suppl. 1): 171–182.

Csanady, G. 1982. Circulation in the Coastal Ocean. Reidel, Amsterdam, The Netherlands.

DeBlois, E.M., and Rose, G.A. 1995. Effect of foraging activity on the shoal structure of cod (*Gadus morhua*). Can. J. Fish. Aquat. Sci. **52**: 2377–2387.

De Young, B., and Davidson, F. 1994. Modelling retention of cod eggs and larvae *Gadus morhua* L. on the Newfoundland Shelf. ICES Mar. Sci. Symp. **198**: 346–355.

Heessen, H.J.L., and Rijnsdorp, A.D. 1989. Investigations on egg production and mortality of cod (*Gadus morhua* L.) and plaice (*Pleuronectes platessa* L.) in the southern and eastern North Sea in 1987 and 1988. Rapp. P.-v. Réun. Cons. Int. Explor. Mer, **191**: 15–20.

Helbig, J., Mertz, G., and Pepin, P. 1992. Environmental influences on the recruitment of Newfoundland/Labrador cod. Fish. Oceanogr. **1**: 39–56.

Houde, E.D. 1987. Fish early life dynamics and recruitment variability. Am. Fish. Soc. Symp. **2**: 17–29.

Lough, R.G., and Bolz, G.R. 1989. The movement of cod and haddock larvae onto the shoals of Georges Bank. J. Fish Biol. **35**(A): 71–79.

Sundby, S., Bjørke, H., Soldal, A.V., and Olsen, S. 1989. Mortality rates during the early life stages and year-class strength of northeast Arctic cod (*Gadus morhua* L.). Rapp. P.-v. Réun. Cons. Int. Explor. Mer, **191**: 351–358.

© 1999 NRC Canada

Relating spatial distributions of acoustically determined patches of fish and plankton: data viewing, image analysis, and spatial proximity

Gordon Swartzman, Richard Brodeur, Jeffrey Napp, Danny Walsh, Roger Hewitt, David Demer, George Hunt, and Elizabeth Logerwell

Abstract: We developed a point-and-click acoustic data viewer (FishViewer) for exploratory comparison of up to three acoustic survey transects (or three frequencies) at a time and other environmental and biological data (e.g., surface temperature and seabird abundance). FishViewer also contains image-processing tools (e.g., morphological and threshold filters) for distinguishing between fish shoals and plankton patches and for patch identification. These tools and methods are illustrated using survey data collected at three frequencies (38, 120, and 200 kHz) near the Pribilof Islands, Bering Sea, during September 1995. Data were also visualized by converting the patches identified in the acoustic images to polygons, showing the boundaries of each patch using a connected component algorithm. Proximity between these fish shoal and plankton patch polygons was examined statistically using an interval-based nonparametric regression model (generalized additive models) and a distance-based proximity measure. The methods presented for data refinement, visualization, and the establishment of fish–plankton patch proximity serve as a paradigm for scale-robust hypothesis formulation and testing of spatial patterns of fish and plankton.

Résumé : Nous avons mis au point un visualiseur de données acoustiques à pointage-cliquage (FishViewer) permettant la comparaison exploratoire de trois transects de détection acoustique (ou de trois fréquences) à la fois, et d'autres données environnementales ou biologiques (p.ex. la température de surface et l'abondance des oiseaux de mer). Le FishViewer comporte aussi des outils de traitement des images (p.ex. un filtre morphologique et un filtre de seuillage) permettant de différencier les bancs de poissons et les essaims de plancton, et de les identifier. Nous illustrons ces outils et méthodes à l'aide de données acoustiques recueillies à trois fréquences (38, 129 et 200 kHz) près des îles Pribilof, en mer de Béring, en septembre 1995. Nous avons aussi visualisé les données en convertissant en polygones les taches identifiées sur les images acoustiques, et en représentant les limites de chaque tache à l'aide d'un algorithme des composantes reliées. La proximité entre ces polygones des bancs de poissons et des essaims de plancton a été examinée statistiquement à l'aide d'un modèle de régression non paramétrique à intervalles (modèles additifs généralisés) et une mesure de proximité basée sur la distance. Les méthodes présentées pour raffiner et visualiser les données et établir la proximité des bancs de poissons et des essaims de plancton servent de paradigme pour la formulation d'hypothèses robustes quelle que soit l'échelle et pour la mise à l'essai des régimes spatiaux des poissons et du plancton.

[Traduit par la Rédaction]

Introduction

Pelagic fish and plankton spatial distributions in ocean ecosystems are influenced by hydrologic features such as ocean fronts and eddies, thermal stratification, and upwelling (Mann and Lazier 1991; Mullin 1993). As a result of the interaction between animal behavior and these physical processes, large patches of zooplankton develop and are maintained. These patches may attract planktivorous fish (Mackas et al. 1985, 1997; Barange 1994). These in turn serve as attractors to piscivorous fish, seabirds, and marine mammals. The large spatial scale in oceanic systems and the lack of consistent methods for acoustically distinguishing fish shoals from plankton patches have allowed only limited study of the spatial interrelationship of fish and zooplankton in the open ocean.

In this paper, we introduce methods for describing the spatial interrelationship of fish shoals and plankton patches. Our objectives are to (*i*) describe a point-and-click acoustic data viewer (FishViewer) and its utility for visualizing and

Received October 20, 1997. Accepted September 8, 1998.
J14264

G. Swartzman.[1] Applied Physics Laboratory, 355640 University of Washington, Seattle, WA 98195, U.S.A.
R. Brodeur and J. Napp. Alaska Fisheries Science Center, NMFS, Seattle, WA 98115, U.S.A.
D. Walsh. Statistics Department, University of Washington, Seattle, WA 98195, U.S.A.
R. Hewitt, D. Demer, and E. Logerwell. Southwest Fisheries Science Center, NMFS, La Jolla, CA 92038-0271, U.S.A.
G. Hunt. Department of Ecology and Evolutionary Biology, University of California, Irvine, CA 92697, U.S.A.

[1]Author to whom all correspondence should be addressed. e-mail: gordie@alava.apl.washington.edu

© 1999 NRC Canada

Fig. 1. Pribilof Island study region in the eastern Bering Sea showing the locations of the A, B, C, and D transect lines.

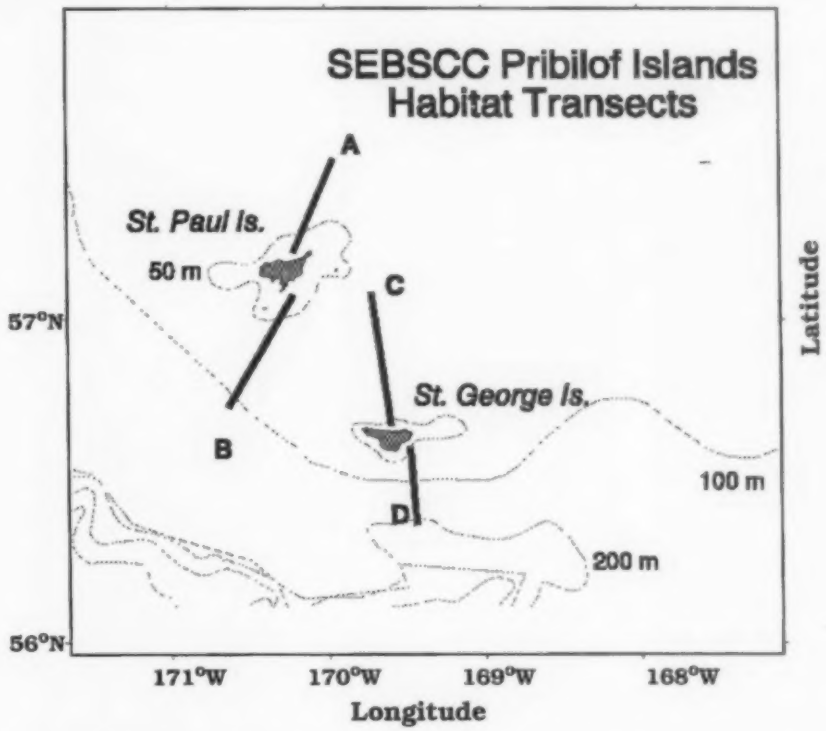

exploring multivariable spatial data sets, (*ii*) introduce recent developments in proximity analysis for describing the spatial interrelationships between predators and prey, and (*iii*) compare two proximity methods and insights into juvenile walleye pollock (*Theragra chalcogramma*) and zooplankton spatial relationships in the eastern Bering Sea (Fig. 1) during September 1995 (Brodeur et al. 1997).

Because of the large amount of data collected by acoustic surveys and the intensive computational nature of the image-processing methods used to identify plankton and fish aggregations, we have developed a viewer to display the different types of data and aid experimentation with the analysis methods used. This viewer has allowed us to develop and evaluate aggregation detection methods as well as to provide a visual exploratory analysis tool.

A major challenge of our work has been to develop and test methods to establish the degree of proximity among plankton, juvenile fish, and seabirds. We desired a proximity measure that considers the patchy nature of both fish and plankton as well as other factors such as the diel migration of plankton and the diel feeding pattern of the birds. In the study area the patches are large enough that they "fill" a significant portion of the surveyed transects; therefore, they cannot be treated as points in space, as is common with spatial statistical measures of interpatch distance. Proximity is complicated by the differential diel movements of plankton and fish such that the patches may be vertically separated at certain times of the day, even though they are horizontally close in space. A proximity measure that addresses how predators orient relative to prey patches should include features of patch size, orientation, and edge-to-edge, rather than center-to-center, distance. Also, the measure of proximity should include a randomness null hypothesis (i.e., the plankton and fish patches are randomly distributed in space relative to each other) and a method for testing the empirical distribution against the null hypothesis.

Methods

Exploratory viewing of acoustic and environmental data

Exploratory analysis of the acoustic data and supporting environmental and biological data collected along the study transects was made possible through the development of FishViewer (Fig. 2), a point-and-click display tool. FishViewer was developed following a prototype system (Lascara 1997) used to display oceanographic data from a towed recorder system. FishViewer adds many features specific to acoustic data and their analysis. It is written in the PV-WAVE echogram-processing programming language and allows the following operations: (*i*) loads transect acoustic echograms into any of three display panels, (*ii*) overlays seabird, surface temperature, salinity, or fluorescence or CTD isotherms along the transect filters on any echogram, (*iii*) performs morphological filtering with a choice of structuring elements and operations, (*iv*) performs pixel-by-pixel differencing between any two compatible echograms, (*v*) allows changing color tables for the acoustic displays, (*vi*) allows examination of the entire acoustic transect using slider bars, and (*vii*) samples backscatter at a point or along a line and displays backscatter values or histograms.

© 1999 NRC Canada

Fig. 2. FishViewer point-and-click acoustic echogram viewer showing data from 1995 transect A at three frequencies. Data were collected from two vessels in close proximity. Bird locations and isotherms can be overlaid on any of the acoustic echogram panels.

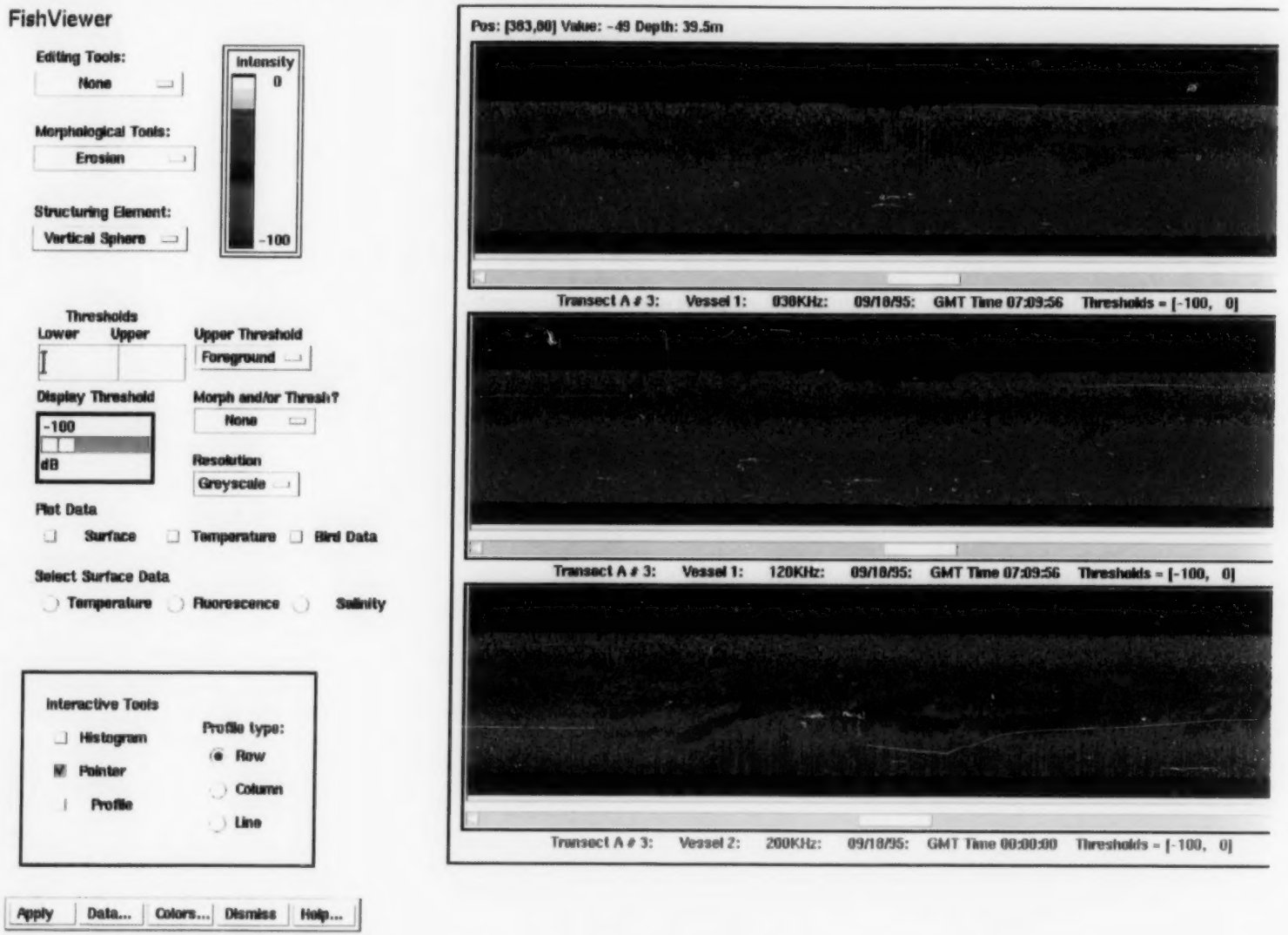

© 1999 NRC Canada

Acoustic surveys

Data for the demonstration of FishViewer and spatial analysis of fish and zooplankton are from acoustic surveys near the Pribilof Islands (Brodeur et al. 1997). Briefly, National Oceanographic and Atmospheric Administration research vessels *Miller Freeman* and *Surveyor* sampled hydrography, nekton, plankton, and seabird distributions in tandem along a 50-km transect extending north from St. Paul Island, Alaska (transect A, Fig. 1), during September 1995. Nominal separation of the two ships was 0.4 km, and speed ranged from 8 to 16 km·h^{-1}. Echo integration and target strength measurements (Simrad EK-500 split-beam echosounder and BI-500 analysis software) were collected for three frequencies (38 and 120 kHz on the *Miller Freeman* and 120 and 200 kHz on the *Surveyor*). Prior to the survey, system gains were calibrated using the standard sphere method (Foote et al. 1987). For each transect, measurements of volume backscatter strength (S_v, decibels per cubic metre, 1 µPa at 1 m) at each frequency were recorded each second. The acoustic data were subsampled to produce acoustic echograms with a horizontal resolution of 1000 pixels per 8 km (about 8 m per pixel) and a depth resolution of 0.5 m.

Shoal and patch identification

Fish shoal identification methods used 38-kHz data (Swartzman et al. 1994*a*), while the plankton patch identification used 120- and 200-kHz data. The algorithms required that patches comprise contiguous pixels, with a clearly defined boundary, in a backscatter range indicative of the target species or group (e.g., greater than –54 dB for walleye pollock and between –72 and –55 dB for zooplankton). The backscatter range was chosen with a threshold filter (all pixels outside the expected backscatter range were set to the background level). Morphological filters were then used to highlight patches in the resulting images. Morphological filters are image-processing methods used to separate clearly bounded objects from background noise (Haralick and Shapiro 1992). They apply dilation and erosion operations, using a predefined structuring element, to an image. Filters can be either binary (0–1) or grayscale. The dilation operation can be visualized as increasing the value of pixels surrounded by pixels at a higher level, up to the level of the surrounding pixels, while erosion lowers the value of pixels surrounded by pixels at a lower level to that level. This morphological filter fills small holes, emphasizes the boundary of the patches, breaks small isthmuses between patches, and eliminates small patches (smaller than the structuring element). The influence of surrounding pixels depends on the size (and shape) of the structuring element chosen. By applying dilation and erosion operations in sequences called openings and closings, the morphological filters can clearly define and distinguish bounded objects consisting of contiguous pixels (i.e., patches) from background noise without smearing or smoothing the shape of the object.

Prior to threshold and morphology filtering, the pixels below the bottom and within the bubble layer (about 5 m below the hull mounted echosounders) were removed from the echograms. All operations were programmed in the PV-WAVE higher level, matrix-oriented programming language (Precision Visuals 1992).

For fish shoals, we used a target threshold of pixels above –54 dB in the 38-kHz echogram, based on previous studies of juvenile walleye pollock target strength (Brodeur and Wilson 1996; Traynor 1996). We used a three-pixel horizontal and two-pixel vertical (3 × 2) grayscale structuring element as our morphological filter with a closing and opening operation (Haralick and Shapiro 1992). We then multiplied a binary version of the resultant echogram (0 for background and 1 for included pixels) by the original 38-kHz echogram. The resulting echogram had backscatter levels from the original echogram for all the pixels in identified patches and background backscatter levels (–100 dB) for all pixels not in patches.

To identify zooplankton patches comprising the acoustic backscatter, we took the difference in mean S_v at two frequencies ($S_{v200} - S_{v120}$). If the dominant scatterers contained gas bladders (e.g., juvenile fish) or were large relative to both wavelengths (backscattering cross section >0.75 and 1.25 cm, respectively), then the S_v differences were expected to be negative (due to the resonant effects) or slightly positive (due to geometric scattering). If, on the other hand, animals were smaller than both wavelengths (e.g., copepods and euphausiids), then Rayleigh scattering would be observed and we would expect a positive difference ($S_{v200} - S_{v120} > 0$, Clay and Medwin 1977). We first used a background threshold range of –72 to –54 dB for plankton (everything outside the range was set to the background value) in the 200- and 120-kHz echograms. We then performed a pixel-by-pixel differencing in backscatter between the echograms (200 – 120 kHz) and used morphological filters on the resultant binary echogram with pixels having positive differences greater than or equal to 2 dB (to eliminate pixels with small positive differences due to geometric scattering). We applied an opening and a closing with a 3 × 2 pixel binary structuring element, and the resulting echogram was multiplied by the original 200-kHz echogram. This method assumes that organisms such as euphausiids and copepods produce higher backscatter at 200 kHz than at 120 kHz, as indicated by various theoretical models of acoustic backscatter from fluid spheres and bent cylinders (Greenlaw 1979; Holliday and Pieper 1980; Stanton et al. 1993).

An example of FishViewer, using the above acoustic data and shoal and patch identification algorithms, is displayed in Fig. 2. Echograms of the same nighttime transect at three frequencies highlight that (*i*) the strongest backscatter of fish (red pixels) occurs at 38 kHz and (*ii*) plankton patches are not visible at 38 kHz and are most apparent at 200 kHz (blue pixels). The fish are seen as a layer between 20 and 30 m depth, while the plankton appear as a more amorphous patch below and moving into the fish layer. A depth scale (0–60 m), on the left side of the image, is not visible on the part of the display panels shown in Fig. 2, which are lined up to display a feature in the front region of transect A.

FishViewer was used not only to compare acoustic transects at different frequencies, times of day, years, and regions (i.e., different transects), but also to experiment with different morphological operations as a tool in developing and communicating the shoal and plankton patch identification algorithms. Figure 3 shows, in the top two panels, part of a daytime pass of transect A on September 11, 1995, at 120 and 200 kHz. On both panels, background thresholds between –72 and –54 dB were applied, a range suggestive of plankton S_v at these frequencies. All pixels outside this range were set to the background level (–100 dB) and appear as background (black) on the echograms. The bottom panel shows the result of differencing the 200- and 120-kHz echograms (after thresholds), using the same color table as used for the other echograms and then applying closing and opening morphological filters consecutively to the echogram after thresholding at +2 dB. The algorithm located a large patch near the bottom (polygonal boundary highlighted in green in Fig. 2) and a narrow patch near the top of the image (e.g., around 10 m depth).

Establishing plankton–fish proximity

Acoustic data abstraction

While FishViewer provides an effective means for data exploration, the size of the echogram files (about 1 megabyte apiece) makes statistical and quantitative comparative analysis computationally prohibitive, especially for most fisheries acoustic surveys. Our approach has been to extract the patch information from the echograms in the form of descriptive patch tables. A connected component algorithm (Haralick and Shapiro 1992) was used to locate each identified patch, and various descriptive parameters were

© 1999 NRC Canada

Fig. 3. Display panels from FishViewer illustrating the application of the plankton identification algorithm. The top two panels show 120- and 200-kHz acoustic backscatter images for a daytime pass of transect A with a threshold between –54 and –72 dB. The bottom image shows the difference between the 120- and 200-kHz images with a threshold filter at +2 dB and a morphological closing and opening with a 3 × 2 pixel structuring element. The pixels remaining after these operations are assumed to be plankton patches. The convex hull boundary of the large patch in the bottom image is shown in green.

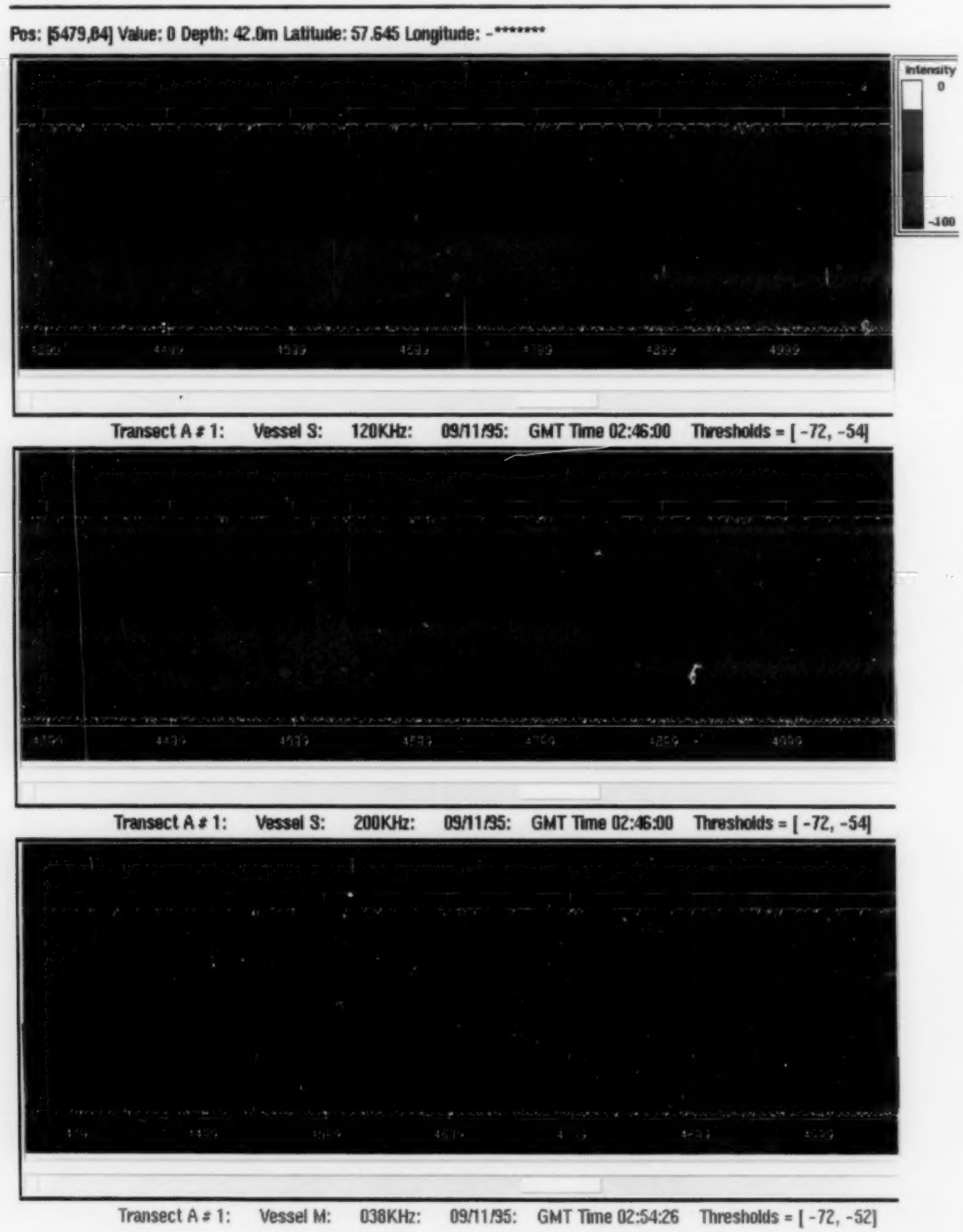
Pos: [5479,84] Value: 0 Depth: 42.0m Latitude: 57.645 Longitude: -*******
Intensity
0
-100
Transect A # 1: Vessel S: 120KHz: 09/11/95: GMT Time 02:46:00 Thresholds = [-72, -54]
Transect A # 1: Vessel S: 200KHz: 09/11/95: GMT Time 02:46:00 Thresholds = [-72, -54]
Transect A # 1: Vessel M: 038KHz: 09/11/95: GMT Time 02:54:26 Thresholds = [-72, -52]

© 1999 NRC Canada

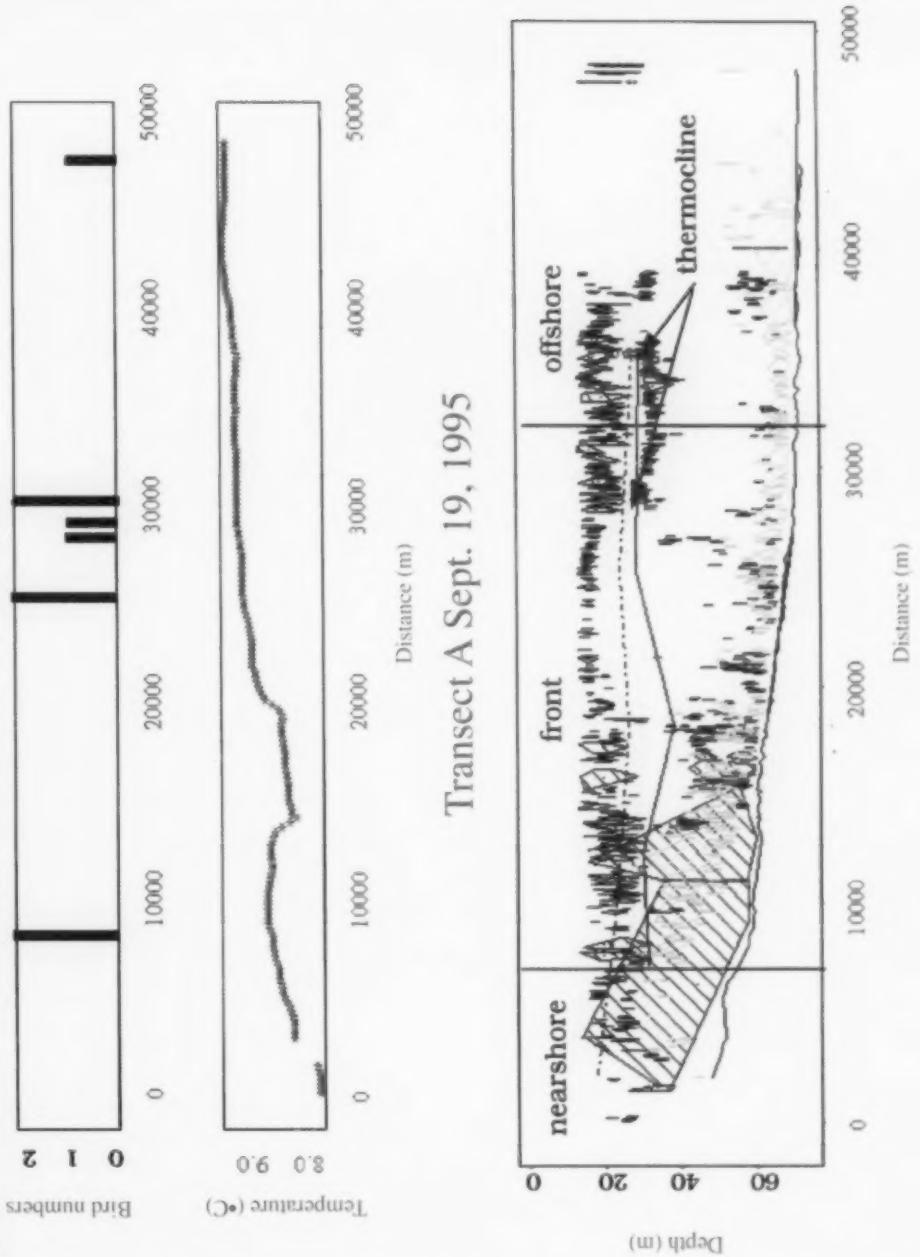

Fig. 4. Polygons showing the shape and location of fish shoals (blue) and plankton patches (orange) in the lower panel, with isotherms along transect A. Surface temperature (middle panel) and the locations of bird sightings (top panel) are also shown. There are no patches visible above 14 m because of the transducer depth. Murre numbers are shown in the top panel.

extracted (Nero and Magnuson 1989) including location parameters (patch depth, latitude, longitude, and distance of the patch center from the start of the transect), size and shape parameters (patch area, width, length, vertices of an eight-sided polygon convex hull enclosing the patch, elongation, and fractal dimension), backscatter parameters (average, maximum, minimum, and variance in patch backscatter), and environmental parameters (depth of the water column below the patch). This table provided a concise description of each patch that was used for display and further analysis of the spatial proximity of plankton and fish patches. Tabular information was entered into the Splus statistical programming language (Becker et al. 1988) for further analyses (described below). Figure 4 shows an example of a daytime pass of transect A on September 19, 1995, with polygons representing the locations of fish shoals and plankton patches (an example of such a polygon is shown in Fig. 3), isotherms calculated from CTD data, and the bottom contour overlaid on the panel. Panels above show surface temperature and the location of birds observed within 300 m of the transect line. This gives a synoptic view of the biota and environmental conditions below and above (i.e., birds) the surface over a 50-km transect.

Binning and generalized additive models

The most straightforward approach to examining spatial proximity between biota is to separate the identified shoals and patches

© 1999 NRC Canada

into horizontal bins or intervals, summing biomass index[2] for all the patches within each bin (Rose and Leggett 1990). Most commonly, within-bin correlations between predator and prey biomass index have been used as a measure of spatial proximity through spectral analysis (Rose and Leggett 1990; Horne and Schneider 1994) or simple correlation calculation (Brown and Morgan 1995). However, these methods are useful only if the relationship between the biota is monotonic. Unspecified nonlinear and nonmonotonic relationships between fish shoals and plankton patches can be included using a nonparametric regression technique, generalized additive models (GAM) (Hastie and Tibshirani 1990). GAM has been used effectively to establish relationships between adult walleye pollock spatial distribution and environmental conditions in the Bering Sea (Swartzman et al. 1994*b*) and between shoals of Pacific hake and environmental conditions in the Eastern Pacific Boundary Current (Swartzman 1997) and herring in the North Sea (Maravelias and Reid 1997). Besides generalizing the assumptions of linearity commonly made in regression and monotonicity made in correlation, GAM also allows a general assumption about the underlying probability distribution, allowing any distribution from the exponential family, which includes the normal, Poisson, binomial, and gamma distributions.

Before using GAM, the data were first binned into horizontal 250-m intervals. A range of intervals from 100 m to 1 km were also used, but the overall results did not change over the range of interval lengths considered. Since many patches spanned several intervals, the fish shoal and plankton patch biomass index was distributed uniformly among all bins that they spanned (assuming that the biomass index was horizontally uniformly distributed within the patch). The data were assumed to have an underlying gamma distribution. The GAM used was

$$\text{Abundance}_{\text{walleye pollock}} = \mu + s(\text{abundance}_{\text{plankton}})$$

where μ is the overall mean and the $s(x)$ are unspecified smooths of the effect of covariate x on the dependent variable. The smoothing in GAM was done using spline smoothers. Visual inspection of the data (e.g., Fig. 4) suggested that the relationship of walleye pollock to plankton was likely to be different in different hydrographic regions. As such, the GAM analysis was done separately for each hydrographic region: a nearshore, tidally mixed region, an offshore, stratified region, and a partially stratified front or transition region. The boundaries between the regions were determined from CTD data using a thermocline-based algorithm that separated the stratified region offshore from the front region and the front from the nearshore region (Stabeno et al. 1999).

Distance-based proximity

An alternative measure of proximity is based explicitly on the distance between patches. Because the plankton diel migrate, it might be misleading to establish that fish and plankton are in the same horizontal bin when they are in fact above and below the thermocline, respectively, although in this case the plankton diel migrate and may be seen as proximate to fish if they are in the same horizontal bin. Alternatively, a fish shoal may be quite far from the center of a plankton patch but quite close to its edge, even when they are not in the same bin. With mobile predators like walleye pollock, we could argue that maintaining proximity does not require being right on top of a prey patch but only within searching distance of the patch. Because of the size of the patches (some plankton patches are over 10 km in horizontal extent), a fish shoal could be some distance from the center of a plankton patch and still have a good chance of encountering it during a feeding period.

Because of the large spatial extent of many plankton patches and fish shoals, a measure of distance between them should not simply be the center-to-center distance, commonly used in spatial statistics as a distance measure between points. Similarly, the measure of proximity of a fish shoal to plankton patches should not simply be the number of plankton patches at different distances from the shoal (however distance is computed) because this ignores the size of or biomass index in the patches. Finally, in order to ascertain whether the observed proximity between fish shoals and plankton patches is "random" or whether prey are clustered around or dispersed away from fish shoals (or vice versa), some measure of randomness is needed.

Our proximity index was based on Ripley's K (Diggle 1983; Cressie 1993), which calculates the number of points inside a circle of radius h from each point in the sample for a range of values of h. Error bounds for randomness are provided by Monte Carlo distribution of the points at random 100 times and repeating the computation of K after each random distribution. Whenever the empirical K goes outside the error bounds, it indicates nonrandomness and shows either clustering (empirical distribution above the error bounds) or inhibition (empirical distribution below the error bounds) in the underlying spatial proximity.

For our study, we replaced the center-to-center distance with an algorithm for computing distance from the edge of a patch to reflect the fact that contact between patches is a function of their edge-to-edge rather than center-to-center distance. We constructed a polygon at distance h from the edge of a patch (analogous to radius h used in Ripley's K) to represent the region at distance h from that patch. Three alternative measures of distance from a patch were considered as follows. (*i*) Construct a polygon h metres both horizontally and vertically away from each patch-edge-polygon vertex. This method allows the mostly horizontally attenuated polygons (Fig. 4) to expand both horizontally and vertically. (*ii*) Construct a polygon h metres out from each patch-edge-polygon vertex along a line from the center of the patch. This method allows proportional growth of the polygon. (*iii*) Ignore vertical distance and take a distance h only in the horizontal direction. This method overcomes the difficulty that gradients in the horizontal and vertical direction are differently perceived by fish and plankton by ignoring the vertical direction entirely.

To identify patches within a distance h from the base polygon, we included those patches having edge vertices (i.e., wholly or partially contained) within the expanded polygon h meters from the original. Instead of counting the number of such patches, we either summed the biomass index for all such patches (or parts of patches) within the expanded polygon or summed the overlap of the patches (or parts of patches) with the original polygon (not the expanded polygon). The overlap measure used was

$$\text{Overlap} = \frac{\text{patch area} + \text{shoal area}}{2(\text{convex hull area})}$$

where the convex hull is a polygon that entirely encloses all boundary points of both original polygons in such a way that a line connecting any two points in either of the enclosed polygons is entirely inside the convex hull polygon. The patch area is the area in square metres of the plankton patch and the shoal area is that of the fish shoal. The overlap measure for any two patches takes a value between 0 and 1. A value of 1 occurs when two patch polygons have 100% overlap, while the value approaches 0 as the patches get farther apart, are more perpendicular to each other in orientation, or are smaller. Figure 5 is a construction of two patches and their convex hull for two contrasting cases. It shows how the overlap changes as edge-to-edge patch distances change.

[2] Biomass index is used as a measure of patch biomass. It is equal to the patch area times the average S_v for the patch and has not been standardized to true biomass, although it is proportional to patch biomass.

© 1999 NRC Canada

Fig. 5. Example of the convex hull (dotted region plus striped regions) for two patches (*a*) partially overlapping and (*b*) farther apart. The overlap measure is close to 1.0 for the patches in Fig. 5*a* and less than 0.5 for those in Fig. 5*b*.

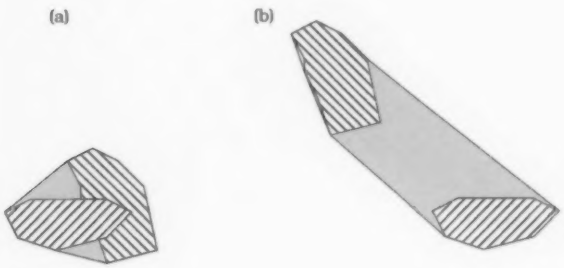

We estimated error bounds for testing the distance-based proximity measure for randomness using a Monte Carlo method. Keeping the original fish shoal locations, plankton patches were uniformly distributed over the region of interest[3] 100 times. The overlap measure was computed for each of these 100 randomizations by growing each fish shoal polygon by distance h between 100 m and 1 km and computing the average overlap with patches, over all shoals, as a function of h. Random distribution of the patches involved changing the horizontal center of each patch without changing its depth or its shape. This specified "random" to mean a set of patches having the same shape and size as the original patches but being randomly distributed horizontally. As such, it does not address questions about whether the patches have random sizes or are at random depths. We decided to accept depth conditions, as influenced by diel migration, and the existing size distribution of the patches as givens rather than testable factors in the proximity context (i.e., we do not consider what the effect would be if the plankton were not near the bottom during the daytime or what the effect of having a different size distribution of plankton would be on proximity).

The distance-based proximity measure was used to examine the spatial relationship of walleye pollock shoals to plankton patches for the same transect data. Each walleye pollock shoal was "grown" in increments of 100 m from 0 to 1 km as a measure of distance from the shoal. The horizontal measure of distance was used. Thus, we emphasized spatial interrelationships over the same spatial scale used in the GAM study (although only the 250-m interval results were shown). Larger scale overlap (i.e., larger than 1 km) could be investigated, but given the limited size of the transect in each region (e.g., 20 km for the front region), larger scale (i.e., 5–10 km) relationships might not be observable because there would be too few intervals in each region.

Results

Figure 4 shows polygons representing (in iconified form) the size and daytime orientation of fish and plankton patches for a single pass of transect A. Surface temperature and bird abundance are shown by panels on top of the main display, while temperature isotherms are overlaid on the main panel. The transect has a well-mixed nearshore region (no stratification), a front region with partial stratification, and a well-stratified offshore region with a well-defined and narrow thermocline. The distribution of fish and plankton for this day differed among these three regions. The nearshore region (to about 6000 m from the start of the transect) contained small shoals and few plankton. The front region (6000 – 32 000 m) contained many smaller fish shoals above the thermocline with small plankton patches below the thermocline and two large fish shoals below the thermocline (examination of target strengths around these shoals indicated that they were not juvenile walleye pollock). The offshore region had fewer fish shoals but extensive plankton patches rising up from the bottom near the end of the transect (near dusk), showing that many plankton are close to the bottom during daytime.

GAM results show the effect of plankton biomass index on walleye pollock biomass index in each bin, along with 95% confidence limits, obtained by bootstrap resampling of the data (Fig. 6). Regressions were significant for the front (p = 0.001) and offshore (p = 0.0009) regions, suggesting that age-0 walleye pollock biomass index increased with increasing plankton biomass index up to 0.01 and then decreased with higher plankton levels and subsequently increased at high plankton levels only in the offshore region. There were too few data in the nearshore region for a meaningful GAM regression.

Results for the distance-based proximity measure for each of the transect A regions are given in Fig. 7. There was significant clustering of plankton around the fish shoals in the nearshore and front regions (the empirical curve is above the upper 95% confidence limit), while in the offshore region, which contained large plankton patches, the distribution was random (the empirical curve is between the upper and lower 95% confidence limits), except at h between 0 and 100 m (Fig. 7*c*). Since this was a daytime transect, there tended to be separation of the plankton and fish, with fish being in the upper water column and plankton near the bottom (Fig. 4). Despite this separation, there is evidence that the fish remained closer to the plankton than would be indicated by a random horizontal distribution of the plankton patches, especially in the nearshore and front regions. Alternatively, from a fish shoal's spatial perspective, there were more plankton patches in the nearshore and front regions within 1 km of the fish shoals than there would have been if the zooplankton patches had been randomly distributed.

The GAM results are consistent with findings of the distance-based proximity. Both suggested a stronger association between fish shoals and plankton patches when plankton biomass was lower. The random distribution of plankton patches around fish shoals and the reduction in fish shoal biomass index at high plankton density, as was observed in the offshore region, both suggest that there was a threshold density of plankton above which there was no small-scale spatial association between fish and plankton. Considering the existence of large plankton patches in the offshore region (Fig. 4), the lack of small-scale proximity between walleye pollock and zooplankton is not surprising. Because these findings are based on only a single transect pass, interpretation of these results must be considered preliminary, and a more complete analysis of this survey data, with a compari-

[3] The distribution is complicated by an edge effect to correct for patches that might partially lie outside the region of interest. This is accomplished by limiting the generated patch locations such that their edges must lie within the study region.

© 1999 NRC Canada

Fig. 6. GAM results for 250-m bins for transect A, September 19, 1995, daytime. Smooths show the effect of plankton on walleye pollock biomass index in the (*a*) front and (*b*) offshore regions. The rug (tick marks) along the bottom of each graph shows the location of the data points. The 95% confidence limits are shown with broken lines.

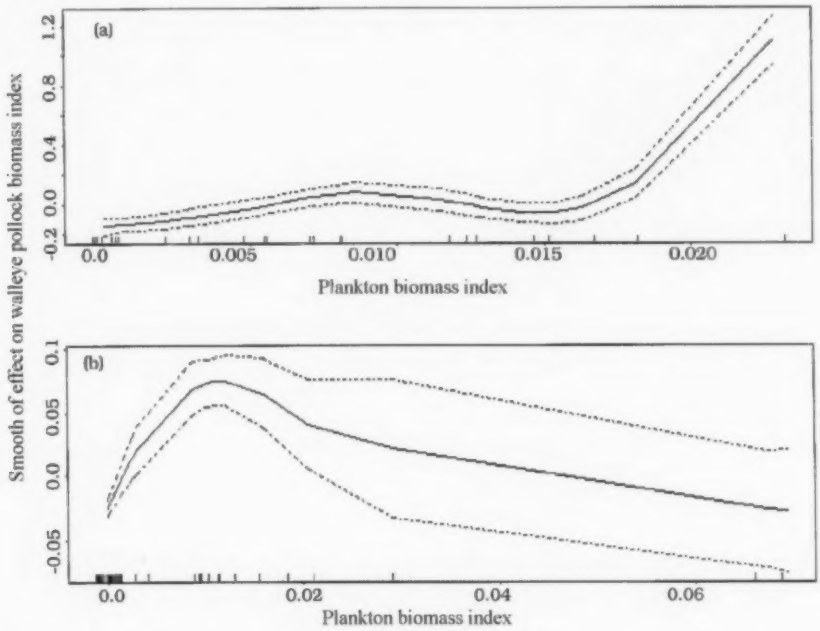

Fig. 7. Results of horizontal proximity measure for a daytime pass of transect A on September 19, 1995, in the (*a*) nearshore, (*b*) front, and (*c*) offshore regions. The nearshore and front regions show clustering of plankton patches around fish shoals, while in the offshore region the plankton patches appear to be randomly distributed around the fish shoals, except between 0 and 100 m distance (clustered). The empirical proximity measures are shown with solid lines and the 95% upper and lower confidence limits are shown with broken lines.

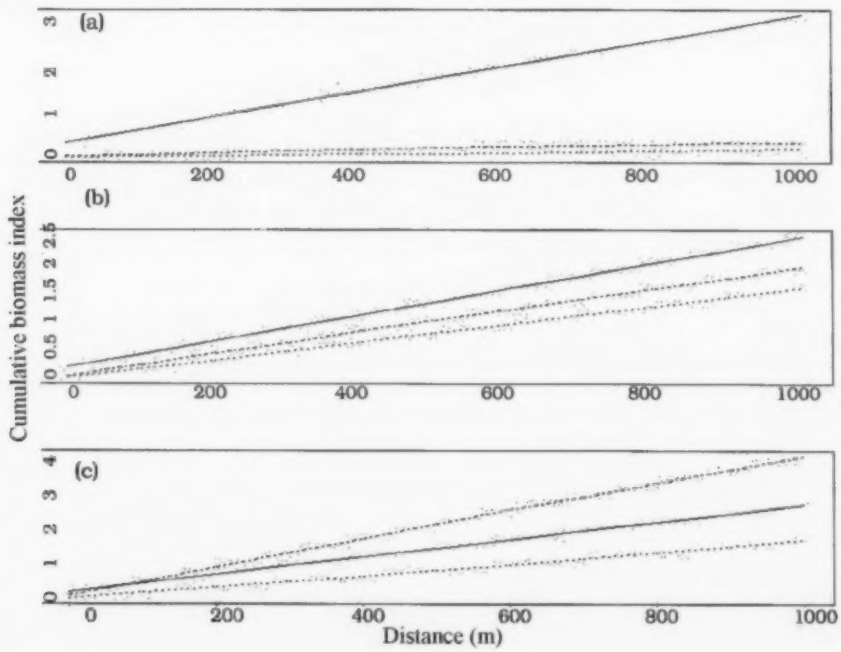

© 1999 NRC Canada

son between transects, day and night passes, and years, is needed.

Discussion

As our ability to effectively distinguish between acoustic measures of fish and plankton in marine ecosystems improves, we are confronted with new challenges in describing and testing their spatial relationship with a view to understanding marine feeding strategies and its repercussions for population dynamics and energetics. The amount of data and the computational demands of processing these data engender a need for visual display tools that can help scientists to examine their data in an explicit spatial context and can allow them to examine and critique the analysis tools used. The FishViewer point-and-click acoustic data viewer presented here is one such tool, hopefully a precursor of many such exploratory data analysis aids for acoustic and accompanying oceanographic and biological data.

We have found the development of algorithms to delineate plankton from juvenile fish patches in acoustic data to be a challenge. We have reported on our current algorithm in the hope that it will be tested and improved with application to other data sets, as has already occurred with the fish identification algorithm that we used (Reid and Simmonds 1993; Swartzman et al. 1994*a*). Our plankton delineation algorithm used data at two frequencies and depended on smaller organisms like plankton giving higher backscatter at higher frequencies, while juvenile fish have very small frequency dependence in their target strengths at these frequencies. A test of the algorithm could be made by comparing the depth distribution of acoustically determined plankton with the depth distribution of zooplankton sampled by accompanying net samples. A stronger test would involve doing the forward calculation on the net survey plankton (Greenlaw 1979; Stanton et al. 1993) to predict what the backscatter from the net-sampled organisms ought to be. We could then ascertain whether the predicted backscatter (in limited areas where net samples were available) agrees with the observed backscatter.

Establishing and interpreting spatial proximity between fish and plankton is complicated by the patchy nature of their spatial organization and temporal change in their distribution (daily, seasonal, and annual). Binning data represents one approach to examining such proximity but has the distinct disadvantage of defining proximity only by horizontal overlap and not distance or depth overlap. In cases where many of the patches are large, as they were in this survey, a distance-based proximity measure including the shape, orientation, and location is desirable. The distance-based proximity test combines a measure of distance between patches with a measure of patch size (biomass index). It extends the strictly biomass index based GAM measure of overlap over horizontal space to examine proximity within a wider area of influence. Furthermore, the distance-based measure takes the existing patches as a baseline measure and examines how proximity would change if the same patches were randomly arranged horizontally over the area of interest. The GAM interval-based measure achieves its confidence limits through bootstrap resampling (not random reorientation) of both the plankton patches and the fish shoals. A more significant GAM relationship derives from narrower confidence limits. Significance in the distance-based proximity measure is also dependent on the confidence limits because wide confidence limits are more likely to lead to the distribution being random.

The two measures define different aspects of proximity. The interval-based measure (GAM) indicated biomass index ranges for the covariate (plankton biomass index) over which the dependent variable (fish biomass index) increased and beyond which it decreased. This could suggest a density threshold above which feeding rate is maximum, thereby necessitating no spatial association. Alternatively, it could suggest depletion of plankton by higher fish biomass index concentrations. The distance-based measure suggested clustering of plankton patches around fish shoals in the nearshore and front regions. The degree of clustering was highest in the nearshore region (as indicated by the empirical curve being much higher than the upper 95% confidence limit), where plankton biomass index was lowest (Fig. 7). In the offshore region, with the highest plankton biomass index (Fig. 4), the plankton were randomly distributed about the fish shoals (the empirical curve is between the upper and lower 95% confidence limits), except at 0 distance (Fig. 7). This also suggests that at higher plankton densities, there was no spatial association between fish and plankton over a horizontal distance range from 100 m to 1 km.

We have chosen to examine the distance-based proximity of plankton patches to fish shoals. We could also examine the proximity of fish shoals to plankton patches — a prey spatial view of their predator. The two measures are not symmetric. We chose the former approach because we perceived the feeding age-0 walleye pollock as more likely to make a behavioral choice around association with their prey that involved horizontal swimming than would the plankton, who appear to use diel migration as a defense against predation.

Horizontal distance and vertical distance are clearly perceived differently by fish and plankton. Thus, we considered several alternative distance measures, although none of them addresses the nonlinearity of the vertical thermocline barrier. One option not considered is to treat above- and below-thermocline biota separately. However, this would neglect the diel migration of plankton. Thus, some of the plankton below the thermocline during the daytime, although they have no physical overlap with the above-thermocline fish, will at night move up near the thermocline and become accessible to these fish. So the daytime proximity measure, if spatial association is the desired criterion, might well ignore the vertical separation, as we did with the walleye pollock – plankton data by using the horizontal distance measure.

Differences in the magnitude of the distance-based proximity measure can be used to compare how much plankton biomass is available to fish shoals in different regions, at different times of the year, or in different years. Such comparisons are possible in a multiyear, multiple-transect study. For example, the low biomass index in the nearshore region (Fig. 7*a*) corroborates that there were fewer prey available for walleye pollock than in the front and offshore regions (Brodeur et al. 1997). As such, we would expect that walleye pollock were less abundant in the nearshore region, which they were.

The proximity tests (both the overlap and biomass indexes) may have general applicability in ecology, particu-

© 1999 NRC Canada

larly in areas where biota aggregate, such as burrowing animals, flocking birds, and herding animals. In fisheries, many juvenile pelagic fish, both marine and freshwater, shoal. For these aggregative groups, distance-based proximity measures may help uncover spatially explicit feeding phenomena not observable with interval-based measures of overlap. The two measures, taken together, can supplement each other to strengthen hypotheses and provide possible insight into spatial interactions between organisms. Working with a proximity index that combines distance, shape, and size of patches has considerable appeal in a situation where the patches cover a significant amount of the study region. Results from the current study, and the widespread nature of aggregation in marine ecosystems, warrant further proximity measure development, analysis, and testing.

Acknowledgments

This is contribution No. B-311 to the Fisheries–Oceanography Cooperative Investigation (FOCI). Funding for this project was provided by the National Oceanographic and Atmospheric Administration (NOAA) Coastal Ocean Program (COP) as part of the Southeast Bering Sea Carrying Capacity Project (SEBSCC). The authors wish to thank Phyllis Stabeno and Sigrid Salo for providing valuable interpretation of oceanographic data and Lorenzo Ciannelli for helpful comments on earlier drafts of this paper. Helpful and incisive reviews were provided by Pierre Petitgas and an anonymous reviewer. Finally, we greatly appreciate the thoughtful editorial and organizational suggestions by series editor Doran Mason.

References

Barange, M. 1994. Acoustic identification, classification and structure of biological patchiness on the edge of the Agulhas Bank and its relation to frontal features. S. Afr. J. Mar. Sci. **14**: 333–347.

Becker, R.A., Chambers, J.M., and Wilks, A.R. 1988. The new S Language. Wadsworth, Pacific Grove, Calif.

Brodeur, R.D., and Wilson, M.T. 1996. Mesoscale acoustic patterns of juvenile walleye pollock (*Theragra chalcogramma*) in the western Gulf of Alaska. Can. J. Fish. Aquat. Sci. **53**: 1951–1963.

Brodeur, R.D., Wilson, M.T., Napp, J.M., Stabeno, P.J., and Salo, S. 1997. Distribution of juvenile pollock relative to frontal structure near the Pribilof Islands, Bering Sea. *In* Proceedings of the International Symposium on the Role of Forage Fishes in Marine Ecosystems. Alaska Sea Grant Publ. AK-SG-97-01. pp. 573–589.

Brown, J.S., and Morgan, R.A. 1995. Effects of foraging behavior and spatial scale on diet selectivity — a test with fox squirrels. Oikos, **74**: 122–136.

Clay, C.S., and Medwin, H. 1977. Acoustical oceanography. John Wiley & Sons, Inc., New York.

Cressie, N.A.C. 1993. Statistics for spatial data. John Wiley & Sons, Inc., New York.

Diggle, P.J. 1983. Statistical analysis of spatial point patterns. Academic Press, London, U.K.

Foote, K.G., Knudsen, H.P., Vestnes, G., MacLennan, D.N., and Simmonds, E.J. 1987. Calibration of acoustic instruments for fish density estimation: a practical guide. Int. Counc. Explor. Sea Coop. Res. Rep. No. 144.

Greenlaw, C.F. 1979. Acoustical estimation of zooplankton populations. Limnol. Oceanogr. **24**: 226–242.

Haralick, R., and Shapiro, L. 1992. Image analysis. VI. Addison-Wesley, New York.

Hastie, T., and Tibshirani, R. 1990. Generalized additive models. Chapman and Hall, London, U.K.

Holliday, D.V., and Pieper, R.E. 1980. Volume scattering strengths and zooplankton distributions at acoustic frequencies between 0.5 and 3 MHz. J. Acoust. Soc. Am. **67**: 135–146.

Horne, J.K., and Schneider, D.C. 1994. Lack of spatial coherence of predators with prey: a bioenergetic explanation for Atlantic cod *Gadus morhua* feeding on capelin *Mallotus villosus*. J. Fish Biol. **45**(Suppl. A): 131–142.

Lascara, K. 1997. SCANFISH transect visualization tool. http://www.ccpo.odu.edu/~lascara/Ties/ties.html.

Mackas, D.L., Denman, K.L., and Abbott, M.K. 1985. Plankton patchiness: biology in the physical vernacular. Bull. Mar. Sci. **37**: 652–674.

Mackas, D.L., Kieser, R., Saunders, M., Yelland, D.R., Brown, R.M., and Moore, D.F. 1997. Aggregation of euphausiids and Pacific hake (*Merluccius productus*) along the outer continental shelf off Vancouver Island. Can. J. Fish. Aquat. Sci. **54**: 2080–2096.

Mann, K.H., and Lazier, J.R.N. 1991. Dynamics of marine ecosystems. Blackwell Scientific Publications, Cambridge, Mass.

Maravelias, C.D., and Reid, D.G. 1997. Identifying the effects of oceanographic features and zooplankton on prespawning herring abundance using generalized additive models. Mar. Ecol. Prog. Ser. **147**: 1–9.

Mullin, M.M. 1993. Webs and scales: physical and ecological processes in marine fish recruitment. Univ. Wash. Sea Grant Publ. WSG-IS-93-01.

Nero, R.W., and Magnuson, J.J. 1989. Characterization of patches along transects using high-resolution 70-kHz integrated acoustic data. Can. J. Fish. Aquat. Sci. **46**: 2055–2064.

Precision Visuals. 1992. Command language users guide. Precision Visuals, Boulder, Co.

Reid, D.G., and Simmonds, E.J. 1993. Image analysis techniques for the study of fish school structure from acoustic survey data. Can. J. Fish. Aquat. Sci. **50**: 886–893.

Rose, G.A., and Leggett, W.C. 1990. The importance of scale to predator–prey spatial correlations: an example of Atlantic fishes. Ecology, **71**: 33–43.

Stabeno, P.J., Schumacher, J.D., Salo, S.A., Hunt, G.L., and Flint, M. 1999. The physical environment around the Pribilof Islands. *In* The Bering Sea: physical, chemical and biological dynamics. *Edited by* T.R. Loughlin and K. Ohtani. Alaska Sea Grant Press, Anchorage, Alaska. In press.

Stanton, T.K., Chu, D., Wiebe, P.H., and Clay, C.S. 1993. Average echoes from randomly oriented random-length finite cylinders: zooplankton models. J. Acoust. Soc. Am. **94**: 3463–3472.

Swartzman, G.L. 1997. Analysis of the summer distribution of fish schools in the Pacific Eastern Boundary Current. ICES J. Mar. Sci. **54**: 105–116.

Swartzman, G.L., Stuetzle, W., Kulman, K., and Wen, N. 1994*a*. Modeling the distribution of fish schools in the Bering Sea: morphological school identification. Nat. Resour. Model. **8**: 177–194.

Swartzman, G., Stuetzle, W., Kulman, K., and Powojowski, M. 1994*b*. Relating the distribution of pollock schools in the Bering Sea to environmental factors. ICES J. Mar. Sci. **51**: 481–484.

Traynor, J.J. 1996. Target strength measurements of walleye pollock (*Theragra chalcogramma*) and Pacific whiting (*Merluccius productus*). ICES J. Mar. Sci. **53**: 253–258.

Wiebe, P.H, Greene, C.H., Stanton, T.K., and Burczynski, J. 1990. Sound scattering by live zooplankton and micronekton: empirical studies with a dual-beam acoustical system. J. Acoust. Soc. Am. **88**: 2346–2360.

© 1999 NRC Canada

ASSIGNMENT OF COPYRIGHT

Ms. No. _____

To: NATIONAL RESEARCH COUNCIL OF CANADA ("NRC") Research Press

From: _____

_____

_____

_____

(name and address of author signing this form)

This refers to the manuscript entitled: _____

_____

written by myself and the following additional author(s): _____

_____

for publication in: _____

1. I declare that the list of authors fairly conforms to academic conventions about who should be listed. I declare that the manuscript, or its equivalent, has not been submitted for publication elsewhere. If it is accepted for publication by the National Research Council of Canada, I will ensure that it, or its equivalent, is not submitted for publication elsewhere.

2. I declare that I am (check ONE):

☐ (a)	the sole owner of the copyright relating to the manuscript, and →	I **assign** to NRC the entire copyright.
☐ (b)	a part owner of the copyright, in conjunction with interests held by co-authors or their employers, and →	I **assign** to NRC my entire interest in the copyright, and I expect the co-authors to also sign a form like this one.
☐ (c)	an agent of my employer with authority to assign the copyright owned by the employer, who is: _____, and →	I **assign** to NRC, on behalf of my employer, my employer's entire interest in the copyright relating to the manuscript, and I expect the co-authors to also sign a form like this one.
☐ (d)	a public servant in Canada (federal, provincial or territorial) or the United Kingdom, so that the copyright is owned by Her Majesty, and →	I have obtained the approval of my employer, according to the terms of my employment, to grant NRC **non-exclusive permission** to publish the manuscript and administer the copyright.
☐ (e)	a public servant of the United States of America, and subject to the law that creates no U.S. copyright for the manuscript, and →	I **assign** to NRC, on behalf of my employer, my employer's entire interest in any copyright that may exist outside the U.S., and I expect the co-authors to sign a form like this one.

3. I understand that my submission of this document does not guarantee publication, and that publication will not occur until **all authors** have provided a copyright transfer. If the manuscript is not published within 2 years after I sign this, the assignment is revoked.

Signed at _____ on _____

(City and Province/State) (Date)

_____

(Signature)

[Standard NRC form; alterations not acceptable.]

Comments on Copyright Transfer
(with extracts from the *Copyright Act*, Revised Statutes of Canada 1985, chapter C-42, as amended)

The publisher is not permitted to publish the manuscript without permission or an assignment of ownership of copyright. For greatest flexibility, and to be prepared to deal with future uses of the published material, the publisher requires ownership.

The owner may assign the right, but that assignment must be in writing:

13.(4) The owner of the copyright in any work may assign the right, either wholly or partially, and either generally or subject to territorial limitations, and either for the whole term of the copyright or for any other part thereof, and may grant any interest in the right by licence, but no assignment or grant is valid unless it is in writing signed by the owner of the right in respect of which the assignment or grant is made, or by his duly authorized agent.

The owner may be the author, but in many cases, the owner is the author's employer:

13.(3) Where the author of a work was in the employment of some other person under a contract of service or apprenticeship and the work was made in the course of his employment by that person, the person by whom the author was employed shall, in the absence of any agreement to the contrary, be the first owner of the copyright, but where the work is an article or other contribution to a newspaper, magazine or similar periodical, there shall, in the absence of any agreement to the contrary, be deemed to be reserved to the author a right to restrain the publication of the work, otherwise than as part of a newspaper, magazine or similar periodical.

The only exception to taking ownership arises when the manuscript is covered by Crown copyright owned by a Canadian government.

12. Without prejudice to any rights or privileges of the Crown, where any work is, or has been, prepared or published by or under the direction or control of Her Majesty or any government department, the copyright in the work shall, subject to any agreement with the author, belong to Her Majesty and in that case shall continue for the remainder of the calendar year of the first publication of the work and for a period of fifty years following the end of that calendar year.

Governments, and in particular the federal government, do not have a simple mechanism for assigning ownership of this particular type of Crown asset. Therefore, when an author is a public servant so that there is Crown copyright in the manuscript, a simple permission to use is acceptable to the publisher, if it is granted by a person with appropriate authority.

CESSION DU DROIT D'AUTEUR

Document n° _____

Au : CONSEIL NATIONAL DE RECHERCHES DU CANADA («CNRC») - Presses scientifiques
De : _____
_____
_____
_____
(nom et adresse de l'auteur qui signe le présent formulaire)

La présente cession porte sur le document intitulé : _____
_____

rédigé par moi, en collaboration avec l'auteur/les auteurs suivant(s) : _____
_____

aux fins de publication dans : _____

1. Je déclare que la liste des auteurs ci-dessus respecte les pratiques usuelles de rédaction savante quant aux personnes dont le nom doit être cité. Je déclare que le document ou son équivalent n'a pas été soumis à quelque autre organisme aux fins de publication. Si le CNRC accepte de publier le document, je m'assurerai que celui-ci ou son équivalent n'est soumis à aucun autre organisme aux fins de publication sans en obtenir la permission préalable du CNRC.

2. Je déclare être (UN SEUL choix) :

☐ (a)	le seul titulaire de droit d'auteur afférent au document,	et →	je **cède** le droit d'auteur intégral au CNRC.
☐ (b)	un titulaire partite du droit d'auteur, de concert avec des coauteurs ou leurs employeurs,	et →	je **cède** ma part du droit d'auteur au CNRC et m'attends à ce que les coauteurs signent une entente comparable.
☐ (c)	un agent de mon employeur ayant l'autorité de céder le droit d'auteur appartenant à l'employeur, nommément : _____,	et →	je **cède** au CNRC, au nom de mon employeur, la part entière du droit d'auteur afférent au document appartenant à mon employeur, et m'attends à ce que les coauteurs signent une entente comparable.
☐ (d)	un fonctionnaire du Canada (fédéral, provincial ou territorial) ou du Royaume-Uni, donc le droit d'auteur appartient à Sa Majesté,	et →	j'ai obtenu de mon employeur, en vertu de mes conditions d'emploi, l'autorisation d'accorder au CNRC la **permission non exclusive** de publier le document et de gérer le droit d'auteur.
☐ (e)	un fonctionnaire des États-Unis d'Amérique, donc sujet à la loi qui n'associe aucun droit d'auteur américain au document,	et →	je **cède** au CNRC, au nom de mon employeur, la part entière de quelque droit d'auteur en vigueur ailleurs qu'aux É.-U. appartenant à mon employeur, et m'attends à ce que les coauteurs signent une entente comparable.

3. Je comprends que la soumission du document ne garantit aucunement sa publication et que la publication ne pourra être réalisée tant que **tous les auteurs** n'auront pas signé une cession du droit d'auteur. Si le document n'est pas publié dans les deux années suivant ma signature des présentes, la cession sera automatiquement révoquée.

Signé à _____, le _____
(ville et province/état) (date)

_____
(signature)

[Formulaire normalisé du CNRC; aucune modification permise.]

Commentaires sur la cession du droit d'auteur
(accompagnés d'extraits de la *Loi sur le droit d'auteur*, Lois révisées du Canada 1985, chapitre C-42 modifié)

L'éditeur ne peut publier un document sans la permission ou une cession du droit d'auteur. Pour des raisons de souplesse et en vue de l'utilisation future du document publié, l'éditeur doit devenir titulaire du droit d'auteur.

Le titulaire peut céder le droit, mais cette cession doit être faite par écrit :

13.(4) Le titulaire du droit d'auteur sur une oeuvre peut céder ce droit, en totalité ou en partie, d'une façon générale, ou avec des restrictions territoriales, pour la durée complète ou partielle de la protection; il peut également concéder, par une licence, un intérêt quelconque dans ce droit; mais la cession ou la concession n'est valable que si elle est rédigée par écrit et signée par le titulaire du droit qui en fait l'objet, ou par son agent dûment autorisé.

Le titulaire peut être l'auteur, mais dans plusieurs cas, le titulaire est l'employeur de l'auteur:

13.(3) Lorsque l'auteur est employé par une autre personne en vertu d'un contrat de louage de service ou d'apprentissage, et que l'oeuvre est exécutée dans l'exercice de cet emploi, l'employeur est, à moins de stipulation contraire, le premier titulaire du droit d'auteur; mais lorsque l'oeuvre est un article ou un autre contribution, à un journal, à une revue ou à un périodique du même genre, l'auteur, en l'absence de convention contraire, est réputé posséder le droit d'interdire la publication de cette oeuvre ailleurs que dans un journal, une revue ou un périodique semblable.

La seule exception dans la cession du droit d'auteur est lorsque le document est associé au droit d'auteur de la Couronne, qui appartient au gouvernement du Canada .

12. Sous réserve de tous les droits ou privilèges de la Couronne, le droit d'auteur sur les oeuvres préparées ou publiées par l'entremise, sous la direction ou la surveillance de Sa Majesté ou d'un ministère du gouvernement, appartient, sauf stipulation conclue avec l'auteur, à Sa Majesté et, dans ce cas, il subsiste jusqu'à la fin de la cinquantième année suivant celle de la première publication de l'oeuvre.

Les gouvernements, en particulier le gouvernement fédéral, ne disposent pas d'un mécanisme simple de cession de droit d'auteur pour ce genre de biens de la Couronne. C'est pourquoi lorsqu'un auteur est un fonctionnaire et que, par conséquent, le droit d'auteur appartient à la Couronne, une simple permission d'usage est suffisante pour l'éditeur, pour autant que celle-ci ait été octroyée par une personne jouissant de l'autorité nécessaire pour ce faire.

NRC·CNRC

Publishing Conference Proceedings?

WE CAN HELP

NRC Research Press...

...offers a ***complete range*** of services to assist you in preparing your Conference Proceedings for publication:

- publication of the program booklet
- publication of an abstracts booklet
- logo and cover design
- publication of your proceedings
- reprints for individual papers
- promotion and marketing
- distribution and sales
- electronic publication of papers or abstracts on the World Wide Web.

NRC Research Press can offer you a package to suit your needs, ranging from production of "print-ready" manuscripts, to fully edited and typeset proceedings in print and electronic formats.

For a price quotation for your publication needs please contact:

Business Manager, NRC Research Press
National Research Council Canada
Building M-55, Ottawa, ON K1A 0R6
Telephone: (613) 993-9093
Fax: (613) 952-7656
E-mail: rp.business@nrc.ca
WWW: http://www.nrc.ca/cisti/journals/

For complete management of all your conference needs, please contact:

Head, Conference Services
Conference Services Office
National Research Council Canada
Ottawa, ON K1A 0R6
Telephone: (613) 993-9432
Fax: (613) 957-9828
E-mail: laurier.forget@nrc.ca

Canada | National Research Council Canada | Conseil national de recherches Canada

CNRC·NRC

Vous publiez des actes de conférences?

COMPTEZ SUR NOUS

Les Presses scientifiques du CNRC...

...offrent une ***gamme exhaustive*** de services qui satisferont tous vos besoins de publication reliés à vos conférences :

- publication de programmes
- publication de brochures de résumés
- conception graphique (logos et pages couvertures)
- publication de comptes rendus de conférences
- tirés à part du texte de présentations particulières
- promotion et marketing
- distribution et ventes
- publication électronique d'articles ou de résumés aux fins de diffusion sur le World Wide Web.

Les Presses scientifiques du CNRC sauront constituer un ensemble de services qui répondra à vos besoins, depuis le simple traitement d'articles jusqu'aux services intégraux de publication traditionnelle ou électronique d'actes de conférences.

Pour discuter de nos tarifs à la lumière de vos besoins particuliers, nous vous invitons à communiquer avec :

Gestionnaire, Activités commerciales
Presses scientifiques du CNRC
Conseil national de recherches Canada, Édifice M-55
Ottawa, ON K1A 0R6
Téléphone : (613) 993-9093
Télécopieur : (613) 952-7656
Adresse électronique : rp.business@nrc.ca
WWW : http://www.nrc.ca/cisti/journals/rjfr.html

Si vous désirez déléguer la gestion de vos conférences, nous vous invitons à communiquer avec :

Chef, Services de conférences
Bureau des services de conférences
Conseil national de recherches Canada
Ottawa, ON K1A 0R6
Téléphone : (613) 993-9432
Télécopieur : (613) 957-9828
Adresse électronique : laurier.forget@nrc.ca

Canada | Conseil national de recherches Canada | National Research Council Canada

Guide to the Parasites of Fishes of Canada. Part IV. Trematoda

David I. Gibson

373 pages
Softcover/Édition brochée
March/mars 1996
ISBN 0-660-16403-5
ISSN 0706-6481
NRC/CNRC 40083
$42.95/42,95 $
Canadian Special Publication of Fisheries and Aquatic Sciences/ Publication spéciale canadienne des sciences halieutiques et aquatiques 124

More than 80 keys leading to the identification of more than 220 species of trematode parasites of Canadian fishes and diagnoses of more than 80 family–group taxa and 130 genera are given. Each genus is illustrated. For each species a Canadian host list, locality data, and any relevant remarks are included. Visit http://www.nrc.ca/cisti/journals/40083/133to136.html at the NRC Research Press Web to view a short chapter of this book.

On retrouve plus de 80 clefs qui permettent d'identifier quelque 220 espèces de trématodes parasites des poissons du Canada et la description de plus de 80 taxums de famille/groupe et de 130 genres. Chaque genre y est illustré. À chaque espèce sont associées des données sur l'emplacement et des remarques particulières. Visitez http://www.nrc.ca/cisti/journals/40083/f133to6.html au site Web des Presses scientifiques du CNRC pour afficher un court chapitre du livre.

To order copies of this publication/Pour commander des exemplaires de ce livre

- Telephone: (613) 993-0151
- Fax: (613) 952-7656
- Mail orders: Monograph Orders, NRC Research Press, National Research Council Canada, Ottawa, Ontario K1A 0R6, Canada
- Internet e-mail: research.journals@nrc.ca
- World Wide Web: http://www.nrc.ca/cisti/journals/formmono.html

Canadian customers please add 7% GST. Orders from Quebec add a further 6.5% QST to the total price including GST. Make cheque or money order payable to "Receiver General for Canada, credit NRC". Note that for all orders outside Canada, rates are in U.S. dollars. All sales are final.

- Téléphone : (613) 993-0151
- Télécopieur : (613) 952-7656
- Par la poste : Monographies, Presses scientifiques du CNRC, Conseil national de recherches Canada, Ottawa (Ontario) K1A 0R6, Canada
- Courrier électronique : research.journals@nrc.ca
- World Wide Web : http://www.nrc.ca/cisti/journals/formmofr.html

Les clients canadiens doivent ajouter la TPS de 7 %. Les clients du Québec doivent ajouter 6,5 % de TVQ au montant total, une fois la TPS additionnée. Libellez le chèque ou le mandat à l'ordre du «Receveur général du Canada, au crédit du CNRC». Pour les clients non canadiens, les prix sont en dollars américains. Aucun remboursement.

Please send me ____ copies of/Veuillez me faire parvenir ____ exemplaire(s) de *Guide to the Parasites of Fishes of Canada: Part IV. Trematoda.*

NRC Research Press

Monograph Program

Presses scientifiques du CNRC

Programme de monographies

NRC·CNRC

PLEASE PRINT/LETTRES MOULÉES

☐ Payment enclosed/Paiement inclus ☐ Charge to/Imputer à ☐ Visa ☐ MasterCard

Account no./ N° de compte | Expiry date/ Date d'expiration

Name/Nom

Signature/Signature

Address/Adresse

City/Ville Province/Province

Postal code/Code postal Country/Pays

Telephone/Téléphone Fax/Télécopieur

e-mail/Courrier électronique Date of order/Date de la commande

Jason D. Stockwell and Brett M. Johnson	**140–151**	Field evaluation of a bioenergetics-based foraging model for kokanee (*Oncorhynchus nerka*)
Geoffrey B. Steinhart and Wayne A. Wurtsbaugh	**152–161**	Under-ice diel vertical migrations of *Oncorhynchus nerka* and their zooplankton prey
Chris Luecke, M. William Wengert, and Roger W. Schneidervin	**162–169**	Comparing results of a spatially explicit growth model with changes in the length–weight relationship of lake trout (*Salvelinus namaycush*) in Flaming Gorge Reservoir
John K. Horne, Paul E. Smith, and David C. Schneider	**170–179**	Comparative examination of scale-explicit biological and physical processes: recruitment of Pacific hake (*Merluccius productus*)
David C. Schneider, Tammo Bult, Robert S. Gregory, David A. Methven, Danny W. Ings, and Vytenis Gotceitas	**180–187**	Mortality, movement, and body size: critical scales for Atlantic cod (*Gadus morhua*) in the Northwest Atlantic
Gordon Swartzman, Richard Brodeur, Jeffrey Napp, Danny Walsh, Roger Hewitt, David Demer, George Hunt, and Elizabeth Logerwell	**188–198**	Relating spatial distributions of acoustically determined patches of fish and plankton: data viewing, image analysis, and spatial proximity

National Research Council Canada
Ottawa, Canada K1A 0R6

Conseil national de recherches Canada
Ottawa, Canada K1A 0R6

Postage paid at Ottawa
Publications mail
Registration No. 1240579

Port payé à Ottawa
Poste-publication
Enregistrement n° 1240579

Canadian Journal of Fisheries and Aquatic Sciences

Volume 56, Supplement 1, 1999

Journal canadien des sciences halieutiques et aquatiques

Volume 56, supplément 1, 1999

Doran M. Mason and Stephen B. Brandt	**1–3**	Space, time, and scale: new perspectives in fish ecology and management
Jerald S. Ault, Jiangang Luo, Steven G. Smith, Joseph E. Serafy, John D. Wang, Robert Humston, and Guillermo A. Diaz	**4–25**	A spatial dynamic multistock production model
Leif Nøttestad, Jarl Giske, Jens Chr. Holst, and Geir Huse	**26–34**	A length-based hypothesis for feeding migrations in pelagic fish
Thomas R. Hrabik and John Magnuson	**35–42**	Simulated dispersal of exotic rainbow smelt (*Osmerus mordax*) in a northern Wisconsin lake district and implications for management
Frank J. Rahel and Nathan P. Nibbelink	**43–51**	Spatial patterns in relations among brown trout (*Salmo trutta*) distribution, summer air temperature, and stream size in Rocky Mountain streams
Timothy E. Essington and James F. Kitchell	**52–60**	New perspectives in the analysis of fish distributions: a case study on the spatial distribution of largemouth bass (*Micropterus salmoides*)
Daniel E. Schindler	**61–70**	Migration strategies of young fishes under temporal constraints: the effect of size-dependent overwinter mortality
E. Conrad Lamon III and C.A. Stow	**71–85**	Sources of variability in microcontaminant data for Lake Michigan salmonids: statistical models and implications for trend detection
Erik R. Zlokovitz and David H. Secor	**86–93**	Effect of habitat use on PCB body burden in Hudson River striped bass (*Morone saxatilis*)
Thomas C. Kline, Jr.	**94–117**	Temporal and spatial variability of $^{13}C/^{12}C$ and $^{15}N/^{14}N$ in pelagic biota of Prince William Sound, Alaska
G.A. Rose and D.W. Kulka	**118–127**	Hyperaggregation of fish and fisheries: how catch-per-unit-effort increased as the northern cod (*Gadus morhua*) declined
David A. Beauchamp, Casey M. Baldwin, Jason L. Vogel, and Chad P. Gubala	**128–139**	Estimating diel, depth-specific foraging opportunities with a visual encounter rate model for pelagic piscivores

Continued on inside back cover / Suite au verso

Canada

Printed in Canada by / Imprimé au Canada par
University of Toronto Press Inc.
Typesetting by / Typographie par
NRC Research Press / Presses scientifiques du CNRC

0706-652X(1999)56+1;1-B

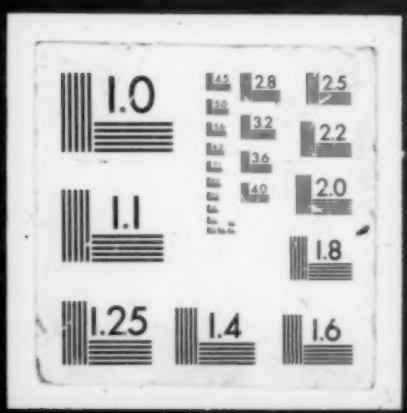
1.0
1.1
1.25
1.4
1.6
2.8
3.2
3.6
4.0
2.5
2.2
2.0
1.8